



**US Army Corps
of Engineers®**
Engineer Research and
Development Center

Initial Research into the Effects of Woody Vegetation on Levees

Volume II of IV: Field Data Collection

Maureen K. Corcoran, John F. Peters, Joseph B. Dunbar, Jose L. Llopis, Fred T. Tracy, Johannes L. Wibowo, Janet E. Simms, Christopher E. Kees, S. Kyle McKay, J. Craig Fischenich, Matthew W. Farthing, M. Eileen Glynn, Bryant A. Robbins, Ryan C. Strange, Martin T. Schultz, Joan U. Clarke, Thomas E. Berry, Charles D. Little, and Landris T. Lee

July 2011

Initial Research into the Effects of Woody Vegetation on Levees

Volume II of V: Field Data Collection

Maureen K. Corcoran, John F. Peters, Joseph B. Dunbar,
Jose L. Llopis, Johannes L. Wibowo, Janet E. Simms,
M. Eileen Glynn, Bryant A. Robbins, Ryan C. Strange,
and Landris T. Lee,

*Geotechnical and Structures Laboratory
U.S. Army Engineer Research and Development Center
3909 Halls Ferry Road
Vicksburg, MS 39180-6199*

Fred T. Tracy

*Information Technology Laboratory
U.S. Army Engineer Research and Development Center
3909 Halls Ferry Road
Vicksburg, MS 39180-6199*

S. Kyle McKay, Martin T. Schultz, Thomas E. Berry,
Joan U. Clarke, and J. Craig Fischenich

*Environmental Laboratory
U.S. Army Engineer Research and Development Center
3909 Halls Ferry Road
Vicksburg, MS 39180-6199*

Christopher E. Kees, Matthew W. Farthing, and Charles D. Little

*Coastal and Hydraulics Laboratory
U.S. Army Engineer Research and Development Center
3909 Halls Ferry Road
Vicksburg, MS 39180-6199*

Final report

Executive Summary

At the request of Headquarters, USACE (HQUSACE), in July 2007, the U.S. Army Engineer Research and Development Center (ERDC) conducted an extensive literature review focusing on the effects of woody vegetation on levees. The review indicated that minimal data exist on the scientific relationship between levees and woody vegetation. Because of the lack of scientific data, HQUSACE concluded that without further research, scientific questions regarding the effects of woody vegetation on levees would remain unanswered. In April 2008, HQUSACE requested that ERDC begin research on this issue. ERDC formed a team consisting of scientists and engineers with geotechnical, environmental, geological, biological and geophysical expertise to assess the impact of woody vegetation on the structural performance of earthen levees using scientific and engineering methods.

The ERDC team prepared a scope of work (SOW) to study the effect of living woody vegetation on slope stability, seepage analyses were used to assess changes in hydraulic conductivity and the effects of the initiation of internal erosion. These particular topics were selected based on input from federal and state agencies, which showed that directing the research toward the effects of woody vegetation on slope stability and internal erosion would advance the understanding of the interaction of roots within an engineered levee. However, the selection of slope stability and seepage for this research does not diminish the need for future research on other topics related to the effects of woody vegetation on levees. Rather, this study should be viewed as an initial research effort into a very complex issue.

This study consists of the following three interrelated components:

1. Site visits, field data collection, and laboratory testing to obtain pertinent information necessary to support subsequent modeling and simulation efforts.
2. Modeling and simulation of the engineering, geological and environmental conditions, and structural performance of the levee system, relative to the initiation of internal erosion and slope stability, under various loading conditions.

3. Developing results and conclusions regarding engineering impacts living of woody vegetation on slope stability and internal erosion.

Site investigations identified root system characteristics using geophysical survey methods, root excavation methods, and root strength (pull-out) tests. Root studies focused on living, healthy woody vegetation. Data collected by these methods were used in the seepage and slope stability analyses. One of the major findings from field investigations was the relative efficacy of electrical resistivity imaging (ERI) measurements in determining the size and extent of tree root balls, relative to other geophysical methods, such as ground penetrating radar (GPR) or electromagnetic (EM) techniques. Root excavation proved successful for validating GPR in sandy soils.

In addition to identifying root characteristics, field studies included soil permeameter testing for the purpose of calculating hydraulic conductivity to test the hypothesis that tree roots influence soil hydraulic properties. Permeameter tests were performed within the root system and in a nearby control area without a tree but within the same soil horizon. Soil samples were retrieved during permeameter testing for soil classification. Statistical methods were used to calculate and compare the mean values of the two data sets: root system versus the control area. The resulting mean values were not used directly in the model simulations because the modeling was performed prior to the field data collection. However, for consistency the resulting means and ranges of calculated hydraulic conductivities were compared to those found in the site engineering documents as well as the values used for seepage models. The statistical comparison of means did not produce conclusive evidence that tree roots influence the average hydraulic conductivity of a soil layer. Only one test showed evidence of an existing macropore associated with a tree site. These analyses were conducted for Sacramento, CA; Burlington, WA; Portland, OR; Lewisville, TX; Vicksburg, MS; Albuquerque, NM; Boca Raton, FL, and Danville, PA.

Slope stability models and seepage models used both two-dimensional (2-D) and three-dimensional (3-D) finite element computer codes. The stability analysis uses limit equilibrium methods for 2-D analyses and deformational analyses in three dimensions. Seepage models included analysis for internal erosion.

The ERDC research used SEEP2D for three analysis in the seepage analyses. These analyses included conducting a sensitivity analysis for hydraulic

conductivity as it affects the groundwater flow field, producing a random macropore heterogeneity in a block of soil representing a root system, and representing a root as a defect extending from the surface to the base of the blanket. The extended root system was depicted as a uniform area of low hydraulic conductivity, which is an extreme representation that may not reflect actual field conditions. The results from these analyses are specific only to the levees studied for this research.

In the first approach, extensive 2-D sensitivity analyses were performed where the hydraulic conductivity of the woody vegetation zone was systematically varied from the surrounding soil by a factor of β , ranging from 1,000 to 0.001. When β is equal to 1.0, the analysis simulates a levee without woody vegetation. In these analyses, the woody vegetation (tree) zone was modeled as a continuum of porous media with dimensions 6 ft wide by 5 ft deep. Various hydraulic loadings were also applied in the sensitivity analyses using steady state and transient conditions.

Sensitivity analyses also investigated the influence of woody vegetation location on model output. Simulations included woody vegetation zones located at the levee toe, beyond the levee toe, levee slope, and levee crest on both the riverside and landside of the studied levees. Pore pressure and the phreatic surface from the seepage analysis were used in the slope stability model to determine effective stresses for strength computations. Two-dimensional analyses were conducted for Sacramento, CA; Burlington, WA; Portland, OR; and Albuquerque, NM.

The second seepage analysis recognized the heterogeneity of macropores within both a root system and surrounding soil matrix by randomly distributing hydraulic conductivity throughout the rectangular configuration representing a root system. Velocity vectors show that a random heterogeneous zone can have flow paths that support large flow velocities. However, research does not exist on whether high velocities result in the initiation of internal erosion.

The third approach in the seepage analysis considers the probability of a tree root creating a seepage exit thereby initiating internal erosion in the soil foundation. This analysis follows the procedure described by Schaefer et al. (2010). Results from this analysis are specific only to the levees studied for this research. Because of the complexity of processes related to seepage and piping and the lack of research supporting such processes, only

the initiation of processes leading to internal erosion is addressed in this research. Analyses were conducted for Burlington, WA, Portland, OR, and Albuquerque, NM. Based on these analyses, the probability of initiation of internal erosion is negligible from woody vegetation at the toe of the levee for the Burlington and Portland sites. The results for Albuquerque yielded a factor of safety slightly higher than 1.0 but the probability of internal erosion occurring is negligible to 0.25.

Two-dimensional stability analyses were conducted using the Spencer Limit Equilibrium Method available within the UTEXAS4 slope stability software. Fixed input parameters for the analysis were soil properties, levee geometry, and root properties. Root reinforcement properties were derived from field test data collected by ERDC for this research. Variable input parameters included: tree position on the levee slope, tree weight, pore pressure, phreatic surface, river elevation, wind load, and failure criteria. In a simplified slope stability analysis, effective stresses for strength is to use the phreatic surface from the seepage analysis, and rather than using the pore pressures computed in the finite element analysis, an assumption is made as to what the pore pressures are below the phreatic surface. However, in the ERDC study, an accurate method of using pore pressures, as computed from the seepage flow analysis, in the slope stability analysis is used. Tree weights and wind loads are divided by 6 based on the 6-ft width because only one foot-wide slice is considered. Because tree root growth is variable, even for a given species in the same region, the root extent used in the models was varied to accommodate the inconsistent patterns of root growth. In general, this study observed that trees on the upper part of the slope decreased the factor of safety because they add weight. Trees near the toe increased the factor of safety because of the reinforcing effects of the roots and the increased counterweight effect of the tree to slope movement. Trees at midslope had lesser effect on the factor of safety because they acted as a load, but not a counterweight, and the roots are too shallow to reach the failure zone within the midslope region.

The objectives of the 3-D seepage and stability analyses were to validate the results of the more simplified 2-D model simulation. The 2-D model geometry and material properties of the woody vegetation zone were imported into the 3-D model. These analyses were made for the Sacramento, CA, and Burlington, WA, sites. The 3-D model modified the geometry to include three woody vegetation zones located at the toe (landslide toe, Sacramento; riverside toe, Burlington) and positioned 20 ft

apart, thereby creating a 3-D version of the 2-D model simulating a row of trees. Only steady state simulations were considered. Local 3-D effects were observed in the flow field around the zones, but resulted change was not apparent to the global flow field, location of the seepage face, or pore pressure gradients. The lack of change is attributed to the particularly shallow depth of the zones relative to the deeper confining layers.

Trees and their root systems were found to have an effect on overall levee stability. Results indicated that a tree can increase or decrease the factor of safety with respect to slope stability depending on the location of the tree on the levee. Additionally, when wind speeds greater than 40 MPH are considered, the factor of safety decreases for all tree locations evaluated for this study (top of slope, midslope, and toe of slope). In this study, reductions in factor of safety reflect specific conditions and may not represent the worst case scenario at these sites. Because of the extreme variability in geology, tree species, climate, and soils, the impact of trees on levees must be analyzed on a case-by-case basis. However, this study does reveal that the tree weight, tree location, root system, and wind loads are all significant parameters that must be taken into account when evaluating the effect of a tree on slope stability for a particular site.

There are many other possible effects of woody vegetation on a levee that were not studied in this research. These are equally important in attempting to fully understand the impact of woody vegetation on levee integrity as those selected for the ERDC research. The possibility of dead or decaying root systems providing preferential flow paths for piping to occur is a topic that requires further study. In addition, the seepage analysis is limited to studying the onset of internal erosion through addressing the contributing factors. Additional research is needed outside the ERDC scope of work to fully evaluate the progression of piping. Until advances are made in this area, it is difficult to fully assess the impact of woody vegetation on the progression of piping.

Efforts reported in this research were focused on living, healthy woody vegetation. Results from numerical analyses were based on models from sandy or silty sand levees. Levees consisting of clay were not included in the ERDC numerical analyses. This research did not address performance of levee systems with the presence of dead, woody vegetation and decaying roots. Other areas of concern that lie outside the scope of work are the contribution, if any, of windthrow and animal burrows to seepage; the

impact of woody vegetation within a levee channel on the hydraulic conveyance of a river; biological impacts, such as the prevention of growth of protective grass cover beneath a tree; and the contribution of woody vegetation to scour and erosion. The effect of woody vegetation on levee inspection, maintenance, and accessibility to the levee for flood fighting were not considered in this study. To have a more complex understanding of potential impacts of woody vegetation on levees, further research in these areas is needed.

DISCLAIMER: The contents of this report are not to be used for advertising, publication, or promotional purposes. Citation of trade names does not constitute an official endorsement or approval of the use of such commercial products. All product names and trademarks cited are the property of their respective owners. The findings of this report are not to be construed as an official Department of the Army position unless so designated by other authorized documents.

DESTROY THIS REPORT WHEN NO LONGER NEEDED. DO NOT RETURN IT TO THE ORIGINATOR.

Contents

Executive Summary	ii
Figures and Tables.....	xiv
Preface	xxxii
Unit Conversion Factors.....	xxxiii
Acknowledgements.....	xxxiv
1 Introduction.....	1
2 Study Sites.....	3
Site assessments	4
3 Geology	8
Data collection and approach	8
Sacramento, CA	10
<i>Introduction</i>	10
<i>Geological setting</i>	10
<i>Previous geotechnical investigations and geology studies</i>	15
<i>Levee failure mechanisms in point bar deposits</i>	17
<i>Cross section at Site B</i>	23
<i>Laboratory soils data</i>	26
<i>Hydraulic conductivity values</i>	30
<i>Groundwater conditions</i>	33
<i>Troxler measurements</i>	33
Burlington, WA	67
<i>Introduction</i>	67
<i>Previous studies</i>	67
<i>Geological setting</i>	67
<i>Levee failure mechanisms</i>	70
<i>Levee profiles</i>	70
<i>Laboratory soils data</i>	71
<i>Hydraulic conductivity</i>	74
<i>Groundwater conditions</i>	77
Albuquerque, NM.....	77
<i>Introduction</i>	77
<i>Previous studies</i>	81
<i>Geological setting</i>	82
<i>Levee failure mechanisms</i>	82
<i>Levee profile</i>	84
<i>Laboratory soils data</i>	90
<i>Hydraulic conductivity</i>	90

<i>Groundwater conditions</i>	90
<i>Troxler measurements</i>	90
Portland, OR	126
<i>Introduction</i>	126
<i>Previous studies</i>	128
<i>Geological setting</i>	128
<i>Levee failure mechanisms</i>	129
<i>Levee profiles</i>	129
<i>Laboratory soils data</i>	131
<i>Hydraulic conductivity</i>	133
<i>Groundwater conditions</i>	133
New Orleans, LA	133
<i>Introduction</i>	133
<i>Study area</i>	135
<i>Geological setting</i>	138
<i>Levee profile</i>	139
<i>Root excavation</i>	140
Boca Raton, FL	141
<i>Introduction</i>	141
<i>Geologic setting</i>	141
<i>Laboratory soils data and hydraulic conductivity</i>	145
<i>Groundwater conditions</i>	145
<i>Troxler measurements</i>	145
Danville, PA.....	172
<i>Introduction</i>	172
<i>Geologic setting</i>	174
<i>Danville Borough levee assessment and results</i>	176
<i>Laboratory soils data and hydraulic conductivity</i>	180
<i>Groundwater conditions</i>	180
<i>Troxler measurements</i>	181
Vicksburg, MS.....	181
<i>Introduction</i>	181
<i>Geologic setting</i>	204
<i>Laboratory soils data and hydraulic conductivity</i>	208
<i>Groundwater conditions</i>	208
<i>Troxler measurements</i>	209
4 Root Characterization.....	216
<i>Geophysical investigation</i>	216
<i>Electrical resistivity imaging</i>	216
<i>Electromagnetic (EM) surveys</i>	222
<i>Ground-penetrating radar (GPR)</i>	223
<i>3-D-Radar Geoscope</i>	224
<i>GPR system</i>	226
<i>GPR interpretation</i>	226
<i>Study locations</i>	227
<i>Sacramento, CA</i>	227

<i>Background</i>	227
<i>Geophysical survey methods</i>	229
<i>Electrical resistivity imaging (ERI)</i>	229
<i>2-D data acquisition and processing</i>	229
<i>Data interpretation: 2-D</i>	230
<i>Data interpretation: Quasi 3-D</i>	233
<i>3-D data acquisition and processing</i>	233
<i>Data interpretation</i>	235
<i>ERI results</i>	236
<i>EM survey</i>	237
<i>Data acquisition and processing</i>	237
<i>Data interpretation</i>	237
<i>GPR survey</i>	241
<i>Data acquisition and processing</i>	241
<i>Data interpretation</i>	242
<i>Comparison of GPR data with 3-D resistivity study</i>	244
<i>Conclusions</i>	244
<i>Portland, OR</i>	248
<i>Background</i>	248
<i>Geophysical survey methods</i>	248
<i>ERI survey</i>	249
<i>2-D data acquisition and processing</i>	249
<i>Data interpretation: 2-D</i>	250
<i>Data interpretation: Quasi 3-D</i>	251
<i>3-D data acquisition and processing</i>	252
<i>Data interpretation</i>	253
<i>Summary of ERI results</i>	255
<i>EM survey</i>	256
<i>Data acquisition and processing</i>	256
<i>Data interpretation</i>	256
<i>GPR</i>	257
<i>Data acquisition and processing</i>	257
<i>Data interpretation</i>	257
<i>Summary of GPR surveys</i>	261
<i>Conclusions</i>	267
<i>Burlington, WA</i>	267
<i>Background</i>	267
<i>Geophysical survey methods</i>	269
<i>ERI survey</i>	269
<i>Data interpretation: 2-D</i>	271
<i>Data interpretation: Quasi 3-D</i>	271
<i>3-D data acquisition and processing</i>	272
<i>Data interpretation</i>	273
<i>EM survey</i>	275
<i>Data acquisition and processing</i>	275
<i>Data interpretation</i>	275
<i>Summary of ERI and EM Results</i>	276
<i>GPR</i>	276
<i>Data acquisition and processing</i>	276
<i>Data interpretation</i>	279
<i>Summary of GPR surveys</i>	280
<i>Conclusions</i>	282
<i>Albuquerque, NM</i>	285
<i>Background</i>	285
<i>Data acquisition and processing</i>	286
<i>Results and interpretation</i>	287
<i>Site 1</i>	287
<i>Site 2</i>	289
<i>Conclusions</i>	290
<i>Lewisville Dam, Lewisville, TX</i>	291
<i>Background</i>	291

Geophysical investigation	293
Geophysical survey methods.....	293
ERI.....	293
Data acquisition and processing	293
Results and interpretation	295
EM survey	299
Data acquisition and processing	299
Results and interpretation	299
Conclusions	301
New Orleans, LA	303
Background	303
Inner Harbor Navigation Canal (IHNC) site	303
EM survey	303
Data acquisition and processing	303
Data interpretation	304
GPR survey.....	305
Data acquisition and processing	305
Data interpretation	306
Data interpretation	306
17th Street Canal site	307
EM survey	308
Data acquisition and processing	308
Data interpretation	308
GPR survey.....	312
Data acquisition and processing	312
Data interpretation	312
Summary.....	313
Vicksburg, MS.....	314
Background	314
Study site	315
Geophysical survey methods.....	315
ERI survey	315
Data acquisition and processing	315
Data interpretation	317
GPR survey.....	319
Data acquisition and processing	319
Data interpretation	319
450-MHz Data.....	321
900-MHz Data.....	321
Conclusions	321
In situ root architectural subsampling	323
Sample design.....	323
Field data collection	330
Soil analysis.....	332
Post-processing of root architectural data	333
Root architecture analysis	335
Bulk properties of root system	347
Comparison of GPR data with root characterization.....	349
Summary	349
Calibration of GPR.....	357
Methods.....	357
Study site	357
Ground-penetrating radar.....	358
In situ measurement.....	359
Laboratory analyses.....	361
Results.....	361
Ground-penetrating radar.....	361

<i>In situ measurement</i>	363
Conclusions	368
<i>Opportunities for future research</i>	368
Geo-referenced LiDAR collection for root characterization	371
<i>Background</i>	371
<i>Method</i>	371
<i>Tree canopy and ground scan</i>	372
<i>Partial excavation and root scan</i>	373
<i>Full excavation and root scan</i>	374
Conclusions	375
5 In Situ Hydraulic Conductivity Tests.....	376
Objectives	376
Approach.....	377
Background	378
<i>Definition of hydraulic conductivity</i>	378
<i>Measurement of in situ hydraulic conductivity</i>	379
<i>Test plan</i>	381
Equipment selection	382
<i>Permeameter</i>	382
<i>Soil moisture probe</i>	383
<i>Density soil sampling auger kit</i>	384
Test procedures.....	385
<i>Determining meaningful test boundaries</i>	385
<i>Borehole testing and sampling protocol</i>	387
<i>Calculation of field saturated hydraulic conductivity</i>	392
Field test results.....	392
<i>Sacramento, CA</i>	393
<i>Burlington, WA</i>	393
<i>Albuquerque, NM Site 1</i>	393
<i>Albuquerque, NM Site 2</i>	398
<i>Portland, OR</i>	398
<i>Boca Raton, FL</i>	405
<i>Lewisville, TX</i>	405
<i>Danville, PA</i>	410
<i>Vicksburg, MS</i>	410
<i>Summary of field tests for hydraulic conductivity</i>	415
Statistical analysis of the hydraulic conductivity test data	415
<i>Equality of variances</i>	418
<i>Comparison of tree and control data</i>	418
<i>Correlation of hydraulic conductivity and distance from tree</i>	420
Results of statistical analyses	420
<i>Comparison of tree and control data</i>	420
<i>Correlation of hydraulic conductivity and distance from tree</i>	422
Conclusions of statistical analysis	422
6 Root Reinforcement for Slope Stability	425

Purpose.....	425
Root pullout device development.....	425
Root pullout testing procedure.....	427
<i>Site preparation</i>	427
<i>Equipment preparation</i>	427
<i>Testing execution</i>	428
Root pullout field test.....	428
Root pullout test results.....	428
Statistical analysis of root pullout data.....	433
References.....	444
Appendix A: Troxler Data.....	461
Appendix B: IHNC Levee Report.....	489
Appendix C: Geophysical Data	502
Appendix D: Hydraulic Conductivity Values for Test Sites.....	629
Appendix E: Field Trip Reports	636
Appendix F: Histograms of In situ-Permeability Data Sets	667
Appendix G: Root Pullout Test Results	673
Appendix H: Glossary.....	680

Figures and Tables

Figures

Figure 1. Overview of data acquisition and application for noninvasive and invasive mapping.....	2
Figure 2. Google Earth (2009) aerial view of the ERDC study site in the Pocket Area. Bottom photograph is the landside levee slope with valley oaks on the landside slope, and a walnut tree at the toe of the levee.....	11
Figure 3. Major physiographic features in the Central Valley of California includes the Sacramento and San Joaquin valleys (Shlemon and Begg 1973). Site B is located in the Pocket Area along the East Bank of the Sacramento River. Rivers draining the Sierra Nevada Mountains area are captured by the Sacramento and San Joaquin rivers and drain into the delta region.....	12
Figure 4. Generalized geological map of the greater Sacramento study area and the Pocket Area showing major boundaries: flood basin, point bar, alluvial terrace. Pocket Area is located on the east bank (point bar side) of the river. (Mulder 2009).....	14
Figure 5. Typical cross section of the levee and soil-bentonite-cement (SBC) slurry cutoff wall for the Pocket Area, Sacramento River (Wahler and Associates 1989a).....	16
Figure 6. Geology map by William Lettis and Associates (URS 2010a) showing CPT locations and natural levee and point bar deposits within the Site B river reach.....	18
Figure 7. Geological cross section from Station 1450 to 1500 for the DWR urban levee assessment (URS 2010a). Section is upstream of Site B with Boring B-8 at upstream edge of Site B.....	19
Figure 8. Geological cross section from Station 1500 to 1550 for the DWR urban levee assessment (URS 2010a). CPT VM0009-16C (CPT-16C) corresponds to the location and lithology used for the levee analysis at Site B. The CPT-16C boring log is shown in Figure 10.....	20
Figure 9. Cross section and levee profile developed from CPT WM0009-16C and existing elevation and bathymetry data.....	24
Figure 10. Drilling log for CPT-WM0009-16C and subdivision of the soil data into levee fill, top blanket, and substratum (URS 2010a). CPT data are classified according to relationships by Robertson and Campanella (1983) between sleeve friction and tip resistance of the cone.....	25
Figure 11. The locations of six borings within 1,000 ft of Site B (URS 2008).....	26
Figure 12. USACE (2005a) cross section through the Site B reach (at dashed red line) showing the soils within the levee and foundation. Laboratory soils data summarized in the table of this figure.....	27
Figure 13. Levee profile used for 2005 seepage evaluation near Site B (USACE 2005a). Hydraulic conductivity used for soil layers is presented in the table.....	29
Figure 14. The location of the geophysical grid in Sacramento, CA, used for Troxler measurements.....	35
Figure 15. Grid system and transect lines for Troxler measurements in Sacramento, CA.....	36
Figure 16a. Dry density (lb/ft ³) from Troxler measurements for Sacramento, CA.....	38

Figure 16b. Wet density ((lb/ft ³) from Troxler measurements for Sacramento, CA.....	39
Figure 16c. Moisture content (lb/ft ³) from Troxler measurements for Sacramento, CA.....	40
Figure 16d. Moisture (%) from Troxler measurements for Sacramento, CA.....	41
Figure 17a. Dry density (lbs/ft ³) verses depth (in.) and distance (ft.) from Troxler measurements for, North Transect,Sacramento, CA.....	43
Figure 17b. Wet density (lbs/ft ³) verses depth (in.) and distance (ft.) from Troxler measurements for, North Transect,Sacramento, CA.....	44
Figure 17c. Moisture content (lbs/ft ³) verses depth (in.) and distance (ft.) from Troxler measurements for, North Transect,Sacramento, CA.....	45
Figure 17d. Moisture (%) verses depth (in.) and distance (ft.) from Troxler measurements for, North Transect, Sacramento, CA.....	46
Figure 18a. Dry density (lbs/ft ³) verses depth (in.) and distance (ft.) from Troxler measurements for, South Transect, Sacramento, CA.....	48
Figure 18b. Wet density (lbs/ft ³) verses depth (in.) and distance (ft.) from Troxler measurements for, South Transect, Sacramento, CA.....	49
Figure 18c. Moisture content (lbs/ft ³) verses depth (in.) and distance (ft.) from Troxler measurements for, South Transect, Sacramento, CA.....	50
Figure 18d. Moisture (%) verses depth (in.) and distance (ft.) from Troxler measurements for, South Transect, Sacramento, CA.....	51
Figure 19a. Dry density (lbs/ft ³) verses depth (in.) and distance (ft.) from Troxler measurements for, East Transect, Sacramento, CA.....	53
Figure 19b. Wet density (lbs/ft ³) verses depth (in.) and distance (ft.) from Troxler measurements for, East Transect, Sacramento, CA.....	54
Figure 19c. Moisture content (lbs/ft ³) verses depth (in.) and distance (ft.) from Troxler measurements for, East Transect, Sacramento, CA.....	55
Figure 19d. Moisture (%) verses depth (in.) and distance (ft.) from Troxler measurements for, East Transect, Sacramento, CA.....	56
Figure 20a. Dry density (lbs/ft ³) verses depth (in.) and distance (ft.) from Troxler measurements for, Transect 1, Sacramento, CA	58
Figure 20b. Wet density (lbs/ft ³) verses depth (in.) and distance (ft.) from Troxler measurements for, Transect 1, Sacramento, CA	59
Figure 20c. Moisture content (lbs/ft ³) verses depth (in.) and distance (ft.) from Troxler measurements for, Transect 1, Sacramento, CA	60
Figure 20d. Moisture (%) verses depth (in.) and distance (ft.) from Troxler measurements for, Transect 1, Sacramento, CA.....	61
Figure 21a. Dry density (lbs/ft ³) verses depth (in.) and distance (ft.) from Troxler measurements for, Transect 2, Sacramento, CA	63
Figure 21b. Wet density (lbs/ft ³) verses depth (in.) and distance (ft.) from Troxler measurements for, Transect 2, Sacramento, CA	64
Figure 21c. Moisture content (lbs/ft ³) verses depth (in.) and distance (ft.) from Troxler measurements for, Transect 2, Sacramento, CA	65
Figure 21d. Moisture (%) verses depth (in.) and distance (ft.) from Troxler measurements for, Transect 2, Sacramento, CA.....	66
Figure 22. The ERDC study site, outlined by the red box, in Burlington, WA.....	68
Figure 23a. Aerial photograph of the reach of Skagit River under study at Burlington, WA, (Google Earth Image 2010). Close-up view of the study area presented in Figure 23b.....	69

Figure 23b. Close-up view of the Burlington, WA, study site (Google Earth image 2010).	69
Figure 24a. Cross sections E and F used for the geotechnical evaluation (Golder Associates 2009). Levee fill in cross section F-F' is a section proposed to be added as part of the planned improvements. Only current levee conditions were modeled by ERDC.	72
Figure 24b. Cross section G-G' used for the geotechnical evaluation (Golder Associates 2009). Levee fill (dark brown) identified in the bottom profile corresponds to new levee to be added as part of the planned improvements. Only current levee conditions were modeled by ERDC.....	73
Figure 25a. Right bank cross sections through the study reach showing USCS soils in subsurface and stratigraphy according to environments of deposition (Golder Associates 2009). Orientation of each section is with view looking to the west (downstream edge on left side and right edge corresponding to upstream side). Note the location of perpendicular profiles E and F in the ERDC study and soils at each location. Legend to cross sections is presented in Figure 25b.	75
Figure 25b. Right bank cross section through the study reach showing USCS soils in subsurface and stratigraphy according to environments of deposition (Golder Associates 2009). Orientation of each section is with view looking to the west (downstream edge on left side and right edge corresponding to upstream side). Note the location of perpendicular profile F used in the ERDC study and soils at each location.	76
Figure 26. Location of two sites evaluated by the ERDC study (Sites 1 and 2). Components of the levee system are based on phases of construction begun in 1954 (base map from U.S. Army Corps Engineers, Albuquerque District).....	79
Figure 27. Location of Site 1, Albuquerque, NM.....	80
Figure 28. Geological map of the study area showing general soils and their age (Connell 2008).	83
Figure 29. Albuquerque Levee profile showing toe drain and irrigation canal on landside (USACE 1954a).....	85
Figure 30a. Profile of the west levee at Station 535 showing idealized case from plans and specs (top) and current condition as determined from LiDAR data and Google Earth image (bottom profile).....	86
Figure 30b. Typical profile identified for the Corrales Levees (USACE 1993, plates 7 and 9). Levee characteristics include slopes of 1V 2.5 H, 12-ft-wide crest, and ground surface at approximately 4,976 ft amsl. Datums for the elevation are referenced to NGVD 1929.....	87
Figure 31. LiDAR image (top) and profile (bottom) from Station 535 (or Station 104,529) showing elevation of top of levee, banks of canal, and landside and flood side ground surface.	89
Figure 32. Profile developed for the west Rio Grande Levee from geotechnical and LiDAR data. Trees were modeled along various locations across the levee profile.	91
Figure 33. Boring log from RGL-8A2S-51.	92
Figure 34. Grain size data for boring RGL-8A2S-51.	93
Figure 35. Location map of Site 1 and Site 2, Albuquerque, NM.....	95
Figure 36. Levee locations for Site 1 and Site 2, Albuquerque, NM.	96
Figure 37. East levee at Site 1 showing the floodplain, Albuquerque, NM.	97
Figure 38. East levee at Site 1 showing the wooded area, Albuquerque, NM.	98
Figure 39. West levee at Site 2, Albuquerque, NM.	99
Figure 40a. Dry density (lb/ft ³) verses depth (in.) and distance (ft.) from Troxler measurements for, Site 1 and 2, Albuquerque, NM.	101

Figure 40b. Wet density (lb/ft ³) verses depth (in.) and distance (ft.) from Troxler measurements for, Site 1 and 2, Albuquerque, NM.....	102
Figure 40c. Moisture content (lb/ft ³) verses depth (in.) and distance (ft.) from Troxler measurements for, Site 1 and 2, Albuquerque, NM.....	103
Figure 40d. Moisture (%) verses depth (in.) and distance (ft.) from Troxler measurements for, Site 1 and 2, Albuquerque, NM.....	104
Figure 41a. Dry density (lb/ft ³) verses depth (in.) and distance (ft.) from Troxler measurements for, all levees, Albuquerque, NM.....	107
Figure 41b. Wet density (lb/ft ³) verses depth (in.) and distance (ft.) from Troxler measurements for, all levees, Albuquerque, NM.....	108
Figure 41c. Moisture content (lb/ft ³) verses depth (in.) and distance (ft.) from Troxler measurements for, all levees, Albuquerque, NM.....	109
Figure 41d. Moisture (%) verses depth (in.) and distance (ft.) from Troxler measurements for, all levees, Albuquerque, NM.....	110
Figure 42a. Dry density (lb/ft ³) verses depth (in.) and distance (ft.) from Troxler measurements for, floodplain, Albuquerque, NM.....	112
Figure 42b. Wet density (lb/ft ³) verses depth (in.) and distance (ft.) from Troxler measurements for, floodplain, Albuquerque, NM.....	113
Figure 42c. Moisture content (lb/ft ³) verses depth (in.) and distance (ft.) from Troxler measurements for, floodplain, Albuquerque, NM.....	114
Figure 42d. Moisture (%) verses depth (in.) and distance (ft.) from Troxler measurements for, floodplain, Albuquerque, NM.....	115
Figure 43a. Dry density (lb/ft ³) verses depth (in.) and distance (ft.) from Troxler measurements for, wooded area, Albuquerque, NM.....	117
Figure 43b. Wet density (lb/ft ³) verses depth (in.) and distance (ft.) from Troxler measurements for, wooded area, Albuquerque, NM.....	118
Figure 43c. Moisture content (lb/ft ³) verses depth (in.) and distance (ft.) from Troxler measurements for, wooded area, Albuquerque, NM.....	119
Figure 43d. Moisture (%) verses depth (in.) and distance (ft.) from Troxler measurements for, wooded area, Albuquerque, NM.....	120
Figure 44a. Dry density (lb/ft ³) verses depth (in.) and distance (ft.) from Troxler measurements for, west levee at site 2, Albuquerque, NM.....	122
Figure 44b. Wet density (lb/ft ³) verses depth (in.) and distance (ft.) from Troxler measurements for, west levee at site 2, Albuquerque, NM.....	123
Figure 44c. Moisture content (lb/ft ³) verses depth (in.) and distance (ft.) from Troxler measurements for, west levee at site 2, Albuquerque, NM.....	124
Figure 44d. Moisture (%) verses depth (in.) and distance (ft.) from Troxler measurements for, west levee at site 2, Albuquerque, NM.....	125
Figure 45. Google Earth image of the Portland study area, top photo shows the Willamette River converging with the Columbia River, bottom photo shows close-up and profile location (red box in top photo) (Google Earth 2010).....	127
Figure 46a. Geologic map of the Portland Quadrangle (Beeson et al. 1991). The legend is presented in Figure 46b.....	130
Figure 46b. Map legend for Figure 46a.....	131
Figure 47. Typical levee profile from NE Marine Drive and corresponding flood elevations (Dickenson et al. 2000). This profile was further modified to reflect the actual site	

conditions based on Google Earth (2010) imagery, LiDAR data, and Columbia River bathymetry (2009 data). Boring data for C-1, profile S-1 were used to describe the subsurface soils and existing laboratory data were used to describe the engineering properties of the various soil layers.....	132
Figure 48. Profile used to model levee and foundation conditions for the Portland site (Dickenson et al. 2000). Levee is composed of sandy soils and the foundation contains a fine-grained top blanket of silt and clay, underlain by pervious substratum composed of silty sands and sands.	134
Figure 49a. Location of the 17th Street Canal study site.....	136
Figure 50. New Orleans surface geology map showing major depositional environments (i.e., point bar (Hpm1), natural levee (Hnl), swamp (Hds), and marsh (Hdl)), woody vegetation study sites (blue rectangles), and the major Hurricane Katrina canal levee failures (red circles) (Saucier 1994). Natural levees from the Mississippi River and abandoned distributary channels (i.e., Bayou Des Families, Metarie, Sauvage, Gentilly) correspond to high ground in the greater New Orleans area.....	139
Figure 51. View of typical levee and I-wall flanking the drainage and harbor canals in the greater New Orleans area. View is from the west levee at IHNC. Photograph shows woody vegetation being removed from the right-of-way and stacked along levee slope for later pick-up and disposal.	140
Figure 52. Study site at Boca Raton, FL, where a fig tree was evaluated.....	142
Figure 53. View of fig trees studied at the Boca Raton, FL. Top photo is view looking south on east side of canal. This tree was tested for soil permeability using the permeameter. Bottom photo is view looking north and shows another fig tree adjacent to entrance into wildlife park. Levee is to the right of photo. Both trees were measured with the Troxler neutron density gage for soil moisture and density.	143
Figure 54. View looking south of the levee system adjacent to the Arthur R. Marshall Loxahatchee National Wildlife Refuge. Top photo shows canal on protected side and marsh on flood side. Pervious nature of the levee soils are reflected by seepage at levee toe on landside. Water level in the marsh was about 1 to 2 ft higher than protected side.	144
Figure 55. Location map for the three sites in Boca Raton, FL.	146
Figure 56a Dry density (lbs/ft ³) from Troxler measurements for Boca Raton, FL.....	148
Figure 56b. Wet density (lbs/ft ³) from Troxler measurements for Boca Raton, FL.....	149
Figure 56c. Moisture content (lbs/ft ³) from Troxler measurements for Boca Raton, FL.....	150
Figure 56d. Moisture (%) from Troxler measurements for Boca Raton, FL	151
Figure 57a. Dry density (lbs/ft ³) verses depth (in.) and distance (ft.) from Troxler measurements for, flagged region, Boca Raton, FL.....	153
Figure 57b. Wet density (lbs/ft ³) verses depth (in.) and distance (ft.) from Troxler measurements for, flagged region, Boca Raton, FL.....	154
Figure 57c. Moisture content (lbs/ft ³) verses depth (in.) and distance (ft.) from Troxler measurements for, flagged region, Boca Raton, FL.....	155
Figure 57d. Moisture (%) verses depth (in.) and distance (ft.) from Troxler measurements for, flagged region, Boca Raton, FL.....	156
Figure 58a. Dry density (lbs/ft ³) verses depth (in.) and distance (ft.) from Troxler measurements for, tree 1, Boca Raton, FL.....	158
Figure 58b. Wet density (lbs/ft ³) verses depth (in.) and distance (ft.) from Troxler measurements for, tree 1, Boca Raton, FL.....	159

Figure 58c. Moisture content (lbs/ft ³) verses depth (in.) and distance (ft.) from Troxler measurements for, tree 1, Boca Raton, FL.....	160
Figure 58d. Moisture (%) verses depth (in.) and distance (ft.) from Troxler measurements for, tree 1, Boca Raton, FL.....	161
Figure 59a. Dry density (lbs/ft ³) verses depth (in.) and distance (ft.) from Troxler measurements for, tree 2, Boca Raton, FL.....	163
Figure 59b. Wet density (lbs/ft ³) verses depth (in.) and distance (ft.) from Troxler measurements for, tree 2, Boca Raton, FL.....	164
Figure 59c. Moisture content (lbs/ft ³) verses depth (in.) and distance (ft.) from Troxler measurements for, tree 2, Boca Raton, FL.....	165
Figure 59d. Moisture (%) verses depth (in.) and distance (ft.) from Troxler measurements for, tree 2, Boca Raton, FL.....	166
Figure 60a. Dry density (lbs/ft ³) verses depth (in.) and distance (ft.) from Troxler measurements for, levee, Boca Raton, FL.....	168
Figure 60b. Wet density (lbs/ft ³) verses depth (in.) and distance (ft.) from Troxler measurements for, levee, Boca Raton, FL.....	169
Figure 60c. Moisture content (lbs/ft ³) verses depth (in.) and distance (ft.) from Troxler measurements for, levee, Boca Raton, FL.....	170
Figure 60d. Moisture (%) verses depth (in.) and distance (ft.) from Troxler measurements for, levee, Boca Raton, FL.....	171
Figure 61. Study area along the Susquehanna River at Danville, Pennsylvania. Close-up view in bottom of photo shows the levee center line and the site studied at Station 122 + 90. Note the trees growing at the edge of the VFZ.....	173
Figure 62. View of Danville levee looking southwest at Station 122 + 90. Silver maple stumps along edge of the vegetation free zone were removed in 2009.....	175
Figure 63a. Center line boring from Station 122 + 90, continued (Schnabel 2010).....	177
Figure 64. The study site in Danville, PA.....	182
Figure 65a. Dry density (lbs/ft ³) from Troxler measurements for Danville, PA.....	184
Figure 65b. Wet density (lbs/ft ³) from Troxler measurements for Danville, PA.....	185
Figure 65c. Moisture content (lbs/ft ³) from Troxler measurements for Danville, PA.....	186
Figure 65d. Moisture (%) from Troxler measurements for Danville, PA.....	187
Figure 66a. Dry density (lbs/ft ³) verses depth (in.) and distance (ft.) from Troxler measurements for, Transect 1, Danville, PA.....	189
Figure 66b. Wet density (lbs/ft ³) verses depth (in.) and distance (ft.) from Troxler measurements for, Transect 1, Danville, PA.....	190
Figure 66c. Moisture content (lbs/ft ³) verses depth (in.) and distance (ft.) from Troxler measurements for, Transect 1, Danville, PA.....	191
Figure 66d. Moisture (%) verses depth (in.) and distance (ft.) from Troxler measurements for, Transect 1, Danville, PA.....	192
Figure 67a. Dry density (lbs/ft ³) verses depth (in.) and distance (ft.) from Troxler measurements for, Transect 2, Danville, PA.....	194
Figure 67b. Wet density (lbs/ft ³) verses depth (in.) and distance (ft.) from Troxler measurements for, Transect 2, Danville, PA.....	195
Figure 67c. Moisture content (lbs/ft ³) verses depth (in.) and distance (ft.) from Troxler measurements for, Transect 2, Danville, PA.....	196

Figure 67d. Moisture (%) verses depth (in.) and distance (ft.) from Troxler measurements for, Transect 2, Danville, PA.....	197
Figure 68a. Dry density (lbs/ft ³) verses depth (in.) and distance (ft.) from Troxler measurements for, Transect 3, Danville, PA.....	199
Figure 68b. Wet density (lbs/ft ³) verses depth (in.) and distance (ft.) from Troxler measurements for, Transect 3, Danville, PA.....	200
Figure 68c. Moisture content (lbs/ft ³) verses depth (in.) and distance (ft.) from Troxler measurements for, Transect 3, Danville, PA.....	201
Figure 68d. Moisture (%) verses depth (in.) and distance (ft.) from Troxler measurements for, Transect 3, Danville, PA.....	202
Figure 69. Location of the Vicksburg, MS, study site in relationship to the City of Vicksburg and the Mississippi River. The study site was in a gravel pit south of Vicksburg in hills bordering the Mississippi River Alluvial Valley. These hills are composed of Tertiary sediments veneered by wind blow silt (loess) derived from exposed fine-grained Mississippi River sediments from melting Pleistocene glaciers in the northern latitudes.	203
Figure 70. Aerial view of the local gravel pit where an oak tree and pine tree were studied. Geophysical surveys were performed at both sites. LiDAR surveys were performed only at the oak site. Excavation of roots was performed at both tree sites. Hamer Creek is the local drainage and is tributary to the Big Black River, which in turn drains into the Mississippi River.	204
Figure 71. Close-up view of the oak tree where LiDAR and geophysical surveys were conducted.	206
Figure 72. Top photo is view of pine tree at the Warren County gravel pit used to test ground penetrating radar for mapping roots. Bottom photo shows the underlying sand and gravel foundation being mined for aggregate. The tree being studied is the farthest tree in the right side of photograph.	207
Figure 73. Location of transect for Troxler measurements in Vicksburg, MS.	210
Figure 74a. Dry density (lbs/ft ³) verses depth (in.) and distance (ft.) from Troxler measurements for Vicksburg, MS.	212
Figure 74b. Wet density (lbs/ft ³) verses depth (in.) and distance (ft.) from Troxler measurements for Vicksburg, MS.	213
Figure 74c. Moisture content (lbs/ft ³) verses depth (in.) and distance (ft.) from Troxler measurements for Vicksburg, MS.	214
Figure 74d. Moisture (%) verses depth (in.) and distance (ft.) from Troxler measurements for Vicksburg, MS.	215
Figure 75. Advanced Geosciences SuperSting R8 electrical resistivity meter.	221
Figure 76. Geonics EM38-MK2 terrain conductivity meter.	223
Figure 77. 3-D-Radar B1831 antenna array with 31 antenna pair.	225
Figure 78. Towed configuration of the 3-D-Radar B1831 antenna array.	226
Figure 79. Location of Site B, Sacramento, CA.	228
Figure 80. 2-D resistivity survey layout, Site B, Sacramento, CA.	229
Figure 81. Layout of 2-D lines used for quasi 3-D processing, Site B, Sacramento, CA.	230
Figure 82. Inversion results for 2-D lines 6 through 11, Site B, Sacramento, CA. Ovals mark approximate tree root locations.	231
Figure 83. Inversion results for 2-D lines 0 through 4, Site B, Sacramento, CA.	232
Figure 84. Quasi 3-D inverted resistivity image, Site B, Sacramento, CA.	234

Figure 85. 3-D resistivity survey layout, Site B, Sacramento, CA.....	234
Figure 86. 3-D inverted resistivity image, Site B, Sacramento, CA. The black oval indicates the tree location.....	235
Figure 87. EM38 survey line layout, Site B, Sacramento, CA.....	238
Figure 88. EM38-MK2 conductivity survey results, 0.5-m inter-coil separation, vertical dipole mode, Site B, Sacramento CA.....	239
Figure 89. EM38-MK2 conductivity survey results, 1.0-m inter-coil separation, vertical dipole mode, Site B, Sacramento, CA.....	239
Figure 90. EM38-MK2 in-phase survey results, 0.5-m inter-coil separation, vertical dipole mode, Site B, Sacramento,CA.....	240
Figure 91. EM38-MK2 in-phase survey results, 1.0-m inter-coil separation, vertical dipole mode, Site B, Sacramento, CA.....	240
Figure 92. Survey area at Site B, Sacramento, CA. The yellow flags in the foreground are spaced 1 m apart. The valley oak tree in the foreground (Tree 2) is the one used for the GPR root characterization study. Cables on the ground are those used for a 3-D resistivity survey.....	241
Figure 93. (a) Antenna swaths along survey lines parallel to the crest. The survey was conducted north to south along lines 1W through 12W, with limited data collected along line 6W and no data collected along line 7W because of the tree location (circle). (b) Antenna swaths along survey lines perpendicular to the crest. The survey was conducted west to east along lines 1N through 14N, with no data collected along lines 6N through 7N because of the tree location (circle).	242
Figure 94. Radargrams parallel and perpendicular to the crest at depth z = 5 cm (actual 0.49 cm) (a) and x and y time slices bounding the tree location (b). The circles in (a) represent the location of the tree.....	243
Figure 95. Time slices showing near-surface influence of the tree. (a) East-west extent 1.71 m (5.62W to 7.33W). (b) North-south extent 1.41 m (7.92S to 9.33S). Data from collection parallel to levee crest.....	245
Figure 96. Radar images showing possible roots extending from near-surface influence of the tree shown in Figure 92.	246
Figure 97. Comparison of GPR data and 3-D resistivity data. The white rectangles on the radar plots correspond to the area imaged in the resistivity survey. The circles/oval on all plots mark the location of the tree (Tree 2).	247
Figure 98. Geophysical test site location, Portland, OR.	248
Figure 99. View, looking east, of the test site showing the trees and levee, Portland, OR.	249
Figure 100. 2-D resistivity survey layout, Portland, OR.....	250
Figure 101. Two-dimensional inversion results, looking up slope, for resistivity lines 0 through -6, Portland, OR.....	251
Figure 102. Two-dimensional inversion results, looking up slope, for lines -8 through -12, Portland, OR.....	252
Figure 103. Quasi 3-D inverted resistivity image, Portland, OR.....	253
Figure 104. Three-dimensional resistivity survey layout, Portland, OR.....	254
Figure 105. Three-dimensional resistivity inversion image, Portland, OR.	255
Figure 106. EM38 survey line layout, Portland, OR.	256
Figure 107. EM38-MK2 conductivity survey results, 0.5-m inter-coil separation, vertical dipole mode, Portland, OR.	258

Figure 108. EM38-MK2 conductivity survey results, 1.0-m inter-coil separation, vertical dipole mode, Portland, OR	258
Figure 109. EM38-MK2 in-phase survey results, 0.5-m inter-coil separation, vertical dipole mode, Portland, OR	259
Figure 110. EM38-MK2 in-phase survey results, 1.0-m inter-coil separation, vertical dipole mode, Portland, OR.....	259
Figure 111. Survey grid (a) and photographs (b) of the stand of cottonwood trees within the survey grid and the two trees of primary interest on Portland levee in Portland, OR. The circles represent the cottonwood trees.	260
Figure 112. Comparison of non-migrated (a) and migrated (b) depth sections at $y = 9.458$ m S. Circles show hyperbola that has been refocused to a point in the migrated section.....	261
Figure 113. GPR data collected parallel (a-c) and perpendicular (d) to the levee. The white circles mark the tree locations. (a) Plan view of parallel radar section at 2.5-cm depth (2.075 ns). The corresponding time of 2.075 ns is a two-way travel time. To obtain the correct depth, divide the two-way time by 2 and multiply by the EM wave velocity (0.219 ns \div 2 \times 0.095 m/ns). (b) Depth profile along line 3.7S. (c) Same as (a) but with interpreted location of shallow roots (red lines). (d) Plan view of perpendicular radar section at 2.6-cm depth (2.197 ns).....	262
Figure 114. Depth slices from data collected parallel to the levee showing interpreted location of possible tree roots. The white circles mark the tree locations; red lines are possible roots.....	263
Figure 115. Location of possible tree roots interpreted from GPR data (parallel to the levee) collected around cottonwood trees on the Portland Levee, Portland, OR. The black circles mark the tree locations; red lines are possible roots.....	265
Figure 116. Depth slices from data collected perpendicular to the levee showing interpreted location of possible tree roots on the Portland Levee, Portland, OR. The white circles mark the tree locations; red lines are possible roots.....	265
Figure 117. Location of possible tree roots interpreted from GPR data (perpendicular to the levee) collected around cottonwood trees on the Portland Levee, Portland, OR. The black circles mark the tree locations; red lines are possible roots.	266
Figure 118. Location of possible tree roots interpreted from GPR data (parallel and perpendicular to the levee) collected around cottonwood trees on Portland levee, Portland, OR. The black circles mark the tree locations; red lines are possible roots.	267
Figure 119. Burlington, WA.	268
Figure 120. View of the test site, looking north, showing the cedar tree and levee, Burlington, WA.	269
Figure 121. 2-D resistivity survey layout, Burlington, WA.	270
Figure 122. Inversion results for 2-D lines 0 through -6, Burlington, WA.....	270
Figure 123. Inversion results for 2-D lines -8 through -12, Burlington, WA.	271
Figure 124. Quasi 3-D inverted resistivity image, Burlington, WA.	272
Figure 125. Three-dimensional resistivity survey layout, Burlington, WA.	273
Figure 126. Three-dimensional Inverted resistivity image, Burlington, WA.	274
Figure 127. EM survey layout, Burlington, WA.	275
Figure 128. EM38 conductivity survey, 0.5-m inter-coil separation, Burlington, WA.....	276
Figure 129. EM38 conductivity survey, 1.0-m inter-coil separation, Burlington, WA.....	277

Figure 130. EM38 in-phase survey, 0.5-m inter-coil separation, Burlington, WA.....	277
Figure 131. EM38 in-phase survey, 1.0-m inter-coil separation, Burlington, WA.....	278
Figure 132. GPR survey grid, Burlington, WA. The circle represents the location of the cedar tree.....	279
Figure 133. Comparison of non-migrated (a) and migrated (b) depth sections at $y = 8.518$ m, Burlington, WA. Circles show hyperbola that has been refocused to a point in the migrated section.....	280
Figure 134. GPR data collected parallel (a-c) and perpendicular (d) to the levee, Burlington, WA. The white circle marks the tree location; the boxes are the locations of the root characterization cells. (a) Plan view of parallel radar section at 0.8-cm depth (0.219 ns). The corresponding time of 0.219 ns is a two-way travel time. To obtain the correct depth, divide the two-way time by 2 and multiply by the EM wave velocity (0.219 ns \div 2 \times 0.078 m/ns). (b) Same section as (a), but with location of possible flooding/deposition events shown. (c) Depth profile along line 7.6E. (d) Plan view of perpendicular radar section at 0.8-cm depth (0.219 ns).....	281
Figure 135. Depth slices from data collected parallel to the levee showing interpreted location of possible tree roots, Burlington, WA.....	283
Figure 135. Concluded.....	285
Figure 136. Location of possible tree roots interpreted from GPR data collected around a cedar tree on the Burlington Levee, Burlington, WA.....	285
Figure 137. Locations of test Sites 1 and 2, Albuquerque, NM.....	286
Figure 138. 3-D ERI layout, Site 1, Albuquerque, NM.....	287
Figure 139. 3-D ERI layout, Site 2, Albuquerque, NM.....	288
Figure 140. 3-D resistivity inversion image, Site 1, Albuquerque, NM.....	289
Figure 141. 3-D resistivity inversion image, Site 2, Albuquerque, NM.....	290
Figure 142. Lewisville Dam, Lewisville, TX.....	292
Figure 143. Location of study tree relative to Lewisville Dam, Lewisville, TX.....	292
Figure 144. Location of study tree relative to the service road and Lewisville Dam toe, Lewisville, TX.....	293
Figure 145. Plan view of 3-D ERI test layout, Lewisville Dam, Lewisville, TX.....	294
Figure 146. Drilling holes in asphalt service road for electrode emplacement, Lewisville Dam, Lewisville, TX.....	294
Figure 147. 3-D ERI layout showing the extent of lines 0 through 7, Lewisville Dam, Lewisville, TX.....	296
Figure 148. 3-D ERI layout showing the extent of lines 4 through 11, Lewisville Dam, Lewisville, TX.....	296
Figure 149. ERI inversion image, Lewisville Dam, Lewisville, TX.....	297
Figure 150. EM survey layout, Lewisville Dam, Lewisville, TX.....	299
Figure 151. EM38-MK2 conductivity survey results, 0.5-m inter-coil separation, vertical dipole mode, Lewisville Dam, Lewisville, TX.....	300
Figure 152. EM38-MK2 conductivity survey results, 1.0-m inter-coil separation, vertical dipole mode, Lewisville Dam, Lewisville, TX.....	300
Figure 153. EM38-MK2 in-phase survey results, 0.5-m inter-coil separation, vertical dipole mode, Lewisville Dam, Lewisville, TX	302

Figure 154. EM38-MK2 in-phase survey results, 1.0-m inter-coil separation, vertical dipole mode, Lewisville Dam, Lewisville, TX.....	302
Figure 155. IHNC and 17th Street geophysical study sites, New Orleans, LA.....	304
Figure 156. Geophysical test grid on levee slope near recently cut test tree, IHNC Site, New Orleans, LA.....	305
Figure 157. EM38 conductivity results, 0.5-m, IHNC Site, New Orleans, LA.....	306
Figure 158. EM38 conductivity results, 1.0-m, IHNC Site, New Orleans, LA.....	306
Figure 159. EM38 in-phase results, 0.5 m, IHNC Site, New Orleans, LA.....	307
Figure 160. EM38 in-phase results, 1.0 m, IHNC Site, New Orleans, LA.....	307
Figure 161. Survey area (a) and photograph looking towards the southeast (b), IHNC Site, New Orleans, LA. The GPR survey line locations (a) are represented by blue lines; the green and red squares mark the start and end, respectively, of a GPR survey line. The black circle indicates the tree stump location.....	308
Figure 162. Plan view (top) of radar section at approximately 8-cm depth. The circle marks the location of the stump. Depth section (bottom) along line 0.44E (location of line in the top section), IHNC Site, New Orleans, LA.....	309
Figure 163. Location of 17th Street Canal Site, New Orleans, LA.....	309
Figure 164. EM38 survey line layout, 17th Street Canal Site, New Orleans, LA.....	310
Figure 165. EM38 conductivity results, 0.5 m, 17th Street Canal Site, New Orleans, LA.....	311
Figure 166. EM38 conductivity results, 1.0 m, 17th Street Canal Site, New Orleans, LA.....	311
Figure 167. EM38 in-phase results, 0.5 m, 17th Street Canal Site, New Orleans, LA.....	312
Figure 168. EM38 in-phase results, 1.0 m, 17th Street Canal Site, New Orleans, LA.....	312
Figure 169. Survey area (a) and photograph (b) at 17th Street Canal, New Orleans, LA. The GPR survey lines (a) are represented by blue GPS-derived dots; the dots off of the survey line are outlier GPS points; the green and red squares mark the start and end, respectively, of a survey line. The circles indicate the stump locations; black squares the drain grates.....	313
Figure 170. 17th Street Canal Site: (a) Plan view of radar section at approximately 6-cm depth. The solid white circles mark the locations of the stumps; black squares are drain grates. (b) Inline section along line 7E at 777429.534 (white line in a).	314
Figure 171. Location of test site, Vicksburg, MS.....	315
Figure 172. Test grid layout and test tree, Vicksburg, MS.....	316
Figure 173. 3-D ERI layout, Vicksburg, MS.....	316
Figure 174. Location of electrical resistivity lines relative to the test tree, Vicksburg, MS.....	317
Figure 175. 3-D inverted resistivity image, Vicksburg, MS.....	318
Figure 176. GPR survey line layout, Vicksburg, MS.....	319
Figure 177. Typical GPR cross section showing hyperbolas presumably caused by tree roots.....	320
Figure 178. Stratified, random sample design for invasive measurement in: (a) Sacramento, (b) Albuquerque – Site 1, (c) Albuquerque – Site 2, and (d) Burlington. Cell colors indicate low-density root domain (green), high-density root domain (blue), tree location (red), cells excluded to prevent damage to the tree (tan), and cells excluded to prevent damage to the levee road (yellow).	328
Figure 179. Stratified, random sample design for invasive measurement in Vicksburg, MS.....	329
Figure 180. Invasive subsampling using (a) manual excavation and (b) compressed air.	330

Figure 181. Excavation and digitization of subsamples: (a) unclipped roots, (b) clipped roots, (c) roots labeled and marked for digitization, and (d) digitization of subsample.....	330
Figure 182. Excavation of a complete root system in Vicksburg, MS: (a) excavation of tree, (b) tree following compressed air excavation, (c) mechanical removal of remaining root system, and (d) digitization benchmarks.....	332
Figure 183. Photographs and digital renderings of invasive subsample locations in Sacramento (a/b) Cell B60, (c/d) Cell B86, (e/f) Cell B105, and (g/h) Cell B140.....	337
Figure 184. Photographs and digital renderings of invasive subsample locations in Albuquerque – Site 1 (a/b) Cell 52, (c/d) Cell 58, (e/f) Cell 74, and (g/h) Cell 136.	338
Figure 185. Photographs and digital renderings of invasive subsample locations in Albuquerque – Site 2 (a/b) Cell 52, (c/d) Cell 76, (e/f) Cell 96, and (g/h) Cell 124.	339
Figure 186. Photographs and digital renderings of invasive subsample locations in Burlington (a/b) Cell 24, (c/d) Cell 41, (e/f) Cell 103, and (g/h) Cell 142.	340
Figure 187. Comparative photograph (a) and digital rendering (b) of invasive root architecture data collection in Vicksburg, MS.	341
Figure 188. Example of numerical representation of root cross section: (a) triangular digitization of irregular root, (b) circumscription of circle around triangular data, (c) octagonal fitting of circle, and (d) comparison of sample root cross section to octagon.....	347
Figure 189. Location of the root characterization cells.....	350
Figure 190. GPR depth slices at 40 cm (actual 39.3 cm) parallel and perpendicular to the crest with outline of root characterization cells and tree position (circle).	351
Figure 191. Comparison of GPR sections and photographs of root characterization cells at 40-cm depth.	352
Figure 192. GPR depth slices at 60 cm (actual 59 cm) parallel and perpendicular to the crest with outline of root characterization cells and tree position (circle).	353
Figure 193. Comparison of GPR sections and photographs of root characterization cells at 60-cm depth.	354
Figure 194. GPR depth slices at 80 cm (actual 81.1 cm) parallel and perpendicular to the crest with outline of root characterization cells and tree position (circle).	355
Figure 195. Comparison of GPR sections and photographs of root characterization cells at 80-cm depth.	356
Figure 196. Aerial (top) and panoramic (bottom) photographs of the study site, Vicksburg, MS.	358
Figure 197. (a) Survey grid located on the east side of the pine tree divided into nine 1-m × 1-m cells. (b) Schematic of sampling grid showing local coordinate system (blue arrows) and cells selected for excavation (red font).	359
Figure 198. Sensors and Software pulseEkko 1000 antenna system using a wheel odometer to measure distance traveled.....	359
Figure 199. GPR profiles showing data acquired with the three antenna frequencies, and the difference in depth of signal penetration and resolution for each frequency.....	362
Figure 200. GPR depth images showing an improvement in target resolution with an increase in antenna frequency.	362
Figure 201. 900 MHz (15.3-18.1 cm) depth images illustrating the dependence of root delineation on the direction of survey traverse.	363
Figure 202. Select depth images of the combined 900 MHz GPR data.	364

Figure 203. Root interpretations between the depth range 0 to 50 cm for GPR data collected with the 450-, 900-, and 1,200-MHz antennae.....	365
Figure 204. (a) Comparison of interpreted roots with excavation photographs for depth ranges 0 to 25 cm and 25 to 50 cm. (b) Photograph of excavated roots >2 cm.....	366
Figure 205. Error in 60 digitization measurements at 13 local benchmarks with increasing distance between transmitter and received: (a) standard deviation and (b) range.....	367
Figure 206. Virtual representation of the study root system generated from electromagnetic digitizer (a) and calibrated photographic modeling (b).	368
Figure 207. Qualitative comparison of root detection techniques: photographs of sampling area (a/d), GPR data (b) and interpreted roots (e), electromagnetic digitization (c), and calibrated photographic modeling (f).	370
Figure 208. (a) Photograph of the southern red oak prior to the LiDAR scan, and (b) the LiDAR scan of the tree canopy and ground prior to soil excavation.	373
Figure 209. (a) Photograph of the southern red oak with tree canopy removed and soil excavated to 0.5 m, and (b) LiDAR scan after partial excavation.	374
Figure 210. (a) Photograph of the southern red oak tree after full excavation, and (b) LiDAR scan of tree trunk and exposed roots.	375
Figure 211. Diagram of the Guelph Permeameter constant head, in situ, hydraulic conductivity measuring device (modified from Reynolds and Elrick 1986).	381
Figure 212. Plan view of hydraulic conductivity field test locations plotted in polar coordinates. The tree's center is located at the origin of the plot, and test locations are plotted along random azimuths and radii.....	383
Figure 213. Schematic diagram of the Geulph Permeameter (Reynolds and Elrick 1986).	384
Figure 214. M-300 soil moisture probe.	385
Figure 215. Eijkelkamp soil core sampler and ring (ring dimensions are 53-mm diam by 51-mm length).	386
Figure 216. Surveying test locations for permeameter tests, Burlington, WA.....	388
Figure 217. Measurement of in situ moisture content measurement using the M-300 Aquaterr, Burlington, WA.....	389
Figure 218. Handheld drill with auger used to drill a hole for placement of permeameter, Vicksburg, MS.	390
Figure 219. Removal of grab sample prior to permeameter test, Burlington, WA.	390
Figure 220. Guelph Permeameter seated inside boring and ready to test boring interval at 3 ft, Burlington, WA.	391
Figure 221. Undisturbed soil sample collected for laboratory analysis, Burlington, WA.	391
Figure 222a. Hydraulic conductivity calculated from in situ permeameter tests at a depth of 3.0 ft, Sacramento, CA.	394
Figure 222b. The locations of the random samples for permeameter tests in Sacramento, CA. The x-y axes are in feet.	394
Figure 223a. Hydraulic conductivity calculated from in situ permeameter tests at a depth of 5.0 ft, Sacramento, CA.	395
Figure 223b. The locations of the random samples for permeameter tests in Sacramento, CA. The x-y axes are in feet.	395
Figure 224a. Hydraulic conductivity calculated from in situ permeameter tests at a depth of 3.0 ft, Burlington, WA.	396

Figure 224b. The locations of the random samples for permeameter tests in Burlington, WA. The x-y axes are in feet.....	396
Figure 225a. Hydraulic conductivity calculated from in situ permeameter tests at a depth of 5.0 ft, Burlington, WA.....	397
Figure 225b. The locations of the random samples for permeameter tests in Burlington, WA. The x-y axes are in feet.....	397
Figure 226a. Hydraulic conductivity calculated from in situ permeameter tests at a depth of 1.5 ft. Albuquerque, NM 1	399
Figure 226b. The locations of the random samples for permeameter tests in Albuquerque, NM 1. The x-y axes are in feet	399
Figure 227a. Hydraulic conductivity calculated from in situ permeameter tests at a depth of 2.5 ft, Albuquerque, NM 1	400
Figure 227b. The locations of the random samples for permeameter tests in Albuquerque, NM 1. The x-y axes are in feet	400
Figure 228a. Hydraulic conductivity calculated from in situ permeameter tests at a depth of 1.5 ft, Albuquerque, NM 2.	401
Figure 228b. The locations of the random samples for permeameter tests in Albuquerque, NM 2. The x-y axes are in feet.....	401
Figure 229a. Hydraulic conductivity calculated from in situ permeameter tests at a depth of 2.5 ft, Albuquerque, NM 2.	402
Figure 229b. The locations of the random samples for permeameter tests in Albuquerque. NM 2. The x-y axes are in feet.....	402
Figure 230a. Hydraulic conductivity calculated from in situ permeameter tests at a depth of 3.0 ft, Portland, OR.....	403
Figure 230b. The locations of the random samples for permeameter tests in Portland, OR. The x-y axes are in feet	403
Figure 231a. Hydraulic conductivity calculated from in situ permeameter tests at a depth of 5 ft, Portland, OR.	404
Figure 231b. The locations of the random samples for permeameter tests in Portland, OR. The x-y axes are in feet	404
Figure 232a. Hydraulic conductivity calculated from in situ permeameter tests at a depth of 1.0 ft, Boca Raton, FL.....	406
Figure 232b. The locations of the random samples for permeameter tests in Boca Raton, FL. The x-y axes are in feet	406
Figure 233a. Hydraulic conductivity calculated from in situ permeameter tests at a depth of 2.0 ft, Boca Raton, FL.....	407
Figure 233b. The locations of the random samples for permeameter tests in Boca Raton, FL. The x-y axes are in feet	407
Figure 234a. Hydraulic conductivity calculated from in situ permeameter tests at a depth of 3.0 ft, Lewisville, TX.	408
Figure 234b. The locations of the random samples for permeameter tests in Lewisville, TX. The x-y axes are in feet	408
Figure 235a. Hydraulic conductivity calculated from in situ permeameter tests at a depth of 5.0 ft, Lewisville, TX.	409
Figure 235b. The locations of the random samples for permeameter tests in Lewisville, TX. The x-y axes are in feet	409

Figure 236a. Hydraulic conductivity calculated from in situ permeameter tests at a depth of 3.0 ft, Danville, PA.....	411
Figure 236b. The locations of the random samples for permeameter tests in Danville, PA. The x-y axes are in feet.	411
Figure 237a. Hydraulic conductivity calculated from in situ permeameter tests at a depth of 5.0 ft, Danville, PA.....	412
Figure 237b. The locations of the random samples for permeameter tests in Danville, PA. The x-y axes are in feet.	412
Figure 238a. Hydraulic conductivity calculated from in situ permeameter tests at a depth of 3.0 ft, Vicksburg, MS.	413
Figure 238b. The locations of the random samples for permeameter tests in Vicksburg, MS. The x-y axes are in feet.....	413
Figure 239a. Hydraulic conductivity calculated from in situ permeameter tests at a depth of 5.0 ft, Vicksburg, MS.	414
Figure 239b. The locations of the random samples for permeameter tests in Vicksburg, MS. The x-y axes are in feet.....	414
Figure 240. Difference between mean hydraulic conductivities for shallow depth (1 to 3 ft) for the tree and control sites with 95% confidence interval.....	420
Figure 241. Chart showing difference between tree and control mean hydraulic conductivities and the 95% confidence intervals for tests conducted at 5 ft. Vicksburg is shown with and without the outlier included in the data set. The Vicksburg data without the outlier (Vicksburg *) shows a smaller confidence interval.	421
Figure 242. Schematic diagram of the ERDC root pullout device.	426
Figure 243. Field operation of the ERDC root pullout device.....	426
Figure 244. Two trees, cottonwood and Oregon ash, selected for root pullout tests, in Portland, OR, approximately 10 miles east of Portland Airport, near Columbia River.....	429
Figure 245. Three trees, two maples and one cedar, selected for root pullout tests, east of Burlington, WA, along the Skagit River.	429
Figure 246. Three trees, alder, cottonwood, and cedar, selected for root pullout tests, east of Burlington, WA, along the Skagit River.	430
Figure 247. Five cottonwood trees, selected for root pullout tests, in Albuquerque, NM, approximately 4 miles northwest of the intersection of I-25 and I-40, near the Rio Grande River.....	430
Figure 248. Four cottonwood trees, selected for root pullout tests, in Albuquerque, NM, approximately 5 miles northwest of the intersections of I-25 and I-40, near the Rio Grande River.....	431
Figure 249. Pullout force vs. displacement of a cottonwood, Portland, OR.	432
Figure 250. Pullout force vs. displacement of a cottonwood, Albuquerque, NM.	432
Figure 251. Comparison of ERDC and Abernathy and Rutherford (2001) pullout stress vs. root diameter tests.	435

Tables

Table 1. Data gathered and analyses conducted for each site studied in the ERDC research.	6
Table 2. Stratigraphy at Site B Pocket Levee, Sacramento River.	24

Table 3. Recommended hydraulic conductivity (K) values for use in base case and initial seepage analyses for the Natomas Levee improvement program.....	32
Table 4. Hydraulic conductivity values assigned to layer soils in Figure 9.....	33
Table 5. Statistical data for Troxler measurements in Sacramento, CA, north transect 2-, 4-, 6-, 8-, 10-, and 12-in. depths.....	37
Table 6. Statistical data for Troxler measurements in Sacramento, CA, north transect: 2-, 4-, 6-, 8-, 10-, and 12-in. depths.....	42
Figure 7. Statistical data for Troxler measurements in Sacramento, CA, south transect: 2-, 4-, 6-, 8-, 10-, and 12-in. depths.....	47
Table 8. Statistical data for Troxler measurements in Sacramento, CA, east transect: 2-, 4-, 6-, 8-, 10-, and 12-in. depths.....	52
Table 9. Statistical data for Troxler measurements in Sacramento, CA, transect 1: 2-, 4-, 6-, 8-, 10-, and 12-in. depths.....	57
Table 10. Statistical data for Troxler measurements in Sacramento, CA, transect 2: 2-, 4-, 6-, 8-, 10-, and 12-in. depths.....	62
Table 11. Hydraulic conductivity values used in the Albuquerque, NM, levee model.....	94
Table 12. Statistical data for Troxler measurements in Albuquerque, NM: 2-, 4-, 6-, 8-, 10-, and 12-in. depths.....	100
Table 13. Statistical data for Troxler measurements in Albuquerque, NM, transect on levees: 2-, 4-, 6-, 8-, 10-, and 12-in. depths.....	106
Table 14. Statistical data for Troxler measurements in Albuquerque, NM, transect on floodplain 2-, 4-, 6-, 8-, 10-, and 12-in. depths.....	111
Table 15. Statistical data for Troxler measurements in Albuquerque, NM, transect in wooded area: 2-, 4-, 6-, 8-, 10-, and 12-in. depths.....	116
Table 16. Statistical data for Troxler measurements in Albuquerque, NM, Site 2: 2-, 4-, 6-, 8-, 10-, and 12-in. depths.....	121
Table 17. Hydraulic conductivity values for Portland.....	135
Table 18. Statistical data for Troxler measurements in Boca Raton, FL: 2-, 4-, 6-, 8-, 10-, and 12-in. depths.....	147
Table 19. Statistical data for Troxler measurements in Boca Raton, FL, flag area: 2-, 4-, 6-, 8-, 10-, and 12-in. depths.....	152
Table 20. Statistical data for Troxler measurements in Boca Raton, FL, Tree 1: 2-, 4-, 6-, 8-, 10-, and 12-in. depths.....	157
Table 21. Statistical data for Troxler measurements in Boca Raton, FL, Tree 2: 2-, 4-, 6-, 8-, 10-, and 12-in. depths.....	162
Table 22. Statistical data for Troxler measurements in Boca Raton, FL, levee: 2-, 4-, 6-, 8-, 10-, and 12-in. depths.....	167
Table 23. Stratum designation for the SEEPW analysis of the Danville levee system (Schnabel 2010).....	179
Table 24. Statistical data for Troxler measurements in Danville, PA: 2-, 4-, 6-, 8-, 10-, and 12-in. depths.....	183
Table 25. Statistical data for Troxler measurements in Danville, PA, Transect1: 2-, 4-, 6-, 8-, 10-, and 12-in. depths.....	188
Table 26. Statistical data for Troxler measurements in Danville, PA, Transect 2: 2-, 4-, 6-, 8-, 10-, and 12-in. depths.....	193

Table 27. Statistical data for Troxler measurements in Danville, PA, Transect 3: 2-, 4-, 6-, 8-, 10-, and 12-in. depths.....	198
Table 28. Statistical data for Troxler measurements in Vicksburg, MS: 2-, 4-, 6-, 8-, 10-, and 12-in. depths.....	211
Table 29. Summary of conditions at sites used in the ERDC research.....	217
Table 30. Electrical resistivity values of some common rocks and minerals (Keller and Rischknecht 1966).....	219
Table 31. Maximum detectable lateral and vertical influence of tree root zones based on results of 2-D, 3-D and quasi 3-D inversion methods, Site B, Sacramento, CA.....	237
Table 32. Maximum detectable lateral and vertical extent of tree root zone based on resistivity and GPR survey results, Sacramento, CA.....	247
Table 33. Maximum detectable lateral influence of tree root zone based on ERI and EM methods, Burlington, WA.....	278
Table 34. Maximum detectable anomaly range and maximum resistivity magnitude for selected slices normal to the x-axis, Lewisville Dam, Lewisville, TX.....	298
Table 35 Maximum detectable anomaly range and maximum resistivity magnitude for selected slices normal to the y-axis, Lewisville Dam, Lewisville, TX.....	298
Table 36. Summary of the geophysical methods and results of the application of these surveys.....	324
Table 37. Summary of soil analysis for Sacramento.....	333
Table 38. Summary of soil analysis for Albuquerque Site 1.....	334
Table 39. Summary of soil analysis for Albuquerque Site 2.....	335
Table 40. Summary of soil analysis for Burlington, WA.....	336
Table 41. Summary of root specific gravity.....	336
Table 42. Summary of root properties – Sacramento, CA.....	342
Table 43. Summary of root properties – Albuquerque, NM – Site 1.....	343
Table 44. Summary of root properties – Albuquerque, NM – Site 2.....	344
Table 45. Summary of root properties – Burlington, WA.....	345
Table 46. Summary of root properties – Vicksburg, MS.....	346
Table 47. Root properties from invasive subsamples.....	348
Table 48. Location of root characterization cells relative to tree.....	350
Table 49. Coarse root properties.....	367
Table 50. Summary of soil and fine root properties.....	369
Table 51. Locations of in situ hydraulic conductivity tests.....	376
Table 52. Values of hydraulic conductivity for typical soils (Freeze and Cherry 1979).....	379
Table 53. Root characteristics as documented by Coder (after Marks and Tschantz 2002).....	387
Table 54. Details of locations used for in situ hydraulic conductivity tests.....	416
Table 55. Difference of log means and confidence intervals plotted in Figures 240 and 241.....	419
Table 56. Summary of calculated mean hydraulic conductivities per tree and control site.....	422
Table 57. Pullout tests summary.....	434
Table 58. Displacement increment data for pullout tests at Albuquerque, NM, Burlington, WA, and Portland, OR.....	436

Table 59. Analysis of covariance for root pullout data collected in Albuquerque, NM, Burlington, WA, and Portland, OR.....	443
---	-----

Preface

This research of the effects of woody vegetation on the structural integrity of levees was sponsored by Headquarters, U.S. Army Corps of Engineers (HQUSACE).

This investigation was conducted during the period of October 2009 to September 2010. The project manager for the study was Dr. Maureen K. Corcoran, Engineer Research and Development Center (ERDC), Geotechnical and Structures Laboratory (GSL). Dr. John F. Peters, GSL, provided the technical oversight. The principal investigators for the research were Dr. Joseph B. Dunbar, M. Eileen Glynn, Jose L. Llopis, Dr. Janet E. Simms, and Dr. Johannes Wibowo, GSL, Dr. Christopher Kees, ERDC, Coastal and Hydraulics Laboratory, S. Kyle McKay and Dr. J. Craig Fischenich, ERDC, Environmental Laboratory, and Dr. Fred T. Tracy, ERDC, Information Technology Laboratory.

The research direction was provided by Dr. Michael K. Sharp, ERDC Technical Director for Water Resources Infrastructure (WRI) and Dr. Maureen K. Corcoran, Associate Technical Director for WRI. This publication was prepared under the general supervision of Dr. William P. Grogan, Deputy Director, GSL, and Dr. David W. Pittman, Director, GSL.

At the time of publication of this report COL Kevin J. Wilson was Commander and Executive Director of ERDC, and Dr. Jeffery P. Holland was Director.

This volume is one of four volumes documenting research conducted by ERDC on the effects of woody vegetation on levees. The fifth volume includes a description of the agency technical review (ATR) process and the comments from the review. The research includes data collected and analyzed during this study, as well as those data previously collected by state and Federal agencies and their contractors. Major components of this project included site selection, characterization, and analysis (including levee location, geometry, geology, and soils within and underlying the levee); field studies (including tree properties and identification), and estimation of root and root ball dimensions using electrical resistivity, electromagnetic induction, and ground-penetrating radar, as well as root excavation); and numerical simulation modeling (including sensitivity and deformation analysis).

Unit Conversion Factors

Multiply	By	To Obtain
feet	0.3048	meters
inches	2.54	centimeters
inches	0.0254	meters
miles (U.S. statute)	1,609.347	meters
miles	1.61	kilometers

Acknowledgements

The U.S. Army Engineer Research and Development Center (ERDC) would like to acknowledge and greatly thank the support of many individuals who contributed their time and resources to ensure the success of this research. The following engineers and scientists from the U.S. Army Corps of Engineers (USACE) Districts and Divisions were instrumental in providing input on field locations, local knowledge of woody vegetation, field support, and geotechnical reports; U.S. Army Engineer District, Albuquerque (SPA) – Ondrea C. Hummel, William J. Trujillo, Deborah A. Foley, Bruce A. Jordan, Kristopher T. Schafer, Dwayne E. Lillard (retired); U.S. Army Engineer District, Sacramento (SPK) – Mary P. Perlea, Kevin Knuuti, Meegan G. Nagy, Michael D. Ramsbotham, Edward A. Ketchum, Pamlyn K. Hill, Ben Gompers; U.S. Army Division, South Pacific Division (SPD) – Kenneth G. Harrington, Lester Tong (retired); U.S. Army Engineer District, New Orleans (MVN) – Stephen F. Finnegan, Michael L. Stout (Contractor); Mississippi Valley Division (MVD) – Ken Klaus; U.S. Army Engineer District, Portland (NWP) – Les D. Miller; U.S. Army Engineer District, Ft. Worth (SWF) – Anita Hill, Ramanuja C. Kannan, Les Perrin (retired); U.S. Army Engineer District, Seattle (NWS) – Charles H. Ifft, Douglas T. Weber, Catherine A. Desjardin; Northwestern Division (NWD) – Steven J. Fink ; and U.S. Army Engineer District, Jacksonville (SAJ) – Randy L. Rabb.

In addition to the principal investigators listed as authors of this report, the following people at ERDC and its contractors supported field efforts, literature searches, and data analyses and are gratefully acknowledged: Dr. Monte L. Pearson Raju V. Kala, Isaac J. Stephens, Clinton J. Forsha, and Jerry Ballard, ERDC, Geotechnical and Structures Laboratory; Jim A. Dolan, ERDC, Information Technology Laboratory (ITL); Daniel A. Leavell, Bowhead Science & Technology; Dr. David Biedenharn and Dr. Chester Watson, Biedenharn Group; Rae Gore and Chelsea Thomas, Bevilacqua Research Corporation; Daniel Chausse, ERDC-Contractors; Pam Bailey, Bobby W. McComas, Tyler D. Tharp, Megan English, and Leah McMahon, ERDC, Environmental Laboratory.

Cheri T. Loden, InfoPro; Marilyn Holt and Karen Taylor, U.S. Army Corps of Engineers-Information Technology Laboratory, compiled and formatted

the report. Mark Hardenberg, (STEM International), Bill Mullen (Bowhead Science & Technology), and Pamela Harrion (ITL) edited the report.

Agencies and individuals outside of USACE were outstanding in their support of this research. The ERDC field activities could not have been completed without the assistance of the following people and organizations: Danville, PA - Tom Graham, Danville Bureau Secretary, Joe V. Bellini, AMEC, Scott Raschke, Schnabel Engineering; Albuquerque, NM – Jerry Lovato, Albuquerque Metropolitan Arroyo Flood Control Authority, Ray Gomez, Middle Rio Grande Conservation District, Mark Stone and students, (University of New Mexico); Sacramento, CA – Richard E. Marshall (retired), California Central Valley Flood Control Association), Dr. Alison Berry, Shih-Ming Chung, and Jaylee Tuil, University of California (UC)-Davis, Roy Kroll, California Department of Water Resources, and River Partners; Jacksonville, FL – Steve Partney, South Florida Water Management District; Burlington, WA – Chuck Bennett, Skagit River Drainage District No. 12; Portland, OR – Dave Hendricks, Multnomah County Drainage District No. 1; and Vicksburg, MS – James Marble, Vicksburg Sand and Gravel.

The participation of Ben Gouldby, HR Wallingford, UK, and Dr. Kenneth Cumming, National Marine Fisheries Service, in the ERDC/California Science Team workshop is greatly appreciated. The expertise of John Greenwood, University at Nottingham-Trent, UK, on root pullout tests greatly increased our knowledge of the procedure and data analysis. Dr. Philip Soar, University of Portsmouth, UK, is acknowledged for his detailed review of a root system model. We appreciate the time Dr. Natasha Pollen-Bankhead and Dr. Andrew Simon, U.S. Department of Agriculture, Agricultural Research Service, National Sedimentation Laboratory, spent relating their experiences on permeameter tests. Loren Murray, URS Corporation, provided the Light Detection and Ranging (LiDAR) scans for the Pocket Levee in Sacramento, CA.

A special thanks to the California Science Team for the many discussions and their input concerning this research; George Sills, Sills Engineering, Dr. Leslie F. Harder, Jr., HDR Engineering, Inc., Dr. F. Douglas Shields, Jr., Consulting Hydraulic Engineer, Keith Swanson, California Department of Water Resources, Laura Kaplan, Center for Collaborative Policy, Dr. Donald Gray, University of Michigan, Peter Buck and Mick Klasson, Sacramento Area Flood Control Agency, Dr. Alison Berry, UC-Davis, Dr. Chris Peterson,

University of Georgia, Roy Kroll and Mike Inamine, California Department of Water Resources, Dr. Jonathan Bray, University of California, Berkeley, Sujan Punyamurthula, Richard Millet, and Franz Campero, URS Corporation, and Steven Chainey, AECOM.

1 Introduction

This volume describes the study sites and summarizes geological, geophysical, and geotechnical data that were compiled from each location. This volume also describes the methods used to characterize root systems and their properties. Methods evaluated in this study are noninvasive (geophysical surveys) and invasive (in situ root architectural subsampling and Light Detection and Ranging (LiDAR) scans). These data provide input for numerical models used in this research. This volume also describes root pullout tests and in situ hydraulic conductivity measurements. Results from the root pullout tests are used in the slope stability model. Hydraulic conductivity measurements are used in a comparative analysis to identify the effects of roots on hydraulic conductivity.

Although a significant number of procedures exist for collecting root architectural data, these techniques have not been quantitatively compared or calibrated to the extent necessary to permit selection for a particular requirement. Thus, this study sought to: (1) use noninvasive and invasive techniques to characterize a root system, and (2) examine the accuracy of noninvasive techniques (e.g., geophysical surveys) by calibrating these techniques with invasive subsampling approaches. Methods used in this research include ground-penetrating radar (GPR), electrical resistivity, electrical conductivity, invasive subsampling, and digitization. However, not every method was used at each site because of variability in soil conditions.

Noninvasive root characterization is both non-destructive and relatively rapid (compared to invasive measurement). However, its accuracy and limitations are currently poorly defined. Butnor et al. (2001) demonstrated that calibration of GPR data with limited invasive measurement markedly improves the accuracy of the technique. Figure 1 presents a framework for collecting, calibrating, and applying noninvasive root data used in this study. Both uncalibrated and calibrated data are presented to demonstrate the relative advantages of undertaking calibration exercises.

Multiple techniques were used by the U.S. Army Engineer Research and Development Center (ERDC) for measuring root system architecture. Each of these techniques will be described in greater detail in the sections that

follow. Root size will be referred to based on the classification of Danjon et al. (1999) as very large or coarse (>2 cm), large (1 to 2 cm), medium (0.5 to 1 cm), and small (<0.5 cm).

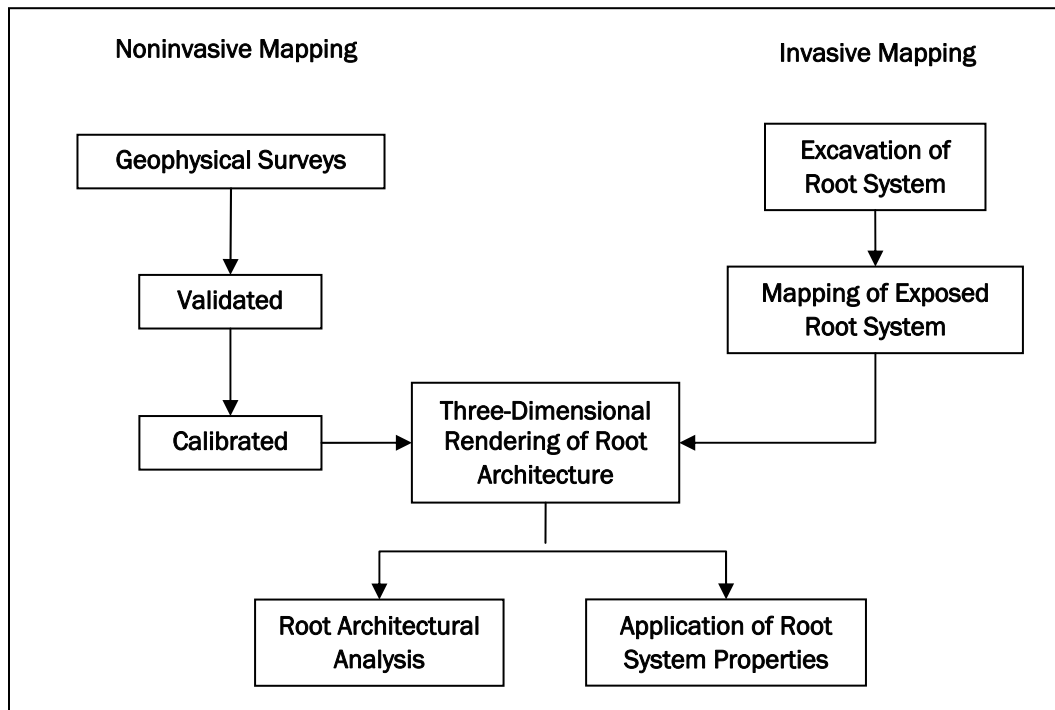


Figure 1. Overview of data acquisition and application for noninvasive and invasive mapping.

2 Study Sites

Woody vegetation on river levee systems in the U.S. are a major problem as opposed to the coastal protection levees from storm surge. Many river levees in the U.S. are legacy systems that were federalized during the Great Depression (1929-early 1940s) or shortly after World War II (1939-1945). Many of these levees were originally intended for agricultural purposes and were not designed using modern soil engineering standards, but rather were built using local practice accepted at the time of construction. However, because of changes in land use patterns, urban areas now occupy what once were agricultural fields. These systems are complex both in terms of their engineering, their hydrology and the local vegetation issues.

Study sites were selected based on an inspection of levees nationwide by the U.S. Army Corps of Engineer (USACE) in 2007, which identified those USACE districts with maintenance deficiencies attributed to the presence of trees within 15 ft from the toe of a levee. In addition to the presence of trees, availability and quality of geotechnical data to permit a detailed site characterization and engineering analysis of the respective reaches were also important to the selection of study sites. Levee geometry, soils, geology, and geographic setting also influenced site selection.

The sites are divided into two categories, site characterization and site assessment, based on the level of research. These categories and the sites for each category are described in the following paragraphs.

Site characterization consists of conducting quantitative field tests to characterize the subsurface environment, including soil type, soil properties, and geology. Geophysical tools were used to define the spatial extent of the root system. However, without further calibration of the geophysical data, the geophysical surveys could only identify a possible root ball. The root ball is defined as the compact section of roots and the soil contained within these roots. A root system includes roots that extend outside the root ball. The exception is the Vicksburg, MS, site. Additional invasive techniques were used to successfully calibrate geophysical data with mapped roots.

Field tests were conducted within the radius of the tree canopy and extended outside the spatial extent of the root system defined by the geophysical assessment. These tests included using permeameters for measuring variation in hydraulic conductivity, soil probes for in situ moisture and unit weight, and pullout tests for measuring root tensile strength. Soil samples were taken for laboratory analyses of engineering properties. Site characterizations varied at each location depending on the quality and quantity of the available data, but generally involved representative geophysical surveys of the trees at each location to determine the root extent and depth and provide stratigraphic models of the local area. Soil sampling was conducted from beneath the tree canopy of representative trees at each location, as well as non-vegetated levee areas, using drive samplers and soil augers to gather data about soil texture, grain size, density, and moisture content. Additionally, shallow 1-m by 1-m soil pits were excavated to verify root extent, depth, and sample the soils within these pits for corroboration of geophysical data.

Site characterizations were conducted at the following sites:

1. Albuquerque, NM: sandy soil, low annual precipitation, sensitive habitat provided by trees
2. Burlington, WA: sandy clay levees, sensitive salmon habitat provided by trees
3. Portland, OR: decommissioned levee available for study
4. Sacramento, CA: legacy non-engineered levees built for removing mine tailings, high sand content, soil-bentonite-cement slurry walls installed in the 1990s, sensitive habitat, highest number of maintenance deficiencies related to woody vegetation

Site assessments

A site assessment is a limited field investigation to mainly gather qualitative information on site conditions and root systems. In areas where trees were removed to meet USACE guidance, qualitative measurements were made and photographs were taken of the root system after tree removal. Soil moisture, unit weight, and hydraulic conductivity were measured in the field at selected locations.

Site assessments were done at the following locations:

1. Danville, PA: highly contrasting soil horizons.

2. Boca Raton, FL: levees constructed on limestone, large number of invasive tree species.
3. Lewisville, TX: a levee was not available for testing in the Dallas/Ft. Worth area because of flood conditions during field tests so a site next to an earth-fill dam was used; different geology than other sites; desiccation is a major problem in this area.
4. New Orleans, LA: high clay content, engineered levees, I-walls, levees built for navigation.
5. Vicksburg, MS: test site for LiDAR scans of root system, and invasive root mapping.

Site characterizations and site assessments included a visit to each site by ERDC. The composition of the ERDC research team was multidisciplinary in nature and included geophysicists, geologists, geological engineers, chemical engineers, civil engineers, hydraulic engineers, computer specialists, biologists, and field technicians. For both site characterizations and site assessments, field testing of in situ soil moisture and density were conducted with a Troxler nuclear density and soil moisture gage to verify the boring data values and access the changes in soil density and moisture under the tree canopy as a function of distance from tree, as well as non-vegetated zones along the levee. Troxler data are shown in Appendix A. Similarly, in situ hydraulic conductivity measurements were taken beneath the tree canopy and in areas without trees to assess changes in physical properties of shallow soils.

The full extent of the data collection, observations, and activities performed are described for both site characterization and site assessments in the following chapters of this volume. The work performed at each site is summarized in Table 1 to gain a better perspective of the comprehensive nature of the data collection efforts at each site.

Three of the study sites examined for the site characterizations are located within the western United States because this is the area with the most deficiencies because of trees. Irrigation and agriculture interests have dominated the historical settlement and development of these areas. Agricultural land use in the past resulted in the wide-scale deforestation of the river's floodplain to accommodate and maximize crop yields by farmers. Subsequently, urbanization of these former agricultural areas within the past half-century has transformed floodplains of the various river systems into flood-protected spaces, as cities have expanded to meet

Table 1. Data gathered and analyses conducted for each site studied in the ERDC research.

increasing population growth. Thus, the river systems that once flowed and migrated unchecked within these different geographical areas have now been transformed into well-regulated flood corridors, which provide public recreation and wildlife habitat areas that are significantly reduced from what once originally existed. The enforcement of USACE vegetation guidelines after the destruction of Hurricane Katrina requires removal of trees from levees raised public concerns about the impacts to environmentally sensitive wildlife habitat within these flood corridors and the reliability of levee systems containing trees.

3 Geology

The focus of this chapter is to describe the geology and geotechnical properties of each study site. This information is used to evaluate impacts of trees on levees by means of engineering models at each site.

Data collection and approach

Historical information was collected for each site from a variety of sources, which include: construction reports, design memorandum, performance data, soil type using the unified soil classification system (USCS) geological maps showing stratigraphy, landforms, and their age or chronology, soil borings of the levee and floodplain, cone penetrometer test (CPT) borings, hydrographic and bathymetric surveys of the river reach, traditional elevation surveys, digital elevation and LiDAR surveys of the study sites and local area, and data from digital Geographic Information System (GIS).

Important sources of imagery for assessing local site conditions were U.S. Geological Survey (USGS) topographic-based digital orthophoto quarter-quadrangles (DOQQs), and high resolution Google Earth imagery of the levee sites.

These data were reviewed and geological cross sections were prepared for each study site that accurately reflect present-day topographical conditions, levee geometry, levee and foundation soils, local stratigraphy, and groundwater conditions, along with the engineering properties of the underlying soils and geological units. Accurate geological and topographical profiles are the basis for modeling the levee profile against hydraulic forces associated with different failure mechanisms that can occur at each site. Backhoe trenches and test pits were used to observe and quantify tree roots of various tree species and to conduct root pullout tests for measurement of tensile strength.

The full extent of the data collection efforts, observations, and field activities are described for each study location. The work done at each site is summarized in the following sections to allow the reader to gain a better perspective on the comprehensive nature of the data collection efforts and site characterization at each site.

Soil moisture and density measurements were made with a Troxler 3451 Nuclear Density Gage at Albuquerque, NM; Boca Raton, FL; Danville, PA;

Sacramento, CA; and Vicksburg, MS, to assess engineering properties (i.e., unit weight and moisture content) of the upper 12 in. of levee and foundation soils. The primary purpose for obtaining in situ unit weight and moisture measurements was to determine variability of these measurements of the near surface at levee and nonleveed areas, as well as barren and woody vegetated areas, to those published in geotechnical investigations. To ensure that the ERDC modeling of the levee or top blanket soils was representative of the actual field conditions reported and studied. Only the deeper Troxler data (i.e., 8 to 12 in.) were used for the purpose of comparing the upper layer (levee or its foundation) properties in the ERDC slope stability and seepage models. Another objective for collecting Troxler data was to see if a tree (and its radius of influence) alters the unit weight and moisture conditions of the levee soils. Data collected by the nuclear density gage are dry density (lb/ft^3), wet density (lb/ft^3), moisture content (lb/ft^3), and percent gravimetric (i.e., unit weight as opposed to volumetric) moisture (%) at 2-, 4-, 6-, 8-, 10-, and 12-in. depths. These data were collected at measured distances from either a representative tree, on the levee (i.e., crest, midslope, and toe), or at an adjacent control site where no trees were present.

It was assumed that the control site adjacent to the woody vegetated area was representative of the same geotechnical reach, with the only exception being the presence of trees. It was beyond the scope of this study to measure the inherent variability within each representative reach in the time allotted to collect the Troxler measurements.

Shallow Troxler data (i.e., measurements between 2 to 6 in.) are generally not representative of the deeper unit weights for the levee or top blanket layer. Shallow data are considered to be more representative of the organic, anthropogenic, and the pedogenic and geomorphic processes. Consequently, shallow data were evaluated separately from the deeper measurements to determine the properties of the shallow subsurface soils and any potential impacts because of woody vegetation.

A series of data tables are presented for each site identifying basic statistical parameters: maximum (max), minimum (min), mean, median, mode, and standard deviation (SD). These tables are grouped for each site to compare all the data (2 to 12 in.) that were collected, for shallow (2 to 6 in.) and deep (8 to 12 in.) measurements and for selected locations at each site. Selected locations include comparison of different levee areas,

floodplain locations with no woody vegetation, grassy control sites, and/or along measured distances from a representative tree trunk and extending outward from the drip line at a fixed spacing. The goal was to compare any trends and variability at the sites studied for sites near the trunk, under the tree canopy, at the drip line, and beyond to some point that was considered outside the influence of the tree.

Sacramento, CA

Introduction

The first section of levee selected for study was designated as Site B. This site contains two valley oaks between 18 to 24 in. in diameter along the landside levee slope and a walnut tree near the levee toe that was adjacent to a wooden fence (Figure 2). Site B is a designation assigned by the Sacramento Area Flood Control Agency (SAFCA) in previous studies. This site is located approximately 5 miles south of downtown Sacramento, CA, in what is locally known as the Pocket Area (PA). Site B is located at approximately Station 292+00 (USACE 2005a) or Station 1508+00 (URS 2008), depending on the geotechnical investigation evaluated. It has been previously studied and characterized in great detail because of poor levee performance during past flood events through-seepage and foundation underseepage. This site was selected because it contains trees on the levee slope that are representative of this geographical area; it has ample geotechnical data to characterize the levee, the foundation soils, and the floodplain geology; and it was easily accessible for the field research conducted by ERDC.

Geological setting

Site B is located in the Central Valley of California (Figure 3) on the east bank of the Sacramento River, at River Mile (RM) 50.4 as measured from the river's mouth (URS 2010a). Alternatively, this site is also located between Levee Mile 5.5 and 5.6 from the reference station at RM 55.9 (USACE 2005a). The Central Valley was created by two major river systems draining the Sierra Nevada Mountain Range over millions of years.

The current drainage system in the Central Valley is the most recent of many river systems that have shaped it during geological time in response to eustatic sea level fluctuations and regional tectonism. The Sacramento and San Joaquin rivers merge southwest of Sacramento to form the latest

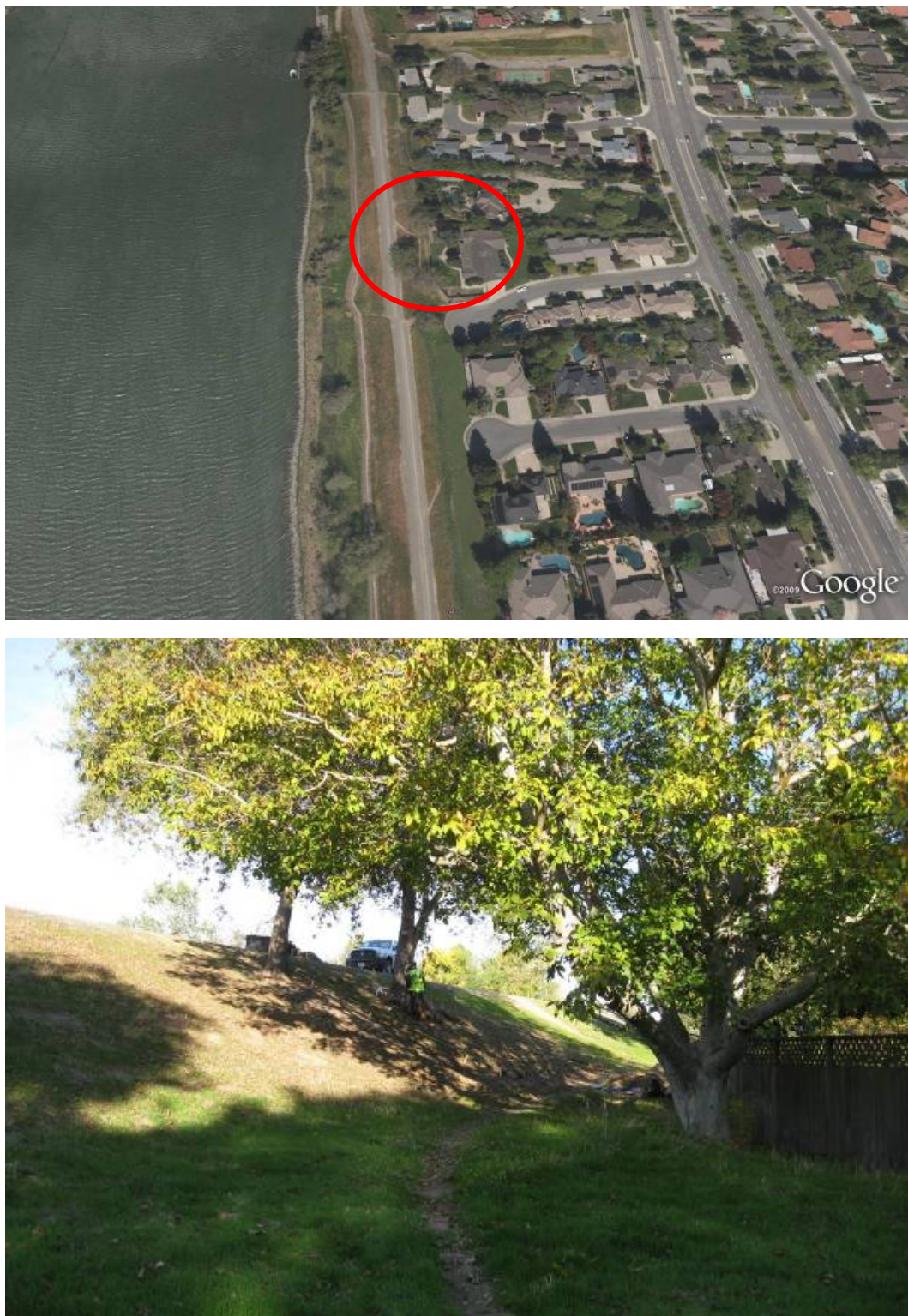


Figure 2. Google Earth (2009) aerial view of the ERDC study site in the Pocket Area.
Bottom photograph is the landside levee slope with valley oaks
on the landside slope, and a walnut tree at the toe of the levee.

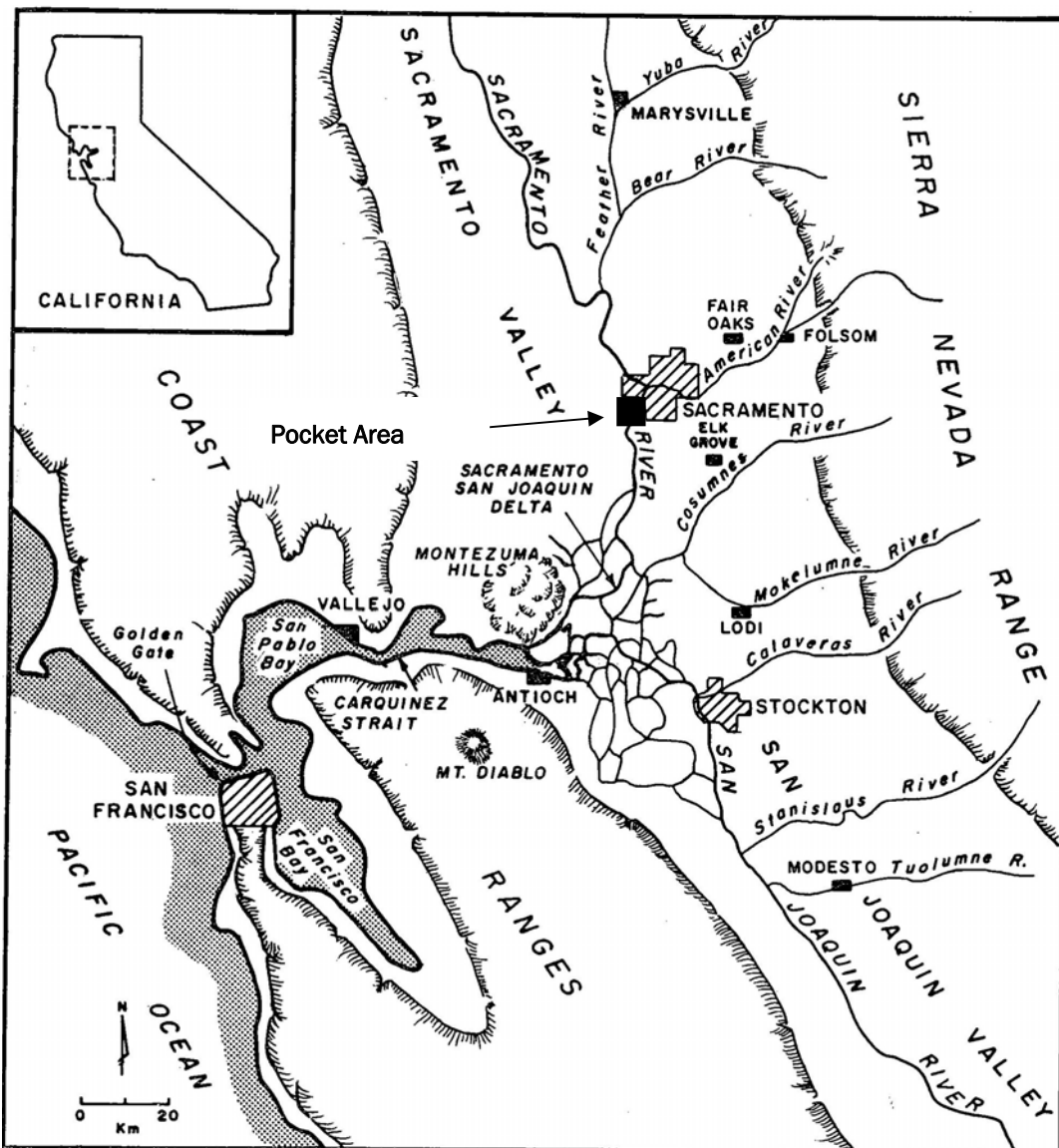


Figure 3. Major physiographic features in the Central Valley of California includes the Sacramento and San Joaquin valleys (Shlemon and Begg 1973). Site B is located in the Pocket Area along the East Bank of the Sacramento River. Rivers draining the Sierra Nevada Mountains area are captured by the Sacramento and San Joaquin rivers and drain into the delta region.

in a series of Sacramento-San Joaquin fluvial-deltaic complexes during the Quaternary [1.8 million years before present (BP)]. The current Sacramento River system drains the northern Sierra Nevada Mountains, while the San Joaquin River drains the southern end of this extensive mountain chain. Major tributary systems immediately upstream of the study area include the Yuba, Bear, Feather, and American rivers as shown in Figure 3.

Regional geological mapping of the Central Valley in the Sacramento area has been conducted by the USGS to characterize the stratigraphy, structure, and chronology of this region (Holley and Harwood 1985a,b). This mapping has recently been integrated into an Environmental Systems Research Institute (ESRI) digital map product by Mulder (2009). A subset of this digital map showing the PA and Site B is presented in Figure 4. The Quaternary evolution and chronology of the American River and Sacramento River systems and associated delta complexes have been studied and described in greater detail by Shlemon (1967; 1971) and Shlemon and Begg (1973).

The geology of the Sacramento area contains deposits associated with the present day floodplain of the American and Sacramento rivers, older floodplain surfaces (i.e., alluvial terraces), and various alluvial fan complexes associated with the different drainage networks that extend from the nearby mountains and flow into the Central Valley. The natural floodplain of the Sacramento River in prehistoric times was much wider than the present day system. This prehistoric floodplain contains floodbasin, lacustrine, and point bar deposits along with abandoned channels and courses of the Sacramento River and its tributaries. Geological mapping and boring data from the PA identifies the floodplain at Site B as being composed of Sacramento River point bar deposits that were deposited approximately 10,000 years BP.

The modern day floodplain has been significantly reduced during the past because of agricultural-related land use. The river is currently restricted to a narrow leveed corridor along the banks of the Sacramento River that was used to flush coarse-grained sediments from the river. These sediments were introduced within the upstream tributary valleys by wide-scale hydraulic gold mining during the mid-1800s. Hydraulic mining was largely discontinued in California in 1879. However, the current system today is still responding to the massive influx of coarse-grained sediment from historical mining activities. The present-day flood protection system for the greater Sacramento area is designed to route major floods away from the Sacramento River through the Yolo Bypass. Several low head weirs upstream of Sacramento divert flood flows from the various tributary systems emptying into the main channel. Additionally, a deepwater ship channel was constructed to facilitate off-river navigation into Sacramento.

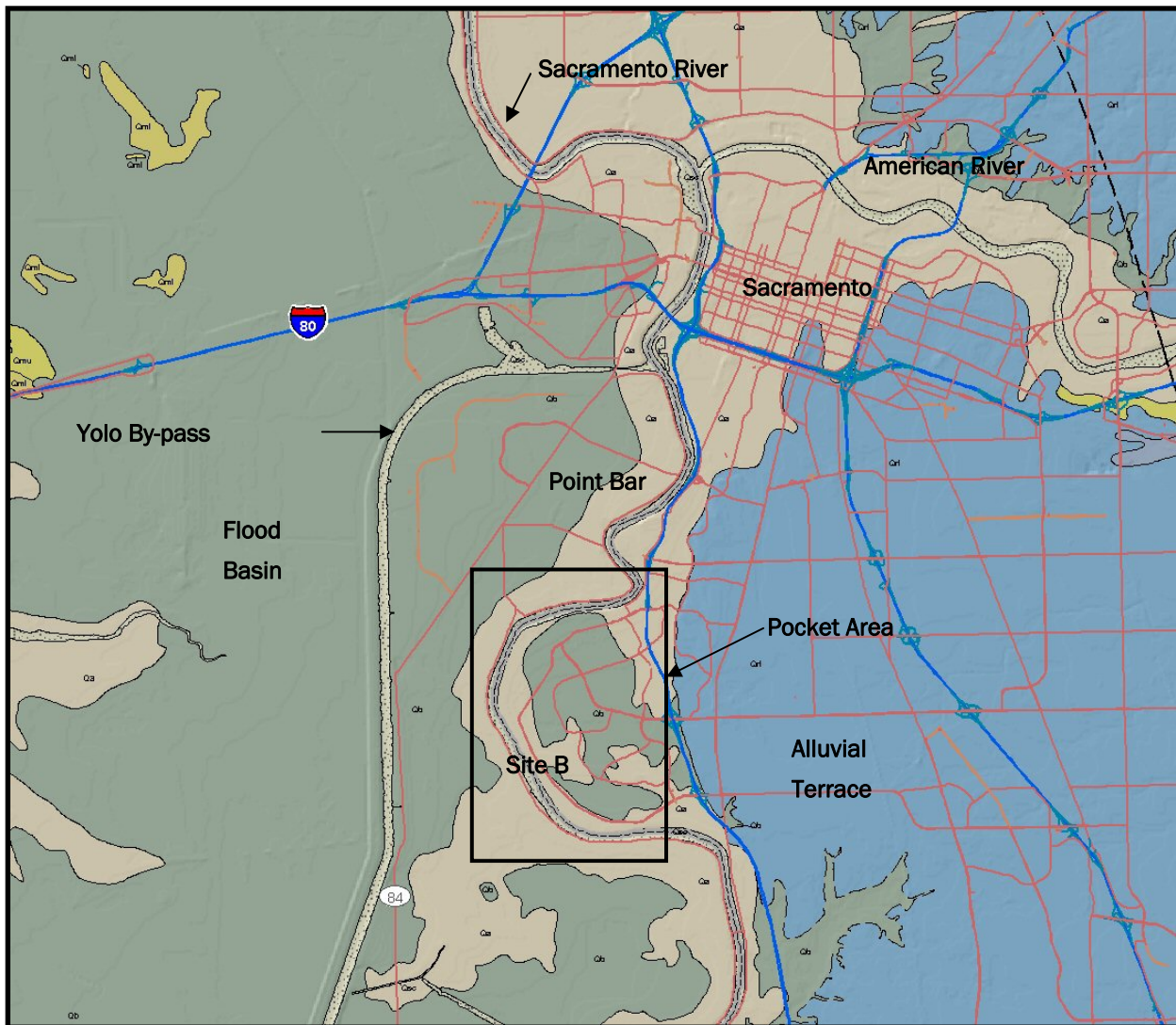


Figure 4. Generalized geological map of the greater Sacramento study area and the Pocket Area showing major boundaries: flood basin, point bar, alluvial terrace. Pocket Area is located on the east bank (point bar side) of the river. (Mulder 2009)

Pocket Area (east bank of the river only) levees were originally constructed to protect agricultural lands by dredging river sediments. Exact levee construction methods at Site B are uncertain, but probably involved using a clam shell bucket and dumping these sediments onto the nearby riverbank. Figure 5 is a typical levee cross section in the PA (Wahler and Associates 1989a). In summary, historical mining, farming, and expanding urban development into the PA has forever changed the Sacramento River in the study area into a canalized corridor that is armored with riprap to prevent future lateral migration of the river from its present course.

Previous geotechnical investigations and geology studies

Critical to the selection of study sites was the availability of geotechnical information to characterize the levee and foundation soils. Numerous engineering borings, associated laboratory soils data, elevation data, and bathymetric surveys of the river channel are available for Site B to adequately develop a representative levee profile for the engineering analyses of tree impacts. These data are presented in various USACE documents (USACE 2004; 2005a) and contractor reports (URS 2010 a,b,c,d; Wahler and Associates 1989 a,b). Boring data from these reports of investigations are used to identify the soils and stratigraphy in the levee and foundation, define the foundation geology, and determine important engineering properties. Soil properties important to the engineering analyses are texture, grain-size distribution, consistency, strength properties, blow count, moisture content, water table position, empirical relationships of grain size and permeability, and the lateral and vertical distribution of major horizons. In summary, available soil boring data from the PA floodplain area provide detailed information to adequately resolve the subsurface deposits and associated engineering properties for evaluating levee stability and underseepage.

Levees in the PA have experienced severe bank erosion and sand boils at the landside levee toe from past floods because of pervious levee and foundation soils (Wahler and Associates 1986). Flood damages from sand boils during the 1986 flood ultimately resulted in the construction of a soil-bentonite-cement (SBC) slurry cutoff wall through the center of the levee during the mid-1990s to prevent levee through-seepage. The slurry wall extends through the center of the levee fill at Site B and terminates in the top stratum to prevent levee through-seepage. The depth of the slurry wall is approximately 20 ft from the top of the levee, and extends to approximately elevation 15 ft at Site B (see Figures 5, 8, 9, and 12). Through-seepage and underseepage were observed at Site B during the 1986 flood (Wahler and Associates 1986). The slurry wall only penetrates the levee and terminates in the underlying fine-grained top stratum. The slurry wall does not restrict levee underseepage in the foundation, which would entail a nearly fully penetrating cutoff wall into the base of the pervious substratum sands. To effectively reduce underseepage in the substratum, the slurry wall would need to fully penetrate nearly 95% of the entire thickness of the substratum aquifer. Consequently, the study area has been characterized by several detailed reports about levee remediation and safety by USACE, Sacramento

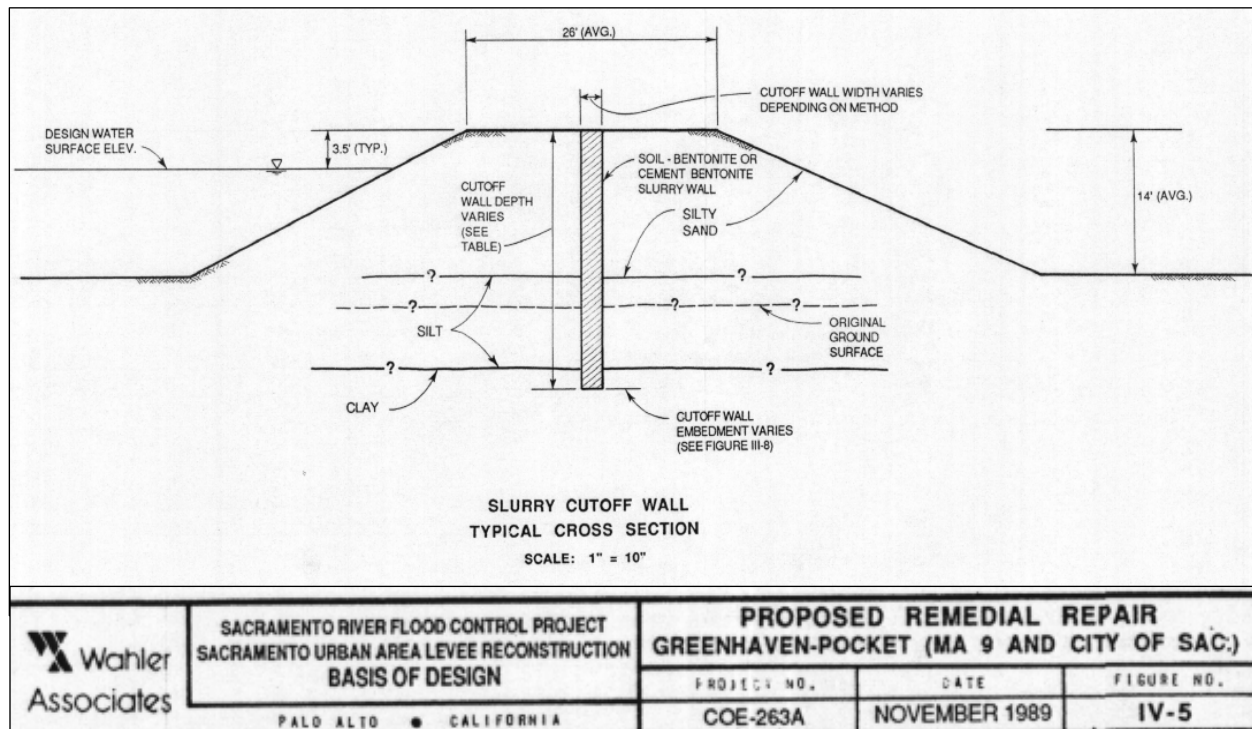


Figure 5. Typical cross section of the levee and soil-bentonite-cement (SBC) slurry cutoff wall for the Pocket Area, Sacramento River (Wahler and Associates 1989a).

District (SPK), and the California Department of Water Resources (DWR).

Reports of studies associated with the construction of the cutoff wall include the work by Wahler and Associates (1989a,b) for USACE and work by USACE to evaluate levee safety for the Federal Emergency Management Agency (FEMA) (USACE 2004; 2005a). More recently, DWR commissioned a study of the entire levee system surrounding metropolitan Sacramento for the Urban Levee Geotechnical Evaluations Program (URS 2010a). Detailed studies by URS (2010a) for DWR in the PA have included compiling all pre-existing geotechnical data, geological studies of the levee surface and foundation, airborne LiDAR surveys, airborne geophysical surveys, and geotechnical analyses of representative levee reaches from the PA. This work evaluates levee stability against sliding, levee through-seepage, and underseepage as part of the comprehensive rehabilitation of the urban levee system by DWR.

As part of the DWR program to evaluate levees, URS (2010a) commissioned William Lettis and Associates to conduct detailed geological mapping in the Pocket Area. Geological maps and cross sections from the Site B reach are presented by URS (2010b,c,d). These cross sections incorporated all

available boring data (USACE 2004, 2005a; Wahler and Associates 1989a,b), as well as new cone penetrometer (CPT) borings drilled specifically for DWR's levee study (Figures 6 through 8). Mapping by William Lettis and Associates (URS 2010b) defines the east riverbank in the PA as being composed of natural levee, point bar, and crevasse splay deposits (Figure 6).

Levee failure mechanisms in point bar deposits

Boring data from the PA identify Site B as being composed of point bar deposits containing a fine-grained top stratum or top blanket and a coarsegrained substratum. The geology beneath the levee at this site is critically important for understanding levee failure mechanisms and the subsequent engineering analyses assessing bank stability. The point bar depositional environment is summarized here to aid in understanding the primary levee failure mechanisms associated with this unique depositional environment and the underlying reasons for subsequent engineering analyses. The listing of failure mechanisms is by no means complete or comprehensive, but provides a general perspective on how this common floodplain depositional environment responds to the hydraulic forces active during high water.

A top blanket or top stratum is a fine-grained layer that overlies a pervious, coarse-grained substratum, and is typical of a meandering fluvial system (Fisk 1944; Saucier 1994). Boring data from the PA show that the top blanket ranges from 10 to 30 ft thick (Figures 6 and 7). The top blanket forms by vertical accretion of fine-grained sediment during flooding. The top blanket includes natural levee deposits, which are usually silts and fine sands that form a topographically distinct ridge adjacent to the main channel. Natural levee deposits are included in the top stratum unit and by vertical accretion of sediment when the river overtops its banks during flooding.

The substratum in contrast forms by lateral accretion of coarse-grained channel sands and gravels onto the point bar (convex) side of the migrating river system. Deposition is entirely restricted within the prism of the channel, and takes place mainly on the low energy or convex side of the active channel. The thickness of substratum deposits usually correspond to the bottom depth of the of the river channel, which forms this coarse-grained unit. The pervious substratum is a pathway for the

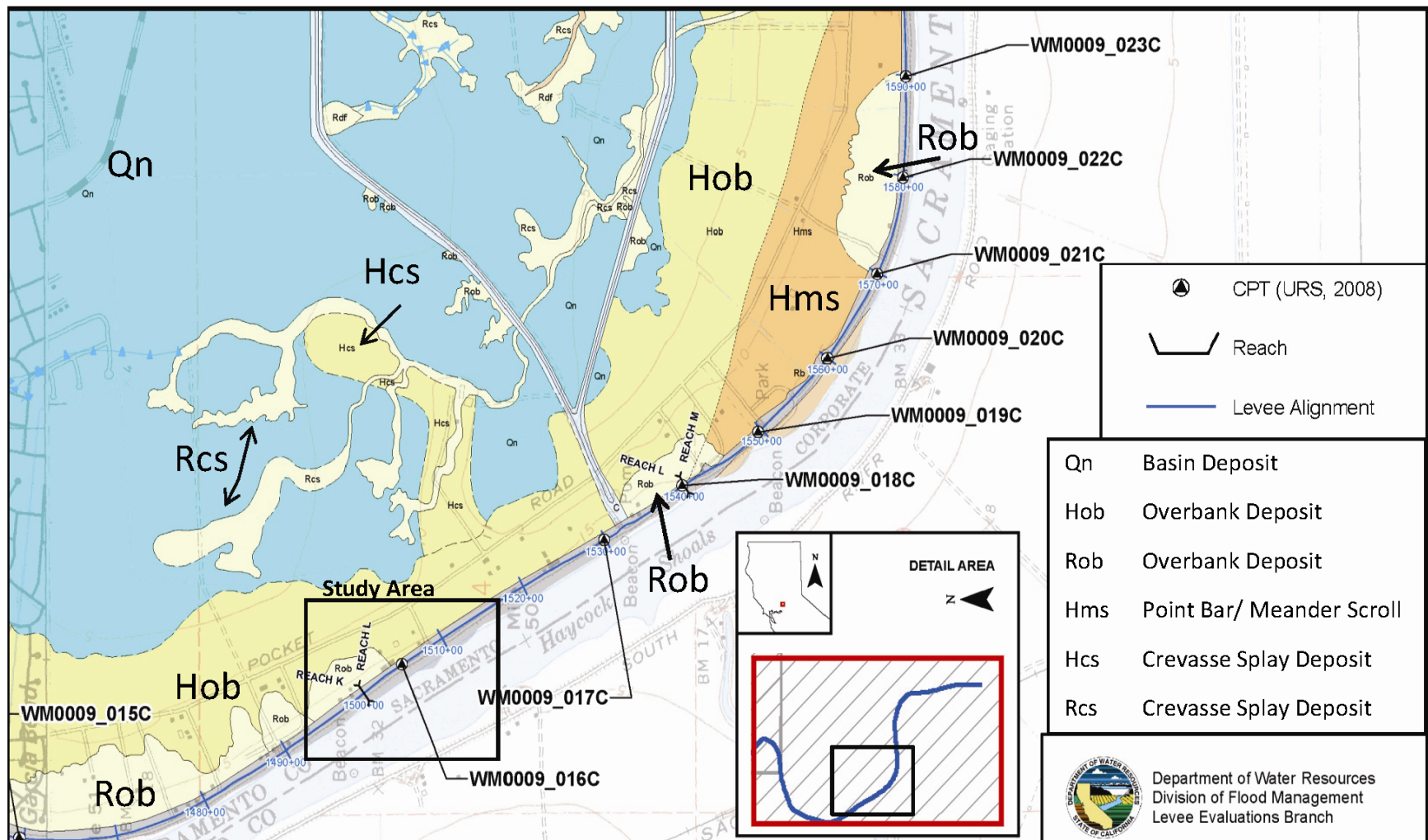


Figure 6. Geology map by William Lettis and Associates (URS 2010a) showing CPT locations and natural levee and point bar deposits within the Site B river reach.

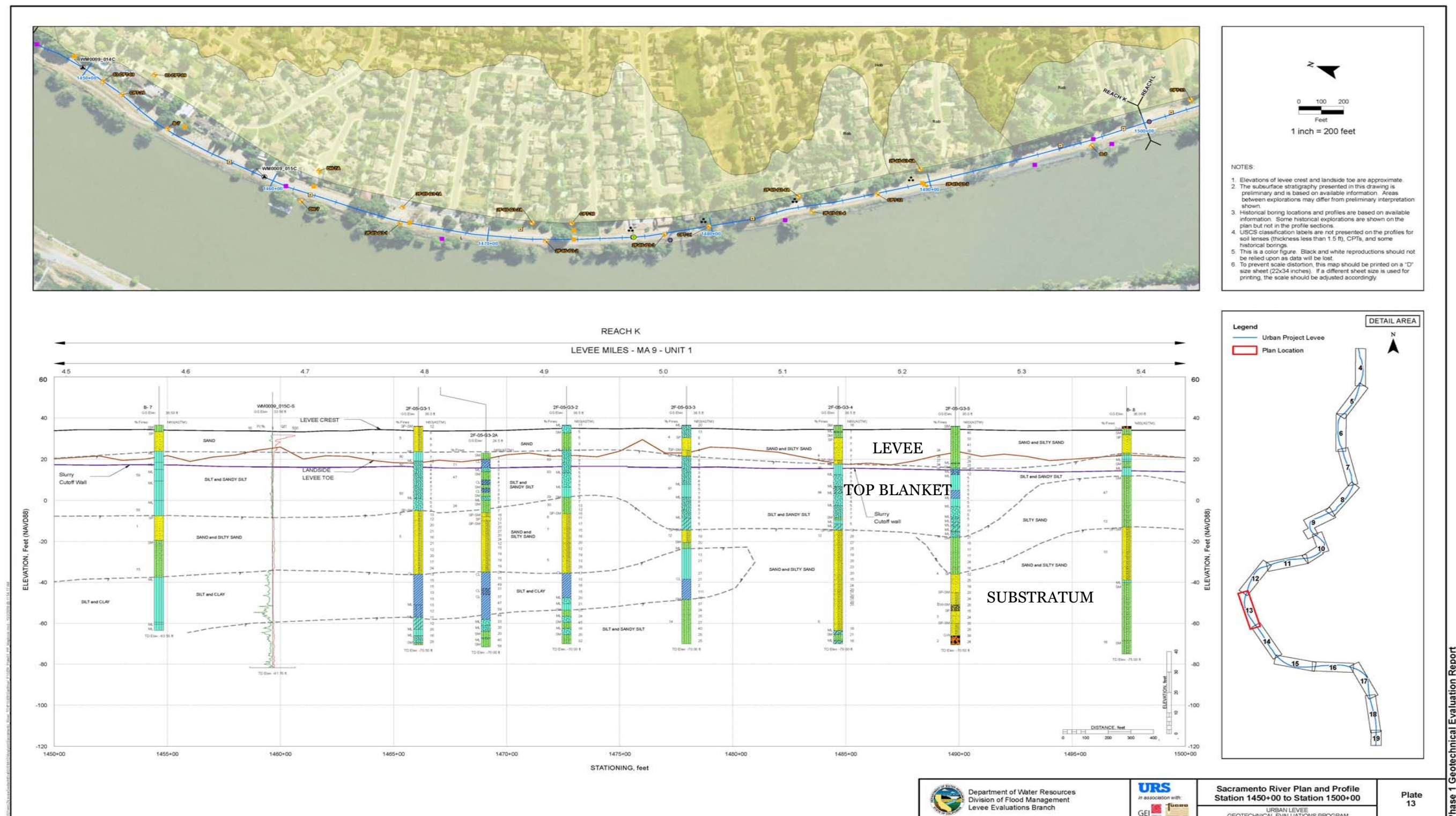


Figure 7. Geological cross section from Station 1450 to 1500 for the DWR urban levee assessment (URS 2010a). Section is upstream of Site B with Boring B-8 at upstream edge of Site B.

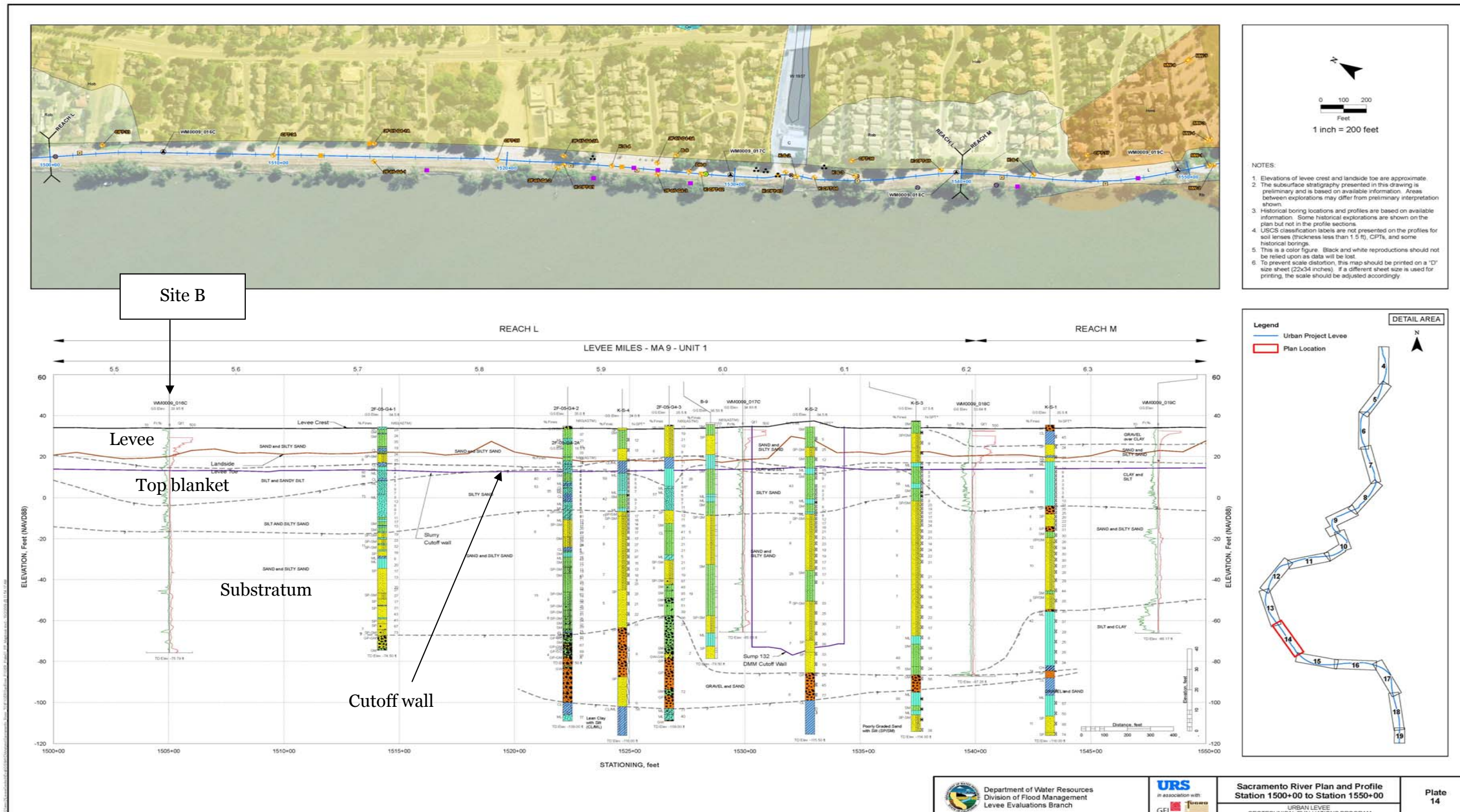


Figure 8. Geological cross section from Station 1500 to 1550 for the DWR urban levee assessment (URS 2010a). CPT VM0009-16C (CPT-16C) corresponds to the location and lithology used for the levee analysis at Site B. The CPT-16C boring log is shown in Figure 10.

movement of water under the levee foundation during flooding. Hydraulic heads generated within this unit can cause heave or rupture of the overlying top blanket at the levee toe, if the weight of the blanket is incapable of containing the underlying hydraulic pressures. Rupture of the top blanket at the levee toe can form sand boils at the levee toe. Excessive hydraulic heads during floods can lead to removal of foundation material from beneath the levee, and cause its eventual collapse, leading to a catastrophic failure. Sand bagging of boils is common engineering practice to help reduce the differential heads between the flood-side and the landside levee toe to pre-vent loss of material from beneath the levee.

In addition to areas where the top blanket is thin, natural and man-made penetrations into the top blanket can cause underseepage and allow boils to form at the levee toe. Man-made penetrations include fence posts, utility poles, utility lines (sewers, electric), and swimming pools. Possible natural penetrations include tree roots, burrowing animals, insects, and other types of biological disturbances. Any place where the landside toe of a levee is penetrated should be carefully monitored to avoid potential problems in seepage prone areas (i.e., areas where the blanket is thin). A complete history of underseepage research in point bar deposits and their engineering treatment is further described in USACE (1941), Mansur et al. (1956), and USACE (2000). Both USACE (1941) and Mansur et al. (1956) describe any type of penetration and specifically root holes in areas of thin top stratum as being especially problematic for causing defects in the clay blanket and pathways for concentrated seepage.

Another important failure mechanism for point bar deposits is slope failures of the riverbank. These generally take place at the cut-bank or the concave side of the river channel, where the thalweg (deepest point in the river) occurs at the toe of the riverbank. The concave side of the riverbank can develop over-steepened slopes, which can undermine the stability of the riverbank and lead to upper slope failure. Normally, this type of failure is a two-stage process. The first part is the loss of the foundation sand by the eroding scour pool, followed by upper bank failure from shear (Krinitzsky 1965; Turnbull et al. 1966). Hardening of a riverbank by stone protection is common engineering practice to prevent the river from migrating laterally, especially in areas where sandy soils (i.e., older point bar deposits) are present. Additionally, vegetation can help reduce surface erosion of erodible soil. Currently, both sides of the riverbank in the vicinity of Site B are armored with riprap to prevent uncontrolled surface erosion of the coarse-

grained riverbank soils and prevent the river from naturally migrating laterally across its floodplain. Site B is located on the convex (point bar) side of the channel as opposed to the concave or cut-bank of the river channel. Consequently, failure mechanisms on the cut-bank side are not addressed by this study.

A third failure mechanism in point bar deposits involves a sudden drawdown of the river stage following prolonged flooding. The added weight of the saturated riverbank and draining of excess pore water from pervious deposits led to a shear failure of the upper bank under the influence of gravity. These types of failures can be fairly deep seated and involve the entire top stratum. However, depending on the depth of the shear surface, trees can also reinforce the bank against shallow seated sliding and slope failures. Further contributing to this failure process is excessive scouring during high water at the riverside toe where levee slopes become too steep to support the weight of the saturated bank. Ordinarily, this type of failure is not critical to public safety unless there is the likelihood of a second flood event that then breaches the weakened levee.

The last failure mechanism that can occur involves only the pervious levee embankment soils. Thus, it is not considered a failure directly in the point bar deposits, but rather in the embankment itself, because of the construction methods and the materials used to build the levees. Because pervious river sand was used to build the PA levees in the early 1900s, using a combination of bucket and hydraulic dredging methods, these levees are prone to through-seepage type failures.¹ Prolonged flooding can cause levee through-seepage, which can lead to water discharge along the lower third of the landside levee slope. This seepage can remove soil particles from the landside slope via hydraulic pressures and eventually lead to piping of material and failure. The presence of woody vegetation and large roots in the embankment on the lower landside slopes may promote pathways for this seepage, and concentrate and destabilize the levee profile during prolonged high water (FEMA 2005). Furthermore, saturation of the levee embankment can soften the soils because of the movement of the wetting front and lead to later problems with flood fighting and access to these areas.

¹ Personal communication. 2010. Mary Perlea and Ed Ketchum, USACE Sacramento District (SPK); Ray Costas, Kleinfelder and Associates; and Les Harder, HDR Company.

In summary, point bar deposits are prone to a variety of failure mechanisms that can affect levee stability. The primary failure mechanisms were briefly reviewed here to help with the understanding of the basic data requirements for the subsequent engineering analyses of these different failure modes. The list of failure mechanisms described here is by no means comprehensive. It merely frames the discussion about the importance of the floodplain geology and how the point bar depositional environment, specifically, is prone to foundation and levee failures from the hydraulic forces within the flood corridor.

Cross section at Site B

A cross section of the levee and riverbank was developed from available boring, survey, bathymetry, and LIDAR data (Figure 9). This section was used for the engineering analysis of trees by ERDC. Table 2 summarizes the layer properties at Site B. This profile incorporates soils data from the existing CPT and boring logs. CPT-WM0009-16C is located at Station 1505+00 and was the closest boring to Site B where the trees were present (Figure 10). This CPT is considered representative of the underlying soils at this location. Soil texture can be interpreted from CPT borings on the basis of measurements of the cone's tip pressure and sleeve friction, which have been correlated to soil types by Robertson and Campanella (1983).

CPT data were compared to other nearby borings (B-8, CPT-33, CPT-34, 2F-05-G4-1, and 2F-05-G4-1A; see plan view in Figure 11). Boring logs from this reach are summarized by the USACE (2005a) cross section in Figure 12, which includes the ERDC study area at Site B. The levee profile in Figure 13 was developed as part of the USACE (2005a) geotechnical investigation for this reach. This profile is entirely consistent with the URS (2008) data that have been collected and reviewed for this site. The cross section presented earlier in Figure 9 and used for the engineering analysis was refined using the available data and field observations by ERDC, SAFCA, and URS (2010 a,b,c,d). The levee profile and underlying stratigraphy are described in the following paragraphs.

The levee at Site B was constructed from river sand with a 1V (Vertical):3H (Horizontal) slope on both the river and landsides (Figure 5). The levee crest was at elevation 32 ft. CPT data from Site B identify the levee as sand, which was 18 ft thick at this location and extended to elevation 14 ft. The base of the levee was approximately 180 ft wide at Site B. The top blanket

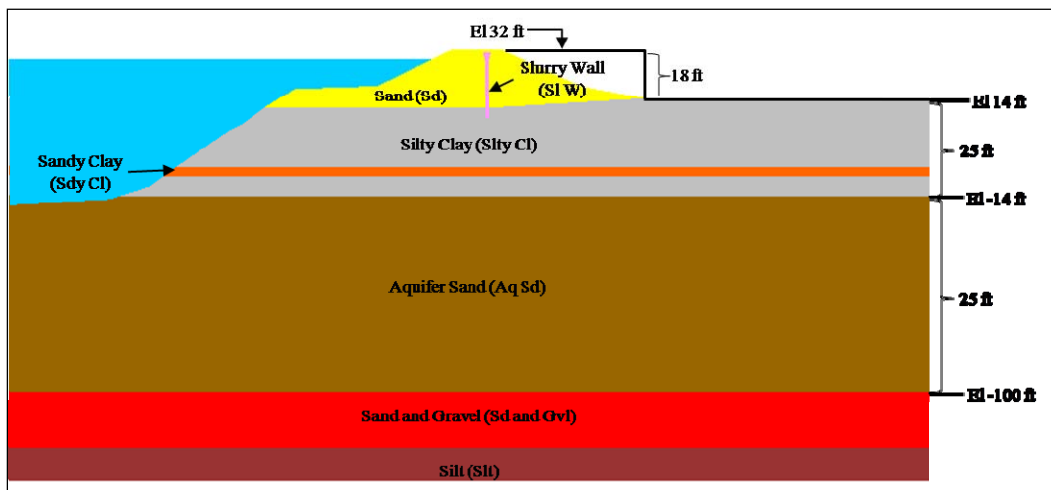


Figure 9. Cross section and levee profile developed from CPT WM0009-16C and existing elevation and bathymetry data.

Table 2. Stratigraphy at Site B Pocket Levee, Sacramento River.

Layer Name	Layer Thickness (Elevation in ft)	Soil Class
Levee	32.0 to 14.0	Stratified Sand
Blanket	14.0 to -4.0	Clay, Silty Clay
Blanket	-4.0 to -7.0	Mixed Sand and Clay
Blanket	-4.0 to -13.0	Clay, Silty Clay
Foundation	-13.0 to -73.0	Sand
Foundation	-73.0 to -100.0	Gravel, poorly sorted

was primarily clay with a mixed sand and clay layer near the base and was nearly 25 ft thick, extending to elevation -14 ft. The underlying substratum was sand (see Figures 9 to 13). Substratum sands were estimated to be nearly 110 ft thick at this location, based on the available boring data. A silty clay layer was encountered at the base of the substratum sands at elevation -100 ft (Figure 8). A 25-ft-thick gravel layer occurred above the base of the substratum sands.

In summary, the levee fill at Site B was composed of sand obtained from the river. The man-made levee was located upon Sacramento River natural levee and point bar deposits (Figure 5). Throughout this reach, the top stratum had a variable thickness, from less than 10 to 30 ft thick (see Figures 7 through 10). CPT boring WM0009-16C was the closest of the CPT data to Site B (Figure 10), and therefore was used to characterize the levee and foundation soils for the cross section that was developed for the engineering analysis. The topography and geometry of the levee section were based on recent bathymetry, elevation, and LiDAR surveys from this

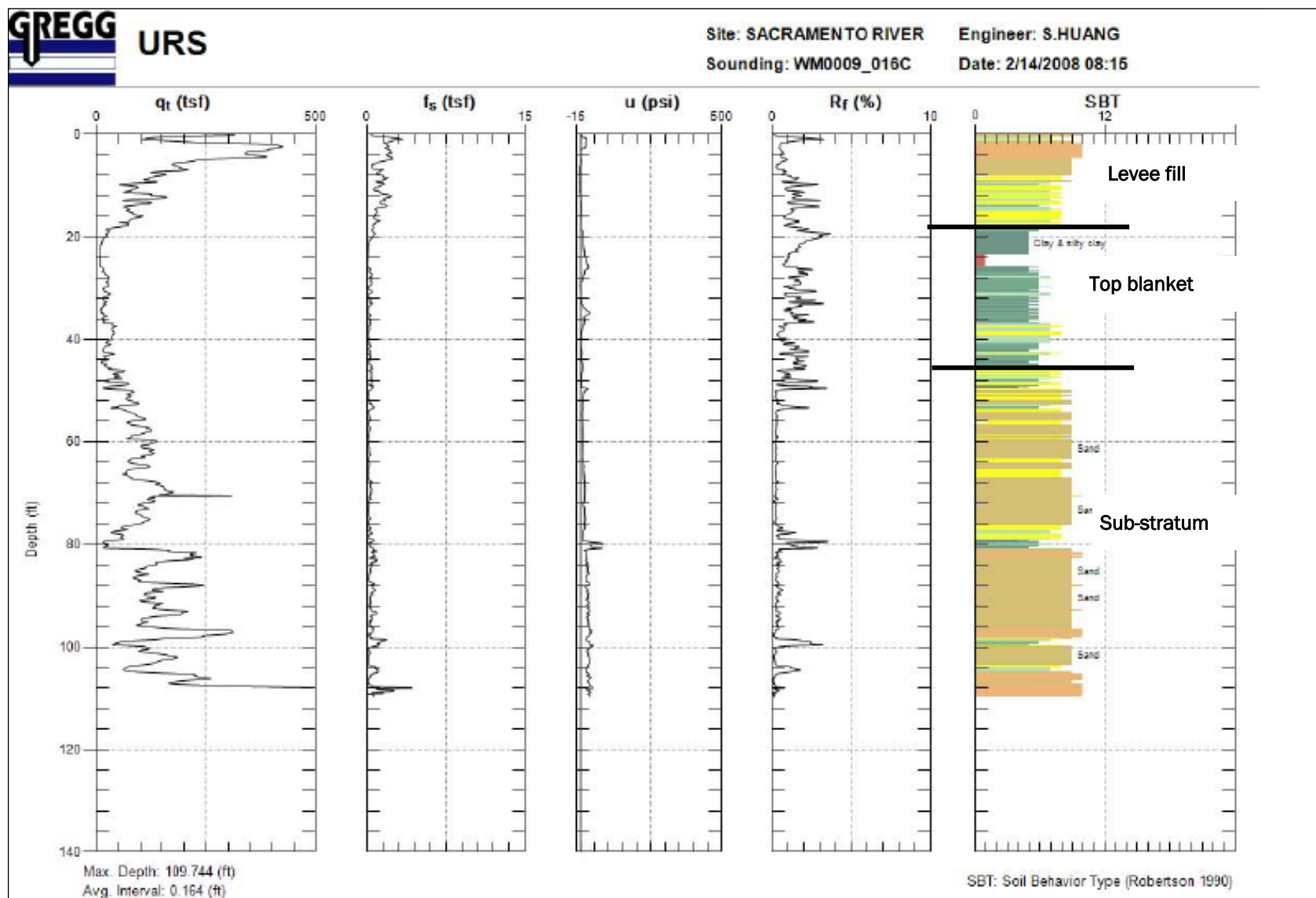


Figure 10. Drilling log for CPT-WM0009-16C and subdivision of the soil data into levee fill, top blanket, and substratum (URS 2010a). CPT data are classified according to relationships by Robertson and Campanella (1983) between sleeve friction and tip resistance of the cone.



Figure 11. The locations of six borings within 1,000 ft of Site B (URS 2008).

reach. The cross section was used in the numerical models for this research. The thickness of the top stratum was varied in the models to determine the effects of subsequent changes and the critical condition from the results of the original cross section. Additionally, hydraulic conductivity or permeability values were varied accordingly to assess their sensitivity to different layer properties and to varying conditions that can be encountered within the PA. The results and variations from the base condition are further described in the appropriate modeling section in Volume III of this report.

Laboratory soils data

Boring data from URS (2010a), USACE (2004; 2005a), and Wahler and Associates (1989a,b) were used to prepare the levee profiles in Figures 7, 8, and 12. These data were primarily derived from undisturbed soil samples (i.e., Shelby tube) taken in the fine-grained top stratum and disturbed samples (i.e., split-spoon) from the pervious substratum. These samples were used to characterize the stratigraphy and provide material for laboratory testing. Soils data in these cross sections are classified using the Unified Soils Classification System (USCS). Soils normally are visually classified during drilling, and field boring logs are produced that document the lithology and sampling process (i.e., soil texture, type samples, blow counts, changes in drilling, stratigraphy, groundwater conditions). In the laboratory, soil samples are again visually classified and subjected to basic, engineering laboratory soils testing. This provides basic data on soil texture, moisture content, grain-size, Atterberg limits, unit weight, and shear strength. These data have been summarized in earlier reports (URS

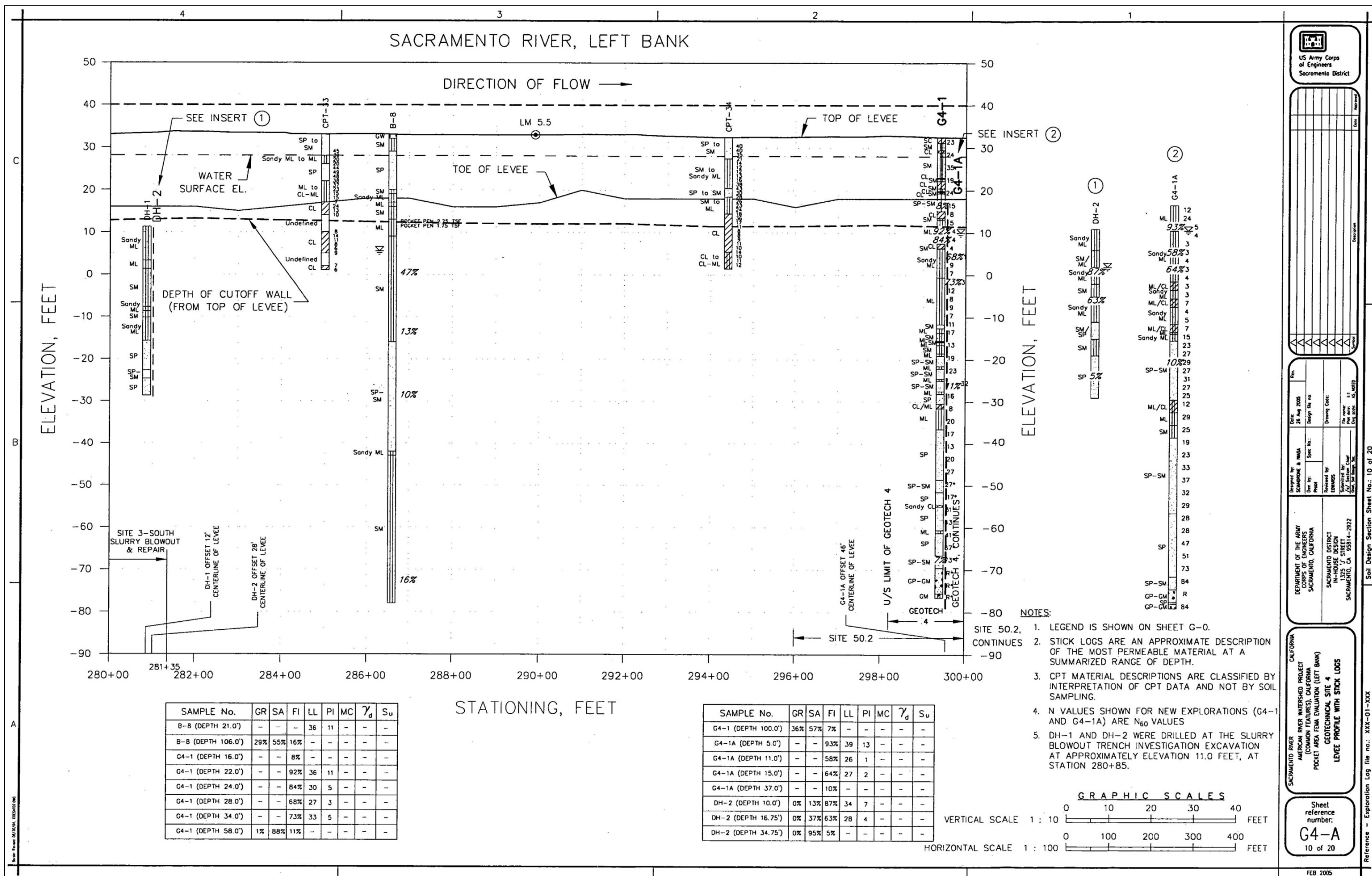
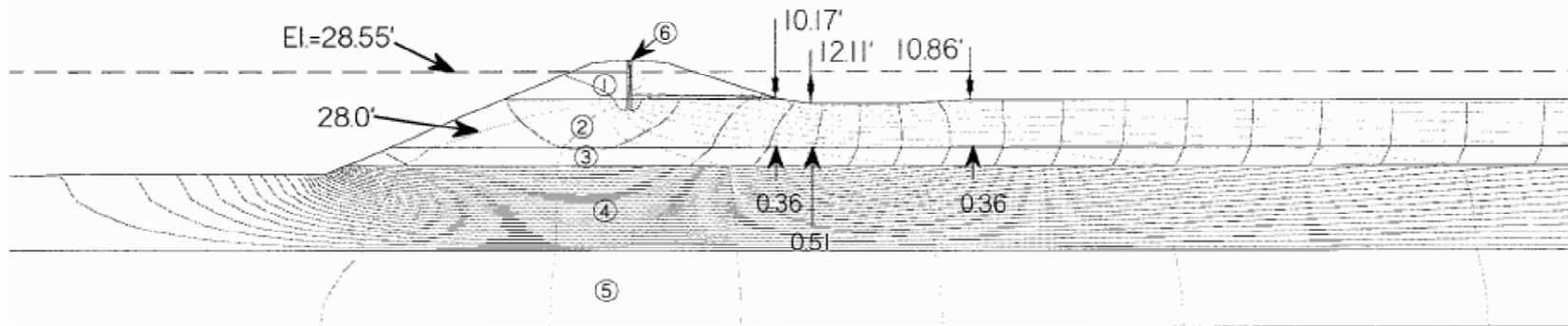


Figure 12. USACE (2005a) cross section through the Site B reach (at dashed red line) showing the soils within the levee and foundation. Laboratory soils data summarized in the table of this figure.

SACRAMENTO RIVER FEMA EVALUATION FOR POCKET AREA
STEADY STATE SEEPAGE MODEL



Hydraulic Conductivity for Soil Layers

Material No.	Material	Permeability (cm/sec)	
		k_v	k_h
1	SP	5×10^{-3}	2×10^{-2}
2	ML/CL, CL/ML, CL, ML	5×10^{-5}	2×10^{-4}
3	SM	2×10^{-4}	8×10^{-4}
4	SP, SP-SM	5×10^{-3}	2×10^{-2}
5	CL, ML, CL/ML	2.5×10^{-5}	1×10^{-4}
6	Cutoff Wall	1×10^{-6}	1×10^{-6}

AMERICAN RIVER WATERSHED PROJECT (COMMON FEATURES) CALIFORNIA
GEOTECH SITE 3 SEEPAGE MODEL STATION 252+00
SEEPAGE RUN NO.: SRG3-3bwsel28-55
SACRAMENTO DISTRICT, CORPS OF ENGINEERS

Figure 13. Levee profile used for 2005 seepage evaluation near Site B (USACE 2005a). Hydraulic conductivity used for soil layers is presented in the table.

2010a; USACE 2004, 2005a; Wahler and Associates 1989a,b). Cross sections presented in Figures 7, 8, and 12 reflect the latest information about the soils and stratigraphy from this reach, based on the various investigations that have been conducted to date.

The stratigraphy for the cross section and levee profile in Figure 9 is summarized in Table 2. Additionally, laboratory soils data from USACE (2005a) are summarized in Figures 12 and 13. Thus, soil layers and topographical data shown in Figure 9 and used in the model studies were compiled from review of previous research in this area.

Hydraulic conductivity values

Selecting hydraulic conductivity or permeability values is an important part of the engineering evaluation of levee through-seepage and underseepage in the substratum sands and gravels. They are ordinarily determined from in situ pump tests, slug tests, or laboratory soils data using empirical relationships derived from sample grain size. Pump and slug tests are generally limited in quantity because of their cost and difficulty, especially in levee research, where hundreds of miles of levees need to be characterized. Packer and slug tests involve the installation of piezometers or placement of packers in boreholes to isolate horizons or zones for testing. In situ testing provides estimates of the borehole permeability of a stratigraphic zone or portions thereof, and represents a localized geographical area. Laboratory permeability tests on soils data, on the other hand, look at point data and thus represent a much smaller area of influence.

Geotechnical reports were the main source of data for estimating hydraulic conductivity (USACE 2005a; URS 2008; URS 2010a,b,c,d). Empirical relationships have been developed to estimate permeability based on grain size data (Hazen 1911; Shepherd 1989). An important parameter for permeability estimates is based on a mean particle size or the D_{10} size from grain-size curves. However, these relationships are usually only valid for a narrow range in grain size, and often break down where the particle size distribution contains fines that are below the No. 200 sieve size. Point bar deposits often contain silty sands, with fines content that can vary between 5 to 30% by weight. The smallest particle sizes are usually the limiting factor in estimating permeability values.

The flow of water through the granular pore space in shallow aquifers is restricted by the fines that are present. Point bar deposits in floodplains typically become finer in texture, from poorly to well graded sands (i.e., geologically, well to poorly sorted) because of the method by which these soils are deposited. Near the base of point bar deposits are gravels that transition upward into clean sands and then silty sands near the top of the pervious substratum unit. This is typical of this floodplain landform. It produces vertical variations in permeability over the thickness of the deposit, which varies texturally with increasing depth. Ordinarily, this type of floodplain deposit has an increase in permeability values with an increase in depth (Figures 7, 8, and 12).

As part of the Urban Levee Geotechnical Evaluation Program of the Sacramento area levee system, DWR developed standard guidelines for the geotechnical engineers evaluating and analyzing the levee system (URS 2007). Because of the limited number of in situ tests that can be reasonably and economically done, DWR standardized the procedures to estimate permeability values from laboratory soils data. This procedure has been accepted by the USACE Sacramento District as well, ensuring a uniform approach to assessing the permeability of levee embankments and foundations for underseepage and through-seepage studies.

The standardized procedure that has been developed by DWR for the Urban Levee Geotechnical Evaluation Program of the Sacramento Levees is based in part on expert opinion and engineering judgment using a table of USCS soil texture versus hydraulic conductivity values (Table 3). This procedure provides a common reference for the subsequent engineering analyses of levee underseepage and through-seepage.² Table 3 identifies the January 2010 draft guidelines for estimating permeability from laboratory soils data.³ Values identified in Table 3 were used to assign permeability values to the soil layers identified in Figure 9. Permeability values are based on the fines content using the laboratory grain size data from the previous geotechnical investigations (USACE 2005a; URS 2008; URS 2010a). Table 4 presents the permeability values that were assigned to the layers at Site B in Figure 9.

² Personal communication. 2010. Ed Ketchum, USACE SPK Geotechnical Branch.

³ Personal communication. 2010. Harder and Sills.

Table 3. Recommended hydraulic conductivity (K) values for use in base case and initial seepage analyses for the Natomas Levee improvement program.

Material Type	Soil Description	K_h (cm/sec)	K_v/K_h	K_v (cm/sec)
Slurry Wall	SCB or CB	1×10^{-6}	1	1×10^{-6}
	SB	1×10^{-7}	1	1×10^{-7}
Clay (CL, CH)	New Compacted Clay Levee	1×10^{-6}	0.25*	2.5×10^{-7}
	New Compacted Clay Berm	1×10^{-6}	0.25*	2.5×10^{-7}
	Clay Layer over 20 feet below ground surface	1×10^{-6}	0.25*	2.5×10^{-7}
	Clay Blanket	1×10^{-5}	0.25*	2.5×10^{-6}
Silt (ML, MH)	Silt or Plastic Silt 80 – 100% fines content, or >50% fines content and PI > 4	1×10^{-5}	0.25*	2.5×10^{-6}
	Sandy Silt 50 – 79% fines content	3×10^{-5}	0.25*	7.5×10^{-6}
	30 – 49% fines content	3×10^{-6}	0.25*	7.5×10^{-7}
	13 – 29% fines content	3×10^{-5}	0.25*	7.5×10^{-6}
Clayey Sand to Sand (SC, SP-SC, SW-SC, SP, SW)	8 - 12% fines content	3×10^{-4}	0.25*	7.5×10^{-5}
	3 - 7% fines content	3×10^{-3}	0.25*	7.5×10^{-4}
	0 - 2% fines content	1×10^{-2}	0.25*	2.5×10^{-3}
	30 – 49% fines content	1×10^{-4}	0.25*	2.5×10^{-5}
	13 – 29% fines content	3×10^{-4}	0.25*	7.5×10^{-5}
Silty Sand to Sand (SM, SP-SM, SW-SM, SP, SW)	8 - 12% fines content	1×10^{-3}	0.25*	2.5×10^{-4}
	3 - 7% fines content	3×10^{-3}	0.25*	7.5×10^{-4}
	0 - 2% fines content	1×10^{-2}	0.25*	2.5×10^{-3}
	30 – 49% fines content	3×10^{-6}	0.25*	7.5×10^{-7}
	13 – 29% fines content	3×10^{-5}	0.25*	7.5×10^{-6}
Clayey Gravel to Sandy Gravel (GC, GP-GC, GW-GC, GP, GW)	8 - 12% fines content	3×10^{-4}	0.25*	7.5×10^{-5}
	0 - 7% fines content	1×10^{-2}	0.25*	$\times 10^{-3}$
	30 – 49% fines content	3×10^{-5}	0.25*	7.5×10^{-6}
	13 – 29% fines content	2×10^{-4}	0.25*	5.0×10^{-5}
Silty Gravel to Sandy Gravel (GM, GP-GM, GW-GM, GP, GW)	8 - 12% fines content	1×10^{-3}	0.25*	2.5×10^{-4}
	0 - 7% fines content	1×10^{-2}	0.25*	2.5×10^{-3}

* Note: The K_v/K_h ratio of 0.25 is intended as an initial value to be considered for seepage analyses. Depending upon the stratifications of the deposits, other ratios may be more appropriate. For example, a K_v/K_h value of 0.5 to 1.0 may be appropriate for clean sandy or gravelly deposits that do not have layers or lenses containing fine material. On the other hand, K_v/K_h values approaching 0.1 may be appropriate for highly stratified or lenticular deposits.

Table 4. Hydraulic conductivity values assigned to layer soils in Figure 9.

Pocket Area Hydraulic Conductivity Values				
Material	K_h (cm/sec)	K_h (ft/day)	K_v (cm/sec)	K_v (ft/day)
Levee sand	8.00E-03	2.27E+01	2.00E-03	5.67E+00
Clay silty clay	8.00E-04	2.27E+00	2.00E-04	5.67E-01
Clay mixed with sand	3.00E-05	8.50E-02	1.00E-05	2.83E-02
Aquifer sand	8.00E-02	2.27E+02	2.00E-02	5.67E+01
Gravel	2.00E-02	5.67E+01	2.00E-02	5.67E+01
Silt	1.00E-04	2.83E-01	1.00E-04	2.83E-01
Slurry wall	1.00E-06	2.83E-03	1.00E-06	2.83E-03

Groundwater conditions

The water table at Site B for the starting model (low water stage) was estimated to be approximately 6 ft below the ground surface for the landside toe of the levee. This elevation level was based on the river stage observed in current Google Earth imagery for the study area. Groundwater levels in the PA vary widely with the river stage because of the pervious nature of the underlying substratum (aquifer) sands.

Residential sections in the PA near the Sacramento River are known for the occurrence of pin boils and moderate to heavy seepage during high river stages. Heavy seepage has been reported and documented in cracks in driveways, sidewalks, roadways and other low-lying areas behind the levee in the PA once the river stage exceeds 15 to 19 ft at the I Street gage. Heavy seepage is defined as the occurrence of pin boils (small pipe openings without sand cones) with running water (Cunny 1987).

Floods in the study reach caused transient to steady-state seepage, depending on the flood stage and duration. A flood hydrograph was used for the input model to determine the loading from the hydraulic forces.

Troxler measurements

Troxler data were collected from a single site (Figure 14) in the Pocket Area of the Sacramento Levee. Geophysical measurements were conducted at this location to map the extent of the root ball and individual roots. A 1-m × 1-m grid (Figure 15) was established for the resistivity survey around a valley oak tree (Box 84 in Figure 15).

Troxler measurements were taken from selected locations within the geophysical grid. Measurement locations are highlighted by the red rectangle in Figure 15 and were usually taken in the center of each grid box. Additionally, a series of transects were developed within the grid. Transects 1 and 2 correspond to a series of fixed distance measurements from the tree and extending upstream on a diagonal line along the levee slope as shown by Figure 15. A grass-covered control site, perpendicular to the levee and approximately 200 ft south of the tree shown in Figure 15, was used for comparison purposes to the location containing the tree. The levees at this site were primarily composed of silty sand (SM).

All of the Troxler data are summarized in Table 5 for the tree site shown in Figures 14 and 15. Plots of these data are shown in Figures 16a to 16d. Data from the north transect are summarized in Table 6, and plots of these data are presented in Figures 17a to 17d. Similarly, data from the south transect is summarized in Table 7 (plots in Figures 18a to 18d), the east transect in Table 8 (plots in Figures 19a to 19d), transect 1 in Table 9 (plots in Figures 20a to 20d), transect 2 in Table 10 (plots in Figures 21a to 21d).

Plots of the two fixed distance transects along the landside levee slope in Figures 20 and 21 were perhaps the most significant findings for the Troxler data collected from this site. Generally, both profiles show the unit weights are much less beneath the tree canopy to the drip line and increase measurably beyond the drip line of the tree. Similarly, the water contents (Figures 20c 20d, 21c and 21d) were low near the trunk, increased toward the drip line, and decreased beyond the drip line as the influence of the tree diminished. The increase in soil moisture under the drip line was attributed to the presence of leaf litter and shade, which likely preserves the moisture in the soil, while the lower values near the trunk may have reflected the depletion of soil moisture around the main part of the root ball.



Figure 14. The location of the geophysical grid in Sacramento, CA, used for Troxler measurements.

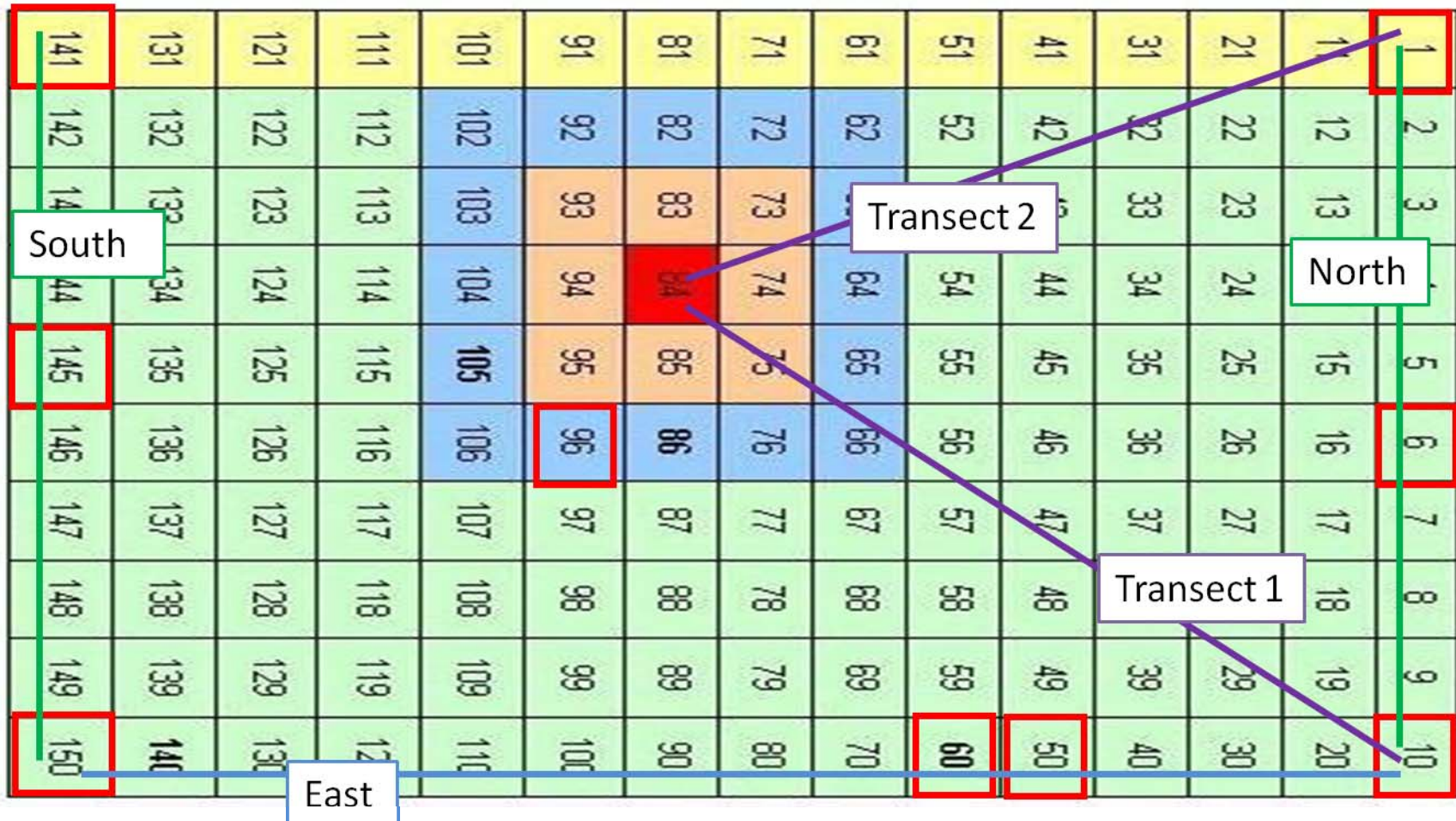


Figure 15. Grid system and transect lines for Troxler measurements in Sacramento, CA.

Table 5. Statistical data for Troxler measurements in Sacramento, CA, north transect 2-, 4-, 6-, 8-, 10-, and 12-in. depths.

North Transect Depth (2-4-6 in.)	Dry Density (lb/ft ³)	Wet Density (lb/ft ³)	Moisture Content (lb/ft ³)	Percent Moisture (%)	North Transect Depth (8-10-12 in.)	Dry Density (lb/ft ³)	Wet Density (lb/ft ³)	Moisture Content (lb/ft ³)	Percent Moisture (%)
Max	102.7	114.2	17.8	40.8	Max	108.2	118.9	18.2	26.6
Min	43.6	61.5	1.9	2.5	Min	65.7	77.2	2.0	2.3
Mean	78.5	87.5	9.0	12.0	Mean	88.5	97.3	8.8	10.3
Median	80.8	88.0	9.0	10.5	Median	88.9	95.8	9.1	9.2
Mode	87.7	96.7	10.1	6.8	Mode	89.5	91.2	6.3	18.5
Standard Deviation	11.6	11.6	4.3	7.3	Standard Deviation	9.0	8.5	4.2	5.6
*#N/A: no central value in data set					*#N/A: no central value in data set				

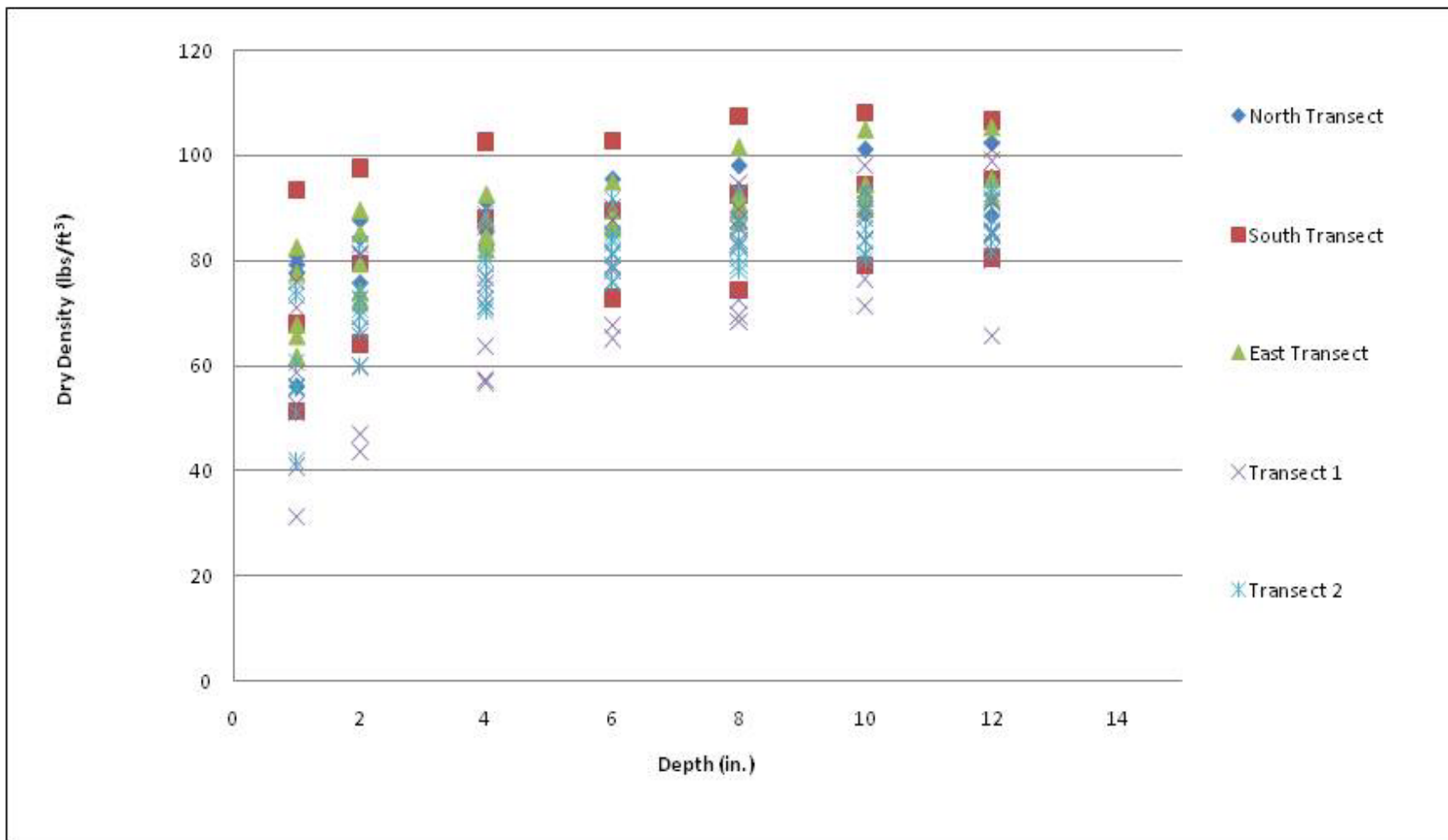


Figure 16a. Dry density (lb/ft³) from Troxler measurements for Sacramento, CA.

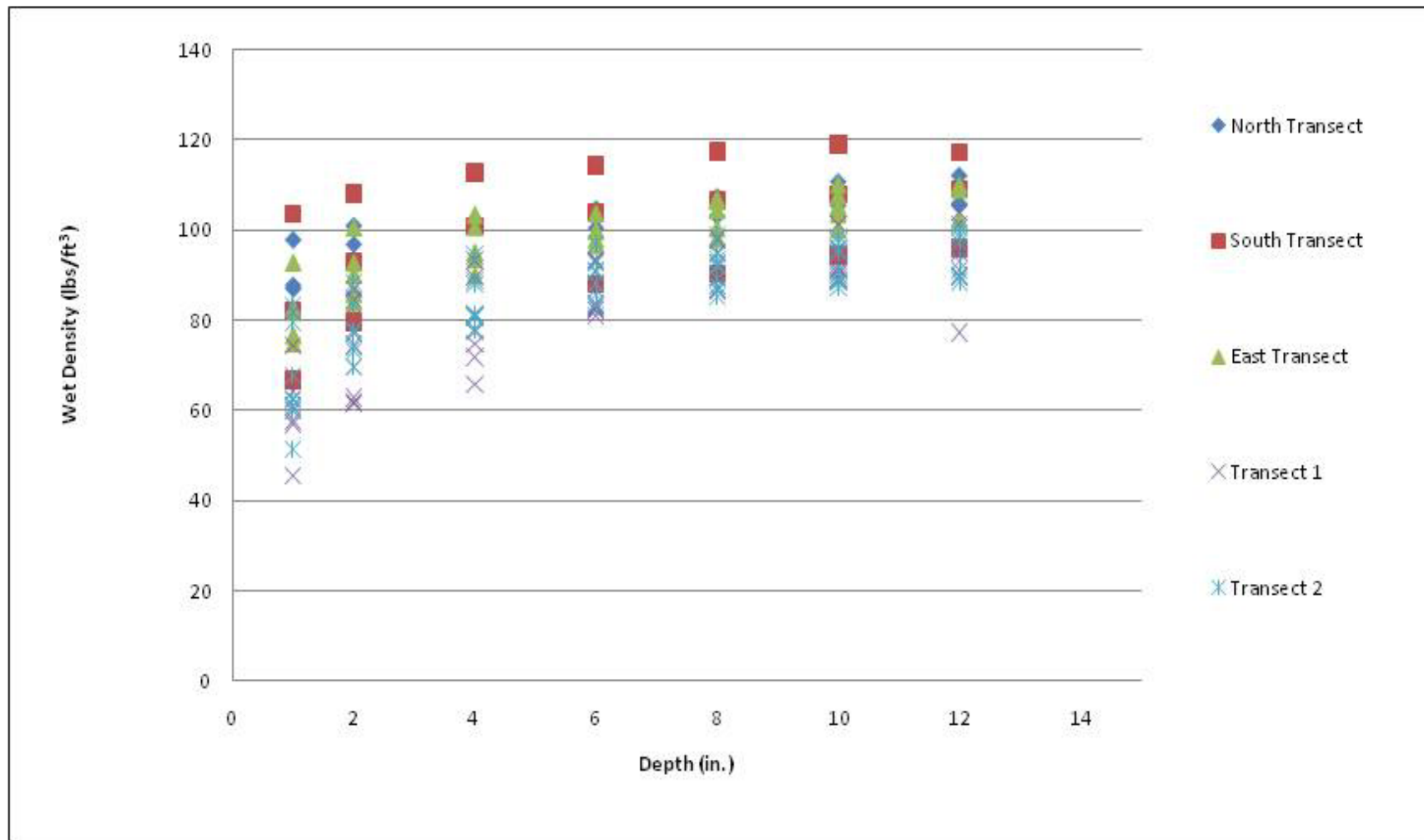


Figure 16b. Wet density ((lb/ft³) from Troxler measurements for Sacramento, CA.

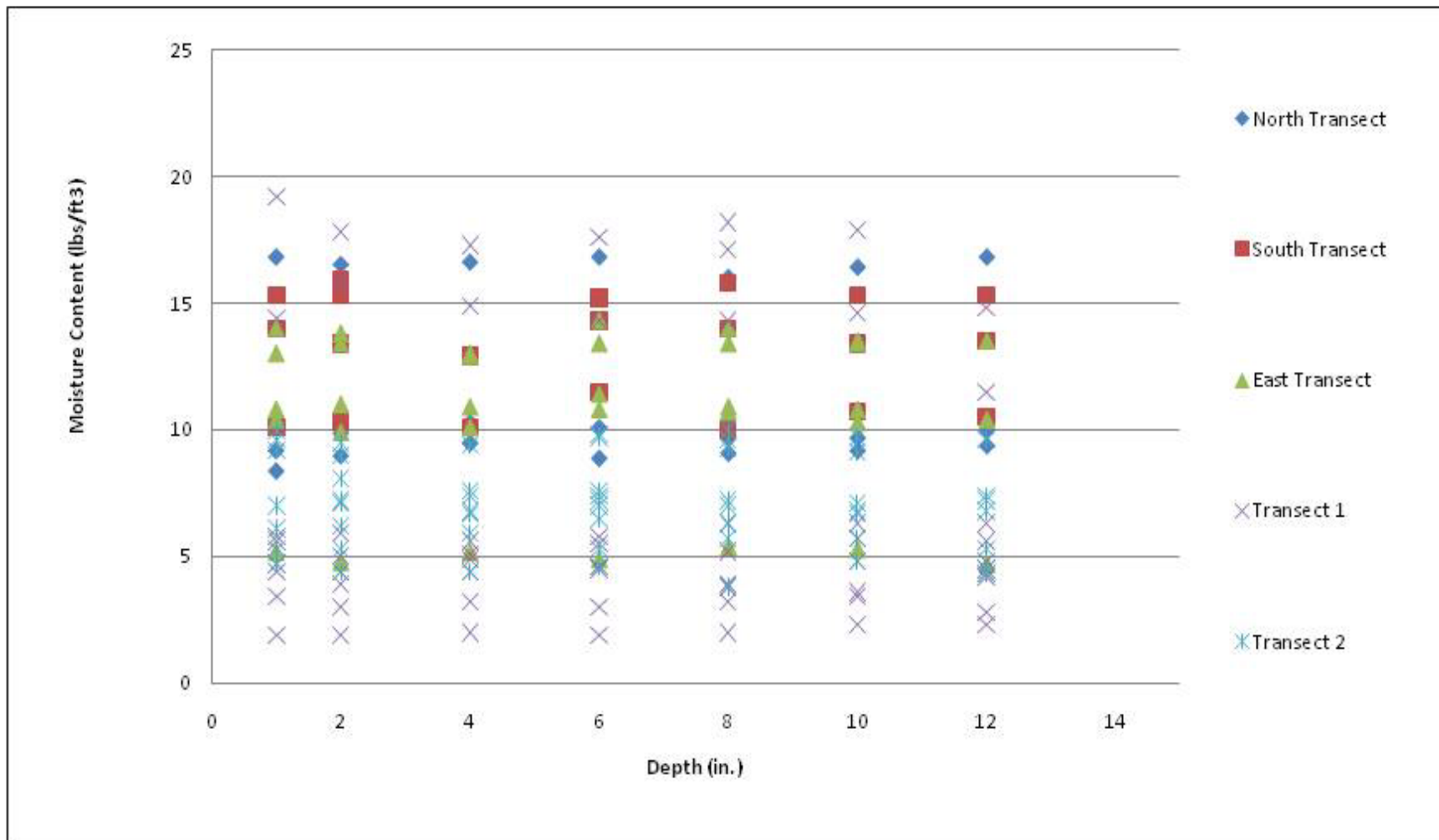


Figure 16c. Moisture content (lb/ft³) from Troxler measurements for Sacramento, CA.

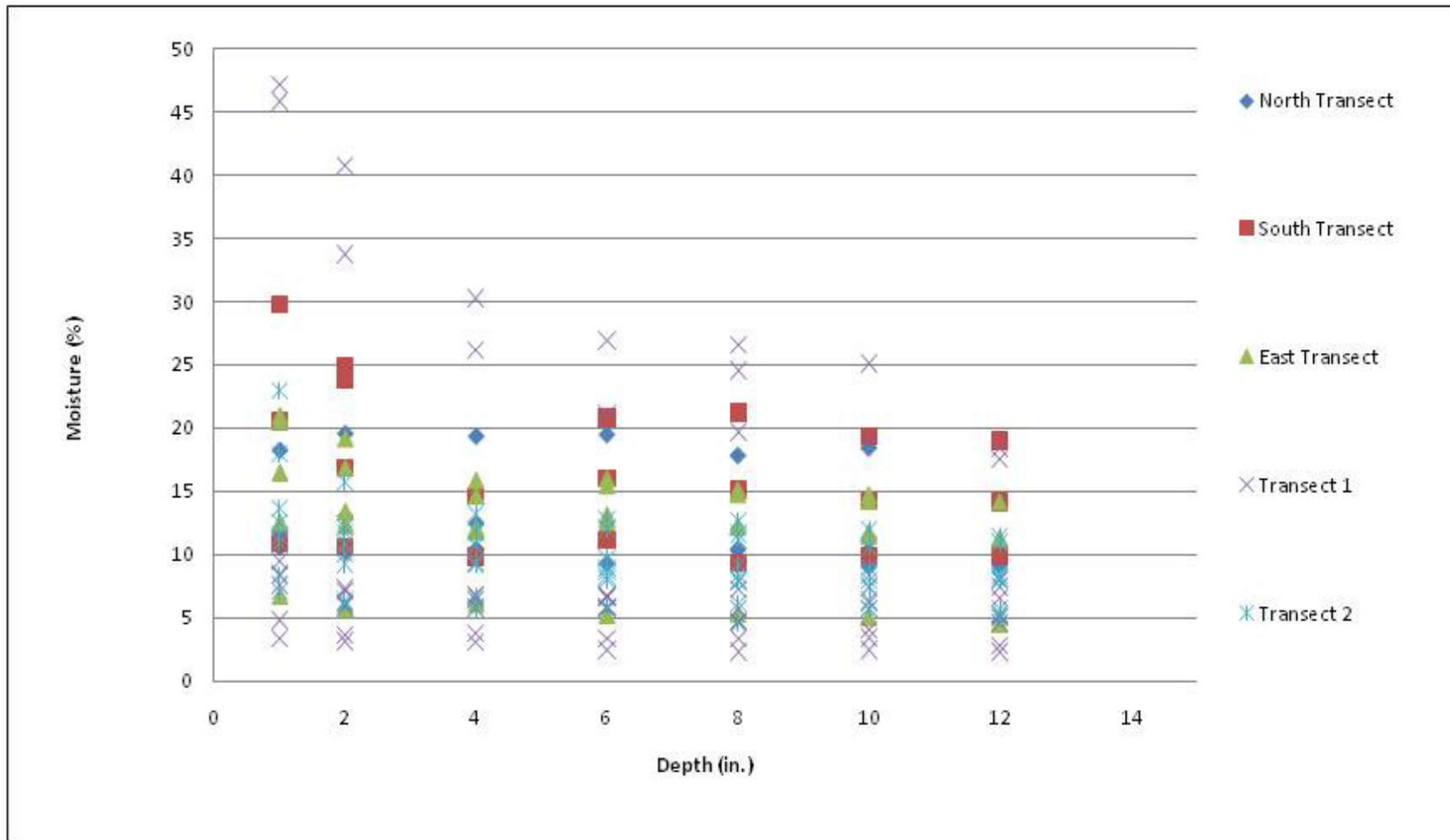


Figure 16d. Moisture (%) from Troxler measurements for Sacramento, CA.

**Table 6. Statistical data for Troxler measurements in Sacramento, CA, north transect:
2-, 4-, 6-, 8-, 10-, and 12-in. depths.**

North Transect Depth (2-4-6 in.)	Dry Density (lb/ft ³)	Wet Density (lb/ft ³)	Moisture Content (lb/ft ³)	Percent Moisture (%)	North Transect Depth (8-10-12 in.)	Dry Density (lb/ft ³)	Wet Density (lb/ft ³)	Moisture Content (lb/ft ³)	Percent Moisture (%)
Max	95.5	104.5	16.8	19.6	Max	102.4	111.9	16.4	18.5
Min	75.7	85.6	8.9	9.4	Min	88.9	103.0	9.1	9.1
Mean	86.5	98.5	12.0	13.9	Mean	95.3	106.5	11.2	11.9
Median	85.9	100.7	10.1	12.5	Median	94.6	105.6	9.7	10.4
Mode	#N/A	#N/A	#N/A	#N/A	Mode	#N/A	#N/A	9.7	#N/A
Standard Deviation	5.6	5.9	3.5	4.3	Standard Deviation	5.0	3.2	3.1	3.9
*#N/A: no central value in data set					*#N/A: no central value in data set				

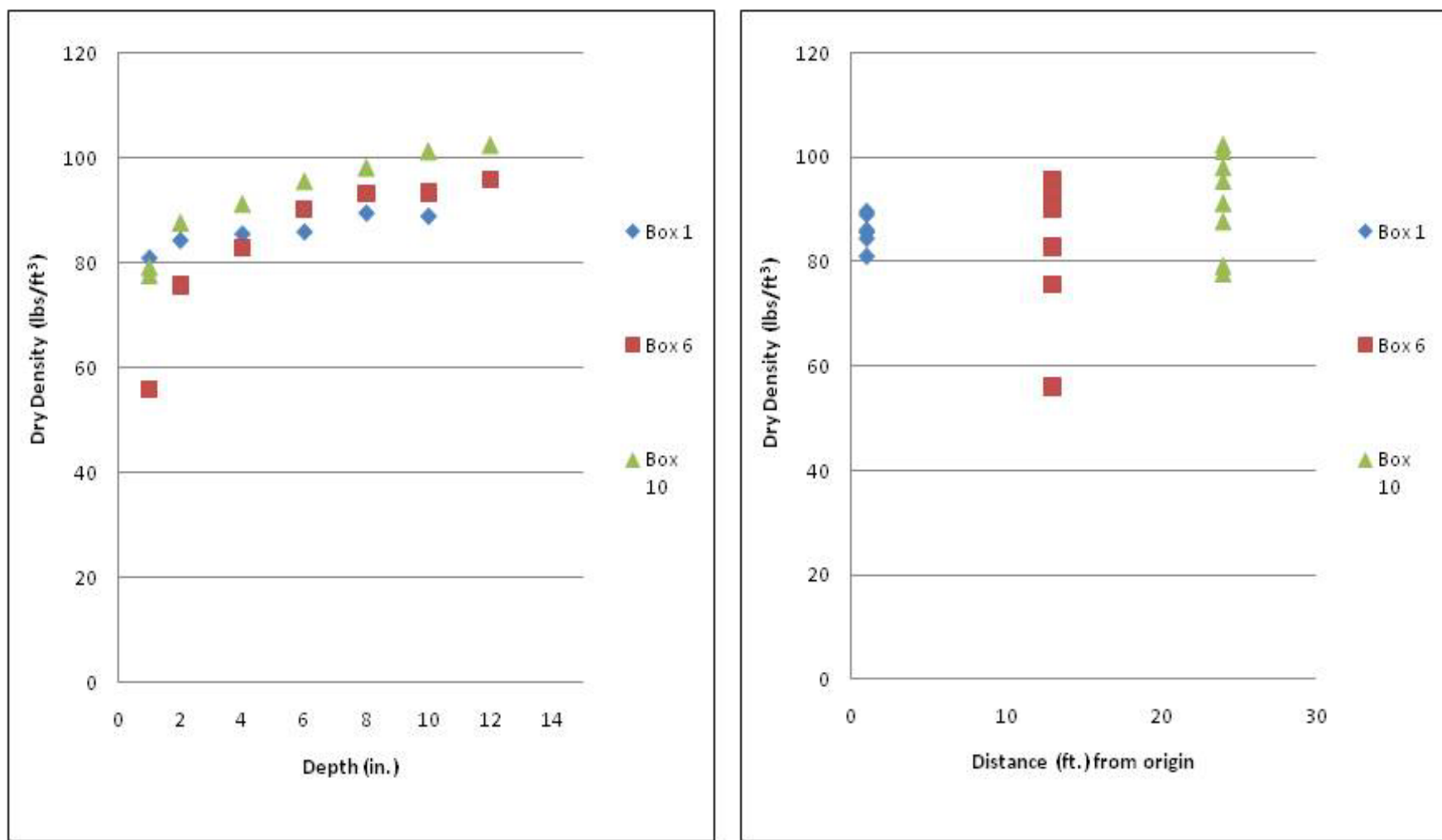


Figure 17a. Dry density (lbs/ft³) verses depth (in.) and distance (ft.) from Troxler measurements for, North Transect,Sacramento, CA.

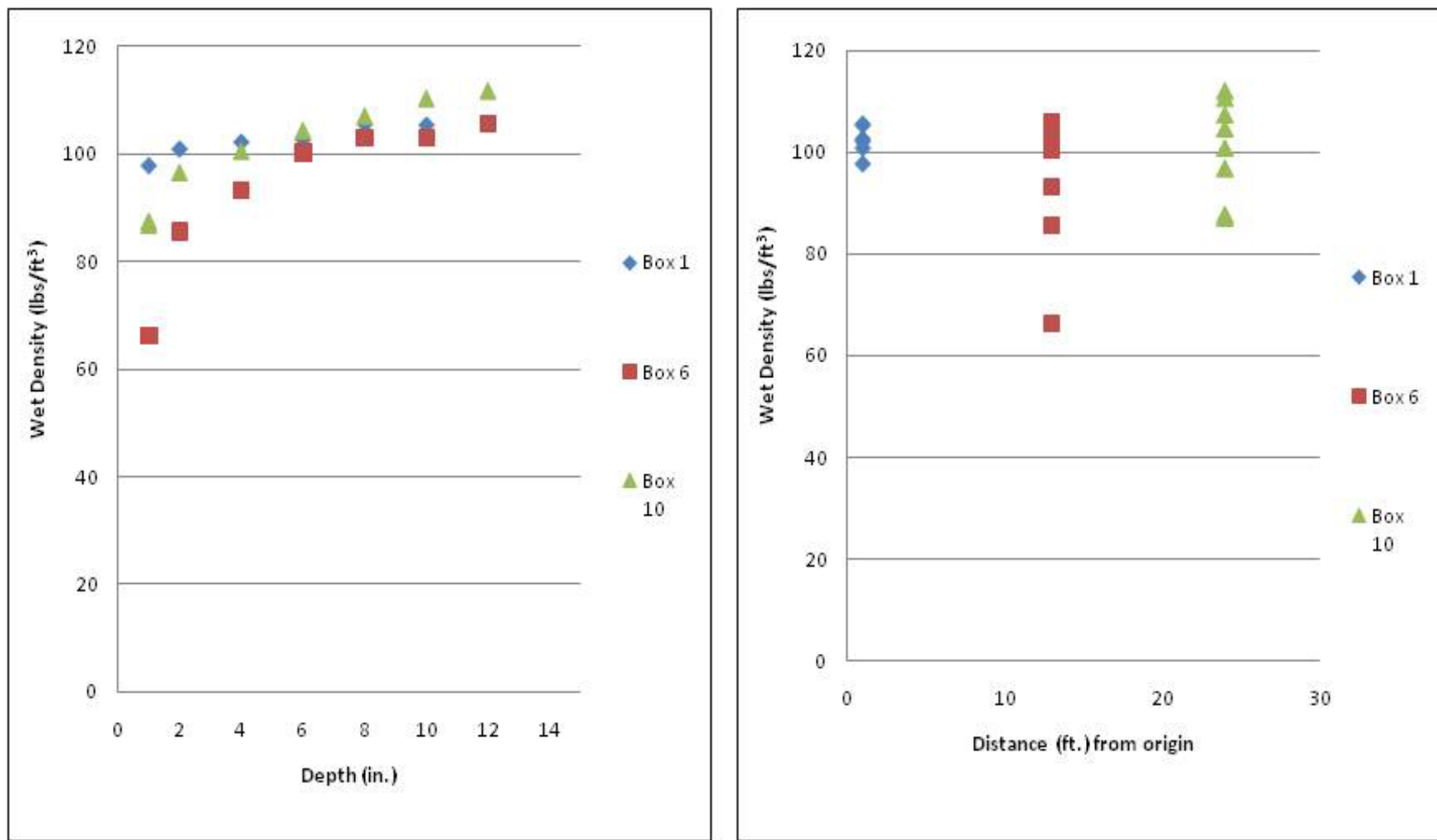


Figure 17b. Wet density (lbs/ft³) verses depth (in.) and distance (ft.) from Troxler measurements for, North Transect,Sacramento, CA.

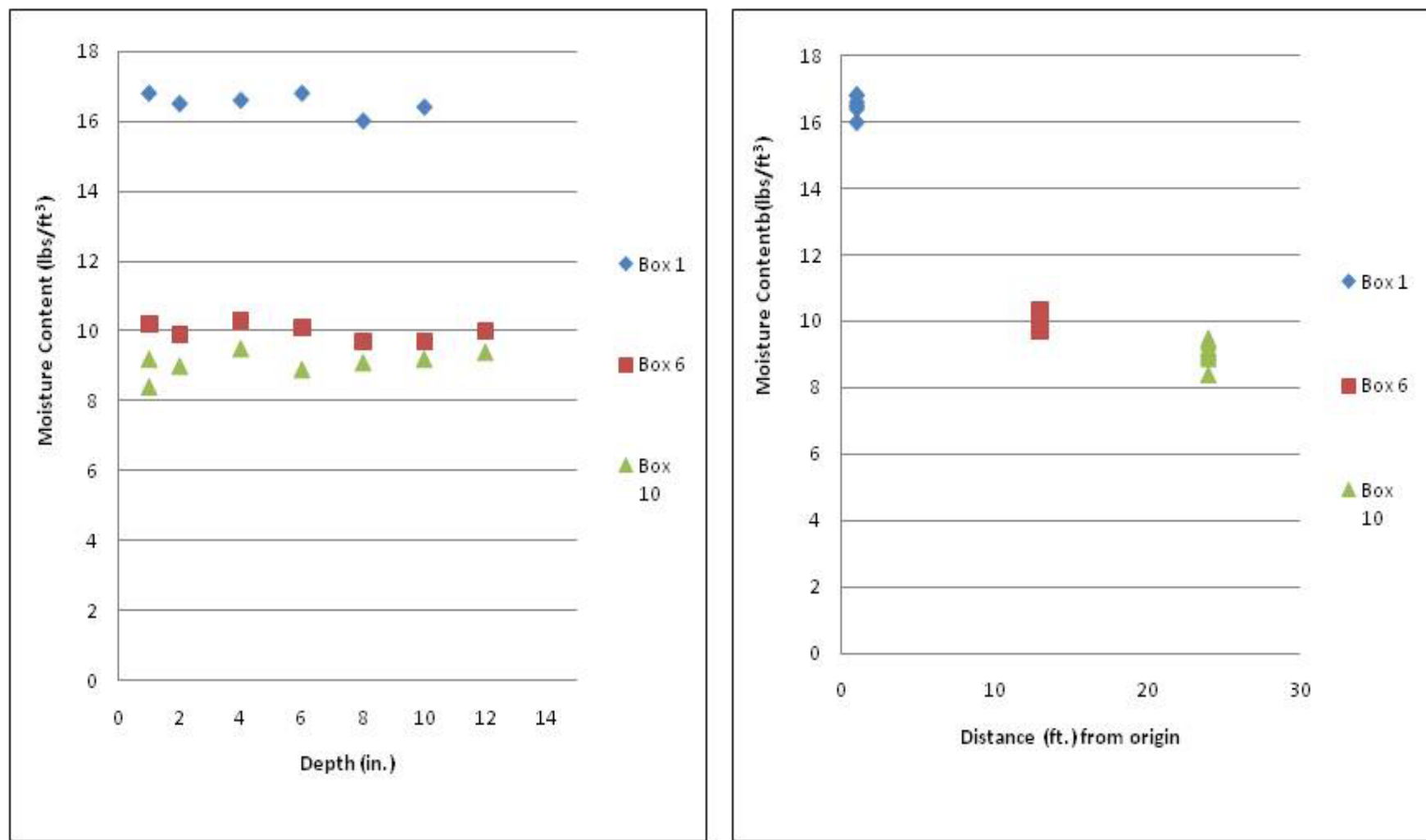


Figure 17c. Moisture content (lbs/ft³) versus depth (in.) and distance (ft.) from Troxler measurements for, North Transect,Sacramento, CA.

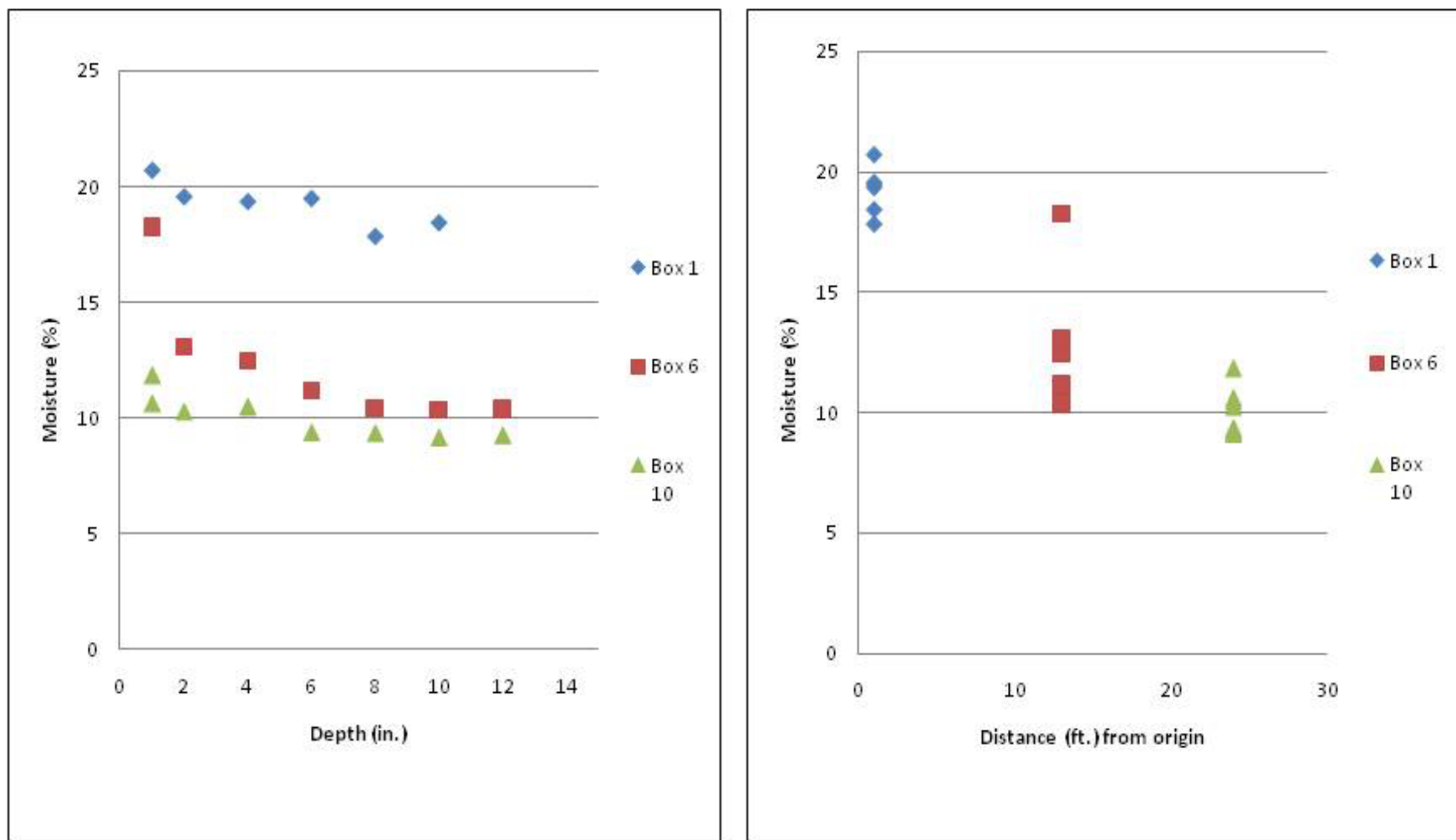


Figure 17d. Moisture (%) verses depth (in.) and distance (ft.) from Troxler measurements for, North Transect, Sacramento, CA.

**Figure 7. Statistical data for Troxler measurements in Sacramento, CA, south transect:
2-, 4-, 6-, 8-, 10-, and 12-in. depths.**

South Transect Depth (2-4-6 in.)	Dry Density (lb/ft ³)	Wet Density (lb/ft ³)	Moisture Content (lb/ft ³)	Percent Moisture (%)	South Transect Depth (8-10-12 in.)	Dry Density (lb/ft ³)	Wet Density (lb/ft ³)	Moisture Content (lb/ft ³)	Percent Moisture (%)
Max	102.7	114.2	15.9	24.8	Max	108.2	118.9	15.8	21.2
Min	64.1	79.5	10.1	9.8	Min	74.4	90.2	10.0	9.3
Mean	84.6	97.7	13.2	16.5	Mean	91.5	105.0	13.5	15.3
Median	87.9	100.7	13.4	16.0	Median	93.5	107.2	13.8	14.7
Mode	#N/A	#N/A	#N/A	#N/A	Mode	#N/A	#N/A	15.3	#N/A
Standard Deviation	15.2	13.3	2.2	5.6	Standard Deviation	12.7	10.6	2.1	4.4
*#N/A: no central value in data set					*#N/A: no central value in data set				

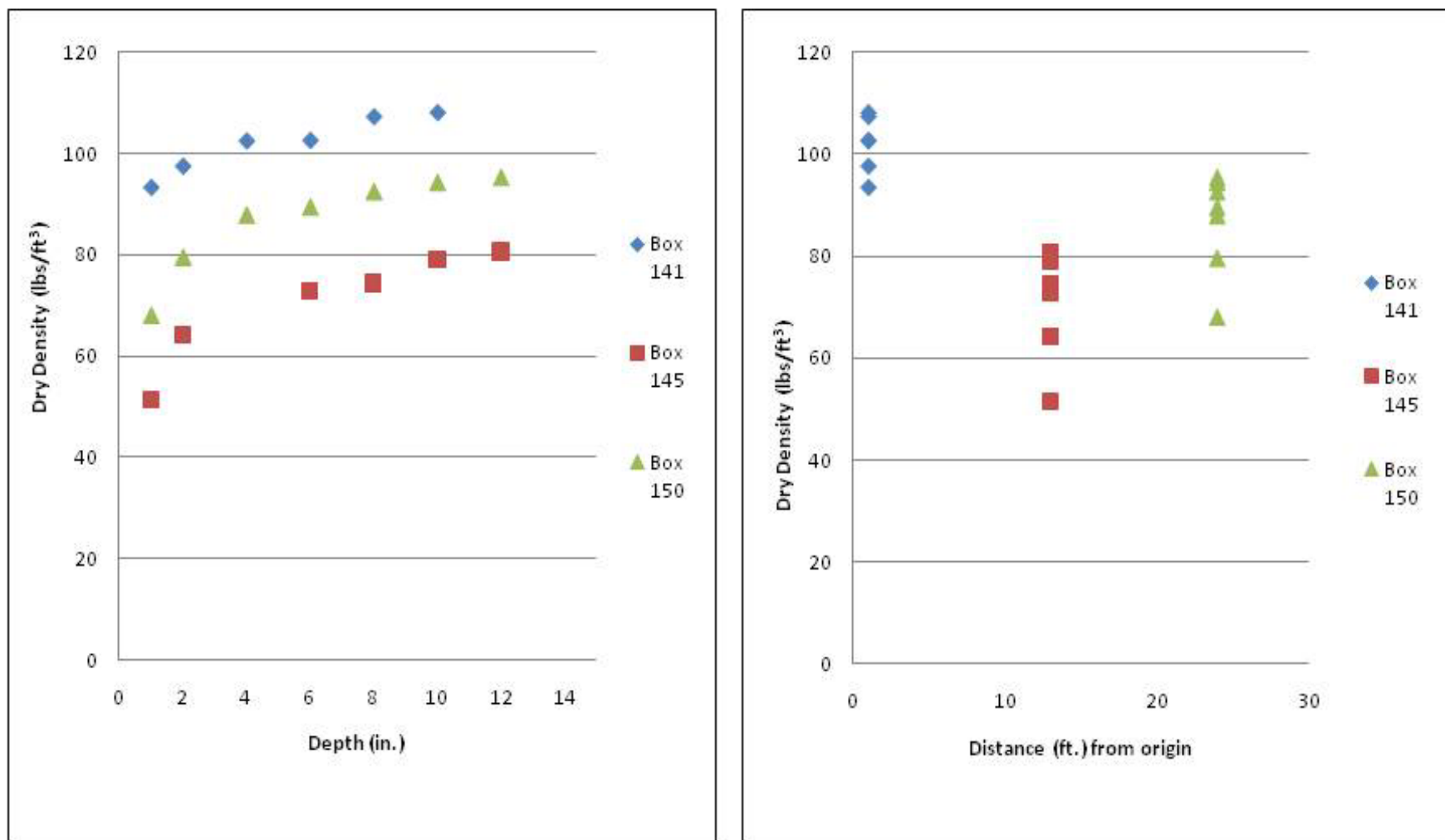


Figure 18a. Dry density (lbs/ft^3) verses depth (in.) and distance (ft.) from Troxler measurements for, South Transect, Sacramento, CA.

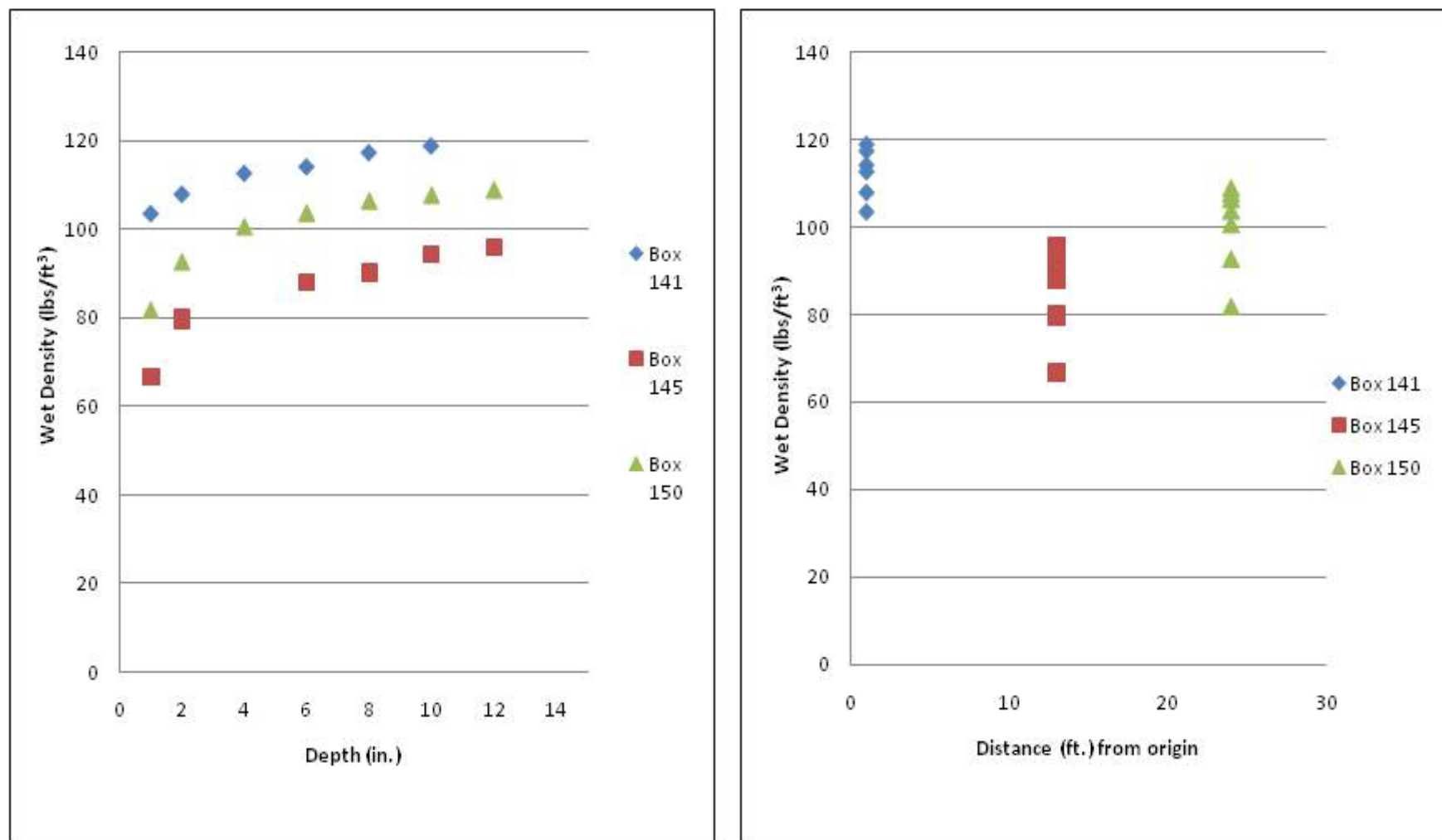


Figure 18b. Wet density (lbs/ft³) versus depth (in.) and distance (ft.) from Troxler measurements for, South Transect, Sacramento, CA.

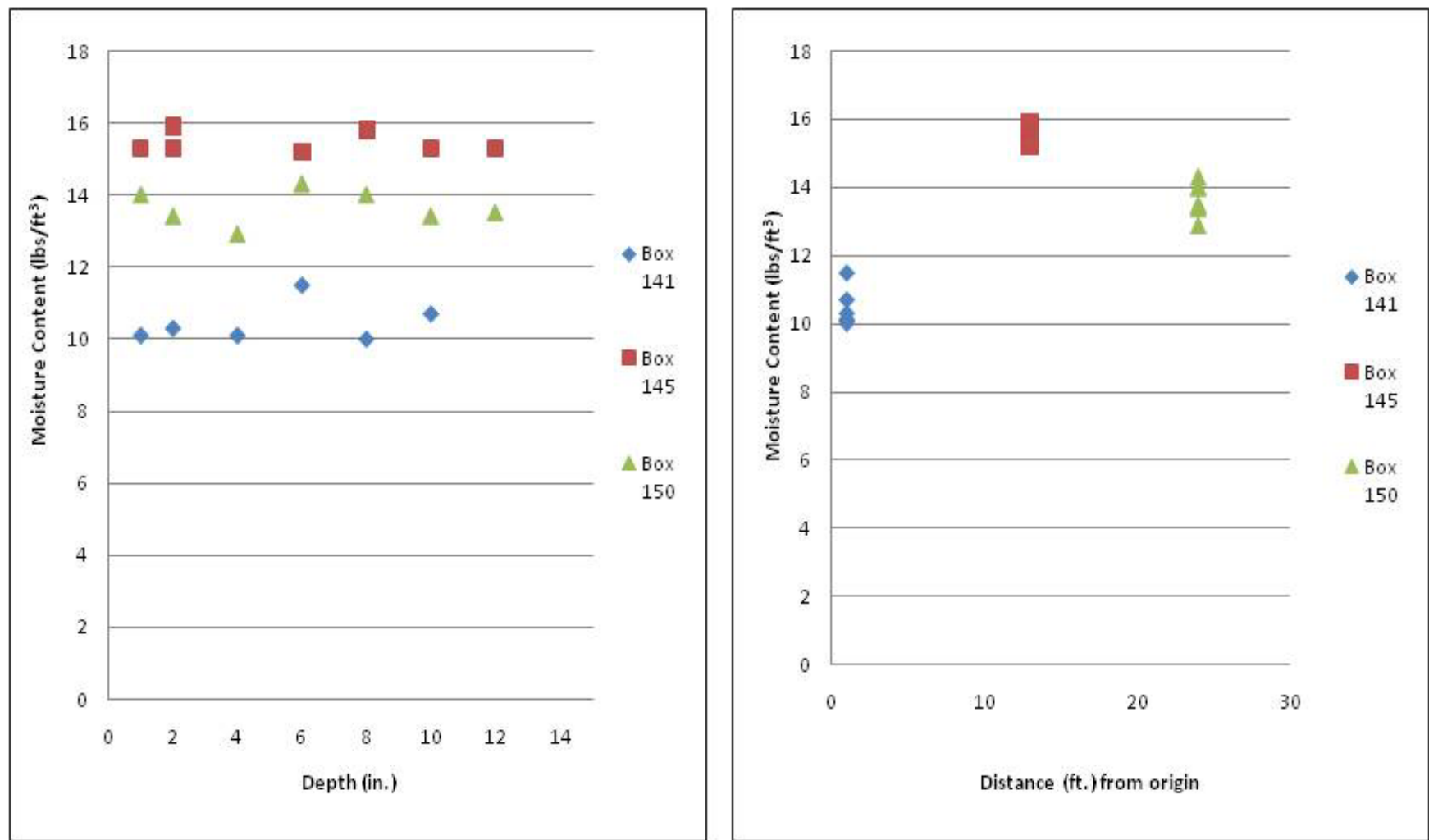


Figure 18c. Moisture content (lbs/ft³) verses depth (in.) and distance (ft.) from Troxler measurements for, South Transect, Sacramento, CA.

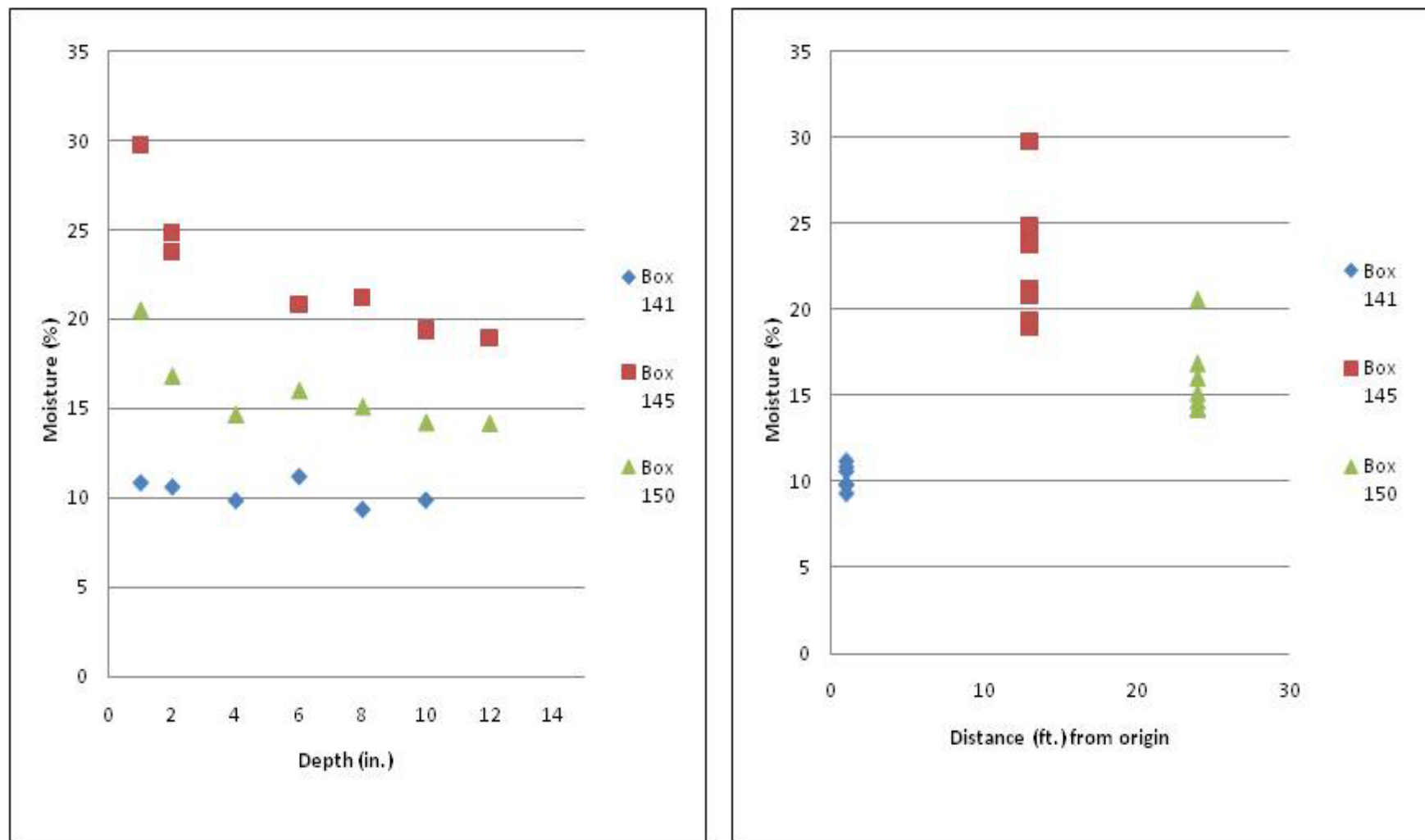


Figure 18d. Moisture (%) verses depth (in.) and distance (ft.) from Troxler measurements for, South Transect, Sacramento, CA.

**Table 8. Statistical data for Troxler measurements in Sacramento, CA, east transect:
2-, 4-, 6-, 8-, 10-, and 12-in. depths.**

East Transect Depth (2-4-6 in.)	Dry Density (lb/ft ³)	Wet Density (lb/ft ³)	Moisture Content (lb/ft ³)	Percent Moisture (%)	East Transect Depth (8-10-12 in.)	Dry Density (lb/ft ³)	Wet Density (lb/ft ³)	Moisture Content (lb/ft ³)	Percent Moisture (%)
Max	95.0	103.8	14.3	19.2	Max	105.3	110.2	14.0	15.1
Min	72.1	84.0	4.8	5.2	Min	87.4	98.1	4.7	4.5
Mean	85.0	95.6	10.7	12.7	Mean	94.4	104.7	10.2	11.0
Median	86.0	96.7	11.0	13.1	Median	92.3	104.9	10.8	12.0
Mode	86.6	99.9	13.4	#N/A	Mode	#N/A	#N/A	13.4	#N/A
Standard Deviation	6.2	6.1	3.2	4.2	Standard Deviation	6.1	3.9	3.4	3.9
*#N/A: no central value in data set					*#N/A: no central value in data set				

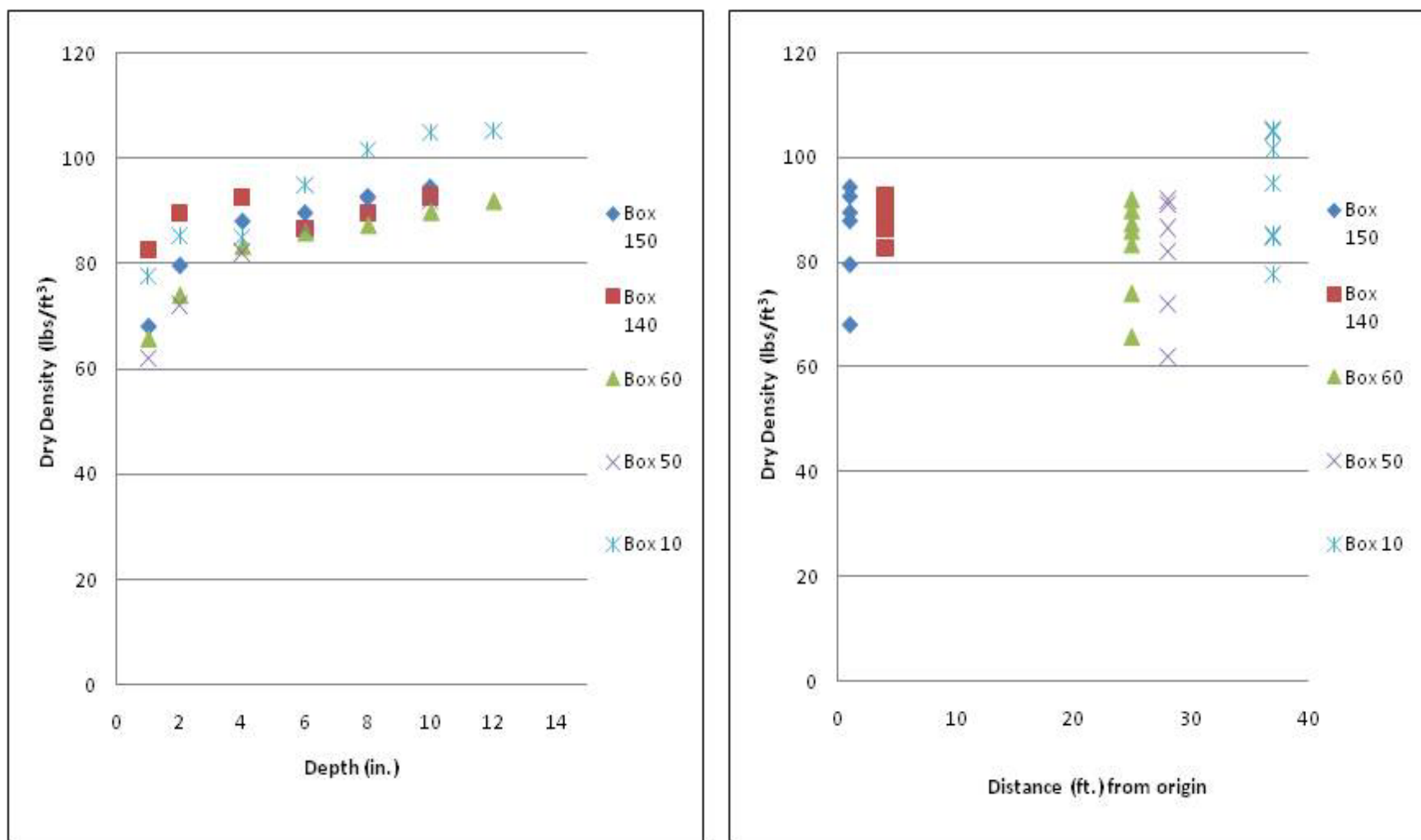


Figure 19a. Dry density (lbs/ft^3) versus depth (in.) and distance (ft.) from Troxler measurements for, East Transect, Sacramento, CA.

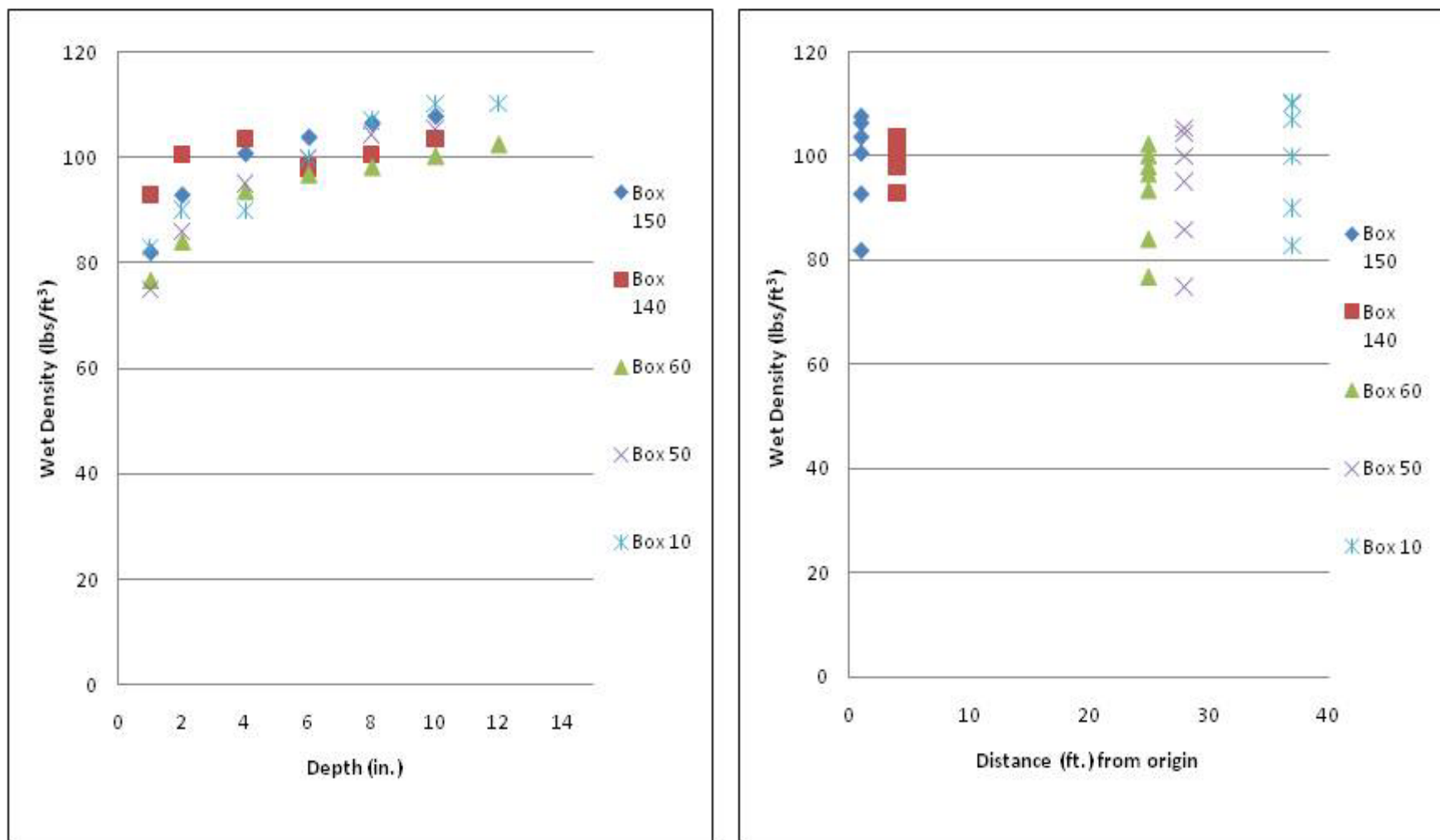


Figure 19b. Wet density (lbs/ft^3) versus depth (in.) and distance (ft.) from Troxler measurements for, East Transect, Sacramento, CA.

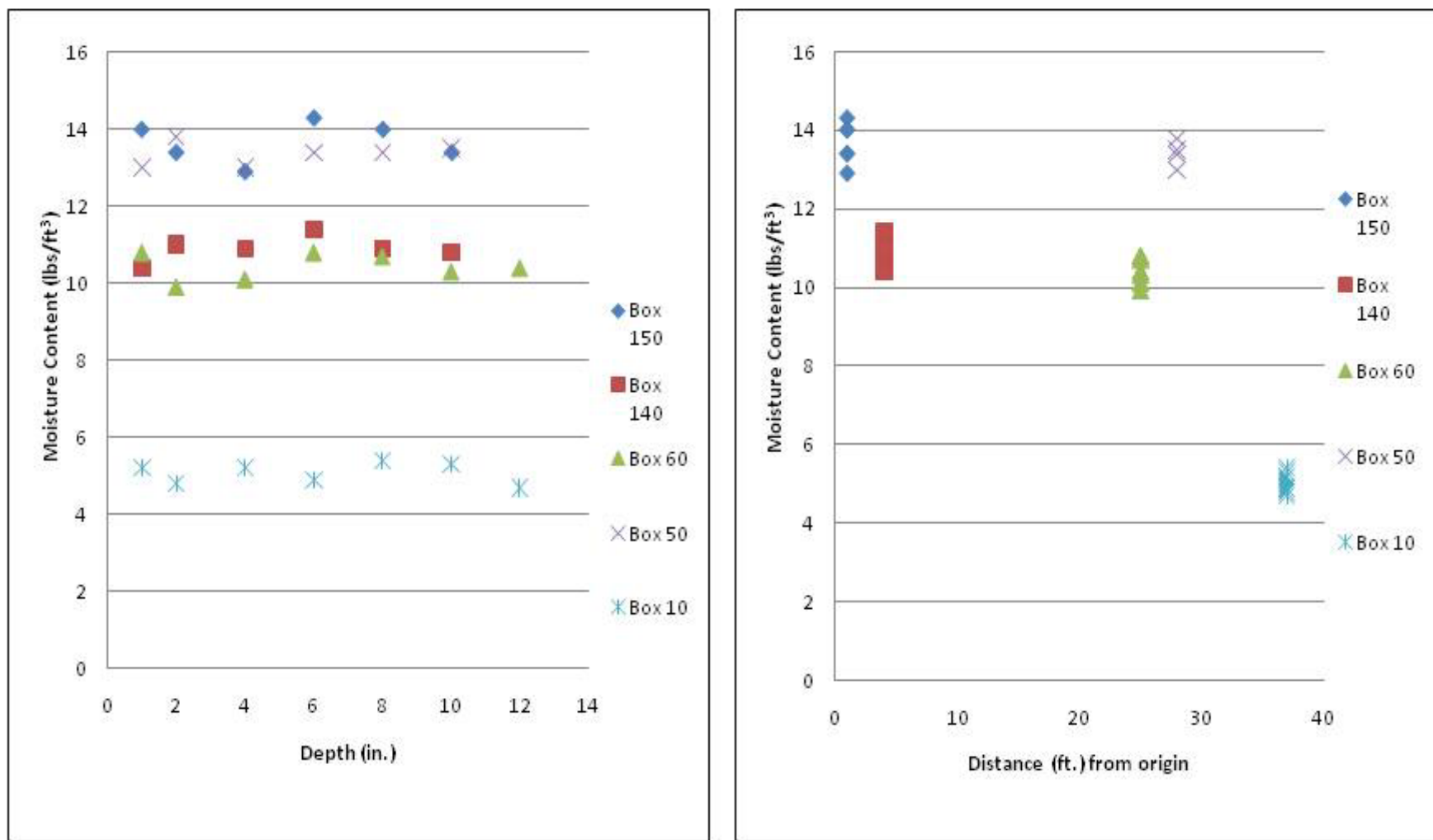


Figure 19c. Moisture content (lbs/ft³) verses depth (in.) and distance (ft.) from Troxler measurements for, East Transect, Sacramento, CA.

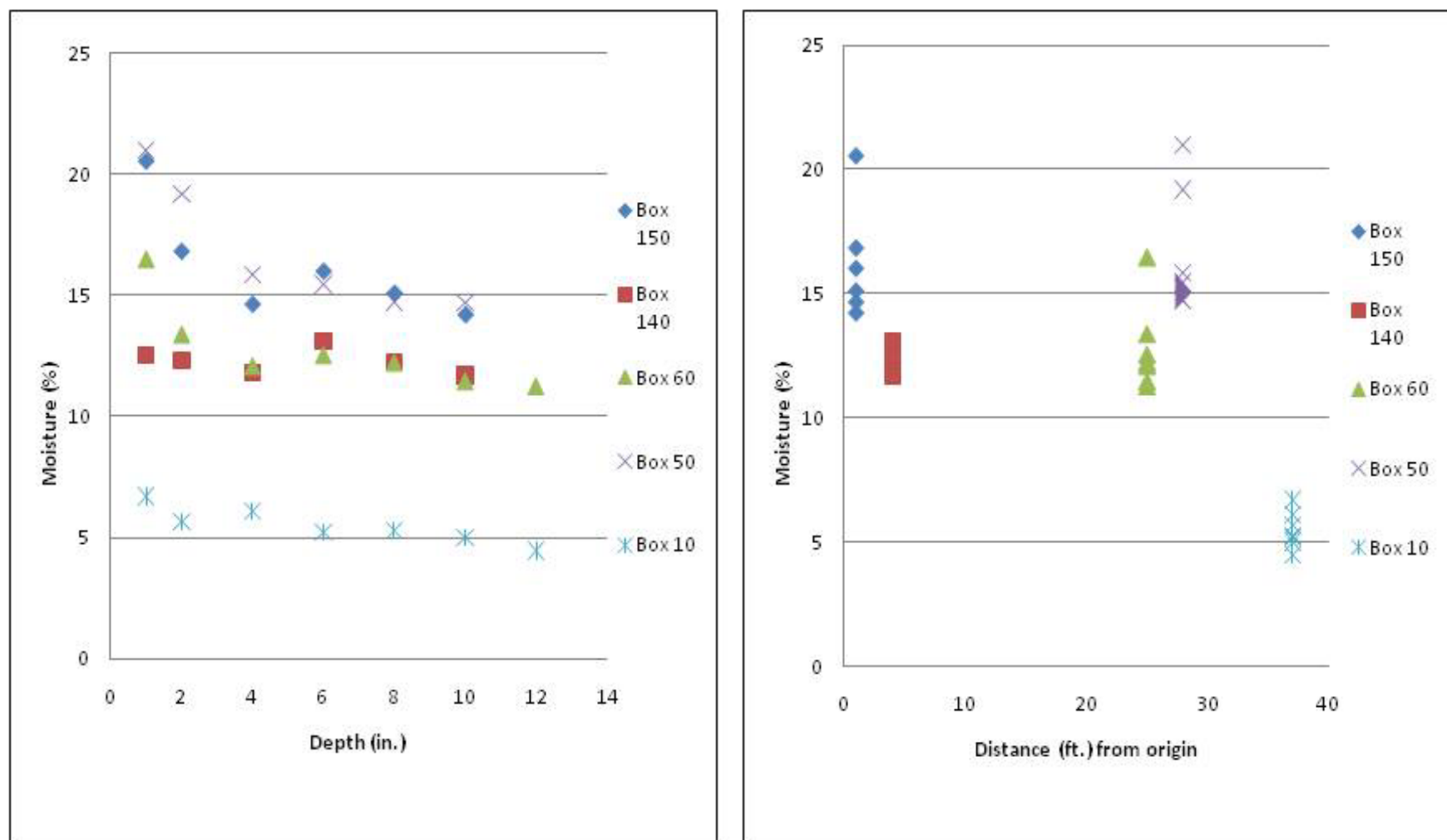


Figure 19d. Moisture (%) verses depth (in.) and distance (ft.) from Troxler measurements for, East Transect, Sacramento, CA.

**Table 9. Statistical data for Troxler measurements in Sacramento, CA, transect 1:
2-, 4-, 6-, 8-, 10-, and 12-in. depths.**

Transect 1 Depth (2-4-6 in.)	Dry Density (lb/ft ³)	Wet Density (lb/ft ³)	Moisture Content (lb/ft ³)	Percent Moisture (%)	Transect 1 Depth (8-10-12 in.)	Dry Density (lb/ft ³)	Wet Density (lb/ft ³)	Moisture Content (lb/ft ³)	Percent Moisture (%)
Max	89.9	93.5	17.8	40.8	Max	101.1	103.9	18.2	26.6
Min	43.6	61.5	1.9	2.5	Min	65.7	77.2	2.0	2.3
Mean	71.9	79.1	7.2	11.5	Mean	84.8	92.1	7.3	9.3
Median	74.2	81.1	5.0	6.5	Median	85.4	91.2	5.0	5.7
Mode	#N/A	#N/A	4.4	6.8	Mode	89.8	91.2	6.3	#N/A
Standard Deviation	12.6	9.7	5.5	11.4	Standard Deviation	9.5	5.7	5.3	7.9
*#N/A: no central value in data set					*#N/A: no central value in data set				

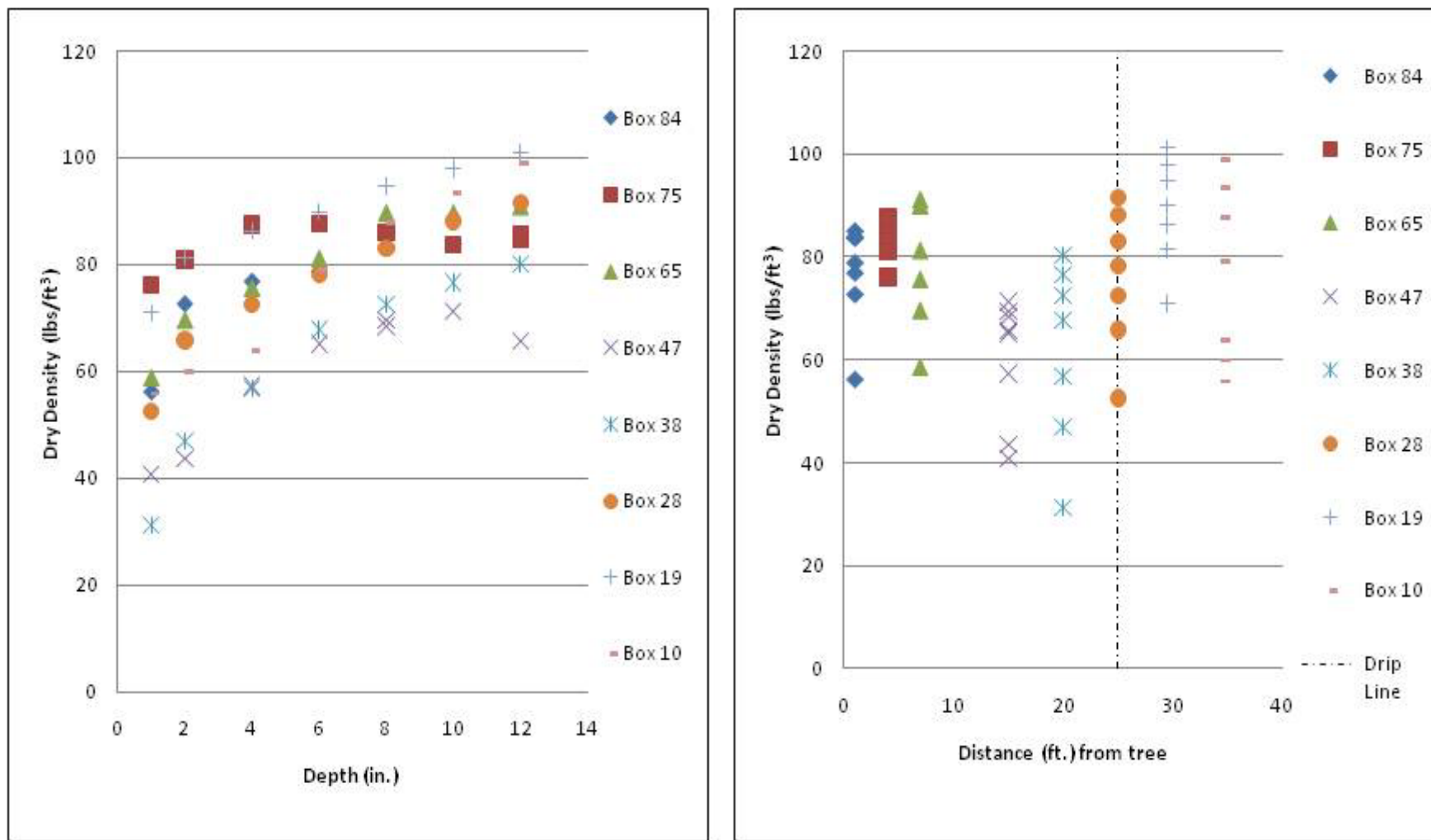


Figure 20a. Dry density (lbs/ft³) versus depth (in.) and distance (ft.) from Troxler measurements for Transect 1, Sacramento, CA.

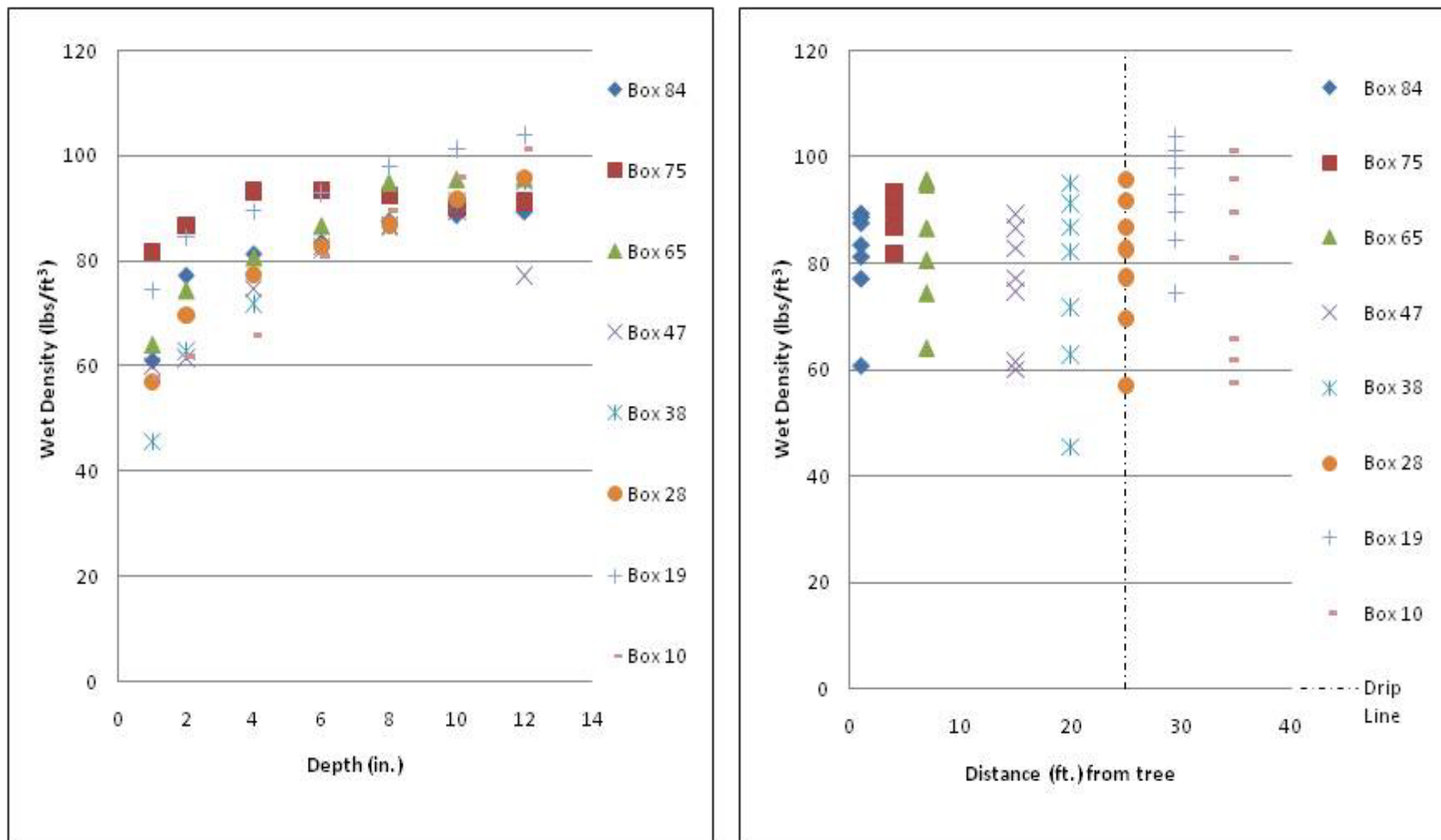


Figure 20b. Wet density (lbs/ft^3) versus depth (in.) and distance (ft.) from Troxler measurements for, Transect 1, Sacramento, CA.

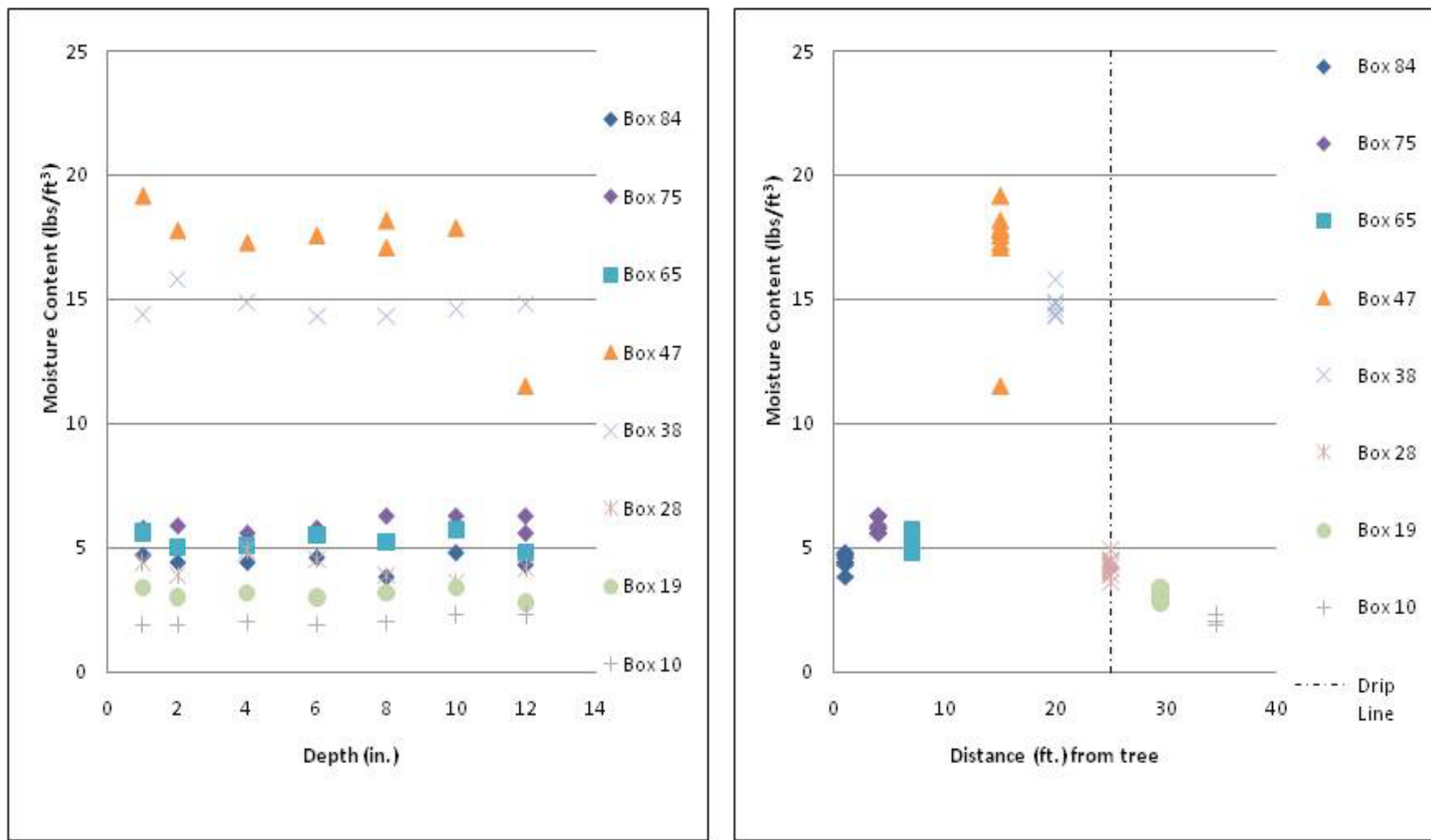


Figure 20c. Moisture content (lbs/ft³) versus depth (in.) and distance (ft.) from Troxler measurements for, Transect 1, Sacramento, CA.

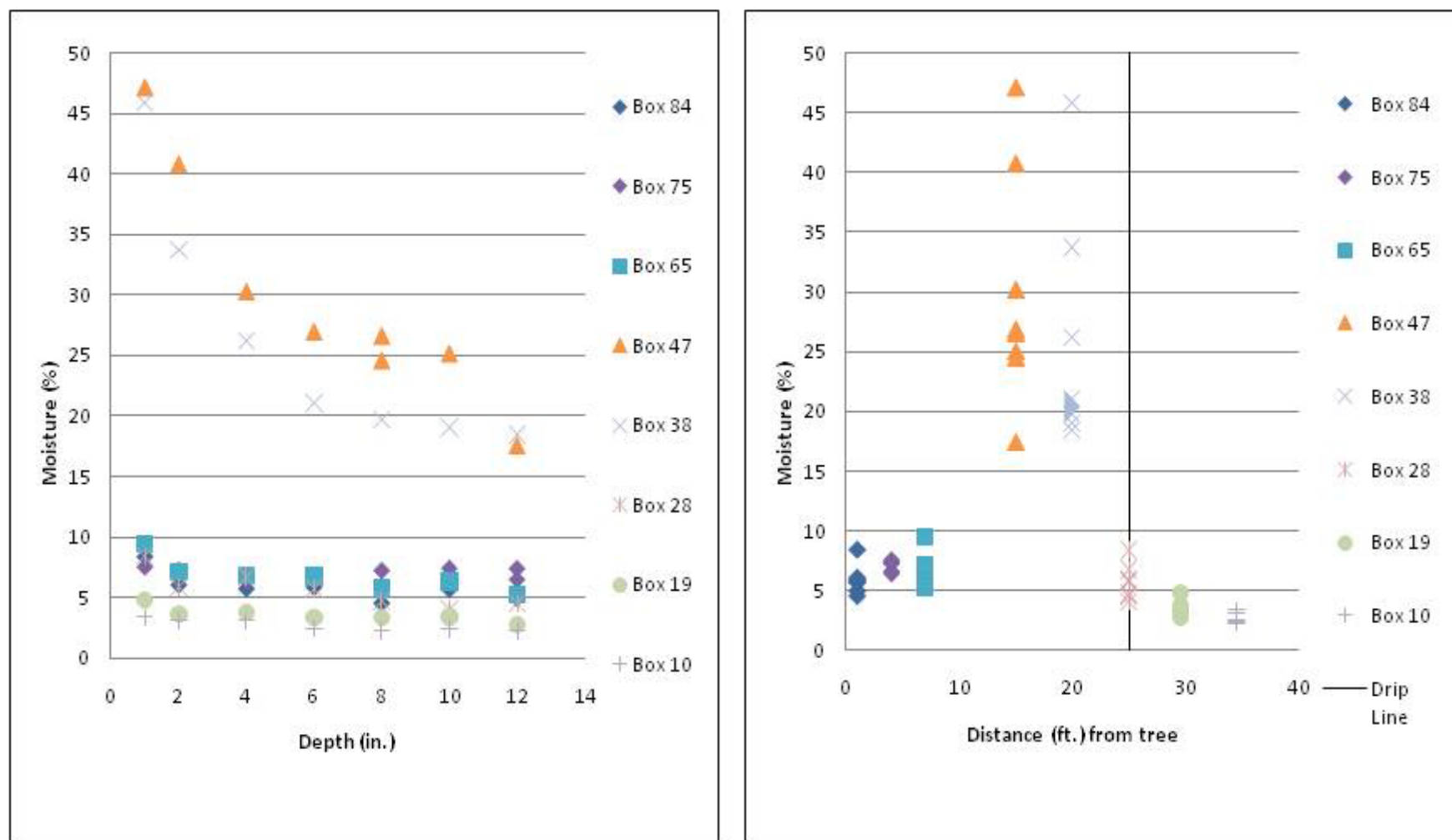


Figure 20d. Moisture (%) versus depth (in.) and distance (ft.) from Troxler measurements for, Transect 1, Sacramento, CA.

**Table 10. Statistical data for Troxler measurements in Sacramento, CA, transect 2:
2-, 4-, 6-, 8-, 10-, and 12-in. depths.**

Transect 2 Depth (2-4-6 in.)	Dry Density (lb/ft ³)	Wet Density (lb/ft ³)	Moisture Content (lb/ft ³)	Percent Moisture (%)	Transect 2: Depth (8-10-12 in.)	Dry Density (lb/ft ³)	Wet Density (lb/ft ³)	Moisture Content (lb/ft ³)	Percent Moisture (%)
Max	91.7	97.0	9.8	15.8	Max	93.9	100.3	10.0	12.7
Min	60.1	69.6	4.4	5.8	Min	79.0	86.9	3.8	4.6
Mean	77.2	84.3	7.2	9.5	Mean	86.3	93.5	7.2	8.4
Median	77.9	84.5	7.2	9.2	Median	85.5	93.3	7.1	8.0
Mode	#N/A	77.7	4.4	#N/A	Mode	#N/A	97.3	9.6	#N/A
Standard Deviation	7.6	7.3	1.8	2.8	Standard Deviation	4.6	4.3	1.9	2.4
*#N/A: no central value in data set					*#N/A: no central value in data set				

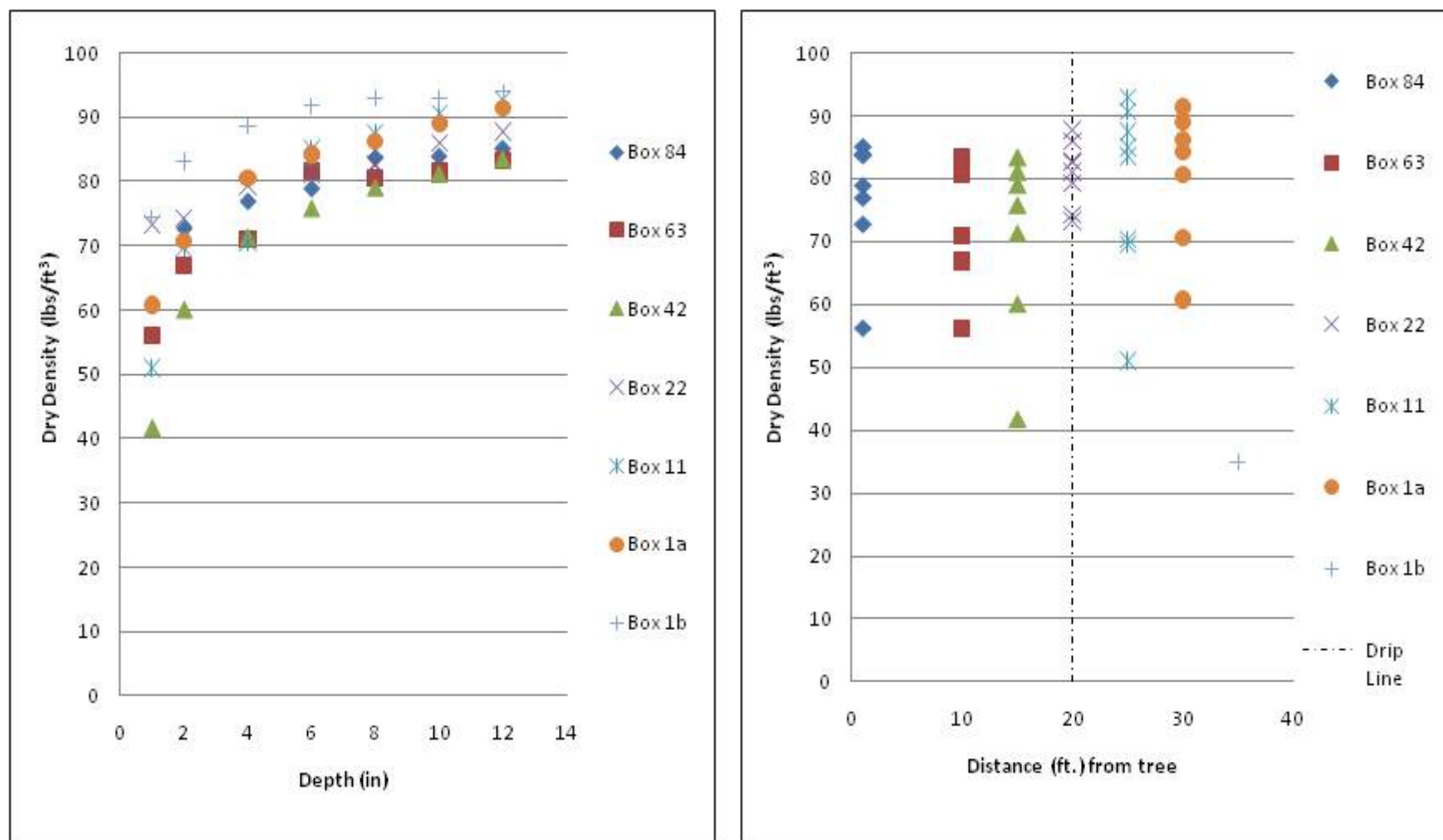


Figure 21a. Dry density (lbs/ft^3) versus depth (in.) and distance (ft.) from Troxler measurements for, Transect 2, Sacramento, CA.

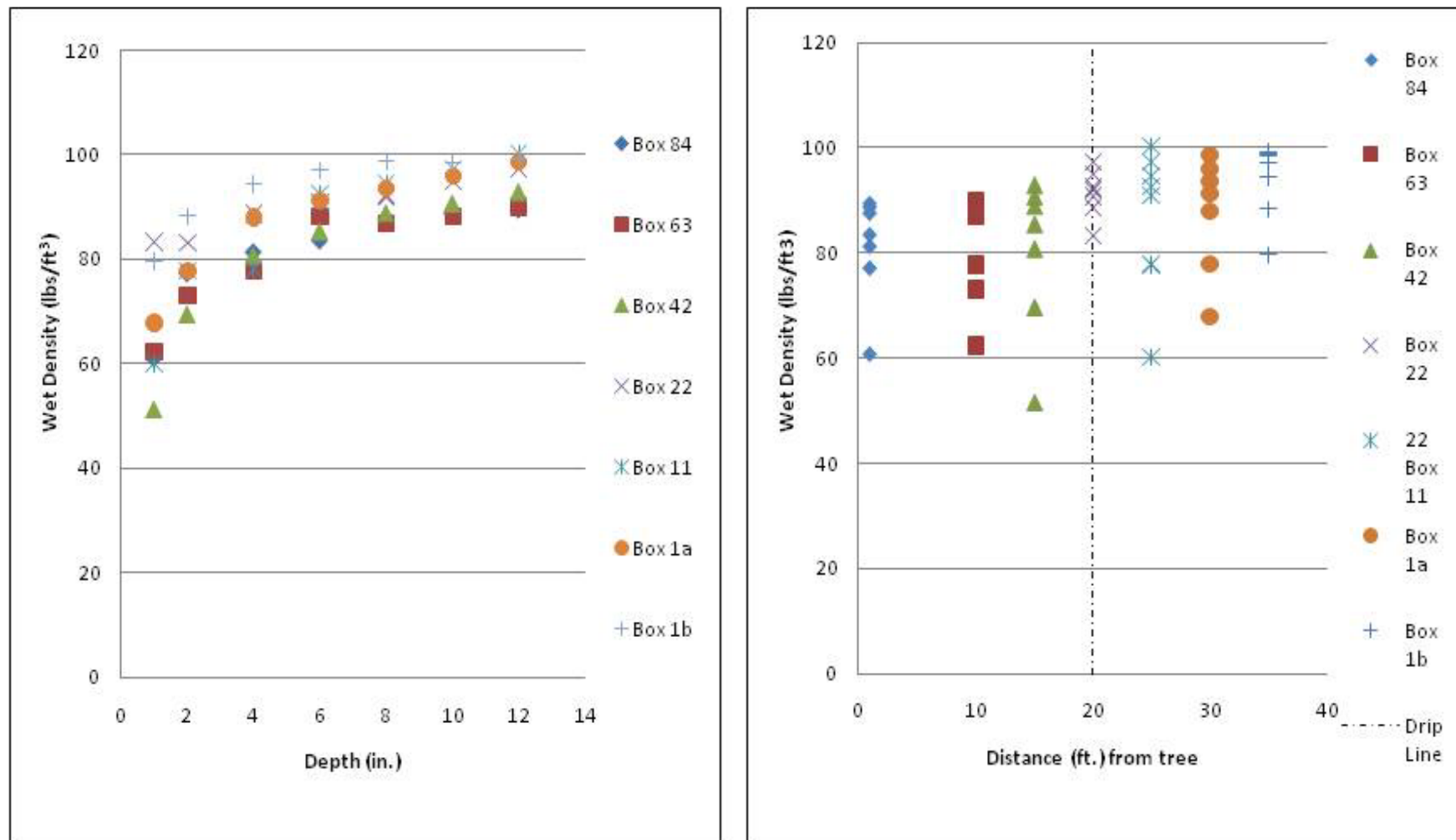


Figure 21b. Wet density (lbs/ft³) verses depth (in.) and distance (ft.) from Troxler measurements for, Transect 2, Sacramento, CA.

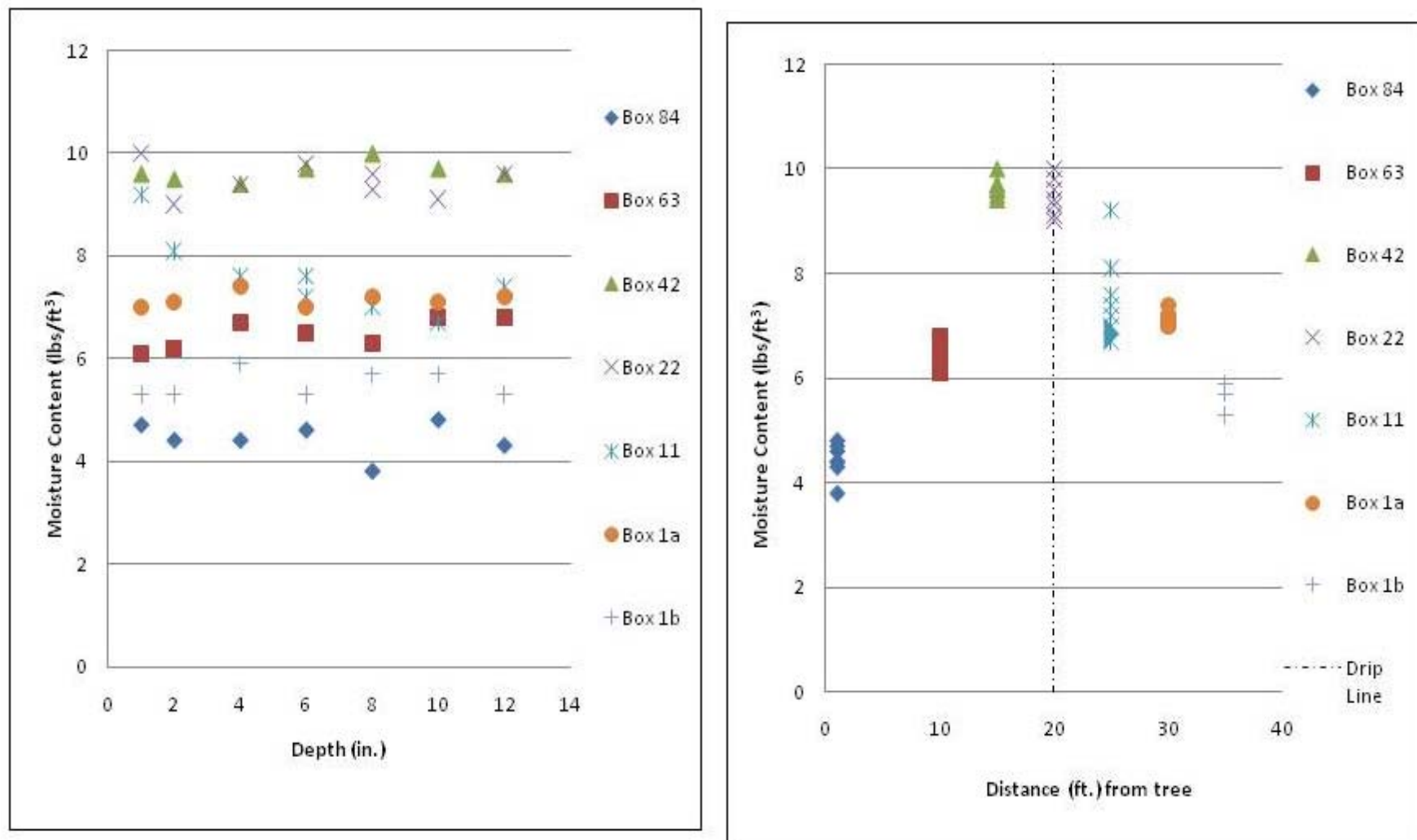


Figure 21c. Moisture content (lbs/ft³) verses depth (in.) and distance (ft.) from Troxler measurements for, Transect 2, Sacramento, CA.

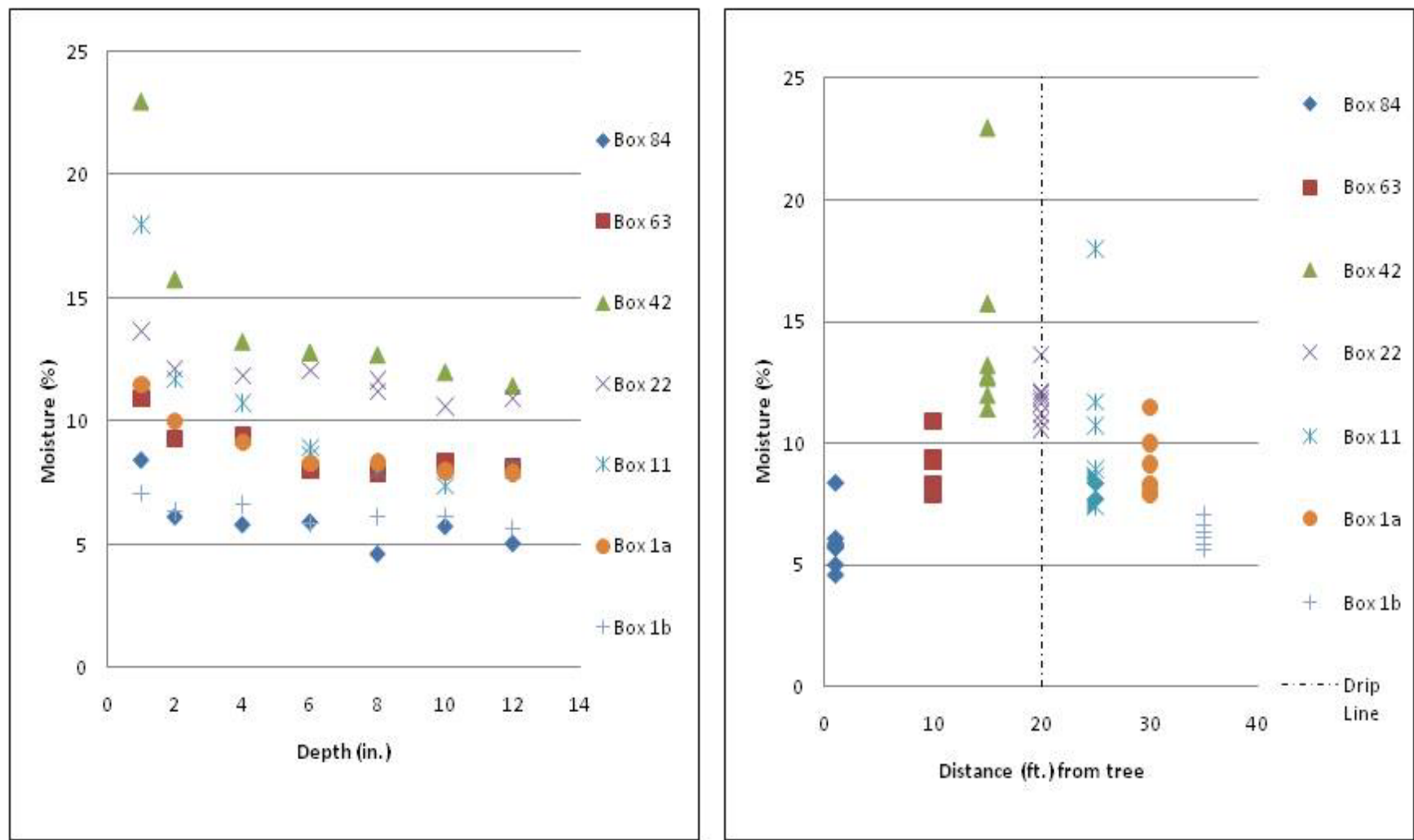


Figure 21d. Moisture (%) verses depth (in.) and distance (ft.) from Troxler measurements for, Transect 2, Sacramento, CA.

Burlington, WA

Introduction

The third study site is located in Burlington, WA, along the west (right) bank of the Skagit River (Figures 22 and 23). This levee is under the jurisdiction of Skagit County Dike District 12. This site was the focus of various geophysical and root pullout studies examining cedar, cottonwood, alder, and maple trees for the ERDC study. The levee system protecting Burlington was designed for a 100-year flood event. The present-day floodplain in the study area has been greatly reduced in extent since settlement and the construction of man-made levees to prevent annual flooding into populated areas. In addition, riverbanks have been hardened with stone or riprap to prevent uncontrolled migration of the Skagit River. Portions of the city of Burlington are located upon the former floodplain and are now protected by the present-day levee system (Figures 22 and 23).

Previous studies

In 2008, the city of Burlington and Dike District 12 commissioned a geotechnical study by Golder Associates (2009) of Redmond, WA, to evaluate the existing levees and to recommend improvements to the levees and construction of new levees as part of the FEMA certification process. This comprehensive study is the primary source of geotechnical data for the Burlington area and the levees studied by the ERDC team. The Golder Associates study compiled previous studies of the levee system by USACE (1979) and provided boring data and information about the geology, soils, stratigraphy, and laboratory engineering properties that are further described here to characterize the Burlington levee reach. The report by Golder Associates, which Dike District 12 provided to the ERDC study team, greatly contributed toward the model development and allowed multiple levee profiles to be examined.

Geological setting

The study area shown in Figures 22 and 23 is situated in the broad, alluvial valley of the Skagit River. The Skagit Valley was carved by the many different glaciers that covered this region during the Pleistocene and the river systems that drained from these glaciers, carrying meltwater and eroded sediments off these glaciers. This created a landscape of elongated north-south orientated uplands and intervening valleys (Golder Associates 2009). Eustatic sea level rise and fall in response to Pleistocene glacial

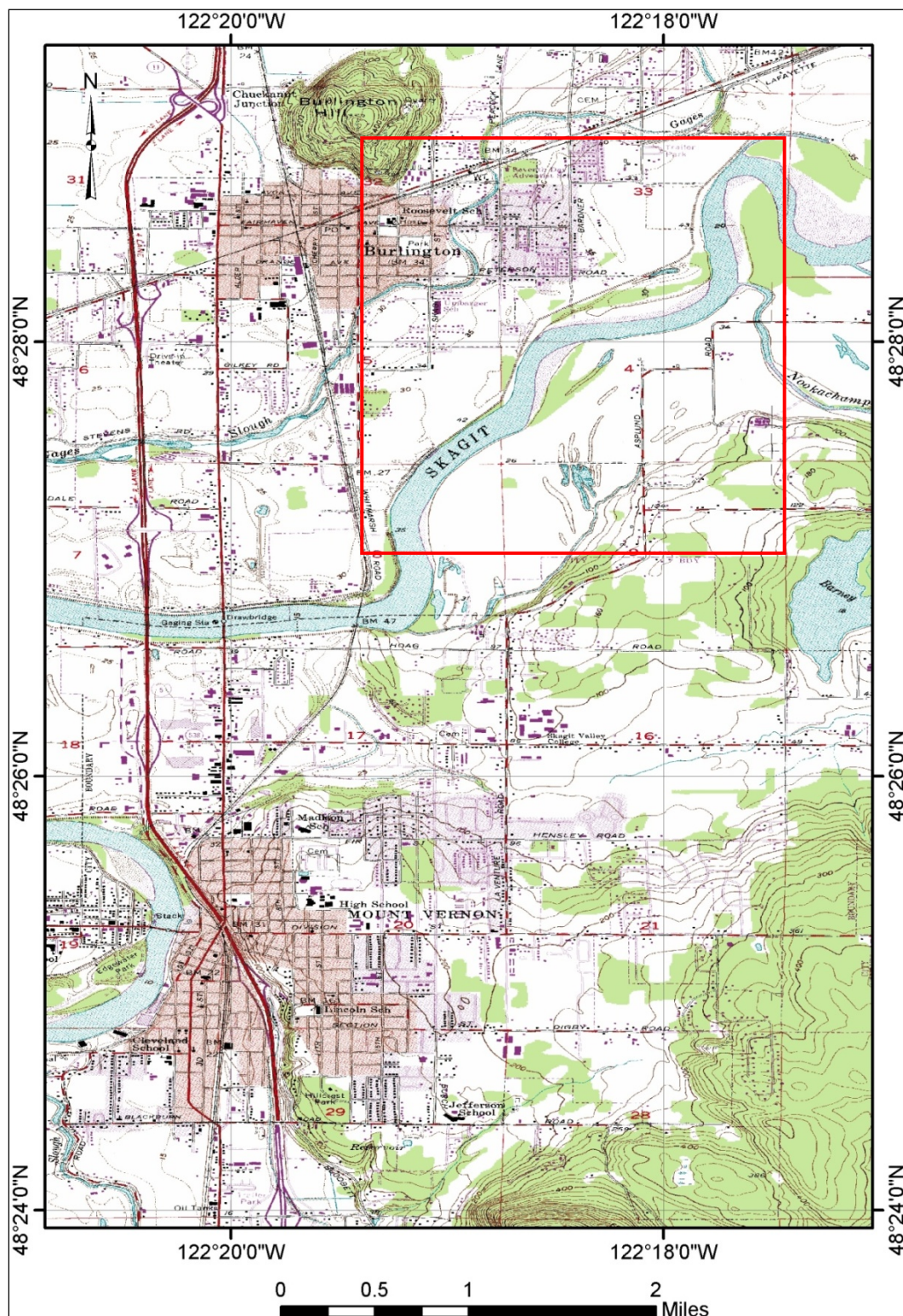


Figure 22. The ERDC study site, outlined by the red box, in Burlington, WA.

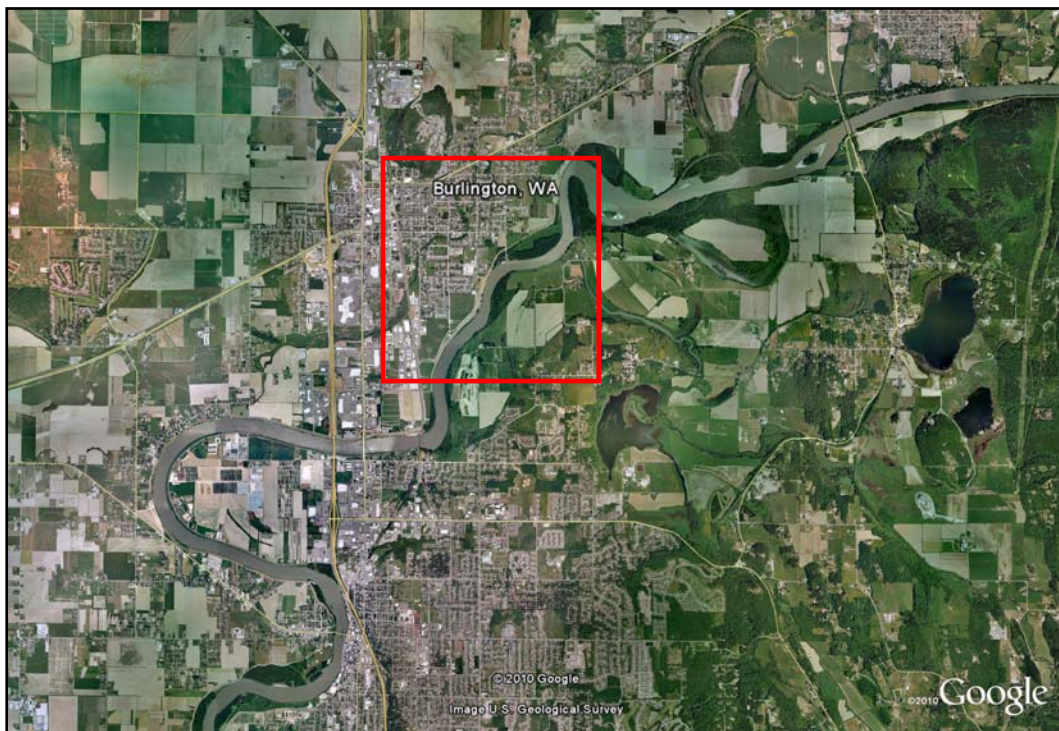


Figure 23a. Aerial photograph of the reach of Skagit River under study at Burlington, WA, (Google Earth Image 2010). Close-up view of the study area presented in Figure 23b.



Figure 23b. Close-up view of the Burlington, WA, study site (Google Earth image 2010).

episodes has carved the aforementioned broad alluvial valley within the study area containing isolated bedrock outcrops, abandoned floodplain surfaces or terraces, and the present-day floodplain.

Levees in the study area were built on Holocene floodplain sediments composed of Skagit River abandoned channel, abandoned course, and overbank (natural levee and flood basin or quiet water) deposits. Before European settlement occurred and the present-day levees were built, the floodplain of the Skagit River contained a meandering river system as evidenced by the presence of abandoned channels, abandoned courses, and the diagnostic ridge and swale topography, which is characteristic of point bar deposits. Many of these geomorphic features are still visible on the topographic map in Figure 22 and photographs of the study area in Figure 23. Boring data from the study area, as well as geological map data (Dethier and Whetten 1981), indicate that the alluvial fill may be in excess of 150 ft thick in the project area.

Levee failure mechanisms

The primary failure mechanisms for point bar deposits have been described in the preceding section about the Sacramento study site. These failure mechanisms are equally applicable to this site, and they include loss of embankment soils owing to levee through-seepage and piping, underseepage within the pervious foundation sands and piping of foundation soils, and slope stability types of failure mechanisms from geomorphic processes operating within the river channel itself (i.e., migration, scouring and resulting over steepened bank slopes leading to shear and flow failures, rapid drawdown, etc.).

Levee profiles

Geotechnical profiles generated by Golder Associates (2009) were used in the ERDC analysis. Because of the availability of this report, its recent publication date, and the comprehensive nature of their study, three levee profiles were evaluated from this site, as opposed to the single profile from the Sacramento site. (Note: Initially, the ERDC team was only able to obtain a copy of the Phase 1 Geotechnical Data report (URS 2008) for the PA as opposed to the final evaluation report (URS 2010a), which contained detailed topographic profiles of representative levee reaches in the PA. Scheduling did not permit the later evaluation of their profiles.)

Thus, the Golder Associates report greatly facilitated the evaluation of multiple sections by the ERDC team).

Profiles E, F, and G (Golder Associates (2009) designation) are shown in Figures 24a and 24b and were easily digitized to develop the topographical and subsurface stratigraphy for the study site. These three sections were used to examine woody vegetation impacts along both the convex (point bar) and concave (cut bank) side of the river. Section E extends through the convex side of the riverbank, while Sections F and G are located on the concave bank. Levee slopes in the Burlington reach are typically 1V:3H.

The subsurface stratigraphy, in terms of floodplain depositional environments, is identified in these three profiles, which extend perpendicular to the levee and riverbank. The down valley extent of these environments is represented by three longitudinal cross sections in Figures 25a and 25b, which identify the locations of the perpendicular sections on the respective longitudinal sections. Available boring data from this area identifies the stratigraphy as primarily man-made fill, overbank (i.e., natural levee and flood basin), and coarse-grained channel (point bar) deposits.

Overbank deposits at profile location G are much thicker than those present in Sections E and F. Profiles F and G are located on the cutbank side of the river, which is eroding into older Skagit River floodplain deposits. An older Skagit River course (Gages Slough) is present north and west of the study site, in what is now the protected part of the city of Burlington (Figures 22 and 23). Overbank deposits are likely associated with this older course and correspond to natural levee and flood basin type deposits from this earlier Holocene course of the river.

Laboratory soils data

Boring data used to develop the cross sections in Figures 24 and 25 represent a composite of USACE levee borings drilled between 1964 and 1978 (USACE 1979), Shannon and Wilson (2000) Riverside Bridge Replacement borings, Landau Associates (2003) borings for the proposed Home Depot store, and Golder Associates (2009) borings and CPTs. Boring and laboratory data from these various studies were contained in the Golder Associates (2009) report. These logs were reviewed to verify the stratigraphy and soils present in the levee fill and foundation.

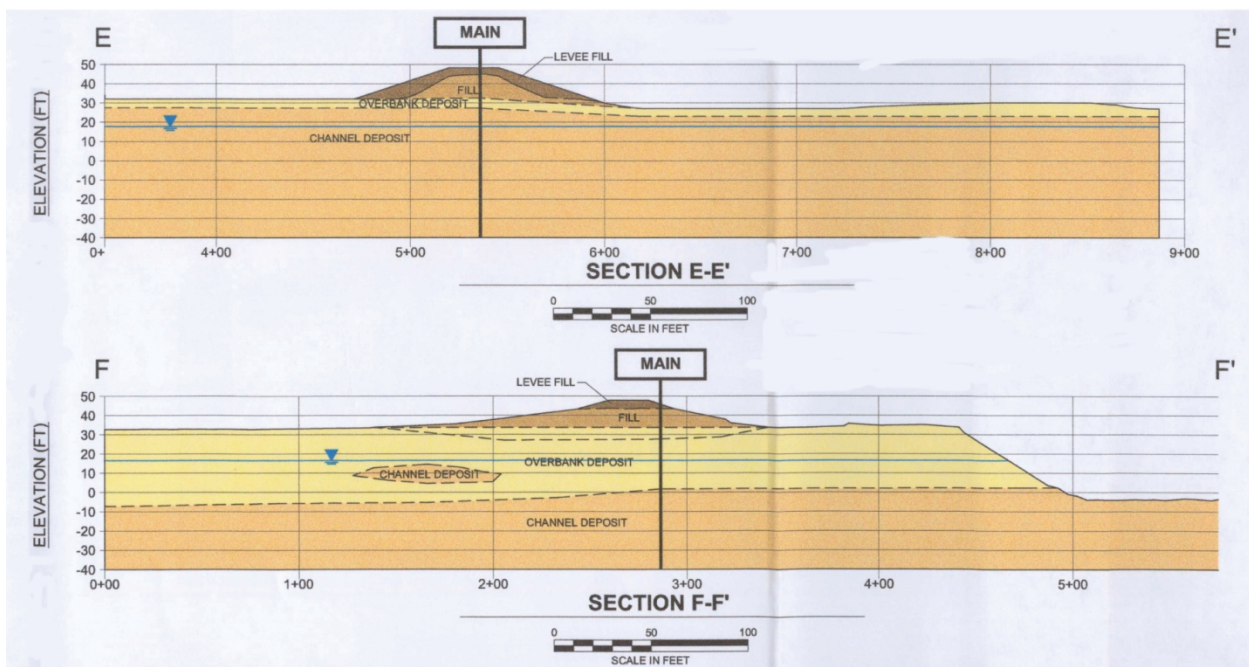
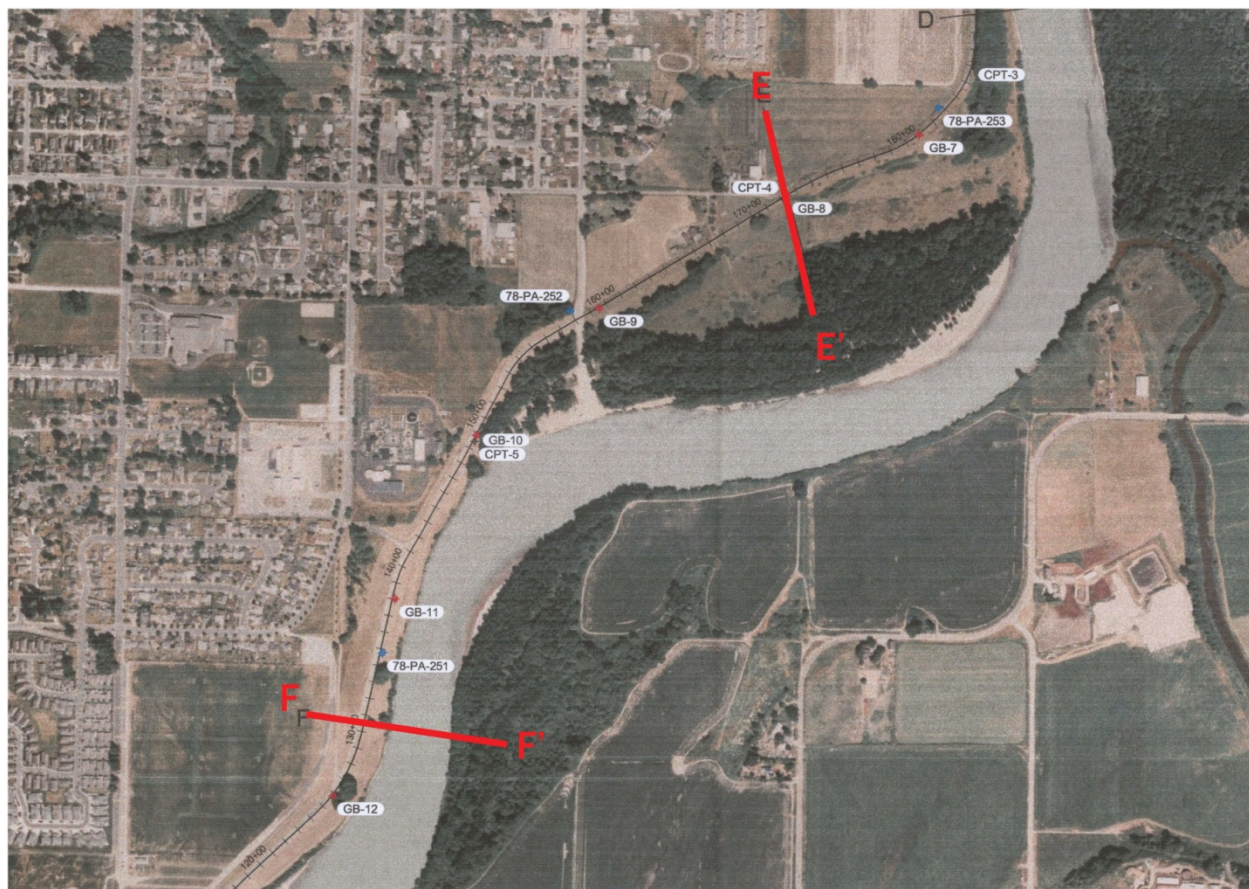


Figure 24a. Cross sections E and F used for the geotechnical evaluation (Golder Associates 2009). Levee fill in cross section F-F' is a section proposed to be added as part of the planned improvements. Only current levee conditions were modeled by ERDC.

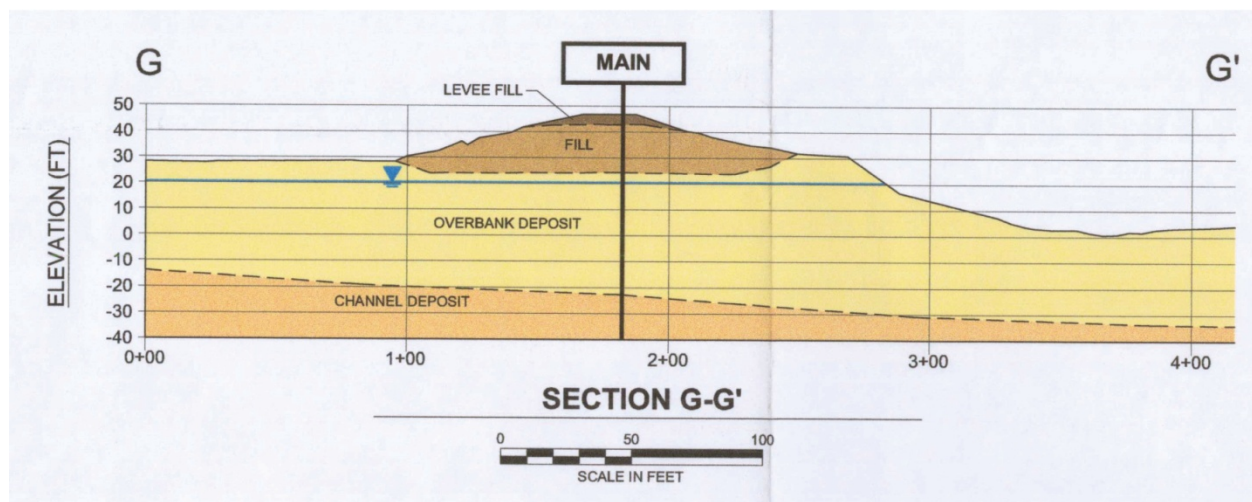


Figure 24b. Cross section G-G' used for the geotechnical evaluation (Golder Associates 2009). Levee fill (dark brown) identified in the bottom profile corresponds to new levee to be added as part of the planned improvements. Only current levee conditions were modeled by ERDC.

USCS soil types forming the right bank and bed of the river in the area of interest are identified by the longitudinal cross sections in Figures 25a and 25b. Boring data in these cross sections reflect a combination of field and laboratory soils data that were compiled from the various past studies. Man-made fill extends into the foundation of the levee, with the fill being composed primarily of silty sand (SM). Boring data summarized in Figures 25a and 25b indicate overbank deposits are primarily silt (ML) to poorly graded fine sand (SP), while point bar or channel deposits are poorly to well graded sand (SP-SW).

Hydraulic conductivity

Grain size data from split-spoon samples taken from the Skagit levees and foundation by Golder Associates (2009) was used to estimate the saturated hydraulic conductivity using both the Hazen (1911) and Massmann (2003) empirical methods. Grain size curves of soil samples from the study area contained in the Golder Associates (2009) geotechnical report were compared to values obtained from the California Guidance procedures for the Natomas levee improvements (Table 3). Results of the three different methods for the various depositional environments are as follows:

- Undocumented Fill
 - Hazen Method: 1.4×10^{-4} cm/sec
 - Massmann Method: 2.2×10^{-3} cm/sec
 - California Guidance: 1.0×10^{-4} cm/sec
- Overbank Deposits
 - Hazen Method: 1.2×10^{-3} cm/sec
 - Massmann Method: 3.6×10^{-3} cm/sec
 - California Guidance: 3.0×10^{-5} cm/sec
- Channel Deposits
 - Hazen Method: 5.8×10^{-2}
 - Massmann Method: 5.9×10^{-2}
 - California Guidance: 1.0×10^{-2} to 3.0×10^{-3}

The California Guidance values for hydraulic conductivity for the different geological units were generally comparable to those obtained by the Hazen and Massman methods used in the geotechnical analysis by Golder Associates (2009) as previously shown. The latter Hazen and Massmann values reflect the average of the calculated hydraulic conductivities for each depositional environment. Values obtained using the D₁₀ grain size and the California Guidance method in Table 3 are the samples that are within or

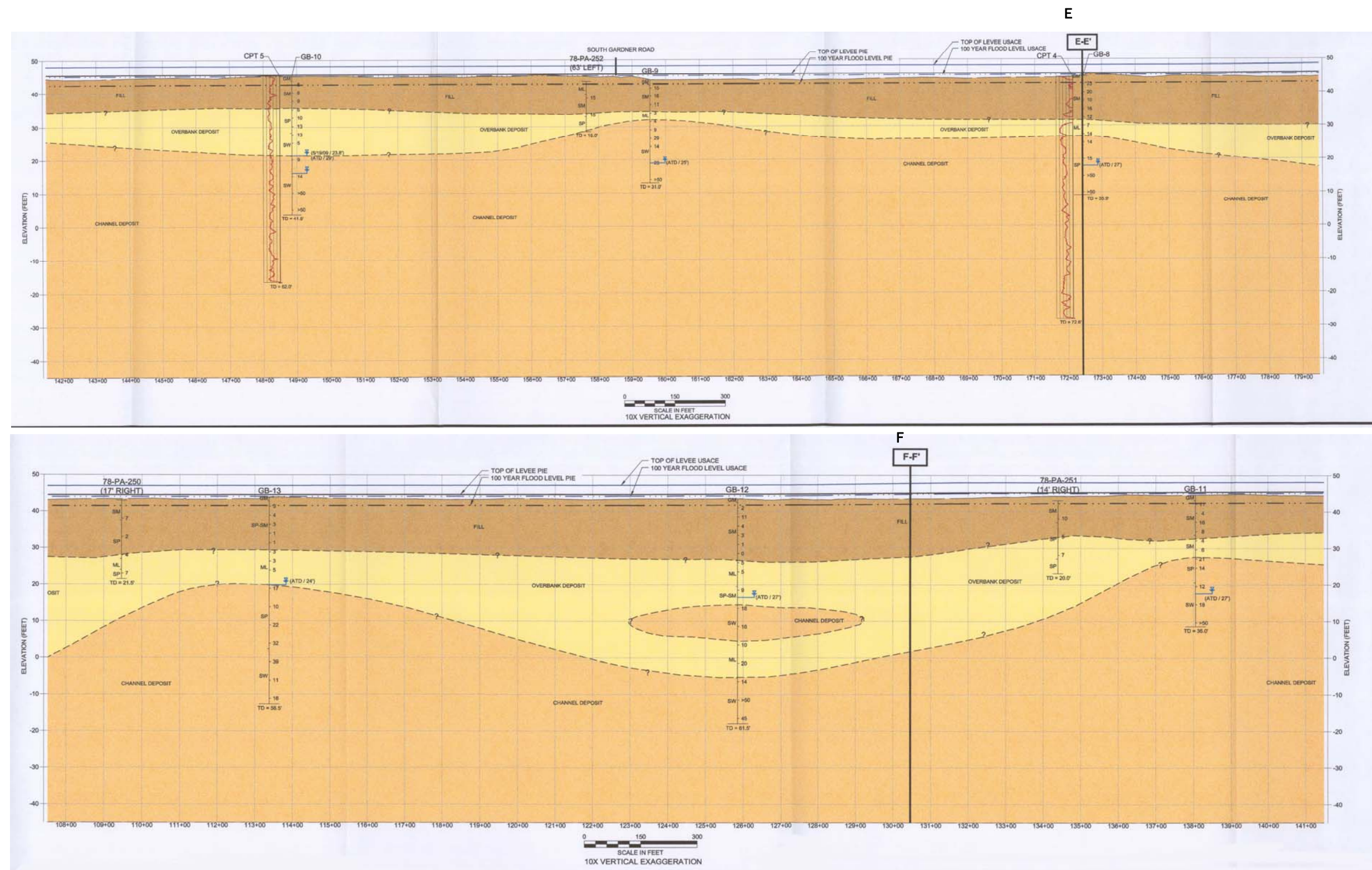


Figure 25a. Right bank cross sections through the study reach showing USCS soils in subsurface and stratigraphy according to environments of deposition (Golder Associates 2009). Orientation of each section is with view looking to the west (downstream edge on left side and right edge corresponding to upstream side). Note the location of perpendicular profiles E and F in the ERDC study and soils at each location. Legend to cross sections is presented in Figure 25b.

G

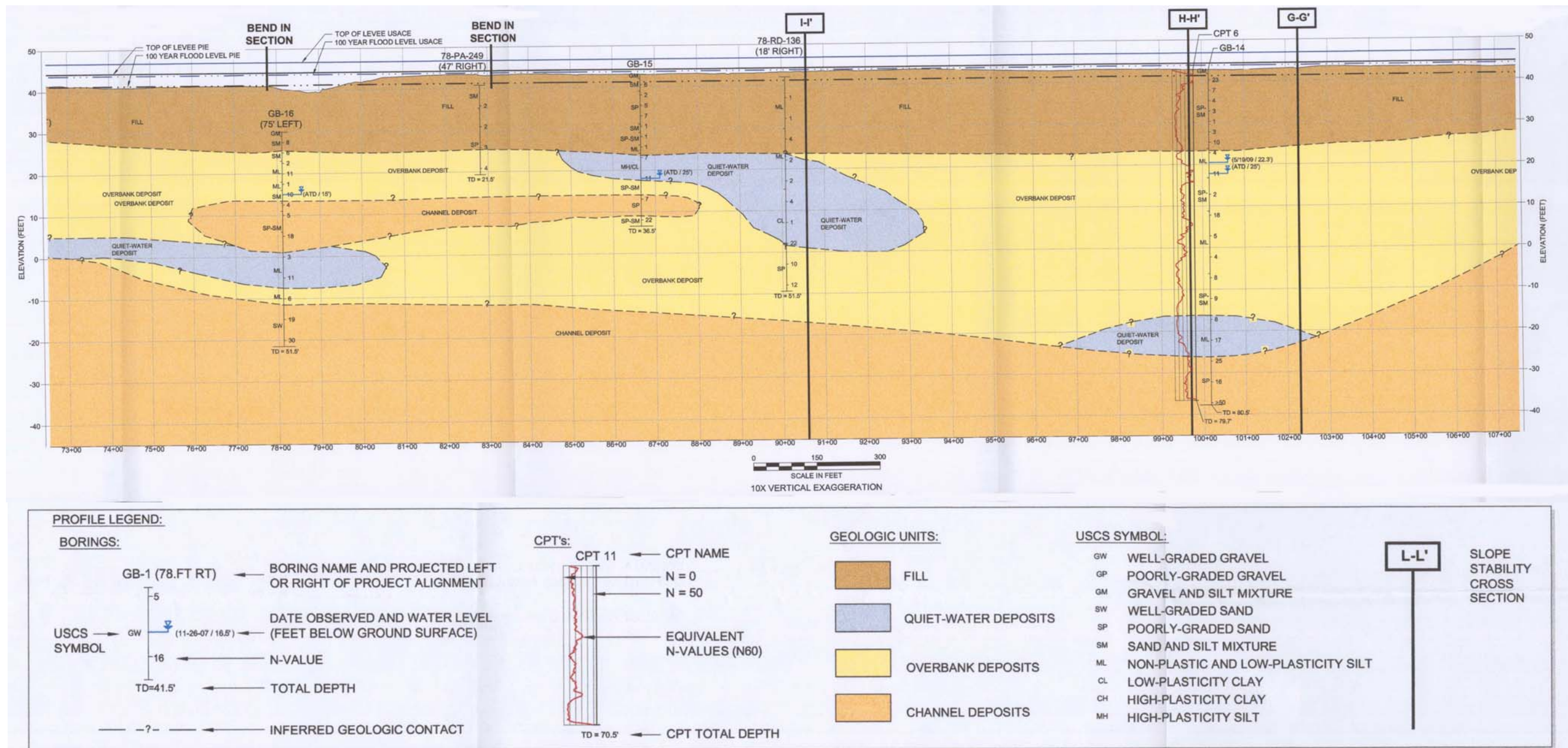


Figure 25b. Right bank cross section through the study reach showing USCS soils in subsurface and stratigraphy according to environments of deposition (Golder Associates 2009). Orientation of each section is with view looking to the west (downstream edge on left side and right edge corresponding to upstream side).

Note the location of perpendicular profile F used in the ERDC study and soils at each location.

near the ERDC profiles of interest. However, it should be noted that only two grain size curves were available from the ERDC study area. One sample was from the fill and the second was from the previous point bar sands at about 30 ft below the surface. The value interpreted for overbank deposited silt (ML) is two orders of magnitude higher than those reported by Hazen and Massmann. However, the empirical relations created using these methods were never intended to be used for samples containing a large percentage of fines passing the No. 200 sieve size. These relations are normally valid for only sands with a specific range in grain size.

Groundwater conditions

Groundwater levels reported in borings drilled for the geotechnical evaluation of the Skagit River levees at Burlington, WA, ranged between 11 and 25 ft above mean sea level (amsl), with a trend of water level increasing in elevation to the northwest (Golder Associates 2009). This increase in groundwater elevation probably reflects the general increase in ground surface elevation. Golder and Associates report the presence of a USGS staff gage on the right bank at approximately 150 ft south of the Burlington Boulevard Bridge (latitude 48°26'42", longitude 122°20'03"). Historical USGS records tell us that the maximum water level recorded was 37.37 ft amsl on 25 November 1990 and the lowest 7.37 ft asml on 26 October 1942.

Albuquerque, NM

Introduction

The next study site area is located on the Rio Grande River at Albuquerque, NM (Figure 26). Two sites (designated as Site 1 and Site 2) were selected at Albuquerque on either side of the river as shown by Figure 26. The first site is a short distance south of the Montaño Bridge, along the eastern side of the Rio Grande. The second site is part of the Corrales levees along the western side of the river (Figure 26). The sites were selected because of different levee geometries along both sides of the Rio Grande, availability of geotechnical data from each site, types of trees present, the ability of ERDC to test the various tree species, particularly root pull out tests, and easy access to the levee areas.

Site 2, located on the right bank approximately midway between the Montaño and the Paso del Norte bridges crossing the Rio Grande, was

chosen for detailed study and evaluation (Figure 27). The reasons for selecting only the western levee site at Albuquerque are as follows. Both Rio Grande levee sites examined have a similar construction history, and both are composed of nearly identical, coarse grained floodplain sediments. However, there is one significant difference between the two sites: the eastern levee system was appreciably widened during the late 1980s for a paved bicycle path. The eastern levee side was nearly doubled in size by construction of the current bike path. Thus, the western side, with the smaller levee footprint, was likely to be more adversely affected by the presence of woody vegetation and was therefore modeled by the ERDC team to study the impacts of vegetation at this site.

The original levees protecting the Albuquerque area from flooding were initially constructed by local farming interests in the late 1800s and early 1900s. These interests eventually merged and formed the Middle Rio Grande Conservancy District (MRGCD) in the 1920s to drain waterlogged lands in the middle Rio Grande Valley to reclaim these areas for agriculture and to provide irrigation, and flood control to valley residents (MRGCD 2010). The Albuquerque levee system is under the jurisdiction of the local levee district, the MRGCD. Between 1930 and 1935, the MRGCD constructed 190 miles of levees as part of their district-wide plan to drain farmlands and to provide flood protection to local residents (Berry and Lewis 1997).

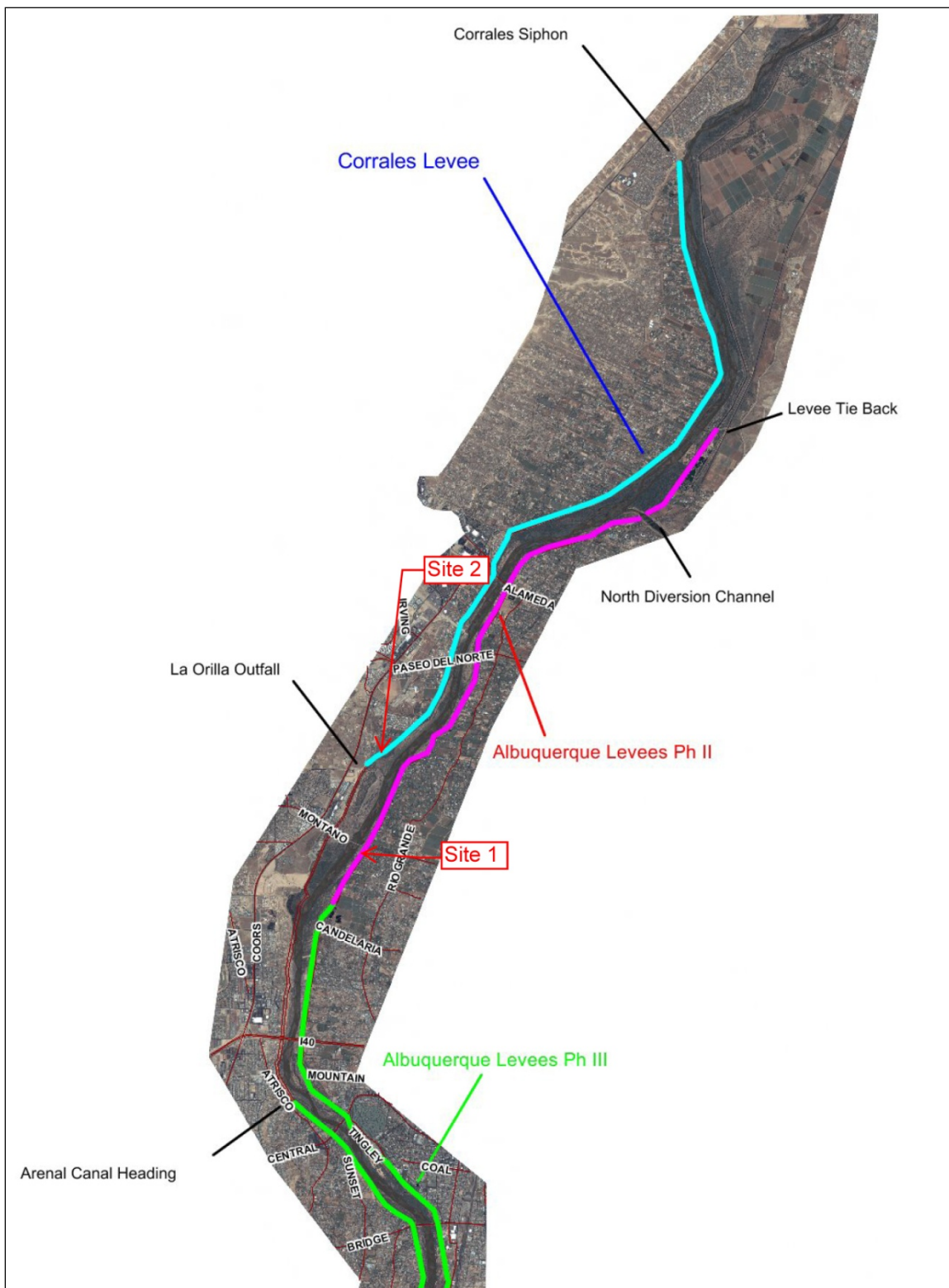


Figure 26. Location of two sites evaluated by the ERDC study (Sites 1 and 2). Components of the levee system are based on phases of construction begun in 1954 (base map from U.S. Army Corps Engineers, Albuquerque District).

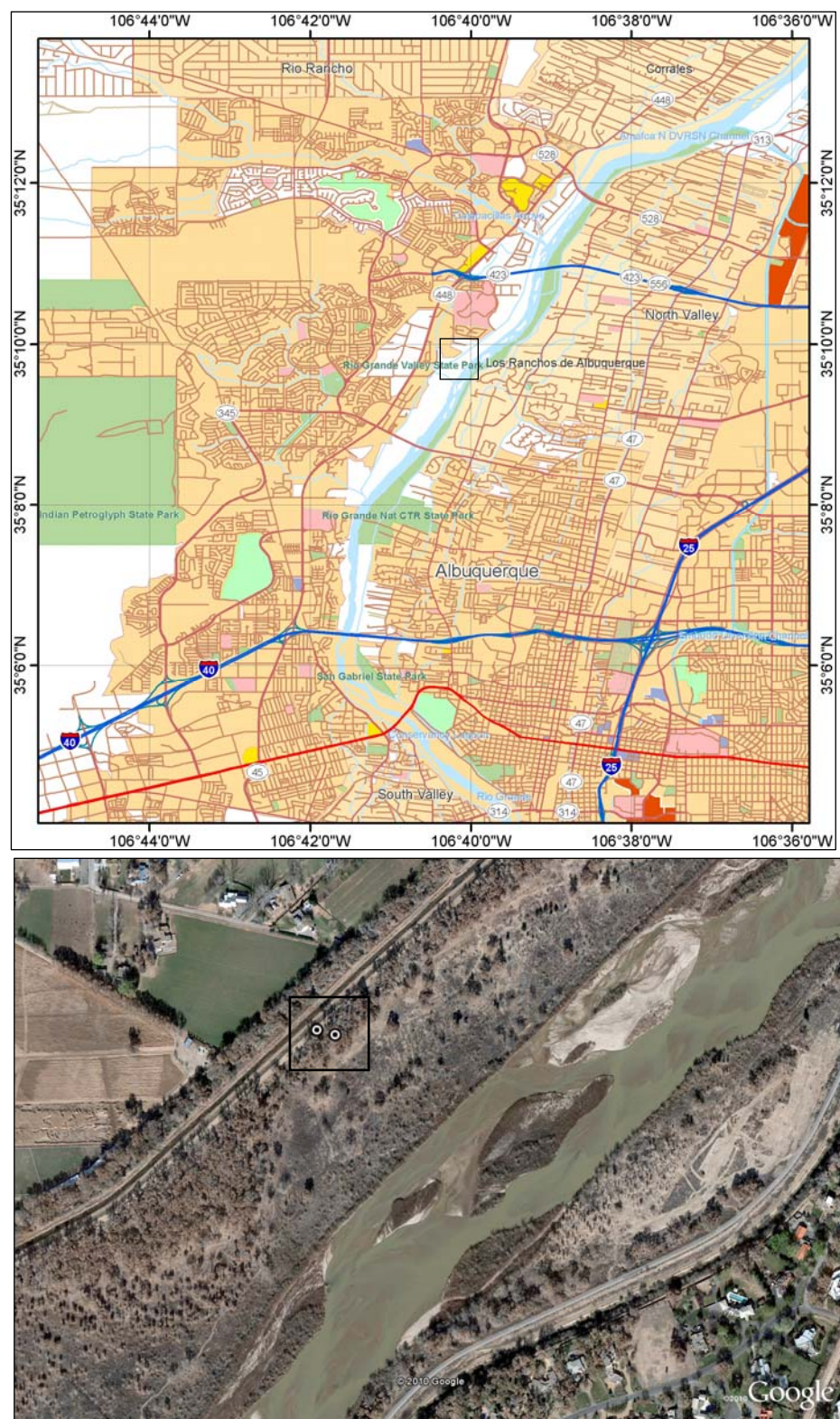


Figure 27. Location of Site 1, Albuquerque, NM.

Federal authority for the Albuquerque levee system was provided by the Flood Control Acts of 1948 and 1950 (USACE 1953). The Albuquerque levees on the eastern side of the river were rebuilt during mid-1950s as part of a comprehensive federal flood protection upgrade of the system. These levees were designed to meet USACE standards for flood protection projects and were built using accepted modern soil mechanics practices. Federal sponsorship and jurisdiction involved the construction of new irrigation canals, levees, and further raising the levee system through the Albuquerque reach under several construction phases (USACE 1953; USACE 1954a,b; USACE 1955). Parts of this levee system are referenced today according to the different phases of the 1950s construction authorization (Figure 26). Levees along the western side of the Rio Grande in the Albuquerque area were built much later, as urban growth expanded into flood-prone areas in the late 1980s. The Corrales levee system was upgraded by USACE in the late 1990s to protect residential and agricultural interests from flooding (USACE 1993, 1996).

An important component of historical bank protection and stabilization efforts on the Rio Grande was the placement of jetty jacks between the 1940s and early 1960s (Grassel 2002). Nearly 115,000 jetty jacks were constructed by 1962 (Lagasse 1980). Peak construction of jetty jacks occurred during the mid- to late-1950s when the current levee system was being rebuilt by USACE and MRGCD. These large steel structures were meant to protect the new levee system, trap sediment, foster the growth of vegetation, and prevent uncontrolled river migration. Jetty jacks were used extensively to control excessive channel migration, before the construction of the main stem dam on the Rio Grande regulated major flood flows on the river. The post-dam era has witnessed the removal of a large number of these jetty jacks. Grassel (2002) concludes that the overall jetty jack program was highly successful in protecting the levees, stabilizing the banks of the Rio Grande, and fostering the growth of woody vegetation in the rivers flood corridor.

Previous studies

Studies of the Albuquerque levee system are presented in various 1950s design memorandum (USACE 1953, 1954a,b, 1955), 1990s design memorandum of the Corrales levee (USACE 1993, 1996), hydraulic analysis (Mussetter Engineering 2006) and a geotechnical analysis for a rebuilt portion of the west levee north of Interstate 25 (AMEC Earth and

Environmental 2008). Geotechnical data in these studies include borings, laboratory analysis of soils data, and survey data on levee height.

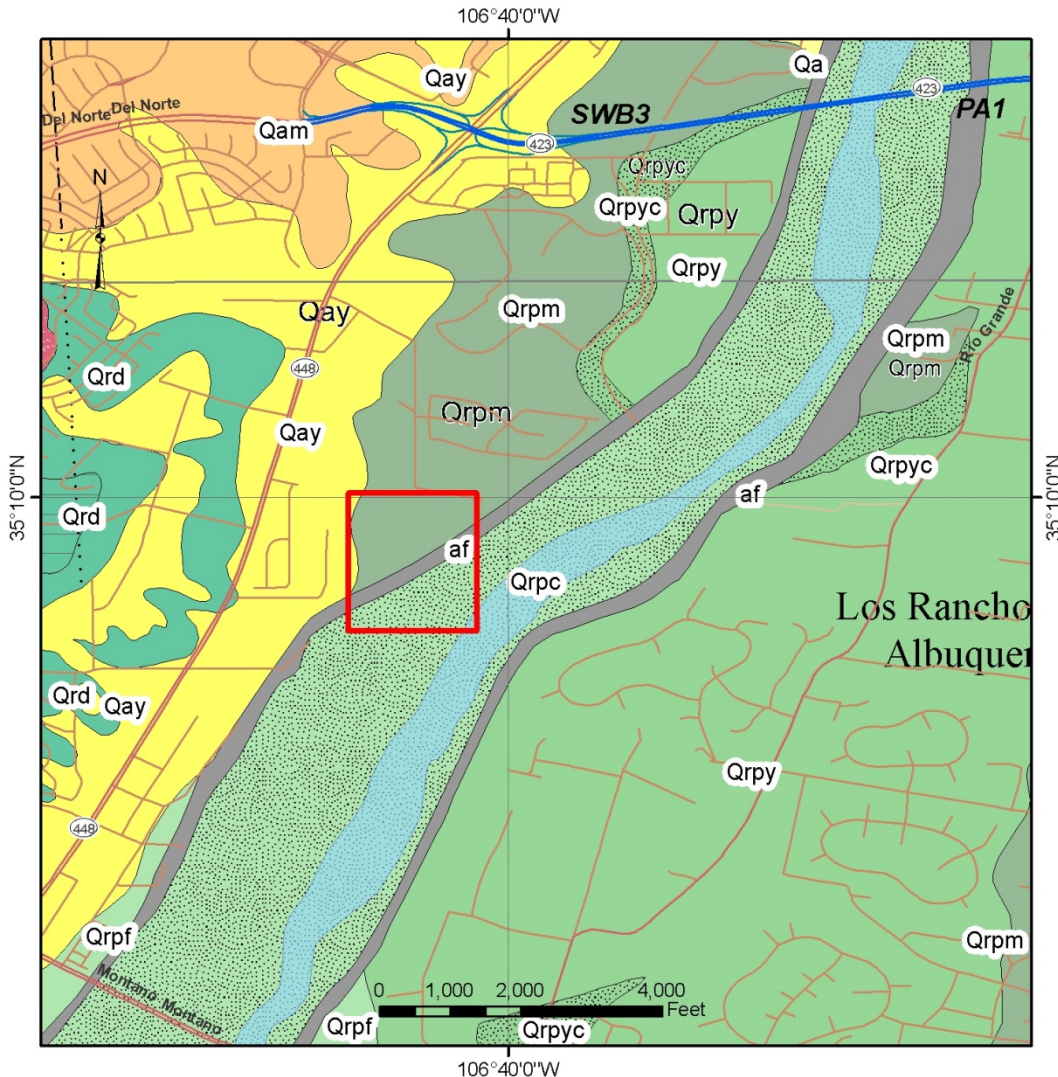
Geological setting

Geological data are presented on various geological quadrangle maps of the Albuquerque area (Connel 1997, 2008; Hawely et al. 1996). The Rio Grande flows through a fault-bounded rift valley, which is tectonically active, as evidenced by nearby Pleistocene volcanoes, lava flows, Pleistocene faults, and large magnitude historical earthquakes. The river has created a distinct floodplain in the Albuquerque area, bordered by older floodplain surfaces or terraces, and alluvial fans created by drainage off the mountain ranges that parallel the river's course. Much of the city of Albuquerque is located upon older Rio Grande terrace deposits on the east side of the valley at the base of the Sandia Mountains.

The foundation of the levee system is composed of coarse-grained Holocene Rio Grande alluvium. A subset of the Albuquerque geological map is presented in Figure 28, showing the spatial distribution of the different geological units in the study area. Floodplain deposits in the study area are mostly coarse grained as defined by the geological map units and levee borings from the USACE (1993) geotechnical report of investigations. Before the levee system was built, the Rio Grande flowed as a series of braided river channels, separated by sand and gravel bars. Past construction of levees, jetty jacks, irrigation canals, tributary dams, and main stem dams on the Rio Grande have regulated major flooding to less than half of their former discharge and shaped the present day character of the river's floodplain and flood corridor. These activities in their aggregate have produced the characteristic single, shallow channel with large midchannel sand and gravel bars that is observed today (Figure 26).

Levee failure mechanisms

As the river sediment and banks are primarily coarse grained, failure mechanisms for this site include the loss of embankment soils due to levee through-seepage and piping, underseepage within the mostly pervious foundation and piping of foundation soils, and scouring of levee slopes by large magnitude flood events. Slope failures from geomorphic processes operating within the main river channel (i.e., bank migration, scouring and resulting over steepened bank slopes leading to shear and flow type failures are not considered a major failure mechanism at this site because



Symbol	Texture	Age	Formation
Qa	Sand, gravel	Holocene	Stream-valley alluvium
af	Sand, gravel	Holocene	Unspecified
Qay	Sand, gravel	Late Pleistocene-Holocene	Stream-valley alluvium
Qrpc	Sand, mud	Late Pleistocene-Holocene	Las Padillas Formation (Fm)
Qrpf	Sand, mud	Late Pleistocene-Holocene	Las Padillas Fm
Qrpm	Sand, mud	Late Pleistocene-Holocene	Las Padillas Fm
Qrpy	Sand, mud	Late Pleistocene-Holocene	Las Padillas Fm
Qrpyc	Sand	Late Pleistocene-Holocene	Las Padillas Fm
Qb2	Basaltic rock	Middle Pleistocene	Albuquerque volcanoes
Qrd	Sand, gravel	Middle Pleistocene	Los Duranes Fm
Qam	Sand, gravel	Middle-Late Pleistocene	Stream-valley alluvium

Figure 28. Geological map of the study area showing general soils and their age (Connell 2008).

of past historical activities (i.e., jetty jacks) to control river migration. The present-day river is located several hundred feet from the floodside toe of the levee. Additionally, the presence of upstream dams has significantly reduced the magnitude and duration of major flooding, and sharply reduced the likelihood of any in-channel related slope failures from occurring at the study site. Jetty jack construction has successfully reduced channel migration within the Albuquerque area since European settlement (Grassel 2002).

A unique feature of the Albuquerque levee system is the presence of a toe drain in the body of the levee that was incorporated into the 1950s levee design to reduce seepage pressures at the toe during high water (Figure 29). Inspection of sections of the toe drains along the east side of the levee system has shown corrosion of the drain pipe, leading to sediment filling and plugging the drain, and the growth of tree roots in the drain itself, reducing the overall integrity of the engineering design (USACE 2005b).

Another unique feature of this levee system, which is not present in any of the other sites previously studied, is the presence of an irrigation canal at the levee toe. A canal is present along both sides of the river. These canals, effectively establish the local groundwater table beneath the levee foundation. Regulated flood flows because of the main stem dams have further reduced the duration of flooding and magnitude of the peak flood stages. Consequently, these factors have significantly reduced the likelihood of through-seepage leading to shallow slides along the bank of the irrigation canals, which potentially can affect the landside toe of the levee if prolonged high groundwater conditions were to cause sloughing of the canal banks towards the levee toe.

Levee profile

Profiles were developed for each site by ERDC using the most current geotechnical, survey, and available LiDAR data. Only the west side of the river is presented here as only this profile was used to model the stability of the levee for the various failure modes described. First return LiDAR data from 2010 were obtained from the Albuquerque District and were used to compare the current conditions to the design levee geometry presented in the Corrales evaluation and hydraulic reports (USACE 1993, 1996; Mussetter 2006). Design conditions and current levee geometry are shown in Figures 30a and 30b. First return LiDAR data from 2010 correspond to the raw laser data, which includes returns from trees,

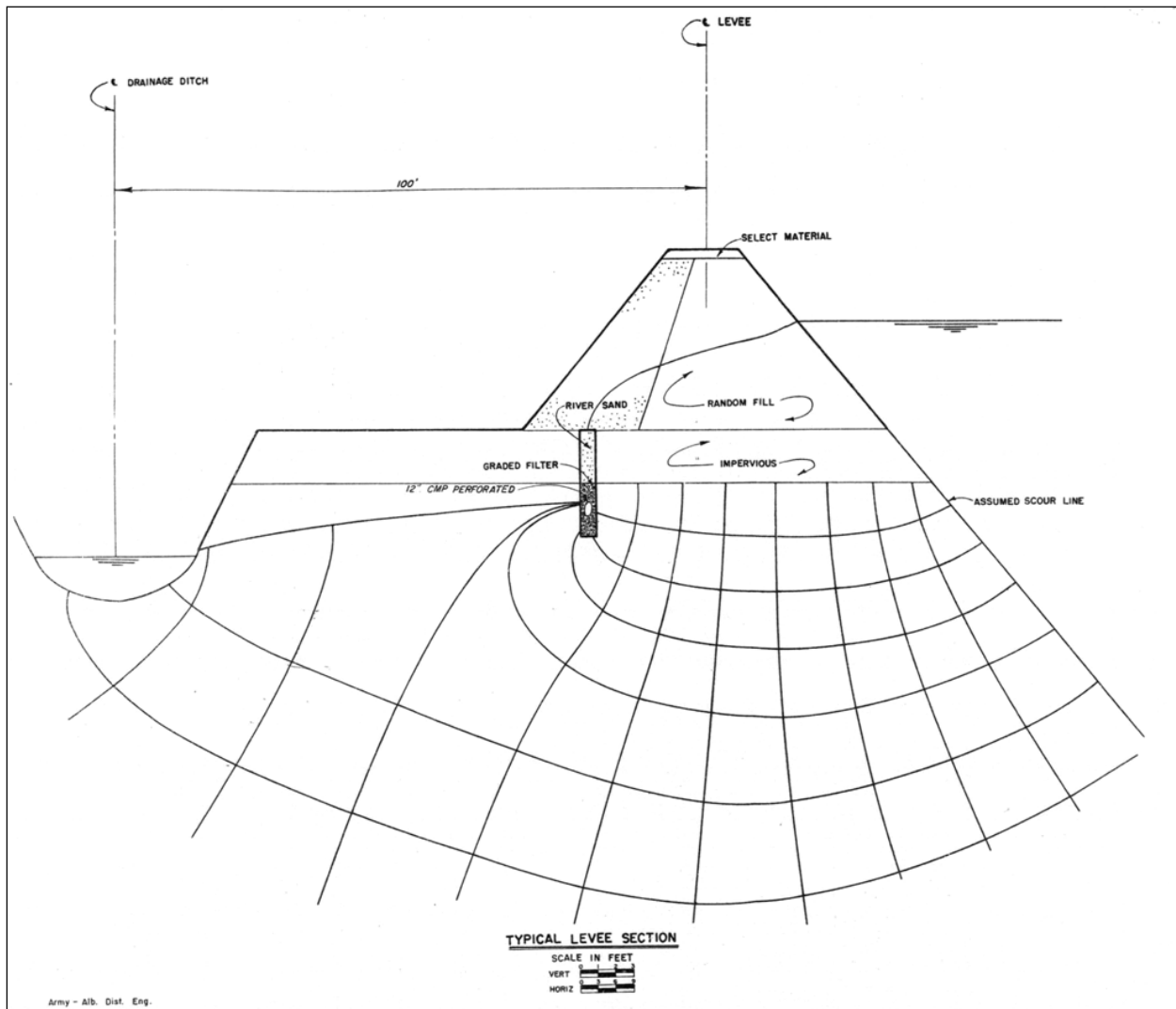


Figure 29. Albuquerque Levee profile showing toe drain and irrigation canal on landside (USACE 1954a).

buildings, and other types of topographical features. A bare earth model is typically developed from these data. Post-processing of the LiDAR data removes the cultural and vegetation features. Only the raw laser data were provided to ERDC to develop accurate levee profiles. These data were used to evaluate current topography. An image of the west levee study area is presented in Figure 30 bottom from the first return data. Trees and the crest of the levee are shown as dark features in the image.

The levee geometry described for Site 2 (approximately Station 535) is identified by the design profile in Figure 30a (USACE 1993). Elevation data for the top of levee at Station 535+00 in Figure 30a (USACE 1993)

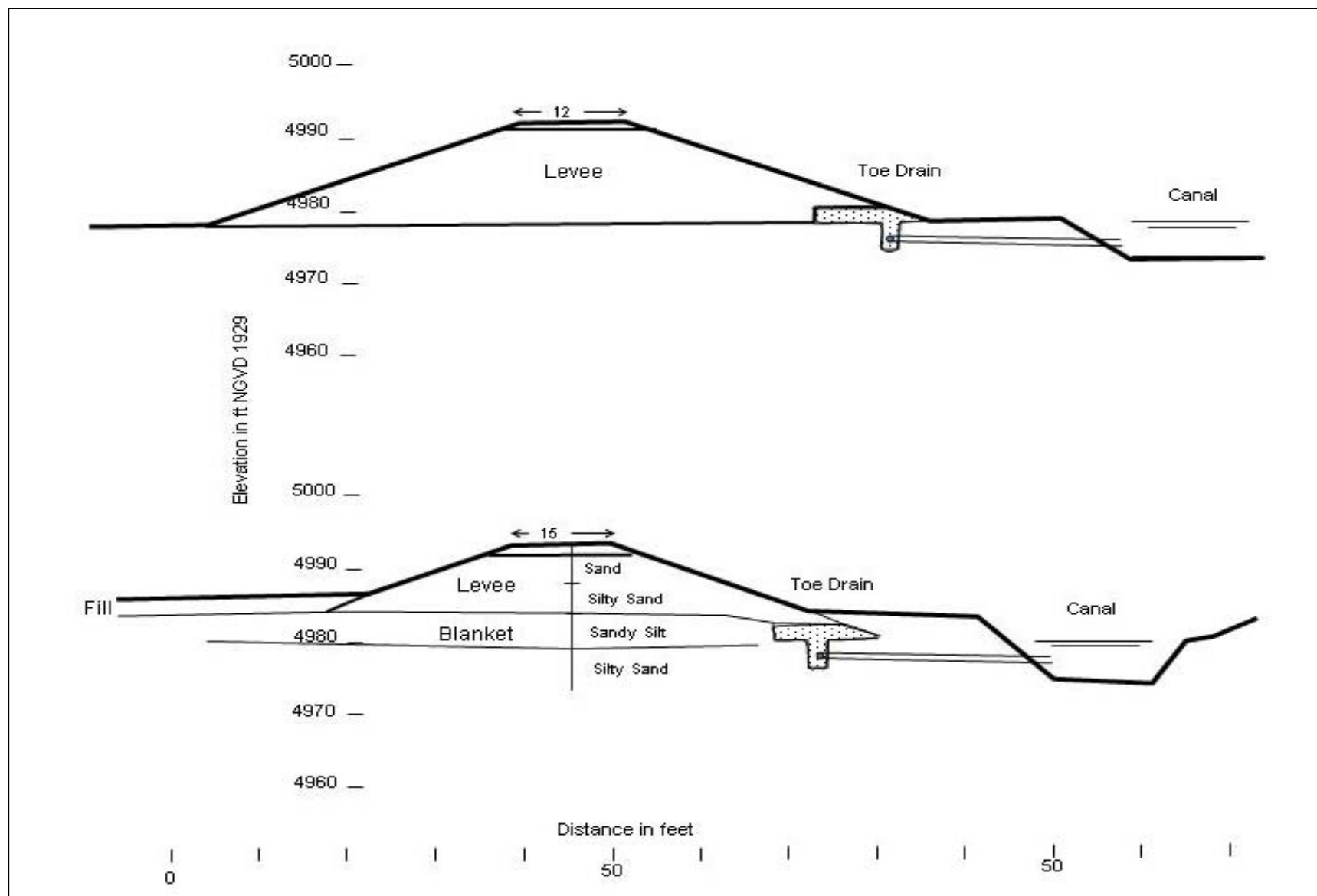


Figure 30a. Profile of the west levee at Station 535 showing idealized case from plans and specs (top) and current condition as determined from LiDAR data and Google Earth image (bottom profile).

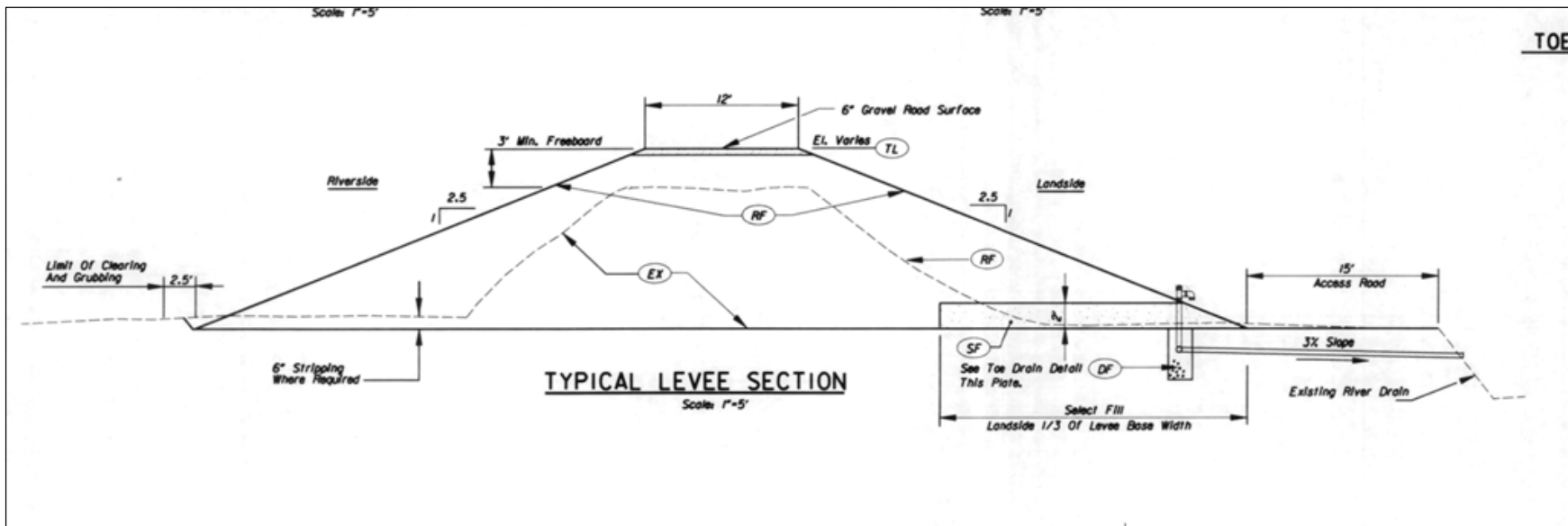


Figure 30b. Typical profile identified for the Corrales Levees (USACE 1993, plates 7 and 9). Levee characteristics include slopes of 1V 2.5 H, 12-ft-wide crest, and ground surface at approximately 4,976 ft amsl. Datums for the elevation are referenced to NGVD 1929.

are given as 4,989.75 ft National Geodetic Vertical Datum (NGVD) 1929. The elevation datum used in the Corrales Levee report is identified as NGVD of 1929 (USACE 1993; 1996). Top of levee elevation identified in the 2006 hydraulic analysis by Mussetter (2006) for the Bureau of Reclamation range lines at Station 104, 529 (near Station 535 under the USACE (1993) designation) is 4,991.4 of 1988 (NAVD88), or a difference of 1.65 ft between the two survey periods. A third measure of the top of levee elevation is provided by the first return, 2010 LiDAR data for Station 535 (near Station 104,529), and corresponds to an elevation of 4,995.9 ft NAVD88. Image and 2-D profile from the LiDAR data are presented in the bottom profile of Figure 30 and show the ground surface elevation, along with the returns from the trees. Disregarding the returns from the tree canopy in this figure, the surface elevation of the levee, landside irrigation canal, and the ground surface from both the protected and flood sides of the river's floodplain is clearly seen. Elevation differences among the three data sets are a combination of datum issues and possible changes to levee height between the different survey events. The correction factor for the older and newer datum is about 2.9 ft¹. Thus, the top of levee height in 1993 was 4,989.75-ft NGVD1929, a 1.6-ft difference from the Mussetter (2006) report, or a 4.25-ft difference from the USACE (1993) report and the 1996 plans and specs for the Corrales Levee (USACE 1996). USGS gage data from the Rio Grande at Albuquerque reference the older NGVD1929 datum.¹ A corresponding correction factor is therefore required to account for the river gage and datum issues for the hydraulic data and the levee profile from the LiDAR elevation data. The profile used to model the levee is presented in Figure 31 and is referenced to the NAVD88 datum.

Another interesting feature of the current hydraulic conditions along the Rio Grande at Albuquerque is the maximum flood event identified for the study reach. The maximum design flood corresponds to a flood that occurred in the late 1940s before Cochiti Dam was built at 42,000 ft³/sec with approximately 2.63 ft of freeboard at the west levee study site (Mussetter 2006). The maximum flood event after Cochiti Dam was built is regulated at less than 8,000 ft³/sec from spring run-off while the maximum flash flood event possible is from local mountain run-off and is estimated to be a short duration event of approximately 21,000 ft³/sec. Thus, new

¹ Personal communication. 2010. Bruce Jordan, U.S. Army Corps, Albuquerque District.

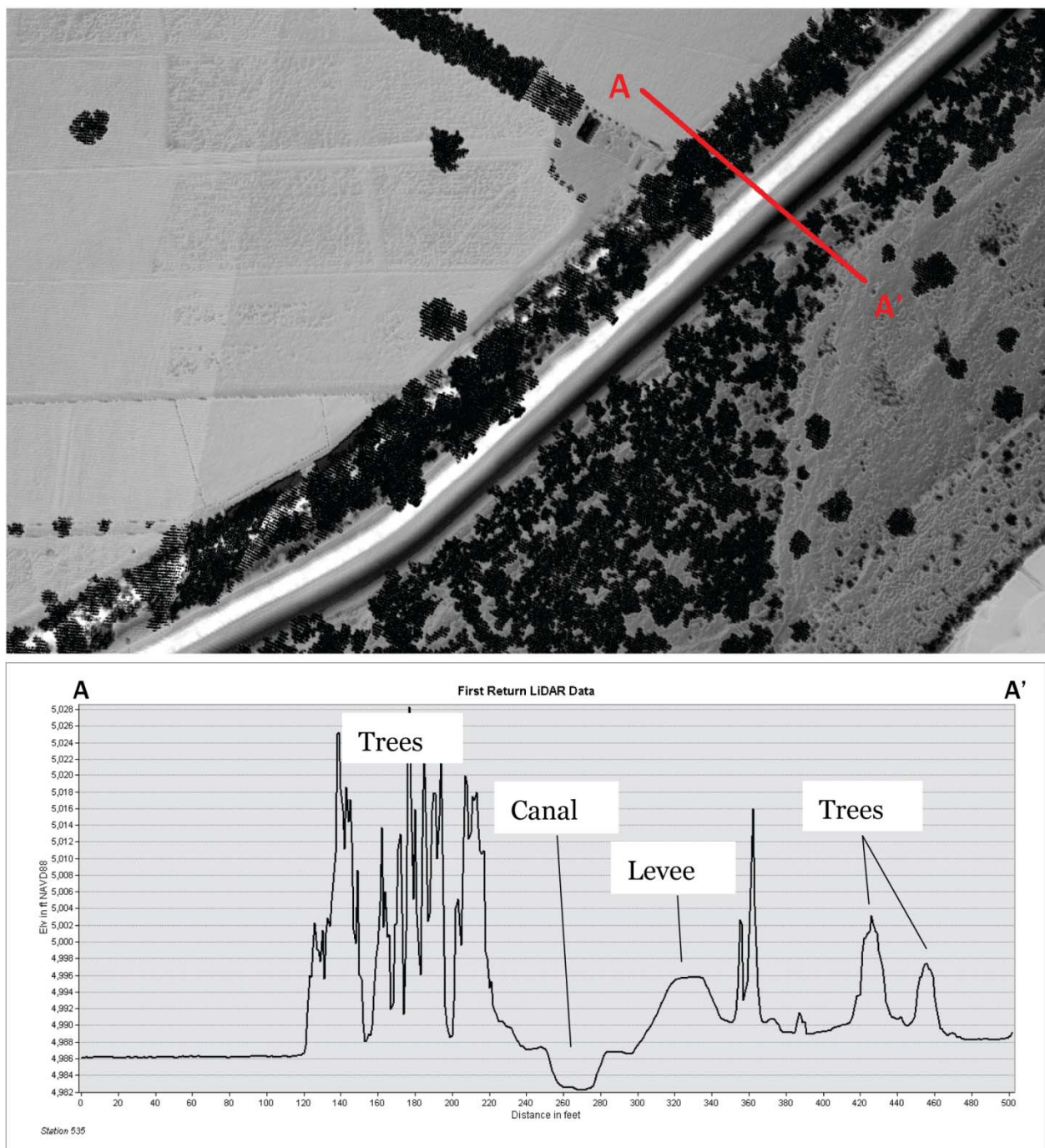


Figure 31. LiDAR image (top) and profile (bottom) from Station 535 (or Station 104,529) showing elevation of top of levee, banks of canal, and landside and flood side ground surface.

normal flood flows through Albuquerque are regulated by Cochiti Dam to be less than 8,000 ft³/sec. The maximum flood event for which the levee was designed and protected by the jetty jack program no longer exists because of dam construction. Thus, the historical flood threat through the Albuquerque area has been significantly reduced because of dam construction on the Rio Grande and its tributaries.

Laboratory soils data

Soils data for the west levee profile were obtained from geotechnical reports for Boring RGL-8A2S-51 drilled at Station 535. This boring identifies mostly sandy soils at this site and shows a thin, sandy-silt topstratum (Figure 32). Boring and laboratory data were incorporated into the levee profile shown in Figure 30 used to model this site. Grain size and Atterberg data were obtained from split-spoon samples taken from boring RGL-8A2S-51 and are presented in Figure 33.

Hydraulic conductivity

Laboratory grain size data in Figure 34 were used to estimate hydraulic conductivity values for the slope stability and underseepage modeling from the California guidance values in Table 3. Values of hydraulic conductivity for the Albuquerque profile in Figure 30 are presented in Table 11.

Groundwater conditions

Groundwater levels can vary widely with the water stage on the Rio Grande because of the pervious nature of the underlying foundation sands. The presence of an irrigation canal at the landside levee toe, and the time of year in relationship to agricultural activities, will govern the local groundwater conditions at the levee site. The irrigation season normally coincides with the spring months and the start of the flood season. As shown by the LiDAR profile in Figure 34b, bank-full stage within the canal corresponds to an elevation of about 4,986 ft NAVD88.

Troxler measurements

Troxler data were obtained from the east and west Rio Grande levees (Figures 35 and 36), from the east side non-vegetated flood plain (Figure 37), and from a wooded region on the east side of the Rio Grande floodplain (Figures 38 and 39). Floodplain and levee soils were identified as being primarily a medium to fine grained silty sand (SM). All the

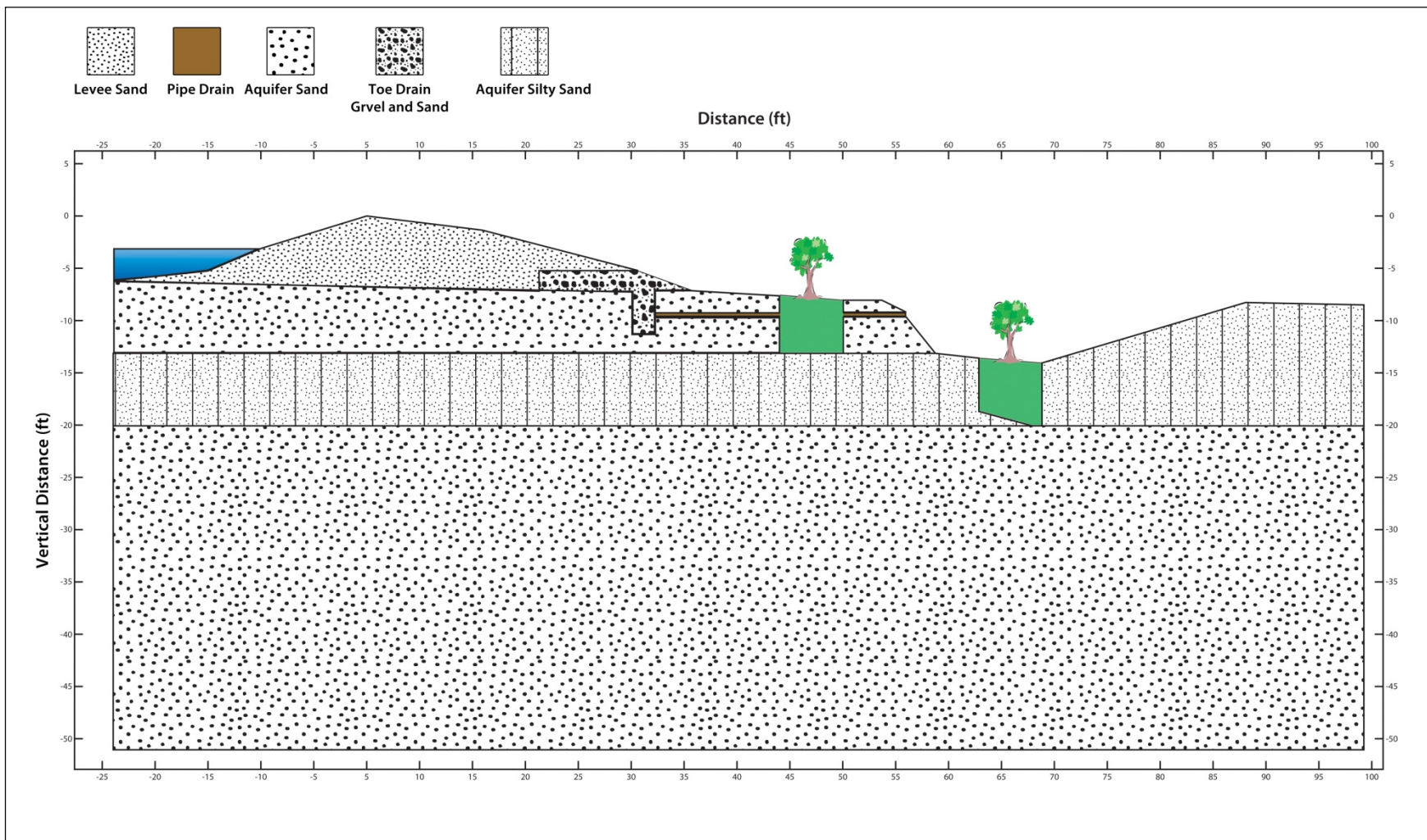


Figure 32. Profile developed for the west Rio Grande Levee from geotechnical and LiDAR data. Trees were modeled along various locations across the levee profile.

				Hole No. RGL-8A2S-51		
DRILLING LOG		DIVISION	SWD	INSTALLATION	SHEET OF SHEETS	
1. PROJECT R.G.L.				SW 4		
2. LOCATION (Coordinates or Station) 2 MI. S. OF CORRALES RD. ON LEVEE				10. SIZE AND TYPE OF BIT 4 TOOTH 6" HOLLOW		
3. DRILLING AGENCY CALIFORNIA TESTING				11. DATUM FOR ELEVATION SHOWN (TBM or MSL)		
4. HOLE NO. (As shown on drawing title and Bore number) RGL-8A2S-51				12. MANUFACTURER'S DESIGNATION OF DRILL MOBILE 80		
5. NAME OF DRILLER DAVID PLA				13. TOTAL NO. OF OVER- BURDEN SAMPLES TAKEN 5	DISTURBED UNDISTURBED	
6. DIRECTION OF HOLE <input checked="" type="checkbox"/> VERTICAL <input type="checkbox"/> INCLINED DEG. FROM VERT.				14. TOTAL NUMBER CORE BOXES		
7. THICKNESS OF OVERBURDEN				15. DEPTH GROUND WATER 13.5 FT		
8. DEPTH DRILLED INTO ROCK				16. DATE HOLE 4/30/84	STARTED COMPLETED 4/30/84	
9. TOTAL DEPTH OF HOLE 20 FT				17. ELEVATION TOP OF HOLE		
ELEVATION	DEPTH	LEGEND	CLASSIFICATION OF MATERIALS (Description)	SPT Blow Count	Mois- ture Content	REMARKS (Drilling time, water loss, depth of weathering, etc., if significant)
*	b	c				
	2		SAND, trace silt, pred. fine, brown		1.6	1) SAMPLE: ① 2 FT ② 5 FT ③ 10 FT ④ 15 FT ⑤ 19 FT
	4			6/13"		
	6		silty SAND, pred. fine non plastic, brown		6.0	
	8					
	10		sandy SILT, low plasticity, lt. brown	9/13"	23.6	
	12					
	14		silty SAND, pred fine nonplastic, brown	10/12"	19.3	
	16					
	18			12/12"	14.2	
ENG FORM 1836 PREVIOUS EDITIONS ARE OBSOLETE. MAR 71 (TRANSLUCENT)				PROJECT	HOLE NO.	
				R.G.L.	342S-51	

Figure 33. Boring log from RGL-8A2S-51.

Project: Rio Grande Levees																	
Hole No.	Depth	Moisture Percent	Sieve Analysis % Passing												Soil Description		
			Atterberg Limits			PI	2"	1-1/2"	1"	3/4"	1/2"	3/8"	#4	#10	#40	#80	#200
50	15'	27.3	NW	NP	-	-	-	-	-	-	-	100	98	68	31	14.8	silty SAND, light brown (SM)
50	19'	35.2	-	-	-	-	-	-	-	-	-	-	100	72	29	10.0	slightly silty SAND, light brown (SP-SM)
51	2'	1.6	-	-	-	-	-	-	-	100	99	96	93	50	19	5.8	slightly silty SAND, brown (SP-SM)
51	5'	6.0	NW	NP	-	-	-	-	-	100	99	98	96	85	66	38.5	silty SAND, brown (SM)
51	10'	23.6	28	5	-	-	-	-	-	-	-	-	100	99	98	85.7	sandy CLAY AND SILT, light brown (CL-ML)
51	15'	19.3	NW	NP	-	-	-	-	-	-	-	-	100	87	40	18.6	silty SAND, brown (SM)
51	19'	14.2	-	-	-	-	-	-	-	-	-	100	96	58	20	5.3	slightly silty SAND, brown (SP-SM)
52	Surface	11.6	NW	NP	-	-	-	-	-	-	-	-	100	96	82	68.8	sandy SILT, brown (ML)
52	1'	10.9	-	-	-	-	-	-	-	-	-	-	100	94	49	3.5	slightly silty SAND, light brown (SP)
52	8'	22.3	-	-	-	-	-	-	-	-	-	-	100	81	16	1.4	SAND, brown (SP)

Figure 34. Grain size data for boring RGL-8A2S-51.

Table 11. Hydraulic conductivity values used in the Albuquerque, NM, levee model.

Material	k_H (cm/sec)	k_H (ft/day)	k_V (cm/sec)	k_V (ft/day)
Levee sand	3.00×10^{-3}	8.50	3.00×10^{-3}	8.50
Levee silty sand	1.00×10^{-4}	0.283	1.00×10^{-4}	0.283
Blanket sandy silt	1.00×10^{-5}	0.0283	1.00×10^{-5}	0.0283
Aquifer silty sand	3.00×10^{-4}	0.850	3.00×10^{-4}	0.850
Aquifer sand	6.00×10^{-3}	17.0	6.00×10^{-3}	17.0
Toe drain	1.00×10^{-3}	2.83	1.00×10^{-3}	2.83
Pipe drain	1.00×10^{-2}	28.3	1.00×10^{-2}	28.3

Albuquerque soil density data are combined and summarized in Table 12 according to the shallow (2-, 4-, and 6-in.) and deep (8-, 10-, 12-in.) measurements. The shallow data are much more variable in Figures 40a to 40d (i.e., dry density, wet density, moisture content, and percent moisture, respectively) and tend to be lower than the deeper density data.

Subsets of the Albuquerque data include shallow and deep measurements from only the levee in Table 13. Levee data are presented according to their depth and distance from the crest in Figures 41a to 41d. Similarly, data obtained only from the floodplain are summarized in Table 14 and according to their depth and distance from an arbitrary origin in Figures 42a to 42d. Presentation of the wooded area measurements on the east side of the Rio Grande floodplain are summarized in Table 15 and by depth and distance from the origin (tree) for three measurement points (identified as 1 to 3) in Figures 43a to 43d. Data from the west levee at Site 2 include a wooded area beyond the levee toe and are summarized in Table 16 and according to depth and distance from the west levee crest in Figures 44a and 44d.

Examining all of the Albuquerque Troxler data in Table 12 and Figures 40a to 40d indicates the levees (no trees present on these levees) have the highest unit weights (both dry and wet), but the lowest moisture contents. Non-vegetated floodplain and forested soils have the lowest unit weights, but the highest moisture contents. The shallow soils data are the most variable in terms of their engineering properties, which is predictable considering the impacts and affects of the local micro-topography, bioturbation of the shallow soil column by organic processes (burrowing organisms), and sedimentation by water and wind.



Figure 35. Location map of Site 1 and Site 2, Albuquerque, NM.



Figure 36. Levee locations for Site 1 and Site 2, Albuquerque, NM.

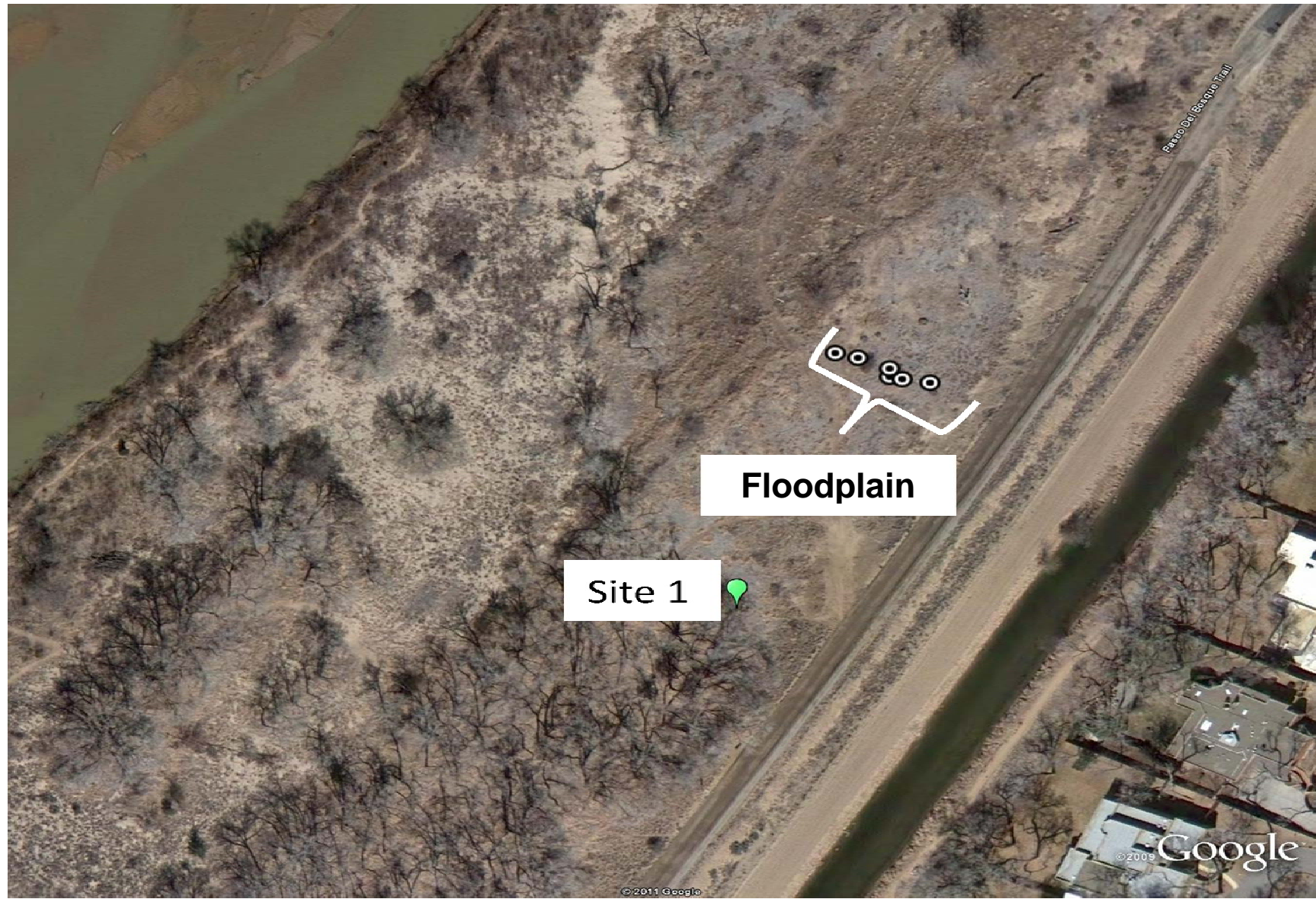


Figure 37. East levee at Site 1 showing the floodplain, Albuquerque, NM.

Figure 38. East levee at Site 1 showing the wooded area, Albuquerque, NM.



Figure 39. West levee at Site 2, Albuquerque, NM.

**Table 12. Statistical data for Troxler measurements in Albuquerque, NM:
2-, 4-, 6-, 8-, 10-, and 12-in.depths.**

Depth (2-4-6 in.)	Dry Density (lb/ft ³)	Wet Density (lb/ft ³)	Moisture Content (lb/ft ³)	Percent Moisture (%)
Max	104.6	111.1	12.4	20.0
Min	44.5	52.9	1.5	2.0
Mean	73.6	80.4	6.8	10.1
Median	73.8	80.2	7.2	10.2
Mode	#N/A	81.5	10.5	17.0
Standard Deviation	15.2	13.8	3.2	5.9
*#N/A: no central value in data set				

Depth (8-10-12 in.)	Dry Density (lb/ft ³)	Wet Density (lb/ft ³)	Moisture Content (lb/ft ³)	Percent Moisture (%)
Max	108.9	114.8	12.3	16.3
Min	64.1	73.1	2.1	2.3
Mean	83.9	91.1	7.2	9.1
Median	80.0	89.9	8.4	9.6
Mode	71.7	93.0	8.4	2.9
Standard Deviation	13.6	11.5	3.1	4.7
*#N/A: no central value in data set				

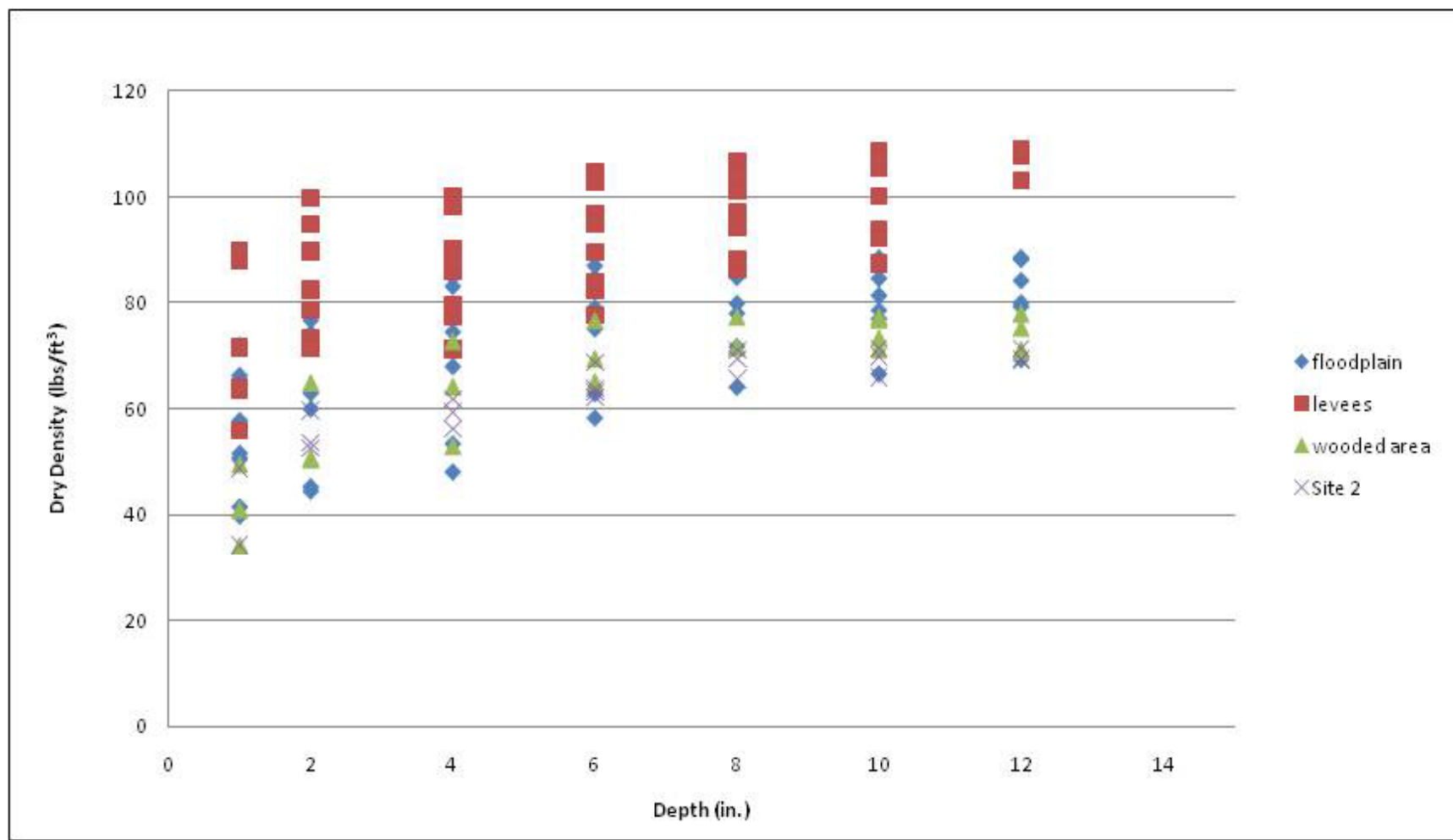


Figure 40a. Dry density (lb/ft^3) verses depth (in.) and distance (ft.) from Troxler measurements for, Site 1 and 2, Albuquerque, NM.

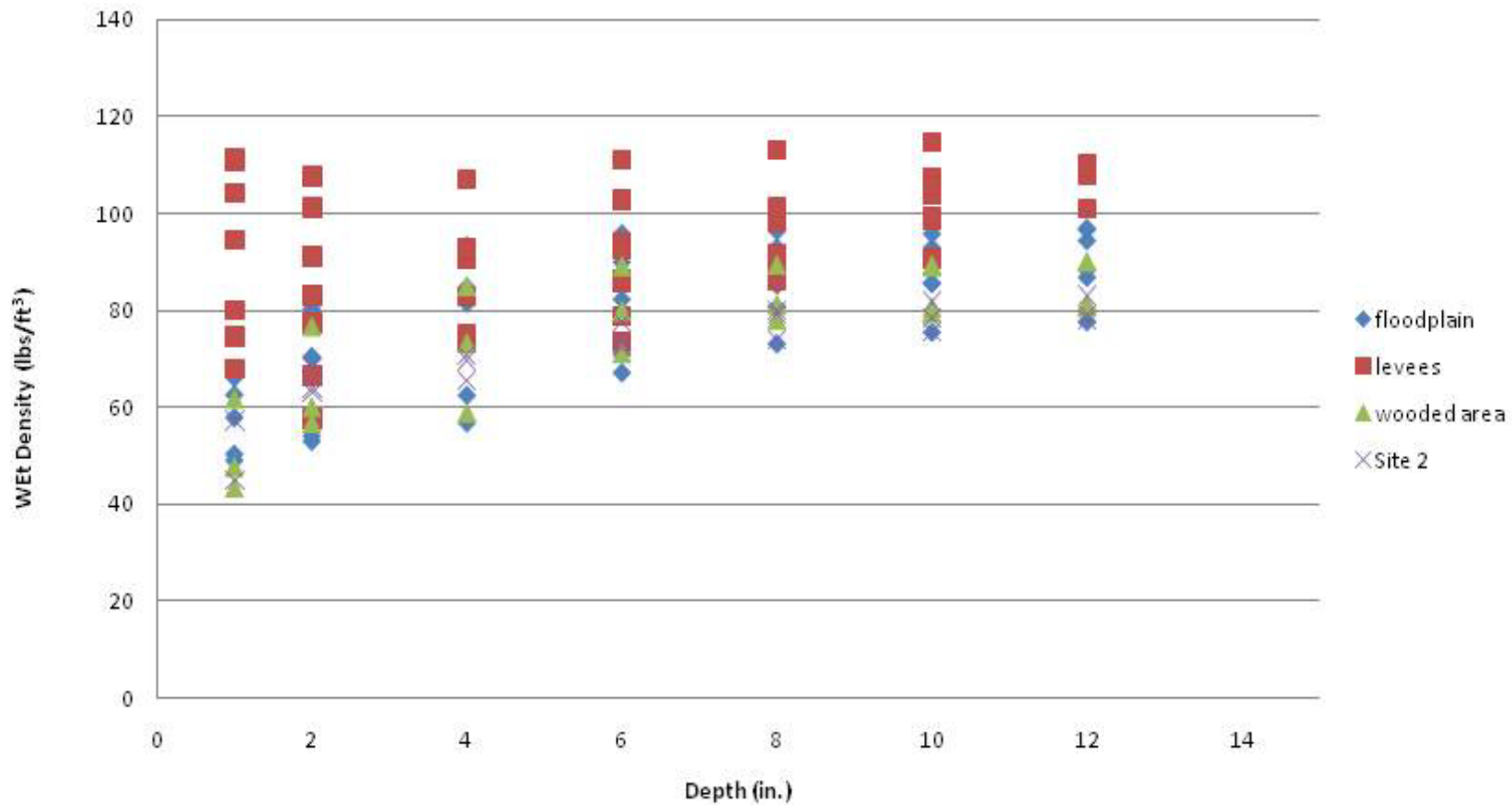


Figure 40b. Wet density (lb/ft³) versus depth (in.) and distance (ft.) from Troxler measurements for, Site 1 and 2, Albuquerque, NM.

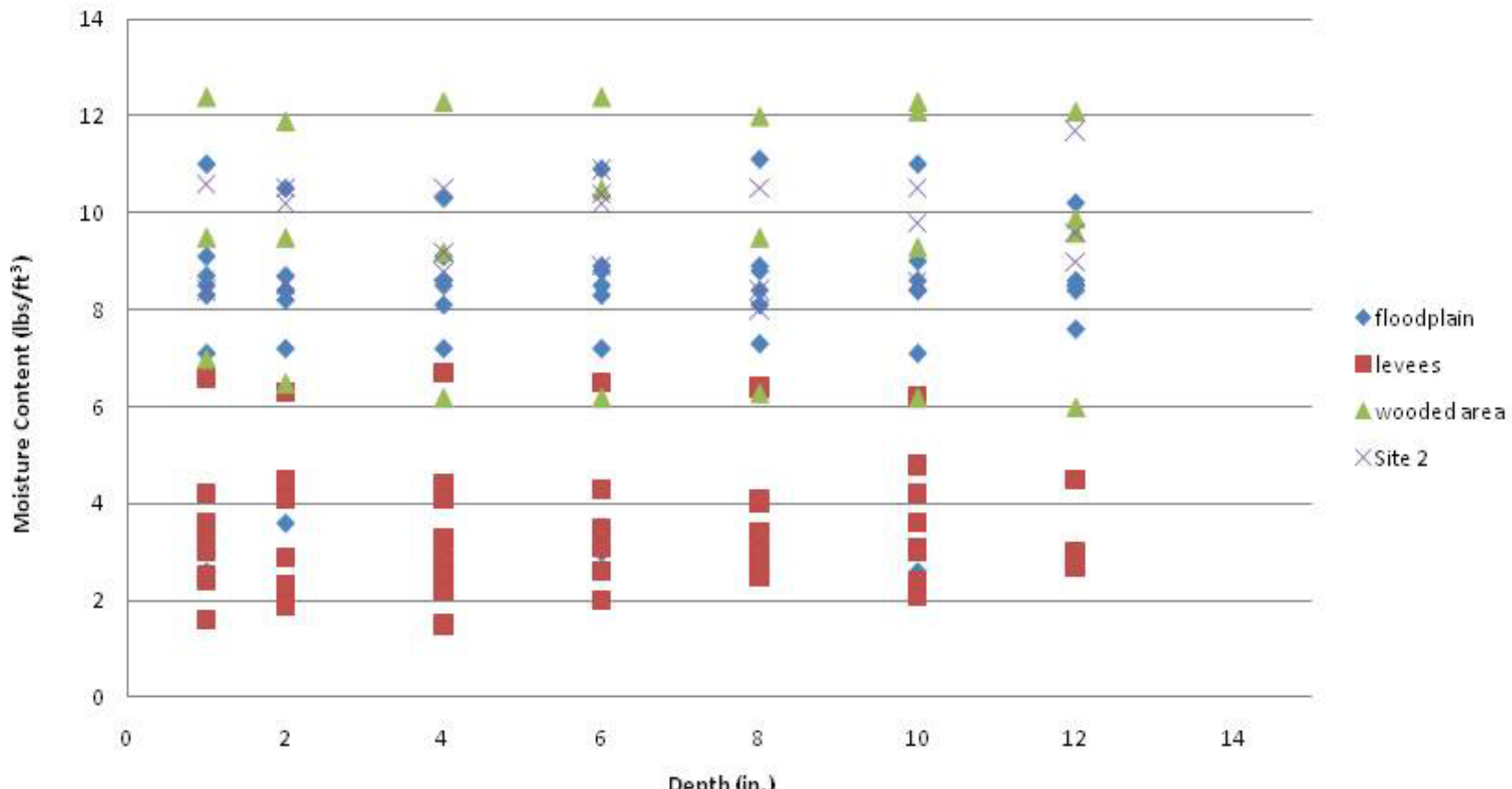


Figure 40c. Moisture content (lb/ft^3) versus depth (in.) and distance (ft.) from Troxler measurements for, Site 1 and 2, Albuquerque, NM.

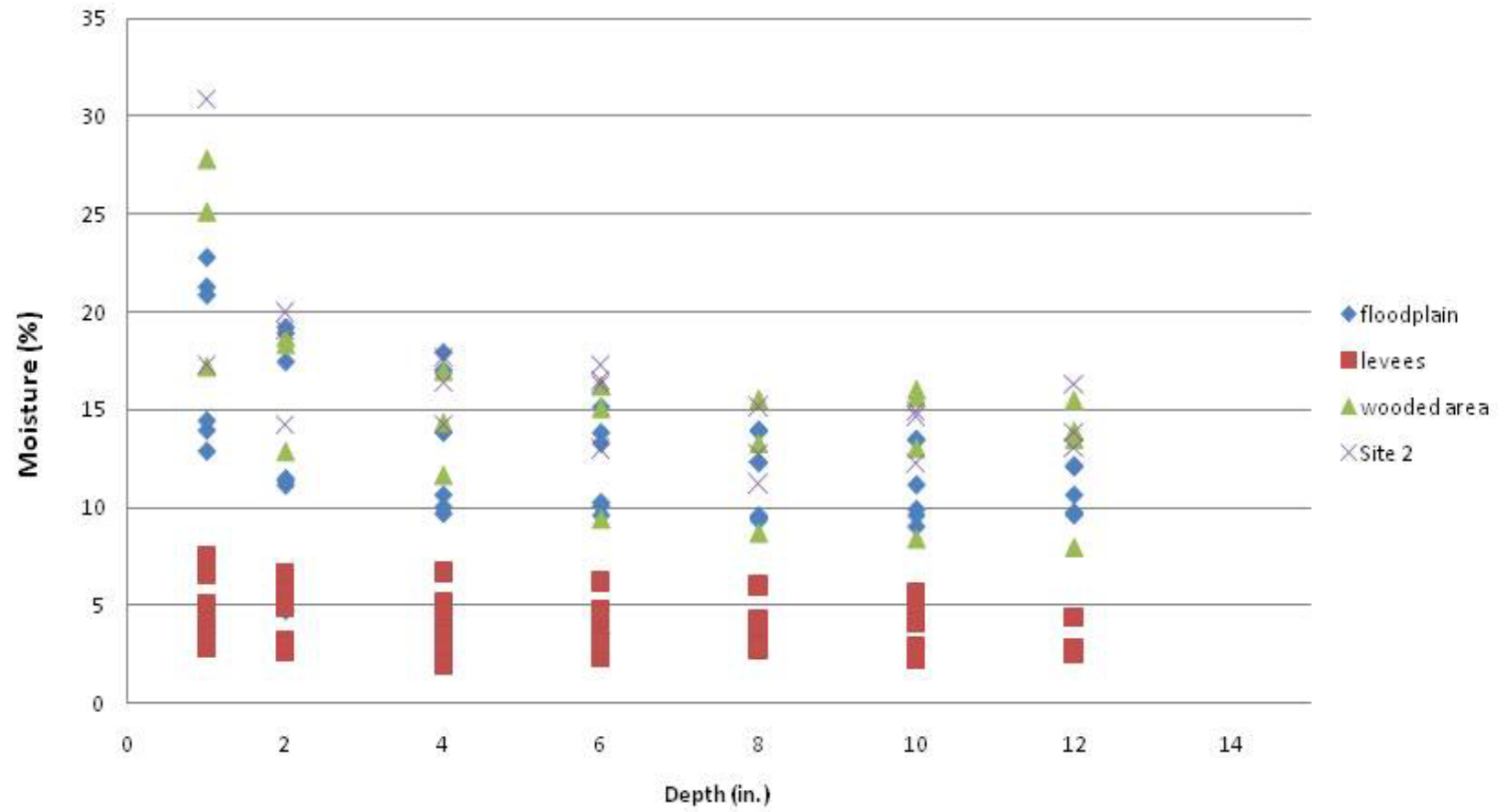


Figure 40d. Moisture (%) versus depth (in.) and distance (ft.) from Troxler measurements for Site 1 and 2, Albuquerque, NM.

Examination of the east and west side levee data in Table 13 and Figures 41a to 41d identifies the crest area as having the highest unit weights. The presence of the roadway on the crest likely contributes to these higher values. The general trend for moisture content is similar for both sides of the levee with the crest having the highest values, followed by the midslope and the toe. A comparison was made between the engineered and non-engineered (i.e., non-Federal agricultural levee) levees (Figure 36) and the engineered levees. The engineered levees have higher values of unit weight overall, but the measure values are not significantly greater.

Near surface floodplain values are the most variable in terms of their distribution (Table 14 and Figures 42a to 42d). Interestingly, the deeper (8- to 12-in.) values increase with closer proximity to the levee toe. Perhaps this increase may be due to a rise in elevation, or local geomorphic conditions due to seasonal sedimentation from wind and or flooding. Comparison of floodplain values (Table 14 and Figures 42a to 42d) to those obtained from the wooded area nearby (Table 15 and Figures 43a to 43d) indicates the unit weights for the floodplain area are slightly higher than the forested area. This trend is similar for the moisture content; with the non-vegetated floodplain soils having slightly higher values than from the forested area (see Tables 14 and 15; Figures 42d and 43d).

Measurements made along a profile on the west side of the Rio Grande at Site 2 from the levee crest to a vegetated area on the floodplain nearly 100 ft perpendicular to the crest, where a tree was present, are summarized in Table 16 and Figures 44a to 44d. Again, the near surface values (<8 in.) are the most variable in terms of their range for the unit weight (Figures 44a and 44b). The engineered levee embankment in this profile has the highest values for the unit weight as compared to the vegetated floodplain area (Figures 44a and 44b), but the lowest moisture content (Figures 44c and 44d).

The Albuquerque data indicate that levees without trees have higher values for unit weight than the non-vegetated floodplain and forested floodplain areas. Soils (i.e., silty sands) are similar for the three areas studied. In situ Troxler measurements for this geographic area indicate that areas that are devoid of woody vegetation have higher unit weights than the forested areas. Levee soils have measurably higher unit weight than other areas on the floodplain, including bare floodplain and forested areas.

**Table 13. Statistical data for Troxler measurements in Albuquerque, NM, transect on levees:
2-, 4-, 6-, 8-, 10-, and 12-in. depths.**

Depth (2-4-6 in.)	Dry Density (lb/ft ³)	Wet Density (lb/ft ³)	Moisture Content (lb/ft ³)	Percent Moisture (%)	Depth (8-10-12 in.)	Dry Density (lb/ft ³)	Wet Density (lb/ft ³)	Moisture Content (lb/ft ³)	Percent Moisture (%)
Max	104.6	111.1	6.7	6.7	Max	108.9	114.8	6.4	6.0
Min	71.2	73.7	1.5	2.0	Min	86.3	89.7	2.1	2.3
Mean	86.9	90.4	3.5	4.0	Mean	100.4	104.0	3.6	3.6
Median	86.7	91.1	3.2	3.8	Median	103.1	107.2	3.1	2.9
Mode	#N/A	101.2	4.1	#N/A	Mode	106.7	#N/A	3.0	2.9
Standard Deviation	10.5	11.2	1.4	1.4	Standard Deviation	7.9	8.1	1.2	1.2
*#N/A: no central value in data set					*#N/A: no central value in data set				

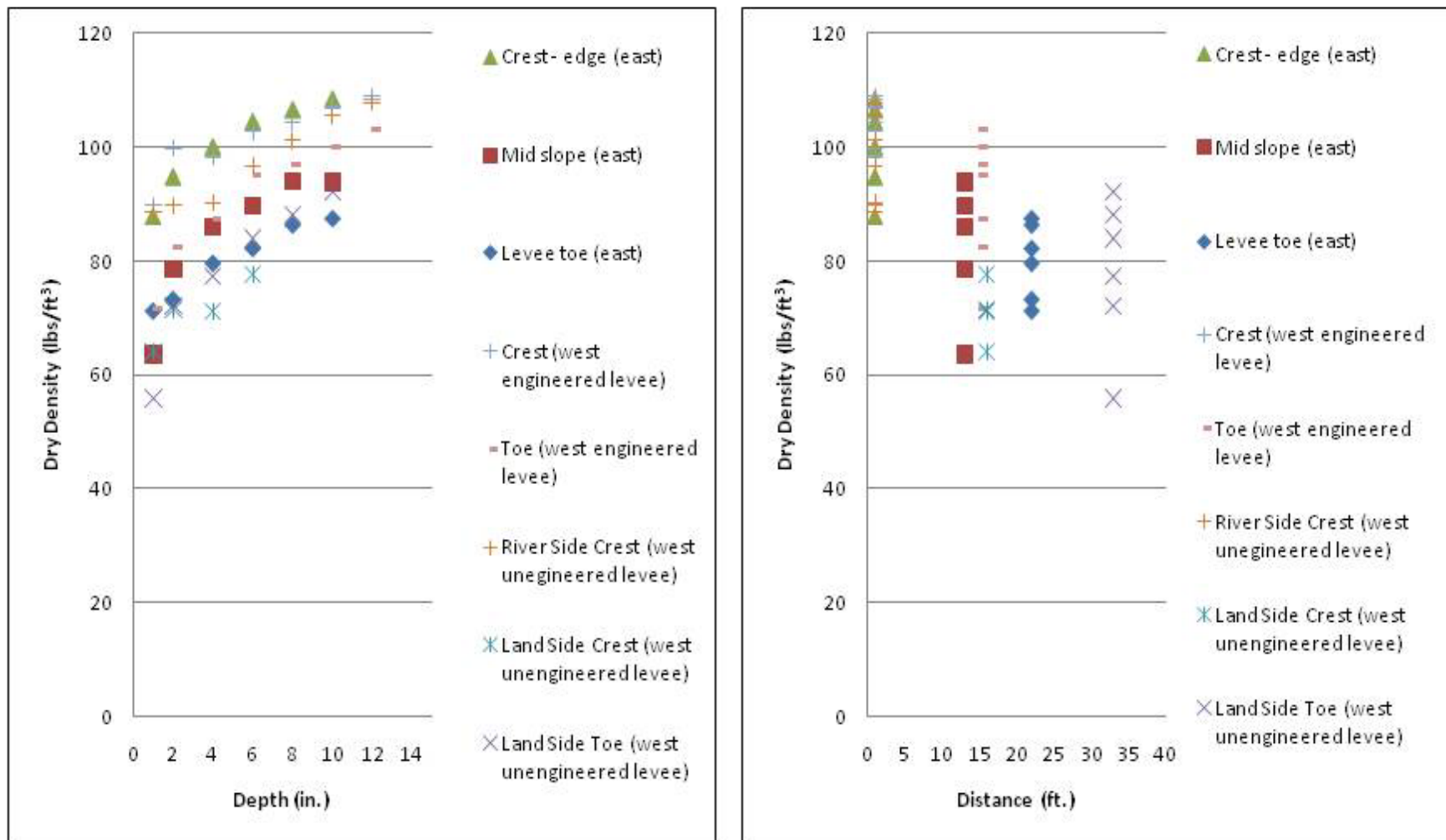


Figure 41a. Dry density (lb/ft³) versus depth (in.) and distance (ft.) from Troxler measurements for, all levees, Albuquerque, NM.

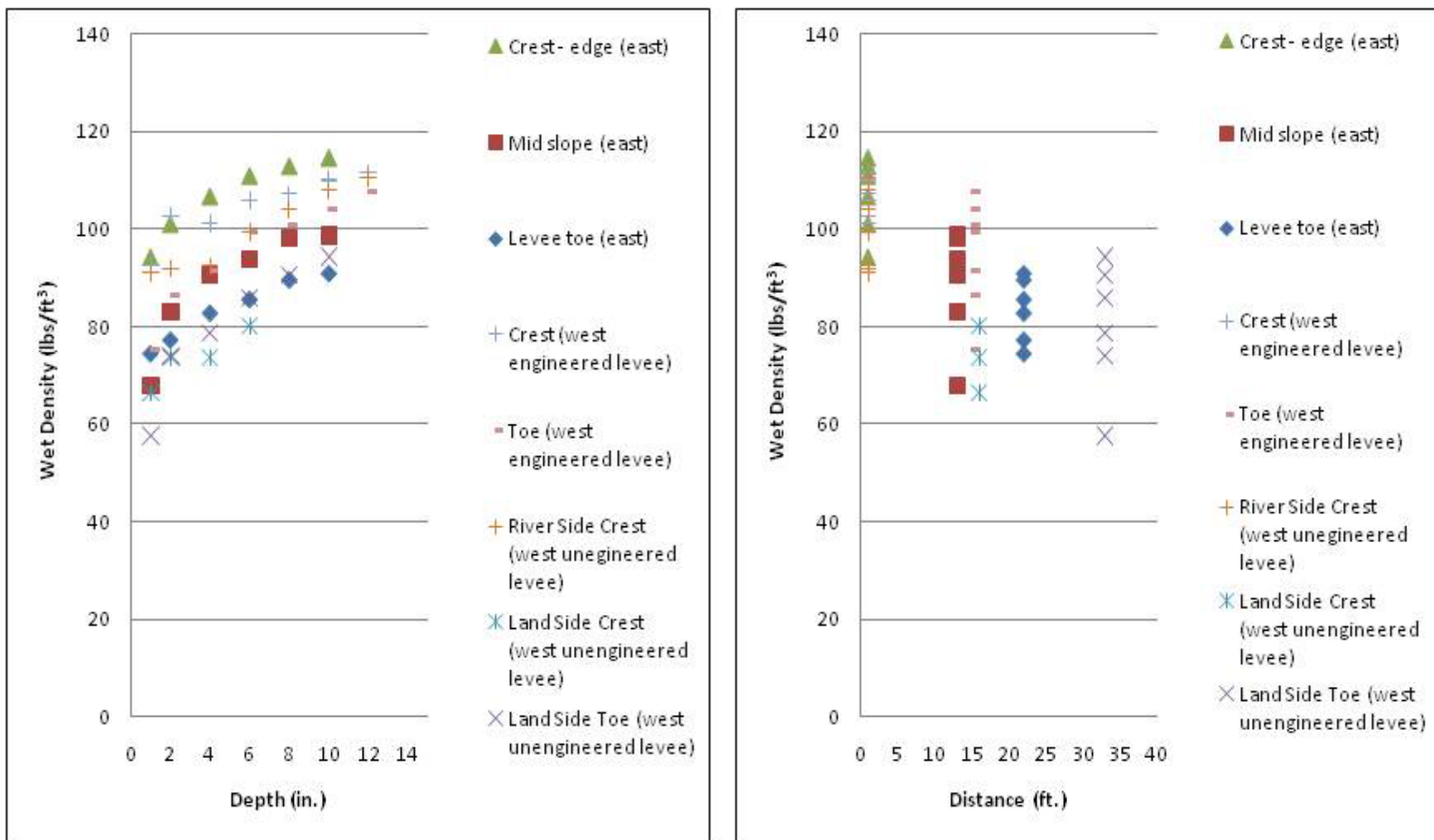


Figure 41b. Wet density (lb/ft³) verses depth (in.) and distance (ft.) from Troxler measurements for, all levees, Albuquerque, NM.

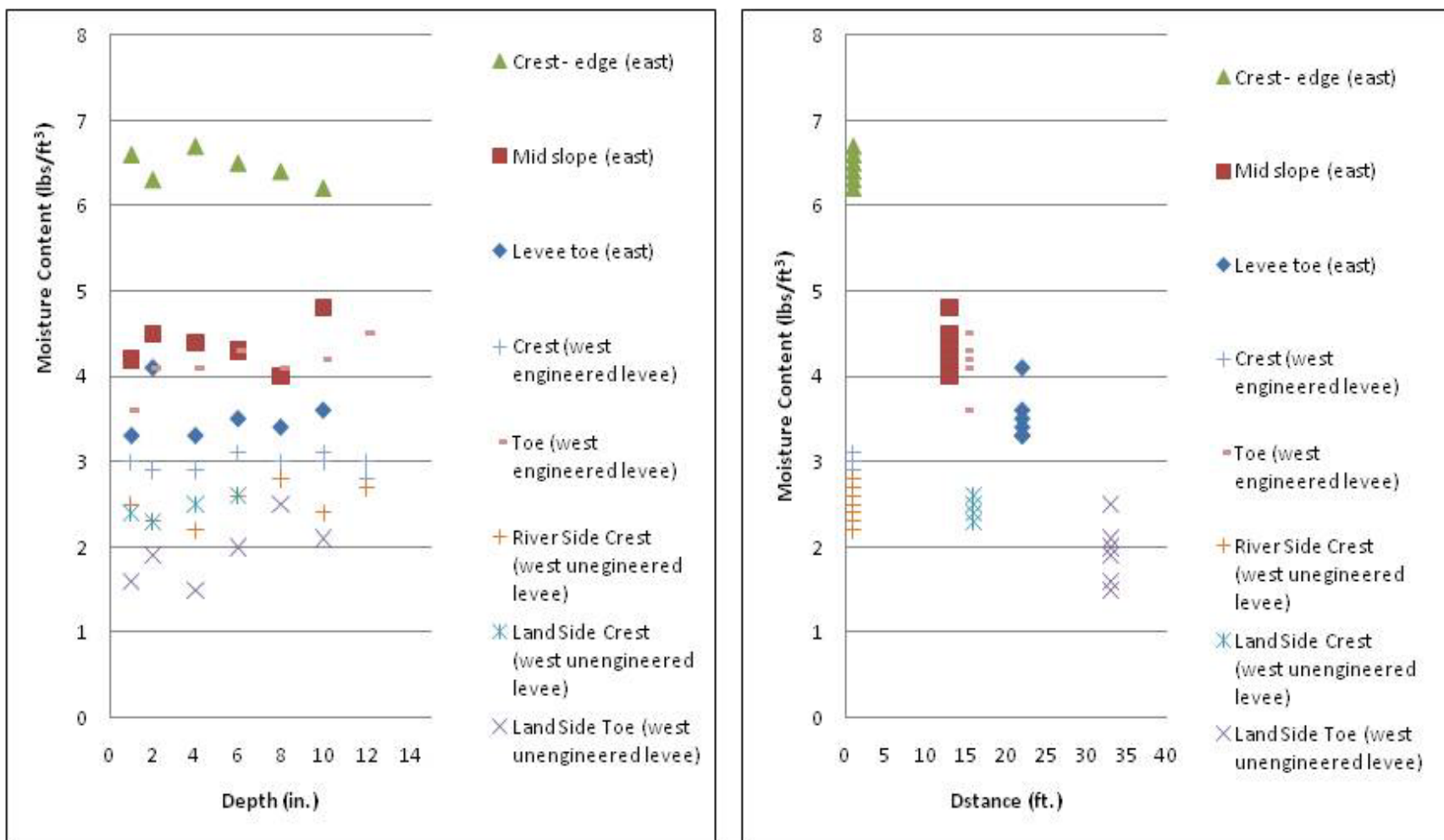


Figure 41c. Moisture content (lb/ft^3) verses depth (in.) and distance (ft.) from Troxler measurements for all levees, Albuquerque, NM.

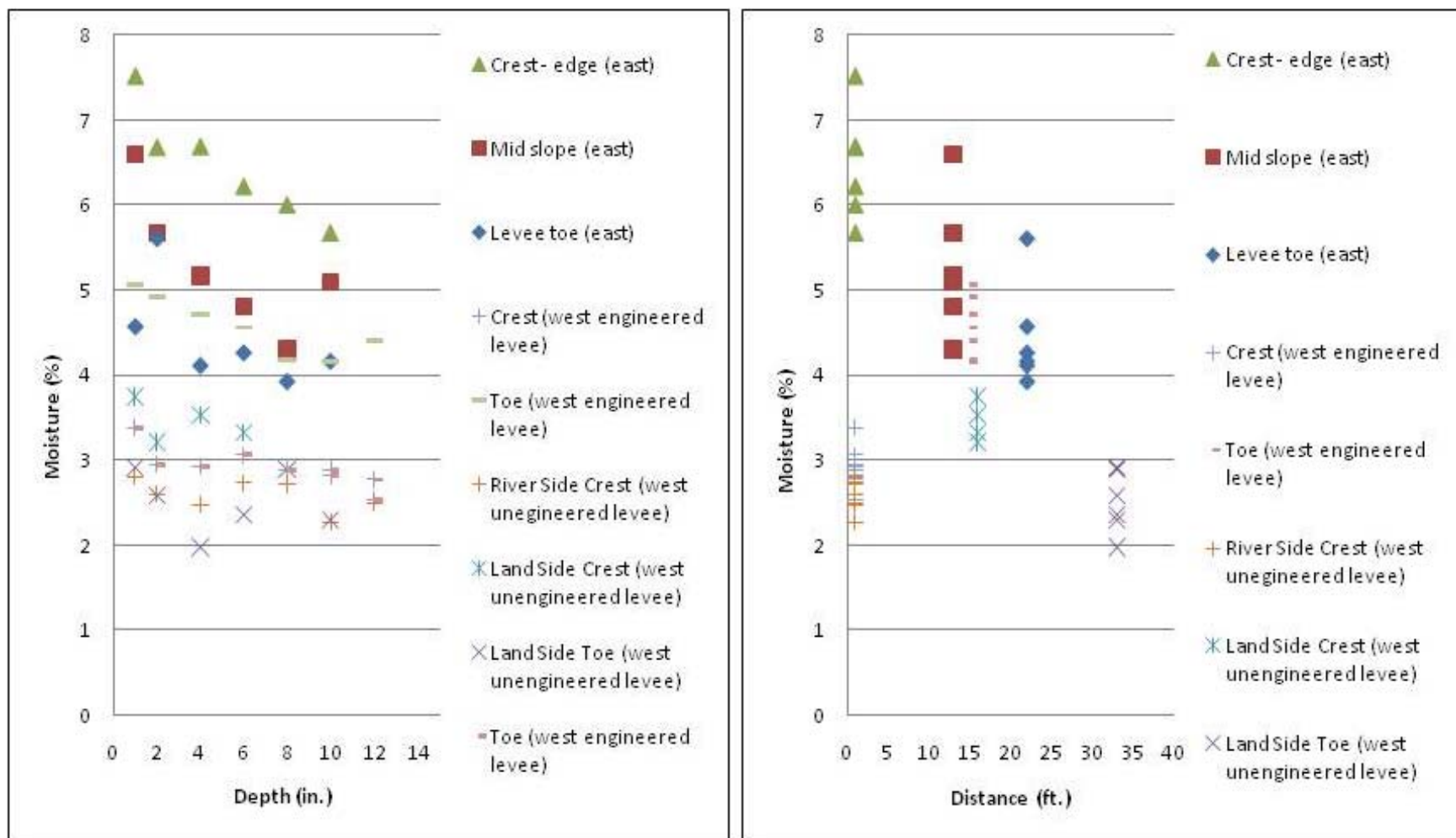


Figure 41d. Moisture (%) versus depth (in.) and distance (ft.) from Troxler measurements for, all levees, Albuquerque, NM.

Table 14. Statistical data for Troxler measurements in Albuquerque, NM, transect on floodplain 2-, 4-, 6-, 8-, 10-, and 12-in. depths.

Depth (2-4-6 in.)	Dry Density (lb/ft ³)	Wet Density (lb/ft ³)	Moisture Content (lb/ft ³)	Percent Moisture (%)	Depth (8-10-12 in.)	Dry Density (lb/ft ³)	Wet Density (lb/ft ³)	Moisture Content (lb/ft ³)	Percent Moisture (%)
Max	87.0	95.9	10.9	19.2	Max	88.5	97.0	11.1	14.0
Min	44.5	52.9	2.5	3.1	Min	64.1	73.1	2.6	3.0
Mean	69.4	77.3	7.9	12.0	Mean	80.4	88.5	8.1	10.3
Median	74.2	81.5	8.4	11.4	Median	80.7	90.5	8.5	9.8
Mode	#N/A	81.5	7.2	#N/A	Mode	88.2	93.0	8.4	13.5
Standard Deviation	13.6	13.2	2.2	4.7	Standard Deviation	7.5	7.2	2.1	2.9
*#N/A: no central value in data set					*#N/A: no central value in data set				

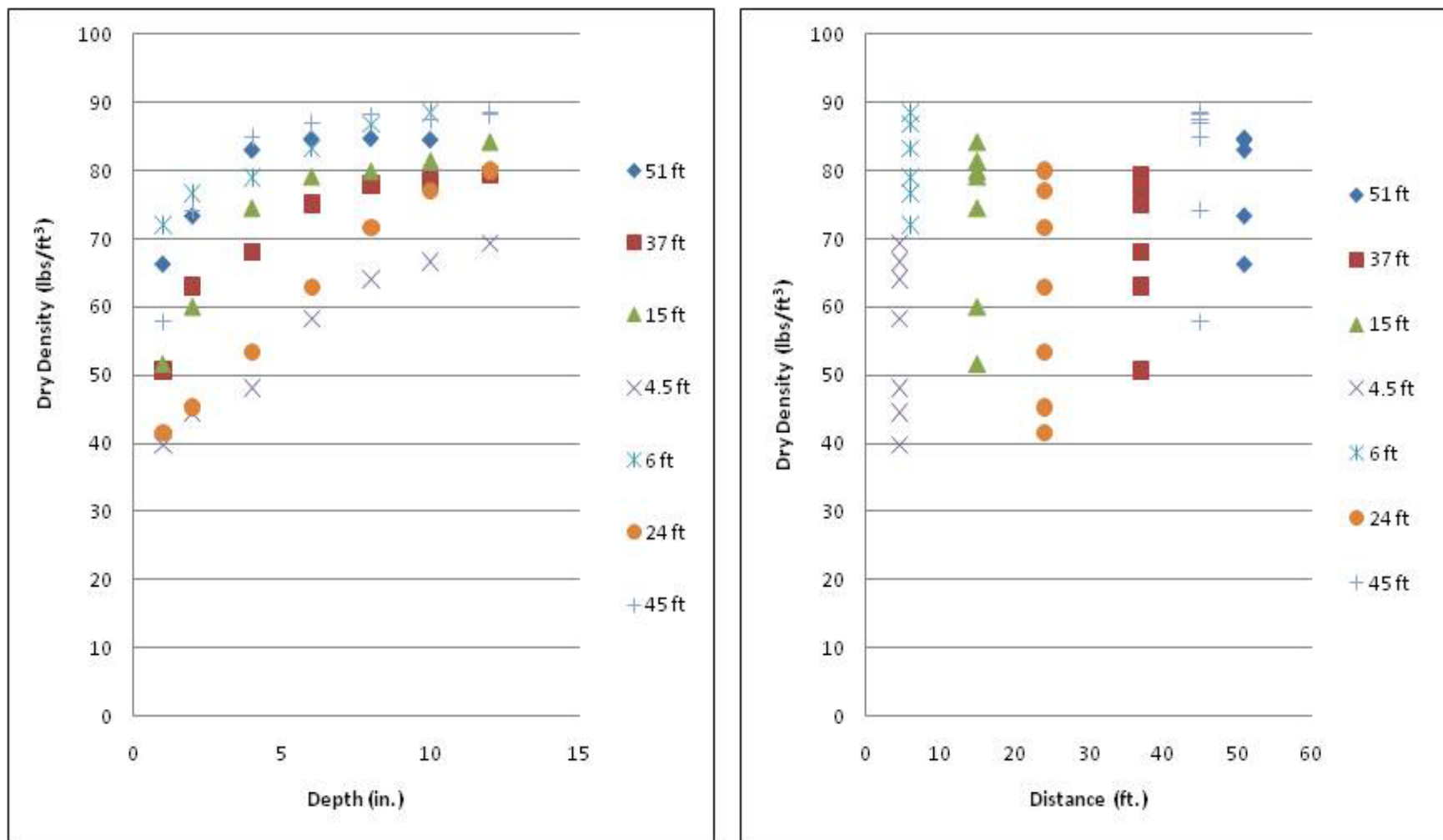


Figure 42a. Dry density (lb/ft^3) versus depth (in.) and distance (ft.) from Troxler measurements for, floodplain, Albuquerque, NM.

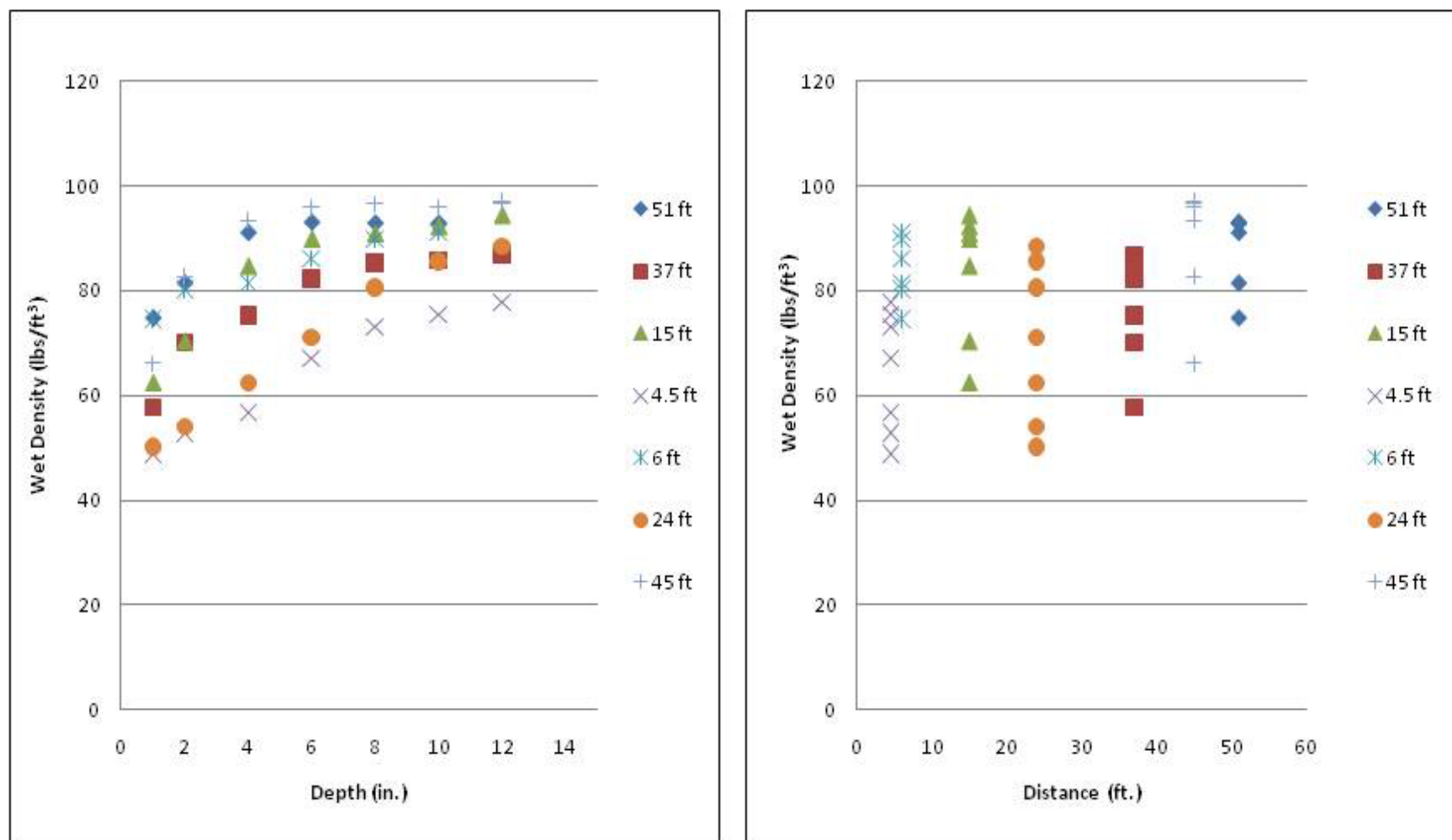


Figure 42b. Wet density (lb/ft^3) verses depth (in.) and distance (ft.) from Troxler measurements for, floodplain, Albuquerque, NM.

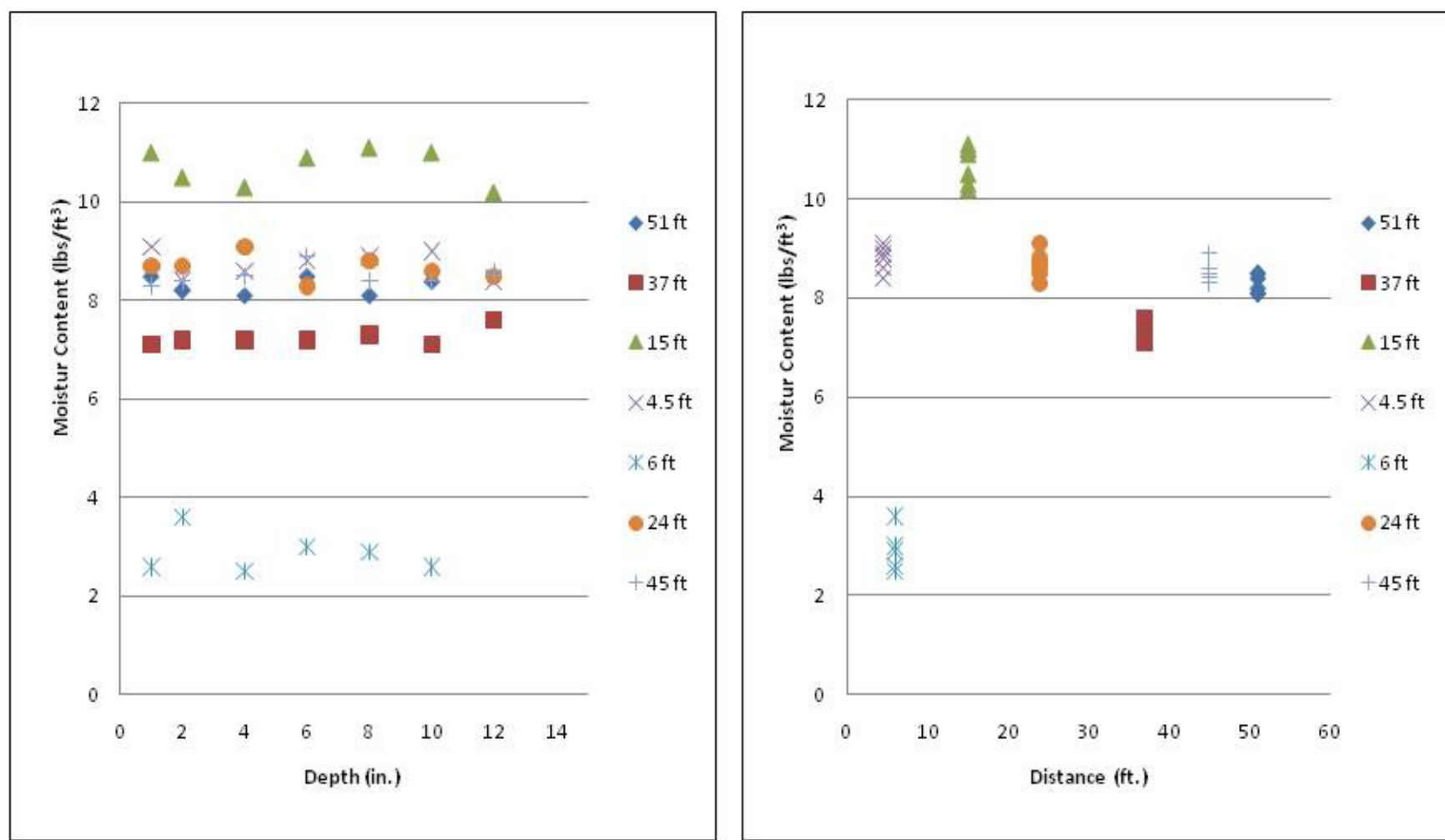


Figure 42c. Moisture content (lb/ft^3) versus depth (in.) and distance (ft.) from Troxler measurements for, floodplain, Albuquerque, NM.

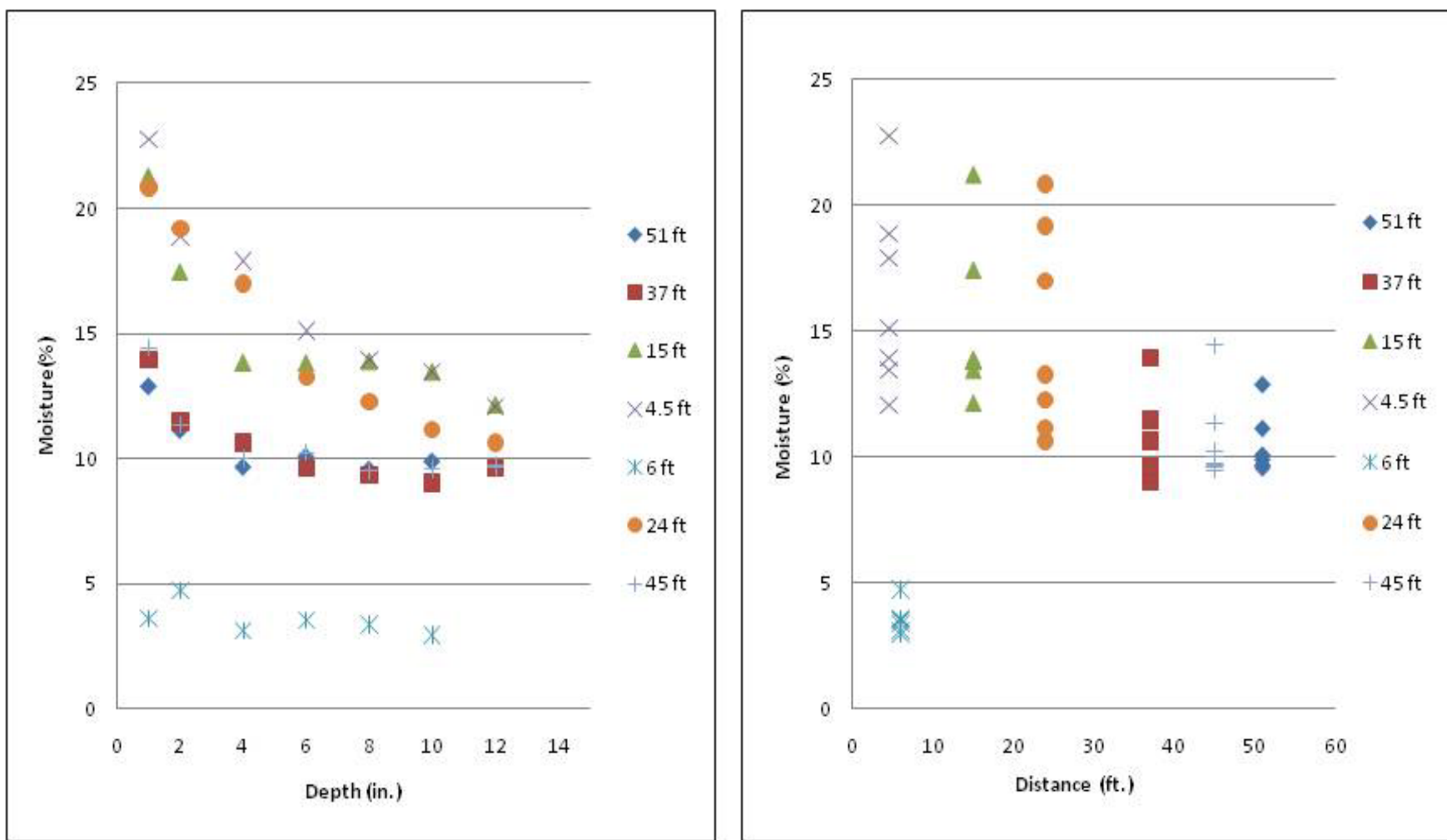


Figure 42d. Moisture (%) versus depth (in.) and distance (ft.) from Troxler measurements for, floodplain, Albuquerque, NM.

**Table 15. Statistical data for Troxler measurements in Albuquerque, NM, transect in wooded area:
2-, 4-, 6-, 8-, 10-, and 12-in. depths.**

Wooded Area Depth (2-4-6 in.)	Dry Density (lb/ft ³)	Wet Density (lb/ft ³)	Moisture Content (lb/ft ³)	Percent Moisture (%)	Wooded Area Depth (8-10-12 in.)	Dry Density (lb/ft ³)	Wet Density (lb/ft ³)	Moisture Content (lb/ft ³)	Percent Moisture (%)
Max	76.6	89.1	12.4	18.7	Max	77.9	90.0	12.3	16.0
Min	50.3	56.8	6.2	9.5	Min	70.8	78.0	6.0	8.0
Mean	62.9	72.3	9.4	14.9	Mean	74.0	83.6	9.6	12.9
Median	64.8	73.3	9.5	15.1	Median	73.3	81.1	9.6	13.5
Mode	#N/A	#N/A	6.2	#N/A	Mode	77.3	#N/A	12.1	#N/A
Standard Deviation	9.7	11.7	2.6	3.1	Standard Deviation	2.9	4.7	2.5	3.1
*#N/A: no central value in data set					*#N/A: no central value in data set				

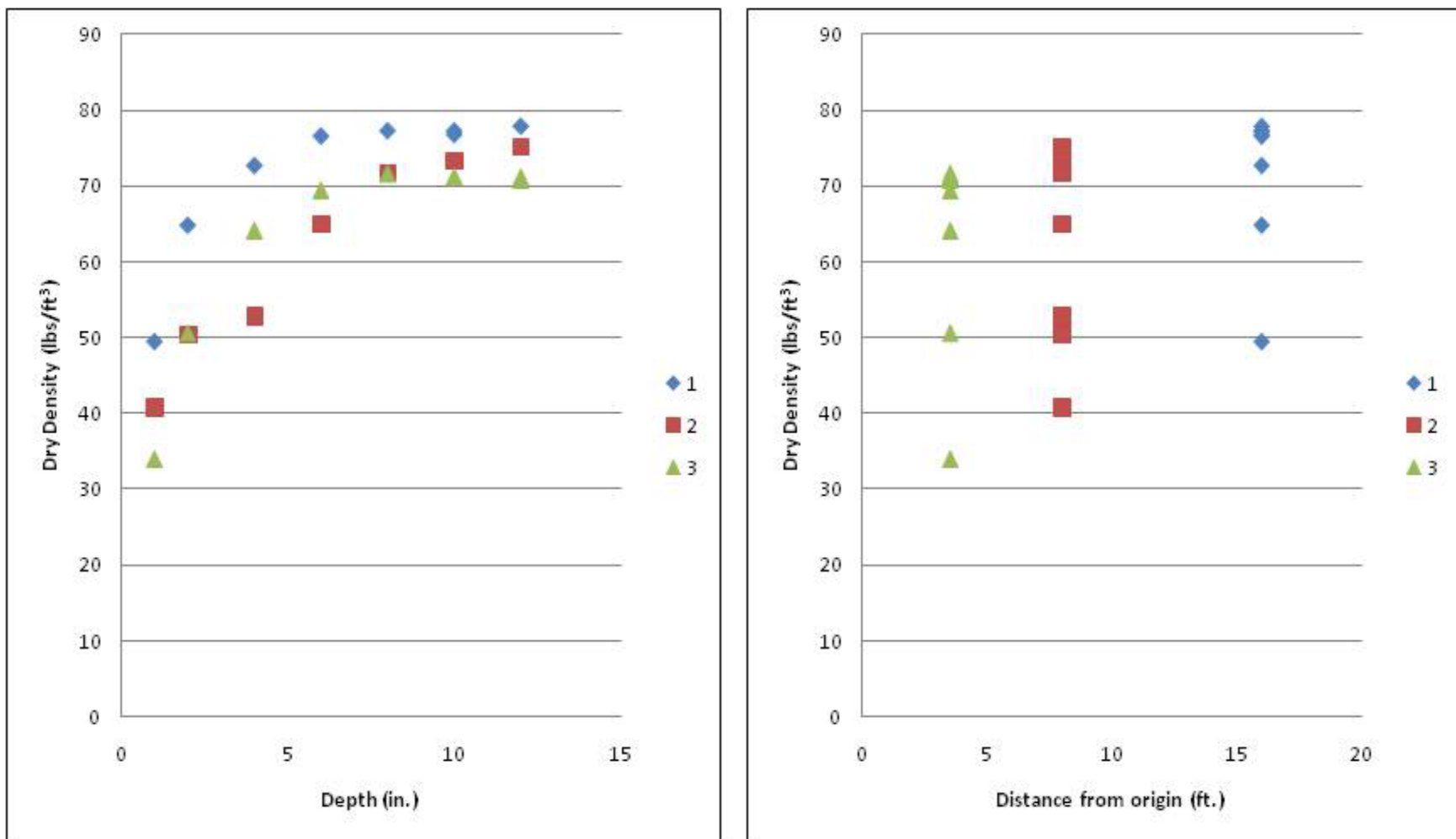


Figure 43a. Dry density (lb/ft³) versus depth (in.) and distance (ft.) from Troxler measurements for, wooded area, Albuquerque, NM.

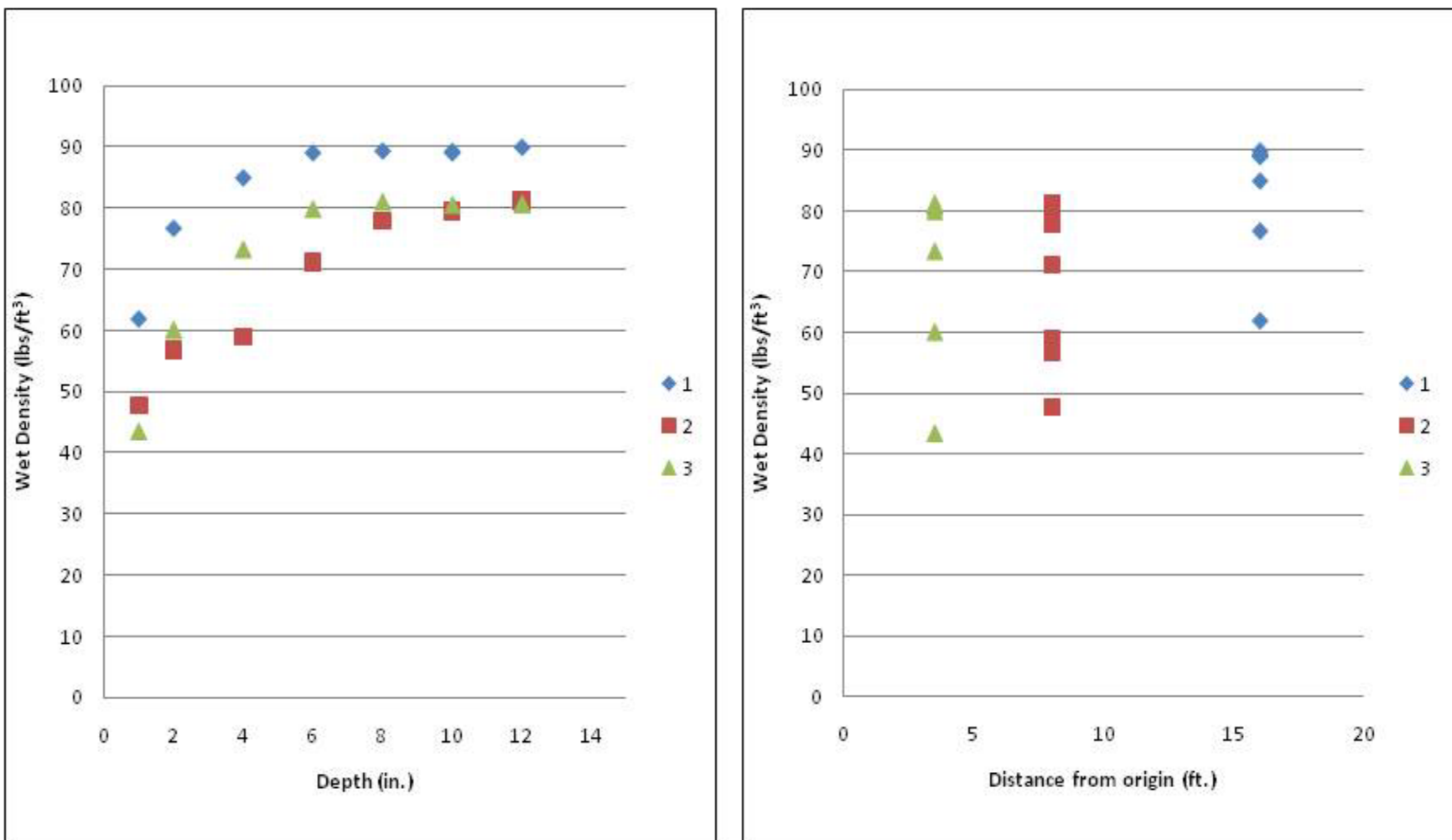


Figure 43b. Wet density (lb/ft^3) versus depth (in.) and distance (ft.) from Troxler measurements for, wooded area, Albuquerque, NM.

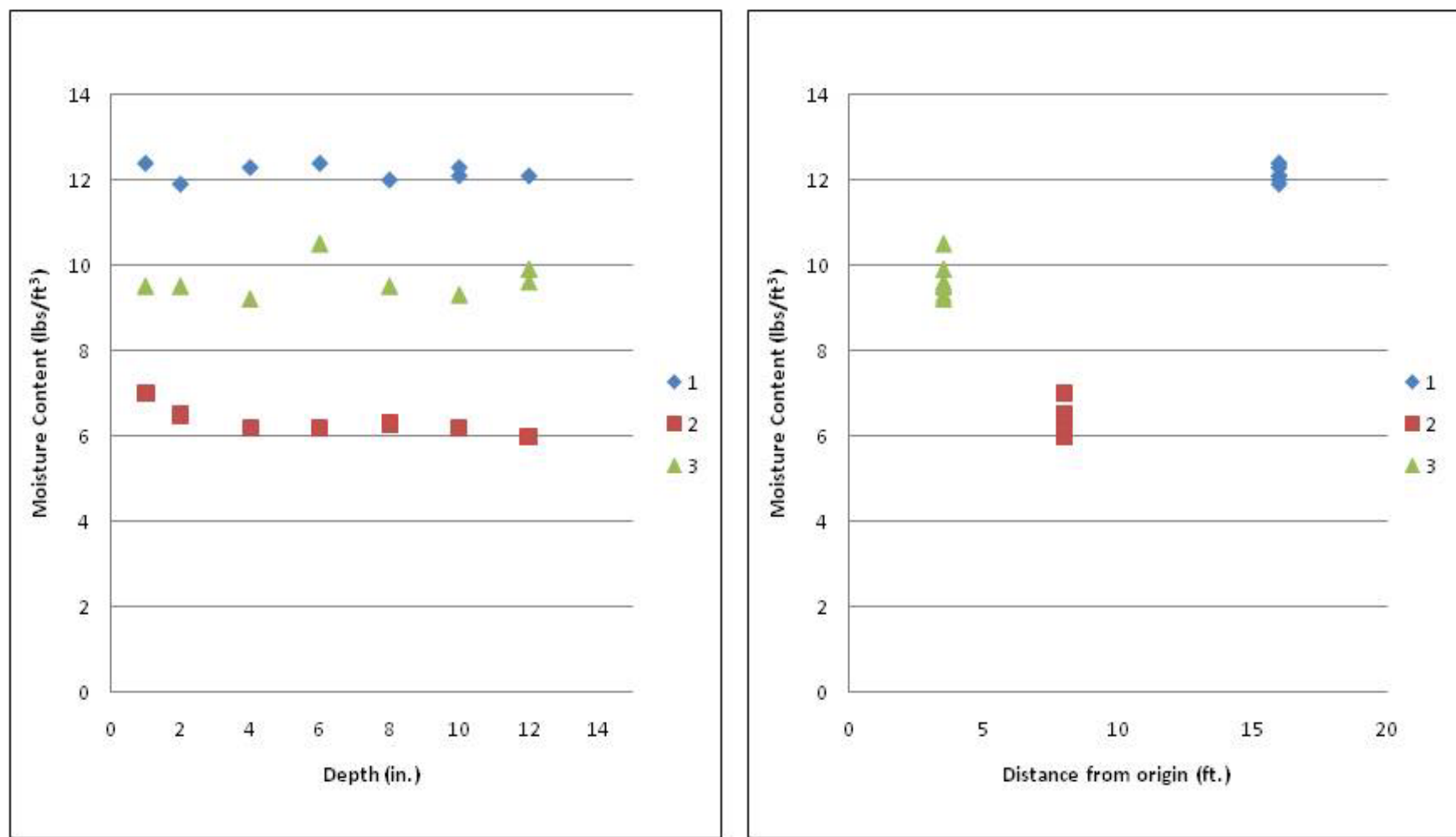


Figure 43c. Moisture content (lb/ft³) versus depth (in.) and distance (ft.) from Troxler measurements for, wooded area, Albuquerque, NM.

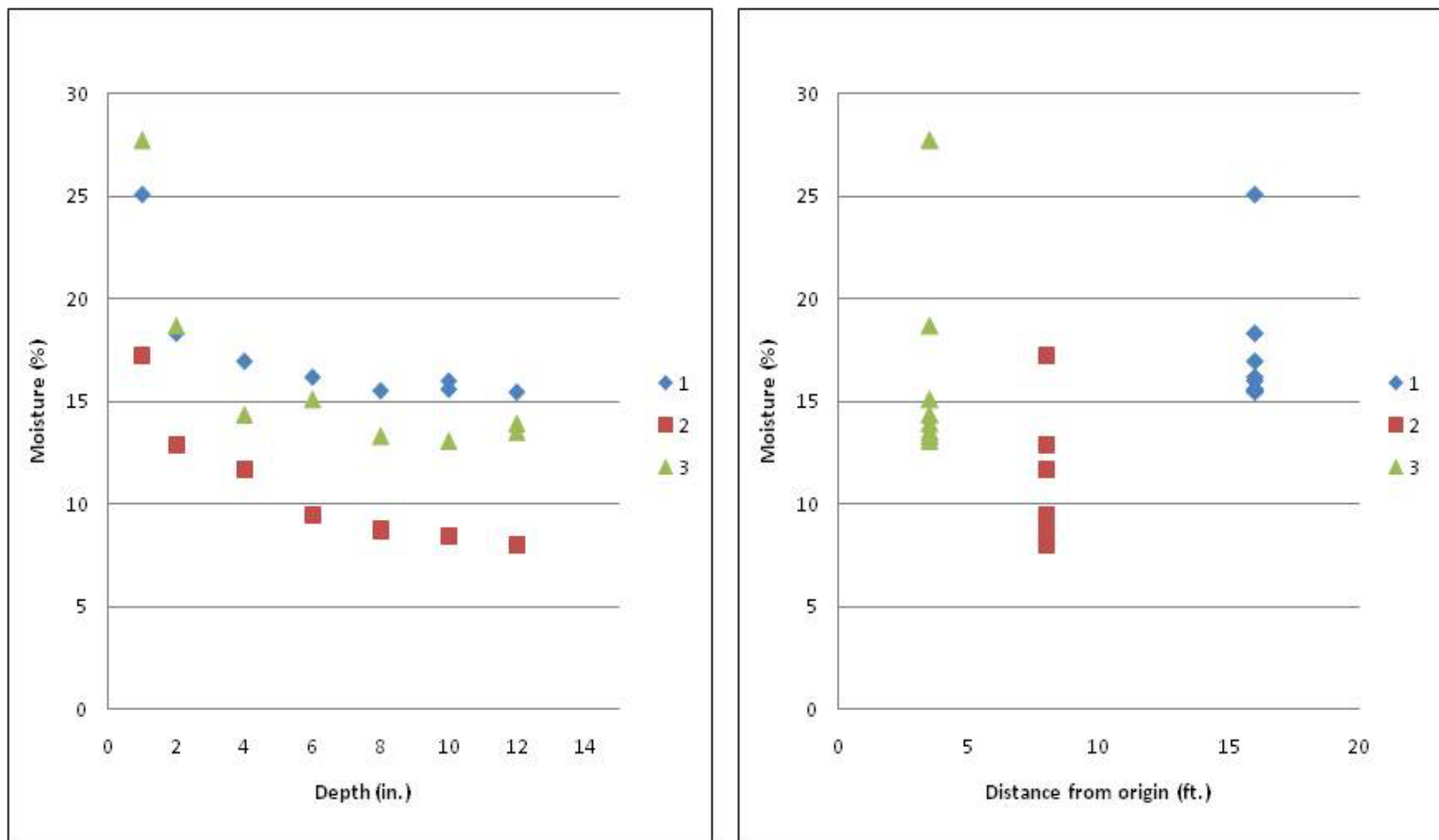


Figure 43d. Moisture (%) verses depth (in.) and distance (ft.) from Troxler measurements for, wooded area, Albuquerque, NM.

**Table 16. Statistical data for Troxler measurements in Albuquerque, NM, Site 2:
2-, 4-, 6-, 8-, 10-, and 12-in. depths.**

Site 2 Depth (2-4-6 in.)	Dry Density (lb/ft ³)	Wet Density (lb/ft ³)	Moisture Content (lb/ft ³)	Percent Moisture (%)	Site 2 Depth (8-10-12 in.)	Dry Density (lb/ft ³)	Wet Density (lb/ft ³)	Moisture Content (lb/ft ³)	Percent Moisture (%)
Max	102.7	105.9	10.9	20.0	Max	108.9	111.6	11.7	16.3
Min	52.6	63.1	2.9	2.9	Min	65.6	74.0	2.8	2.5
Mean	72.9	80.4	7.5	11.7	Mean	85.8	92.5	6.7	8.9
Median	63.4	74.1	8.9	14.2	Median	71.4	83.1	8.0	11.2
Mode	#N/A	#N/A	2.9	#N/A	Mode	69.5	79.1	3.0	#N/A
Standard Deviation	18.1	15.1	3.2	6.6	Standard Deviation	18.4	15.3	3.3	5.5
*#N/A: no central value in data set					*#N/A: no central value in data set				

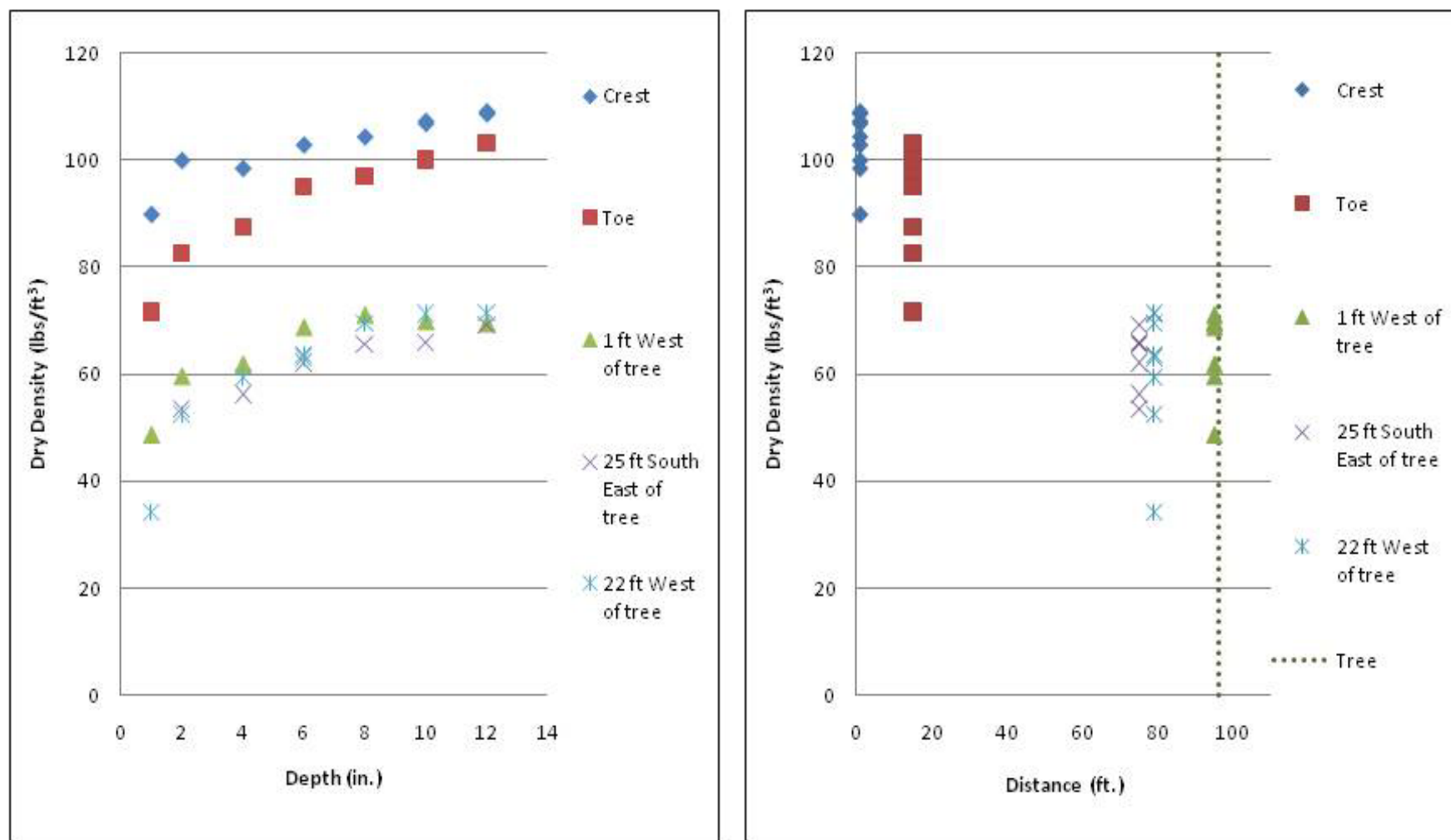


Figure 44a. Dry density (lb/ft³) versus depth (in.) and distance (ft.) from Troxler measurements for, west levee at site 2, Albuquerque, NM.

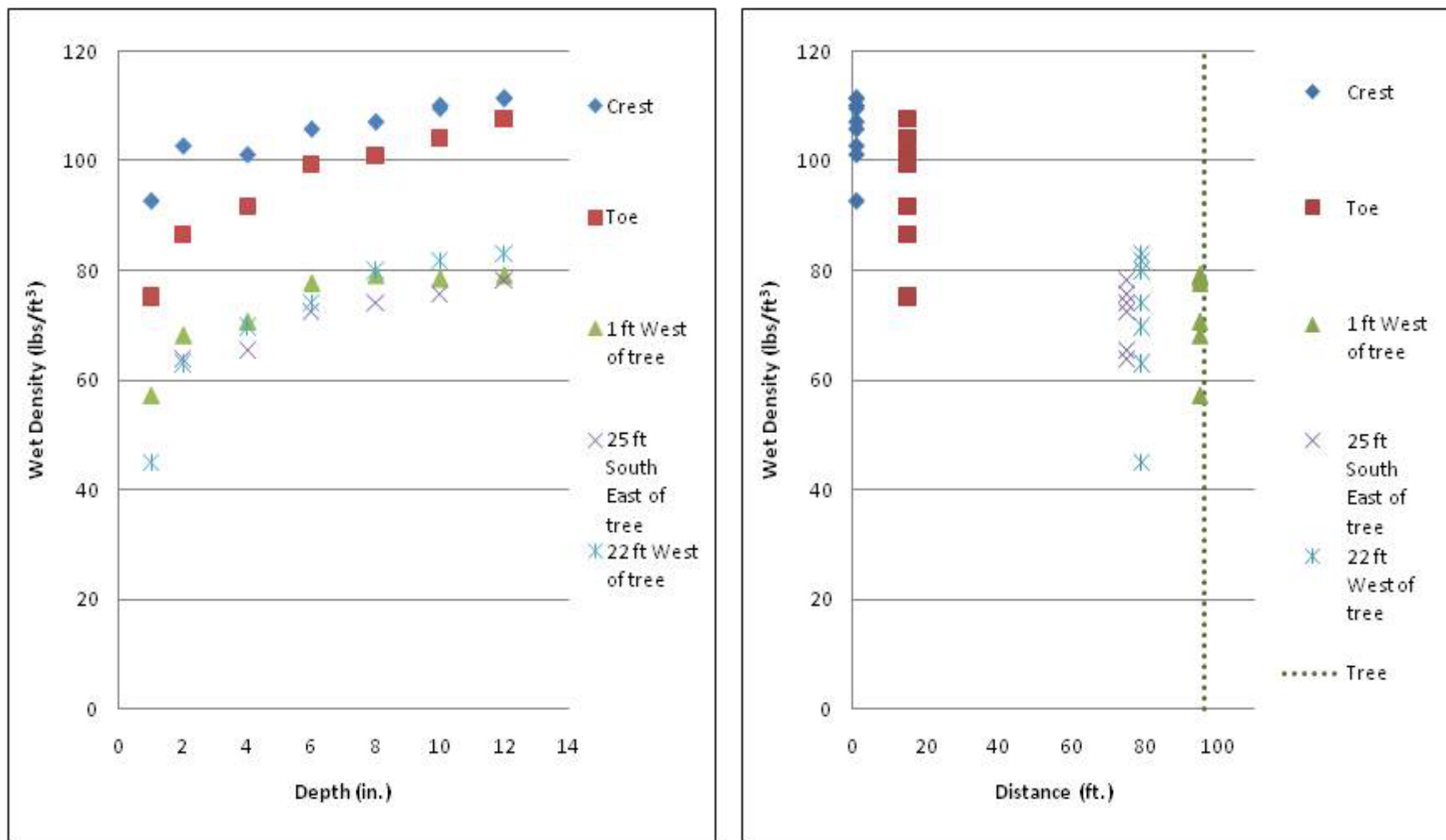


Figure 44b. Wet density (lb/ft³) versus depth (in.) and distance (ft.) from Troxler measurements for, west levee at site 2, Albuquerque, NM.

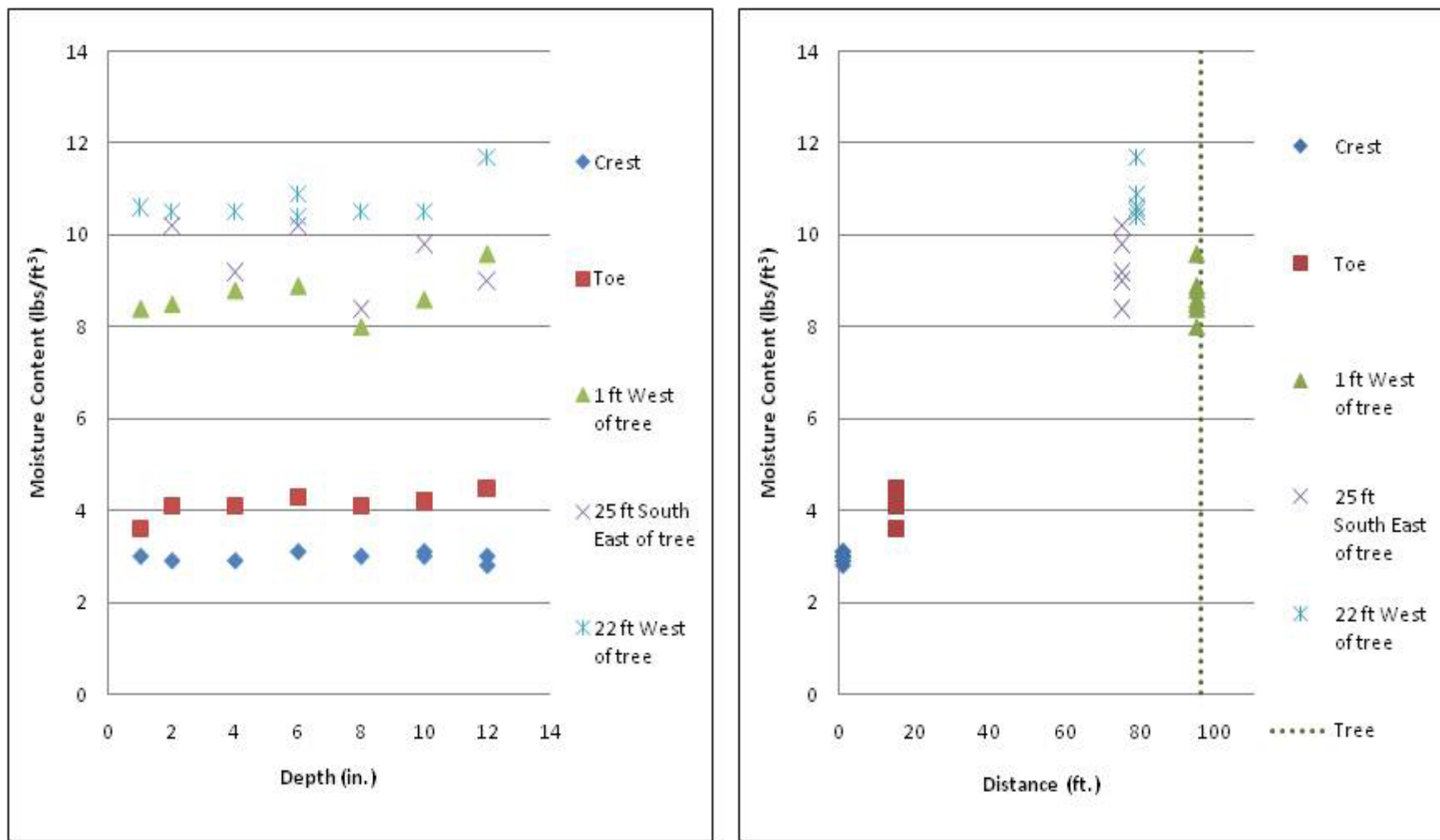


Figure 44c. Moisture content (lb/ft³) versus depth (in.) and distance (ft.) from Troxler measurements for, west levee at site 2, Albuquerque, NM.

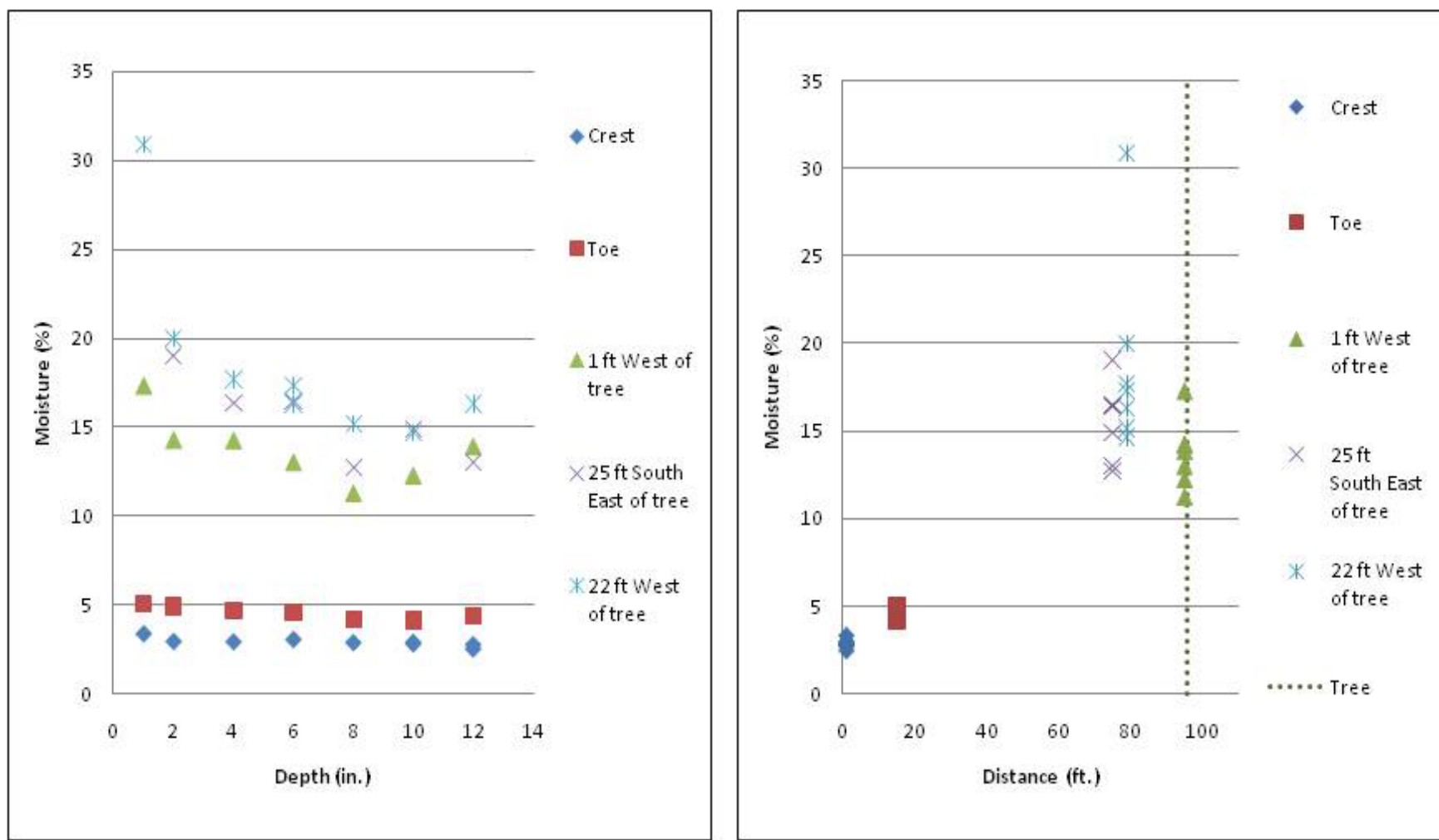


Figure 44d. Moisture (%) versus depth (in.) and distance (ft.) from Troxler measurements for, west levee at site 2, Albuquerque, NM.

Portland, OR

Introduction

The next site of interest is located in Portland, OR, adjacent to the Portland International Airport (Figure 45). The reach of river under study is located on the left bank of the Columbia River, at approximately RM 109. The levee is situated adjacent to NE Marine Drive. This road becomes part of the levee embankment east of the airport. The area examined does not include the roadway portion of the levee. This levee reach is under the jurisdiction of the Multnomah County Drainage District No. 1 (MCDD1) and the U.S. Army Engineer District, Portland.

Flood protection in the Portland area was built intermittently between the early 1900s and 1950s and is a combination of levees, canals, tide boxes, and pumping plants (USACE 2001). The MCDD1 was organized in 1917 and constructed the current flood protection system with assistance from the City of Portland and USACE. Nearly 100 federal, public, and private dams have been built on the Columbia River basin since 1930 for power generation, flood control, navigation, and irrigation. These dams have served to regulate the large magnitude floods that were once common during prehistoric times. Historical floods during the past century have resulted in various upgrades (new levees, increases in levee height, new pumps) to the flood protection system because various parts of the system performed poorly during major flood events.

The location that was selected for study is fairly typical of the levees along the Columbia River reach. An important consideration for selecting a study area was the availability of geotechnical data to characterize this site. This levee reach was also the focus of a large-scale tree removal program between 2007 and 2008, which was well documented by the local levee district (Cornforth Consultants 2008). MCDD1 commissioned a comprehensive report on the stump and root removal activities from the levee, including maps, photographs, and descriptions of the trees, stumps, and roots. The Cornforth Consultants report provides detailed information about characteristics of the trees in this reach.



Figure 45. Google Earth image of the Portland study area, top photo shows the Willamette River converging with the Columbia River, bottom photo shows close-up and profile location (red box in top photo) (Google Earth 2010).

Previous studies

In addition to the comprehensive tree removal study by Cornforth Consultants (2008), a geotechnical study was performed as part of a comprehensive seismic evaluation by USACE and the MCDD1 (USACE 2001; Dickenson et al. 2000). Oregon State University (OSU) geotechnical engineers specializing in earthquakes and familiar with the soils and geology from this region did the geotechnical evaluation of the study reach for the USACE and MCDD 1 (Dickenson et al. 2000). The study by OSU included additional geotechnical borings and subsequent laboratory tests of levee and foundation soils.

The OSU study assessed the impacts of flooding concurrent with a large magnitude earthquake, possibly damaging the levee system, which protects important infrastructure. It is noteworthy that USACE policy normally does not consider earthquake loading in levee design, as the risk of both a maximum flood and large magnitude earthquake occurring simultaneously is considered extremely remote (USACE 2000).

Additionally, most flood control levees do not ordinarily hold a permanent pool, which then requires a seismic evaluation for liquefaction potential (USACE 1995). The earthquake evaluation found that under a 100-year flood event, the levee system could withstand damage from a major earthquake with a magnitude of 7 on the moment magnitude scale (M_w), thereby preventing complete levee failure and flooding.

Geological setting

The geology of the study area has been mapped in detail at the 7-1/2-min scale (1:24,000) by the Oregon Department of Geology and Mineral Resources. The study area is presented on geological and seismic hazard maps for the Portland and Mount Tabor 7-1/2-min quadrangles (Beeson et al. 1991; Mabey et al. 1993 a,b,c; 1995). The Columbia and Willamette rivers converge approximately 7 miles downstream of the study area and have shaped the geology of this area during the Quaternary.

The study site is located within a tectonically-controlled, fault-bounded valley, filled with Quaternary alluvial and outwash deposits derived from the melting of nearby continental and alpine glaciers during the Pleistocene Epoch (2.5 million years to 12,000 years BP) and the early Holocene Epoch (10,000 years BP). The Columbia River through the study area was a major drainage way for glacial melt water during the Pleistocene. The current river

system consists of a series of large in-channel lateral sand and gravel bars that form prominent islands within the valley of the Columbia River. Many of these islands have been settled since the 1900s, especially following the construction of various large flood control and power generation dams on the upper Columbia River during the 1930s. These dams, in conjunction with levee construction, have regulated river flows and permitted extensive settlement of the protected floodplain in this area.

The left bank of the river in the vicinity of the study area has been mapped as Quaternary alluvium (Qal) and catastrophic flood deposits [Qtch (channel), Otf (fine-grained), and Otc (coarse grained)] as shown by Figure 46 (Beeson 1991). The presence of an older terrace (i.e., catastrophic floodplain deposits (i.e., Qtch, Otf, and Otc) separating the Columbia and Willamette rivers and relic sloughs still visible within the protected floodplain deposits indicates prehistoric and historic river flows were mainly a braided regime (i.e., anastamosing river channels), with high flows and rapid channel migration through the narrow Columbia River Valley in response to glacial and spring snowmelt from the nearby mountains. These conditions were responsible for deposition of in-channel sand and gravel bars, which are separated by relic sloughs (old channels), and low lying lakes filled with organic sediments.

Levee failure mechanisms

The primary failure mechanisms for this reach are similar to those previously described for point bar deposits earlier in this volume for the PA in Sacramento, CA. As the sediments are primarily coarse grained, failure mechanisms for this site include loss of embankment soils because of levee through-seepage and piping, underseepage within the pervious foundation and piping of foundation soils, and slope stability type failures from geomorphic processes operating within the river channel itself (i.e., migration, scouring and resulting over steepened bank slopes leading to shear and flow failures, rapid drawdown). However, because upstream dams regulate flood flows, the likelihood of channel related slope stability failures is greatly reduced.

Levee profiles

A representative levee profile was developed for this site using a combination of recent LiDAR elevation data for current ground surface conditions, bathymetry data from Columbia River, and hydraulic

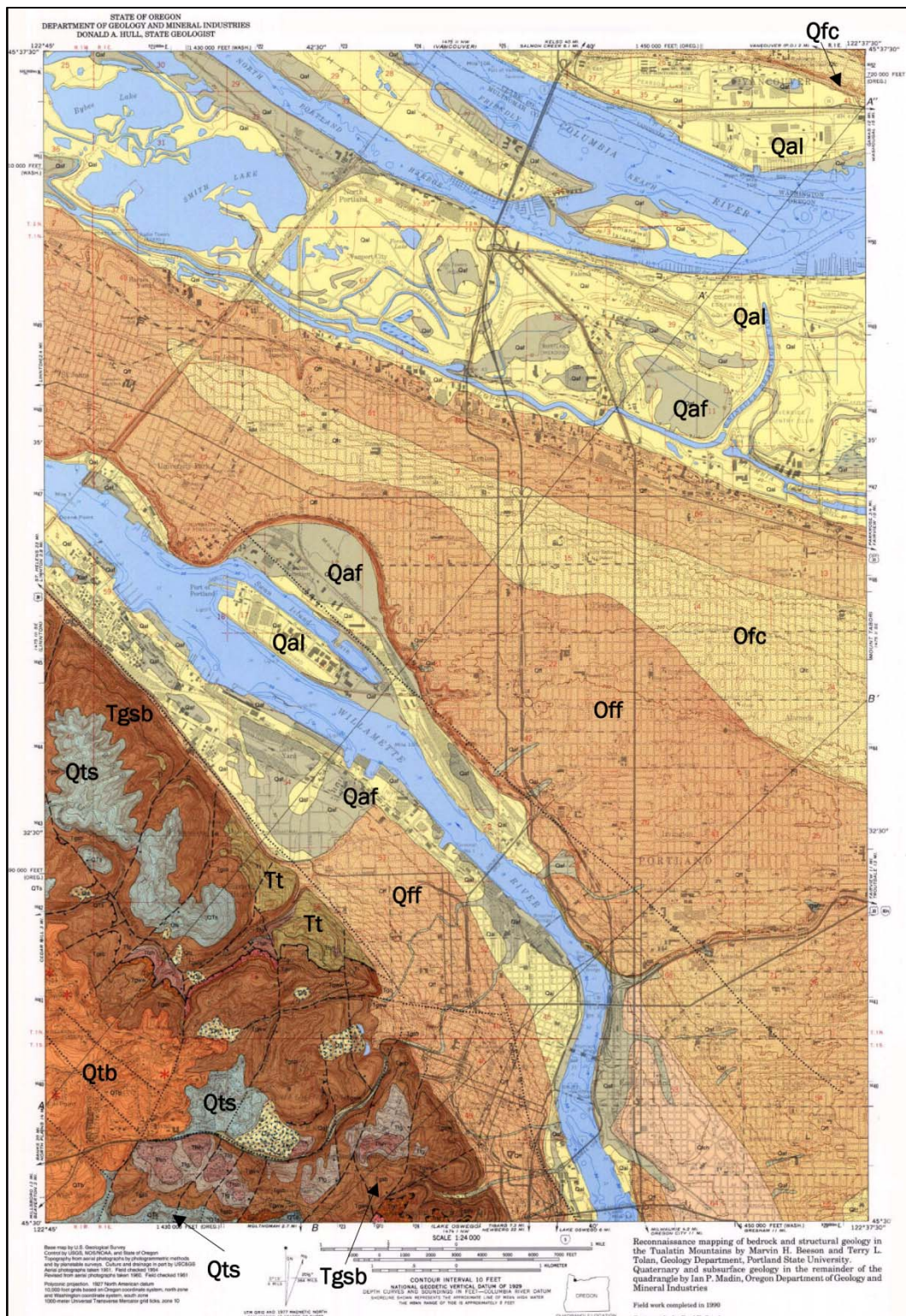


Figure 46a. Geologic map of the Portland Quadrangle (Beeson et al. 1991). The legend is presented in Figure 46b.

Legend			
Holocene			Pleistocene-Tertiary
Qal	Alluvium undifferentiated	Qtb	Boring Lava
Qaf	Artificial fill	Qts	Neogene Mudstone
		Tt	Troutdale Formation
Pleistocene			
Qff	Fine-grained facies	Tertiary	
Qfc	Coarse-grained facies	Tgsb	Sentinel Bluffs flow

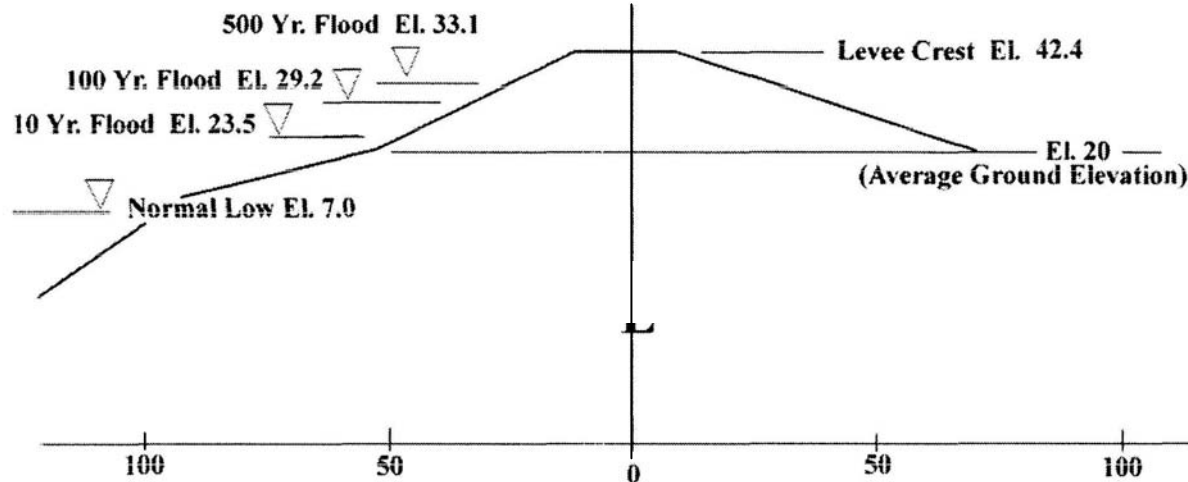
Figure 46b. Map legend for Figure 46a.

and geotechnical data derived from the earthquake evaluation for this reach (Dickenson et al. 2000; USACE 2001). LiDAR and bathymetry data were provided by USACE, Portland District. The profile that was developed corresponds to the location of Boring C-1 and Profile S-1 (Dickenson et al. 2000; USACE 2001). Levee slopes at Portland are 1V:3H. A typical profile from NE Marine Drive is presented in Figure 47. This profile was modified to reflect current site topography and bathymetric conditions using current survey data previously described and Google Earth imagery to obtain present surface conditions (Figure 45).

Laboratory soils data

The soils composing the levee embankment and foundation are identified in Figure 48 and are based on field boring logs, visual classification of soil samples, and laboratory soils testing conducted in the geotechnical report by Dickenson et al. (2000). The levee is composed of pervious sands. The foundation consists of a fine-grained top blanket and pervious substratum as shown by Figure 48. Selected soil samples were obtained from boring C-1 (i.e., levee embankment and foundation substratum) and other representative borings in this reach to classify and characterize the embankment and foundation soil layers identified in Figure 48.

The vertical distribution of soil texture at this location (Figure 48) is similar to point bar deposits observed at the Sacramento and Burlington sites. Braided stream deposits often develop a vertical profile similar to point bar deposits. A fining upward soil texture from coarse grained sands and gravels at the base of the channel environment to more fine-grained



Regulated Flood Elevations at NE Marine Drive

Risk	Flood Event	Elevation (feet NGVD)
0.10 (10%)	10-year	23.5
0.02 (2%)	50-year	27.3
0.01 (1%)	100-year	29.2
0.0025 (0.25%)	400-year	32.7
0.002 (0.2%)	500-year	33.1
-----	Levee Design Flood	34.3
-----	Levee Crest	42.4

Conversion Table for Elevation Data

Conversion	Datum (elevation in feet)				
	NGVD	Mean Sea Level	City of Portland	National Weather Service	NAVD88
	0.0	0.0	1.4	-1.8	3.5

Figure 47. Typical levee profile from NE Marine Drive and corresponding flood elevations (Dickenson et al. 2000). This profile was further modified to reflect the actual site conditions based on Google Earth (2010) imagery, LiDAR data, and Columbia River bathymetry (2009 data). Boring data for C-1, profile S-1 were used to describe the subsurface soils and existing laboratory data were used to describe the engineering properties of the various soil layers.

silt and clay near surface is fairly typical of the point bar depositional regime. Braided stream deposits ordinarily do not have a fine grained top blanket but, if present, is relatively thin. A thick top stratum similar to that shown in Figure 48 is more typical of a meandering type fluvial system. However, the narrow size of the alluvial valley through this reach may constrict the system from developing into a true meandering plan form like those observed in the first two sites studied and prevent the classic abandoned oxbows from forming and becoming well developed across its floodplain. The width of the oxbow channel is normally commensurate to the width of the river forming these abandoned features and these are absent within this river reach. The valley size, present day channel bathymetry, and Quaternary history (i.e., tectonism and Pleistocene glacial record) reflect characteristics of a braided stream regime and associated depositional environments.

Hydraulic conductivity

Grain size and Atterberg data from Shelby tube and split-spoon samples were taken from in the Portland levees and foundation by Dickenson et al. (2000). These data were used to estimate the hydraulic conductivity values for the slope stability and underseepage modeling using the California guidance procedure in Table 3. Values of hydraulic conductivity for the Portland profile in Figure 48 are presented in Table 17.

Groundwater conditions

Groundwater levels vary widely with the Columbia River stage because of the pervious nature of the underlying substratum sands. The normal low water level is identified in Figure 47. This level corresponds to the low water elevation of the river at an elevation of 7 ft amsl.

New Orleans, LA

Introduction

As part of the research into vegetation on levees, opportunities to observe trees being removed from the levee right-of-way in different USACE Districts were taken by ERDC when possible. In May 2010, two areas in the greater New Orleans area, one along the Inner Harbor Navigation Canal (IHNC) and the other along the 17th Street Canal, were commissioned to have trees removed from the vegetation free zone (VFZ) in May 2010. These areas were surveyed by ERDC using geophysical methods before the

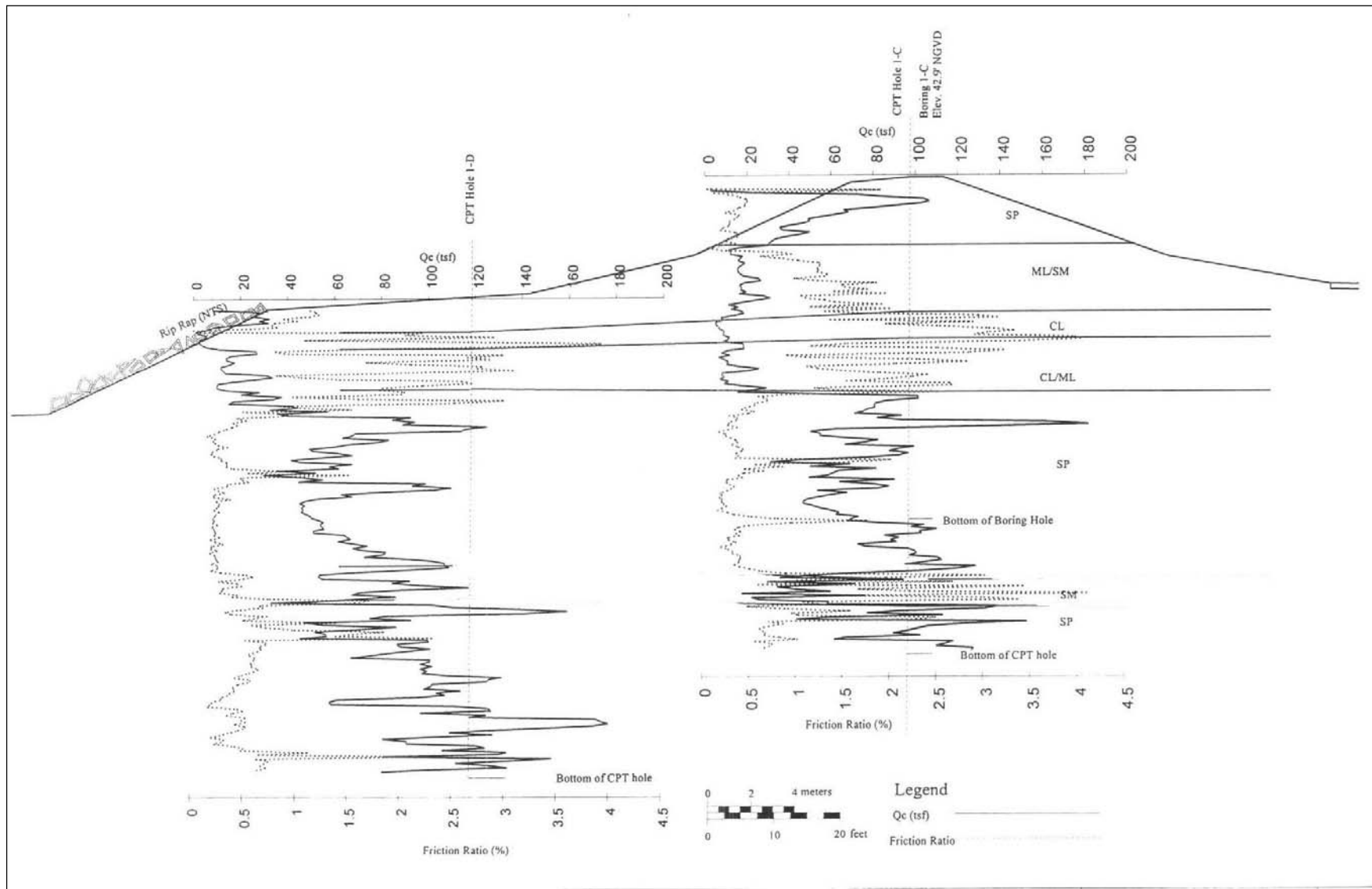


Figure 48. Profile used to model levee and foundation conditions for the Portland site (Dickenson et al. 2000). Levee is composed of sandy soils and the foundation contains a fine-grained top blanket of silt and clay, underlain by pervious substratum composed of silty sands and sands.

Table 17. Hydraulic conductivity values for Portland.

Material	k_H (cm/sec)	k_H (ft/day)	k_V (cm/sec)	k_V (ft/day)
Sand (SP)	1.94×10^{-2}	54.9	9.66×10^{-3}	27.4
Silty sand (SM)	1.94×10^{-3}	5.5	9.52×10^{-4}	2.7
Silt-clay (CL)	7.05×10^{-5}	0.2	3.52×10^{-5}	0.1
Sandy silt (ML)	1.76×10^{-4}	0.5	1.06×10^{-4}	0.3
Sand-silt (SM-ML)	1.94×10^{-3}	5.5	9.52×10^{-3}	2.7
Riprap	0.645	1828.8	0.645	1828.8

trees were excavated from the levee VFZ. ERDC monitored the root ball excavation at one area, after the geophysical surveys were completed, to assess the extent of the tree root impacts into the body of the levee and to measure the root zone properties.

The geology and climate in New Orleans are quite different when compared to those of the other study sites. The sediments in the New Orleans area were formed under fluvial-deltaic type conditions, as opposed to alluvial point bar type deposits associated with a meandering and braided regime in arid and west coast northern latitude settings. Woody vegetation growth in the New Orleans area occurs under conditions of ample monthly rainfall, high humidity, and the growth is mostly in fine-grained soils consisting primarily of highly plastic clays. Additionally, the New Orleans District commissioned a study by JESCO Environmental and Geotechnical Services (2008) to study tree roots and impacts of trees on levees. Their well documented study provides important background data involving trees and levees from this geographical area.

Study area

In May 2009, trees were removed from a reach of levee along the west bank of IHNC, and from the west bank of the 17th Street Canal near the 17th Street pump house (Figures 49a and 49b). The levee in the IHNC area is sited on the west side of the industrial canal and is a combination of earthen embankment and I-wall. The levee reach studied encompasses a 1,000-ft-long zone, parallel to France Road, and extends due north from U.S. Highway 90 to about the vicinity of Mirabeau Avenue. Mostly hackberry trees were removed from the fence row that separates the land-owner's property from the levee corridor.



Figure 49a. Location of the 17th Street Canal study site.



Figure 49b. Reach of levee at the IHNC where trees were removed.

The 17th Street Canal site is a combination of earthen embankment and I-wall. The study site at the 17th Canal pump house is much smaller than the IHNC study site. The 17th Street Canal site had only two large oak within the VFZ trees that died as a result of Hurricane Katrina. The contractor hired to excavate these trees removed them before ERDC had an opportunity to send personnel to New Orleans to observe and document the excavation process. However, geophysical surveys were performed on these trees and the adjacent levee prior to their removal.

Levees at the IHNC and 17th Street Canal sites were rebuilt following Hurricane Betsy in 1965, which flooded portions of New Orleans and included I-wall and T-wall construction along the canals to protect against storm surge from hurricanes. The areas studied and described here were not directly involved in any of the Hurricane Katrina levee failures. The two study site levees did not experience any major structural damages from the storm surge. Woody vegetation did not directly contribute to any of the New Orleans levee failures (IPET 2006). Only the IHNC site was flooded because of levee failures that occurred elsewhere, further to the

south on west side of the IHNC, and west of the study site, at the London Canal at Mirabeau Bridge. Failures in the IHNC area were along the west levee, south of Interstate 10 and about 1.5 miles from the tree area studied. The Mirabeau Bridge failure occurred more than 2 miles west of the IHNC study site. Levee failures along both the IHNC and along London Canal were responsible for this area being flooded after Hurricane Katrina.

Geological setting

The geology of the New Orleans area has been mapped and described in detail by various studies and papers (Kolb and Van Lopik 1958a,b, 1965; Kolb and Saucier 1982; Saucier 1994; Dunbar et al. 1994, 1995; Dunbar and Britsch 2008). The New Orleans area is a spatially complex landscape that has developed in response to sea level rise and the different distributary channels that once flowed through this area as part of the growth and abandonment of the various Holocene Mississippi River deltas. The surface geology within the New Orleans area consists of abandoned distributary channels, natural levees flanking these distributary channels, natural levee associated with the current course of the Mississippi River, and inland swamp and marsh deposits in the low-lying areas between the prominent natural levees (Figure 50). The natural levees from these different channels correspond to the highest ground elevations within the New Orleans area.

Man-made activities in the New Orleans area during the time of European settlement have further contributed to the spatial complexity and affected the elevation of the ground surface across the city. Many parts of New Orleans are below sea level because of man's activities. These activities include construction of drainage and navigation canals, groundwater pumping, hydraulic dredging of sediments, creation of lakefront developments, and construction of levees to prevent the river from flooding into the city. Human activities, local and regional subsidence in this region, long-term sea level rise, combined with the deltaic setting, are responsible for the unique landscape that is present day New Orleans. Levees at the IHNC and 17th Street Canal sites were rebuilt following Hurricane Betsy in 1965. Storm surge protection included I-wall and T-wall construction along the canals to protect against elevated water levels.

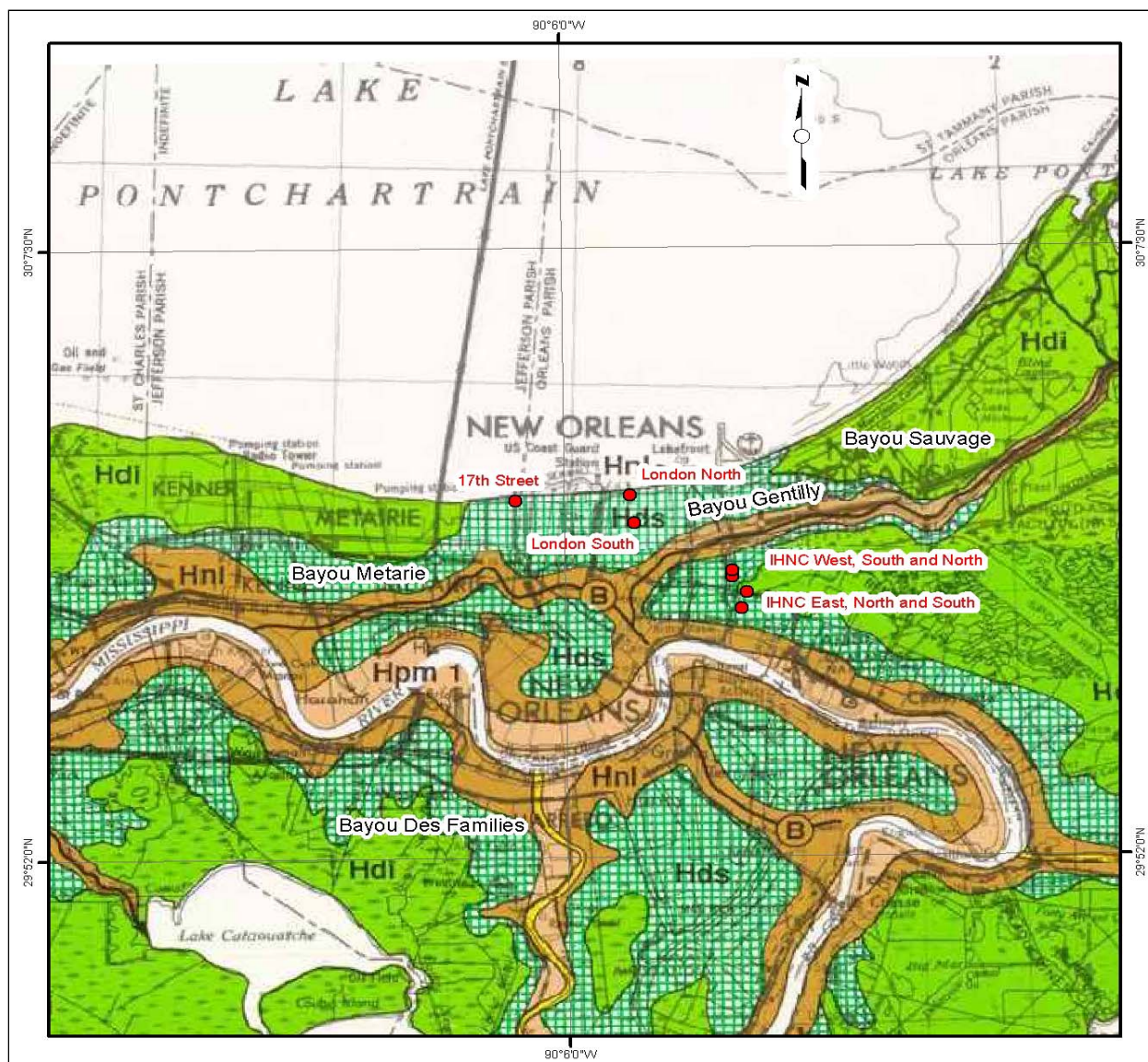


Figure 50. New Orleans surface geology map showing major depositional environments (i.e., point bar (Hpm1), natural levee (Hnl), swamp (Hds), and marsh (Hdi)), woody vegetation study sites (blue rectangles), and the major Hurricane Katrina canal levee failures (red circles) (Saucier 1994). Natural levees from the Mississippi River and abandoned distributary channels (i.e., Bayou Des Families, Metarie, Sauvage, Gentilly) correspond to high ground in the greater New Orleans area.

Levee profile

The levee profile at the two canal levees possesses an earthen embankment with 1V:3H slope and an I-wall through the center of the earthen portion of the levee (Figure 51). The tip of the sheet pile forming the I-wall is variable in length, but typically extends 15 to 20 ft below the levee surface into soft clays that are of shallow water origin. The composition of the levee embankment and foundation at both sites is primarily well compacted clay



Figure 51. View of typical levee and I-wall flanking the drainage and harbor canals in the greater New Orleans area. View is from the west levee at IHNC. Photograph shows woody vegetation being removed from the right-of-way and stacked along levee slope for later pick-up and disposal.

soils (USACE 1968, 1990; Dunbar et al. 1994). Levee foundation soils typically transition from natural levee, to inland swamp, to marsh, and to shallow water type deposits (i.e., interdistributary), which reflect the fluvial-deltaic environments that are responsible for these sediments being deposited. Both woody vegetation sites are south (i.e., seaward) of the buried relic beach (fine sand) ridge that formed 3,000 to 4,000 years ago and was later buried by recent Mississippi River deltaic deposits. This buried beach is responsible for protecting Lake Pontchartrain from complete filling by later Mississippi River distributary channels developing in the New Orleans area.

Root excavation

Monitoring of tree removal activities at the IHNC by ERDC (Appendix B) and studies conducted by JESSCO Environmental and Geotechnical

Services (2008) indicate that the extent of root ball depth is generally limited to less than 3.5 ft in highly plastic clay soils typically found in the New Orleans area. Deep roots into clay levees in the New Orleans area are uncommon, but can exist (JESSCO 2008). Additionally, the JESSCO study found that the roots extend further into the natural soils than into the compacted levee sections for the larger diameter roots. This finding was generally supported by the limited number of observations by ERDC in the IHNC tree removal area.

Boca Raton, FL

Introduction

This study site is located in southern Palm Beach County, near Boca Raton, FL (Figure 52). The site contains a back levee which protects against storm surge from rising water levels in the Arthur R. Marshall Loxahatchee National Wildlife Refuge. This site contains fig trees that were outside of the VFZ (Figure 53), but were representative of vegetation from this region. A view of the levee system is shown in Figure 54. These levees have a crown width of 10 to 12 ft and are about 10 ft in height, with side slopes of 1V:3H.

The levees are owned by the South Florida Water Management District (SFMD), which was originally created in 1949 as the Central and Southern Florida Flood Control District. The District became the SFWMD in 1972 to provide flood protection and irrigation to farmers and overseas Everglade restoration projects. This District has over 1,700 employees and 2,000 miles of canals, levees, pumps, and other types of water-related infrastructure.

Geologic setting

A unique feature of this site, compared to other sites studied, was the presence of shallow limestone bedrock, typically less than 4 ft deep beneath the ground surface. The bedrock for this area is mapped as the Miami Limestone, which is described as white to light gray in color, fossiliferous, contains variable percentage of sand, and often grades into calcareous sand (Scott 1993; Scott et al. 2001). Bedrock was frequently encountered at shallow depths in the auger holes for permeameter testing.



Figure 52. Study site at Boca Raton, FL,
where a fig tree was evaluated.



Figure 53. View of fig trees studied at the Boca Raton, FL. Top photo is view looking south on east side of canal. This tree was tested for soil permeability using the permeameter. Bottom photo is view looking north and shows another fig tree adjacent to entrance into wildlife park. Levee is to the right of photo. Both trees were measured with the Troxler neutron density gage for soil moisture and density.



Figure 54. View looking south of the levee system adjacent to the Arthur R. Marshall Loxahatchee National Wildlife Refuge. Top photo shows canal on protected side and marsh on flood side. Pervious nature of the levee soils are reflected by seepage at levee toe on landside. Water level in the marsh was about 1 to 2 ft higher than protected side.

Soils overlying the bedrock are marsh deposits, fine-grained sand, and shell used for fill. The soils series in the area studied are classified as being either Dania or Lauderhill (USDA 1978). These soils correspond to organic marsh deposits overlying bedrock. This area has been extensively disturbed during historic time by construction of the nearby canal, roads, and the flood protection levees.

Laboratory soils data and hydraulic conductivity

No geotechnical data were obtained for this site to characterize the engineering properties of the levee fill and the shallow foundation. The levee soils were observed to be fairly pervious, containing silty sands and fine-grained sands with shell fragments. The levees were likely built from material dredged from near the toe of the levee.

Groundwater conditions

The water table is at ground surface to less than 3 ft below the ground surface near the canal. As shown by the lower photo in Figure 54, through seepage is ponding at the surface because of the differential head between the flood and protected sides of the levee.

Troxler measurements

Troxler data were taken at three areas in the Arthur R. Marshall Loxahatchee National Wildlife Refuge near Boca Raton, FL (Figure 55). Measurements were made on the east side of the levee system within the grid system used for hydraulic conductivity tests (identified as Tree 1 at the Flag Region in Figure 55), on the west side of the levee beneath a fig tree near the park entrance to the wildlife refuge (Tree 2 in Figure 55) and on the levee south of the two tree sites (identified as the levee in Figure 55). Soils were similar at the three sites, composed of calcareous, gravelly sand (GC-SW). The limestone bedrock was shallow, often less than 3 ft beneath the surface based on the auger holes used to perform hydraulic conductivity testing at the fig tree (Tree 1, Figure 55).

A summary of all the Troxler data for this site is presented in Table 18 and Figures 56a to 56d, for the flagged area in Table 19 and Figures 57a to 57d, for Tree 1 in Table 20 and Figures 58a to 58d, for Tree 2 in Table 21 and Figures 59a to 59d, and the levee area in Table 22 and Figures 60a to 60d. Examination of all the measurement for this area in Table 18 and



Figure 55. Location map for the three sites in Boca Raton, FL.

**Table 18. Statistical data for Troxler measurements in Boca Raton, FL:
2-, 4-, 6-, 8-, 10-, and 12-in. depths.**

Depth (2-4-6 in.)	Dry Density (lb/ft ³)	Wet Density (lb/ft ³)	Moisture Content (lb/ft ³)	Percent Moisture (%)	Depth (8-10-12 in.)	Dry Density (lb/ft ³)	Wet Density (lb/ft ³)	Moisture Content (lb/ft ³)	Percent Moisture (%)
Max	110.4	118.7	27.0	35.6	Max	117.1	125.5	20.2	23.4
Min	46.9	51.1	1.8	2.5	Min	70.6	81.4	1.7	1.9
Mean	77.0	85.7	8.8	11.8	Mean	90.2	98.2	8.1	9.3
Median	74.0	82.9	8.2	10.4	Median	89.3	96.2	8.2	8.6
Mode	73.2	100.7	8.2	3.0	Mode	91.4	87.6	11.7	2.4
Standard Deviation	15.1	15.9	5.2	7.1	Standard Deviation	11.7	11.4	4.5	5.6
*#N/A: no central value in data set					*#N/A: no central value in data set				

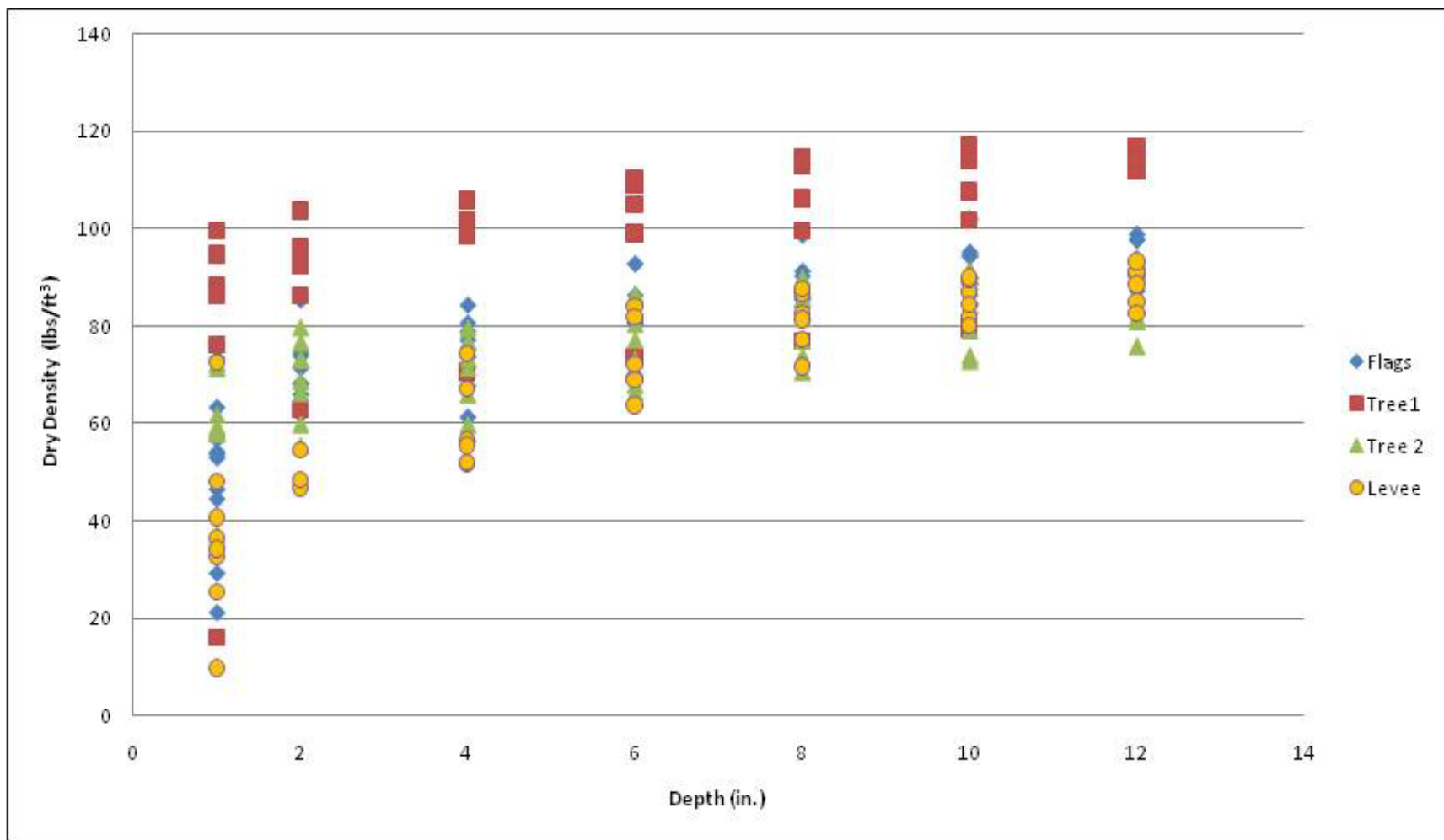


Figure 56a Dry density (lbs/ft³) from Troxler measurements for Boca Raton, FL.

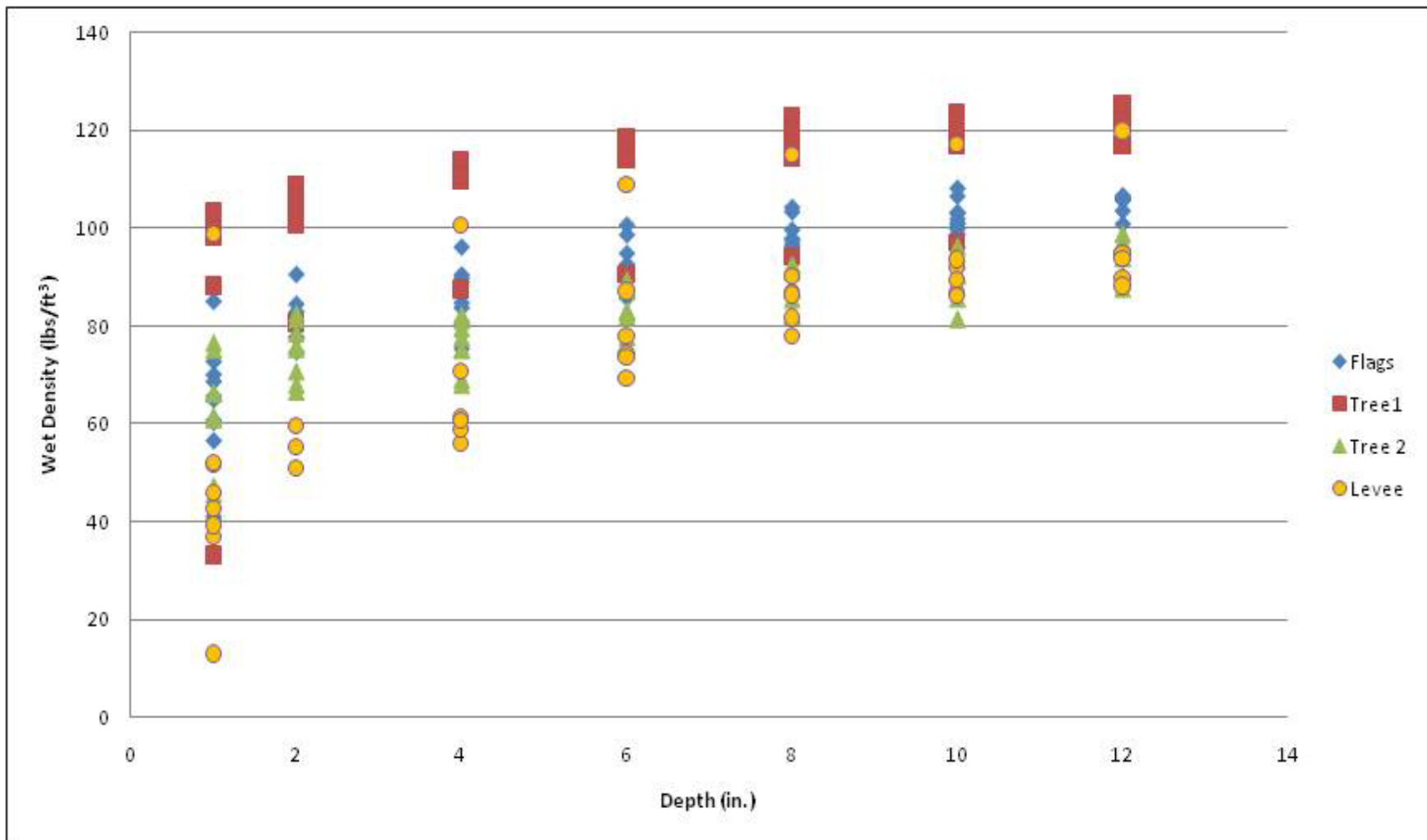


Figure 56b. Wet density (lbs/ft³) from Troxler measurements for Boca Raton, FL.

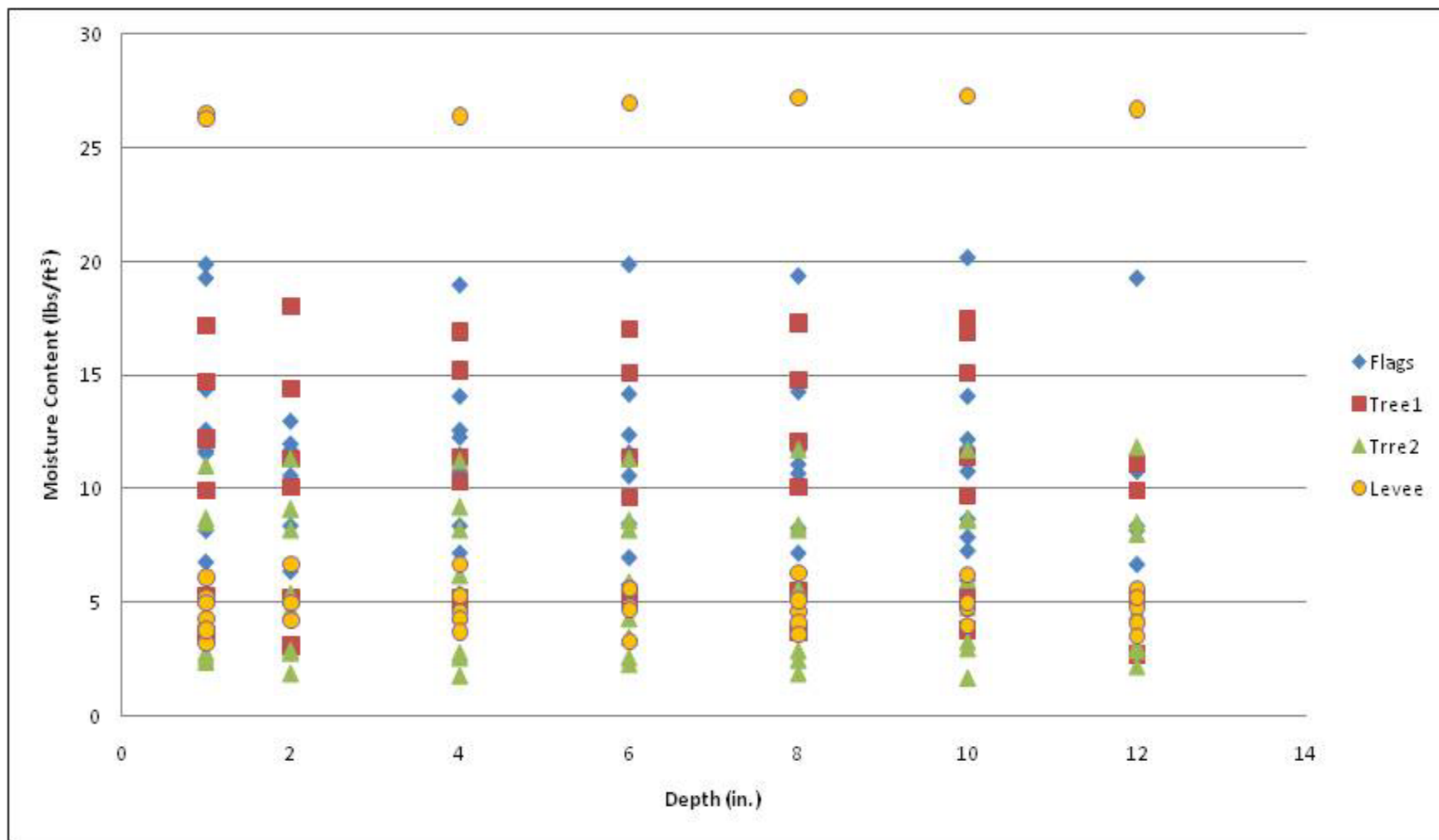


Figure 56c. Moisture content (lbs/ft³) from Troxler measurements for Boca Raton, FL.

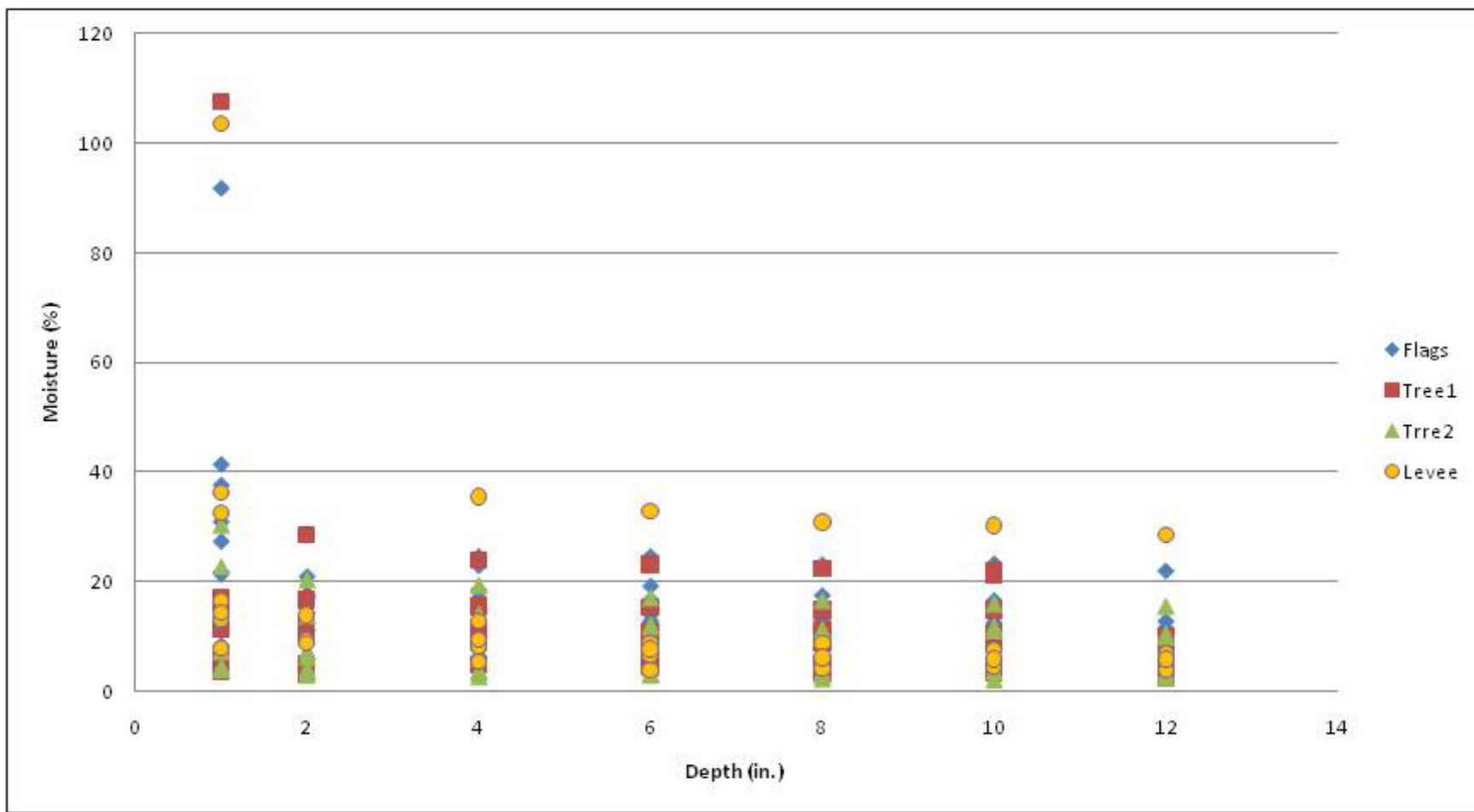


Figure 56d. Moisture (%) from Troxler measurements for Boca Raton, FL.

**Table 19. Statistical data for Troxler measurements in Boca Raton, FL, flag area:
2-, 4-, 6-, 8-, 10-, and 12-in. depths.**

Flags Depth (2-4-6 in.)	Dry Density (lb/ft ³)	Wet Density (lb/ft ³)	Moisture Content (lb/ft ³)	Percent Moisture (%)	Flags Depth (8-10-12 in.)	Dry Density (lb/ft ³)	Wet Density (lb/ft ³)	Moisture Content (lb/ft ³)	Percent Moisture (%)
Max	92.9	100.7	19.9	24.7	Max	102.2	108.2	20.2	23.4
Min	61.3	74.8	5.1	5.9	Min	81.3	93.2	5.5	5.6
Mean	75.5	86.4	10.9	14.8	Mean	90.3	101.3	11.0	12.4
Median	74.0	85.8	11.5	14.5	Median	89.4	101.0	10.8	12.5
Mode	#N/A	92.6	11.7	#N/A	Mode	#N/A	#N/A	10.8	#N/A
Standard Deviation	7.7	7.2	3.7	5.5	Standard Deviation	5.9	4.1	4.0	5.1
*#N/A: no central value in data set					*#N/A: no central value in data set				

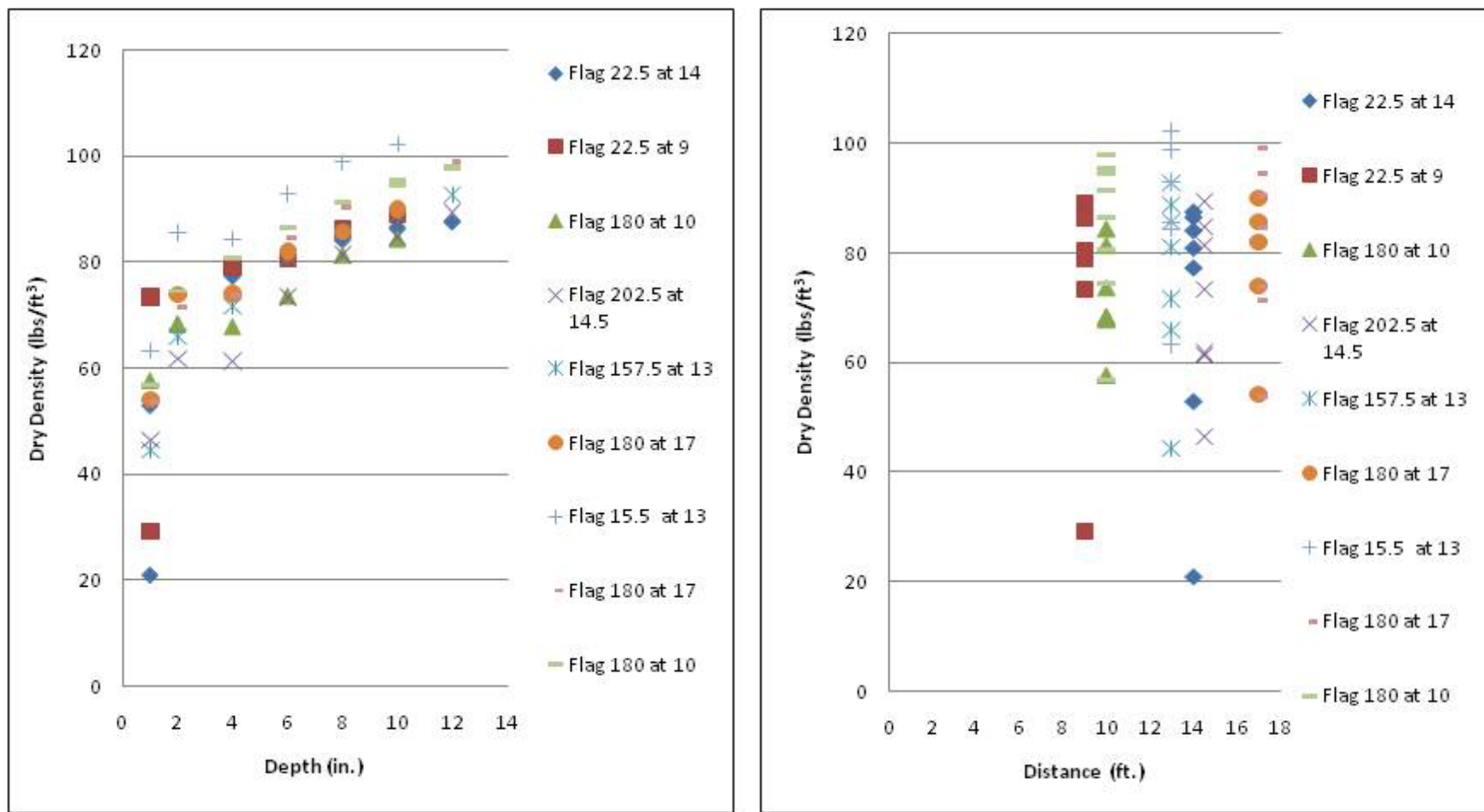


Figure 57a. Dry density (lbs/ft³) versus depth (in.) and distance (ft.) from Troxler measurements for flagged region, Boca Raton, FL.

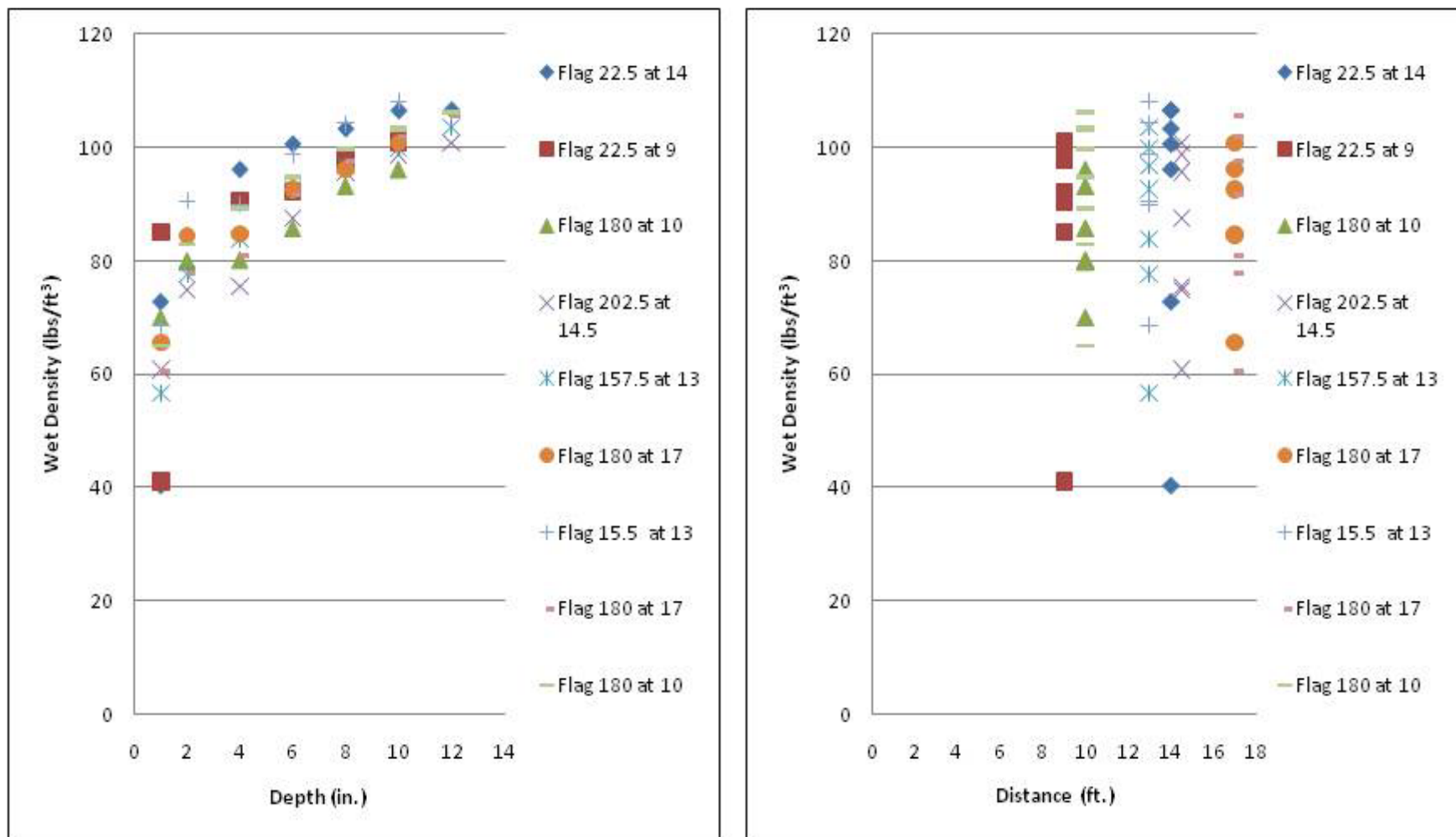


Figure 57b. Wet density (lbs/ft³) versus depth (in.) and distance (ft.) from Troxler measurements for flagged region, Boca Raton, FL.

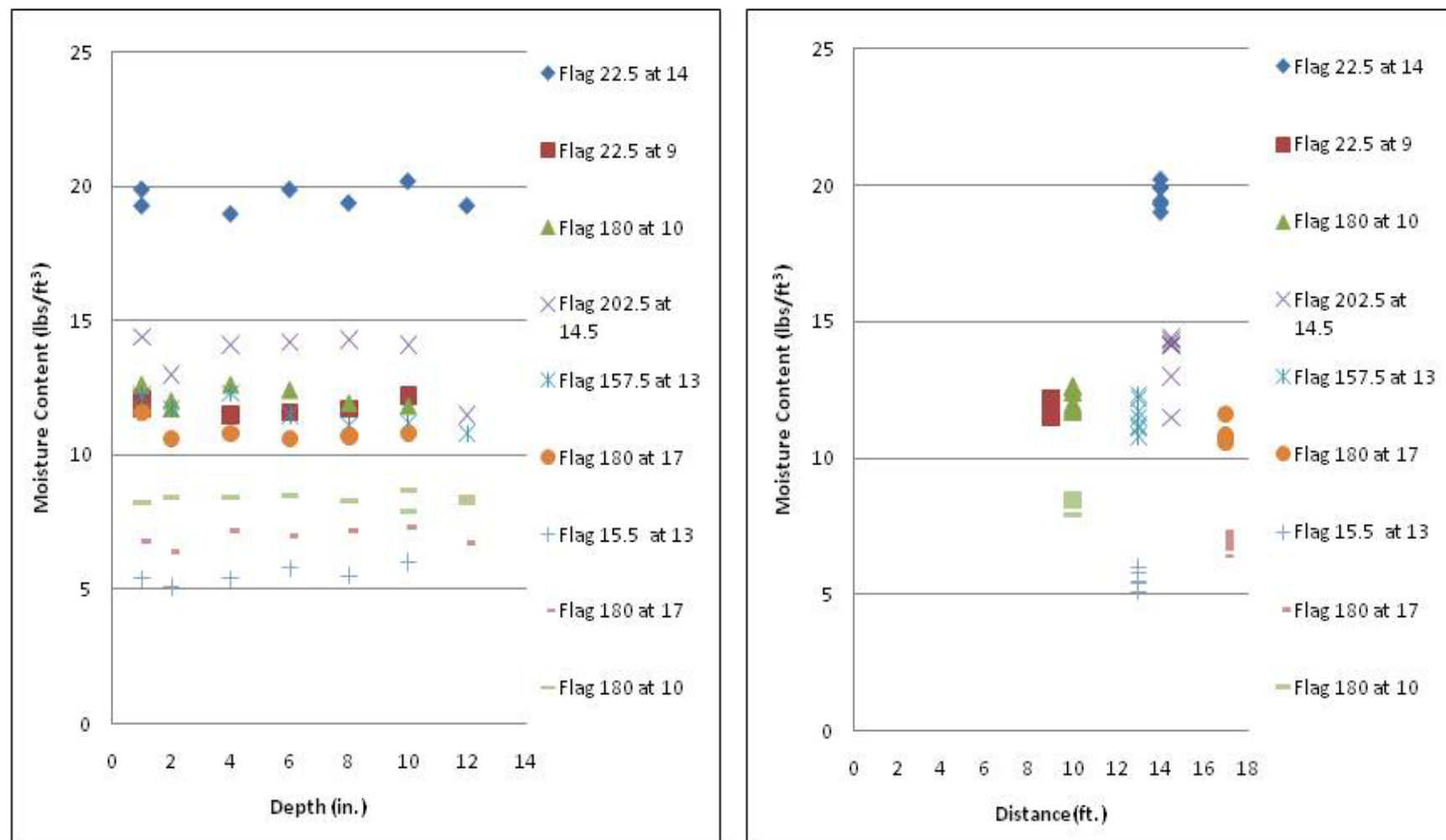


Figure 57c. Moisture content (lbs/ft^3) versus depth (in.) and distance (ft.) from Troxler measurements for, flagged region, Boca Raton, FL.

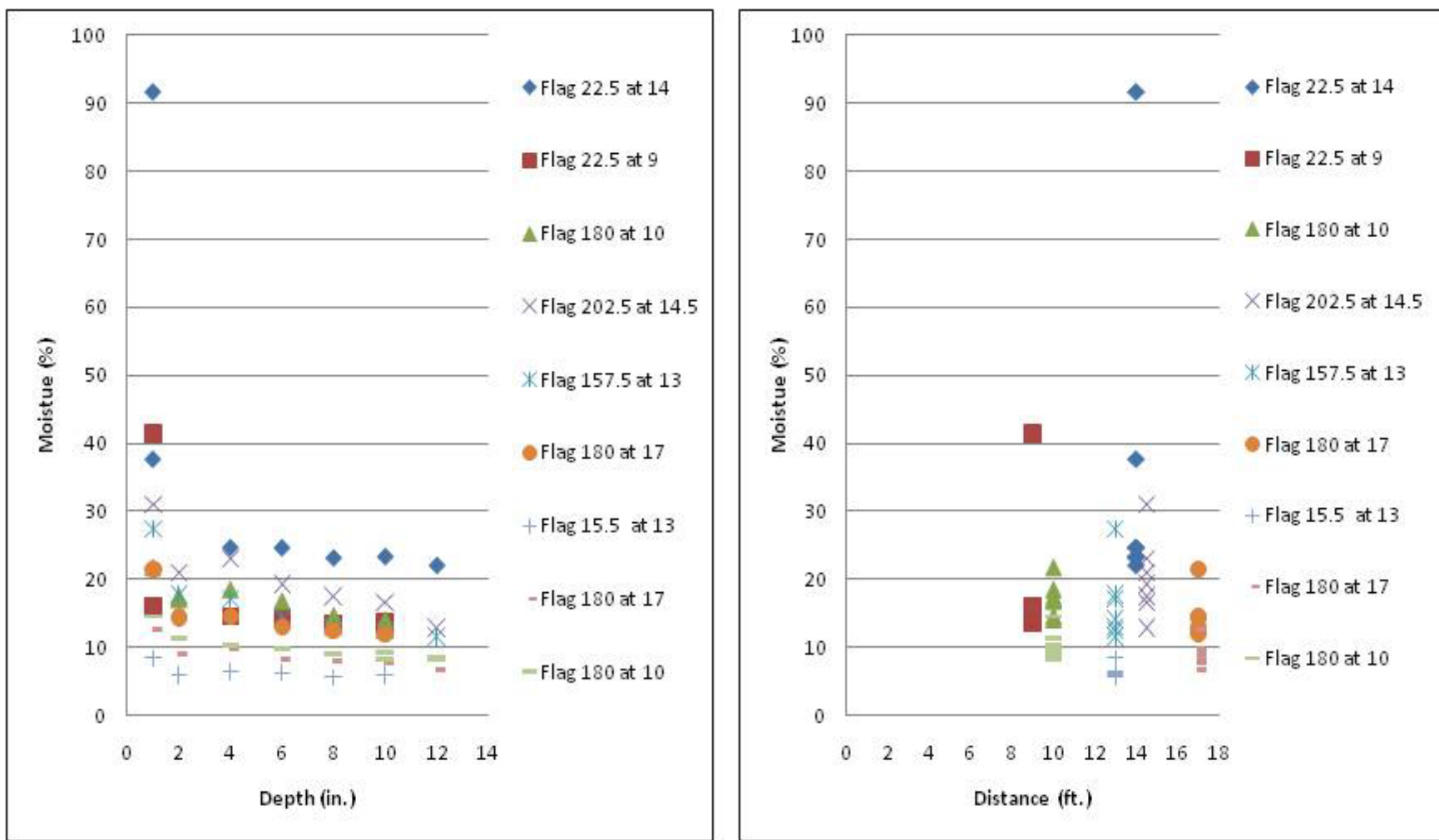


Figure 57d. Moisture (%) verses depth (in.) and distance (ft.) from Troxler measurements for, flagged region, Boca Raton, FL.

Table 20. Statistical data for Troxler measurements in Boca Raton, FL, Tree 1:
2-, 4-, 6-, 8-, 10-, and 12-in. depths.

Tree 1 Depth (2-4-6 in.)	Dry Density (lb/ft ³)	Wet Density (lb/ft ³)	Moisture Content (lb/ft ³)	Percent Moisture (%)	Tree 1 Depth (8-10-12 in.)	Dry Density (lb/ft ³)	Wet Density (lb/ft ³)	Moisture Content (lb/ft ³)	Percent Moisture (%)
Max	110.4	118.7	18.0	28.7	Max	117.1	125.5	17.5	22.5
Min	62.8	80.7	3.1	3.0	Min	76.9	94.2	2.7	2.4
Mean	96.3	106.8	10.5	11.9	Mean	105.8	115.9	10.1	10.3
Median	100.4	110.3	10.8	10.6	Median	113.0	119.0	10.1	9.0
Mode	#N/A	114.1	5.2	#N/A	Mode	115.5	#N/A	5.2	14.9
Standard Deviation	14.1	10.6	4.8	7.5	Standard Deviation	13.8	9.9	5.1	6.7
*#N/A: no central value in data set					*#N/A: no central value in data set				

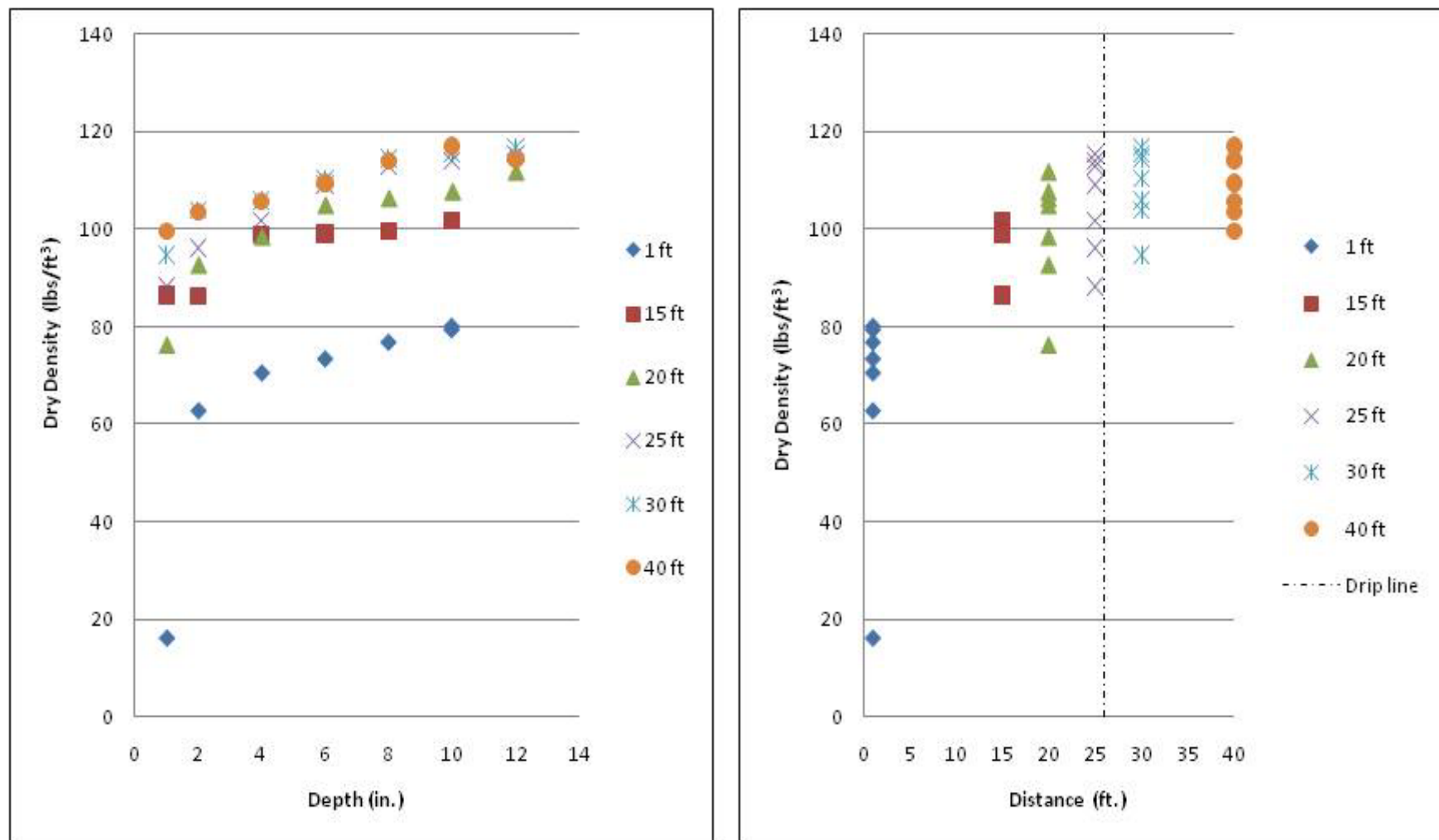


Figure 58a. Dry density (lbs/ft^3) versus depth (in.) and distance (ft.) from Troxler measurements for tree 1, Boca Raton, FL.

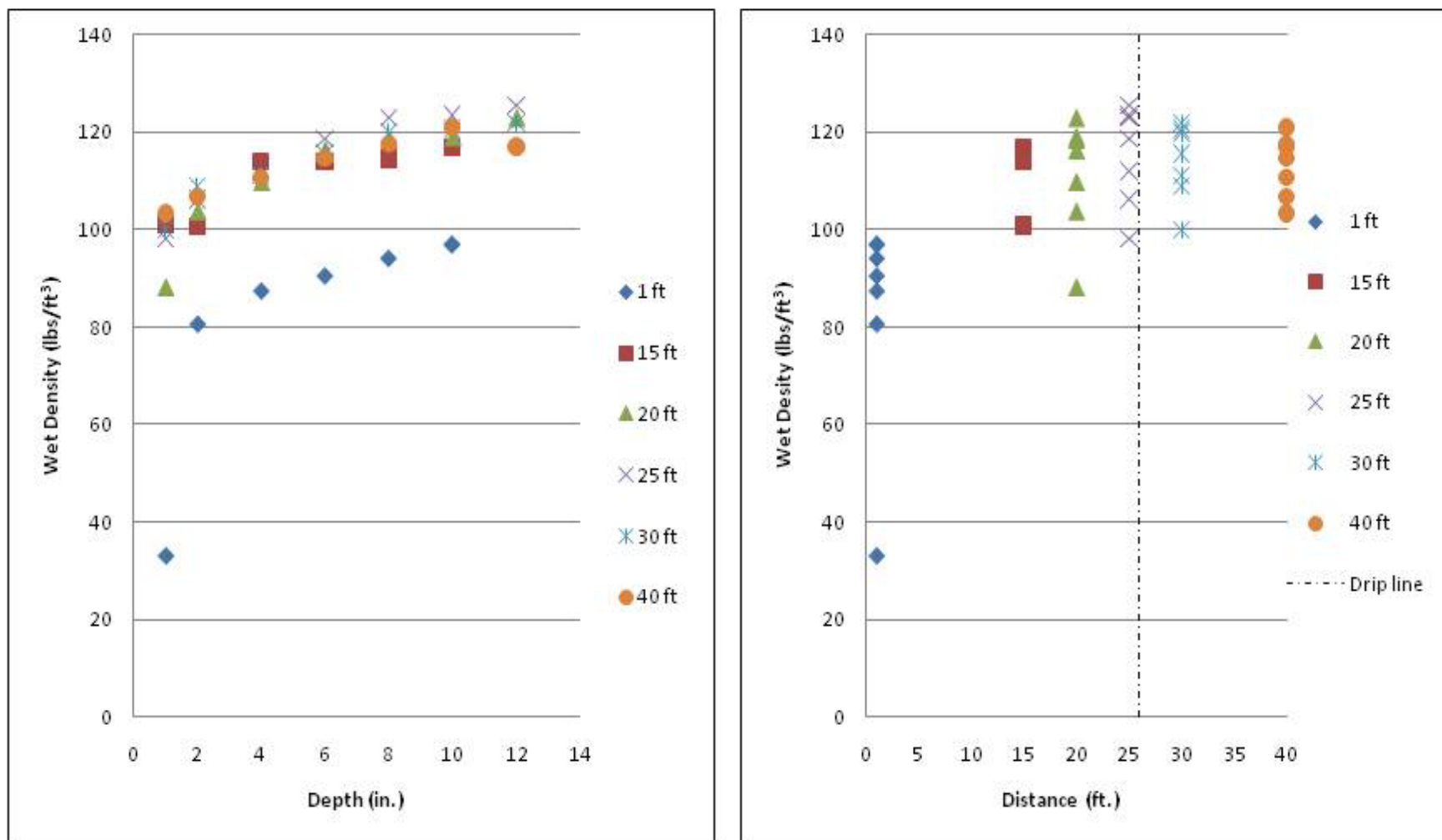


Figure 58b. Wet density (lbs/ft³) versus depth (in.) and distance (ft.) from Troxler measurements for, tree 1, Boca Raton, FL.

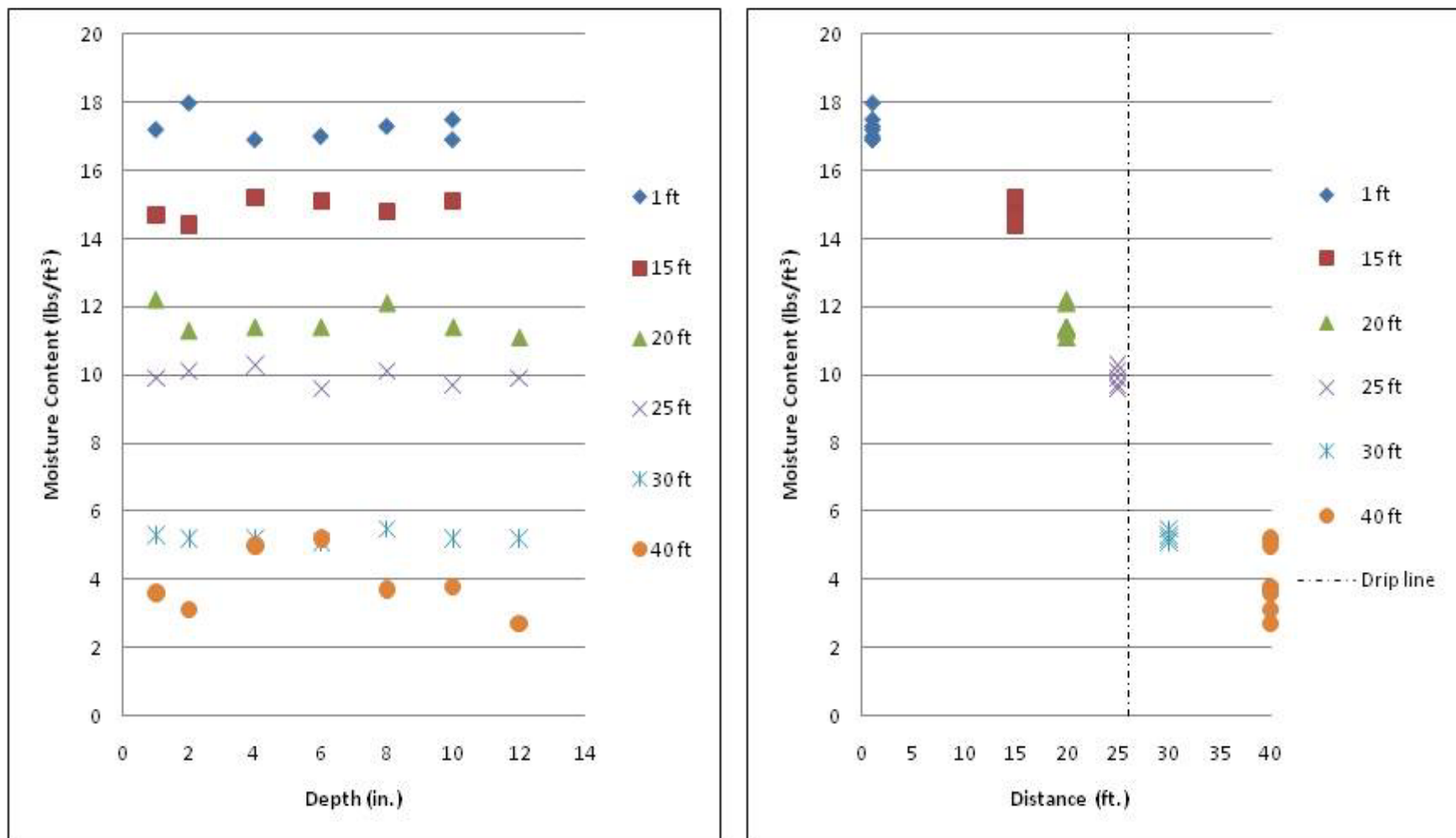


Figure 58c. Moisture content (lbs/ft³) versus depth (in.) and distance (ft.) from Troxler measurements for, tree 1, Boca Raton, FL.

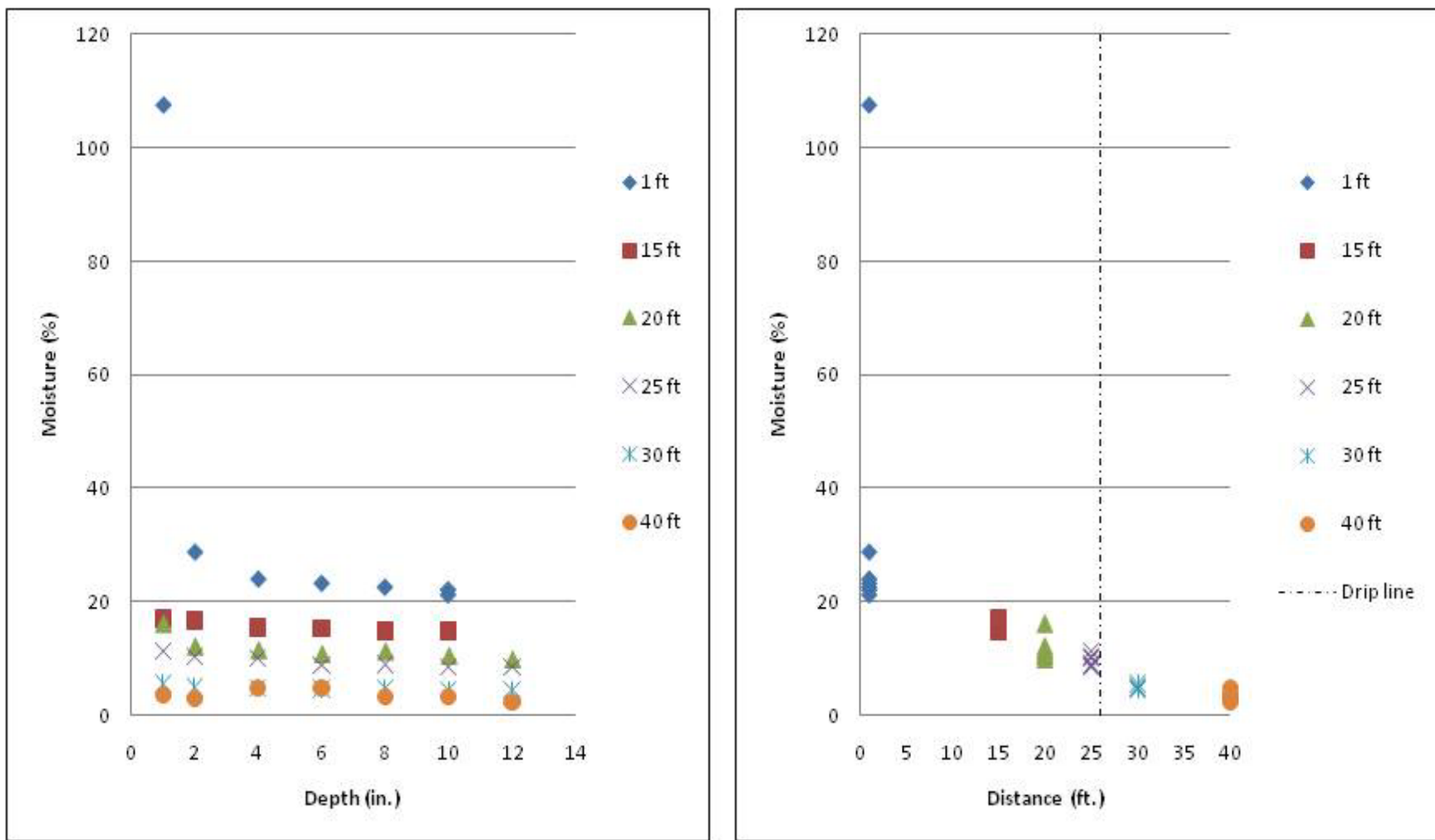


Figure 58d. Moisture (%) versus depth (in.) and distance (ft.) from Troxler measurements for, tree 1, Boca Raton, FL.

**Table 21. Statistical data for Troxler measurements in Boca Raton, FL, Tree 2:
2-, 4-, 6-, 8-, 10-, and 12-in. depths.**

Tree 2 Depth (2-4-6 in.)	Dry Density (lb/ft ³)	Wet Density (lb/ft ³)	Moisture Content (lb/ft ³)	Percent Moisture (%)	Tree 2 Depth (8-10-12 in.)	Dry Density (lb/ft ³)	Wet Density (lb/ft ³)	Moisture Content (lb/ft ³)	Percent Moisture (%)
Max	86.6	89.3	11.3	20.4	Max	94.1	98.7	11.8	16.5
Min	55.3	66.6	1.8	2.5	Min	70.6	81.4	1.7	1.9
Mean	73.2	78.1	5.1	6.8	Mean	86.7	90.6	5.2	5.7
Median	73.2	78.1	5.1	6.8	Median	86.7	90.6	5.2	5.7
Mode	73.2	77.7	8.2	#N/A	Mode	73.8	87.6	5.6	#N/A
Standard Deviation	8.5	6.3	3.2	5.7	Standard Deviation	7.5	4.9	3.3	4.7
*#N/A: no central value in data set					*#N/A: no central value in data set				

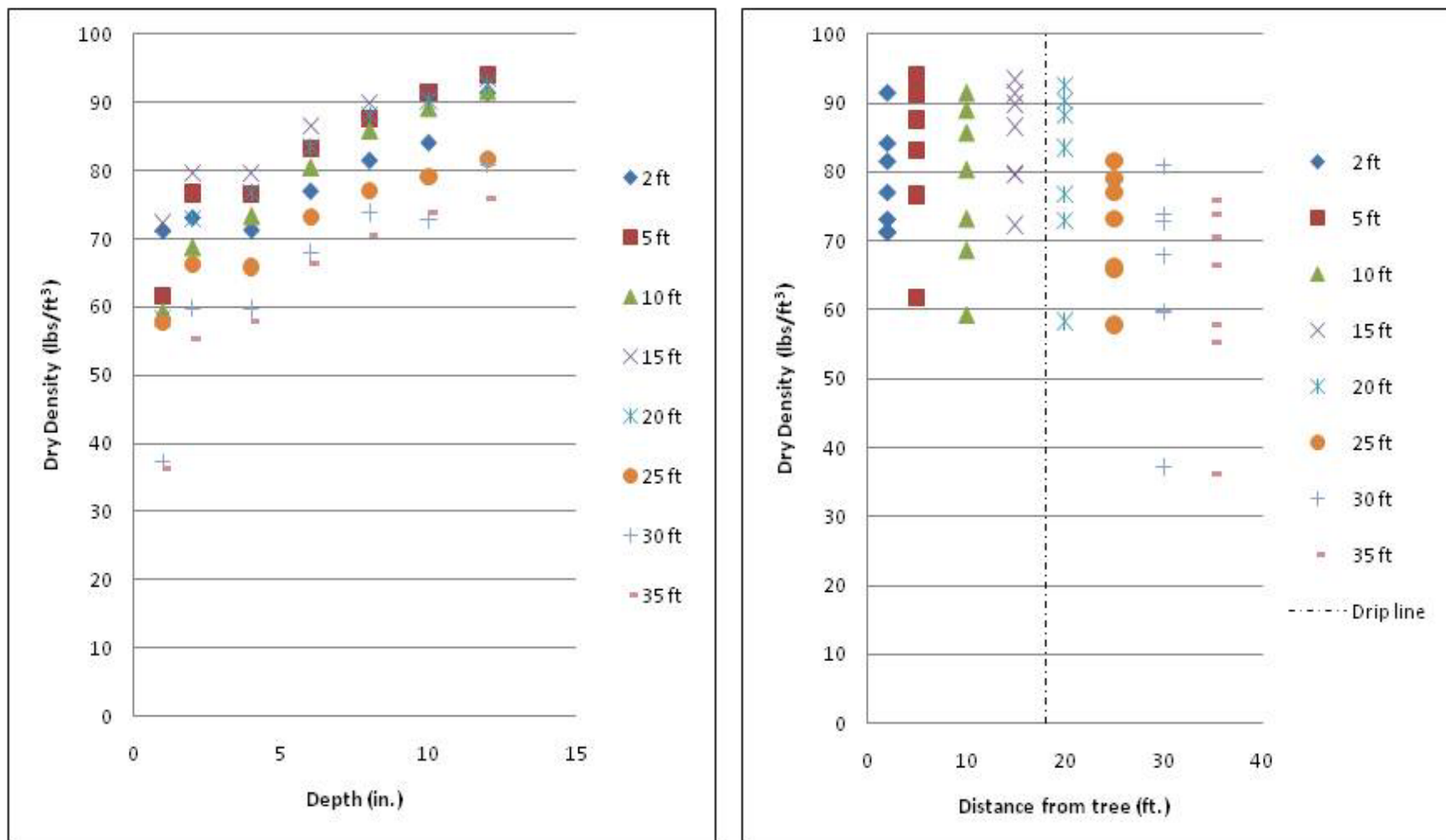


Figure 59a. Dry density (lbs/ft³) verses depth (in.) and distance (ft.) from Troxler measurements for, tree 2, Boca Raton, FL.

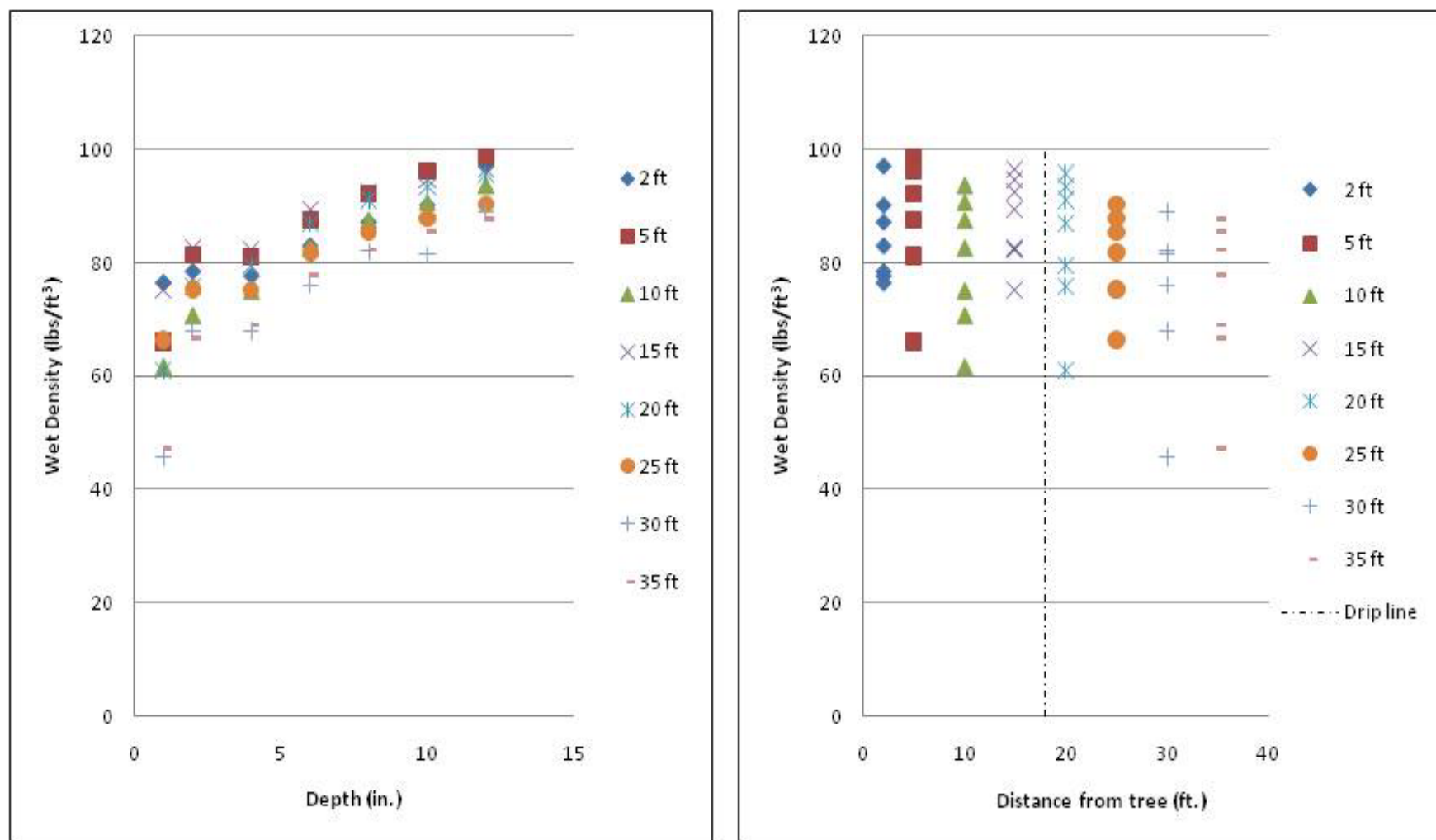


Figure 59b. Wet density (lbs/ft^3) versus depth (in.) and distance (ft.) from Troxler measurements for, tree 2, Boca Raton, FL.

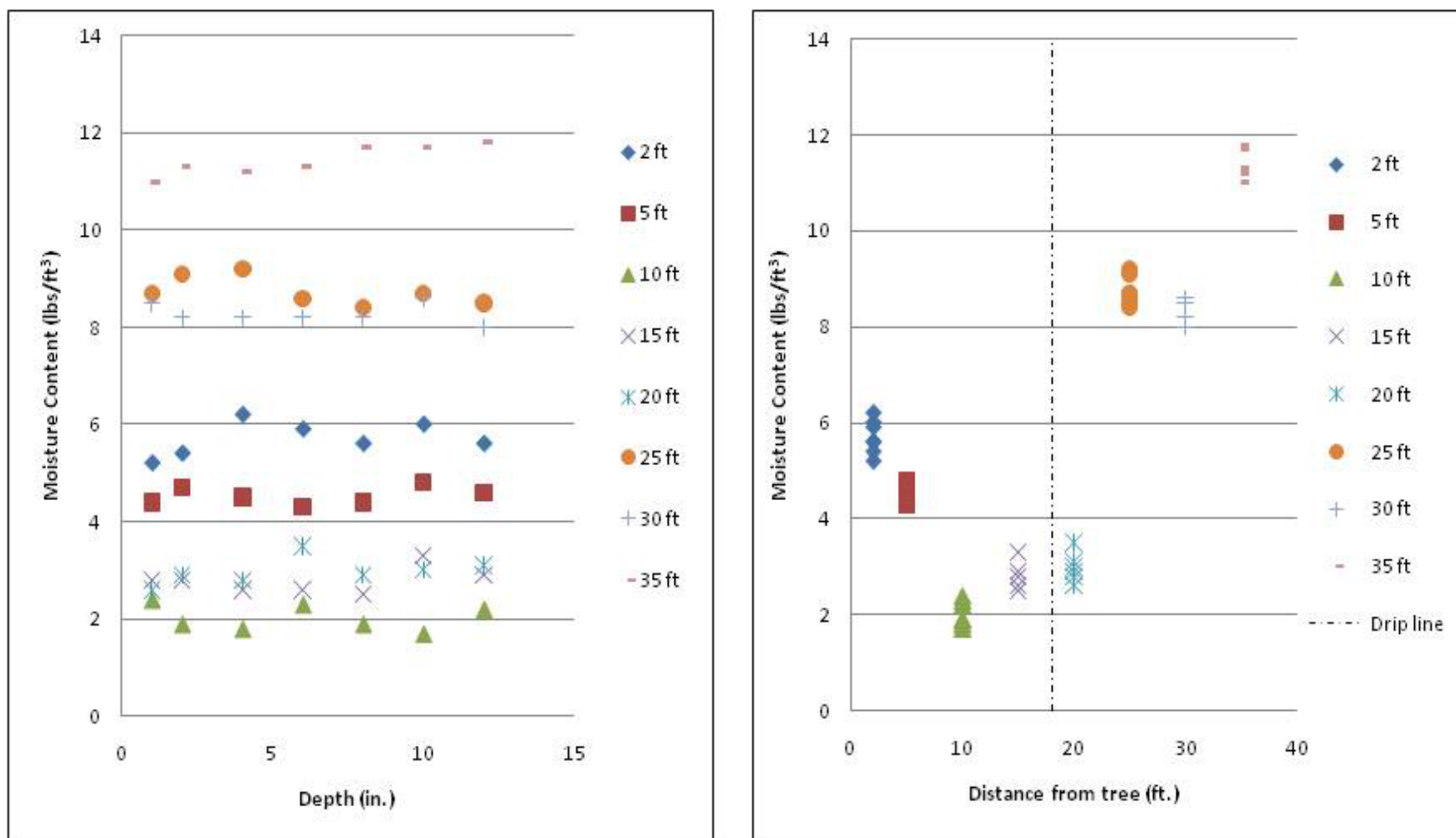


Figure 59c. Moisture content (lbs/ft³) versus depth (in.) and distance (ft.) from Troxler measurements for, tree 2, Boca Raton, FL.

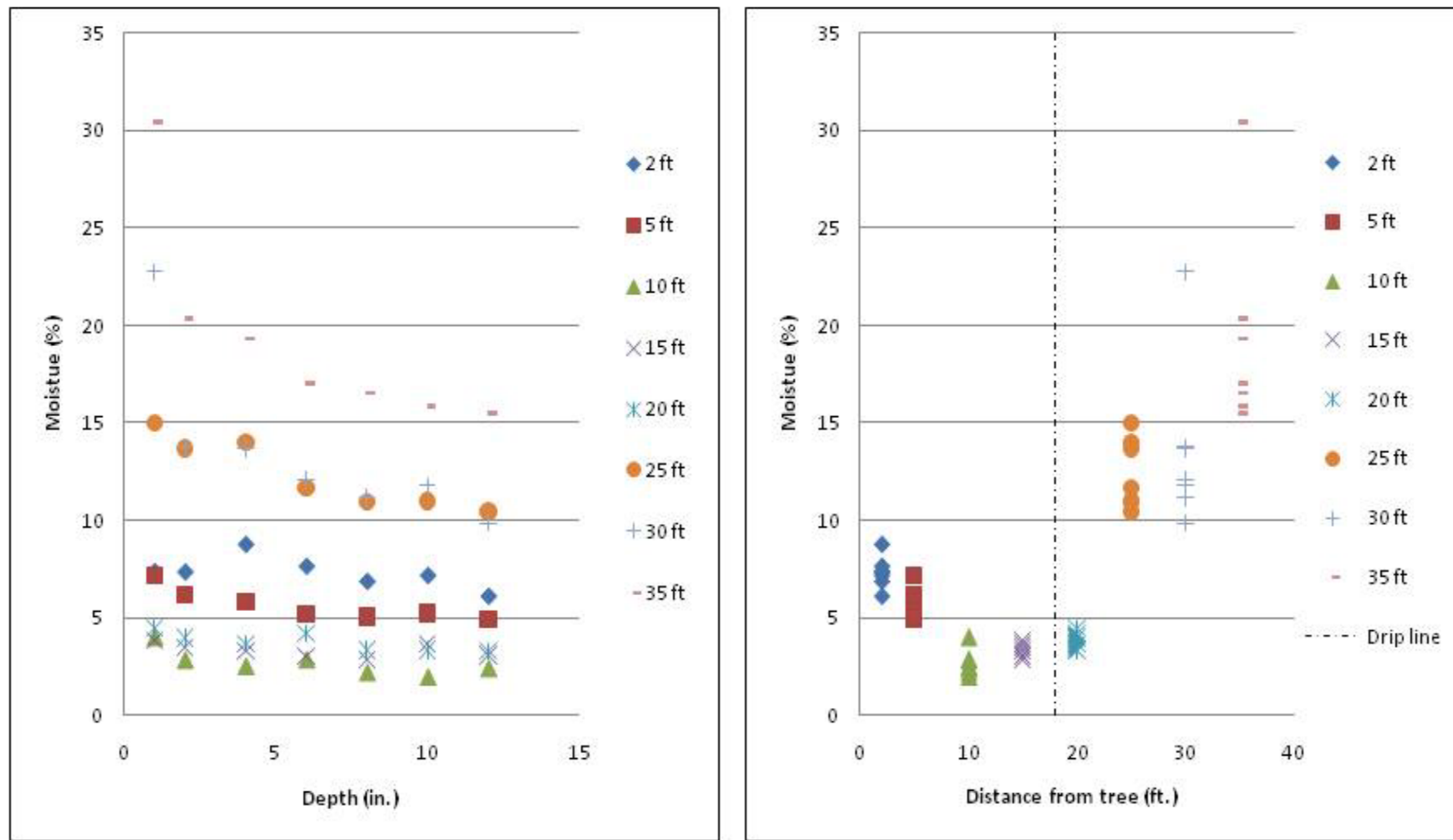


Figure 59d. Moisture (%) versus depth (in.) and distance (ft.) from Troxler measurements for, tree 2, Boca Raton, FL.

Table 22. Statistical data for Troxler measurements in Boca Raton, FL, levee:
2-, 4-, 6-, 8-, 10-, and 12-in. depths.

Levee Depth (2-4-6 in.)	Dry Density (lb/ft ³)	Wet Density (lb/ft ³)	Moisture Content (lb/ft ³)	Percent Moisture (%)	Levee Depth (8-10-12 in.)	Dry Density (lb/ft ³)	Wet Density (lb/ft ³)	Moisture Content (lb/ft ³)	Percent Moisture (%)
Max	84.0	108.9	27.0	35.6	Max	93.3	120.0	27.3	30.9
Min	46.9	51.1	3.3	3.9	Min	71.7	77.9	3.5	3.9
Mean	63.2	71.1	7.9	11.9	Mean	85.1	93.6	8.5	9.8
Median	63.8	69.4	5.0	8.8	Median	85.9	90.1	4.9	5.9
Mode	#N/A	#N/A	6.7	#N/A	Mode	#N/A	86.8	4.8	#N/A
Standard Deviation	11.9	16.9	7.7	9.4	Standard Deviation	5.5	11.8	8.6	9.4
*#N/A: no central value in data set					*#N/A: no central value in data set				

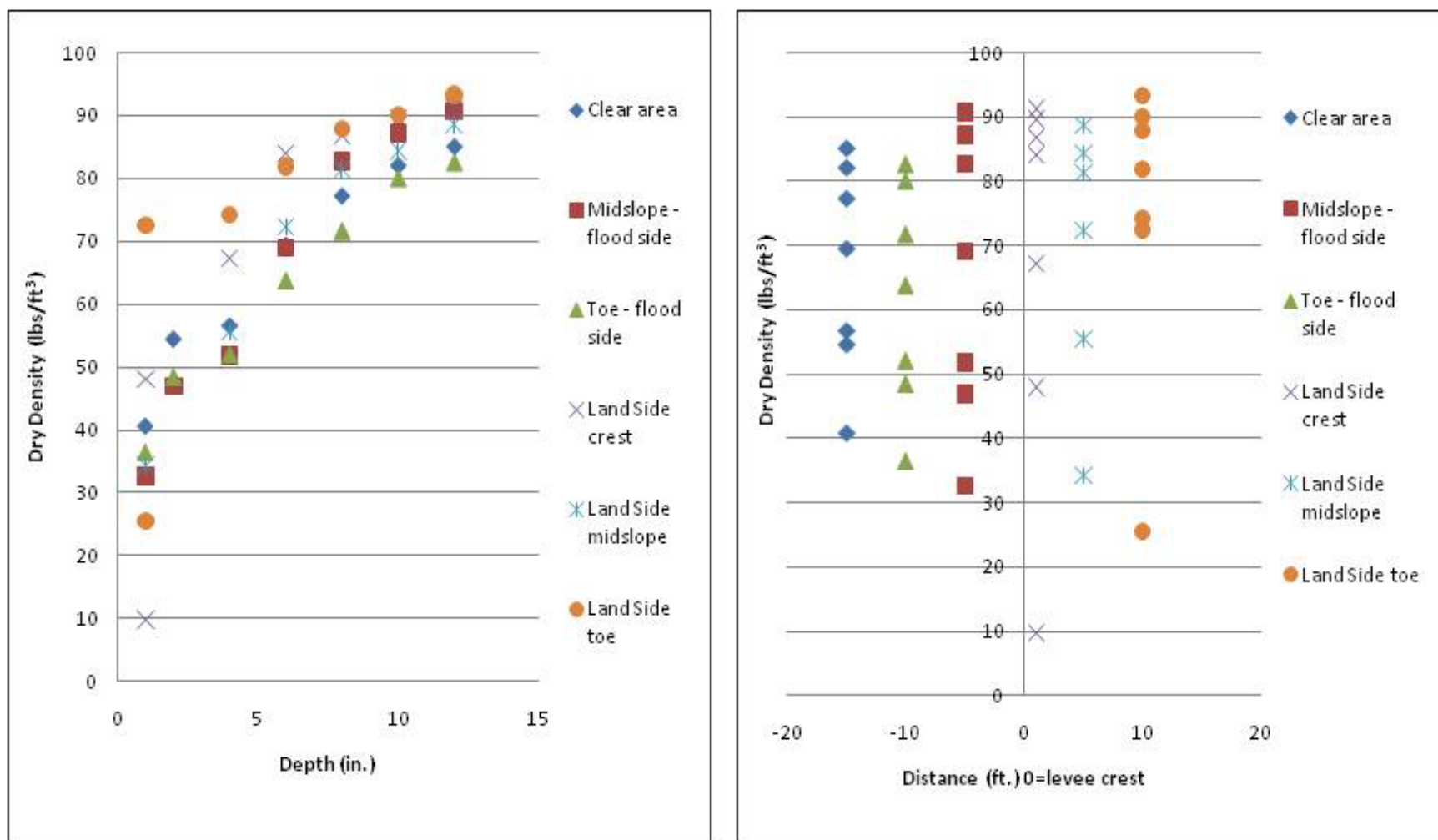


Figure 60a. Dry density (lbs/ft³) versus depth (in.) and distance (ft.) from Troxler measurements for levee, Boca Raton, FL.

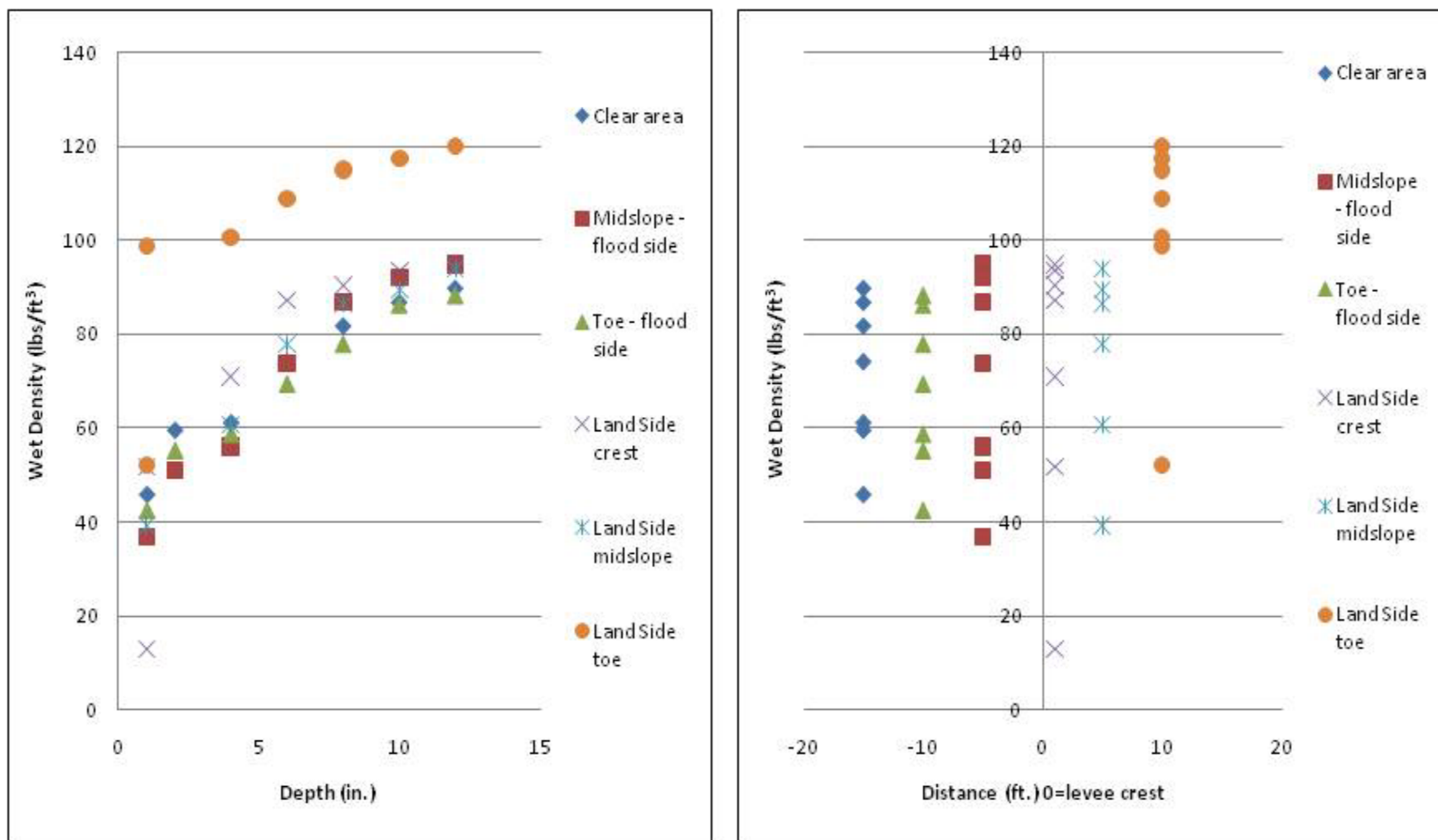


Figure 60b. Wet density (lbs/ft³) verses depth (in.) and distance (ft.) from Troxler measurements for, levee, Boca Raton, FL.

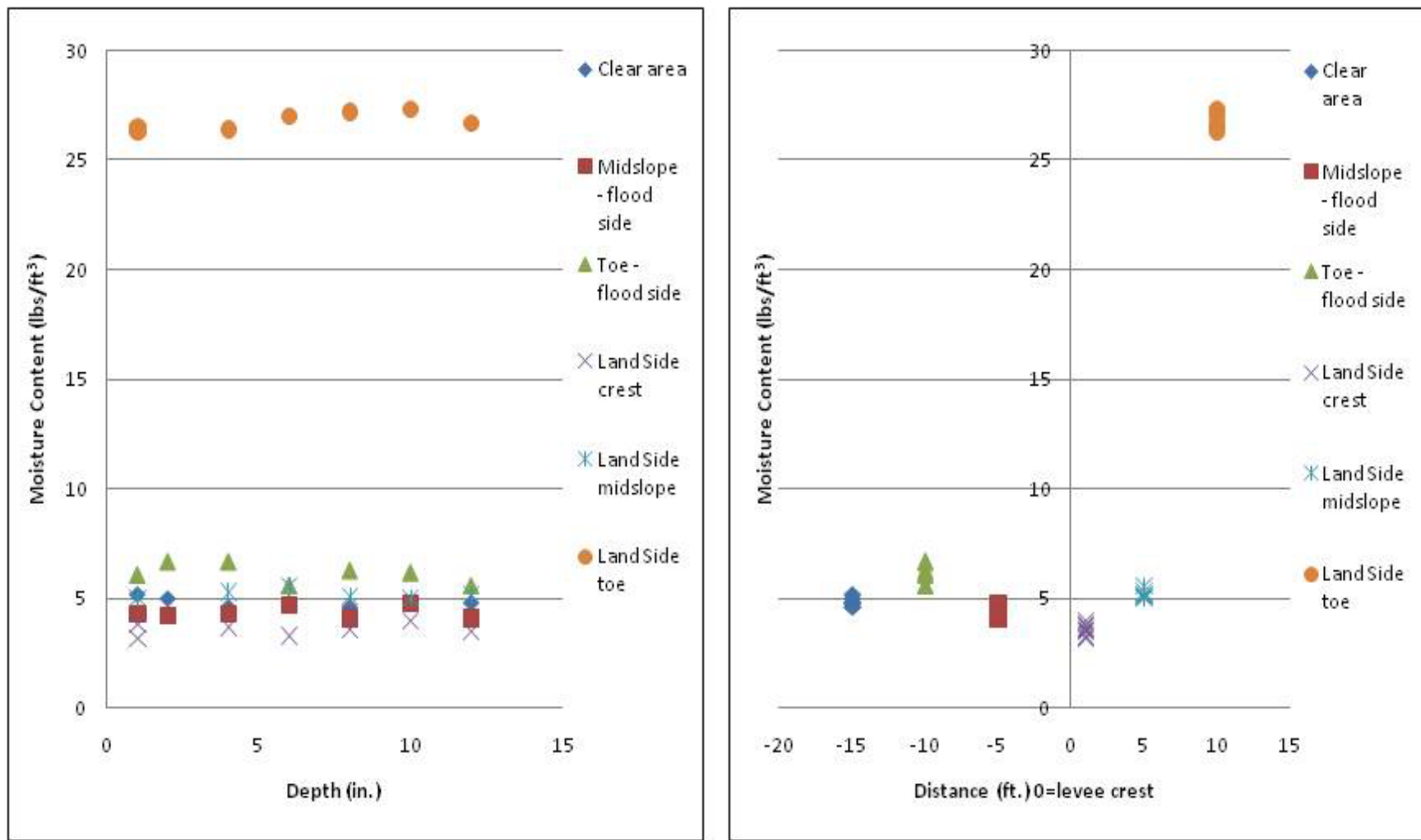


Figure 60c. Moisture content (lbs/ft³) versus depth (in.) and distance (ft.) from Troxler measurements for, levee, Boca Raton, FL.

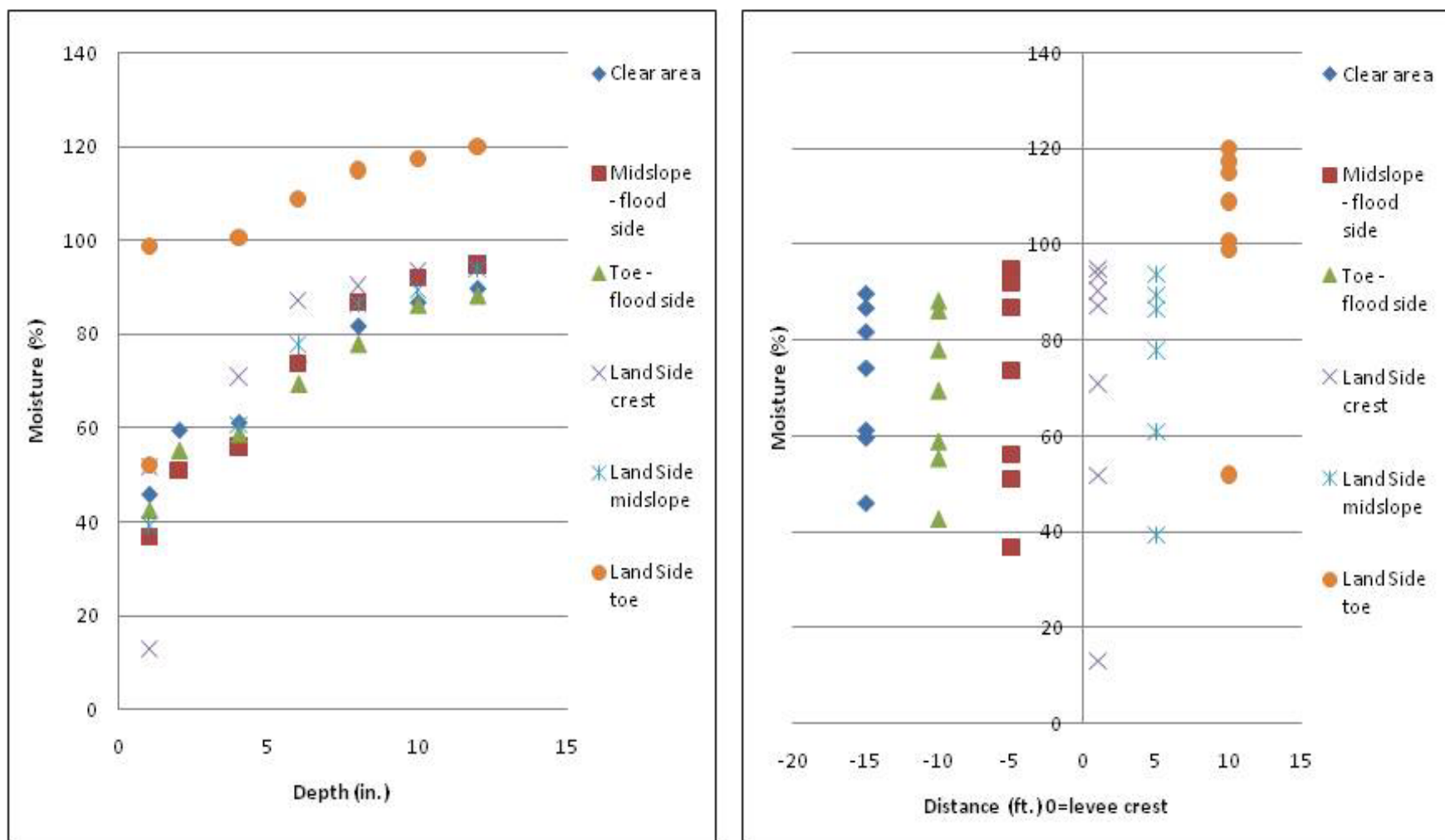


Figure 60d. Moisture (%) verses depth (in.) and distance (ft.) from Troxler measurements for, levee, Boca Raton, FL.

Figures 56a to 56d indicate that the levee has the lowest unit weights, while those from Tree 1 have some of the highest values measured. These high values might be related to the shallow bedrock at this location and the gravel that is present along the roadway. Moisture contents are the lowest at the levee. Profiles at Trees 1 and 2 as a function of distance from the levee show opposite trends for unit weights. The profile for Tree 1 shows unit weights lower near the tree and increase with distance from the tree (Figures 58a and 58b), while those at Tree 2 have the opposite trend, the unit weights decrease with distance from the tree (Figures 59a and 59b). In all cases, the unit weights increase with deeper depths and is the reason for separating the shallow from the deeper data. Unit weights for the levee in Figures 60a and 60b identify the highest values at the landside toe, followed by the riverside and landside crest. The presence of a shell road at the landside toe is responsible for the higher values unit weight, compared to those at the crest. Furthermore, the presence of seepage at the landside of the levee is responsible for the higher values for soil moisture in Figures 60c and 60d.

In general, the low water table combined with abundant rainfall for this area makes soil moisture generalizations to not be very meaningful. The highest values in Figures 56c and 56d are at the landside toe of the levee in an area where through-seepage was occurring. The water level on the flood side was above the toe of the levee during the site visit, reflecting the pervious nature of the levee embankment soils, resulted in seepage being present at the landside toe, which is reflected by the high values in Figures 56c and 56d.

Danville, PA

Introduction

The City of Danville, PA, is located in Montour County on the Susquehanna River (Figure 61). This location was included in the levee sites studied by ERDC because of its eastern U.S. setting, the existence of a comprehensive engineering assessment of the levee system for the FEMA certification process (Schnabel 2010), and the willingness of the levee owner to support ERDCs research effort. The engineering analysis by Schnabel (2010) included a study on the impacts of silver maples to the reliability of the flood protection system.

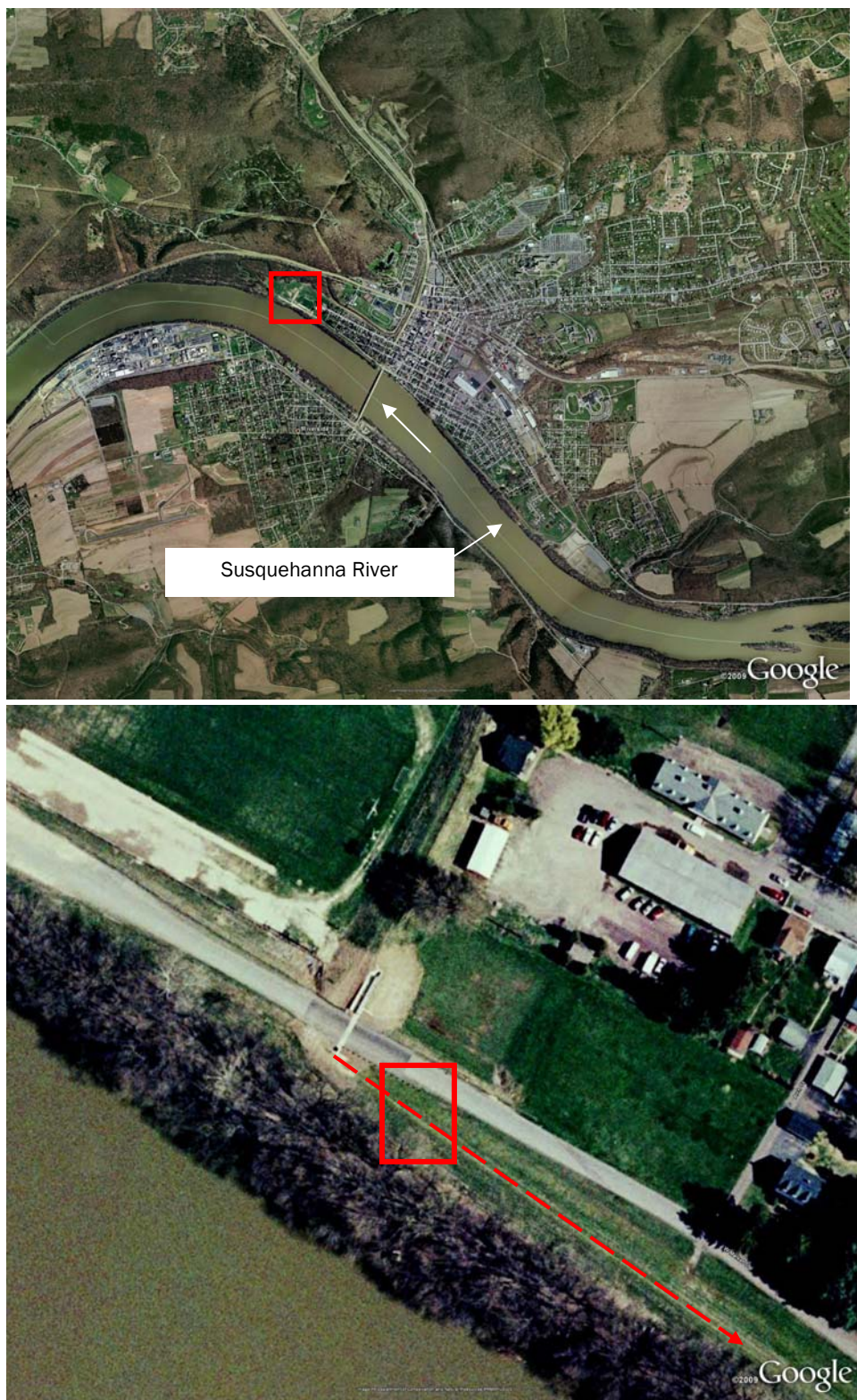


Figure 61. Study area along the Susquehanna River at Danville, Pennsylvania.
Close-up view in bottom of photo shows the levee center line and
the site studied at Station 122 + 90. Note the trees
growing at the edge of the VFZ.

The Danville levee system is owned, operated, and maintained by the local borough. The levee system is approximately 5 miles in length and borders the Susquehanna River. The system provides flood protection from the Susquehanna River and its tributaries flowing within the Borough limits. The flood protection system was originally built in the mid-1950s and has been subsequently upgraded in response to large magnitude flood events over the past 50 years (Schnabel 2010). The levee system involves earthen levees, flood walls, and interior drainage control structures, which pass drainage behind the levee to the Susquehanna River during low water.

The typical levee prism contains a 12-ft-wide crown with side slopes of 1 V and between 2.0 to 2.5 H (Figure 62). To comply with guidance for levee certification, the Borough removed all woody vegetation from the levee toe in 2009 to meet the standards for the vegetation free zone (VFZ) along the levee right-of-way. Most of the woody vegetation deficiencies at Danville involved the presence of mature silver maples within the flood side 15-ft-wide VFZ corridor (Figure 62).

ERDC activities at Danville involved a reconnaissance survey of the levee system and limited study of a site where pre-existing engineering data were available. To support further study, ERDC performed additional data collection at Station 122+90, which was a study profile in the engineering assessment by Schnabel (2010). ERDC personnel obtained hydraulic conductivity, Troxler density, and Troxler soil moisture measurements.

Geologic setting

Danville is located in a narrow alluvial valley cut into sedimentary rocks of Silurian (443 to 416 million years BP) and Devonian (416 to 359 million years BP) by the Susquehanna River during geologic time (Berg et al. 1984; Berg and Dodge 1981; Hoskins 1976a, 1976b; Schnabel 2010). The borough is located in the region of Pennsylvania that was covered by Pleistocene continental glaciers as evidence by the presence of glacial tills in Montour County (Sevon and Braun 2007; USDA 1985). Additionally, this region was further modified by the discharge of glacial melt waters into the Susquehanna River system during the Pleistocene. Boring data drilled for the geotechnical evaluation of the Danville levee system by Schnabel (2010) indicate that the alluvial deposits are generally less than 20 to 30 ft thick. The undisturbed alluvium in descending order consists of a thin top blanket of silt and clay, a pervious substratum of coarse-grained



Figure 62. View of Danville levee looking southwest at Station 122 + 90. Silver maple stumps along edge of the vegetation free zone were removed in 2009.

sand and gravel, a lower coarse gravel unit containing disintegrated bedrock, and rock (Schnabel 2010).

A representative boring from Station 122 + 90 at the levee center line is presented in Figure 63 (Schnabel 2010). This boring is representative of similar conditions for the levee and its foundation for the Danville flood protection system. The levee at this location is approximately 15 ft tall as compared to the toe. The levee embankment is composed of fill material, consisting of sandy clay and silty to clayey sand. The levee foundation is composed of fill, which becomes coarser grained with depth and includes coal, cinders, slag, and ash. The presence of these materials in the levee and foundation fill is a legacy of Danville's history as an important iron manufacturing center during the 1800s to support the development of railroads in the U.S (Schnabel 2010). The fill transitions to natural alluvial sediments at 26-ft depth in the center line boring in Figure 63 and terminates in the coarse gravels above the bedrock contact.

Danville Borough levee assessment and results

The Borough of Danville contracted an engineering assessment of their levee system to AMEC and Schnabel Engineering to comply with the FEMA certification process (Scott Raschke⁵ 2011; Schnabel 2010). The engineering assessment by Schnabel Engineering included drilling additional geotechnical borings in the levee right-of-way (center line, floodside toe, and riverside toe), digging test pits in the levee section, and elevation surveys of representative sections. Furthermore, test pits were dug adjacent to mature silver maple trees to map the root extent and determine the impact to the levee prism. A steady state seepage analyses using SEEPW was performed on representative profile sections to assess underseepage impacts because of pervious geologic conditions, pervious levee soils, and impacts related to woody vegetation growing within the VFZ. Stratigraphic models of the levee and foundation were developed for the SEEPW analysis for the representative profiles evaluated using the boring data as shown by Table 23 and the stratum designation identified on the boring log in Figure 63. ERDC obtained additional field measurements at Station 122 + 90, which was one of the levee sections evaluated by the Schnabel (2010) assessment.

⁵ Personal communication. 2011. Scott Raschke, AMEC.

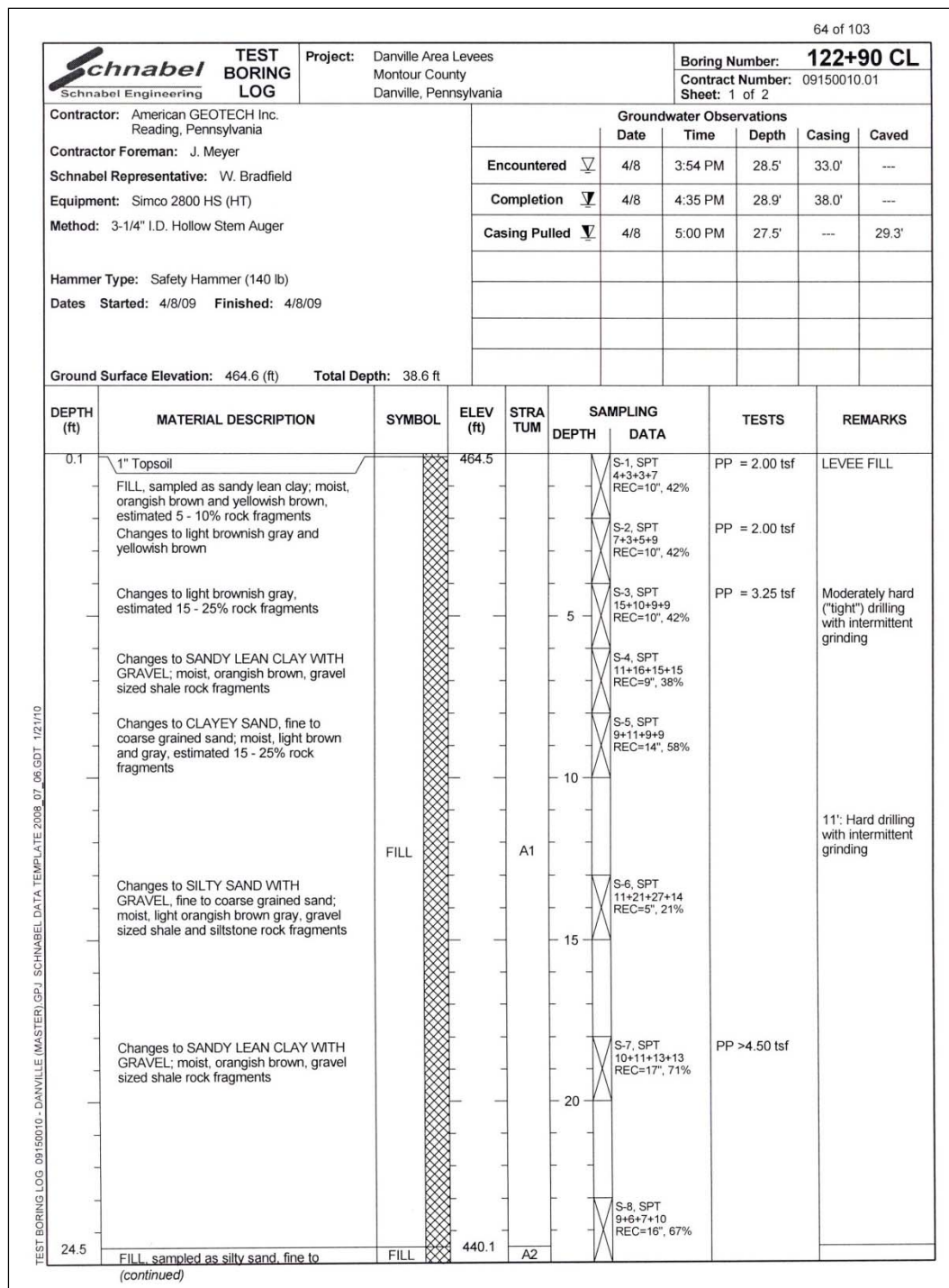


Figure 63a. Center line boring from Station 122 + 90, continued (Schnabel 2010).

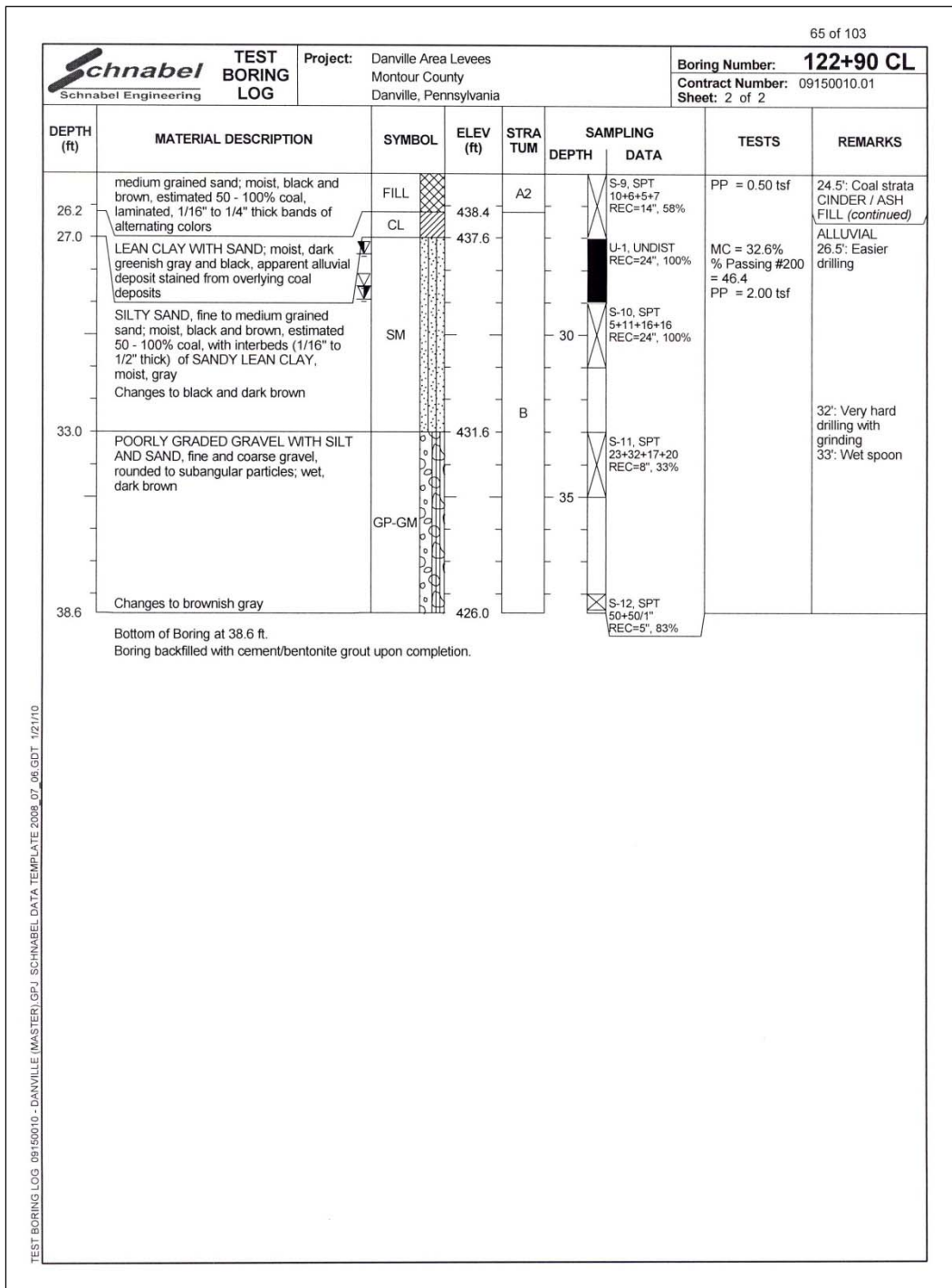


Figure 63b. Concluded.

Table 23. Stratum designation for the SEEPW analysis of the Danville levee system (Schnabel 2010).

Soil Description	Classification ⁽¹⁾	Density ⁽²⁾	Designation on Plates
FILL: Levee Fill (A1)	Fine	Loose/Soft	A1-F-L
	Fine	Dense/Firm	A1-F-D
	Coarse	Loose	A1-C-L
	Coarse	Dense	A1-C-D
FILL: Cinder/Ash Fill (A2)	Coarse	Loose	A2-C-L
	Coarse	Dense	A2-C-D
FILL: Soil Fill (A3)	Fine	Loose/Soft	A3-F-L
	Fine	Dense/Firm	A3-F-D
	Coarse	Loose	A3-C-L
	Coarse	Dense	A3-C-D
ALLUVIAL: Fine-Grained (B1) ⁽³⁾	Low plasticity	Loose/Soft	B1-L-L
	Low plasticity	Dense/Firm	B1-L-D
ALLUVIAL: Coarse-Grained (B2)	SP (poorly-graded sand)	Loose	B2-SP-L
	SP (poorly-graded sand)	Dense	B2-SP-D
	SM (silty sand)	Loose	B2-SM-L
	SM (silty sand)	Dense	B2-SM-D
ALLUVIAL: Coarse-Grained (B3)	GP (poorly-graded gravel)	Loose	B3-GP-L
	GP (poorly-graded gravel)	Dense	B3-GP-D
	GM (silty gravel)	Loose	B3-GM-L
	GM (silty gravel)	Dense	B3-GM-D
DISINTEGRATED ROCK (C)	Disintegrated Rock		C
ROCK (Rx)	Rock		D

(1) Fine – classifies as fine-grained based on gradation (greater than 50% passing the No. 200 sieve).

Coarse – classifies as coarse-grained based on gradation (less than 50% passing the No. 200 sieve).

(2) Indicates the basic consistency/density of a soil based on unit weight/shear strength. Note fine-grained soils are not typically classified as “loose” or “dense,” but this nomenclature was used for simplicity.

(3) Fine-grained alluvial were originally subdivided into low and high plasticity soils, but based on interpretation of the data, the high plasticity designation was not necessary.

Included in the Schnabel (2010) seepage study was a sensitivity analysis to determine the impacts to levee reliability from the root zone of silver maple trees growing into the VFZ and the levee prism. One of the purposes for the sensitivity analysis was to determine the practical root excavation depth needed for the mitigation of woody vegetation and roots growing into the levee slope and the VFZ from encroaching flood side tree growth.

Tree data were obtained from excavation of test pits adjacent to mature silver maples to provide information for the sensitivity modeling and analysis. Test pit excavation was performed with the collaboration of an arborist. The sensitivity analyses used a 1-, 2-, and 3-ft root plate or zone along the floodside to assess the exit gradient and the factor of safety at each representative site evaluated by increasing the permeability of the root zone or plate, in comparison to the underlying embankment levee soils.

Test pit studies indicated that the majority of mature silver maple roots were shallow in nature, being less than 18 in. deep. The maximum root size was limited to about 6 in. in diameter adjacent to the tree and diminished significantly in size within three stump diameters (Schnabel 2010). Furthermore, it was found that silver maple roots, where present, did not penetrate deep into the main body of the levee prism, but rather were confined to only the upper 18 in. Thus, tree mitigation within the VFZ at the levee toe was restricted to cutting the tree and leaving the stump in place (Figure 62), because the seepage analysis indicated only a 5% difference in the factor of safety between areas where trees were present and those without.

Laboratory soils data and hydraulic conductivity

Laboratory soil testing was conducted as part of the Danville levee assessment by Schanabel (2010) to assign engineering properties to the various stratigraphic layers (Table 23) in their SWEEPW cross sections. Test data from selected samples were included on the boring logs (Figure 63). Testing included the standard engineering-related tests for moisture content, grain size distribution, Atterberg limits, dry unit weight, bulk density, hydraulic conductivity, direct shear, and triaxial shear test. Additionally, ERDC supplemented these data with in situ Troxler density, soil moisture, and falling head permeameter tests at levee Station 122 + 90.

Groundwater conditions

As the levee system is located adjacent to the river, groundwater levels are governed by the stage of the Susquehanna River. The pervious nature of the alluvial soils in the levee foundation allow for rapid changes in groundwater elevation as the stage of the river rises or falls. Groundwater was encountered at the base of the fill sequence in the center line boring in Figure 63.

Troxler measurements

Troxler data at Danville, PA, were obtained from three transects or profiles along the levee from the landside to the floodside (Figure 64). No trees were present on any of the levees. Any trees that were present were removed in 2009 by the city to comply with USACE vegetation policy. Levee soils are composed of fill (i.e., coal, cinders, slag, and ash from earlier iron mining and smelting activities) and sandy clay (SC) obtained from the floodplain according to available boring data. Measured unit weights from the Danville area were some of the highest values recorded among all the ERDC sites visited. Examination of all the data in Table 24 and Figures 65a to 65d identifies a maximum unit weight of 126 lb/ft³. These data are presented in Figures 65a and 65b. Moisture contents are between 10 and 50% for the near surface and between 8 and 28% for 12-in. depth. Summary data for the individual profiles are presented in Tables 25, 26, and 27, and Figures 66 (a - d), 67 (a - d), and 68 (a - d), for Profiles 1, 2, and 3, respectively. Typically, the levee crest or center line has the highest values for unit weight. In some cases, the toe or levee midslope has some of the lowest values measured, as compared to the riverside of the floodplain with increasing distance from the levee toe. Highest values of soil moisture occur on the natural floodplain. The levees typically have the lowest moisture values as they have steep slopes (1V:2.5H).

Vicksburg, MS

Introduction

Two sites at a local sand and gravel pit in Warren County, MS, (Figures 69 to 70) were evaluated for targeted studies of trees for mapping individual roots and the rootball. Studies were performed on an oak tree and involved terrestrial LiDAR, GPR, and resistivity surveys beneath the tree. Studies conducted at the pine tree were limited to GPR surveys. Both of the tree sites were later excavated by using an air compressor and air lance to expose the root system to map the roots and to verify the results of the geophysical methods for noninvasive mapping.

The purpose for conducting the LiDAR survey at the oak site was to obtain a detailed morphometric map of the tree and its root system and obtain physical properties of the roots for modeling purposes. Terrestrial LiDAR surveys were performed to obtain a detailed map of the tree canopy and its

Figure 64. The study site in Danville, PA.

**Table 24. Statistical data for Troxler measurements in Danville, PA:
2-, 4-, 6-, 8-, 10-, and 12-in. depths.**

Depth (2-4-6 in.)	Dry Density (lb/ft ³)	Wet Density (lb/ft ³)	Moisture Content (lb/ft ³)	Percent Moisture (%)	Depth (8-10-12 in.)	Dry Density (lb/ft ³)	Wet Density (lb/ft ³)	Moisture Content (lb/ft ³)	Percent Moisture (%)
Max	116.9	132.1	25.90	39.7	Max	126.0	140.5	25.6	30.3
Min	55.8	73.8	9.7	8.7	Min	69.6	86.4	7.9	7.4
Mean	82.1	101.1	19.0	24.2	Mean	93.7	111.8	18.1	19.8
Median	78.6	99.4	18.8	25.5	Median	89.7	110.1	18.2	20.6
Mode	76.9	80.5	22.2	#N/A	Mode	83.7	98.5	18.6	20.6
Standard Deviation	15.3	14.5	4.4	7.5	Standard Deviation	13.9	13.3	4.1	5.6
*#N/A: no central value in data set					*#N/A: no central value in data set				

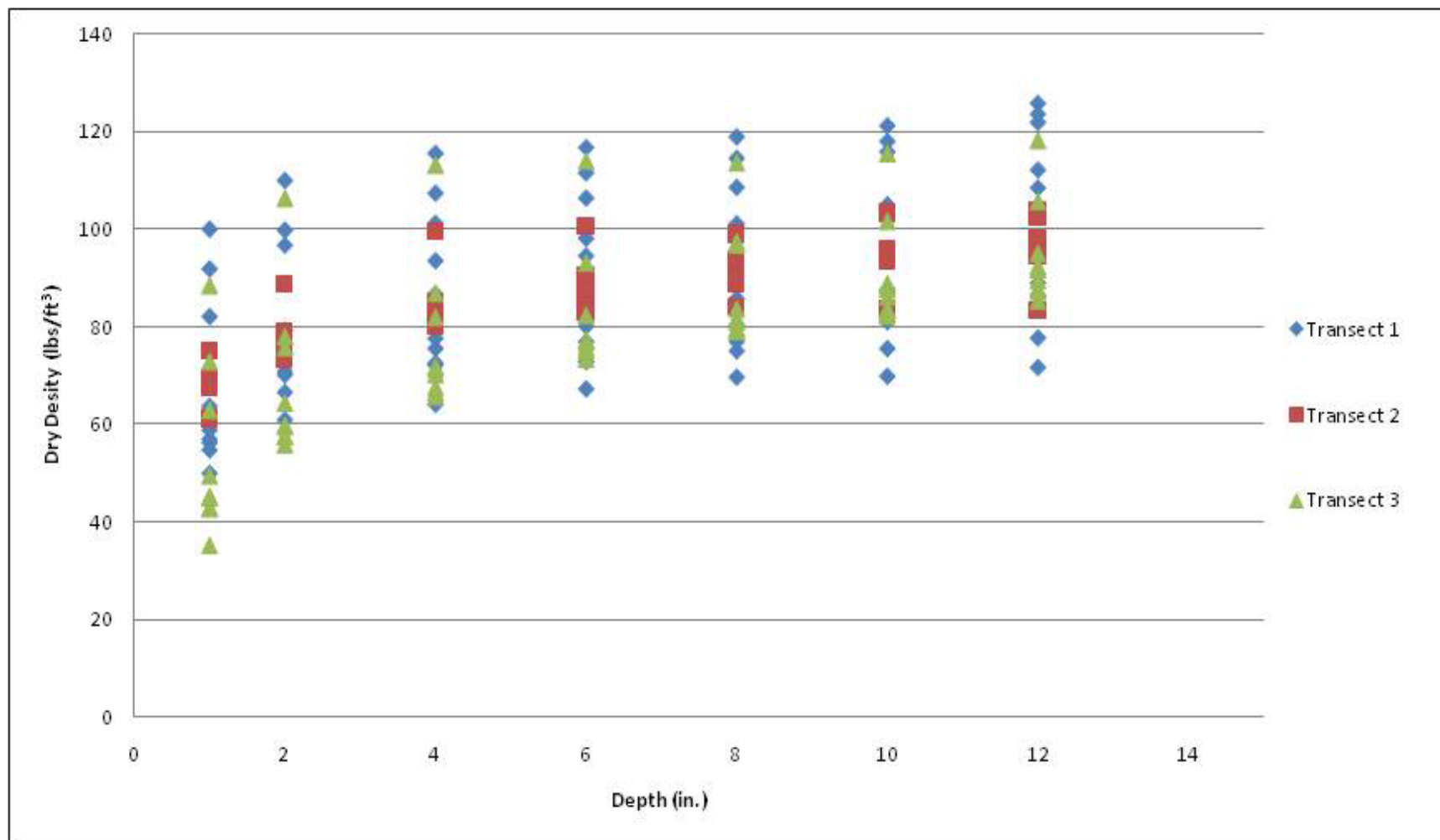


Figure 65a. Dry density (lbs/ft³) from Troxler measurements for Danville, PA.

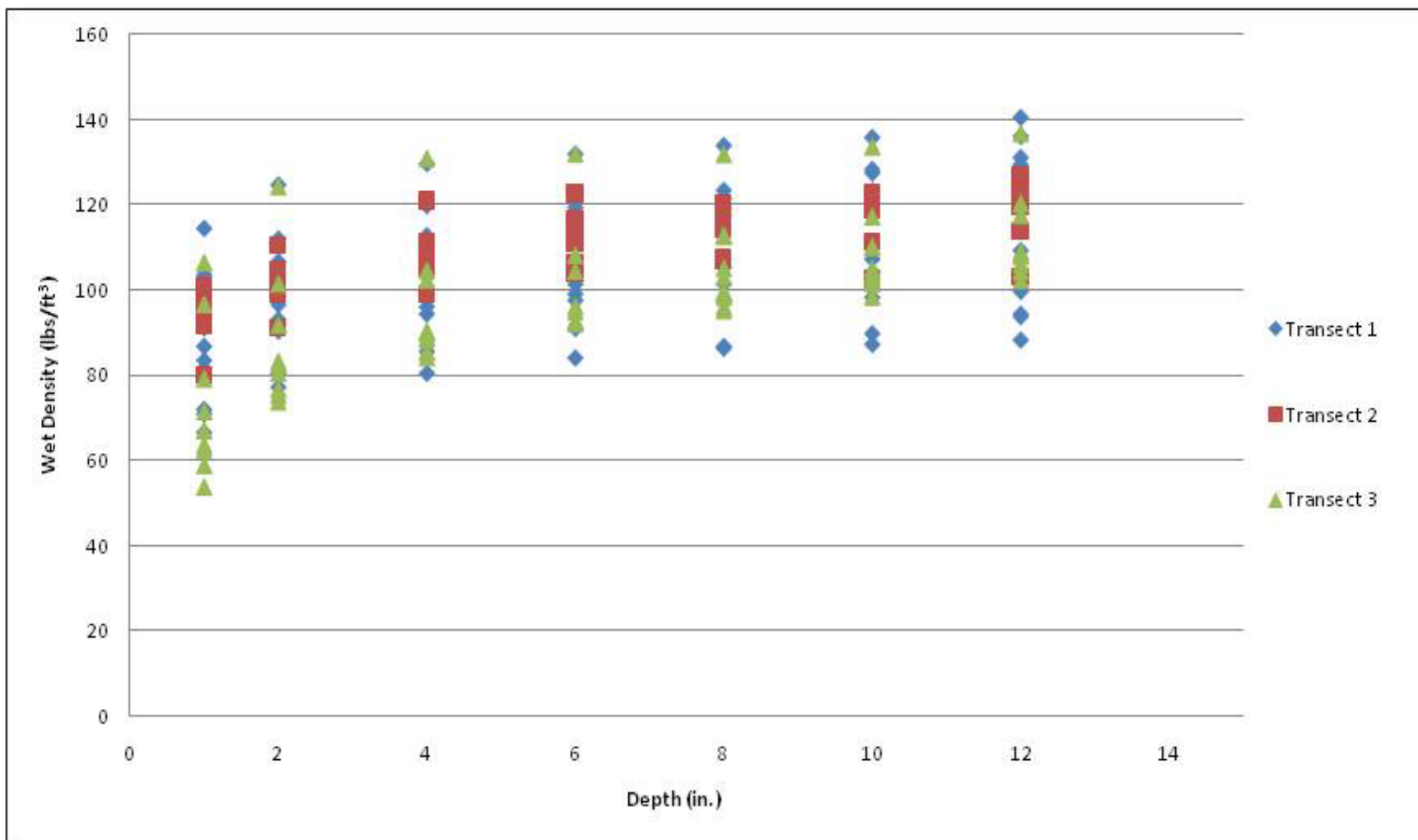


Figure 65b. Wet density (lbs/ft³) from Troxler measurements for Danville, PA.

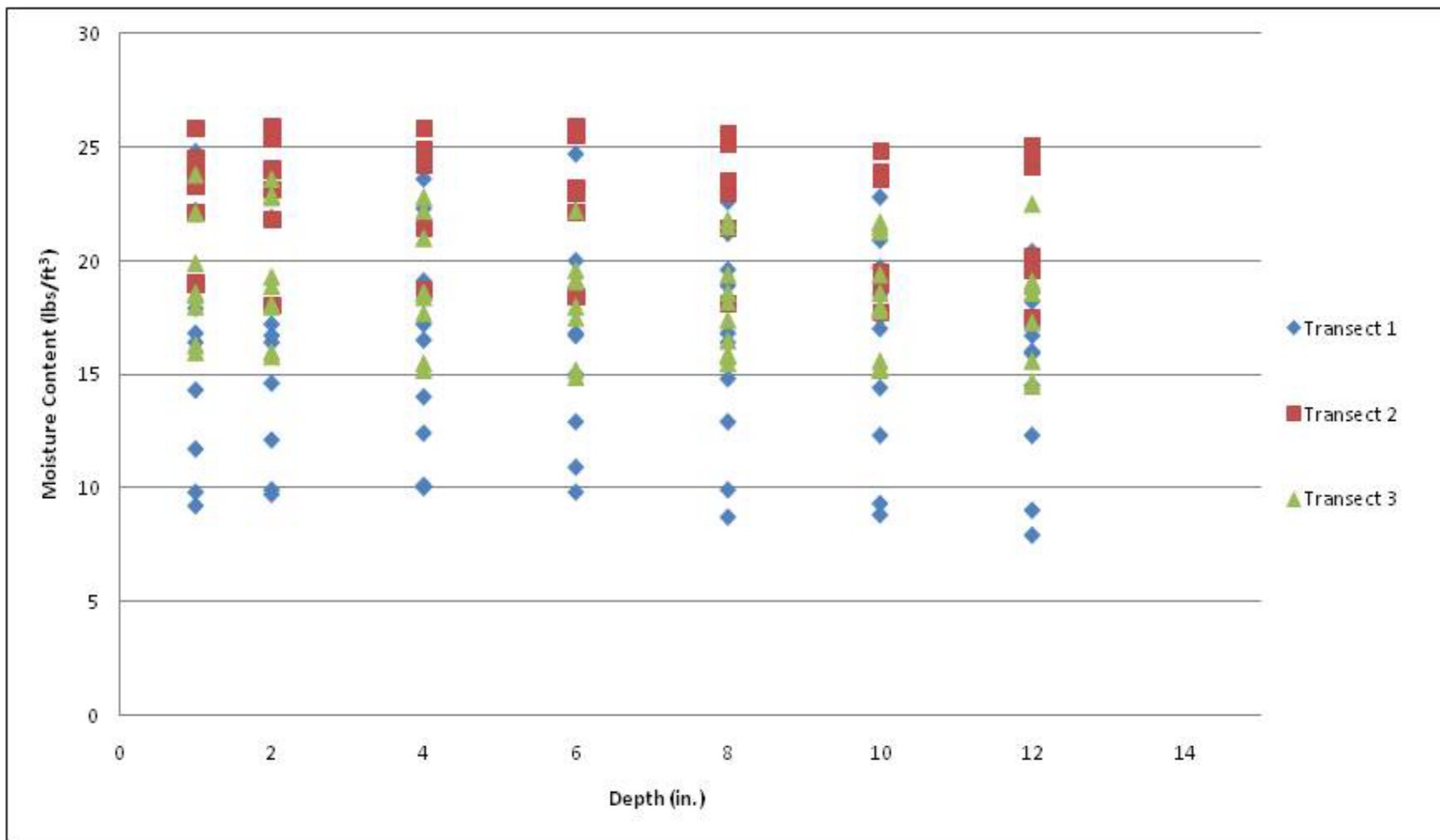


Figure 65c. Moisture content (lbs/ft^3) from Troxler measurements for Danville, PA.

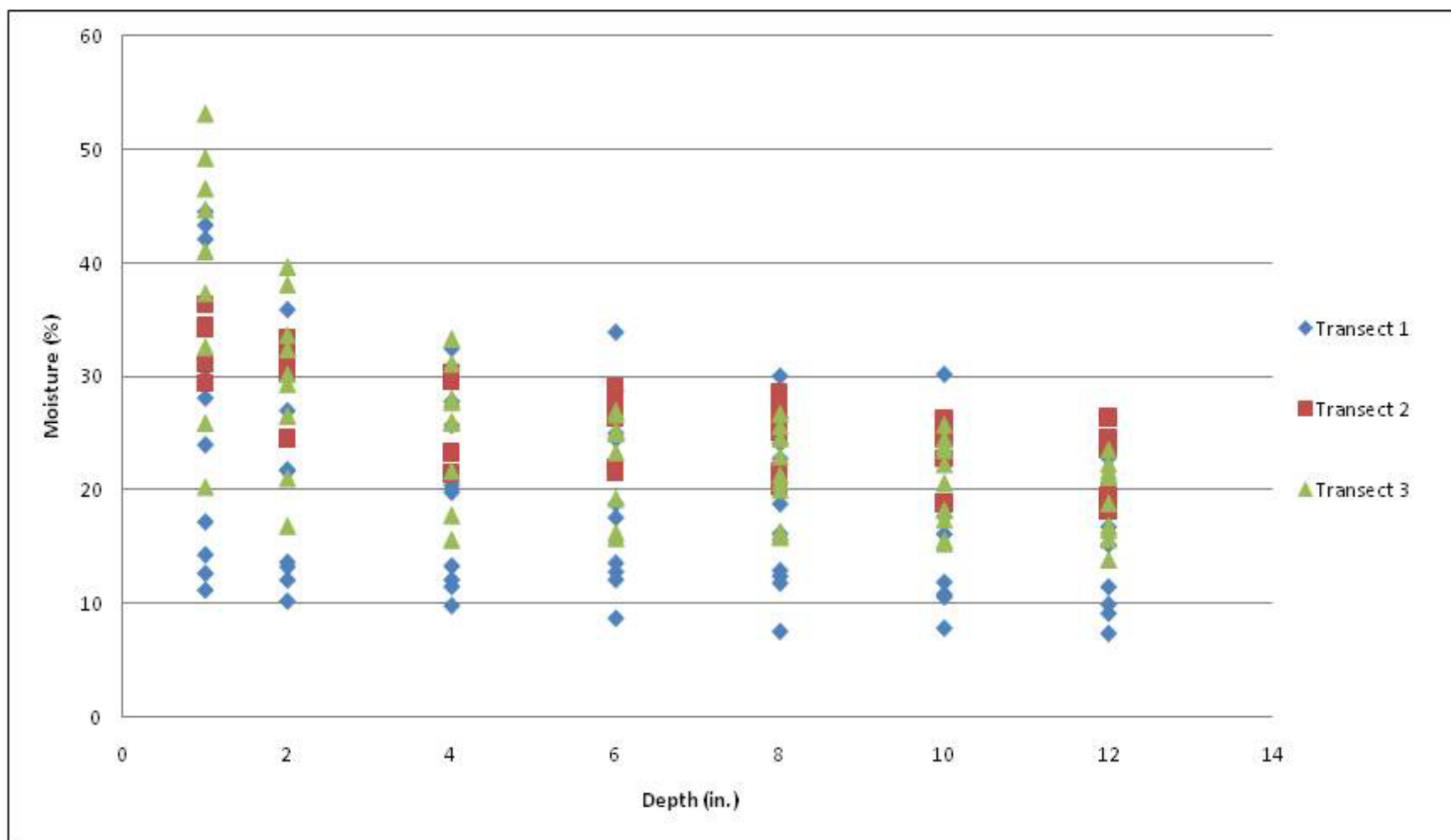


Figure 65d. Moisture (%) from Troxler measurements for Danville, PA.

**Table 25. Statistical data for Troxler measurements in Danville, PA, Transect1:
2-, 4-, 6-, 8-, 10-, and 12-in. depths.**

Transect 1 Depth (2-4-6 in.)	Dry Density (lb/ft ³)	Wet Density (lb/ft ³)	Moisture Content (lb/ft ³)	Percent Moisture (%)
Max	116.9	131.9	24.7	36.0
Min	60.8	77.2	9.7	8.7
Mean	85.9	102.6	16.7	20.6
Median	79.7	99.2	16.7	20.1
Mode	#N/A	80.5	17.2	#N/A
Standard Deviation	16.9	15.0	4.8	8.4
*#N/A: no central value in data set				

Transect 1 Depth (8-10-12 in.)	Dry Density (lb/ft ³)	Wet Density (lb/ft ³)	Moisture Content (lb/ft ³)	Percent Moisture (%)
Max	126.0	140.5	22.8	30.3
Min	69.6	86.4	7.9	7.4
Mean	96.5	112.2	15.7	17.2
Median	94.8	113.5	16.6	16.5
Mode	#N/A	#N/A	12.3	#N/A
Standard Deviation	18.7	17.4	4.4	6.8
*#N/A: no central value in data set				

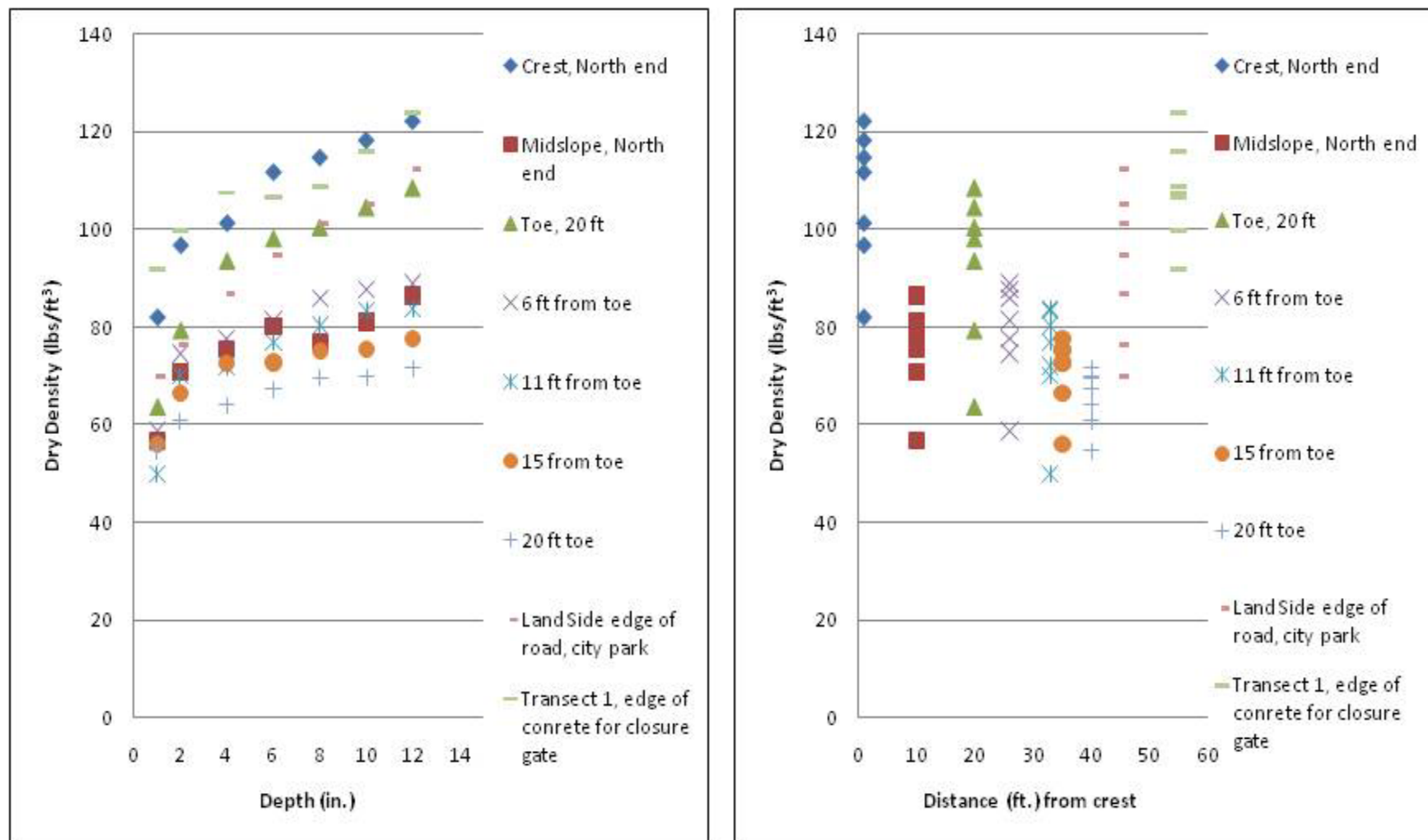


Figure 66a. Dry density (lbs/ft^3) verses depth (in.) and distance (ft.) from Troxler measurements for, Transect 1, Danville, PA.

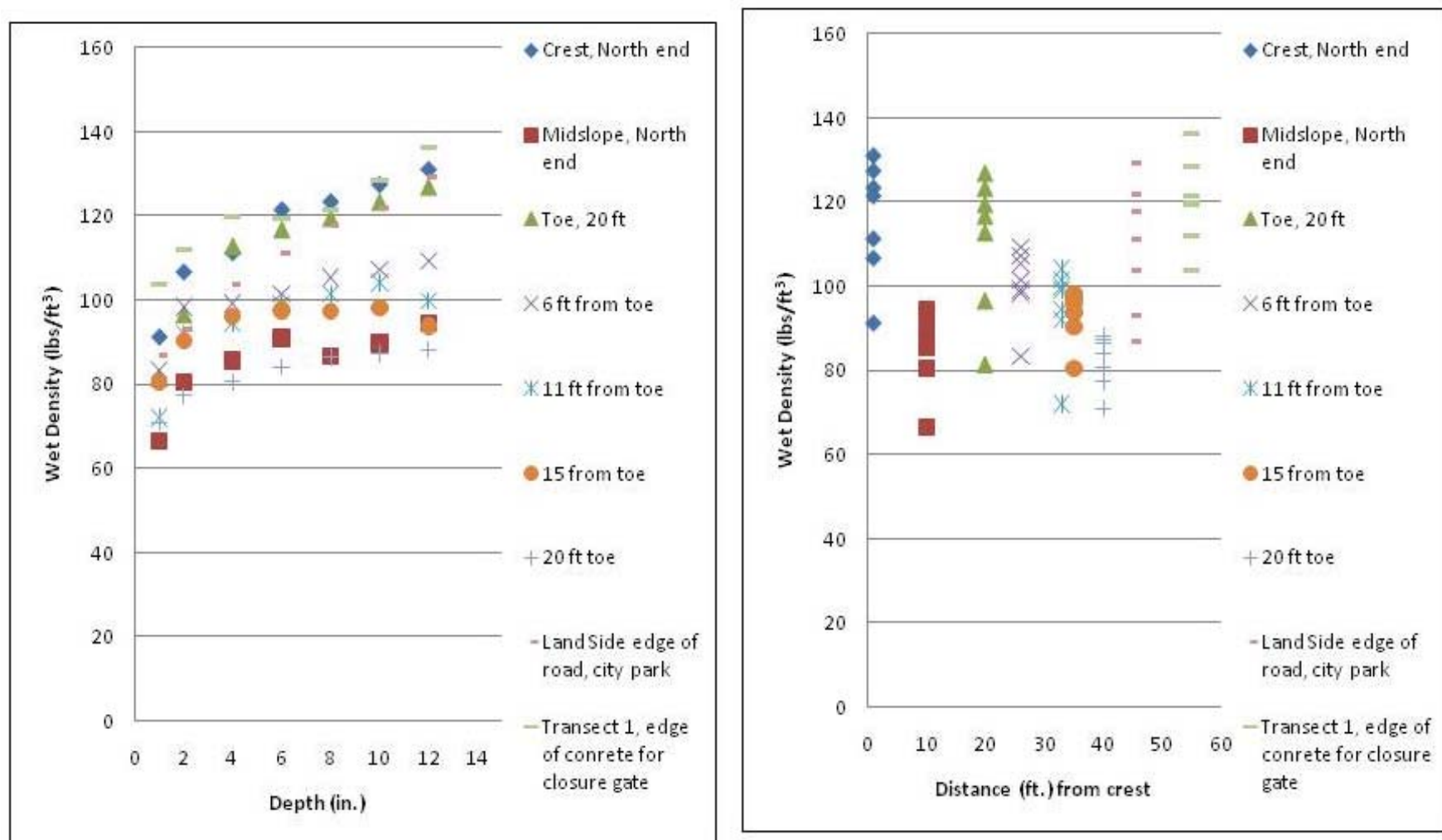


Figure 66b. Wet density (lbs/ft^3) versus depth (in.) and distance (ft.) from Troxler measurements for Transect 1, Danville, PA.

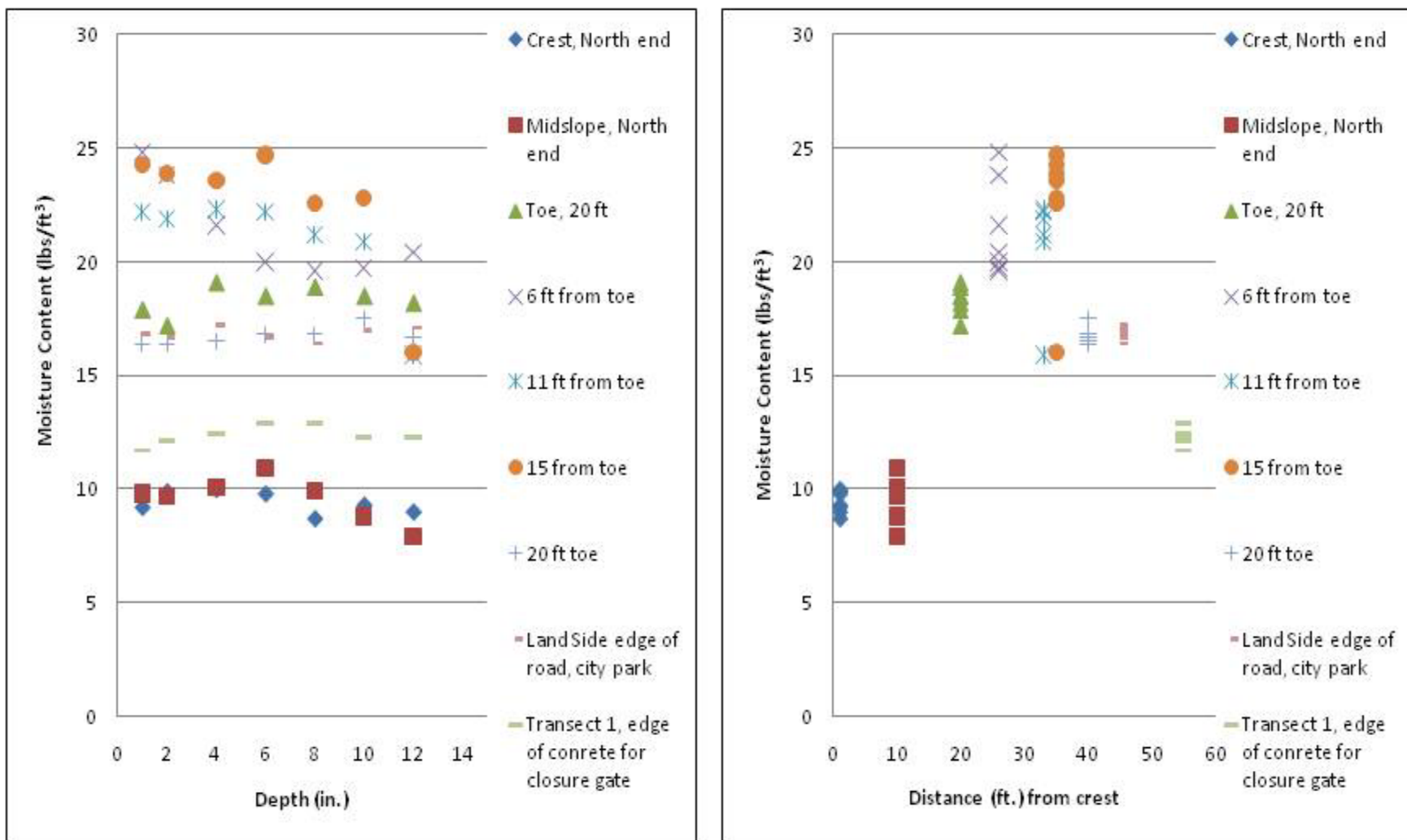


Figure 66c. Moisture content (lbs/ft^3) versus depth (in.) and distance (ft.) from Troxler measurements for Transect 1, Danville, PA.

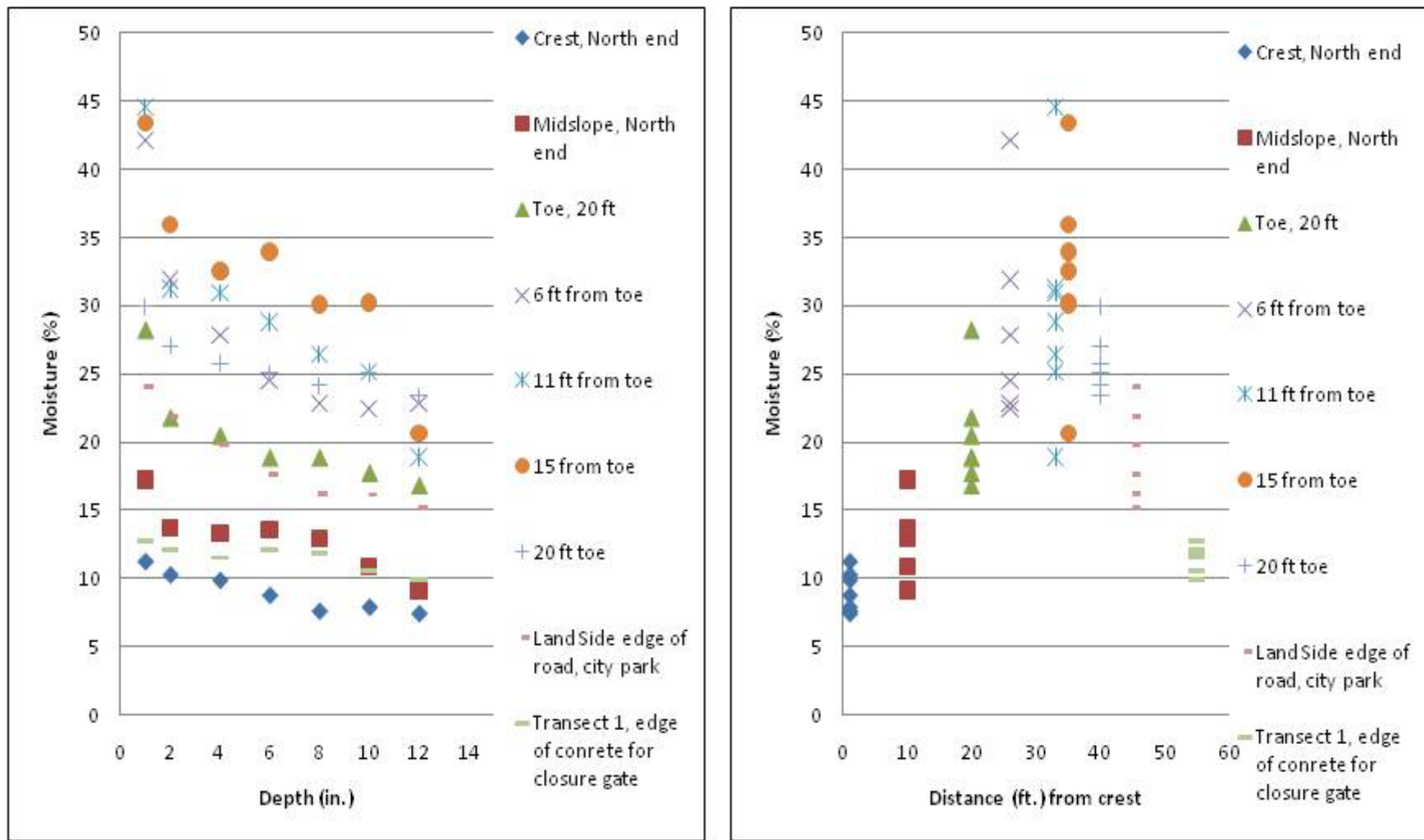


Figure 66d. Moisture (%) versus depth (in.) and distance (ft.) from Troxler measurements for, Transect 1, Danville, PA.

**Table 26. Statistical data for Troxler measurements in Danville, PA, Transect 2:
2-, 4-, 6-, 8-, 10-, and 12-in. depths.**

Transect 2 Depth (2-4-6 in.)	Dry Density (lb/ft ³)	Wet Density (lb/ft ³)	Moisture Content (lb/ft ³)	Percent Moisture (%)	Transect 2 Depth (8-10-12 in.)	Dry Density (lb/ft ³)	Wet Density (lb/ft ³)	Moisture Content (lb/ft ³)	Percent Moisture (%)
Max	100.6	122.7	25.9	33.4	Max	103.9	127.1	25.6	28.6
Min	73.2	91.1	18.0	21.5	Min	83.4	102.7	17.5	18.2
Mean	84.2	107.3	23.1	27.6	Mean	94.0	116.0	22.0	23.5
Median	83.3	106.1	23.6	28.8	Median	94.4	118.9	23.3	24.2
Mode	#N/A	#N/A	25.9	#N/A	Mode	#N/A	118.9	#N/A	#N/A
Standard Deviation	7.6	8.0	2.6	3.9	Standard Deviation	6.3	7.2	2.8	3.3
*#N/A: no central value in data set					*#N/A: no central value in data set				

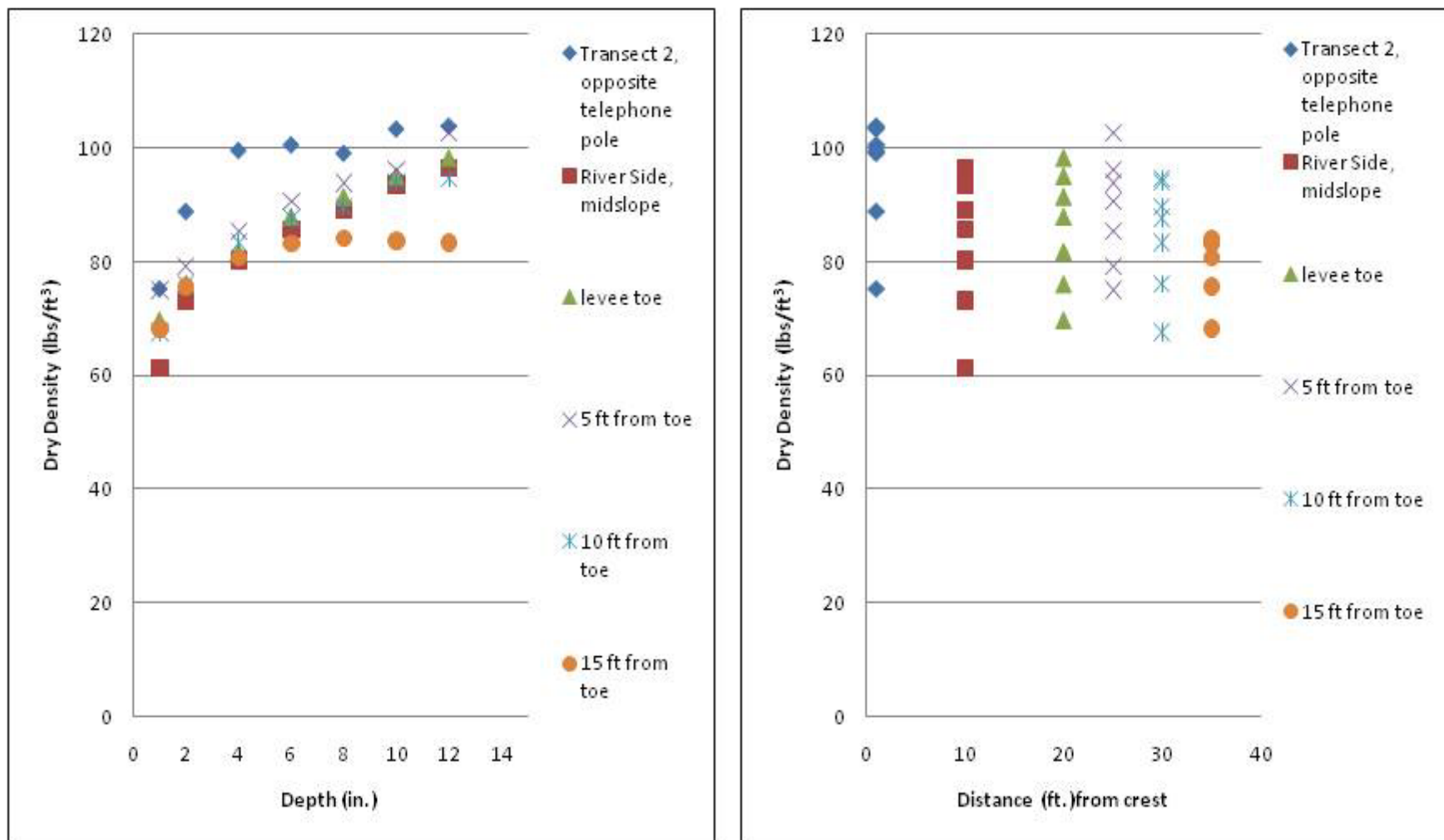


Figure 67a. Dry density (lbs/ft³) verses depth (in.) and distance (ft.) from Troxler measurements for, Transect 2, Danville, PA.

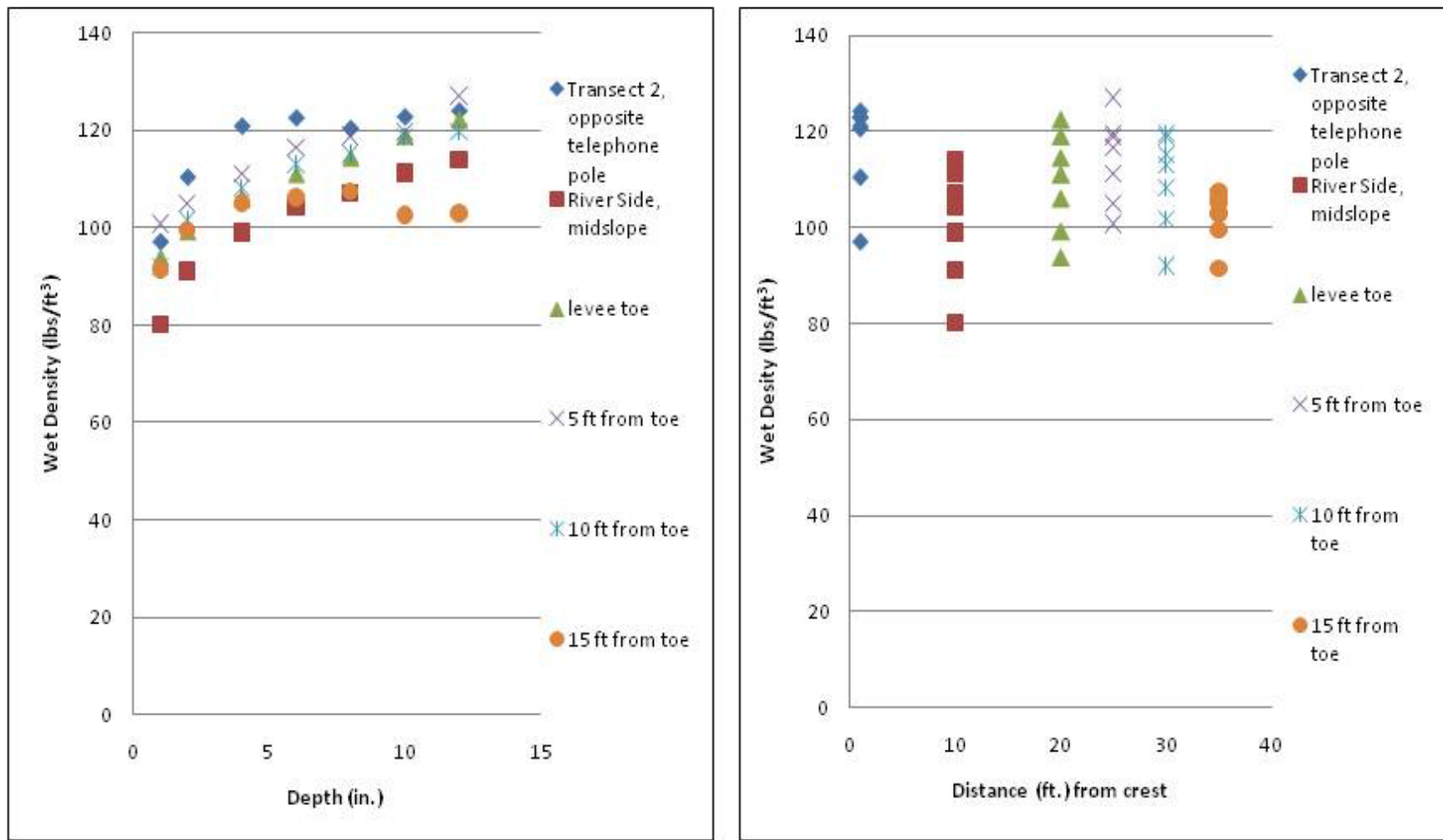


Figure 67b. Wet density (lbs/ft^3) verses depth (in.) and distance (ft.) from Troxler measurements for, Transect 2, Danville, PA.

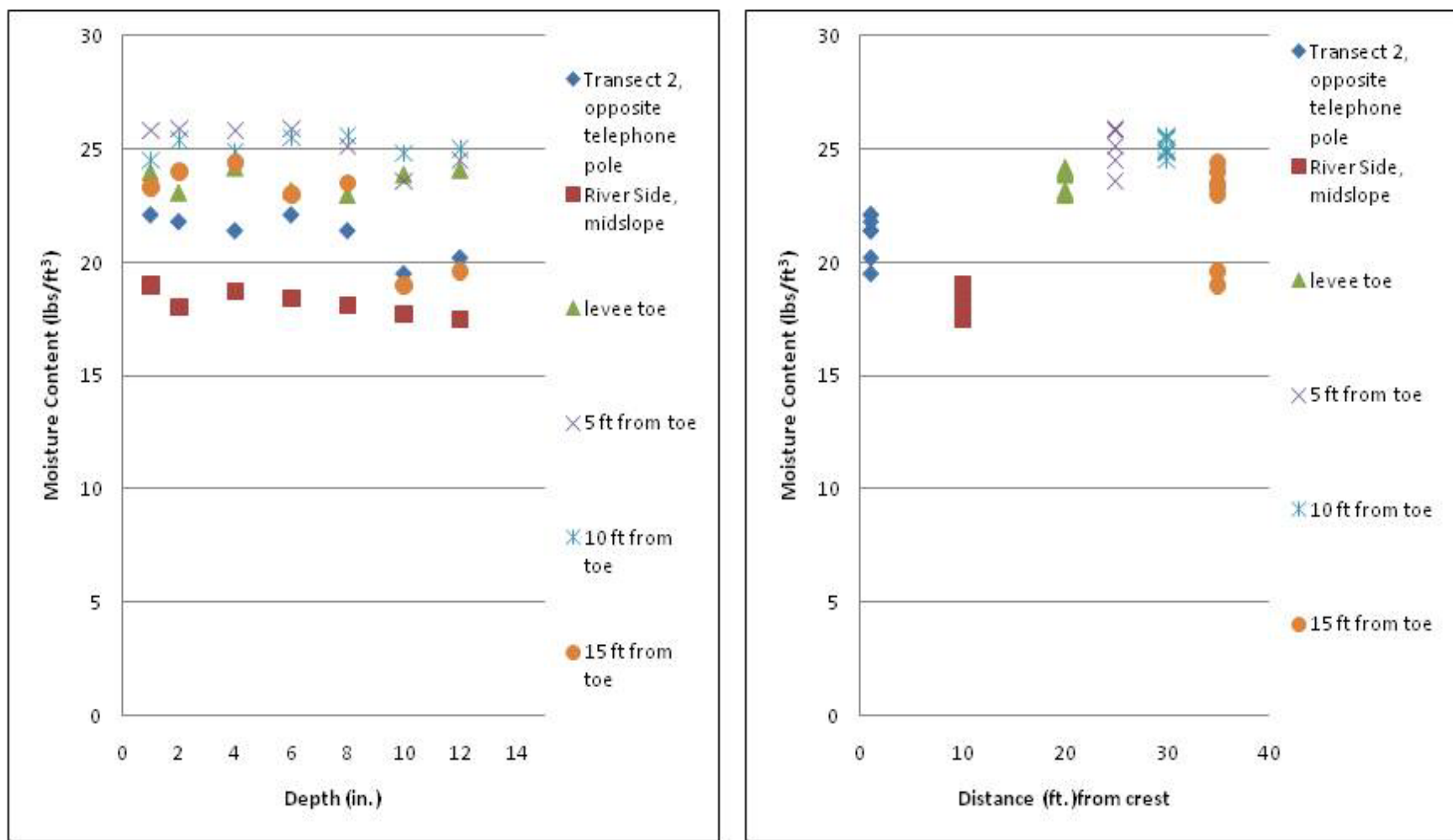


Figure 67c. Moisture content (lbs/ft³) verses depth (in.) and distance (ft.) from Troxler measurements for, Transect 2, Danville, PA.

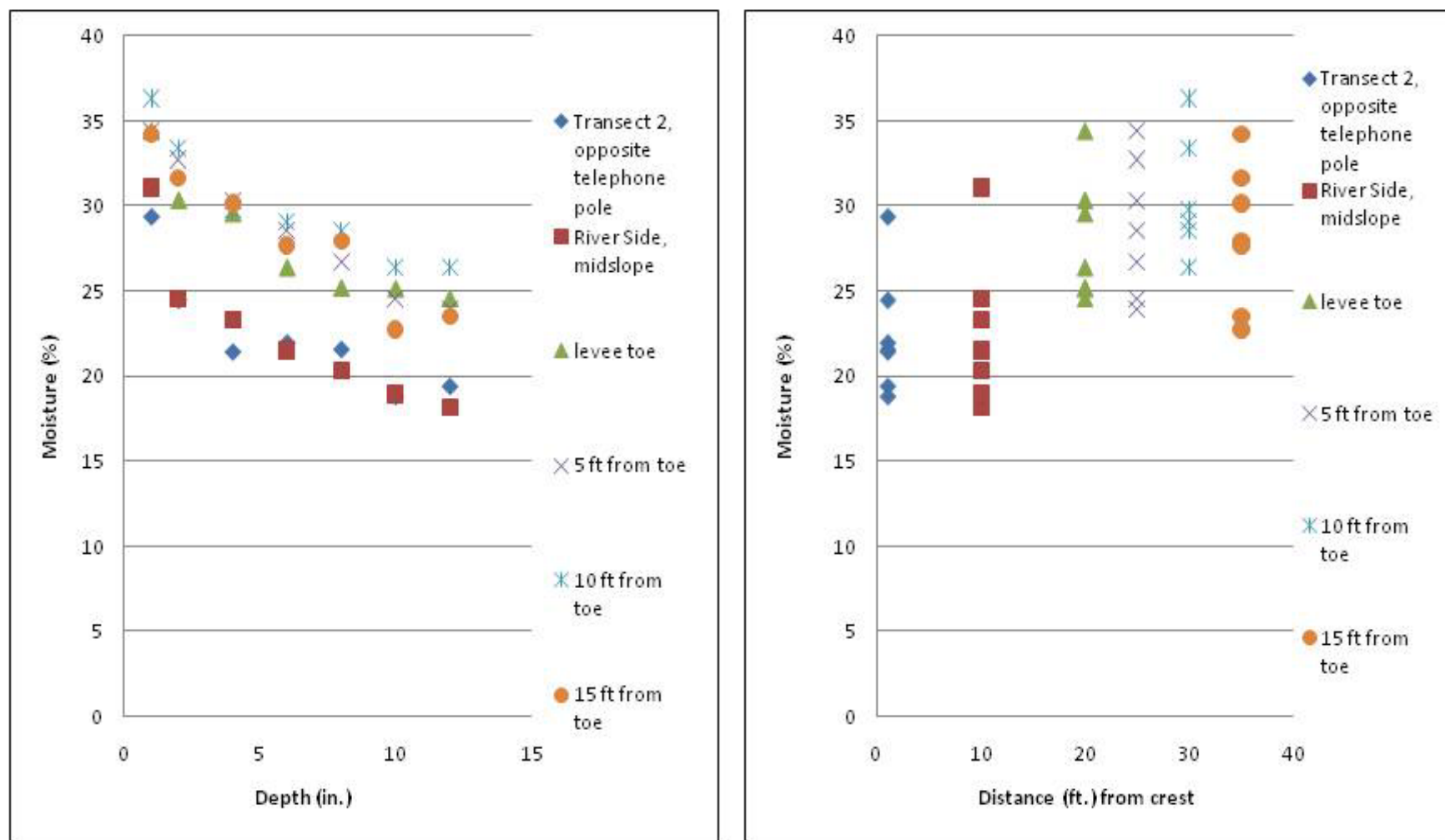


Figure 67d. Moisture (%) verses depth (in.) and distance (ft.) from Troxler measurements for, Transect 2, Danville, PA.

**Table 27. Statistical data for Troxler measurements in Danville, PA, Transect 3:
2-, 4-, 6-, 8-, 10-, and 12-in. depths.**

Transect 3 Depth (2-4-6 in.)	Dry Density (lb/ft ³)	Wet Density (lb/ft ³)	Moisture Content (lb/ft ³)	Percent Moisture (%)	Transect 3 Depth (8-10-12 in.)	Dry Density (lb/ft ³)	Wet Density (lb/ft ³)	Moisture Content (lb/ft ³)	Percent Moisture (%)
Max	114.1	132.1	23.6	39.7	Max	118.4	137.0	22.5	26.8
Min	55.8	73.8	14.9	15.7	Min	79.1	95.3	14.5	13.9
Mean	76.1	95.0	18.9	25.9	Mean	90.7	108.8	18.1	20.3
Median	74.3	92.1	18.6	26.3	Median	87.9	105.2	18.2	20.7
Mode	75.8	#N/A	18.0	#N/A	Mode	83.6	98.5	18.6	#N/A
Standard Deviation	16.0	15.6	2.6	6.6	Standard Deviation	11.0	10.8	2.4	3.8
*#N/A: no central value in data set					*#N/A: no central value in data set				

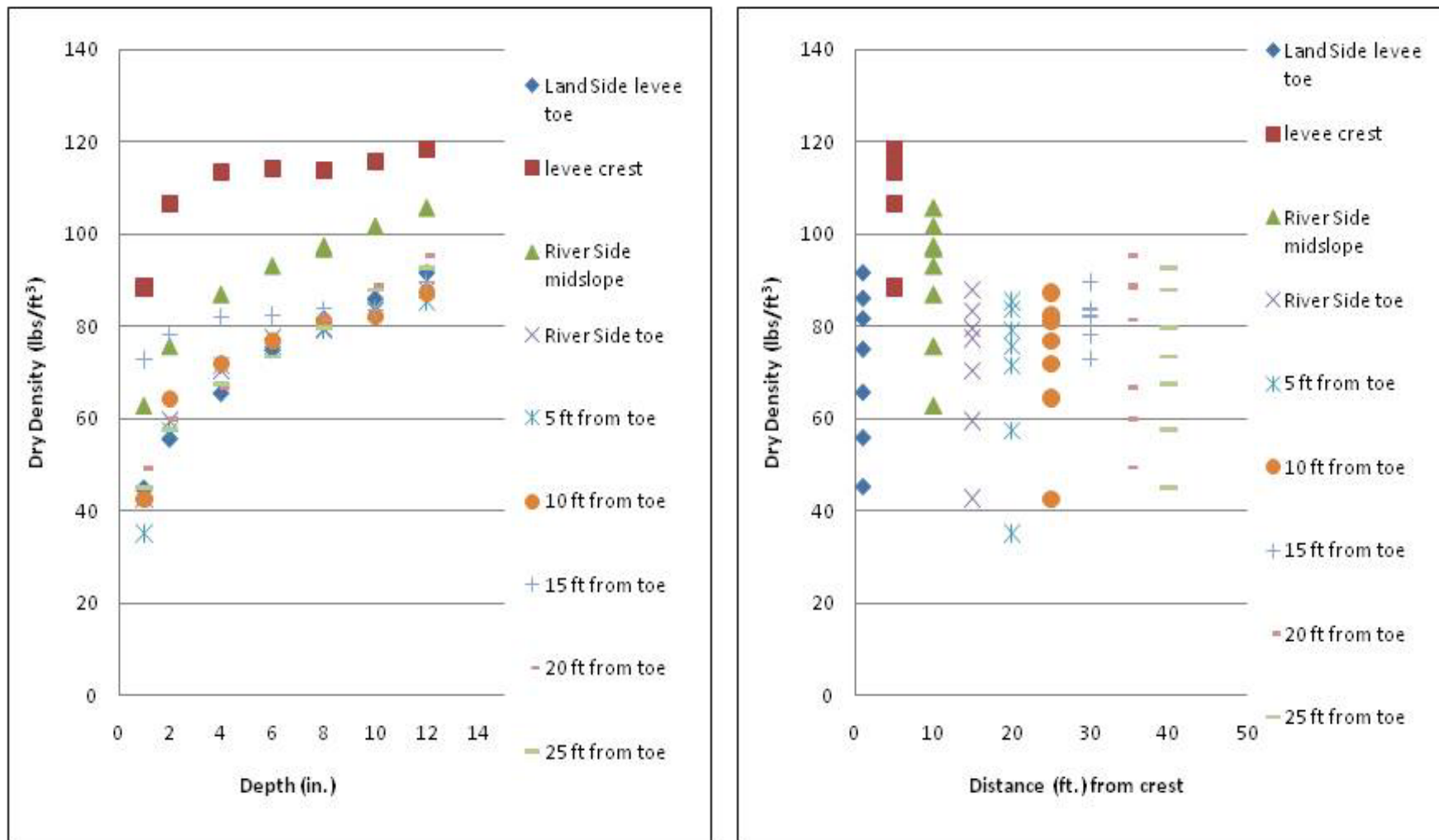


Figure 68a. Dry density (lbs/ft^3) verses depth (in.) and distance (ft.) from Troxler measurements for, Transect 3, Danville, PA.

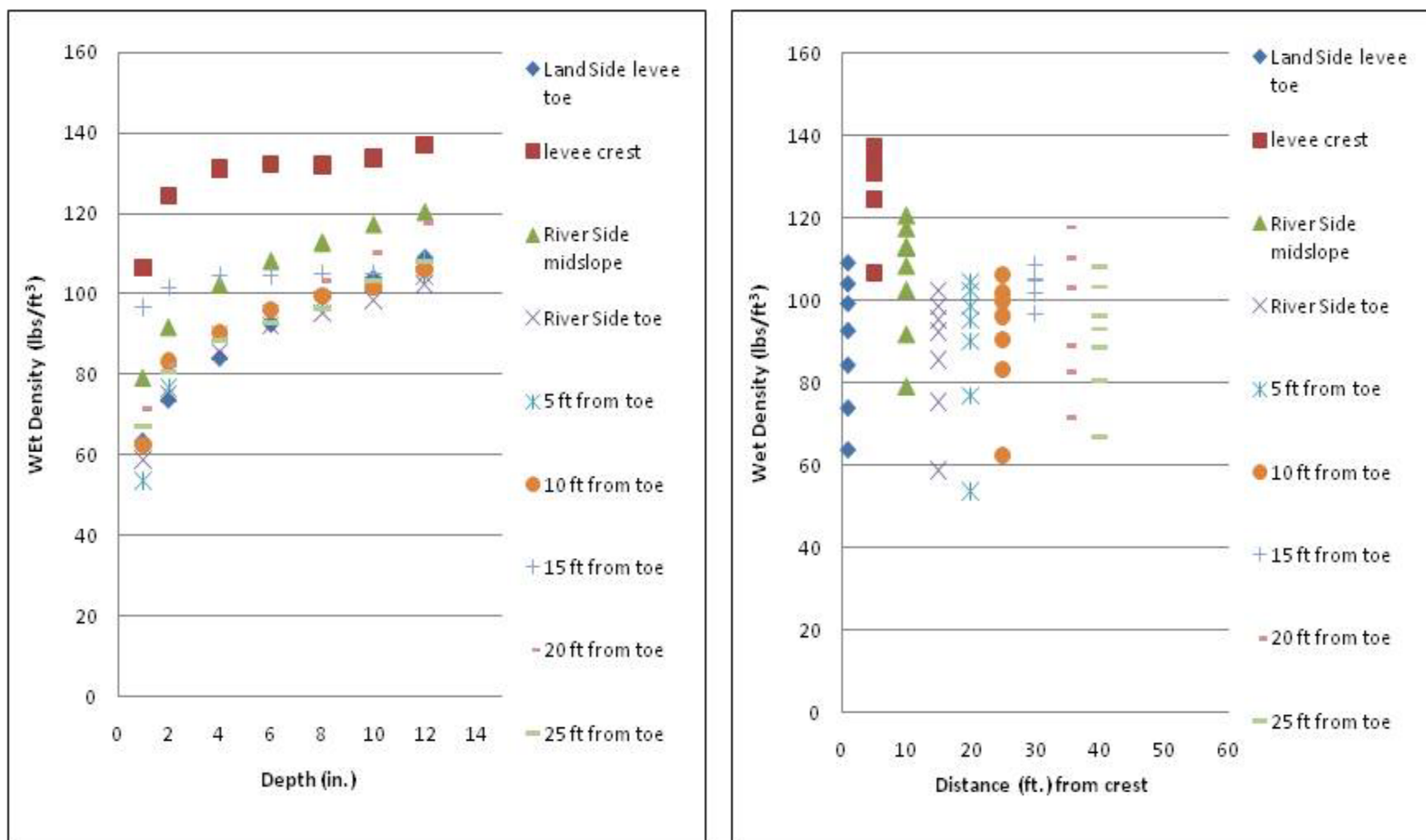


Figure 68b. Wet density (lbs/ft^3) verses depth (in.) and distance (ft.) from Troxler measurements for, Transect 3, Danville, PA.

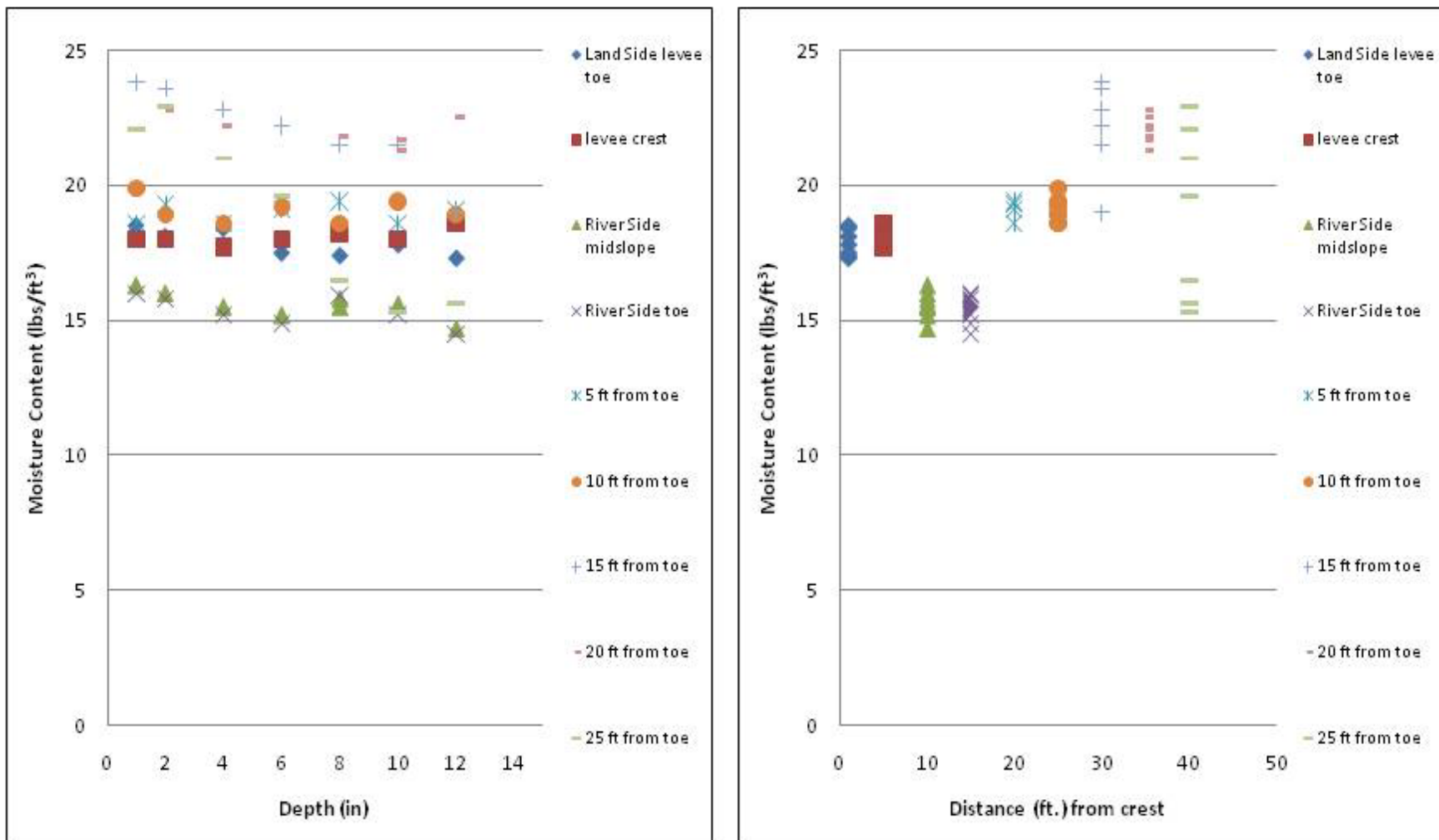


Figure 68c. Moisture content (lbs/ft³) versus depth (in.) and distance (ft.) from Troxler measurements for, Transect 3, Danville, PA.

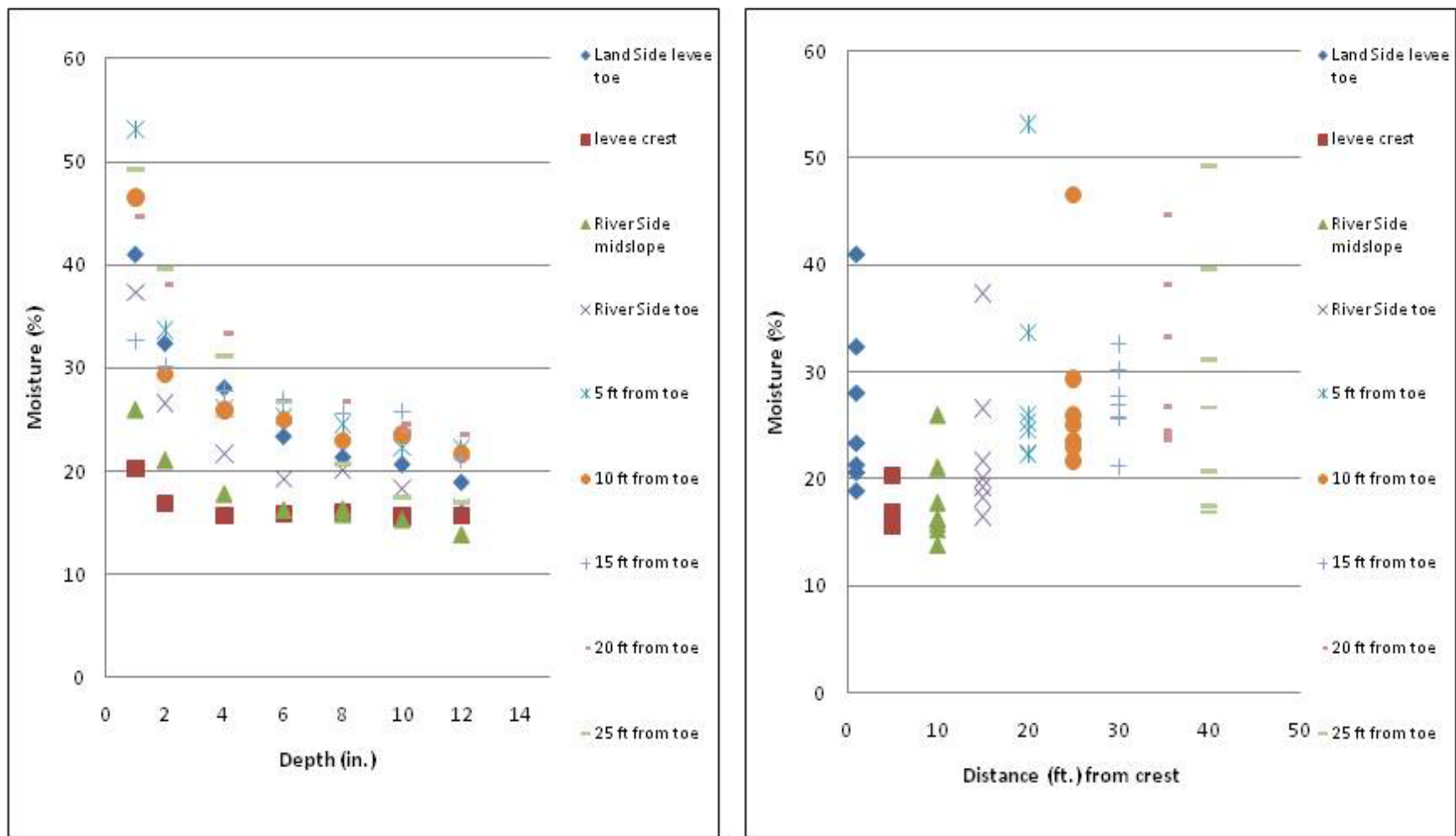


Figure 68d. Moisture (%) versus depth (in.) and distance (ft.) from Troxler measurements for, Transect 3, Danville, PA.



Figure 69. Location of the Vicksburg, MS, study site in relationship to the City of Vicksburg and the Mississippi River. The study site was in a gravel pit south of Vicksburg in hills bordering the Mississippi River Alluvial Valley. These hills are composed of Tertiary sediments veneered by wind blow silt (loess) derived from exposed fine-grained Mississippi River sediments from melting Pleistocene glaciers in the northern latitudes.

rootball after being excavated with the air lance. LiDAR data were incorporated into the geotechnical modeling by providing physical dimensions and characteristics of the tree, the roots, and the rootball extent. GPR and resistivity surveys were used prior to any excavation to determine the worth of these techniques for mapping individual roots and their extent as part of the evaluation of noninvasive techniques for subsurface mapping of woody vegetation. Geophysical surveys were performed adjacent to and around the root zone, before the excavation of the root mass was initiated.

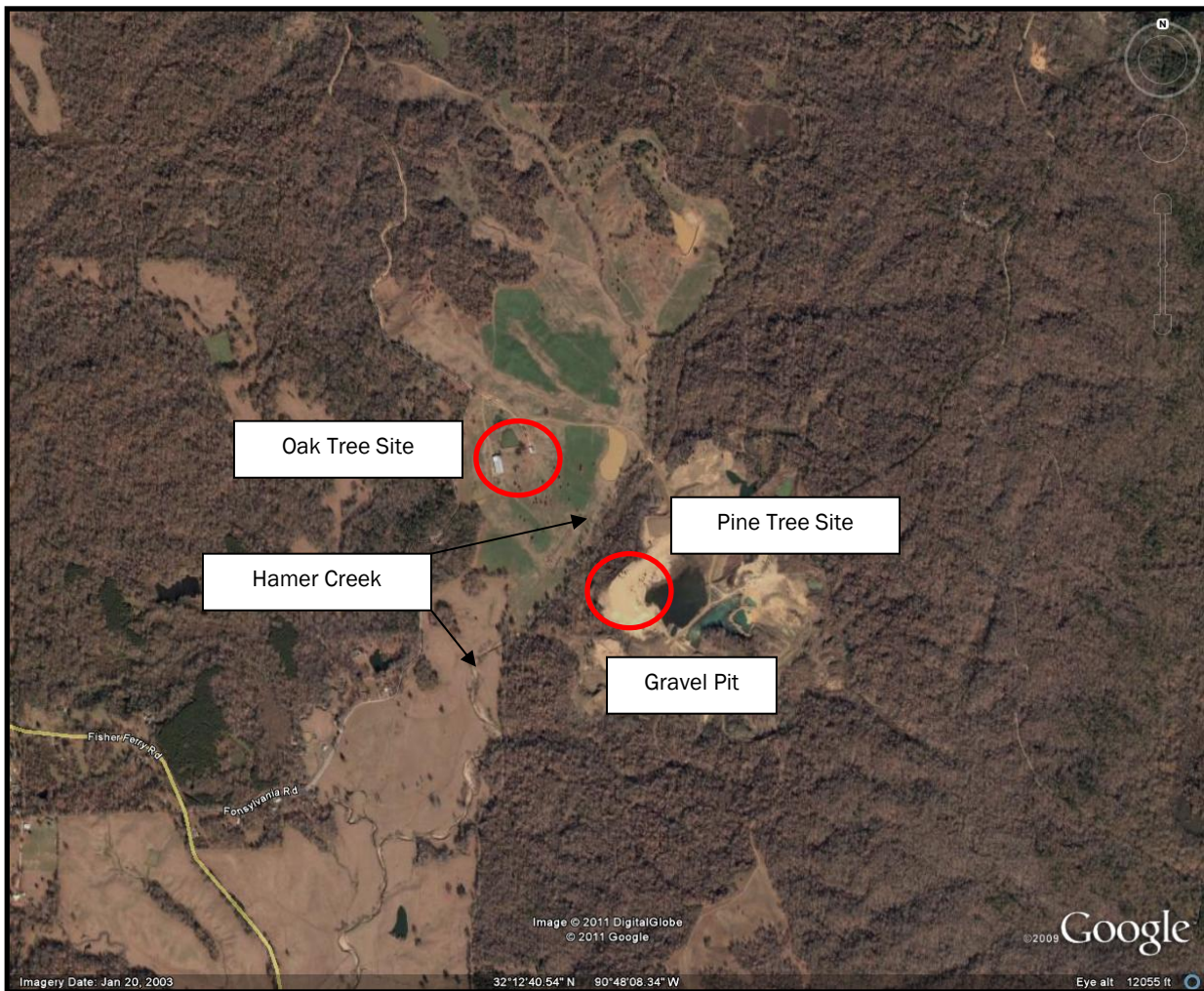


Figure 70. Aerial view of the local gravel pit where an oak tree and pine tree were studied. Geophysical surveys were performed at both sites. LiDAR surveys were performed only at the oak site. Excavation of roots was performed at both tree sites. Hamer Creek is the local drainage and is tributary to the Big Black River, which in turn drains into the Mississippi River.

Geologic setting

The Vicksburg, MS, area is nationally noted for its thick occurrence of loess (windblown silt) soils and is the type locality for one of several different loess sheets in the Mississippi River Alluvial Valley (Clark et al. 1989; Krinitzsky and Turnbull 1967; Kolb and Durham 1967; Saucier 1994). Loess deposits are present along the bluffs bordering the Mississippi River's alluvial valley. These deposits occur as a thick accumulation of windblown dust, composed primarily of silt-sized, quartz particles. The origin for the loess is from fine-grained outwash plain deposits derived from melting continental glaciers during the Pleistocene. The Mississippi River at Vicksburg was a conduit for massive quantities of glacial sediment

transported by the Mississippi and Ohio Rivers during the Pleistocene. Prevailing winds blowing across the alluvial valley entrained silt-sized particles from the exposed outwash plain deposits and transported these sediments onto the high bluffs bordering the present day Mississippi River's alluvial valley. Loess deposits are present along both sides of the bluffs flanking the Mississippi River in the central U.S. Extensive loess deposits are present in Arkansas, Illinois, Louisiana, Mississippi, Missouri, and Tennessee (Krinitzsky and Turnbull 1967; Saucier 1994). Loess deposits decrease in thickness with increasing distance from the Mississippi River's floodplain. In the Vicksburg area, loess deposits can attain a thickness of nearly 100 ft adjacent to the river, as evidenced by road cut exposures and numerous soil borings that have been drilled through the loess (Krintszky and Turnbull 1967; Kolb and Durham 1967; Mellen et al. 1941). The thicker accumulations of loess sediments in the Vicksburg area correspond to multiple periods of deposition, associated with different glacial melting and waning episodes in the Pleistocene. In the Vicksburg area at least three different loess sheets are present.

The age of the different loess sheets in the Vicksburg area was tentatively characterized by Krinitzsky and Turnbull (1967) as ranging from the Early Holocene (8,000 yr BP) to Late Pleistocene (125,000 yr BP). The Warren County gravel pit site south of Vicksburg likely contains the youngest of the loess sheets present in the Vicksburg area, which have been subsequently modified by Holocene pedogenic (i.e., weathering and soil formation) and historic anthropogenic (man-made) processes.

The oak tree in Figures 71 and 72 corresponds to a site situated in loess soils, which were subsequently modified by pedogenic processes. The Warren County soil survey bulletin (USDA 1964) indicates that the tree site is composed of Memphis-Natchez soils on 12 to 17% slopes. The tree site is located on a gentle southeast facing slope overlooking Hamer Creek (Figure 70), which is a tributary to the Big Black and Mississippi Rivers. Silt (ML) and silt loam (CL-ML) are present beneath the oak tree. The total thickness reported for the C-horizon (unmodified parent horizon in soil taxonomy) for Memphis and Natchez soils is estimated to be 10 to 20 ft deep (USDA 1964).

The foundation geology at the pine tree is entirely different compared to the oak tree location. Obvious differences between the two sites are the different tree species and the pine tree is situated on top of highly



Figure 71. Close-up view of the oak tree where LiDAR and geophysical surveys were conducted.



Figure 72. Top photo is view of pine tree at the Warren County gravel pit used to test ground penetrating radar for mapping roots. Bottom photo shows the underlying sand and gravel foundation being mined for aggregate. The tree being studied is the farthest tree in the right side of photograph.

disturbed ground compared to the oak tree location. The pine tree is situated on top of a large man-made gravelly sand (SW) hill, which was stockpiled earlier for the aggregate (Figure 72). The stockpile was derived from a 10- to 40-ft-thick layer of naturally occurring coarse sands and gravels which are located unconformably beneath the loess deposits.

The gravel pit in relationship to Hamer Creek's floodplain (Figure 70) occurs as a pronounced topographic high and is representative of many similar quarrying operations throughout the central Mississippi region and the Southeast Gulf Coastal Plain. These sand and gravel pits typically occupy topographically higher elevations than the surrounding terrain. They are an erosional vestige or remnant of a much larger and geographically-widespread alluvial fan complex, formed by ancestral rivers draining the Appalachian Mountains during the Pliocene and Early Pleistocene (5 to 1.5 million years BP) across much of the southeastern U.S. coastal plain (Ispahordig and Lamb 1971). Local drainage, established after deposition of this coarse grained fan complex in the early to middle Pleistocene, has eroded this extensive fan in response to tectonic uplift and eustatic sea level fluctuations. The end result is the presence of these isolated knolls occupying topographic high areas throughout the central Mississippi and the Vicksburg area. Further to the south in the gulf coast plain, this sand and gravel unit is relatively continuous, extending from Texas to Florida and across southern Louisiana, Mississippi, and Alabama. This unit has been mapped as the Citronelle Formation in Louisiana and Mississippi (Moore 1976; Ispahordig and Lamb 1971).

Laboratory soils data and hydraulic conductivity

Representative soil samples were collected from the two tree sites at the gravel pit to characterize soil texture and their grain-size distribution. These samples classify as clayey silt (ML) beneath the oak tree and gravelly sand (SW) beneath the pine tree. The gravel in the sand was previously washed and concentrated to primarily a pea gravel size with approximately 10 to 15% volume.

Groundwater conditions

The Vicksburg site is much different in comparison to any of the previous sites examined as no levees exit at this location and the site is well removed from the active floodplain. The purpose for studying the Vicksburg gravel pit site was to perform LiDAR and geophysical

experiments locally, in order to develop and improve field data collection methods. Groundwater data were evaluated at previous sites to provide input into underseepage and slope stability assessments at the levee sites studied. Groundwater was observed in the gravel pit as occupying lower elevations than either the oak or pine locations.

Troxler measurements

Troxler data from a single site in Vicksburg, MS, was collected in the same area as the two trees studied in the gravel pit (Figure 73). Soil in this area consists of silty clay (ML) in the top layer and the lower layer soil consisted of yellowish silt. Soil density data for all depths are presented in Table 28 and, Figures 74a to 74d show the plots of this data. Dry density and wet density values increase with depth. Moisture content tends to be consistent with depth for each point. Percent moisture decreases with depth. Dry density values are consistent from the tree to the drip line and drop slightly as distance from the tree increases. Wet density values increase from the tree to the drip line and decrease slightly after the drip line. Moisture content and percent moisture values increase as distance from the tree increases.

Figure 73. Location of transect for Troxler measurements in Vicksburg, MS.

Table 28. Statistical data for Troxler measurements in Vicksburg, MS:
2-, 4-, 6-, 8-, 10-, and 12-in. depths.

Depth (2-4-6 in.)	Dry Density (lb/ft ³)	Wet Density (lb/ft ³)	Moisture Content (lb/ft ³)	Percent Moisture (%)	Depth (8-10-12 in.)	Dry Density (lb/ft ³)	Wet Density (lb/ft ³)	Moisture Content (lb/ft ³)	Percent Moisture (%)
Max	90.4	108.7	23.6	36.6	Max	96.7	115.1	23.4	28.3
Min	64.2	87.7	15.4	17.0	Min	79.9	101.1	15.0	16.0
Mean	82.1	102.0	19.9	24.5	Mean	89.2	109.4	20.2	22.8
Median	82.4	103.2	20.2	24.8	Median	89.2	110.2	21.0	24.0
Mode	#N/A	#N/A	20.8	#N/A	Mode	93.8	112.1	23.4	#N/A
Standard Deviation	6.6	5.3	2.6	4.9	Standard Deviation	4.9	3.6	2.8	4.0
*#N/A: no central value in data set					*#N/A: no central value in data set				

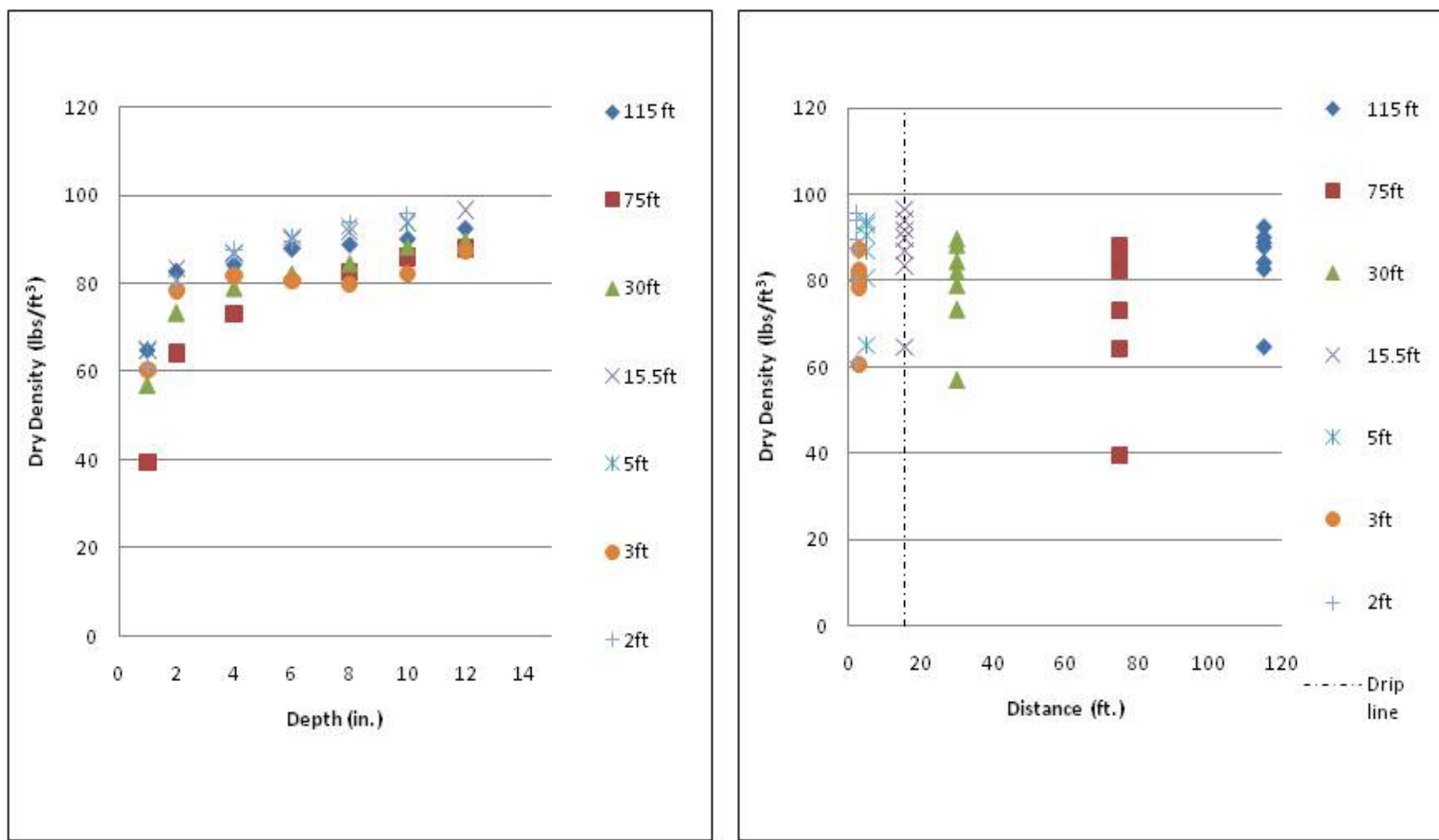


Figure 74a. Dry density (lbs/ft³) versus depth (in.) and distance (ft.) from Troxler measurements for Vicksburg, MS.

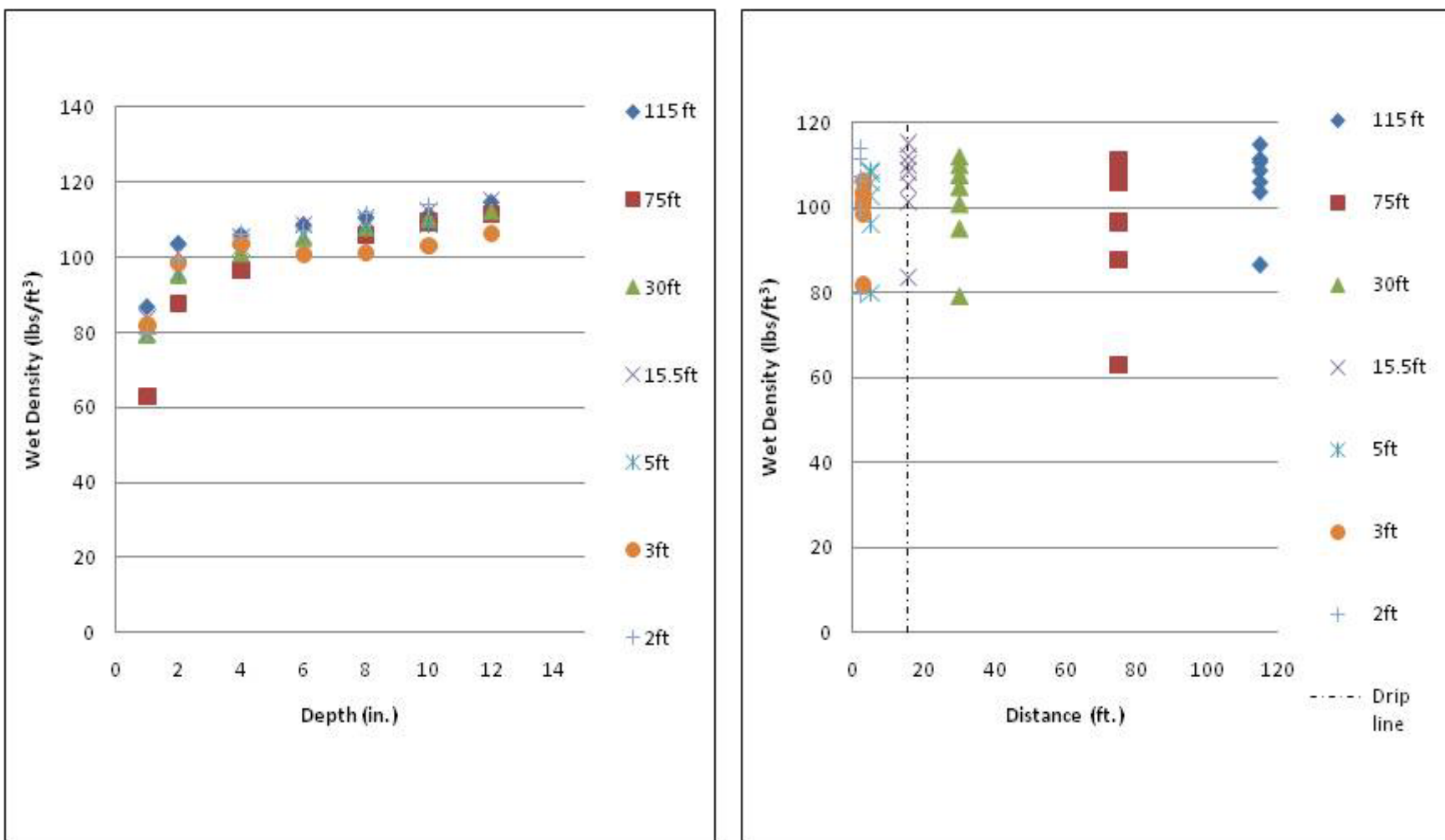


Figure 74b. Wet density (lbs/ft³) versus depth (in.) and distance (ft.) from Troxler measurements for Vicksburg, MS.

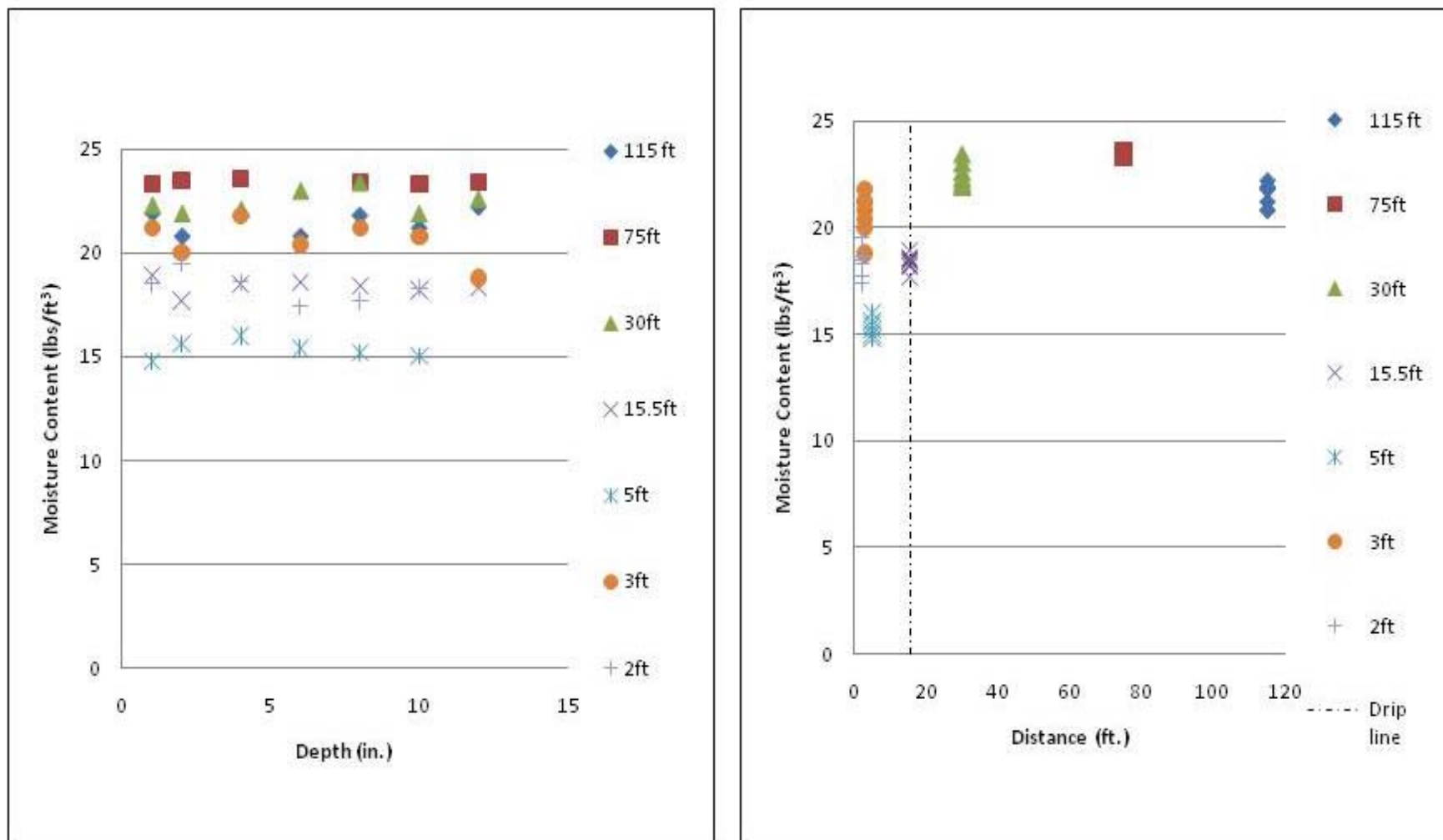


Figure 74c. Moisture content (lbs/ft^3) versus depth (in.) and distance (ft.) from Troxler measurements for Vicksburg, MS.

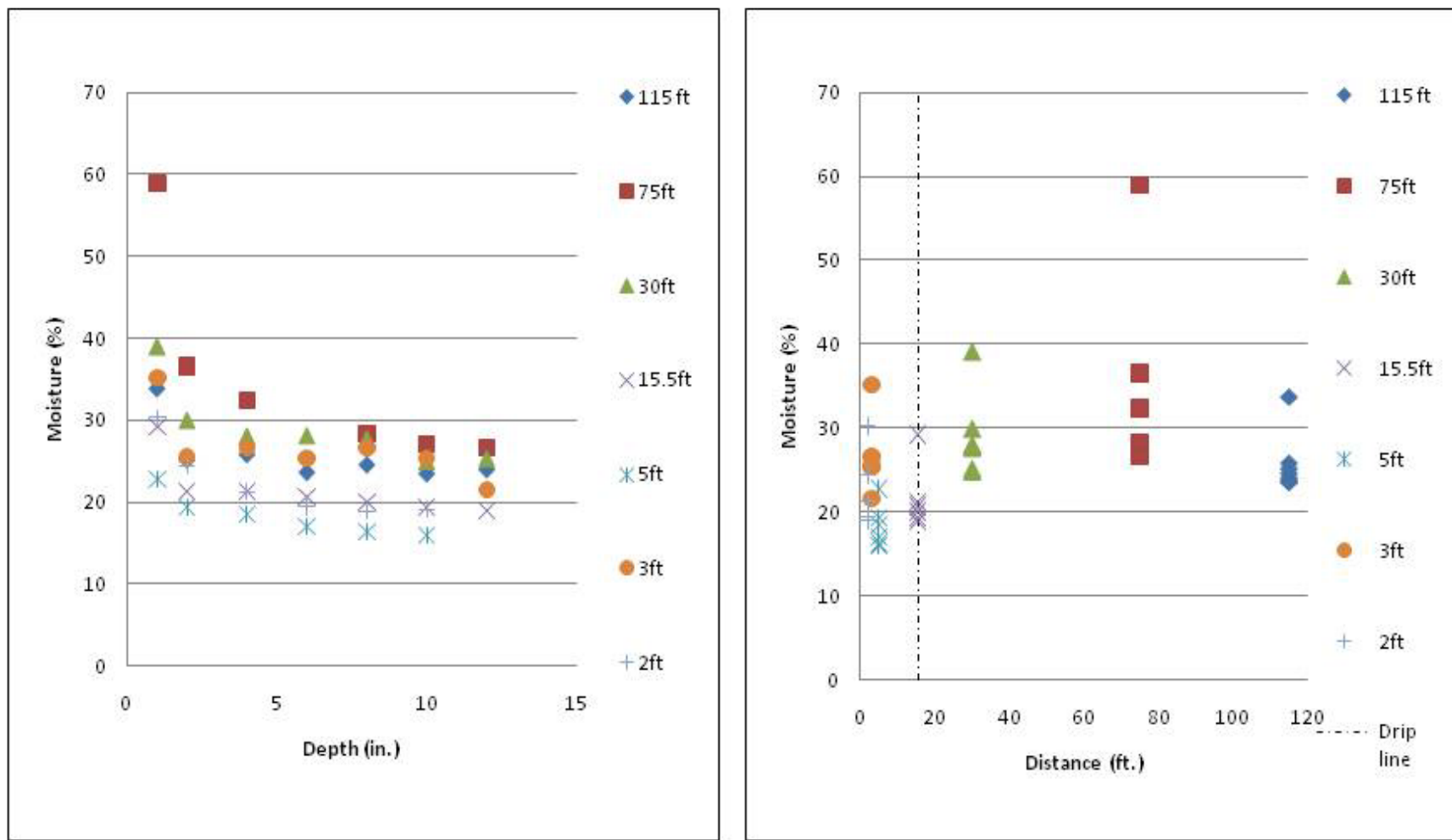


Figure 74d. Moisture (%) versus depth (in.) and distance (ft.) from Troxler measurements for Vicksburg, MS.

4 Root Characterization

Although a significant number of procedures exist for collecting root architectural data, these techniques have not been quantitatively compared or calibrated to the extent necessary to permit selection for a particular need. Thus, this study sought to: (1) compare a variety of these techniques and (2) examine the accuracy of non-invasive techniques, including the potential for calibrating noninvasive methods with invasive subsampling approaches.

Non-invasive root characterization is both non-destructive and relatively rapid (compared to invasive measurement); however, its accuracy and limitations are currently poorly defined. Butnor et al. (2003) demonstrated that calibrating GPR data with limited invasive measurement markedly improves the accuracy of the technique.

Multiple techniques were used for measuring root system architecture under a variety of environmental conditions to assess the strengths, weaknesses, and limitations of the methods. In selecting a test tree, one was chosen that was relatively isolated (more than 2 m from nearest neighbors) for ease of measurement; however, given the emphasis of this study on detection of roots and not recreation of a specific tree's architecture, isolation is not imperative. Relevant botanical properties of the tree and physical properties of the site are detailed throughout this document and summarized in Table 29. Each of the data collection techniques will be described in greater detail in the sections that follow. Rooting conditions will generally be described on the basis of the classification scheme of Danjon et al. (1999) as very large or coarse (>2 cm), large (1 to 2 cm), medium (0.5 to 1 cm), and small (<0.5 cm).

Geophysical investigation

Electrical resistivity imaging

Electrical resistivity is a measure of the degree to which soil conducts an electrical current, and can be used to infer the composition and physical features of subsurface geologic materials. Major factors influencing the resistivity measurement are the amount of pore fluid present, the salinity of the pore fluid, mineralogy, porosity, and the amount of fracturing.

Table 29. Summary of conditions at sites used in the ERDC research.

Location	Site Description ^a	Methods ^b and Sample Taxa
Sacramento, CA 38°29'20"N 121°33'05"W	A reach of sandy levee in urban Sacramento on the east bank of the Sacramento River. The sample tree was located midslope on the landside of the levee. Mean annual temperature is 16.2°C. Mean annual rainfall is 4.5 cm. Prevailing winds are from the south.	GPR, ERI, EM, SME Valley oak <i>Quercus lobata</i> Née 75 cm DBH ^c 16.8 m drip line 15 m height
Albuquerque, NM 35°08'33.35"N 106°40'34.54"W	Site 1 – A reach of sandy levee in urban Albuquerque on the east bank of the Rio Grande River south of Montano Boulevard. The sample tree was located on the waterside of the levee approximately 15 m from the levee toe. Site 2 – A reach of sandy levee in urban Albuquerque on the west bank of the Rio Grande River north of Montano Boulevard. The sample trees were located on the waterside of the levee approximately 10 m from the levee toe. Mean annual temperature is 13.8°C. Mean annual rainfall is 22.6 cm. Prevailing winds are from the north.	ERI, SME Site 1 – Fremont cottonwood <i>Populus fremontii</i> 41 cm DBH ^c 10.7 m drip line 11 m height ERI, SME Site 2 – 2 Fremont cottonwoods <i>Populus fremontii</i> 58 cm DBH ^c 14 m drip line 12 m height 27 cm DBH ^c 9.2 m drip line 9 m height
Burlington, WA 48°27'47"N 122°18'47"W	Sample tree was 5 m from the levee toe on the waterside of the west bank of the Skagit River levee system. Mean annual temperature is 10.5°C. Mean annual rainfall is 83.1 cm. Prevailing winds are from the south-southeast.	GPR, ERI, EM, SME Western red cedar <i>Thuja plicata</i> 143 cm DBH ^c 12.2 m drip line 20 m height
Vicksburg, MS 32°12'41"N 90°48'21"W	Test site was in a rural pasture approximately 14 km south of Vicksburg. Sample tree was on an embankment sloping gently from SW to NE at approximately 5 deg. Mean annual temperature is 18.6°C. Mean annual rainfall is 147.3 cm. Prevailing winds are from the south	GPR, ERI, SME Southern red oak <i>Quercus falcata</i> 29 cm DBH ^c 7.5 m drip line 7.5 m height
New Orleans, LA 30°00'41"N 90°01'52.63"W	IHNC Site – A reach of clay levee on the Inner Harbor Navigation Canal in an urban environment. The studied tree had been cut several days prior to the field study. The tree was located on the toe of the levee.	GPR, EM Hackberry <i>Celtis occidentalis</i> 64 cm DBH ^c

Location	Site Description ^a	Methods ^b and Sample Taxa
29°59'15.33"N 90°07'29.71"W	<p>17th Street Site – A reach of clay levee on the 17th Street Canal. Two oak tree stumps that had been cut approximately 2 years prior to the study were located halfway up the levee slope.</p> <p>Mean annual temperature is 20.3°C, Mean annual rainfall is 157.2 cm. Prevailing winds are from the south.</p>	GPR, EM Oak trees 110 and 90 cm DBH ^c
Portland, OR 45°33'32"N 122°26'14"W	<p>Test site is located approximately half way up the protected slope of a sandy levee. Eight trees, roughly in a 150-ft long line and parallel to the crest of the levee, were sampled.</p> <p>Mean annual temperature is 11.9°C Mean annual rainfall is 112.6 cm. Prevailing winds in summer are from the NNW and from the ESE in the winter.</p>	GPR, ERI, EM 8 Fremont cottonwoods <i>Populus fremontii</i> Diameter range approximately 50-100 cm DBH ^c Overlapping drip lines Height ranges approximately 10-15 m
Lewisville, TX 33°03'51"N 96°59'15"W	<p>The studied tree is located on the toe of the western end of Lewisville Dam. The site consists of clay soils.</p> <p>Mean annual temperature is 17.8°C Mean annual rainfall is 86.6 cm. Prevailing winds are from the south.</p>	ERI, EM Post oak <i>Quercus stellata</i> 110 cm DBH ^c 15 m drip line 10 m height
Danville, PA 40°57'49.45" N 76°37'38.72" W 40°57'18.86" N 76°36'51.99" W	<p>Site 1 – north end of Danville levee system on the Susqueanna River; levees composed of very dense silty sand</p> <p>Site 2 – south end of Danville levee system on the Susqueanna River; levees composed of very dense silty sand</p> <p>Mean annual temperature: Not available Mean annual rainfall: 43.8 in. (111.3 cm) Prevailing winds are generally from the west, but more northerly in the winter and more southerly in the summer.</p>	No geophysical surveys

Location	Site Description ^a	Methods ^b and Sample Taxa
Lake Providence, LA 32°48'26.48" N 91°10'31.53" W	Edge of oxbow lake of the Mississippi River adjacent to Hwy 65. Active sand boils on lake; approximately 0.5 mi from active sand boils adjacent to the Mississippi River levee Tree species/Dimensions Cypress (<i>Taxodium distichum</i>) Climate Mean annual temperature: 64.0 °F (17.8 °C) Mean annual rainfall: 63.47 in. (161.2 cm)	No geophysical surveys

^a Temperature and precipitation values are average annual from the weather station closest to the site. (USDC 2010). Prevailing wind data are from WRCC (2010).

^b GPR – ground-penetrating radar, ERI – electrical resistivity imaging, EM – electromagnetic, induction, SME – sub-sampled manual excavation

^cDBH – diameter at breast height

Table 30 gives the electrical resistivity values of common rocks and earth materials. Electrical resistivity values vary over several orders of magnitude, depending on the type of earth material. Sedimentary rocks, because of their higher porosity and greater water content, have lower

Table 30. Electrical resistivity values of some common rocks and minerals (Keller and Rischknecht 1966).

Material	Resistivity, Ω-m	Conductivity, Siemens/m
Igneous and Metamorphic Rocks		
Granite	$5 \times 10^3 - 10^6$	$10^{-6} - 2 \times 10^{-4}$
Basalt	$10^3 - 10^6$	$10^{-6} - 10^{-3}$
Slate	$6 \times 10^2 - 4 \times 10^7$	$2.5 \times 10^{-8} - 1.7 \times 10^{-3}$
Marble	$10^2 - 2.5 \times 10^8$	$4 \times 10^{-9} - 10^{-2}$
Quartzite	$10^2 - 2 \times 10^8$	$5 \times 10^{-9} - 10^{-2}$
Sedimentary Rocks		
Sandstone	$8 - 4 \times 10^3$	$2.5 \times 10^{-4} - 0.125$
Shale	$20 - 2 \times 10^3$	$5 \times 10^{-4} - 0.05$
Limestone	$50 - 4 \times 10^2$	$2.5 \times 10^{-3} - 0.02$
Soils and Waters		
Clay	$1 - 1000$	0.01 - 1
Alluvium	$10 - 800$	$1.25 \times 10^{-3} - 0.1$
Groundwater (fresh)	$10 - 100$	0.01 - 0.1
Sea water	0.2	5

resistivity values than intact igneous and metamorphic rocks. Wet soils and groundwater have even lower resistivity values. Clayey soil normally has lower resistivity values than sandy soil (Locke 2000).

An electrical resistivity imaging (ERI) survey uses an array of four metal rods or electrodes in contact with the ground surface. The array consists of two current electrodes and two potential electrodes. Current is introduced into the ground through one current electrode (positive electrode) and flows through the subsurface to the other current electrode (negative electrode). The subsurface material acts as a natural resistor, and a potential difference is generated across the two potential electrodes. Knowing the amount of current injected into the ground, the electrode separation, and the potential difference, one can compute apparent resistivity. The unit of electrical resistivity is the ohm-meter ($\Omega\text{-m}$). Resistivity is the reciprocal of electrical conductivity.

After apparent resistivity values are obtained from a field survey, it is necessary to transform the data to provide an image of the subsurface resistivity distribution. This is done using an inversion computer program. The program derives a starting resistivity model and compares those values with the measured apparent resistivity values. Based on the calculated differences, the program adjusts the model and again measures the difference between predicted and measured values. This iterative process continues until an inversion stop criterion is satisfied. The root-mean-squared error gives a measure of this difference.

ERI surveys can be collected using 2-D or 3-D acquisition techniques. The 2-D surveys collect data along straight survey lines, and the results provide a cross section of the distribution of resistivity values beneath the survey line. Because of their simplicity in field use, 2-D resistivity surveys are still used in most investigations; however, they can lead to distorted and misleading results in heterogeneous areas (Gharibi and Bentley 2005). In a 3-D survey, data are collected within a gridded area, unlike a 2-D survey, where electrodes are emplaced along a single straight line. Electrodes are usually placed in a grid pattern in a 3-D survey, within which data can be collected in many directions. A roll-along 3-D survey is a variation of the normal 3-D survey method. In the roll-along method, a 3-D survey is conducted as usual, and when the survey is completed, the electrodes from the back half of the grid are picked up and leap-frogged or rolled-along to the front end of the grid and the survey resumed. The results from these

surveys are typically presented as planes or “slices” in one of three orthogonal directions: X, Y, and Z (depth).

Acquiring true 3-D electrical resistivity data is time consuming and costly when compared with 2-D methods. The quasi 3-D technique, an alternate data collection method, employs closely spaced 2-D survey lines and 3-D inversion software to provide a 3-D-like interpretation of the subsurface (Rucker et al. 2008). The advantage of this technique over a 3-D survey is that it uses data from relatively closely spaced 2-D lines, thus reducing data collection time. Gharibi and Bentley (2005) show that data acquired in a quasi 3-D manner are suitable for processing and interpretation when using the proper geometric constraints, such as line and electrode spacing. In this study, 2-D, quasi-3-D, 3-D and roll-along 3-D methods are used.

Stainless steel rods, driven vertically into the ground, were used as electrodes for the ERI surveys in this investigation. The metal rods, approximately 1 cm in diameter, were driven about 0.3 m into the ground surface. The electrodes were connected to a multiconductor cable that was coupled to a resistivity meter. An Advanced Geosciences, Inc., SuperSting R8 resistivity meter with the Smart electrode switching system was used to collect data (Figure 75). This system allows up to eight pairs of electrodes to be measured simultaneously, thus expediting data collection. Data were collected using 2-D and 3-D ERI survey methods. Programs EarthImager 2-D and EarthImager 3-D (Advanced Geosciences, Inc.) were used to invert the 2-D and 3-D ERI data, respectively.



Figure 75. Advanced Geosciences SuperSting R8 electrical resistivity meter.

ERI was chosen as a testing method based on its capability of measuring contrasts in the electrical properties of the subsurface. An adequate electrical resistivity contrast between a tree's root ball soil mass and the surrounding soil must exist in order for the root ball to be detected and delineated.

Electromagnetic (EM) surveys

Electromagnetic (EM) induction is used to measure the apparent electrical conductivity (inverse of electrical resistivity) of subsurface materials. Electrical conductivity is a measure of the degree to which the soil conducts an electrical current, and can be used to infer the extent and type of geological materials or buried materials. As with ERI, major factors influencing the conductivity measurement are the amount of pore fluid present, the salinity of the pore fluid, the presence of conductive minerals, and the amount of fracturing.

The instrumentation used to measure soil conductivity consists of a transmitter coil (Tx) and a receiver coil (Rx) separated by a fixed distance. An alternating current is passed through the Tx coil, generating a primary time varying magnetic field. This primary field induces eddy currents in subsurface conductive materials. The induced eddy currents are the source of a secondary magnetic field that is detected by the Rx coil along with the primary field.

Two components of the induced magnetic field are measured by the EM system. The first is the quadrature phase, sometimes referred to as the out-of-phase or imaginary component. Apparent ground terrain conductivity is determined from the quadrature component. Disturbances in the subsurface caused by compaction, in-filled abandoned channels, soil removal and fill activities, buried objects, or voids may produce conductivity readings different from background values, thus indicating anomalous areas. The second phase is the in-phase component. The in-phase component is sensitive to metallic objects and therefore is useful when looking for buried metal such as metal rails, rebar, or electrical wires.

A Geonics Ltd. EM38-MK2 conductivity meter, as shown in Figure 76, was used with Tx-Rx coils set at fixed distances of 0.5 and 1.0 m and operated in the vertical dipole mode. This allowed for a depth of investigation of approximately 0.75 and 1.5 m for the 0.5- and 1.0-m coil separations, respectively. The field operator carried the EM38-MK2 at a height of

approximately 5 to 10 cm above the ground surface while slowly walking along each profile line to acquire near-continuous data. The EM data are presented as contour maps of conductivity and in-phase values for the 0.5- and 1.5-m coil separations. The maps show lateral changes in conductivity and in-phase values related to geological and buried features such as caused by tree root zones. Examining the maps from the two different coil separations provides information about changes in conductivity and in-phase values as a function of depth.

Ground-penetrating radar (GPR)

Ground-penetrating radar (GPR) is a geophysical method that uses radar pulses to image the subsurface. This non-destructive method uses electromagnetic radiation in the microwave band of the radio spectrum and detects the reflected signals from subsurface features. GPR can be used in a variety of media, including rock, soil, ice, fresh water, pavements, and structures. It can detect objects, changes in material, and voids and discontinuities.



Figure 76. Geonics EM38-MK2 terrain conductivity meter.

GPR uses transmitting and receiving antennas. The transmitting antenna radiates short pulses of the high-frequency radio waves into the ground. These signals travel from the transmitting antenna, reflect off boundaries with dissimilar electrical properties, objects, or irregular surfaces and are detected by the receiving antenna. These signals are recorded, amplified, processed, and provide a near-continuous profile of the subsurface. The data processing principles involved are similar to reflection seismology.

The depth of penetration and amount of definition that can be expected from the GPR is determined by the electrical properties of the host material being tested as well as the power and frequency of the transmitting antenna. As the soil conductivity increases, the GPR's depth of penetration decreases. This is because the electromagnetic energy is more quickly dissipated into heat, causing a loss in signal strength at depth. Higher frequencies do not penetrate as far as lower frequencies, but provide better resolution. Optimal depth penetration is achieved in dry sandy soils or massive dry materials, such as granite and limestone, where the depth of penetration could be up to 15 m. In moist or clay-laden soils and soils with high electrical conductivity, penetration is sometimes only a few centimeters.

Several researchers have used GPR to detect subsurface tree roots. Barton and Montagu (2004) created a test bed using damp sand and buried roots of different diameters at different depths. Under these near-ideal conditions, they were able to detect and model the roots to estimate their diameter. In field applications, researchers have encountered various levels of success, depending on soil type, moisture state and root size, density and depth (al Hagrey 2007; Hruska et al. 1999; Morelli et al. 2007).

Two GPR systems, a 3-D-Radar Geoscope and a Sensors & Software, Inc. pulseEKKO (pE) 1000, each using different operating principles, were used in this study and are described in the following paragraphs.

3-D-Radar Geoscope

A step-frequency GPR, 3-D-Radar Geoscope with a B1831 antenna array, was employed that has the capability to simultaneously acquire data ranging from 150 MHz to 2 GHz. The system allows the acquisition of three-dimensional (3-D) data. The length of the B1831 antenna array is 1.8 m. The array has 31 Tx-Rx antenna pair, with each pair spaced 5.5 cm apart along the array (Figure 77). The antennae are different sizes,

designated small (16), medium (8), and large (7). The GPR antenna array is typically towed, but can be mounted on a vehicle (Figure 78). A 12-v deep-cycle marine battery powers the Geoscope control unit, both of which are carried in the vehicle. The towed antenna array is typically positioned 10 cm above the ground surface, but can be adjusted to a greater height to accommodate taller surface vegetation or obstacles. Although the array has 31 antenna pair, channels 2 through 30 were used during data acquisition; channels 1 and 31 tend to exhibit higher noise levels and were disabled. The data are acquired at 2-MHz steps over the 150-MHz to 2-GHz frequency range. Because most of the antennae are active during data acquisition, it is necessary to tow the array at a slow walking speed, not to exceed 3 km/hr. The data acquisition software allows a warning to be sounded when the acquisition speed approaches a user-specified level to help prevent lost scans caused by excessive speed.

The recommended survey line separation is 1 m, which gives approximately 50 cm of overlap from line to line. Some overlap is desired and it does not need to be as great as 50 cm. A line separation of 1 m was chosen because it is easy to accommodate when laying out a grid in the field, and a 50-cm overlap does not result in a significant increase in survey time. Data acquisition began at the same end of the test site for each survey line. This facilitates data processing, and it also allows sufficient turn around room when positioning the vehicle and array at the next survey line.

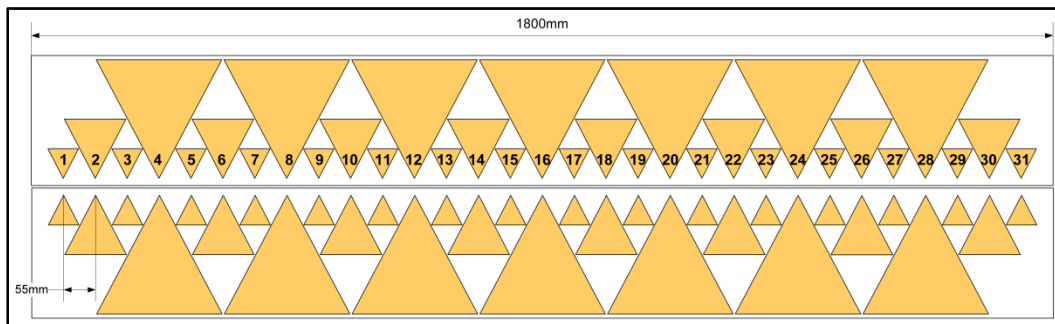


Figure 77. 3-D-Radar B1831 antenna array with 31 antenna pair.



Figure 78. Towed configuration of the 3-D-Radar B1831 antenna array.

The software 3-DR-Examiner that is provided with the 3-D-Radar system is used to process the GPR data. All survey line data are subjected to the same three-step processing procedure: (1) an inverse fast Fourier transform (IFFT) is performed to transform the data from the frequency domain to the time domain; (2) removing background using a mean filter, which subtracts the average trace of a radargram from each individual trace in the radargram; and (3) autoscaling of the data. After processing, the data are exported to the software GPR-Slice for 3-D visualization.

GPR system

GPR interpretation

The interpretation of GPR data is often subjective, with one looking for changes in reflection characteristics, hyperbolic shapes, and discontinuities. Changes in reflection characteristics such as amplitude and reflector thickness indicate differences in electrical properties of a material, layer thickness, and heterogeneity. A hyperbolic response occurs when the radar antenna passes over an object of finite size with a different dielectric permittivity than the surrounding material. The antenna output has an elliptical footprint, therefore a portion of the signal reaches the object prior to

the antenna being directly over the object, resulting in a hyperbolic response. The width of the hyperbola gives a relative indication of the size of an object. The presence of reflection discontinuities can indicate the presence of a trench or geologic feature such as a fault. Knowledge of how the electromagnetic wave responds to different materials (e.g., air, metals, snow/ice, soil types, moisture conditions) and a prior knowledge of site conditions aids the interpreter in deciphering a radargram.

A Sensors & Software, Inc. pE 1000 GPR system was also used in this study. Unlike the 3-D-Radar Geoscope system already described, which can step through a series of frequencies, the pE 1000 is an impulse-type GPR that generates a high voltage pulse of short duration. The GPR antenna radiates this signal into the ground. The operating frequency of the pE 1000 is determined from the center frequency of the bandwidth. The bandwidth and the center frequency of a radar system are primarily determined by the antennas selected. Whereas the 3-D-Radar Geoscope is capable of simultaneously collecting information from a wide range of frequencies, or depths, using multiple antenna pairs, the pE 1000 is limited to collecting information from one antenna pair at a time using a single center frequency. Antenna pairs, of varying frequencies, are swapped-out during a survey to collect information from different depths. Instead of showing the results from a wide frequency range on a single radargram, as is the case with the 3-D-Radar Geoscope system, the pE 1000 presents individual radargrams for a single frequency. The programs EKKO View Deluxe and EKKO View (Sensors & Software, Inc.) were used to analyze and present the GPR data.

Study locations

Geophysical surveys were conducted in New Orleans, LA; Sacramento, CA; Portland, OR; Burlington, WA; Lewisville, TX; Vicksburg, MS; and Albuquerque, NM. The sites are described in chronological order as listed previously from the first survey to the most recent survey.

Sacramento, CA

Background

A geophysical study was conducted from 26 through 31 August 2009 along a stretch of the Sacramento River levee to determine the effectiveness of ERI, EM, and GPR to noninvasively map the tree root distribution of two

trees on the protected slope of the levee. The test site, Site B, is located on the east bank of the Sacramento levee, locally known as the Pocket Levee, and is approximately 11 km south-southwest of Sacramento, CA (Figure 79).

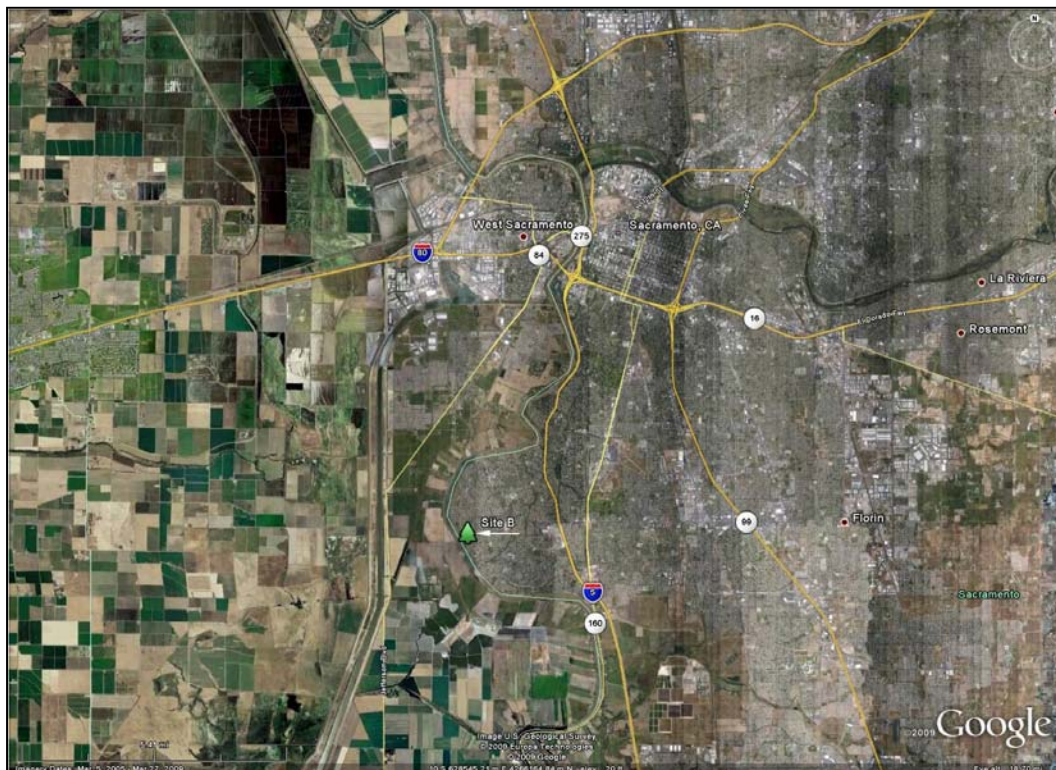


Figure 79. Location of Site B, Sacramento, CA.

The study site is located on the protected slope of the Sacramento River levee and measures approximately 27 m by 11 m. Reportedly, the levee consists of hydraulically-placed material dredged from the Sacramento River and consists chiefly of sandy soils. A 5-ft-thick clay cap, designed to protect the underlying sandy levee soil from erosion, is supposedly present. However, observations of the surficial soils and from shallow excavations tell us that the clay cap appears to be absent in this area. Two valley oaks (*Quercus lobata*), approximately 9 m apart and located about midslope, grow within the site. The height of the levee is approximately 2 m.

Geophysical survey methods

Electrical resistivity imaging (ERI)

ERI data were acquired using 2-D and 3-D survey techniques. Data acquisition and processing techniques are described in the following paragraphs.

2-D data acquisition and processing

Two-dimensional ERI data were collected along twelve 27.5-m-long parallel lines (Figure 80). The lines are located on the slope and oriented parallel to the axis of the levee. Line separation is 1 m and each line consists of 56 electrodes spaced 0.5 m apart. A dipole-dipole electrode array was used to collect the data. The two trees are located between lines 6 and 7 as shown in Figure 80. Tree 1 is located at approximate coordinates $X = 3$ m and $Y = 6.5$ m and Tree 2 at coordinates $X = 11.75$ m and $Y = 6.5$ m.

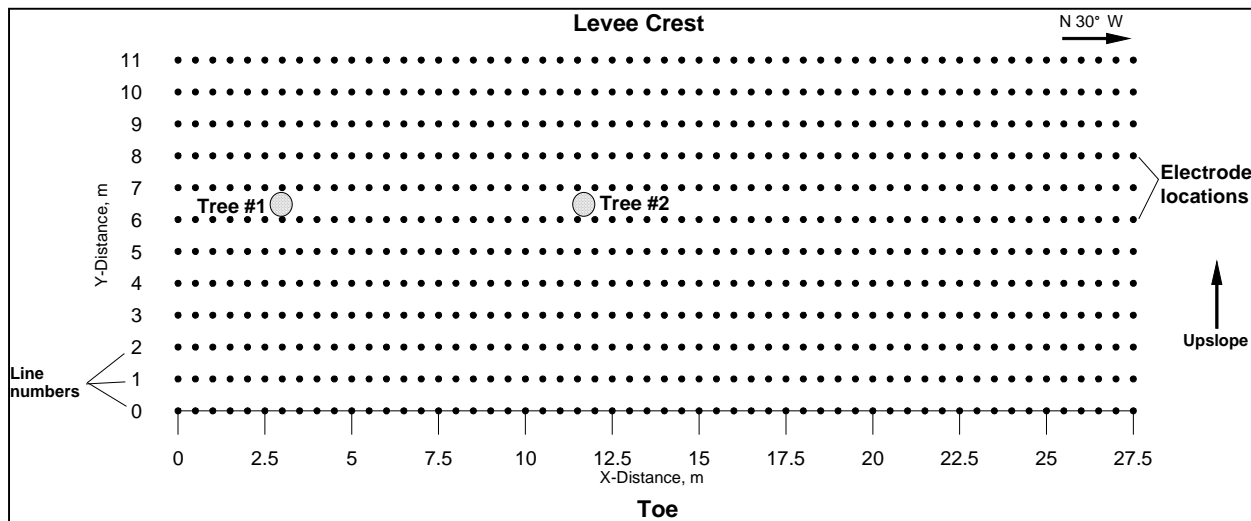


Figure 80. 2-D resistivity survey layout, Site B, Sacramento, CA.

The 2-D data were also processed using the quasi 3-D technique described in Chapter 2 of this volume. The 2-D lines 2 through 9 (Figure 81) were combined into a single 3-D data set and inverted using EarthImager 3-D (Advanced Geosciences, Inc.). Lines 0 to 1 and 10 to 11 were not used in the quasi 3-D inversion to reduce computer processing time. Also, excluding these lines in the inversion is presumed to have only a minor, if any, effect on the inversion results because of the large distance between the omitted lines and the trees. This survey met the criteria for quasi 3-D processing as the electrode spacing (0.5 m) was one half of the line spacing (1 m).

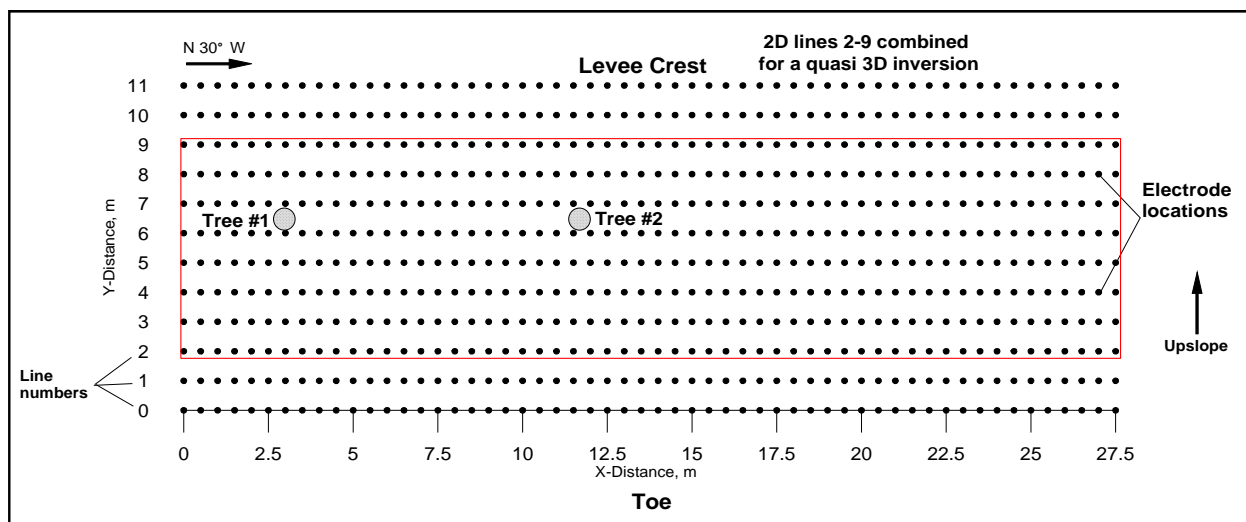


Figure 81. Layout of 2-D lines used for quasi 3-D processing, Site B, Sacramento, CA.

Data interpretation: 2-D

The 2-D data were inverted using EarthImager 2-D software (Advanced Geosciences, Inc.). The inverted resistivity sections for lines 6 through 11 are presented in Figure 82 and lines 0 through 5 are shown in Figure 83. For the ease of comparison, the same resistivity color scale is used for all of the sections (30 to 2500 $\Omega\text{-m}$). Line 11, located on the crest of the levee, is over soil with resistivity values ranging predominantly between 200 and 500 $\Omega\text{-m}$ (Figure 82). The relatively low resistivity values along line 11 are presumed to be caused by the slurry wall within and along the center line of the levee. As the sections progress down slope to line 6, the amount of soil with higher resistivity values gradually increases. Line 10 shows a thin layer (approximately 1 m thick) of higher resistivity soil (yellow and red) extending along the entire line immediately below the surface. In lines 8 and 9, a resistive ($>1000 \Omega\text{-m}$) layer in the approximately upper 1 m, predominates. This layer probably corresponds to a dry sandy soil. Lines 5 through 7 show an approximately 4- to 5-m-thick layer of electrically resistive soil presumed to correspond to dry sandy soil.

Lower-valued resistivity zones, presumed root zones and indicated by the green areas, are present along line 7 at $X = 3$ and $X = 11.5$ to 12.5 m. The maximum depth of the interpreted root zone is approximately 1 m for Tree 1 and 1.3 m for Tree 2. Low-valued zones of similar resistivity are detected along line 6 between $X = 2.5$ to 4 m and $X = 11$ to 12 m. The maximum depth of the interpreted root zones is approximately 0.8 m for Tree 1 and 1.5 m for Tree 2. Root zones could not be interpreted for the results from lines 8 through 11.

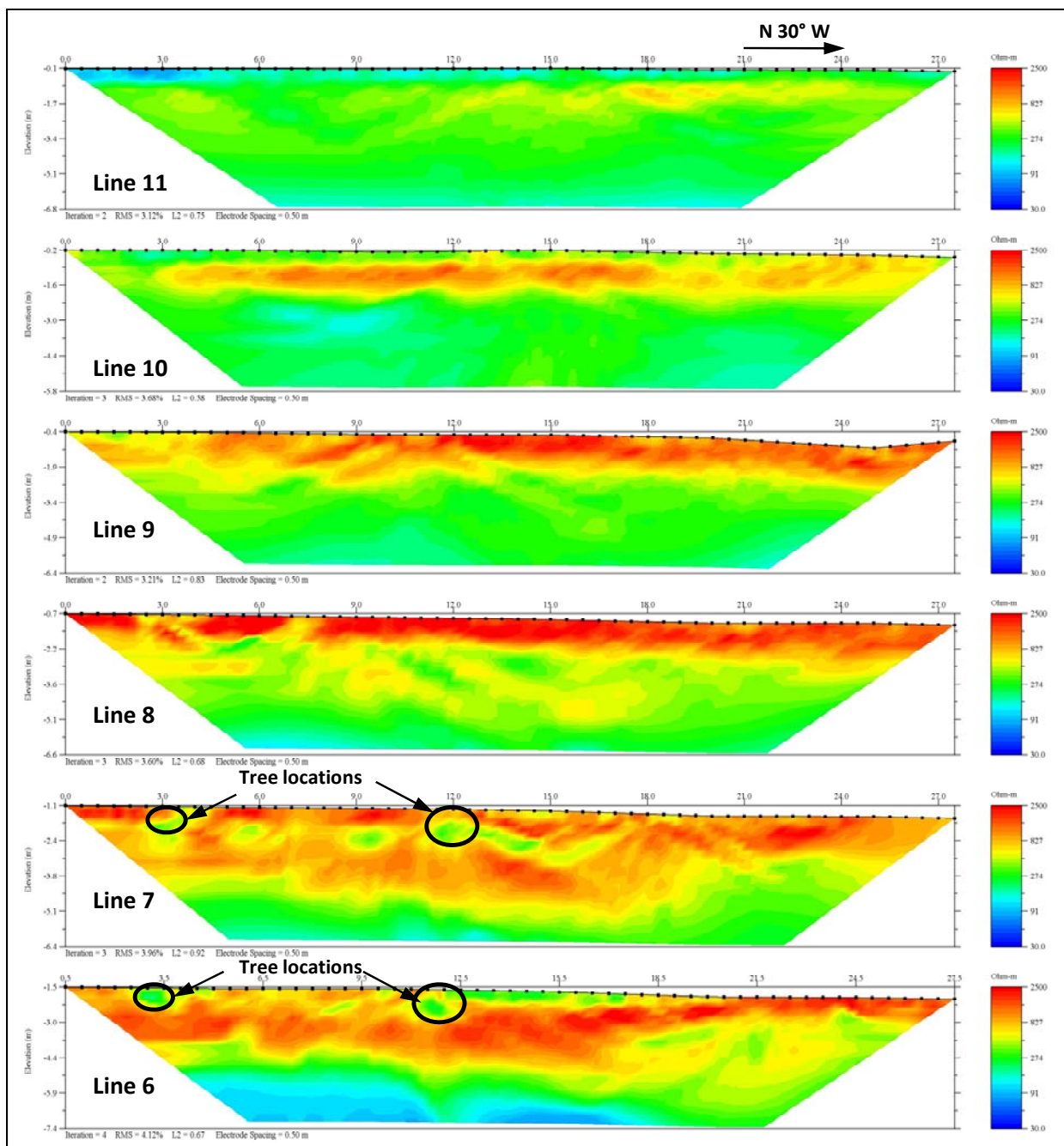


Figure 82. Inversion results for 2-D lines 6 through 11, Site B, Sacramento, CA.
Ovals mark approximate tree root locations.

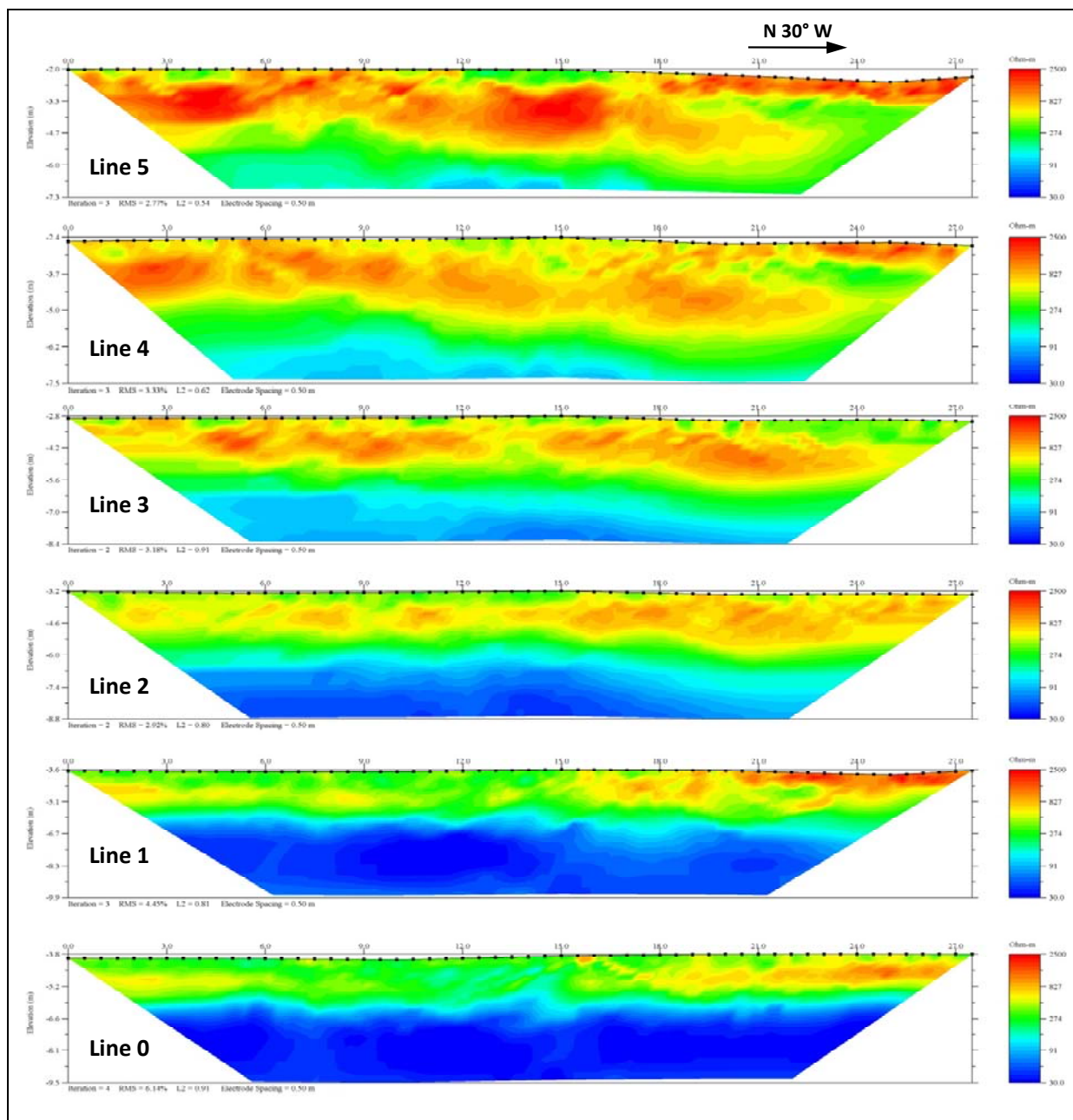


Figure 83. Inversion results for 2-D lines 0 through 4, Site B, Sacramento, CA.

Figure 83 presents the results for lines 0 through 5, which were collected along the lower section of the levee. The same thick, resistive soil layer as found beneath lines 6 and 7 still exists beneath lines 4 and 5 and it quickly thins out towards line 0. Also, note that there is a relatively low-valued resistivity zone below approximate elevation -6.5 m. This zone may correspond with a clay-rich soil or the top of the groundwater table. Evidence of tree roots were not interpreted from the data in lines 0 through 5.

Data interpretation: Quasi 3-D

Figure 84 shows the inverted resistivity image for combined 2-D lines 3 through 9. The black ovals represent the tree locations. Figures C1 through C8, in Appendix C, are depth slices (slices perpendicular to the z-axis) between depths of 0 and 2.34 m. The black ovals represent the tree locations and the white ovals show the vertically projected location of the trees on the depth slice surface. The black dots represent the electrode locations on the ground surface. Relatively low-valued anomalies are evident in the vicinity of Trees 1 and 2 in Figures C1. The maximum depth of the influence of the root zone for Tree 1 is approximately 1.00 m and about 2.10 m for Tree 2.

Figures C9 through C16, in Appendix C, are vertical slices taken along the x-axis (perpendicular to the y-axis). The slices indicate that the horizontal extent of the root zone in the Y direction (perpendicular to the axis of the levee) is between approximately $Y = 5.5$ and 6.5 for Tree 1 and between $Y = 5.0$ and 7.0 . The inversion results also indicate that the root zone for Trees 1 and 2 extend approximately 1.22 and 2.40 m along the x-axis, respectively.

3-D data acquisition and processing

A 3-D ERI grid measuring 13 m by 7 m was established within the 2-D survey area as shown in Figure 85. The rectangular grid consists of 112 electrodes spaced 1 m apart. As with the 2-D survey, the dipole-dipole electrode array was used in this survey. The northern tree, Tree 2, was selected for a thorough investigation and thus the 3-D grid was approximately centered on it. It may have been possible to encompass both trees within the grid. However, because they would have been located near the edges of the grid, there would have been inadequate sampling around each tree. Alternatively, the roll-along survey method could have been conducted to sample both trees with a 3-D survey. The roll-along method, as

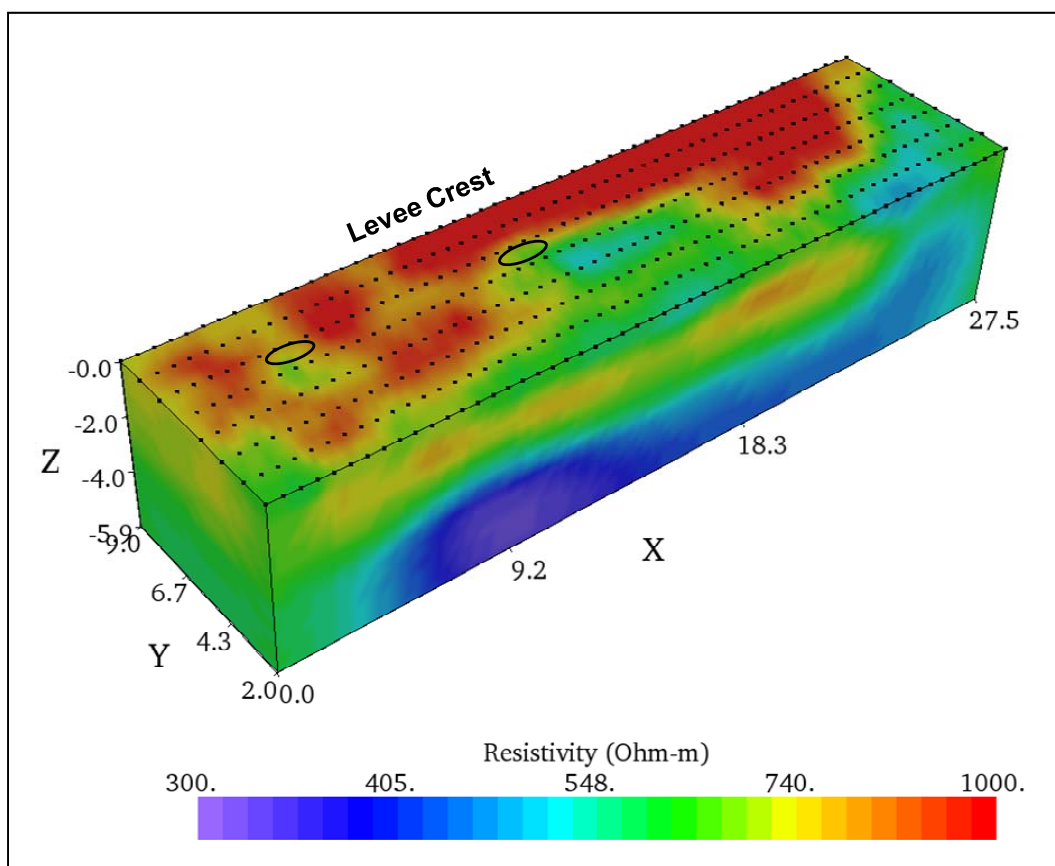


Figure 84. Quasi 3-D inverted resistivity image, Site B, Sacramento, CA.

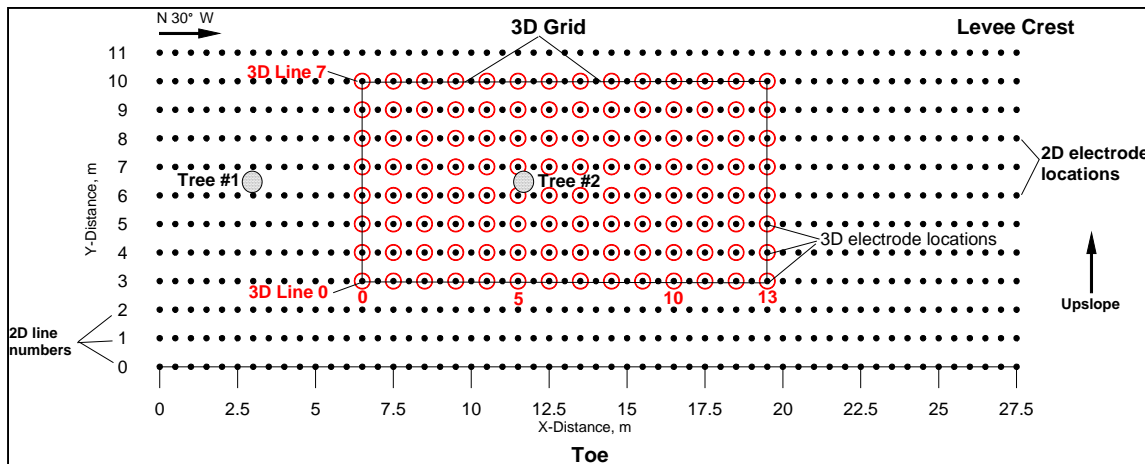


Figure 85. 3-D resistivity survey layout, Site B, Sacramento, CA.

previously mentioned, is time-consuming, and was not considered for this investigation because of time constraints. The 3-D data were collected in September 2009. The 3-D resistivity data were inverted using EarthImager 3-D software (Advanced Geosciences, Inc.).

Data interpretation

The 3-D resistivity inversion image is shown Figure 86. Note that x -axis stations in the 3-D block are translated a positive 6.5 m relative to the 2-D sections. This means that Stations 0 and 13 m on the 3-D block x -axis correspond to Stations 6.5 and 19.5 m, respectively, on the 2-D sections (Figure 8o). Similarly, y -axis stations in the 3-D block are translated a positive distance of 3.0 m along the y -axis relative to the 2-D sections. This means that Stations 0 and 7 m on the 3-D block x -axis correspond to lines 3 and 10 m, respectively, on the 2-D sections.

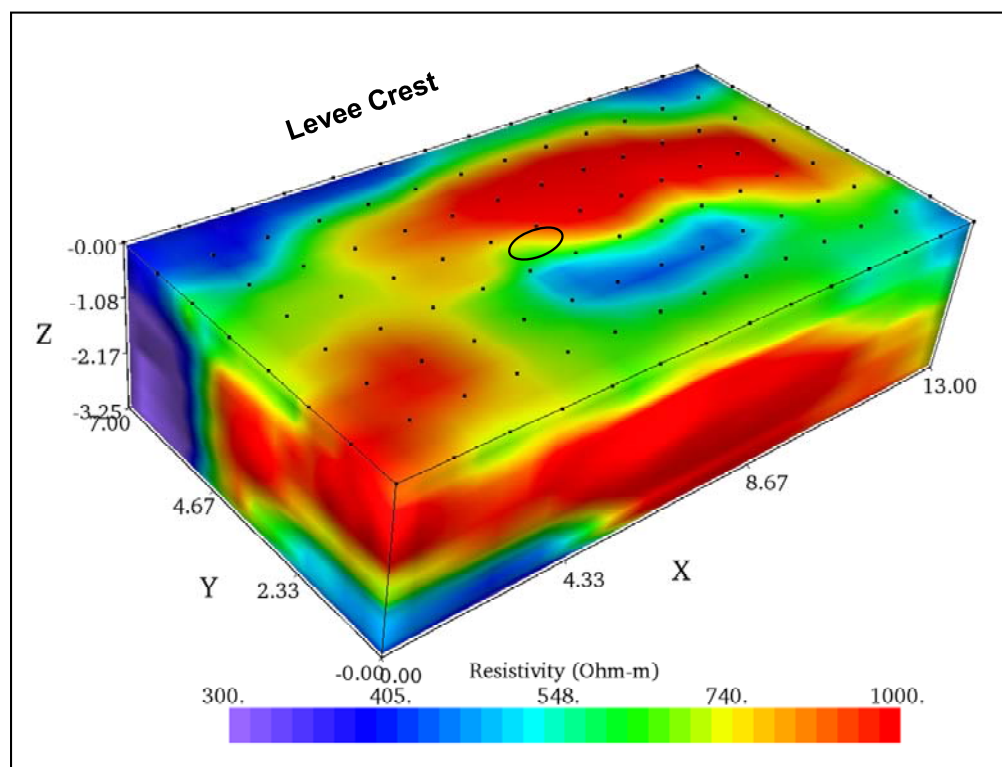


Figure 86. 3-D inverted resistivity image, Site B, Sacramento, CA.
The black oval indicates the tree location.

Figures C17 through C25, in Appendix C, show depth slices at approximate 0.25-m depth intervals between depths of 0.00 and 2.00 m. The black oval represents the approximate location of the tree on the surface of the 3-D block, while the white oval is the projected vertical location of the tree on the depth slice surface. The dots in the Figures C17 through C25 represent the electrodes, which are spaced 1 m apart. A low resistivity anomaly is evident between approximate depths of 0.50 and 1.52 m beneath approximate surface coordinate $X = 5.25$ m and $Y = 2.75$ m. The anomalous area reaches a maximum lateral extent between depths of 0.75 and 1.00 m.

Below 1.00 m, the areal extent of the anomaly gradually diminishes until it is no longer present below a depth of 1.75 m. Between the ground surface and a depth of 0.5 m, the anomaly is difficult to distinguish. The lack of a resistivity contrast may be caused by highly heterogeneous soil in the upper 0.5 m. The data indicate that the maximum areal extent of the anomaly, which occurs at depths between 0.75 and 1.00 m, is approximately 2 m in the *X* direction and 1.5 m in the *Y* direction. The 2-D coordinates that correspond to this anomaly are approximately $X = 11.75$ m and $Y = 5.75$ m. (See Figure 82, line 6, for a vertical representation through this area.)

Figure C26 through C39, in Appendix C, are slices taken parallel to the *x*-axis approximately every 0.25 m between $Y = 1.52$ m and $Y = 4.25$ m. The resistivity values located between $X = 5$ and $X = 6$ m decrease in value between slices taken at $Y = 1.52$ m and $Y = 2.99$ m. At $Y = 2.99$ m the low resistivity area located at approximately $X = 5.4$ m reaches a minimum value (Figure C32). This low resistivity anomaly corresponds to the location of Tree 2. The anomaly at this location extends to a depth of about 1 m. As slices progress up slope, this anomaly becomes smaller until it is no longer noticeable at line $Y = 4.00$ m (Figure C36).

ERI results

Three electrical resistivity inversion methods were used to determine the maximum detectable horizontal and vertical extent of the root zones for the trees located on the protected slope of the levee. Being able to measure a contrast between the root zone and surrounding soil gives the maximum detectable extent of the root system. The actual extent of the root zone most likely extends beyond the distance measured with ERI. Table 31 summarizes the inversion results for the 2-D, 3-D, and quasi 3-D inversion methods. The distance between the two extreme 2-D lines that detect the root zones gives the maximum detectable extent of the root zone perpendicular to the slope of the levee. For example, 2-D lines 6 and 7, which are 1 m apart, detected the presence of the root zone, therefore the maximum horizontal detectable distance of the root zone perpendicular to the slope is 1 m.

The root zone extent for Tree 1 is based on the results of 2-D and quasi 3-D inversions. Both inversion methods are in agreement. The tree root extent for Tree 2 is based on 2-D, 3-D and quasi 3-D inversion results. In the case

Table 31. Maximum detectable lateral and vertical influence of tree root zones based on results of 2-D, 3-D and quasi 3-D inversion methods, Site B, Sacramento, CA.

Inversion Method	Tree 1			Tree 2		
	Maximum Depth, m	Maximum Distance Parallel to Slope, m	Maximum Distance Perpendicular to Slope, m	Maximum Depth, m	Maximum Distance Parallel to Slope, m	Maximum Distance Perpendicular to Slope, m
2-D - Line 6	0.8	1.5	1.0 ^a	1.5	1.0	1.0*
2-D - Line 7	1.0	1.0		1.3	1.0	
3-D	n/a	n/a	n/a	1.5	2.0	1.5
Quasi-3-D	1.0	1.2	1.0	2.1	2.4	2.0
Average	0.9	1.2	1.0	1.6	1.6	1.5

^a The maximum detectable distance perpendicular to the slope is based on the distance between the two 2-D lines with the greatest separation. In this case, Lines 6 and 7 have a 1-m line separation. Thus, the maximum distance perpendicular to the slope is 1 m.

of Tree 2, the quasi 3-D inversion results showed greater values than those from the 2-D and 3-D inversions.

EM survey

Data acquisition and processing

A Geonics Ltd. EM38-MK2 conductivity meter with Tx-Rx coils set at fixed distances of 0.5 and 1.0 m operating in the vertical dipole mode was used. Data were collected along sixteen 28-m-long survey lines spaced 1.0 m apart and oriented parallel to the axis of the levee (Figure 87). Conductivity and in-phase data for both coil separations were collected simultaneously.

Data interpretation

The data are plotted as contour maps of conductivity and in-phase values for the 0.5- and 1.0-m inter-coil separations (Figure 88 and Figure 89). The conductivity results indicate relatively high values along the crest, which is located between approximate lines 10 and 15. The higher values may be caused by a high percentage of clay in the soil or the presence of a cutoff wall located beneath the center of the levee crest. The sloped portion of the site, lines 0 through 10, have relatively lower values, indicating an increase in the amount of sand in the soil or decreasing moisture content, or both. The conductivity results for the 1.0-m coil separation (Figure 89) indicate an increase in conductivity values between lines 0 and 2, the levee toe, whereas the 0.5-m conductivity data do not. The increase in

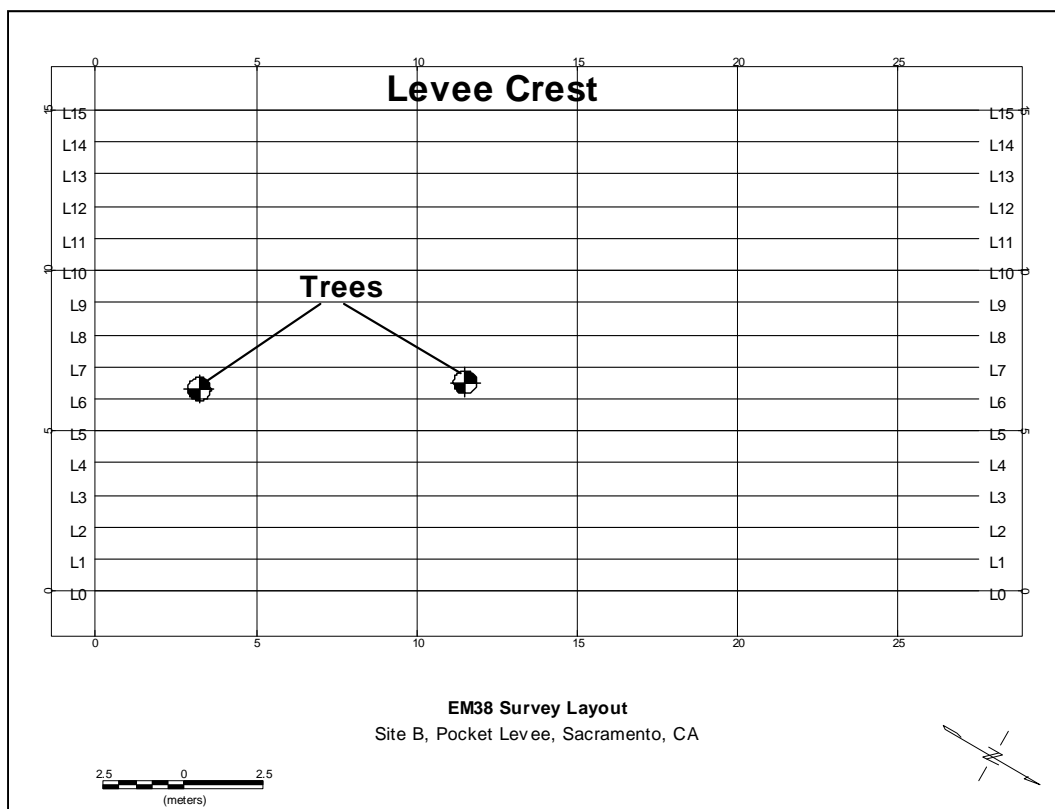


Figure 87. EM38 survey line layout, Site B, Sacramento, CA.

conductivity values in the 1.0-m data is probably caused by an increase in clay content in the soils underlying the levee toe.

The lack of an increase in conductivity values near the toe in the 0.5-m conductivity plot (Figure 88) is presumably attributable to the EM38-MK2 not being able to penetrate through the levee to the underlying higher conductivity valued soils with a 0.5-m coil separation. The 1.0-m coil separation configuration, with a depth of penetration of 1.5 m, however, can. No anomalous conductivity values were interpreted indicating the presence of the root zone of either tree.

Figures 90 and 91 present the in-phase survey results for the EM38-MK2 0.5- and 1.0-m coil spacing, respectively. The in-phase results indicate relatively high values along the crest, which is located between approximate EM lines 10 and 15. The higher in-phase values indicate a change in soil type between the crest and slope. As with the conductivity surveys, no anomalous in-phase values pointing to the presence of the root zone of either tree were interpreted.

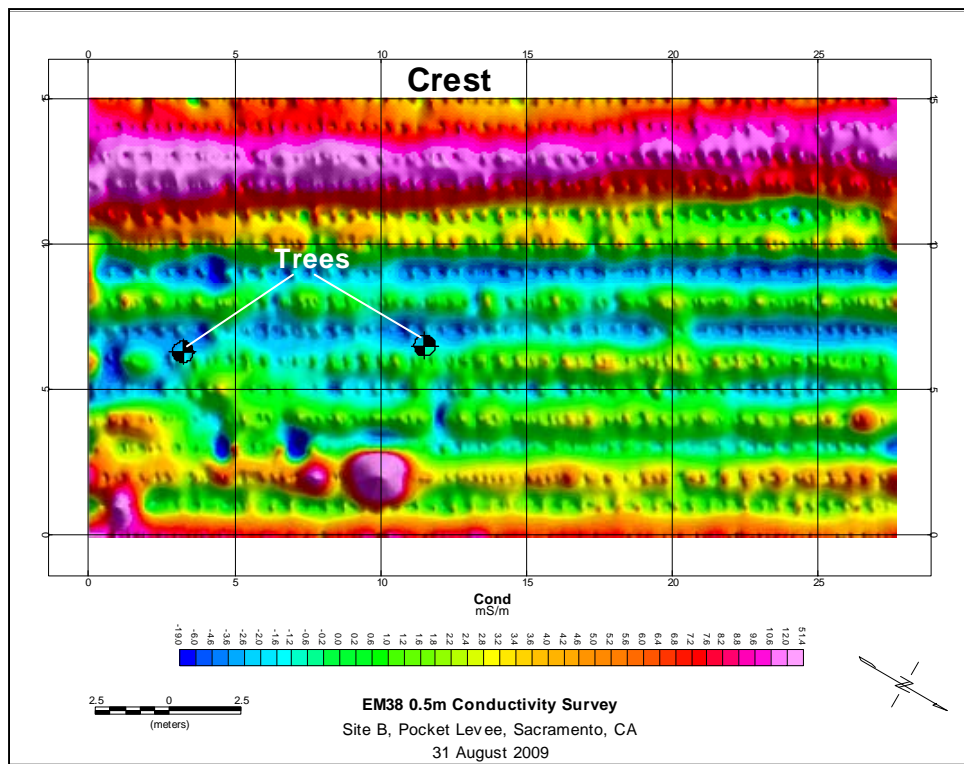


Figure 88. EM38-MK2 conductivity survey results, 0.5-m inter-coil separation, vertical dipole mode, Site B, Sacramento CA.

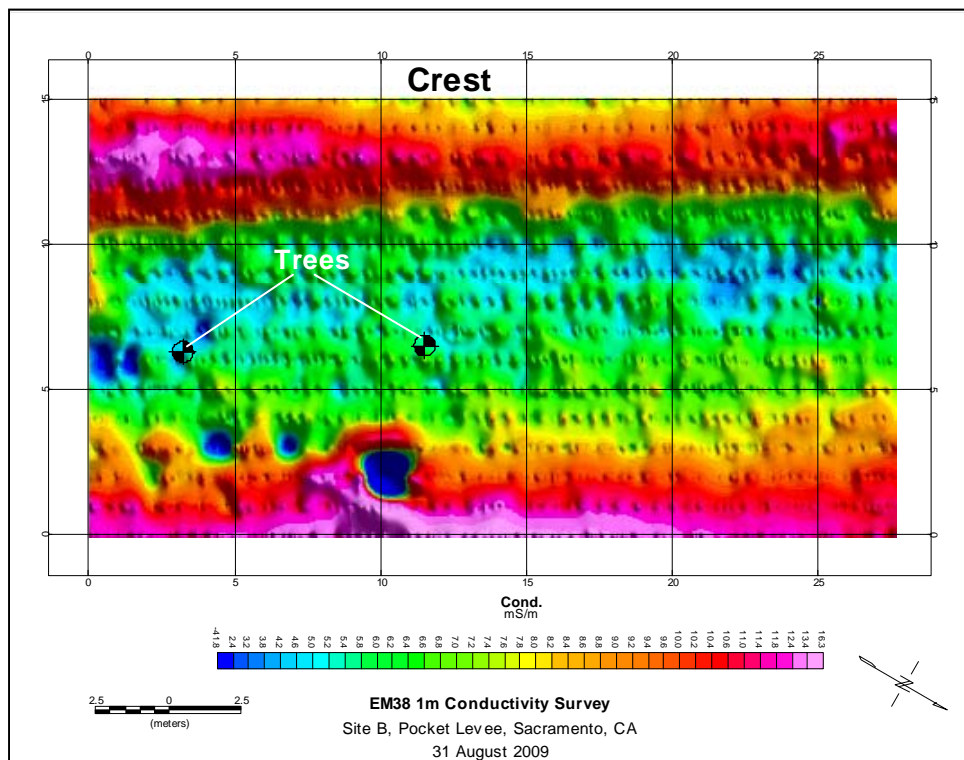


Figure 89. EM38-MK2 conductivity survey results, 1.0-m inter-coil separation, vertical dipole mode, Site B, Sacramento, CA.

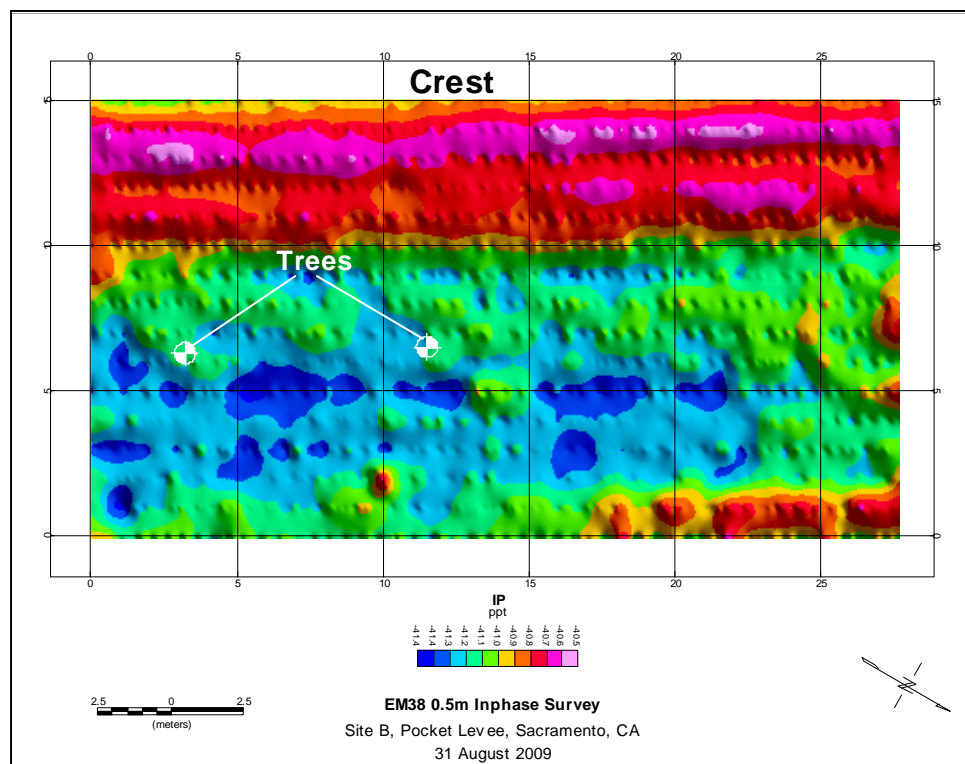


Figure 90. EM38-MK2 in-phase survey results, 0.5-m inter-coil separation, vertical dipole mode, Site B, Sacramento, CA.

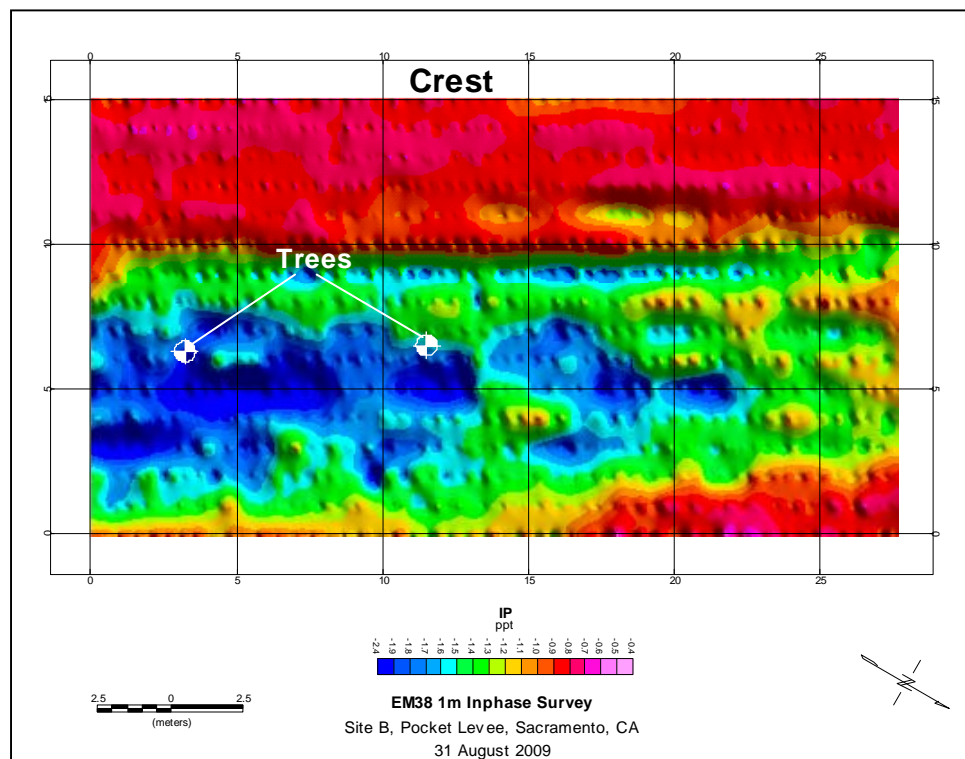


Figure 91. EM38-MK2 in-phase survey results, 1.0-m inter-coil separation, vertical dipole mode, Site B, Sacramento, CA.

GPR survey

Data acquisition and processing

The GPR data were acquired along survey lines both parallel and perpendicular to the levee crest with a 3-D Radar Geoscope using a B1831 antenna array. The survey lines were centered on meter markers and spaced 1.0 m apart (Figure 92). Eleven lines (1W through 12W) were surveyed parallel to the crest (Figure 93a), whereas 12 lines (1N through 14N) were surveyed perpendicular to the crest (Figure 93b). The levee crest is located along the west side of the survey area. A depth of investigation of 1.0 m was achieved, based on a subsurface electromagnetic wave velocity of 0.1 meters per nanoseconds (m/ns). The 3-D Radar Geoscope GPR and the processing steps used in this study are described earlier in this chapter.



Figure 92. Survey area at Site B, Sacramento, CA. The yellow flags in the foreground are spaced 1 m apart. The valley oak tree in the foreground (Tree 2) is the one used for the GPR root characterization study. Cables on the ground are those used for a 3-D resistivity survey.

Data interpretation

Figure 93 shows the antenna swath paths (11 parallel, 12 perpendicular) for the surveys conducted parallel (north to south) and perpendicular (west to east) to the levee crest. Note that the parallel section extends 0 to 13W, whereas the perpendicular section extends to 15W. Figure 94 shows the radargram data at a depth 5 cm, along with the *x* and *y* vertical time-slices bounding the tree location. The strong red circular anomalies at the northern (top) and western (left) edges of the two radargrams in Figure 94a are from the aluminum plates used to mark the start of the survey lines. The weak to strong anomalies that extend the length of the site, between 9W to 10W in the parallel section and 5E to 6E in the perpendicular section, occur at the transition from the gravel-covered crest to the vegetated levee slope. Numerous weak to moderately strong anomalies are visible in the radargrams. Without ground-truth data, it is difficult to say what the anomalies represent. Some could represent variations in soil type or moisture conditions, whereas others could be gravel or rocks, cultural debris, or levee construction materials. Apparent in the parallel section is a weak (west side) to moderately strong (east side) reflection from the tree.

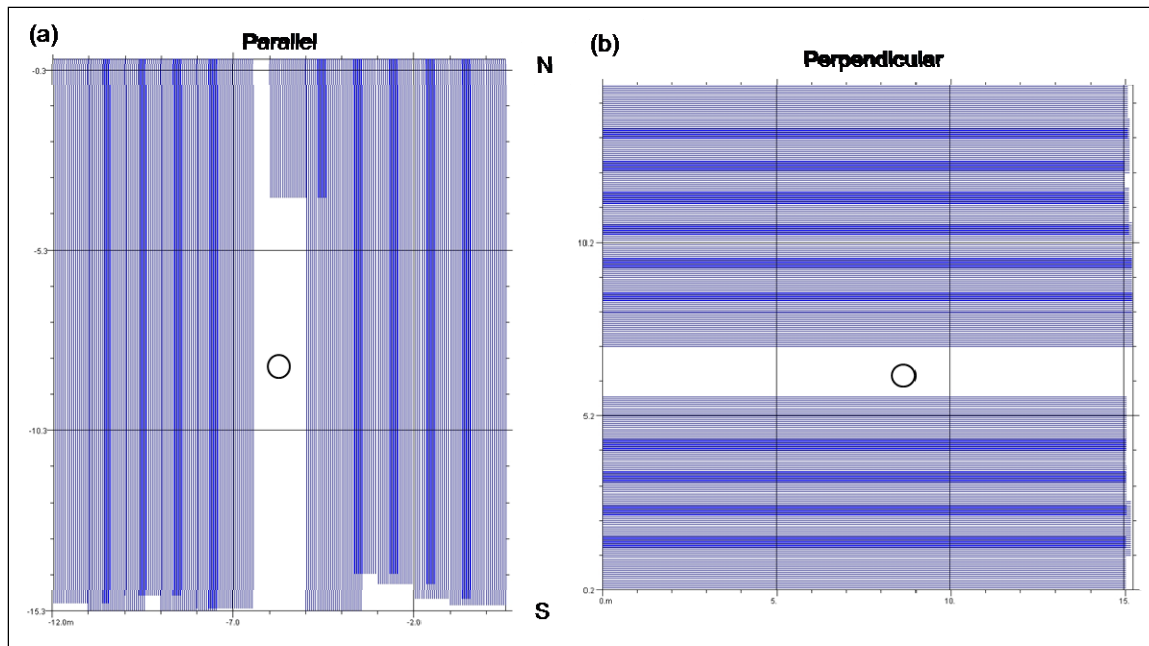


Figure 93. (a) Antenna swaths along survey lines parallel to the crest. The survey was conducted north to south along lines 1W through 12W, with limited data collected along line 6W and no data collected along line 7W because of the tree location (circle). (b) Antenna swaths along survey lines perpendicular to the crest. The survey was conducted west to east along lines 1N through 14N, with no data collected along lines 6N through 7N because of the tree location (circle).

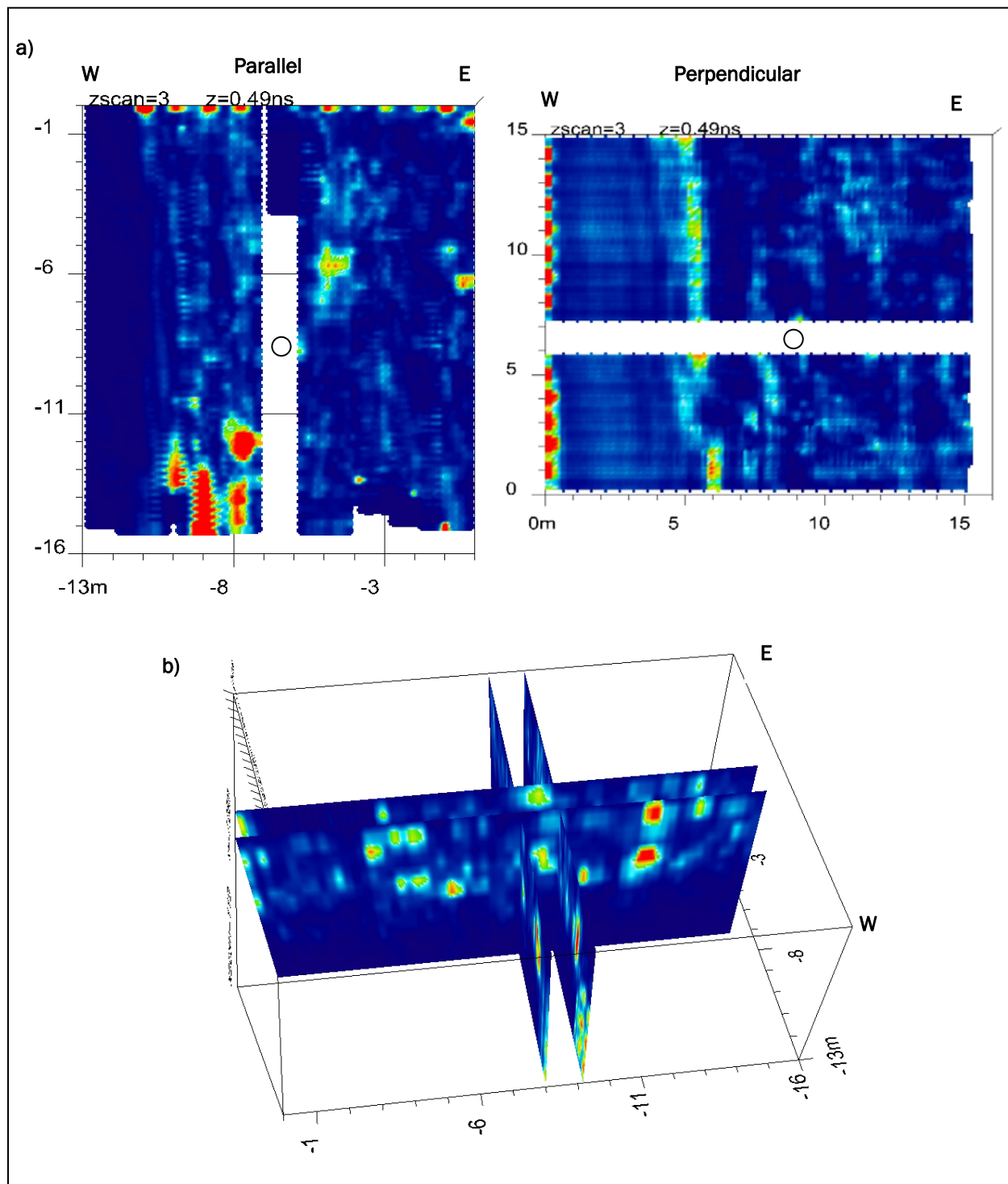


Figure 94. Radargrams parallel and perpendicular to the crest at depth $z = 5$ cm (actual 0.49 cm) (a) and x and y time slices bounding the tree location (b). The circles in (a) represent the location of the tree.

Figure 94b is a view from west to east of the north-south (parallel) GPR time slices acquired adjacent to the tree.

The influence of the tree is apparent immediately around its location in the near surface. Time slices from data collected parallel to the crest tell us that this near-surface signature extends 0.25 m to the west and east (Figure 95a), for a total east-west influence of 1.71 m (from 5.62W to 7.33W). The north-south influence of the tree is 1.41 m, extending from 7.92S to 9.33S (Figure 95b). Time slices along the y-plane may indicate roots extending from the area of influence shown in Figure 95. Figure 96 shows image slices at $y = 8.78$ m south (parallel) and $x = 9.16$ m E (5.84 m W) (perpendicular), and a depth of 29.5 cm.

Comparison of GPR data with 3-D resistivity study

Plots of the radar data collected both parallel and perpendicular to the levee crest and 3-D resistivity data are compared in Figure 97. The GPR data are from a depth of 5 cm, whereas the resistivity is at the surface. Note that the resistivity low in the southwest corner corresponds to a strong reflection in the parallel radar section. A comparison of the zone of root influence determined using the resistivity and GPR techniques is given in Table 32. The lateral maximum detectable extents determined using each method are similar, however there is a significant difference in the vertical extent. This difference is attributed to the ability of the resistivity survey technique to interrogate the region directly under the tree, whereas the GPR method is limited by the surface position of the antenna around the tree.

Conclusions

ERI, EM and GPR surveys were conducted along a section of the Sacramento River levee to determine the effectiveness of these noninvasive geophysical techniques to map the tree root distribution of two trees on the protected slope of the levee.

The maximum detectable lateral and vertical extents of the root zone were determined for the larger of the two trees (Tree 2) based on 2-D, 3-D, and quasi 3-D ERI inversion results. Two-dimensional and quasi 3-D ERI inversion results were used to determine the maximum detectable extent of the smaller tree's (Tree 1) root ball zone. For this site, the tree root zone had significantly lower resistivity values than the surrounding soil. It

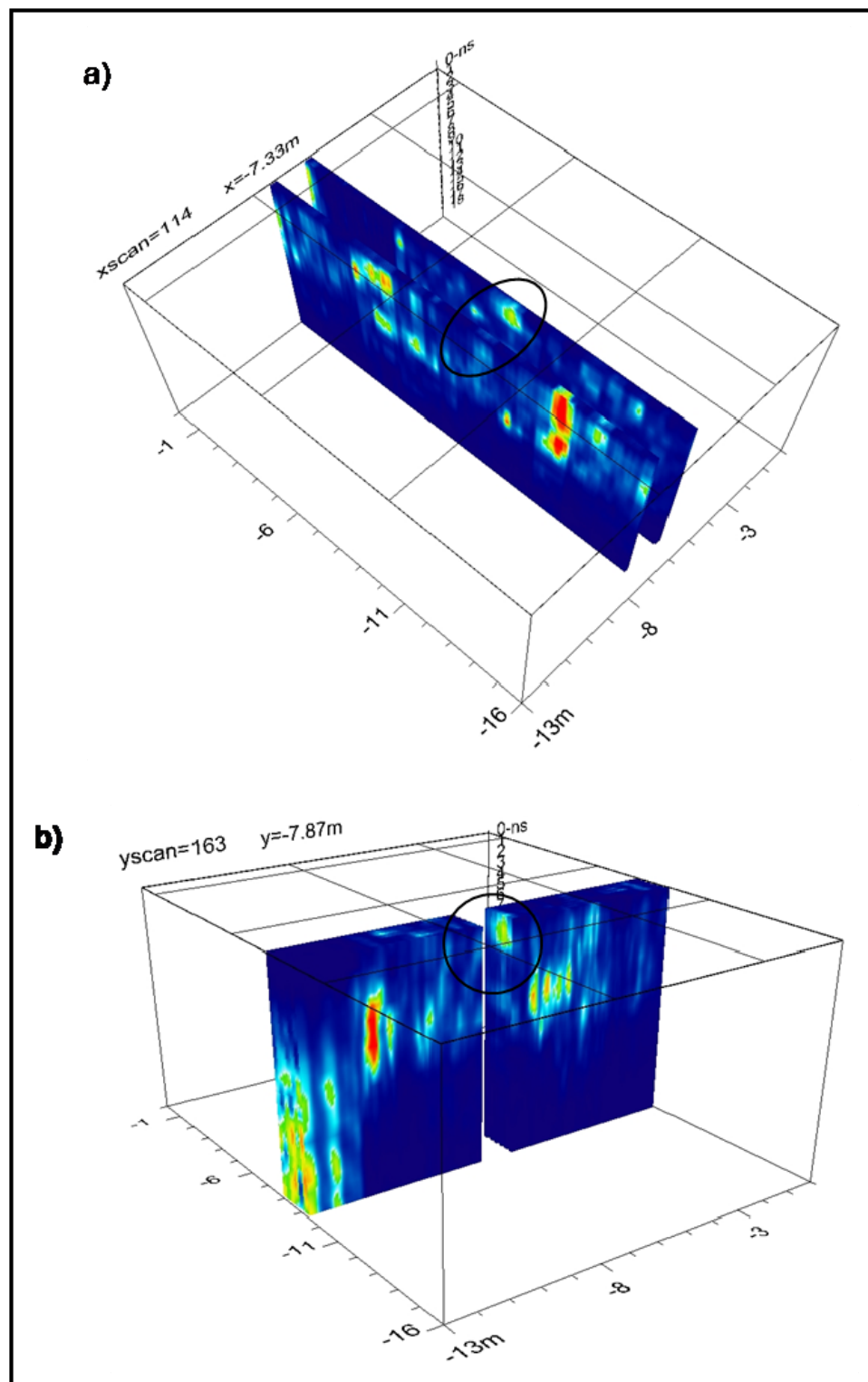


Figure 95. Time slices showing near-surface influence of the tree.
(a) East-west extent 1.71 m (5.62W to 7.33W). (b) North-south
extent 1.41 m (7.92S to 9.33S). Data from collection
parallel to levee crest.

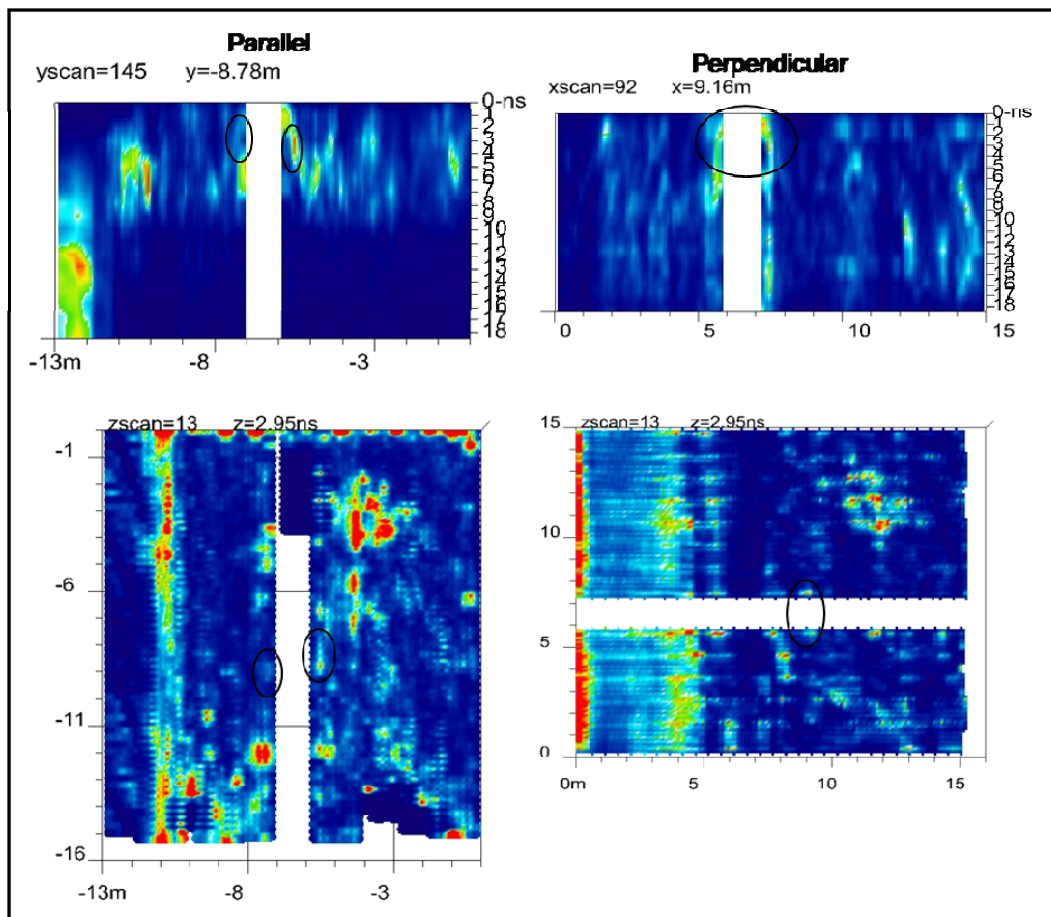


Figure 96. Radar images showing possible roots extending from near-surface influence of the tree shown in Figure 92.

cannot be determined at this time which ERI inversion technique provides the most accurate representation of the root ball zone as these trees, to date, have not been excavated to expose their root architecture.

GPR data were collected parallel and perpendicular to the levee crest using a 31-channel antenna array. There appears to be a significant amount of clutter in the subsurface that hindered the detection of individual roots. The maximum detectable lateral extent of the root zone of influence is comparable to that determined from the ERI survey.

The data collected from the EM surveys conducted near the two trees did not indicate the presence of roots or root ball zone.

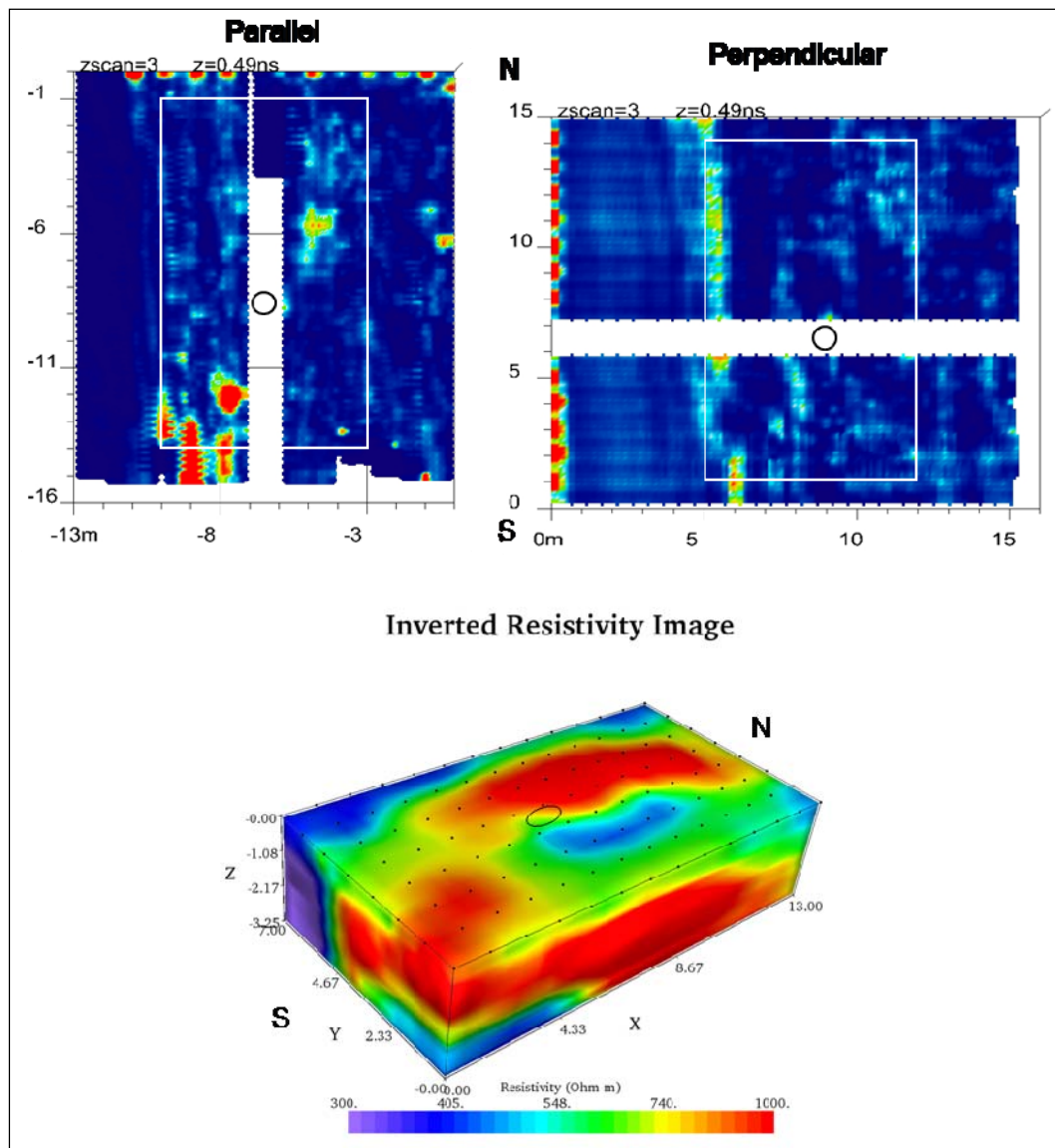


Figure 97. Comparison of GPR data and 3-D resistivity data. The white rectangles on the radar plots correspond to the area imaged in the resistivity survey. The circles/oval on all plots mark the location of the tree (Tree 2).

Table 32. Maximum detectable lateral and vertical extent of tree root zone based on resistivity and GPR survey results, Sacramento, CA.

Geophysical Technique	Tree 2		
	Maximum Detectable Depth, m	Maximum Detectable Distance Parallel to Slope, m	Maximum Detectable Distance Perpendicular to Slope, m
Resistivity (average)	1.6	1.6	1.5
GPR	0.35	1.4	1.7

Portland, OR

Background

Three surface-based geophysical methods, ERI, EM induction, and GPR, were used to determine the extent of the tree root distribution of several cottonwood trees on a levee along the Columbia River, located approximately 19 km east-northeast of Portland, OR (Figure 98). The investigation was conducted by ERDC personnel during 18 through 23 September 2009.

The study site has dimensions of 12 by 43 m and is located on the protected slope of the Columbia River levee (Figure 98). There are eight cottonwood trees located within the study site as shown in Figure 99.

Geophysical survey methods

ERI, EM induction and GPR were used to map the extent of the tree root zone. Principles of operation for these methods are described in Chapter 2 of this volume.



Figure 98. Geophysical test site location, Portland, OR.



Figure 99. View, looking east, of the test site showing the trees and levee, Portland, OR.

ERI survey

ERI data were acquired using 2-D and roll-along 3-D survey techniques. Data acquisition and processing techniques for the 2-D and 3-D methods are described in the following paragraphs. Data were collected using a SuperSting R8 resistivity meter with the Smart electrode switching system.

2-D data acquisition and processing

Two-dimension ERI data were collected along seven 43-m-long, parallel lines as shown in Figure 100. The lines were oriented parallel to the axis of the levee. Line separation was 2 m and each line consisted of 44 electrodes spaced 1.0 m apart. The locations of the trees relative to the 2-D ERI lines are shown in Figure 100. The 2-D data were inverted using EarthImager 2-D.

The 2-D data in this study were also processed using the quasi 3-D technique described in Chapter 2. The survey was designed with 1.0-m electrode and 2-m line spacings, thus meeting the criteria for quasi 3-D

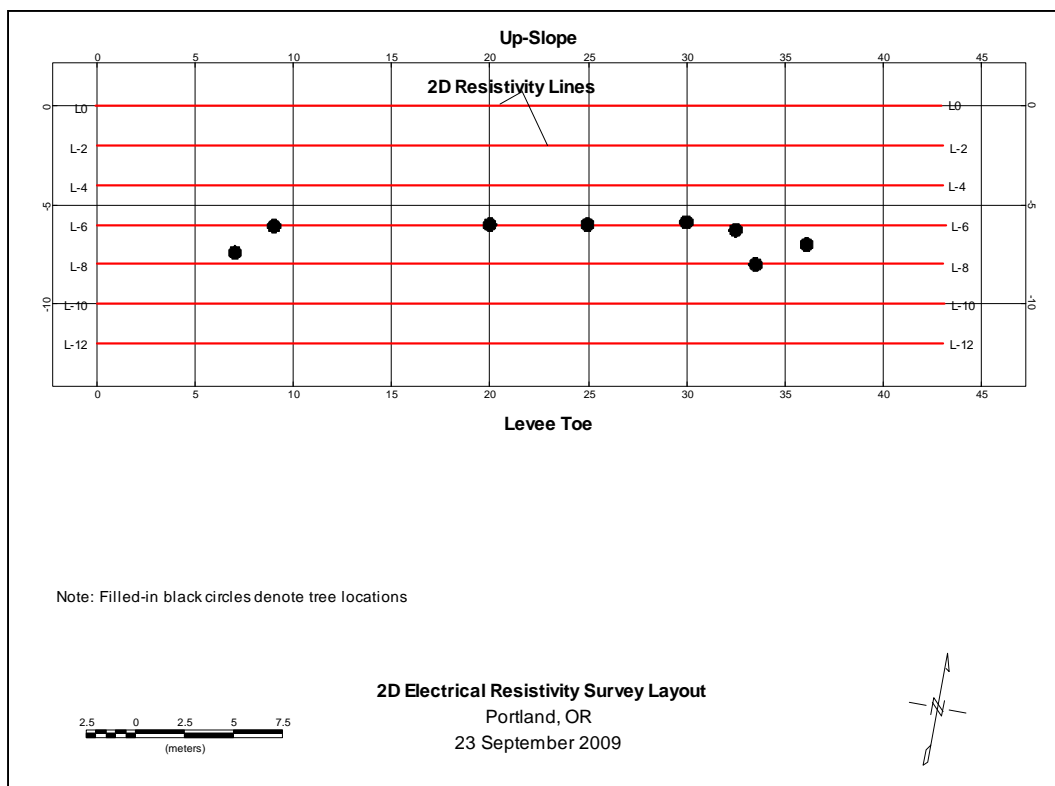


Figure 100. 2-D resistivity survey layout, Portland, OR.

processing. Seven 2-D survey lines, lines o-12 (Figure 100) were combined into a single 3-D data set and inverted using EarthImager 3-D.

Data interpretation: 2-D

The inverted resistivity sections for 2-D lines o through -6 are presented in Figure 101 and the sections for lines -8 through -12 are shown in Figure 102. For easy comparison, the same resistivity scale was used for all of the 2-D sections (25 to 1,000 $\Omega\text{-m}$). Figure 101 shows that the upper 1 to 2 m of soil are highly resistive, with values exceeding 1,000 $\Omega\text{-m}$ and are interpreted as dry sand. As the resistivity profile lines progress down slope, the highly resistive surface layer becomes discontinuous, as seen in lines 6 and 8, and disappears along lines 10 and 12. Along lines 10 and 12, the high resistivity layer is replaced with a 1- to 2-m thick layer having resistivity values ranging between approximately 100 and 200 $\Omega\text{-m}$. Underlying the relatively high resistivity layers is a soil layer approximately 7 to 8 m thick with resistivity values less than 75 $\Omega\text{-m}$. This layer is interpreted as clay. Along lines 6 and 8 where the trees are located, no anomalous resistivity areas indicating the tree locations were noted.

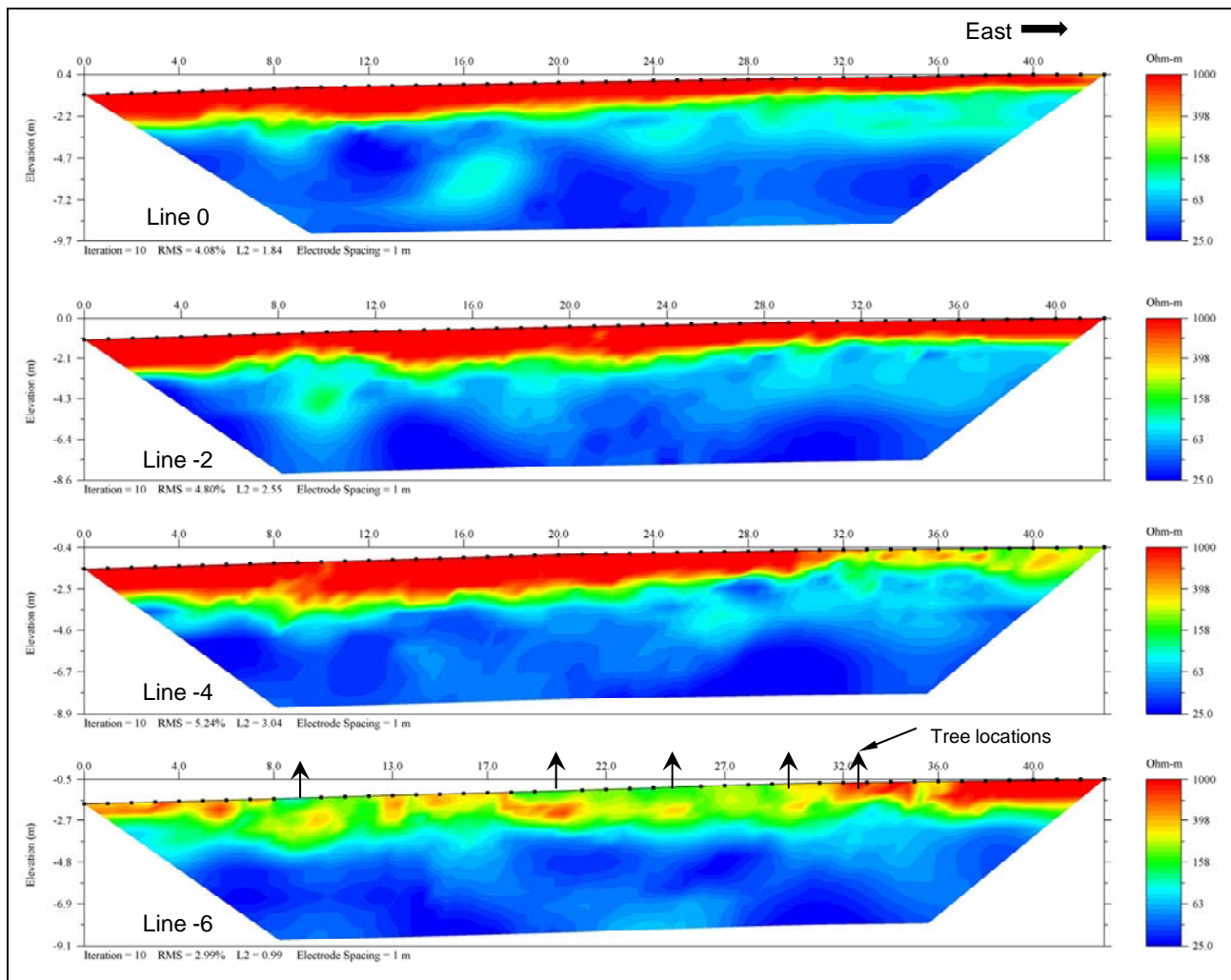


Figure 101. Two-dimensional inversion results, looking up slope, for resistivity lines 0 through -6, Portland, OR.

Data interpretation: Quasi 3-D

Figure 103 is an inverted resistivity image of the combined 2-D lines. Figures C38 through C50, in Appendix C, are depth slices (slices perpendicular to the z-axis) taken every 0.5 m between depths of 0.00 and 3.00 m. The black ovals represent the tree locations on the ground surface. The black dots represent the electrode locations on the ground surface. There is a relatively high resistivity surface layer extending across most of the site. Unlike the highly resistive (greater than 1,000 $\Omega\text{-m}$) surface layer calculated from the 2-D inversion program, the surface layer calculated from the quasi 3-D inversion program has a maximum resistivity of approximately 250 $\Omega\text{-m}$. As the depth slices increase become deeper, the resistive layer recedes up slope.

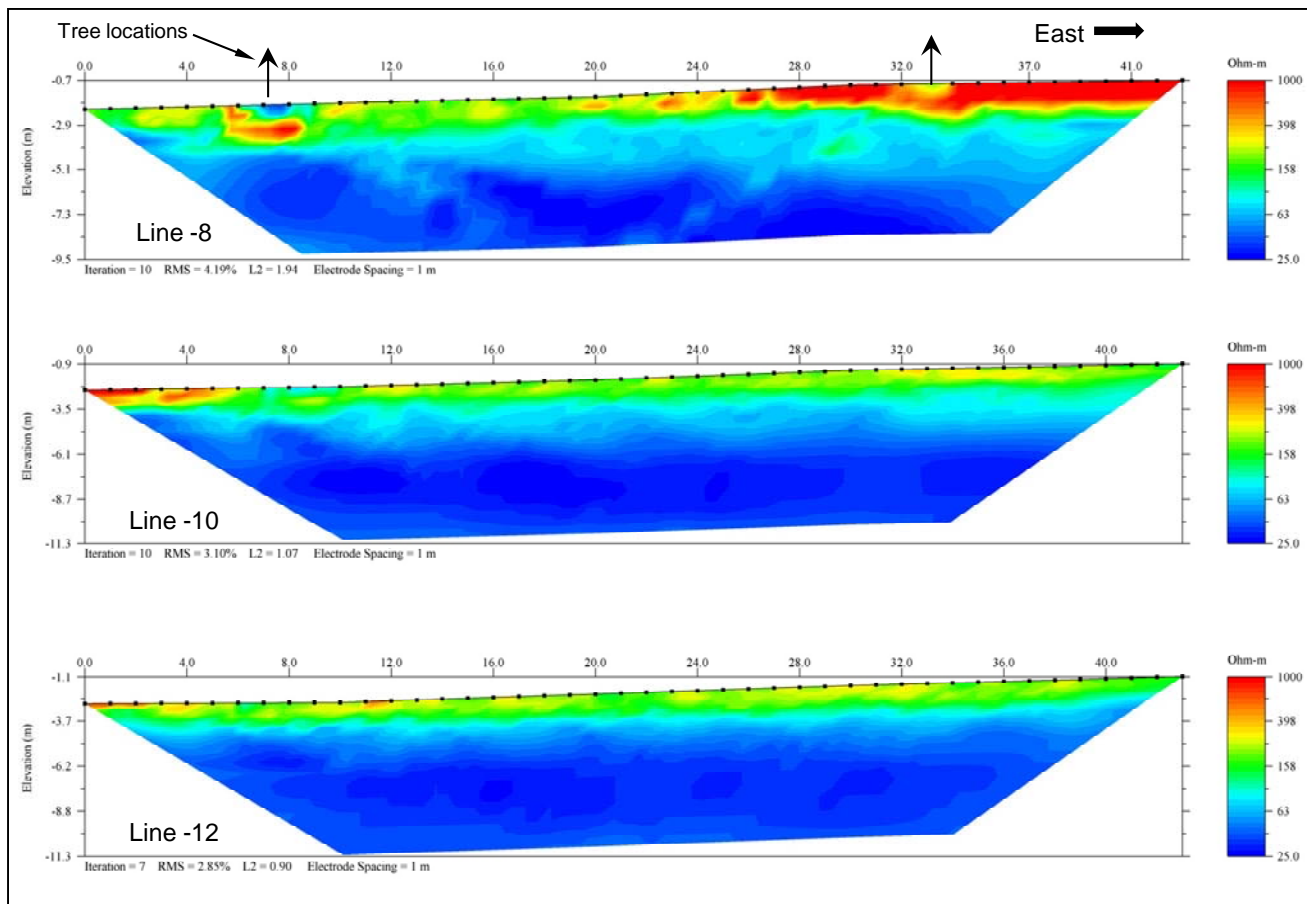


Figure 102. Two-dimensional inversion results, looking up slope, for lines -8 through -12, Portland, OR.

Figures C51 through C61, in Appendix C are vertical slices taken along the x -axis (perpendicular to the y -axis) between $Y = 5.00$ m and $Y = 9.50$ m at 0.50-m intervals. The black ovals represent the locations of the trees on the ground surface. The figures show a relatively high resistivity surface layer approximately 2 m thick overlying a soil with much lower resistivity values. As the slices progress downslope, one can see that the high resistivity overburden becomes discontinuous in the vicinity of $Y = 8.00$ m and has nearly disappeared by the time it reaches $Y = 9.00$ m. No tree roots or root zone locations were interpreted from the quasi 3-D inversion results.

3-D data acquisition and processing

A 3-D ERI grid measuring 11 m by 13 m was established around the two western-most trees as shown in Figure 104. The rectangular grid consists of electrodes positioned 1 m apart. Stainless steel rods, approximately 1 cm in diameter, were driven vertically into the ground to a depth of about 0.3 m and used as electrodes. A roll-along survey method was used to

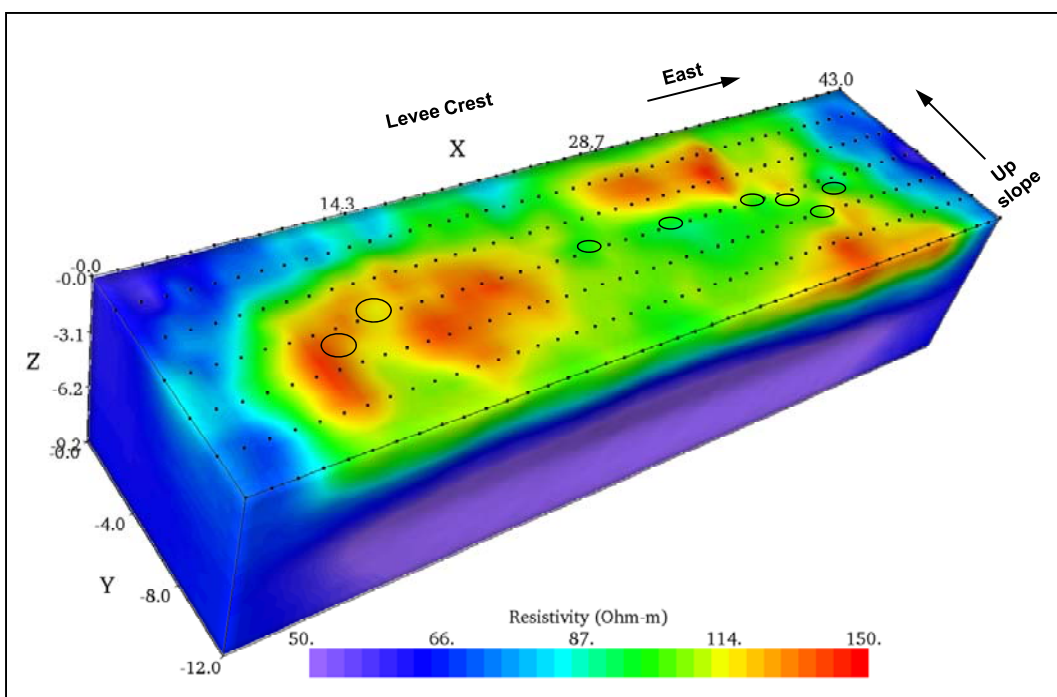


Figure 103. Quasi 3-D inverted resistivity image, Portland, OR.

collect the ERI data. In the roll-along method, a 3-D survey is conducted as usual. Upon completion of the survey, the electrodes from the back half of the grid are picked up and leap-frogged or rolled-along to the front end of the grid and the survey resumed. Figure 104 shows the location of the 3-D survey relative to the locations of the 2-D ERI lines. In this survey, the 3-D grid was leap-frogged in an easterly direction. Three-dimensional data were initially collected from a 13- by 7-m rectangular area. After the initial survey was completed, the four western-most north-south trending cables located between $X = 0$ m and $X = 3$ m were disconnected from the electrodes and rolled-along east to the front of the grid. The four rolled-along cables were then connected to electrodes along lines $X = 8$ m through $X = 11$ m, thus forming another 13- by 7-m grid. The 3-D resistivity data were inverted using EarthImager 3-D software.

Data interpretation

An inverted resistivity image of the 3-D grid is shown in Figure 105. The black ovals on the grid show the approximate position of the eight trees. The dots on the figure represent the electrode locations, which are spaced 1 m apart. The maximum depth of investigation is approximately 3.25 m.

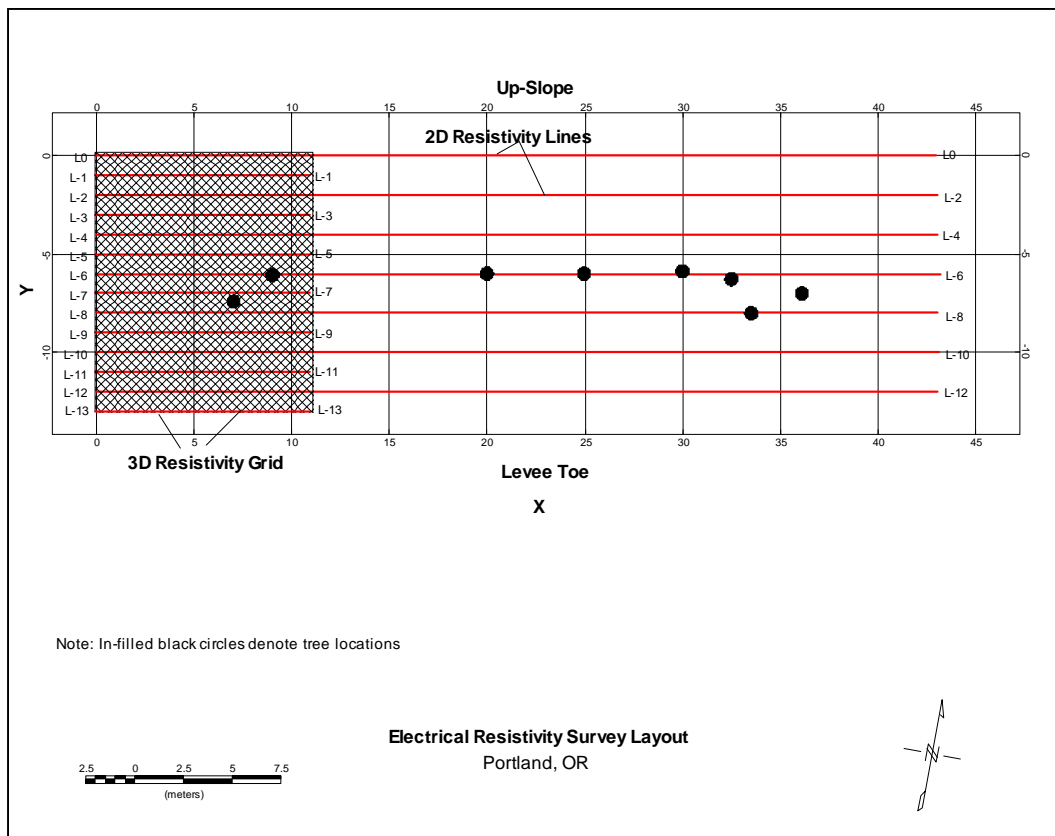


Figure 104. Three-dimensional resistivity survey layout, Portland, OR.

Figures C62 through C68, in Appendix C, show depth slices of the inverted resistivity image taken at 0.50-m depth intervals between depths of 0 and 3.00 m. The black ovals represent the approximate locations of the trees shown on the ground surface of the 3-D block. The white ovals are the projected locations of the trees on the depth slice surface. The black dots on the figures represent the electrode locations on the ground surface.

At a depth of 0.00 m, the two trees, located within the 3-D grid, are situated in a low resistivity area that is relatively localized. Initially, it appears that the tree root zones may be associated with relatively low resistivity values; however, as the depth slices increase become deeper, the soil directly beneath the trees become more resistive. The resistive soil is quite extensive and not limited to only the area immediately beneath the tree. No localized anomalous resistivity areas are apparent beneath the tree related to the tree root zones in the data.

Figures C69 through C80, in Appendix C, show slices of the 3-D inverted resistivity image taken at 0.50-m intervals parallel to the x-axis between $Y = 3.50$ and $Y = 9.00$ m. The white ovals represent the approximate

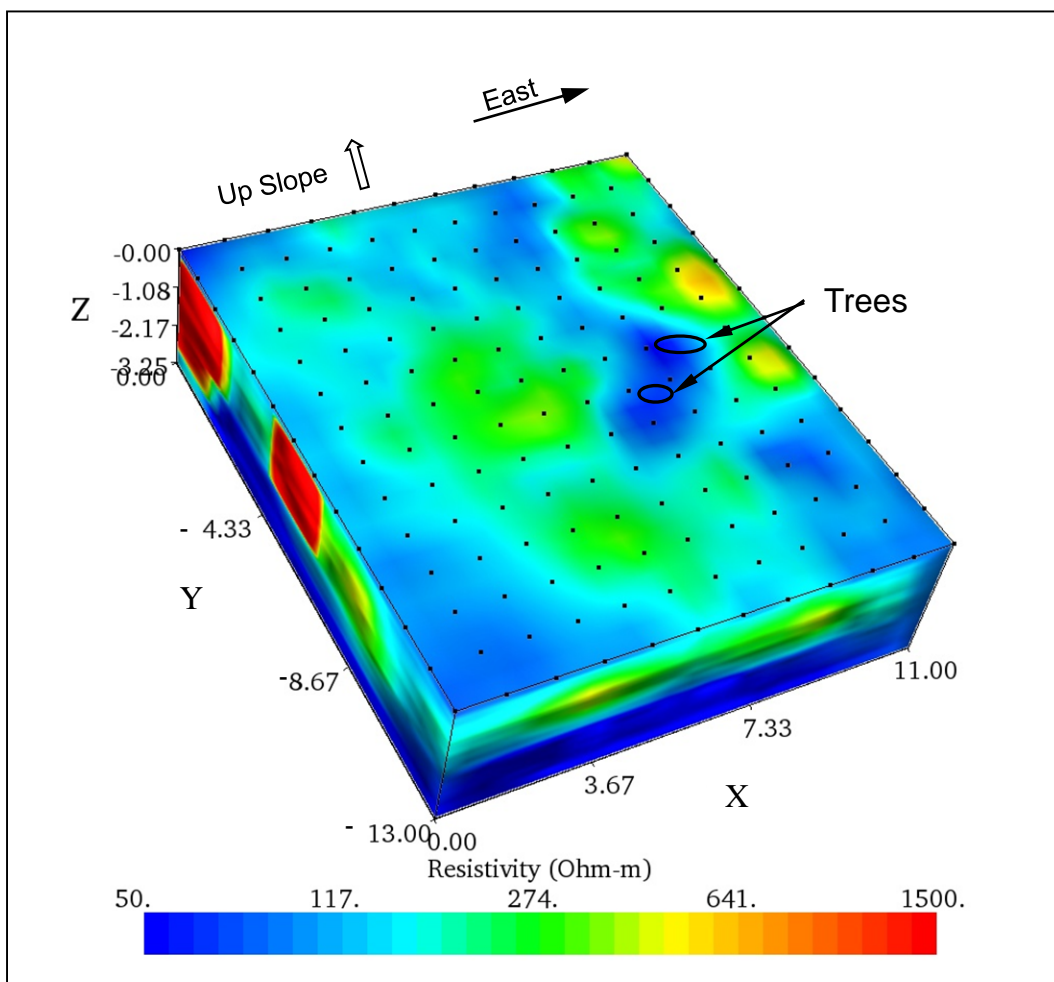


Figure 105. Three-dimensional resistivity inversion image, Portland, OR.

locations of the two trees on the ground surface. The figures show a high resistivity layer approximately 2 m thick overlying a soil with much lower resistivity. As the slices progress from $Y = 3.50$ to $Y = 6.00$ m, the lateral extent of the high resistivity layer increases and then decreases as it approaches $Y = 9.00$ m. No localized anomalous resistivity areas beneath or in the vicinity of the trees associated with the tree root zones were observed.

Summary of ERI results

The 2-D and 3-D ERI surveys were conducted in the vicinity of eight cottonwood trees located on the levee slope. The ERI data show highly variable resistivity values in the upper 2 m caused by heterogeneous soil, thus making it difficult to see differences in resistivity values between the root zone from background soil. Neither 2-D, quasi 3-D nor 3-D processing of ERI data indicated the location of the tree root zones.

EM survey

Data acquisition and processing

An EM survey grid measuring 45 by 12 m was established around the eight trees as shown in Figure 106. A Geonics Ltd. EM38-MK2 conductivity meter was used with Tx-Rx coils set at fixed distances of 0.5 and 1.0 m and operated in the vertical dipole mode. Data were collected along E-W oriented lines spaced 1 m apart. The EM data were contoured and maps of conductivity and in-phase values for the 0.5- and 1.0-m inter-coil separations were plotted.

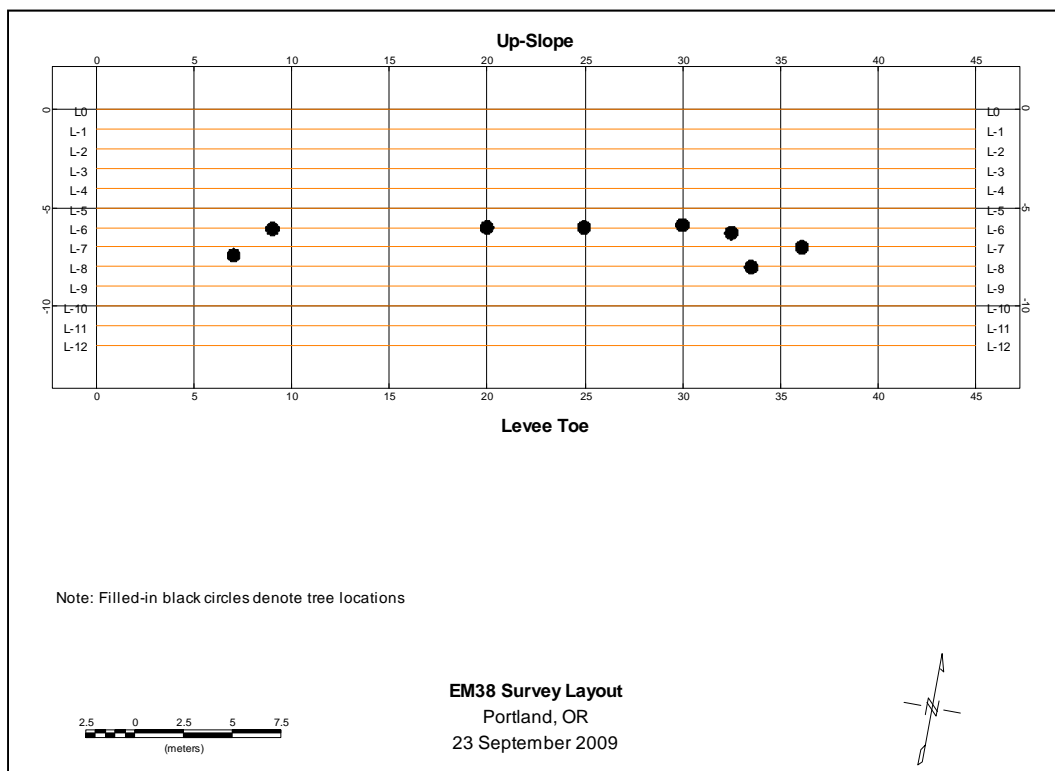


Figure 106. EM38 survey line layout, Portland, OR.

Data interpretation

Figures 107 and 108 present the conductivity survey results for the 0.5- and 1.0-m inter-coil spacings, respectively. Note that it was difficult to calibrate the EM38 at this site because of the extremely low near-surface conductivity values and, consequently, unrealistic negative conductivity values are presented. It is evident that, in general, the conductivity values of the 1.0-m inter-coil spacing are much higher than those for the 0.5-m inter-coil spacing. This indicates that the soil electrical conductivity increases with depth. The increase in conductivity values with depth is

most likely caused by an increase in clay or moisture. The striping seen in the 0.5-m conductivity data is caused by a line spacing interval that was too coarse. No correlation between conductivity and tree location is evident in the data.

Figures 109 and 110 present the in-phase survey results for the EM38 0.5 m and 1.0-m inter-coil spacings, respectively. No correlation between in-phase values and the root zone location from the in-phase surveys was interpreted.

GPR

Data acquisition and processing

The GPR data were acquired along survey lines both parallel and perpendicular to the levee crest. The survey lines were centered on meter markers and spaced 1 m apart. Of the 31 antennae available in the array, only 29 (2 through 30) were used; the two end antenna (1 and 31) were not used because they tend to be noisy. The antennae in the array are spaced 0.055 m. The 29 operational antennae give a single swath width of 1.54 m. There is a 0.5-m overlap between survey lines when using a 1-m survey line spacing. Seven lines (1S-4S, 10S-12S) parallel to the crest were surveyed; twenty-three lines (1E-5E, 11E-18E, 22E-23E, 27E-28E, and 37E-42E) perpendicular to the crest were surveyed. The levee crest is located north of the survey area. Figure 111 shows the location of the cottonwood trees and survey lines. The two cottonwood trees of primary interest (where the electrical resistivity surveys were done) are centered at grid positions (7S, 7E) and (6S, 9E). The processing steps applied to the data are described in Chapter 2.

Data interpretation

The data were migrated to refocus the hyperbolas generated by subsurface anomalies into point features to help us identify possible roots. Figure 112 shows examples of a non-migrated and migrated radargram, where the hyperbola in the non-migrated section has been reduced to a point in the migrated section. It is these “points” that will be connected in depth slices shown later to identify possible roots. Figure 113 shows a plan view of the GPR data collected parallel and perpendicular to the levee just beneath the ground surface (2.5-cm depth) and a radargram along line 3.7S. Depth of investigation is approximately 0.7 m (Figure 3c), based on a subsurface EM wave velocity of 0.095 m/ns. Figure 113b shows the location of roots

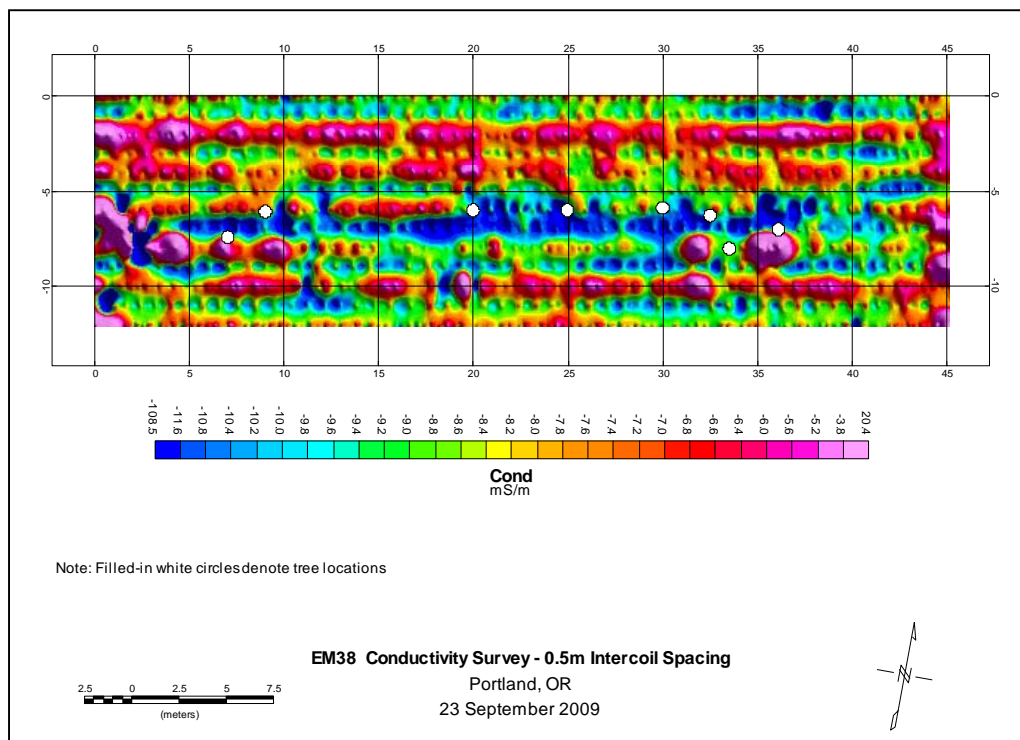


Figure 107. EM38-MK2 conductivity survey results, 0.5-m inter-coil separation, vertical dipole mode, Portland, OR.

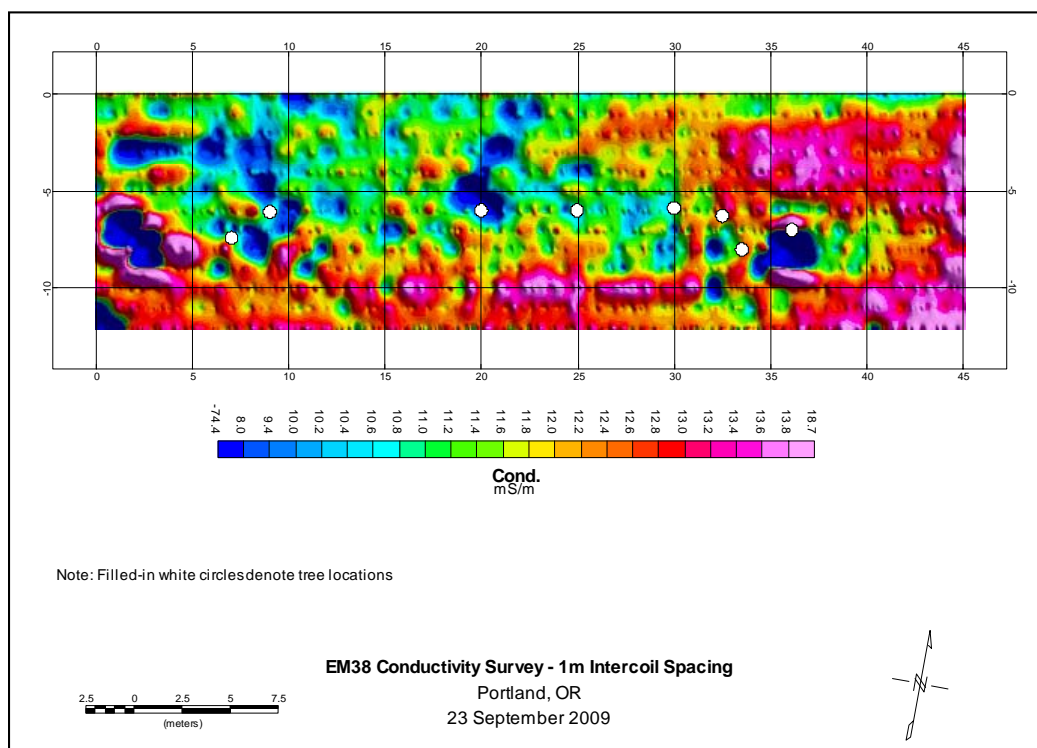


Figure 108. EM38-MK2 conductivity survey results, 1.0-m inter-coil separation, vertical dipole mode, Portland, OR.

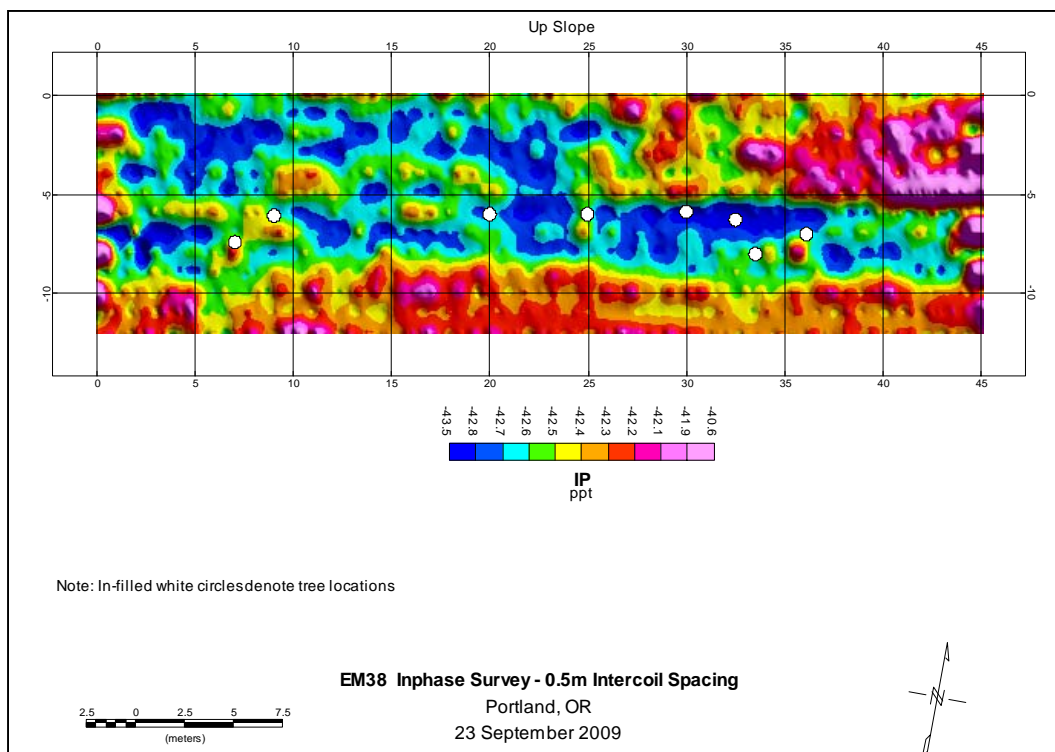


Figure 109. EM38-MK2 in-phase survey results, 0.5-m inter-coil separation, vertical dipole mode, Portland, OR.

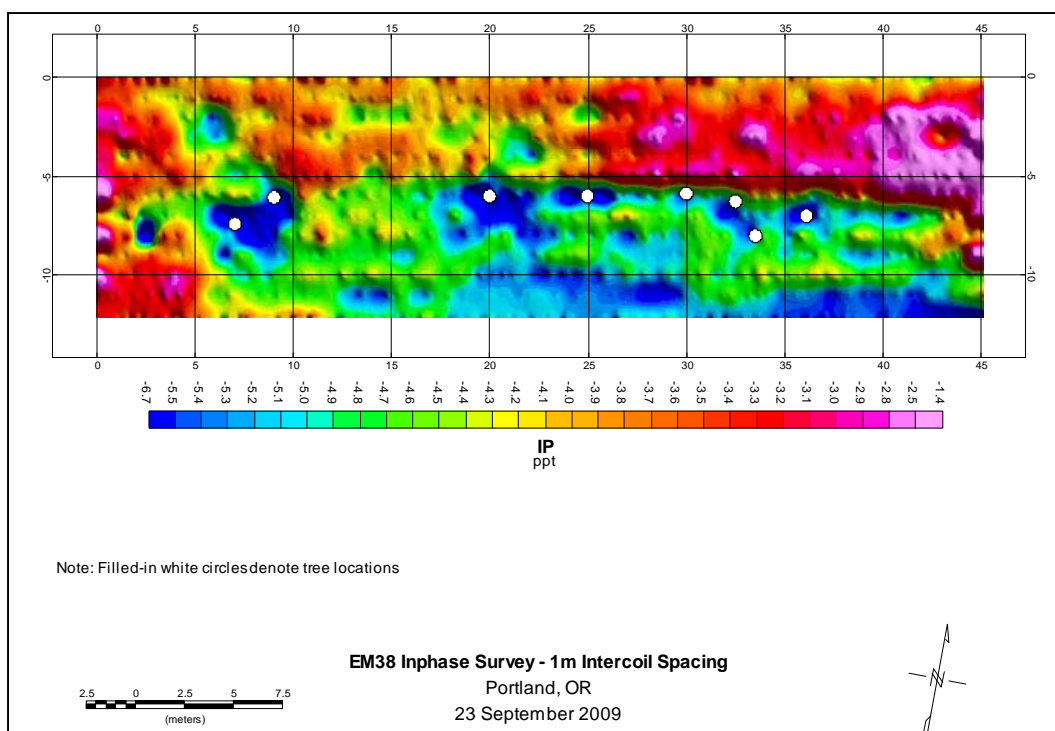


Figure 110. EM38-MK2 in-phase survey results, 1.0-m inter-coil separation, vertical dipole mode, Portland, OR.

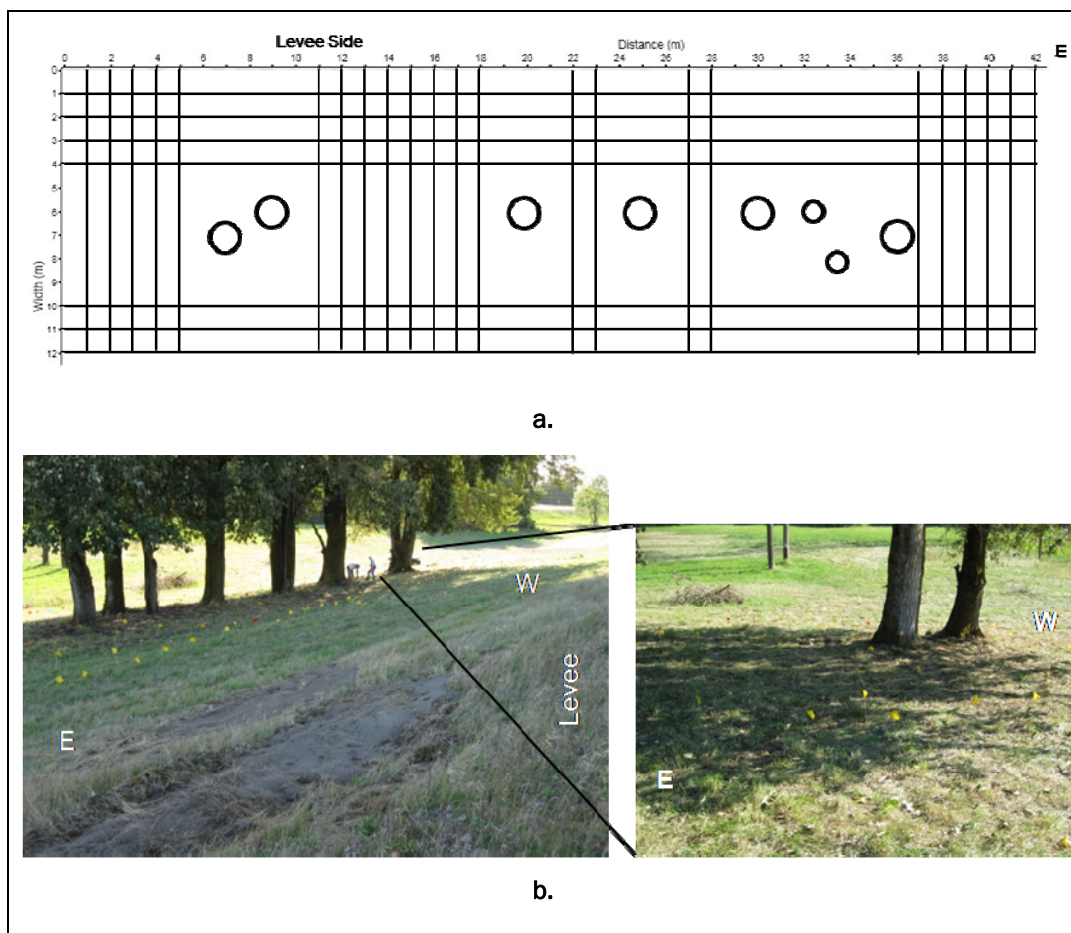


Figure 111. Survey grid (a) and photographs (b) of the stand of cottonwood trees within the survey grid and the two trees of primary interest on Portland levee in Portland, OR. The circles represent the cottonwood trees.

interpreted at this depth. It is likely that others are present. Numerous hyperbolic reflections caused by buried features are present in the shallow depth section shown in Figure 3c. Many of these features “ring” down through the depth profile. For example, the tree roots visible on the ground surface between 19–22E give a strong reflection response at this depth and deeper. It is important to be aware of these ringing effects to avoid misinterpreting them as actual anomalies in deeper sections. Ringing effects can mask weaker anomalies that may be of interest.

The GPR plan view sections (from data collected parallel to the levee) given in Figure 114 are interpreted depth sections with possible root locations. Without ground truth, it is difficult to say if the interpreted anomalies are actual roots. Figure 115 is an overlay of all of the interpreted roots determined from the survey lines parallel to the levee. The interpreted segments tend to be short and some appear to form longer root segments.

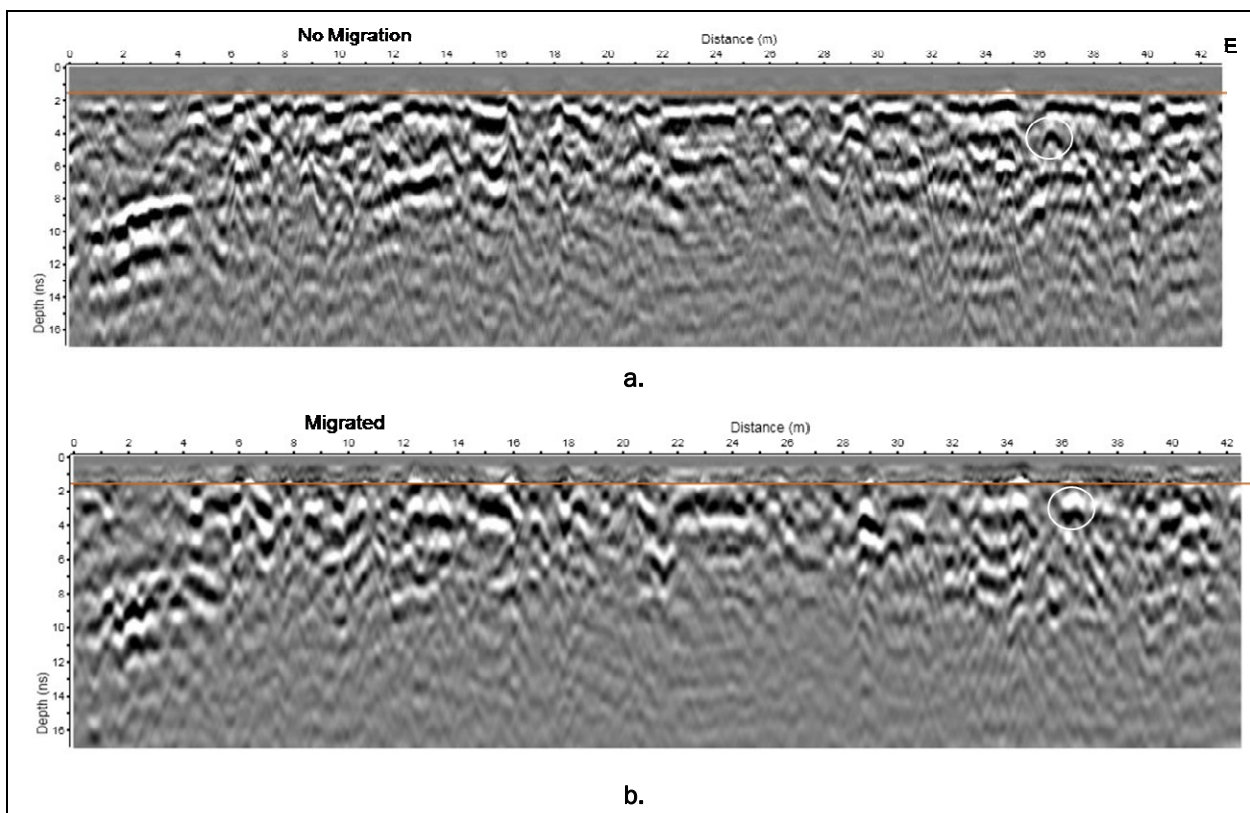


Figure 112. Comparison of non-migrated (a) and migrated (b) depth sections at $y = 9.458$ m. S. Circles show hyperbola that has been refocused to a point in the migrated section.

Figures 116 and 117 are plan view sections for GPR data acquired perpendicular to the levee and the interpreted root locations, respectively. These data fill in the areas not covered by the survey lines acquired parallel to the levee. The interpreted root segments from the parallel and perpendicular GPR surveys are merged in Figure 118. No roots were identified in the data below a depth of 0.5 m. It is likely that there are other tree roots detected by the GPR system that have not been identified. Likewise, it is possible that some of the anomalies identified as tree roots are not roots. The tree roots on the ground surface did provide some knowledge of reflection characteristics; however, without ground truth, it is difficult to state with a high degree of confidence that the anomalies identified as roots are actually roots.

Summary of GPR surveys

GPR data were collected around a line of cottonwood trees to image the larger subsurface roots. Tree roots were visible at the ground surface and the reflection characteristics of these roots aided in mapping possible subsurface roots. Tree root segments were interpreted from the shallow

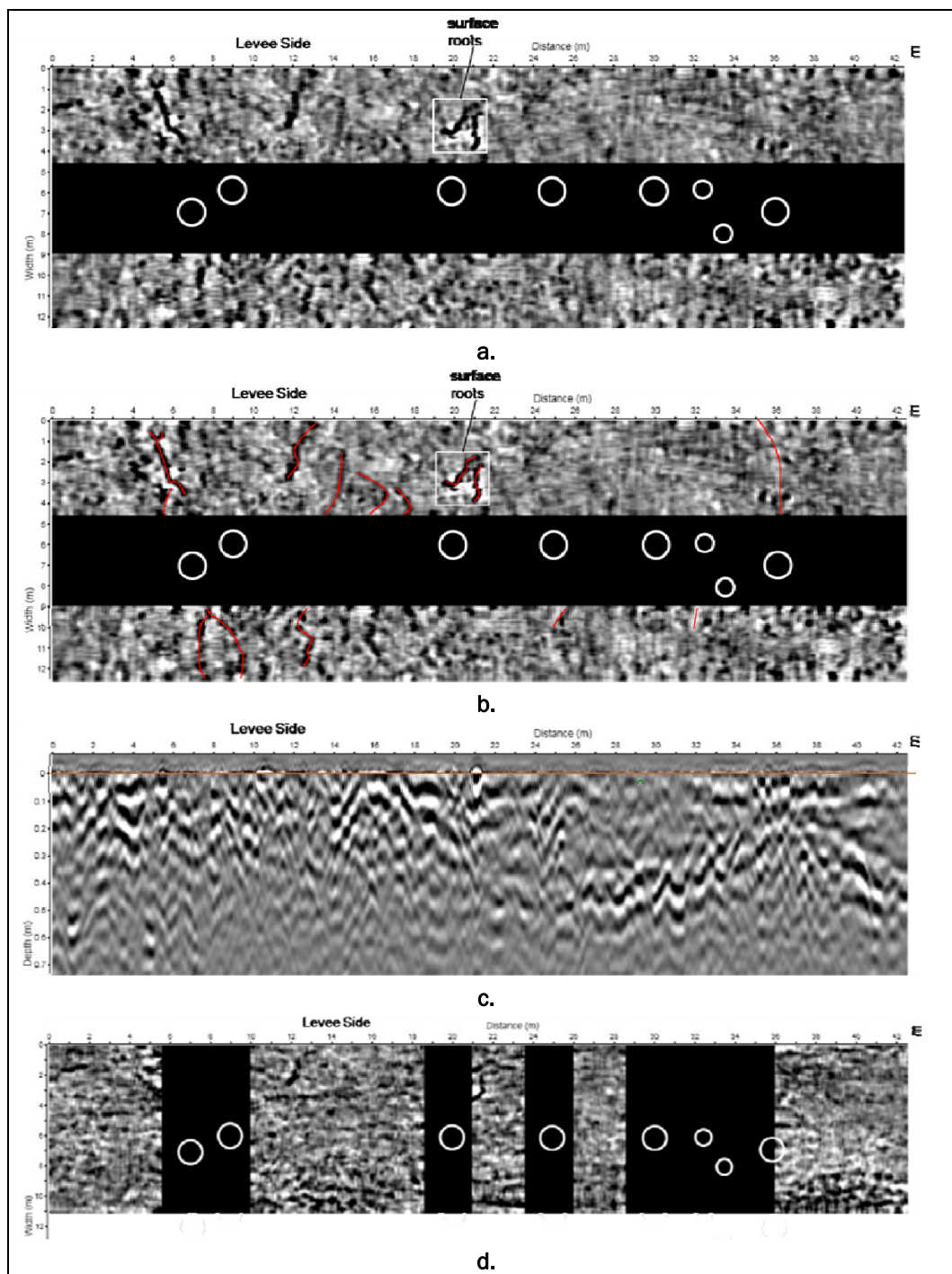


Figure 113. GPR data collected parallel (a-c) and perpendicular (d) to the levee. The white circles mark the tree locations. (a) Plan view of parallel radar section at 2.5-cm depth (2.075 ns). The corresponding time of 2.075 ns is a two-way travel time. To obtain the correct depth, divide the two-way time by 2 and multiply by the EM wave velocity ($0.219 \text{ ns} \div 2 \times 0.095 \text{ m/ns}$). (b) Depth profile along line 3.7S. (c) Same as (a) but with interpreted location of shallow roots (red lines). (d) Plan view of perpendicular radar section at 2.6-cm depth (2.197 ns).

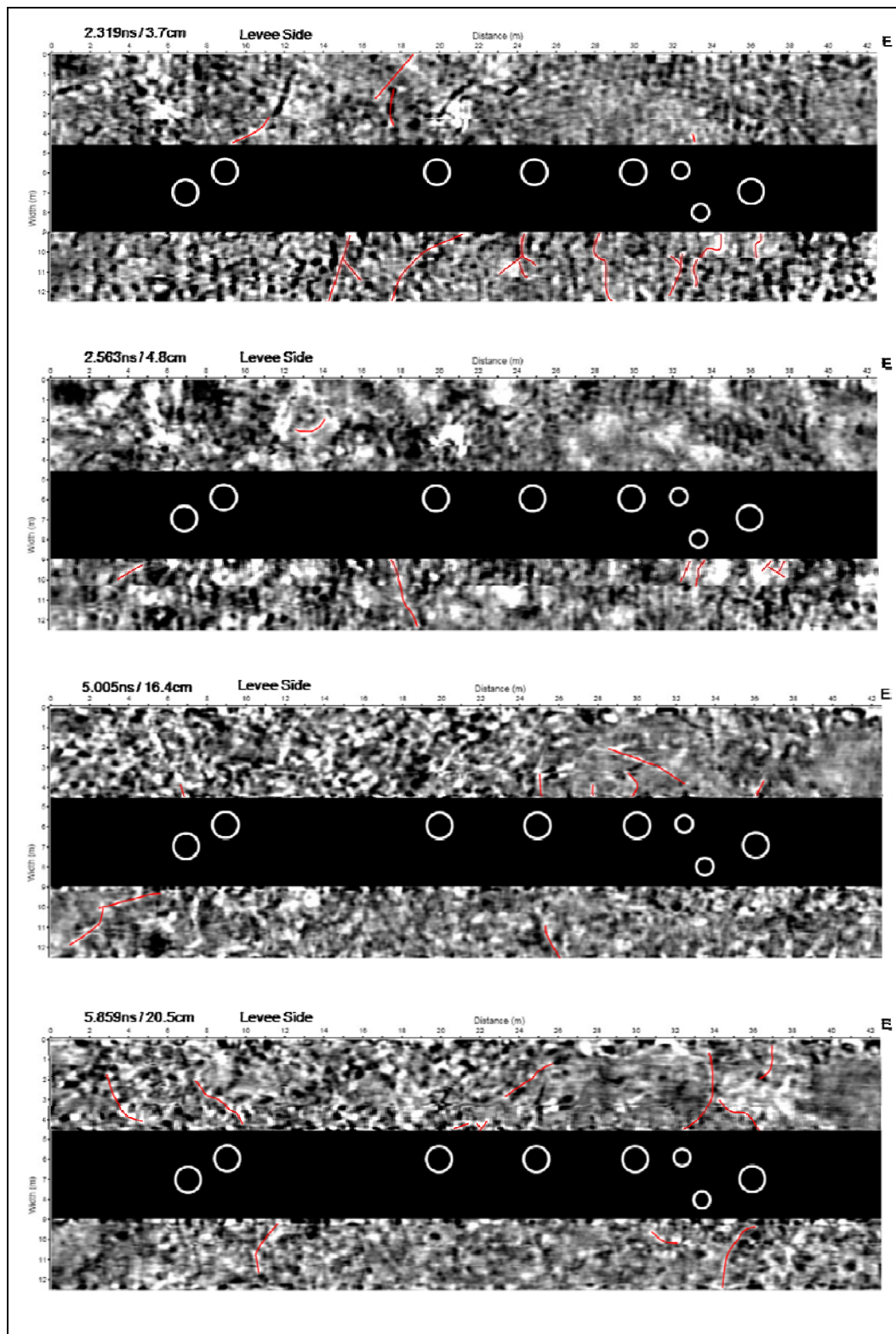


Figure 114. Depth slices from data collected parallel to the levee showing interpreted location of possible tree roots. The white circles mark the tree locations; red lines are possible roots.

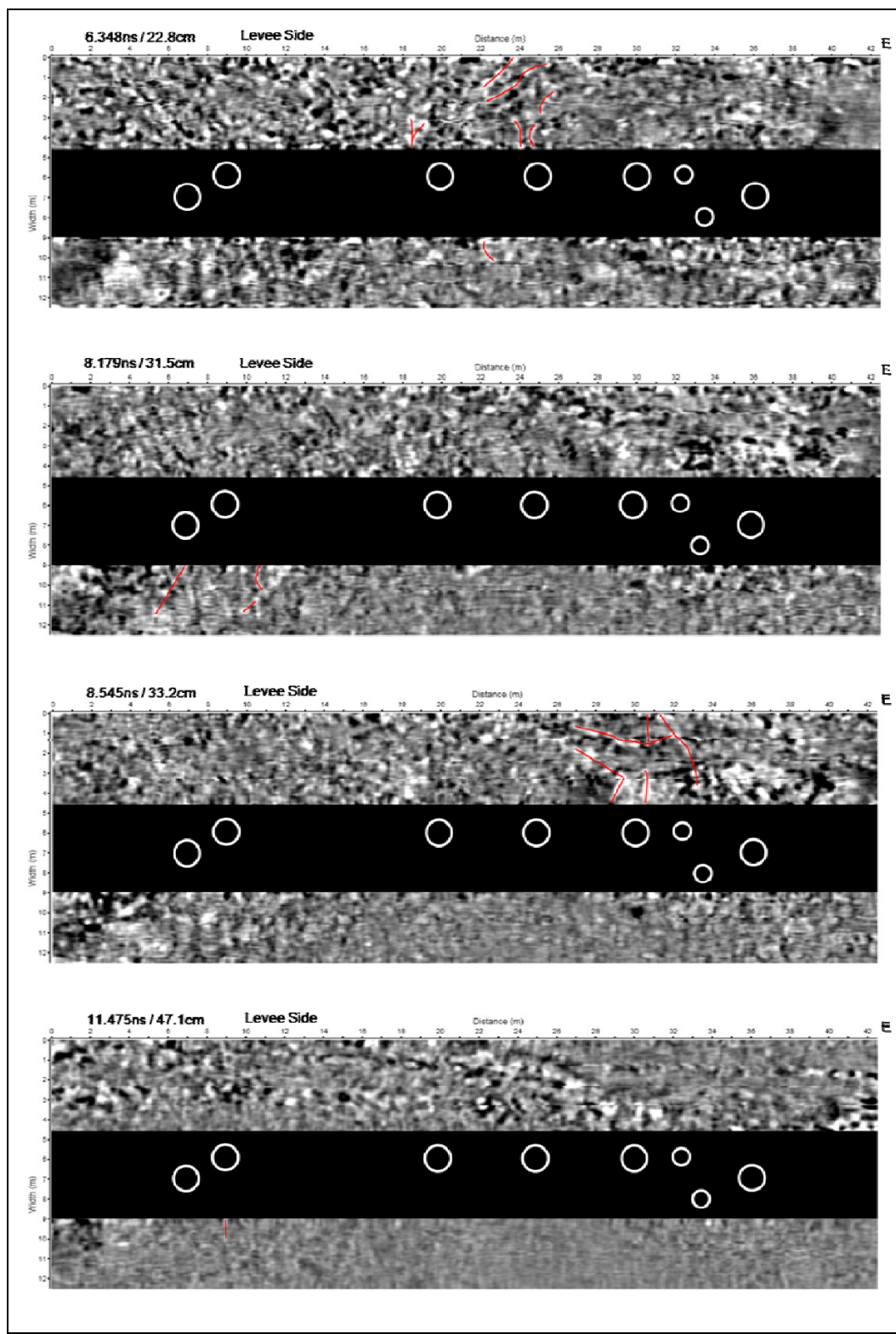


Figure 114. Concluded.

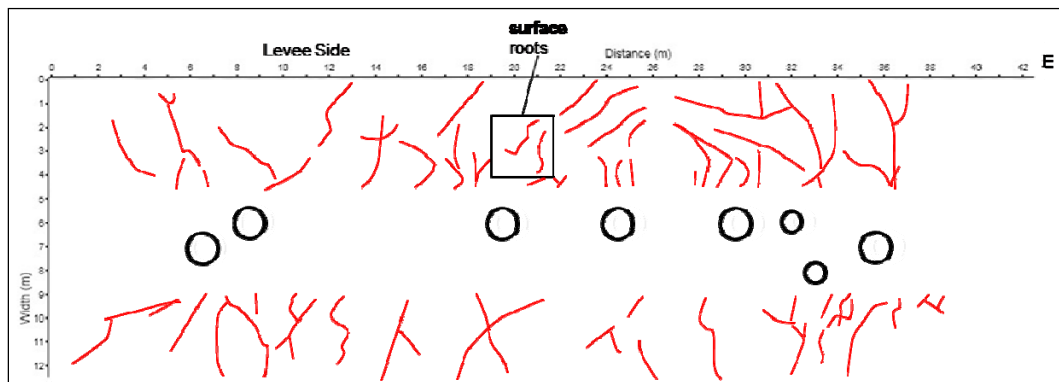


Figure 115. Location of possible tree roots interpreted from GPR data (parallel to the levee) collected around cottonwood trees on the Portland Levee, Portland, OR. The black circles mark the tree locations; red lines are possible roots.

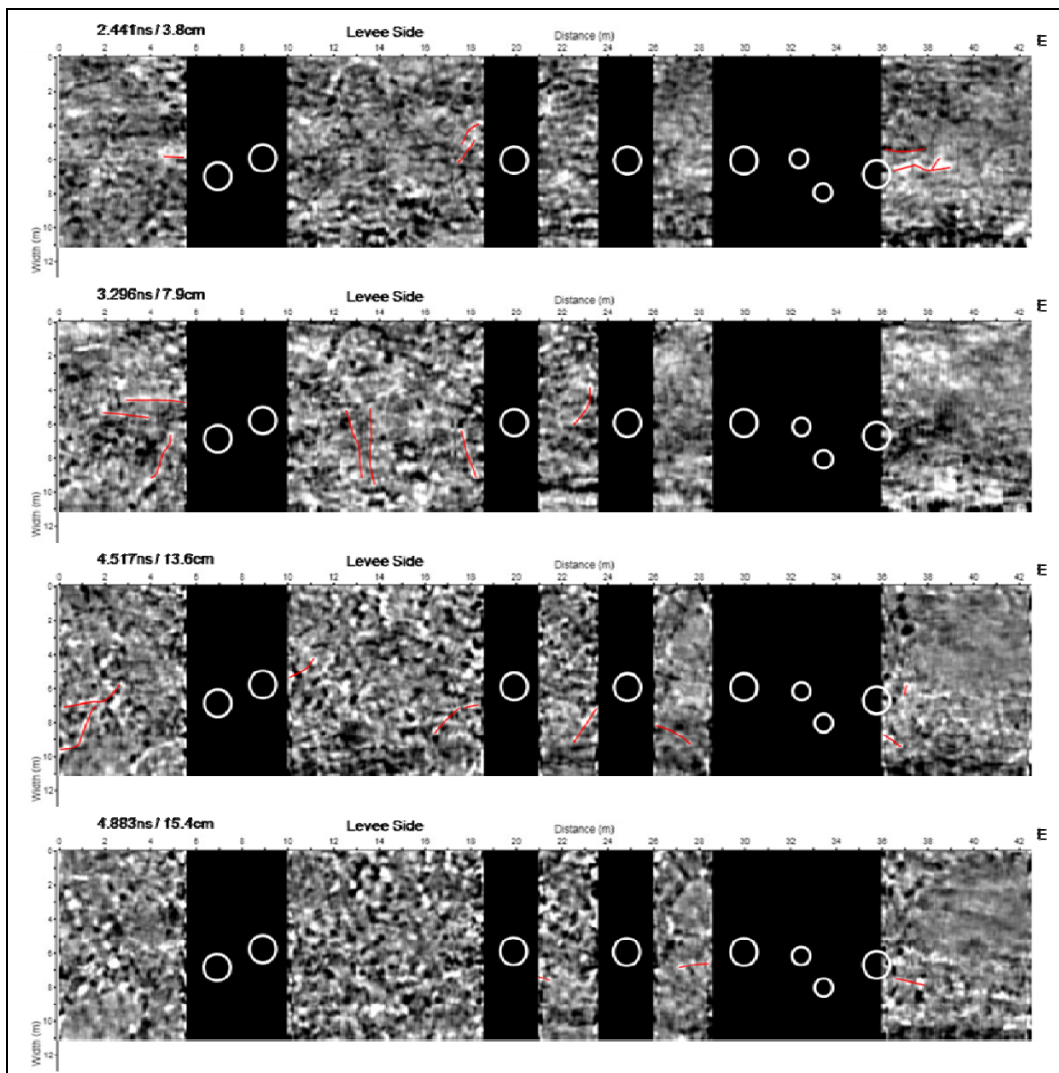


Figure 116. Depth slices from data collected perpendicular to the levee showing interpreted location of possible tree roots on the Portland Levee, Portland, OR. The white circles mark the tree locations; red lines are possible roots.

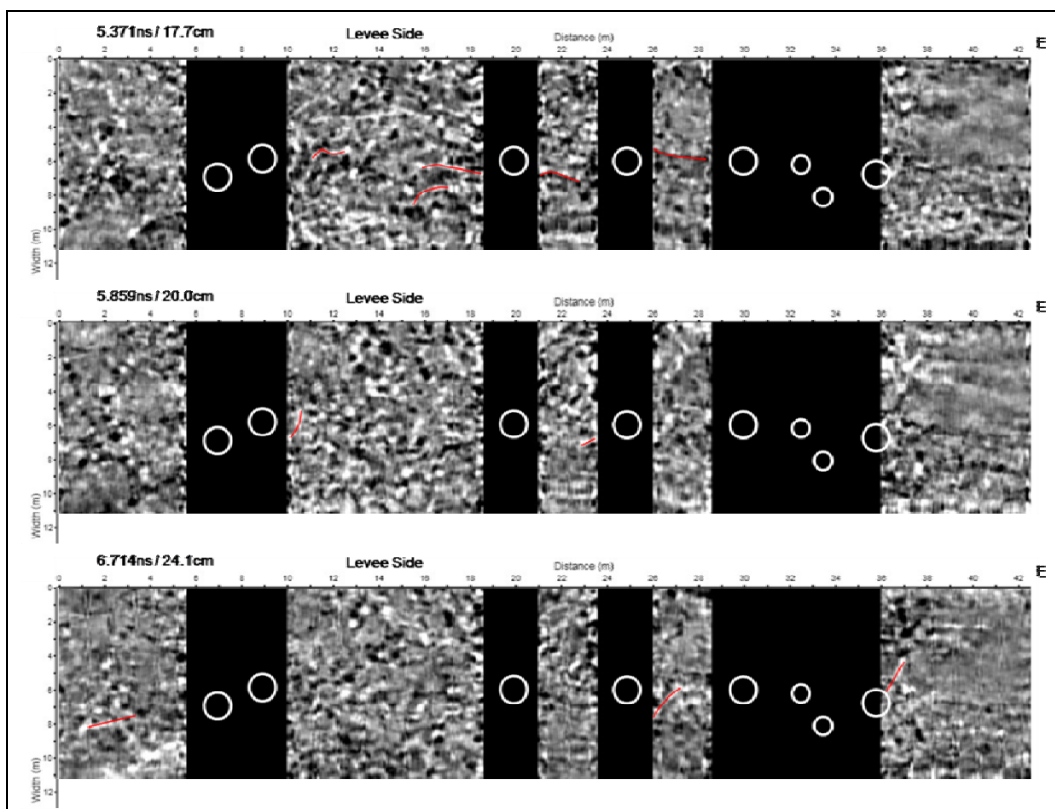


Figure 116. Concluded.

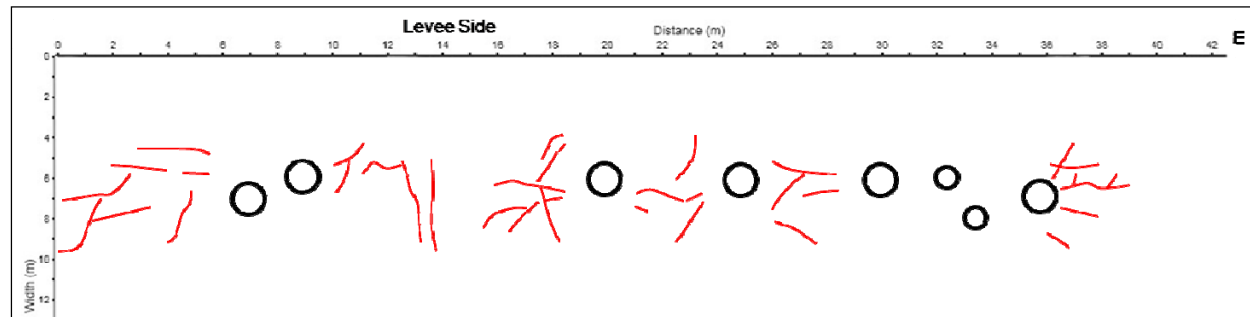


Figure 117. Location of possible tree roots interpreted from GPR data (perpendicular to the levee) collected around cottonwood trees on the Portland Levee, Portland, OR. The black circles mark the tree locations; red lines are possible roots.

surface to a depth of approximately 0.5 m. The GPR survey extended 6 m north and south of the line of cottonwood trees, and possible roots were detected at this distance. It is probable that anomalies present in the data were not identified as tree roots and vice versa; anomalies identified as tree roots are not roots. Without ground-truthing, it is difficult to state with confidence that the mapped anomalies are tree roots.

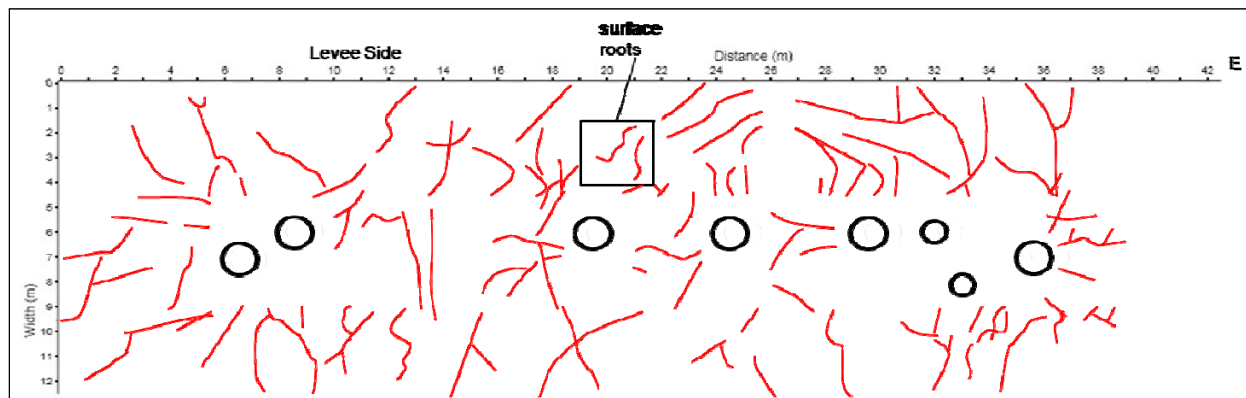


Figure 118. Location of possible tree roots interpreted from GPR data (parallel and perpendicular to the levee) collected around cottonwood trees on Portland levee, Portland, OR. The black circles mark the tree locations; red lines are possible roots.

Conclusions

ERI, EM, and GPR surveys were conducted along a stretch of the Columbia River levee to noninvasively map the tree root distribution of several cottonwood trees on the protected slope of the levee. The ERI results show an approximately 2-m thick overburden layer that is electrically highly resistive and that thins out and becomes discontinuous downslope. The overburden was interpreted as consisting of dry sandy soil because of its high resistivity values. Underlying the resistive overburden are lower resistivity soils presumed to consist of finer-grained soil with higher moisture contents. The ERI results indicate that the upper 2 m are heterogeneous. The EM data also exhibit highly variable conductivity readings across the site to a depth of approximately 1.5 m. No roots or root ball zones were interpreted from the results of the ERI or EM surveys.

GPR reflections, interpreted to be tree roots, were traced from just below the ground surface to an approximate depth of 0.5 m. The reflections were mapped approximately 6 m (limit of testing) in either direction of the line of cottonwood trees. The locations of the reflections will have to be inspected to verify that they are caused by buried tree roots.

Burlington, WA

Background

Three geophysical methods, ERI, EM induction, and GPR were used to determine the maximum detectable extent of the tree root distribution of a western red cedar (*Thuja plicata*) tree. It grows on the bank of the Skagit

River, Burlington, WA, located approximately 95 km north of Seattle, WA. The investigation was conducted by ERDC personnel during 25 through 28 September 2009.

The study site is located on a flat parcel of land between the Skagit River and the levee (Figure 119). An area measuring approximately 13 by 41 m was established around the tree in which to conduct the geophysical surveys. The investigated cedar tree has an approximate crown width of 12 m, an approximate height of 20 m and a trunk diameter of about 1.43 m at chest height (Figure 120).

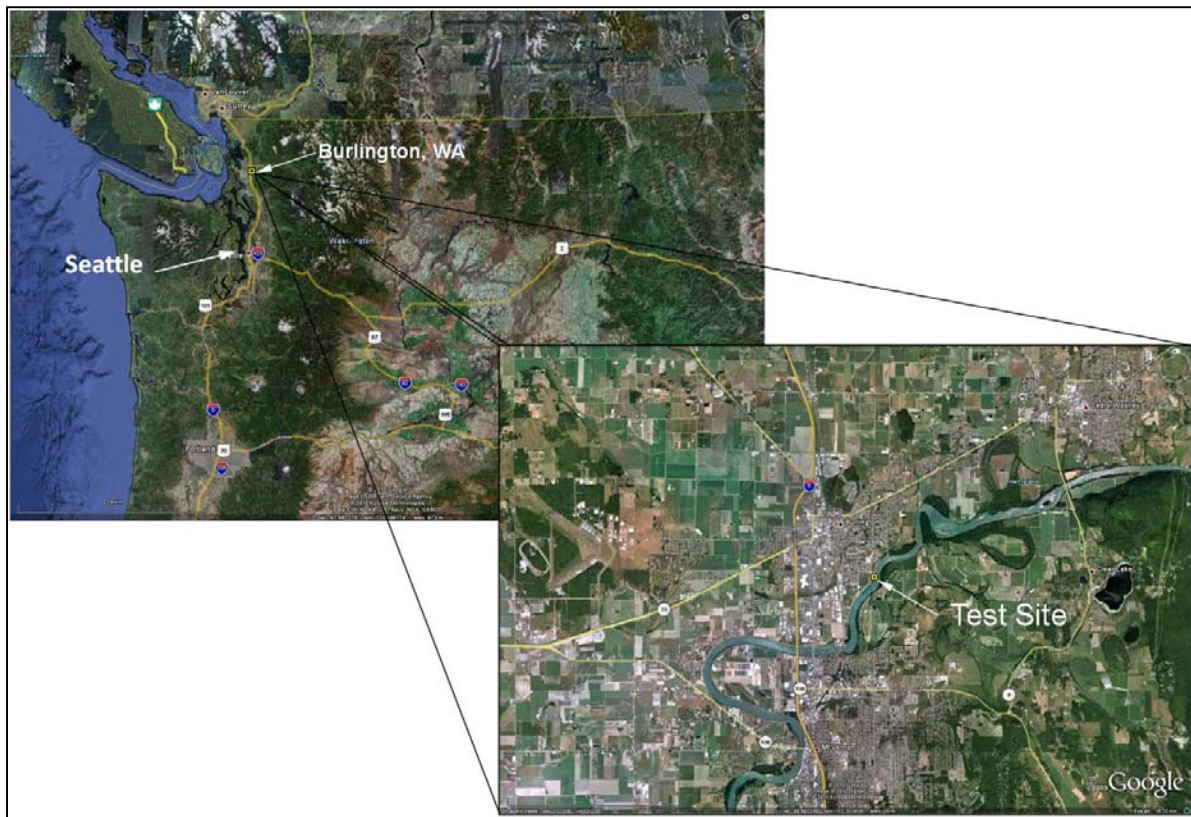


Figure 119. Burlington, WA.



Figure 120. View of the test site, looking north, showing the cedar tree and levee, Burlington, WA.

Geophysical survey methods

ERI survey

ERI data were acquired using 2-D and roll-along 3-D survey techniques as described earlier in this chapter. Data acquisition and processing techniques for the 2-D and 3-D methods are described in the following paragraphs. Data were collected using a SuperSting R8 resistivity meter with the Smart electrode switching system.

Line separation is 2 m and each line consists of 42 electrodes spaced 1.0 m apart. Figure 121 shows the cedar tree location relative to the 2-D ERI lines. The 2-D data were inverted using EarthImager 2-D.

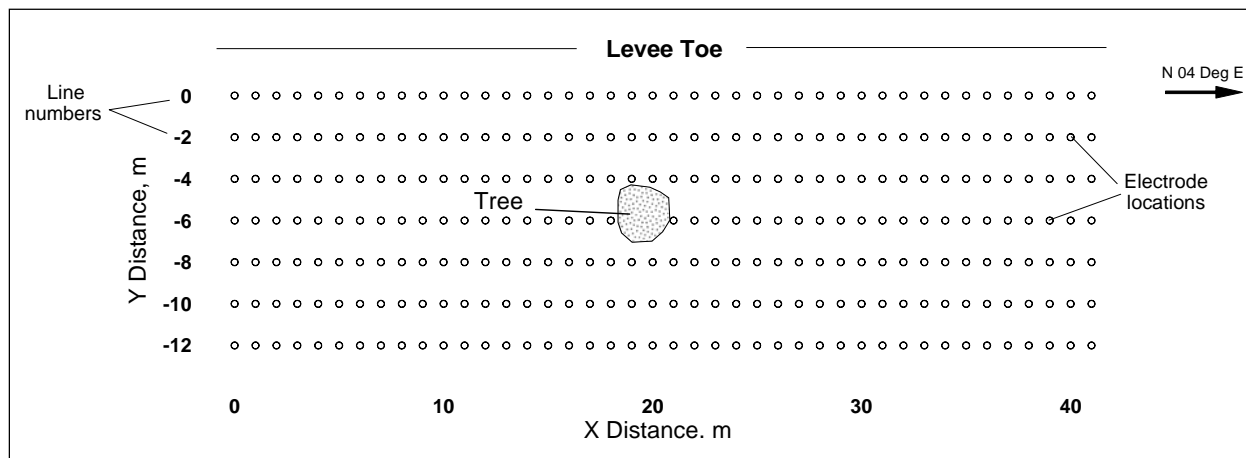


Figure 121. 2-D resistivity survey layout, Burlington, WA.

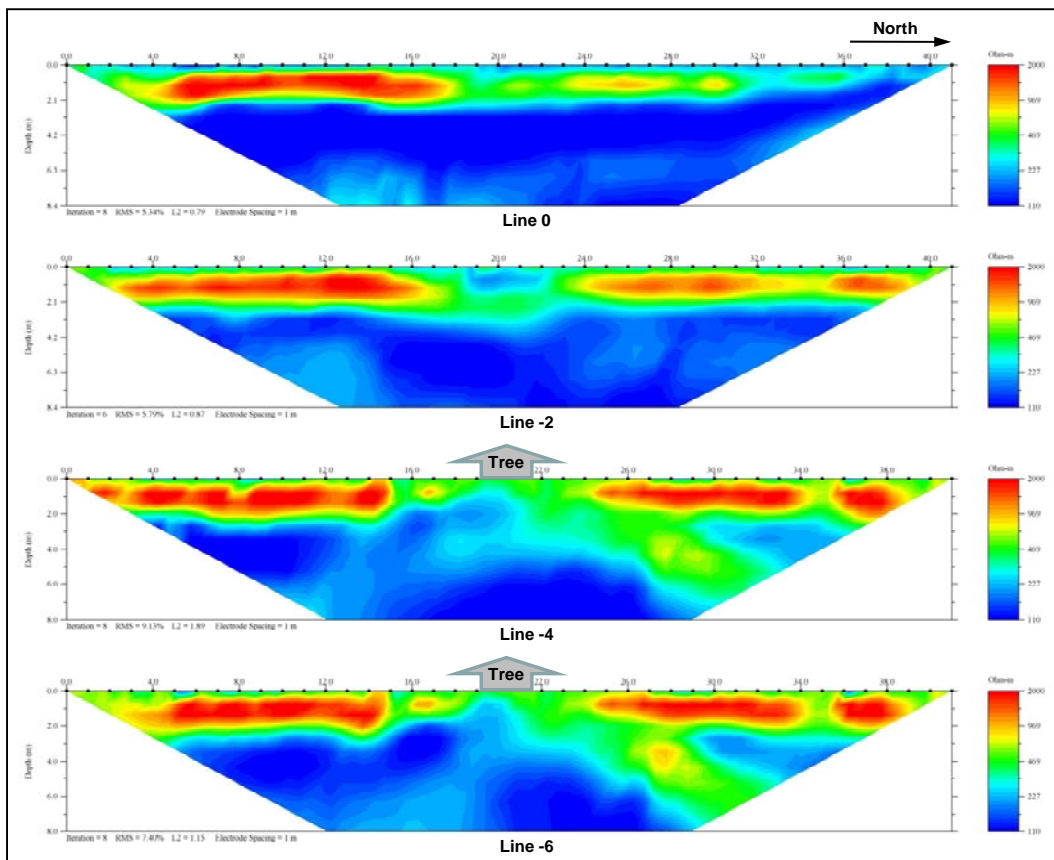


Figure 122. Inversion results for 2-D lines 0 through -6, Burlington, WA.

In this study the 2-D data were also processed using the quasi 3-D technique described in Chapter 2. The survey was designed with a 1.0-m electrode and 2-m line spacing, thus meeting the criteria for quasi 3-D processing. Seven 2-D survey lines, lines 0 through 12 were combined into a single 3-D data set and inverted using EarthImager 3-D.

Data interpretation: 2-D

The inverted resistivity sections for 2-D lines o through -6 are presented in Figure 122. Lines -8 through -12 are shown in Figure 123. For easy comparison, the same resistivity scale (110 to 2,000 $\Omega\text{-m}$) was used for all of the 2-D sections. Line o, the line located closest to the toe of the levee, consists of a high resistivity layer with a thickness of approximately 2 m overlying lower resistivity soil (Figure 122). As the lines progress east towards the location of the cedar tree, the high resistivity overburden material appears to separate in the vicinity of the tree and be replaced by

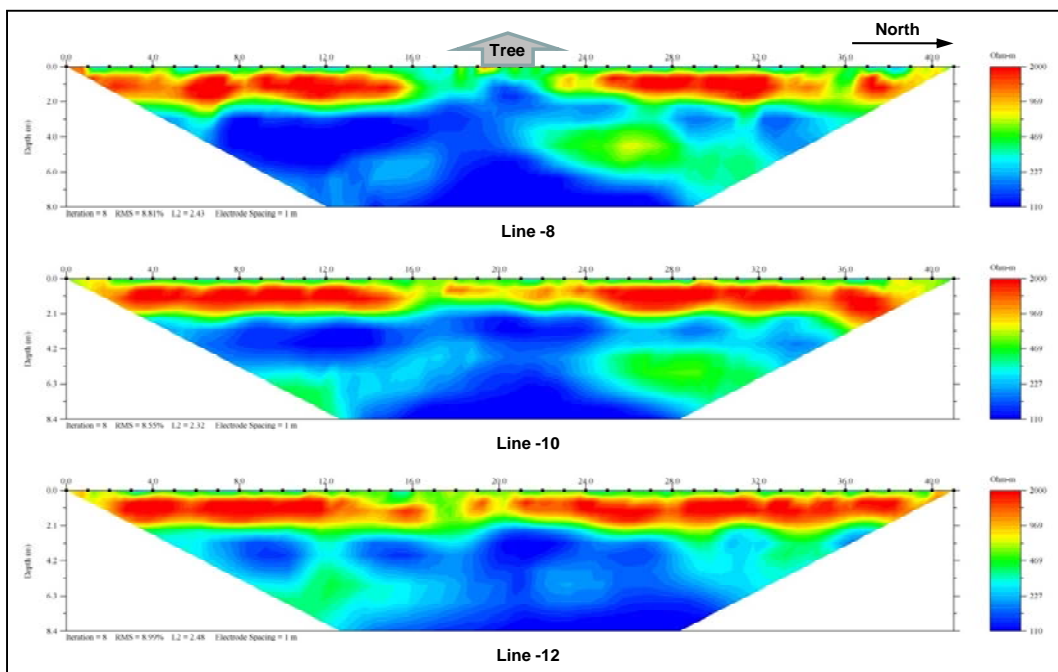


Figure 123. Inversion results for 2-D lines -8 through -12, Burlington, WA.

less resistive material. As the 2-D lines progress past the tree, the high resistivity overburden again becomes continuous along the entire line. The lower resistivity area extends approximately between lines o and -10 (eastwest direction) and the maximum north-south extent occurs between approximately 15 and 24 m along lines -2 and -6. The average diameter of the low resistivity zone centered on the tree is approximately 9.5 m.

Data interpretation: Quasi 3-D

Figure 124 is an inverted resistivity image of the combined 2-D lines. Figures C81 through C95, in Appendix C, are depth slices (slices perpendicular to the z-axis) taken every 0.5 m between depths of 0 and 7.0 m. The gray oval represents the tree location on the ground surface

and the violet oval shows the projected surface location of the tree on the depth slice surface. The black dots represent the electrode locations on the ground surface. Similar to the 3-D resistivity survey results, a highly resistive burden extends to a depth of between 2.00 and 2.50 m, where a lower resistivity layer is encountered. Also noted is a circular zone of relatively lower resistivity centered on the base of the tree that extends through the resistive overburden. The diameter of the low resistivity zone ranges between approximately 8 and 10 m.

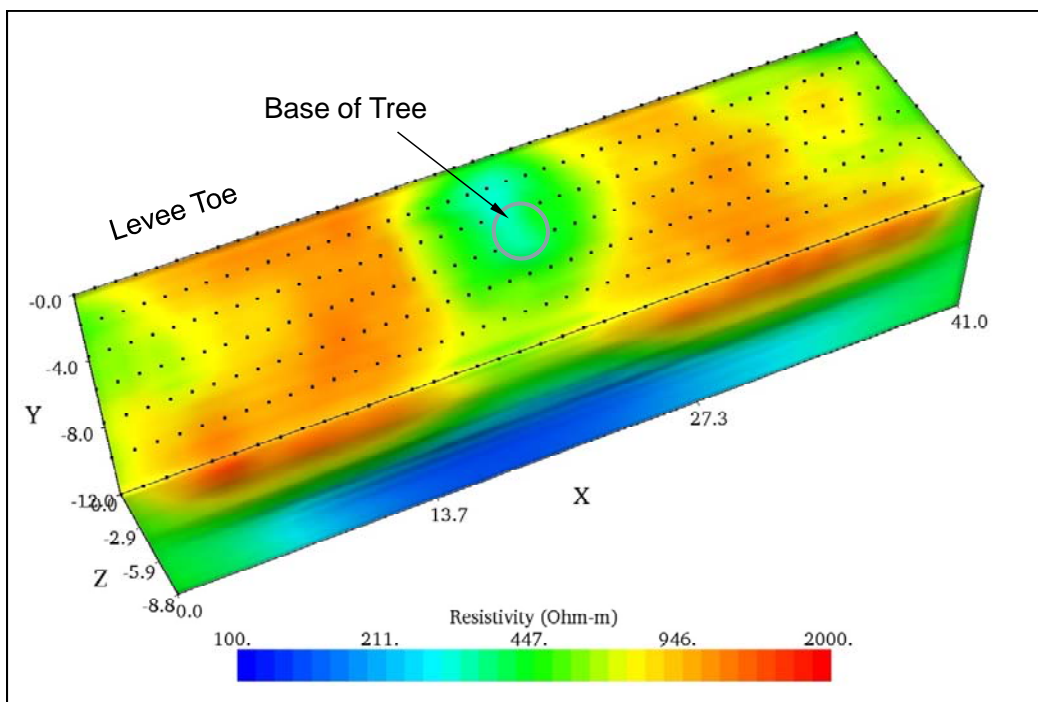


Figure 124. Quasi 3-D inverted resistivity image, Burlington, WA.

Figures C96 through C120, in Appendix C, are vertical slices taken along the x -axis (perpendicular to the y -axis) at 0.50-m intervals. The light blue oval represents the location of the tree on the ground surface. The figures show a high resistivity layer approximately 2 m thick overlying a soil with much lower resistivity values. As the slices progress from $Y = 0.00$ to $Y = -12.00$ m, the high resistivity overburden becomes discontinuous in the vicinity of the cedar tree and is replaced with soil with much lower resistivity.

3-D data acquisition and processing

A 3-D ERI grid measuring 11 by 13 m was established around the study tree (Figure 125). The rectangular grid consists of electrodes positioned 1 m apart. Stainless steel rods, approximately 1 cm in diameter, were

driven vertically into the ground to a depth of about 0.3 m and used as electrodes. A roll-along survey method was used to collect the 3-D ERI data as described in Chapter 2. Figure 125 shows the location of the 3-D survey relative to the locations of the 2-D ERI lines. In this survey, the 3-D grid was leap-frogged in a northerly direction. The 3-D data were initially collected from electrodes along E-W trending lines $X = 15$ through $X = 22$ m. At the end of the initial survey, cables along lines $X = 15$ through $X = 18$ were disconnected from the electrodes and rolled-along to the front of the grid. The four rolled-along cables from lines were then connected to electrodes along lines $X = 23$ through $X = 26$ m, allowing collection of ERI data from lines $X = 19$ through $X = 26$ m, the last section of the survey. The 3-D resistivity data were inverted using EarthImager 3-D software.

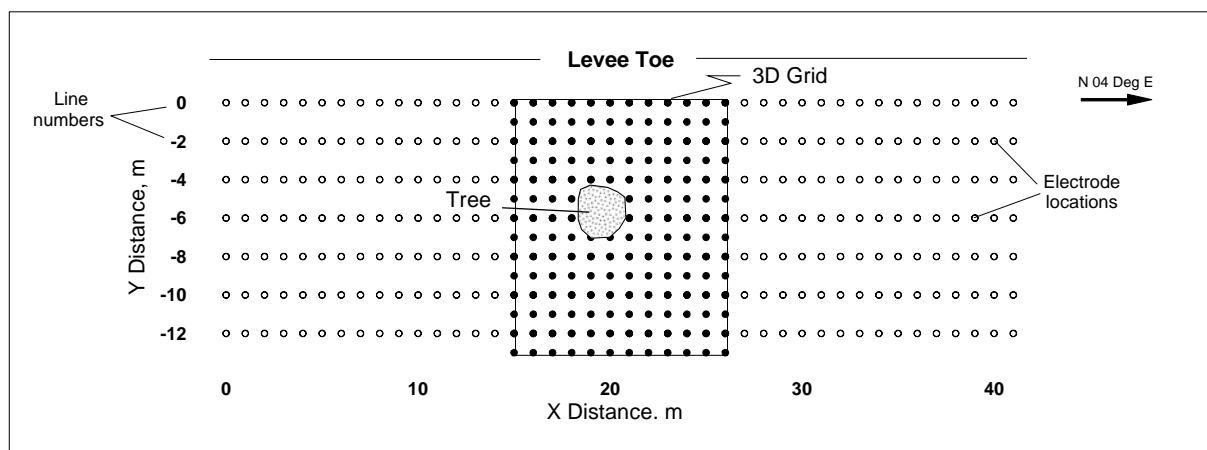


Figure 125. Three-dimensional resistivity survey layout, Burlington, WA.

Data interpretation

An inverted resistivity image of the 3-D grid is shown in Figure 126. The white oval in the center of the grid shows the tree's approximate position. The dots on the figure represent the electrode locations, which are spaced 1 m apart. The maximum depth of investigation is approximately 3.25 m.

Figures C121 through C127, in Appendix C, show depth slices of the inverted resistivity image taken at approximate 0.50-m depth intervals between depths of 0 and 3.00 m. The white oval represents the approximate location of the tree shown on the ground surface of the 3-D resistivity inversion image and the gray oval is the projected surface location of the tree on the depth slice surface. The dots on the figures represent the electrode locations which are spaced 1 m apart.

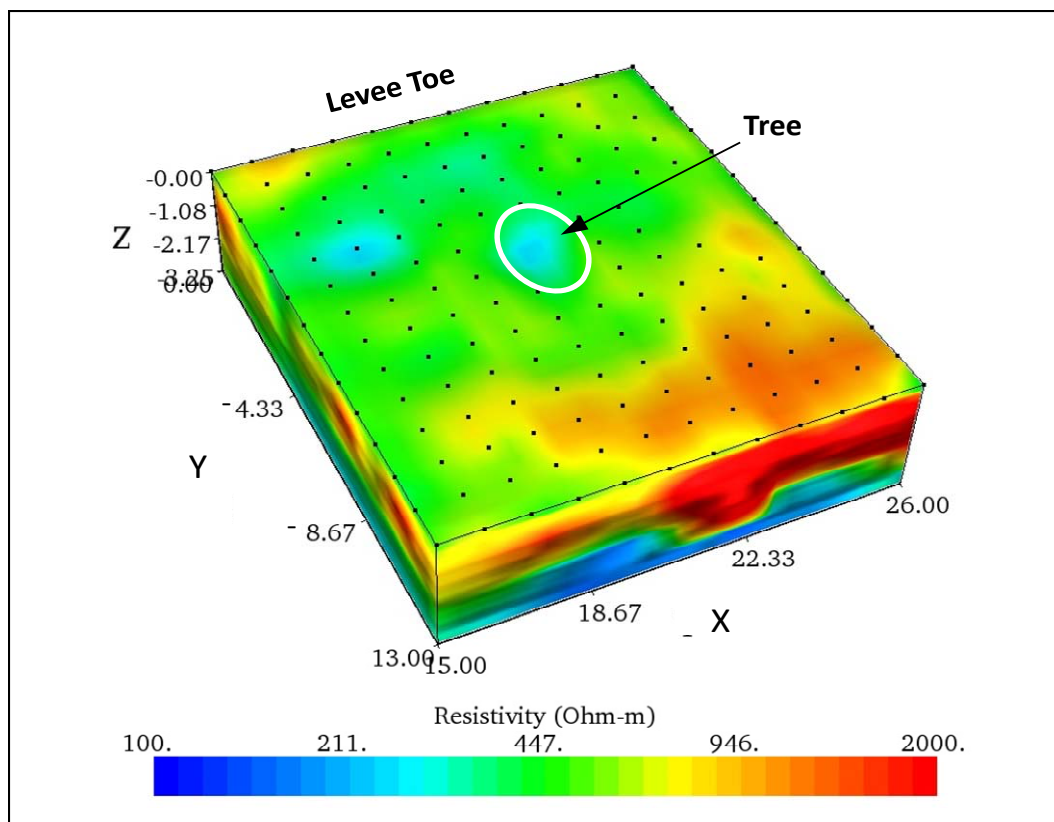


Figure 126. Three-dimensional Inverted resistivity image, Burlington, WA.

A prominent, roughly circular, relatively low resistivity zone, centered on the cedar tree, is evident between depths of 0.50 and 1.50 m. This low resistivity “window” penetrates the entire 2.00-m-thick resistive overburden. The soil resistivity decreases in value below a depth of 2.00 m, possibly because of an increase in fine-grained soil or an increase in soil moisture.

Figures C128 through C154, in Appendix C, show slices of the inverted resistivity image taken at 0.50-m intervals perpendicular to the y -axis. The white oval represents the location of the tree on the ground surface. The figures show a high resistivity layer approximately 2 m thick overlying a soil with much lower resistivity values. As the slices progress from $Y = 0.00$ to $Y = -13.00$ m, the high resistivity overburden becomes discontinuous in the vicinity of the cedar tree and is replaced with soil having a much lower resistivity.

EM survey

Data acquisition and processing

An EM survey grid measuring 40 by 13 m was established around the study tree (Figure 127). A Geonics Ltd. EM38-MK2 conductivity meter was used with Tx-Rx coils set at fixed distances of 0.5 and 1.0 m and operated in the vertical dipole mode. Data were collected along N-S oriented lines. The EM data were contoured and maps of conductivity and in-phase values for the 0.5-m and 1.0-m inter-coil separations plotted.

Data interpretation

Figures 128 and 129 present the conductivity survey results for the 0.5- and 1.0-m inter-coil spacings, respectively. Note that it was difficult to calibrate the EM38 at this site because of the extremely low conductivity values and, consequently, unrealistic negative conductivity values are presented. Comparing Figures 128 and 129, it is evident that, in general, the conductivity values of the 1.0-m inter-coil spacing are significantly higher than those for the 0.5-m inter-coil spacing. This indicates that the soil's electrical conductivity increases with depth, which is consistent with the ERI survey results. The increasing conductivity is most likely caused by an increase in clay or moisture with depth. The two conductivity plots show an area approximately 8 to 10 m in diameter with anomalously high conductivity values centered on the tree.

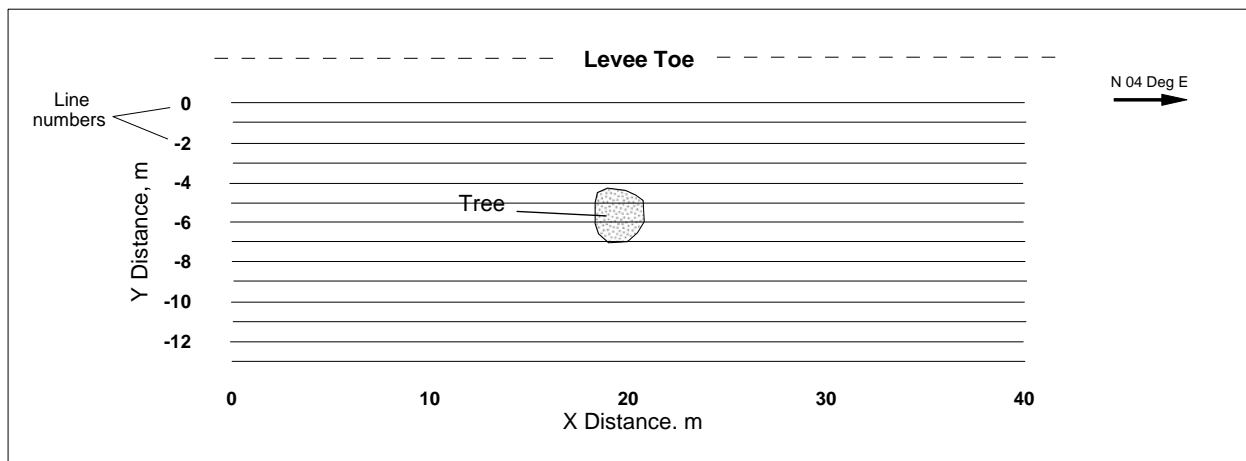


Figure 127. EM survey layout, Burlington, WA.

Figures 130 and 131 present the in-phase survey results for the EM38 0.5- and 1.0-m inter-coil spacings, respectively. No correlation between in-phase values and the root zone location are apparent.

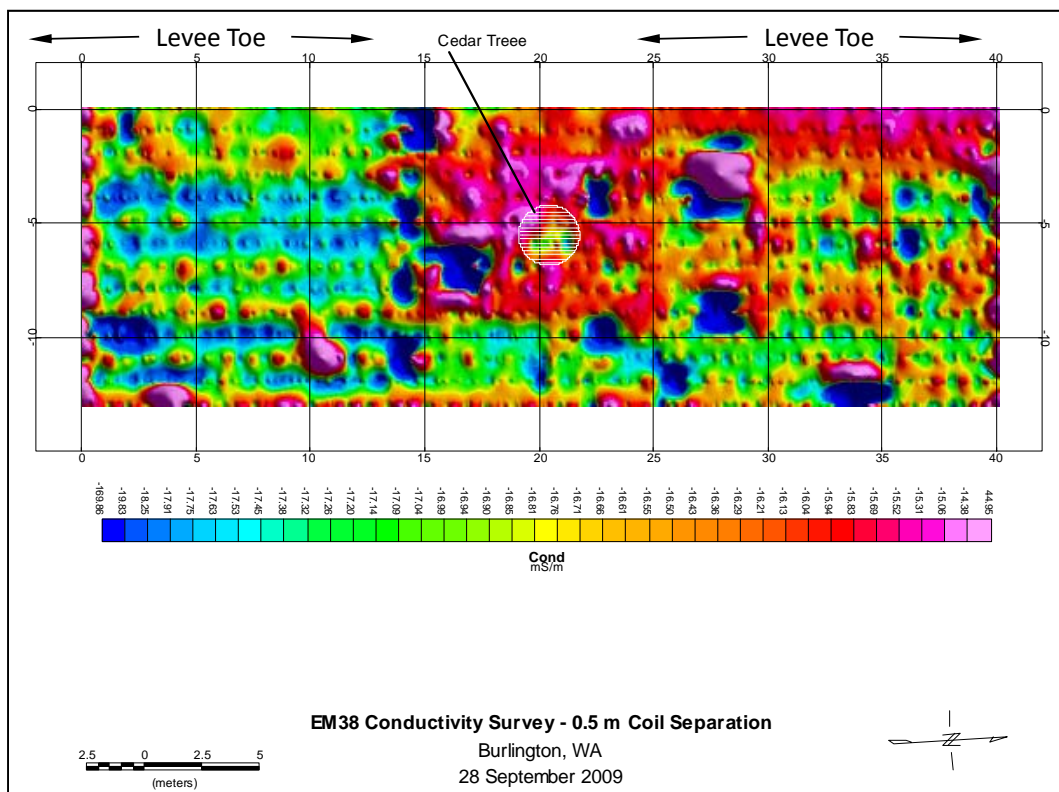


Figure 128. EM38 conductivity survey, 0.5-m inter-coil separation, Burlington, WA.

Summary of ERI and EM Results

ERI and EM methods were used to determine the maximum detectable horizontal extent of the root zone of a cedar tree located on the protected toe of the levee. Table 33 summarizes the results for the 2-D, 3-D, and quasi 3-D inversion methods as well as EM38 survey results. The geophysical results indicate a lateral, roughly circular, anomalous area of lower resistivity centered on the tree. The anomalous area is presumed to indicate the extent of the tree's measureable root zone. It is also possible that the anomalous zone is better suited to the growth of the cedar tree and that its tree roots may only occupy a part of the anomaly.

GPR

Data acquisition and processing

The GPR data were acquired along survey lines both parallel and perpendicular to the levee crest. The survey lines were centered on meter markers and spaced 1 m apart. Of the 31 antennae available in the array, only 29 (2 through 30) were used; the two end antenna (1 and 31) were not used because they tend to be noisy. The antennae in the array are spaced

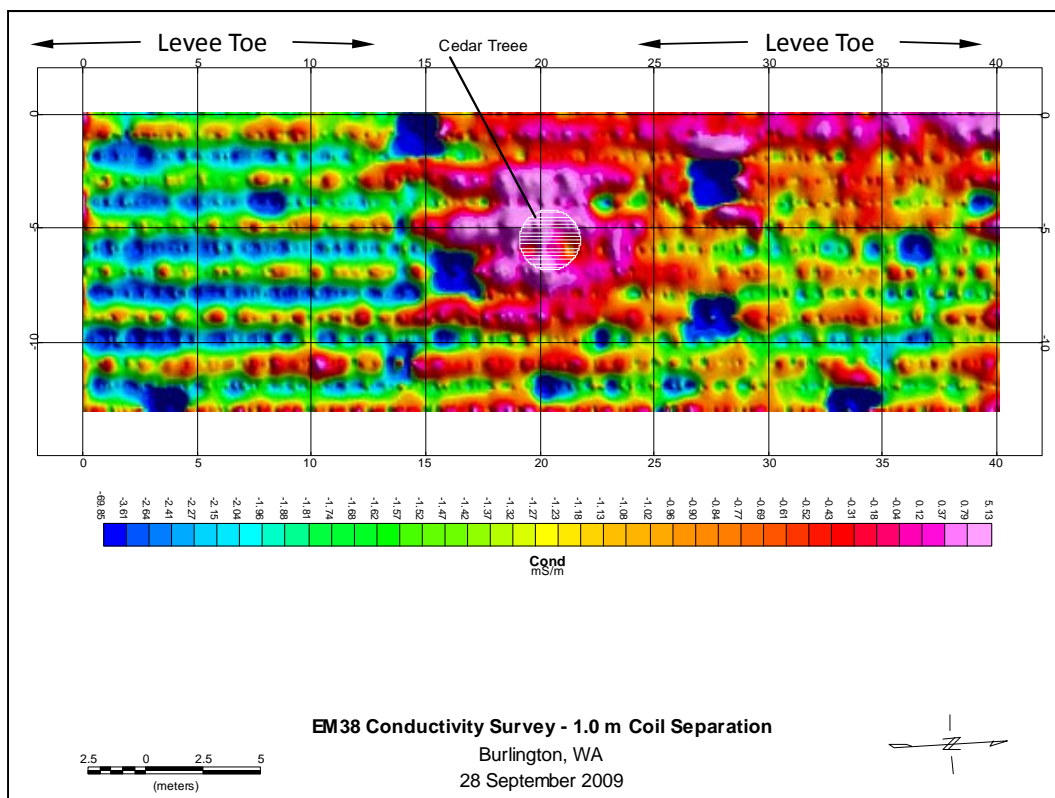


Figure 129. EM38 conductivity survey, 1.0-m inter-coil separation, Burlington, WA.

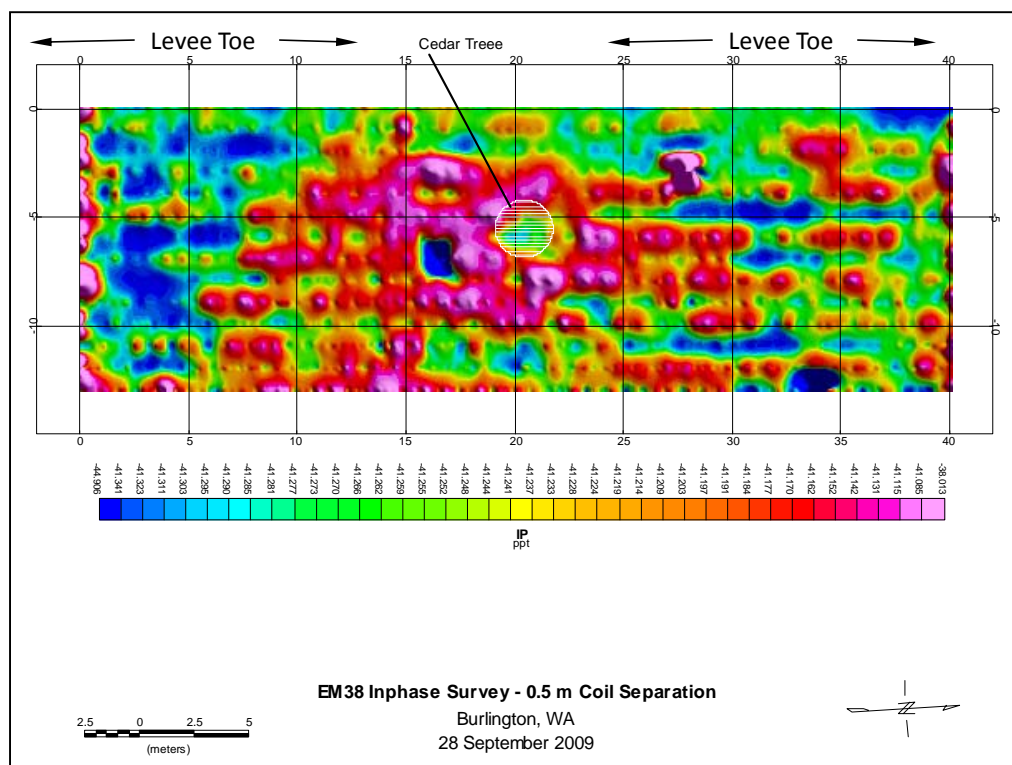


Figure 130. EM38 in-phase survey, 0.5-m inter-coil separation, Burlington, WA.

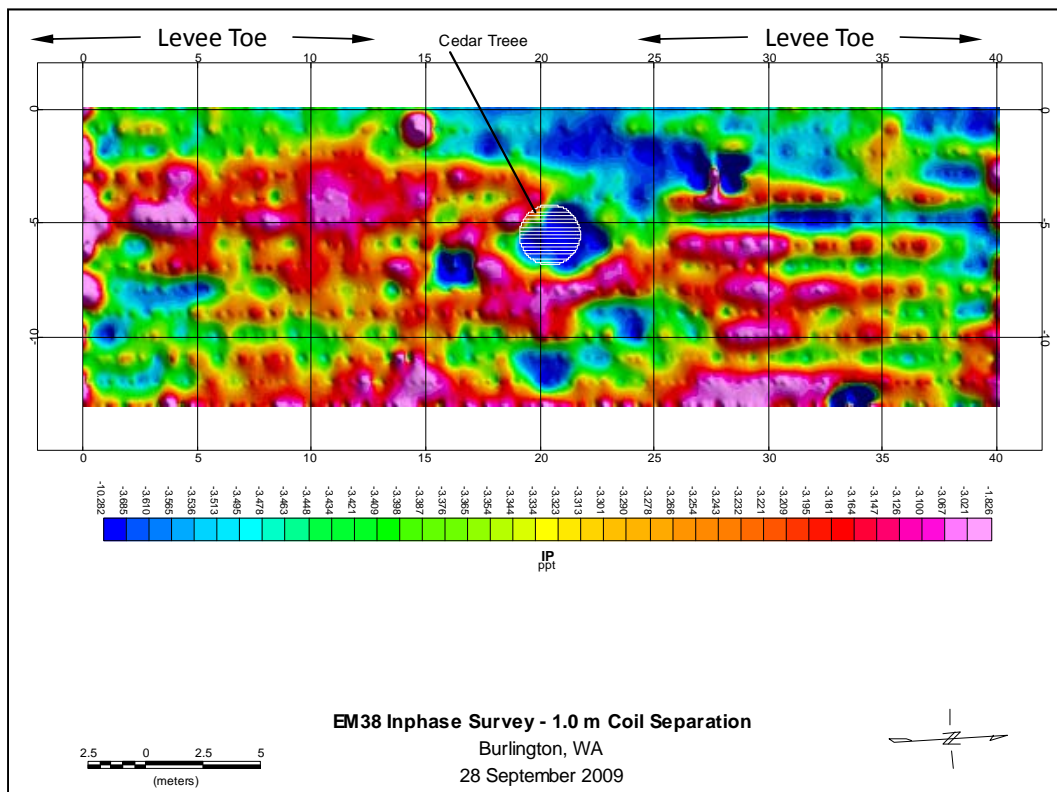


Figure 131. EM38 in-phase survey, 1.0-m inter-coil separation, Burlington, WA.

Table 33. Maximum detectable lateral influence of tree root zone based on ERI and EM methods, Burlington, WA.

Geophysical Method	Maximum Detectable Anomaly Diameter in N-S Direction (parallel to levee toe), m	Maximum Detectable Anomaly Diameter in E-W Direction (perpendicular to levee toe), m
ERI 2-D Inversion	9	8
ERI 3-D Inversion	10	10
ERI Quasi-3-D Inversion	10	12
EM38	10	10

0.055 m. For 29 operational antennae, this gives a single swath width of 1.54 m. There is a 0.5-m overlap between survey lines when using a 1-m survey line spacing. Eight lines (1E-3E, 8E-12E) parallel to the levee crest were surveyed; sixteen lines (10N-18N, 24N-30N) perpendicular to the levee crest were surveyed. The levee crest is located west of the survey area. Figure 132 shows the location of the cedar tree and survey lines. The cedar tree was centered at grid position (6E, 20N). The processing steps applied to the data are described earlier in this chapter.

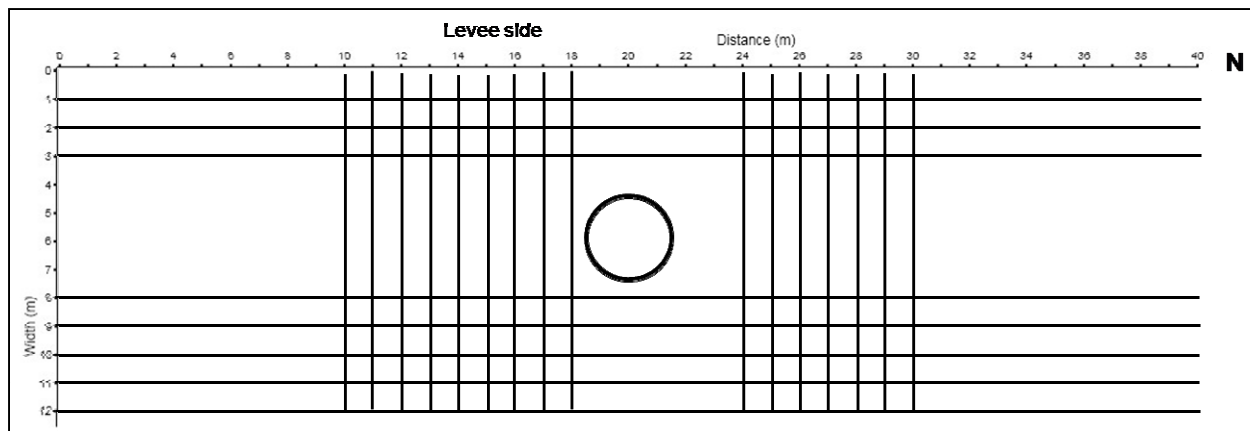


Figure 132. GPR survey grid, Burlington, WA. The circle represents the location of the cedar tree.

Data interpretation

The data were migrated to refocus the hyperbolas generated by subsurface anomalies into point features to aid in identifying possible roots. Figure 133 shows an example of non-migrated and migrated radargrams, where the hyperbola in the non-migrated section has been reduced to a point in the migrated section. It is these “points” that will be connected in depth slices shown later to identify possible roots. Figure 134 shows a plan view of the GPR data collected parallel and perpendicular to the levee, directly beneath the ground surface (0.8-cm depth) and a radargram along line 7.6E. Depth of investigation is approximately 1.4 m (Figure 134), based on a subsurface EM wave velocity of 0.078 m/ns. Subsurface layering is observed, along with numerous hyperbolic reflections caused by buried features. A circular feature with a diameter of about 15 m is observed around the tree location (Figure 134a). This feature appears to coincide with the grass-free area under the tree (Figure 120). Also apparent in the depth slice (Figure 134b) are parallel linear features that are at an angle to the levee. These linear features may be related to past flooding and deposition. Note in Figure 134a that there are numerous anomalies (white “dots,” linear features, circular expressions, etc.) present in this shallow depth section. Many of these features “ring” down through the depth profile (Figure 134c, i.e., strong near-surface anomaly adjacent to the tree at 20N). It is important to be aware of these ringing effects to avoid misinterpreting them for actual anomalies in deeper sections. Ringing effects can mask weaker anomalies that may be of interest. The longer GPR survey lines acquired parallel to the levee provide better images than the shorter lines perpendicular to the levee, so only parallel depth slices will be presented.

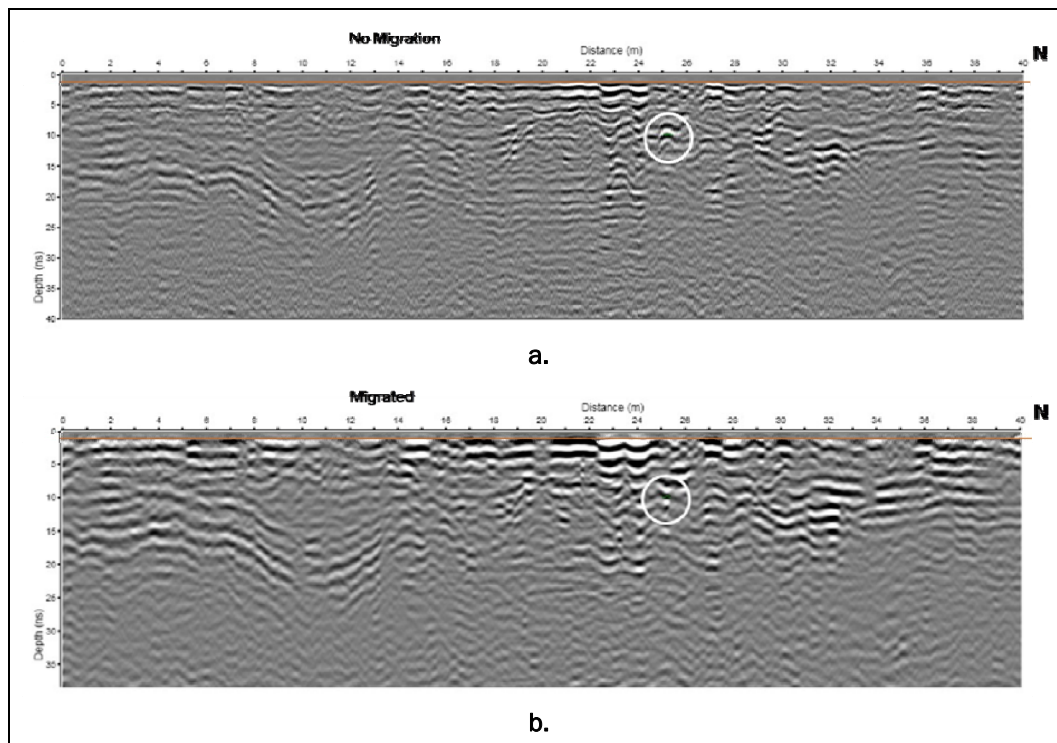


Figure 133. Comparison of non-migrated (a) and migrated (b) depth sections at $y = 8.518$ m, Burlington, WA. Circles show hyperbola that has been refocused to a point in the migrated section.

The GPR plan view sections (from data collected parallel to the levee) given in Figure 135 are interpreted depth sections with possible root locations. Without ground truth it is difficult to say if the interpreted anomalies are actual roots. Figure 136 is an overlay of all of the interpreted roots. The interpreted segments tend to be short and some appear to form longer root segments.

Summary of GPR surveys

GPR data were collected around a cedar tree on the Skagit River levee Burlington, WA, to image the larger subsurface roots. No obvious root structures were observed in the data; however, possible root segments were interpreted from the shallow surface to a depth of approximately 62 cm. These root segments extend a radius of about 6 m about the tree. This area is similar to that observed in the electrical resistivity data (10- to 12-m diam).

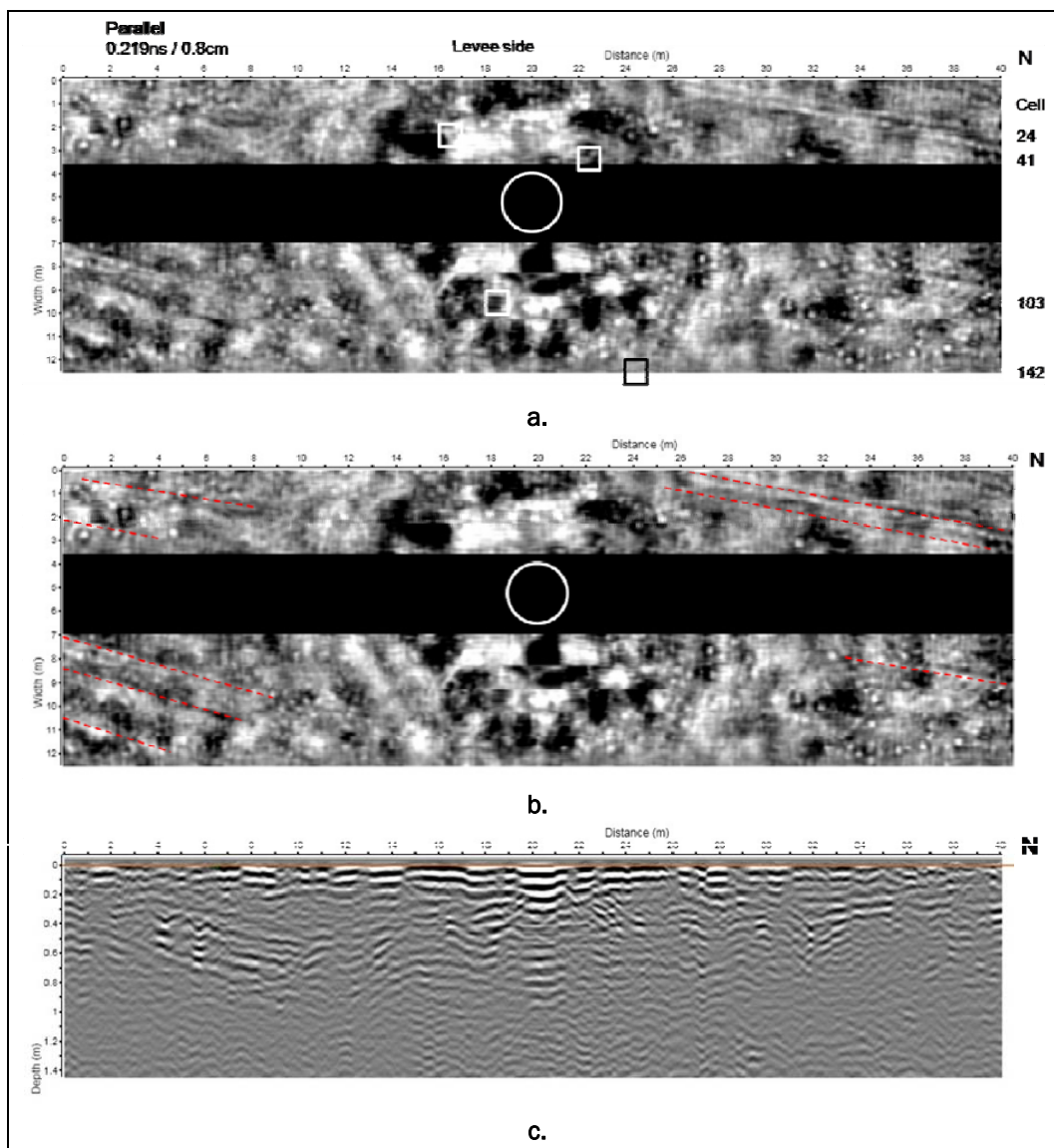


Figure 134. GPR data collected parallel (a-c) and perpendicular (d) to the levee, Burlington, WA. The white circle marks the tree location; the boxes are the locations of the root characterization cells. (a) Plan view of parallel radar section at 0.8-cm depth (0.219 ns). The corresponding time of 0.219 ns is a two-way travel time. To obtain the correct depth, divide the two-way time by 2 and multiply by the EM wave velocity ($0.219 \text{ ns} \div 2 \times 0.078 \text{ m/ns}$). (b) Same section as (a), but with location of possible flooding/deposition events shown. (c) Depth profile along line 7.6E. (d) Plan view of perpendicular radar section at 0.8-cm depth (0.219 ns).

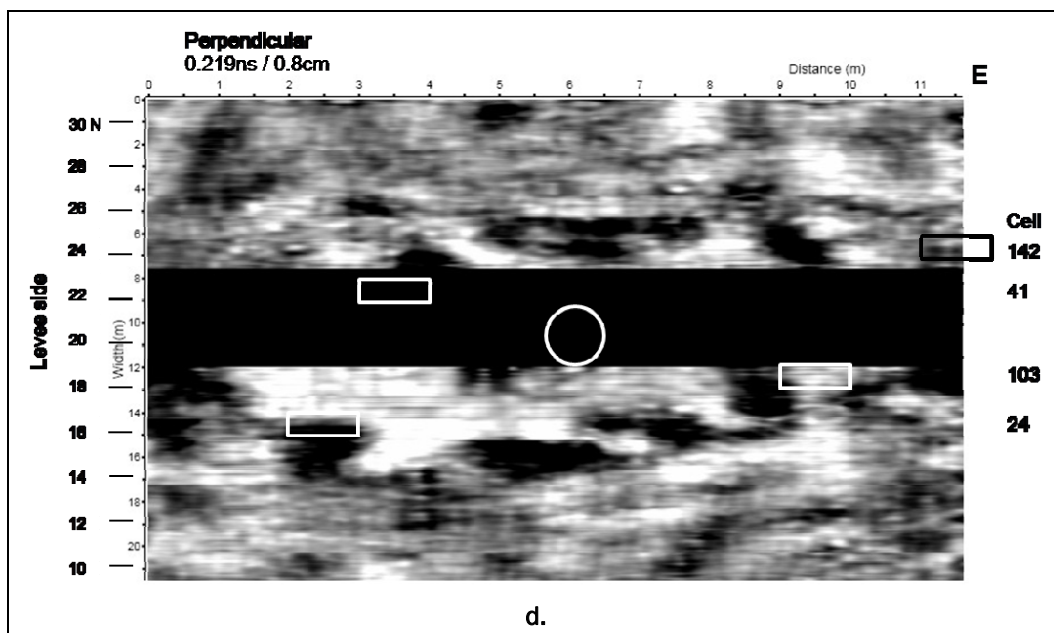


Figure 134. Concluded.

Conclusions

ERI, EM induction, and GPR surveys were used along a part of the Skagit River levee, Burlington, WA, to noninvasively map the tree root distribution of a cedar tree on the protected levee toe.

Seven, parallel, 41-m-long 2-D ERI survey lines, spaced 2 m apart and with 1-m electrode spacing, were run on the toe of the unprotected side of the levee. The lines were oriented approximately parallel to the levee axis. A 13- by 11-m 3-D ERI survey grid, with 1-m electrode spacing, was established around the base of the tree. The 3-D grid survey collected resistivity data from many horizontal surface electrode configurations and provides a 3-D image of the distribution of resistivity values. The 2-D survey lines were also analyzed using a quasi 3-D inversion technique to provide 3-D results. An EM38 survey consisting of 14 parallel, 40-m-long lines, spaced 1 m apart, was conducted over the same area covered by the 2-D resistivity survey.

The ERI survey results indicate a 2-m-thick overburden layer that is electrically highly resistive, extending across much of the site. The overburden is interpreted as consisting of dry sandy-gravelly soil because of its high resistivity value. Underlying the overburden, are lower resistivity soils presumed to consist of finer-grained material with higher moisture

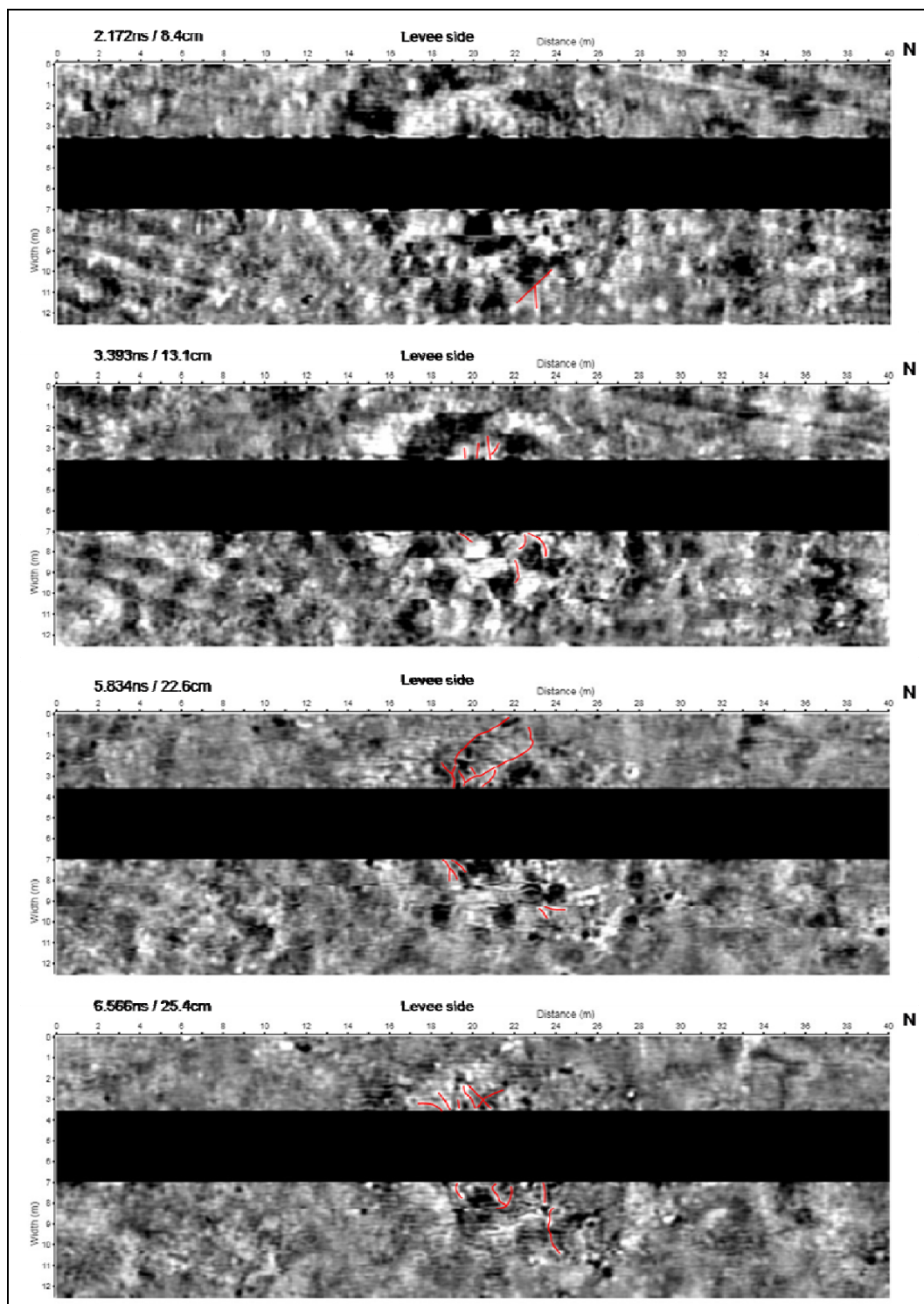


Figure 135. Depth slices from data collected parallel to the levee showing interpreted location of possible tree roots, Burlington, WA.

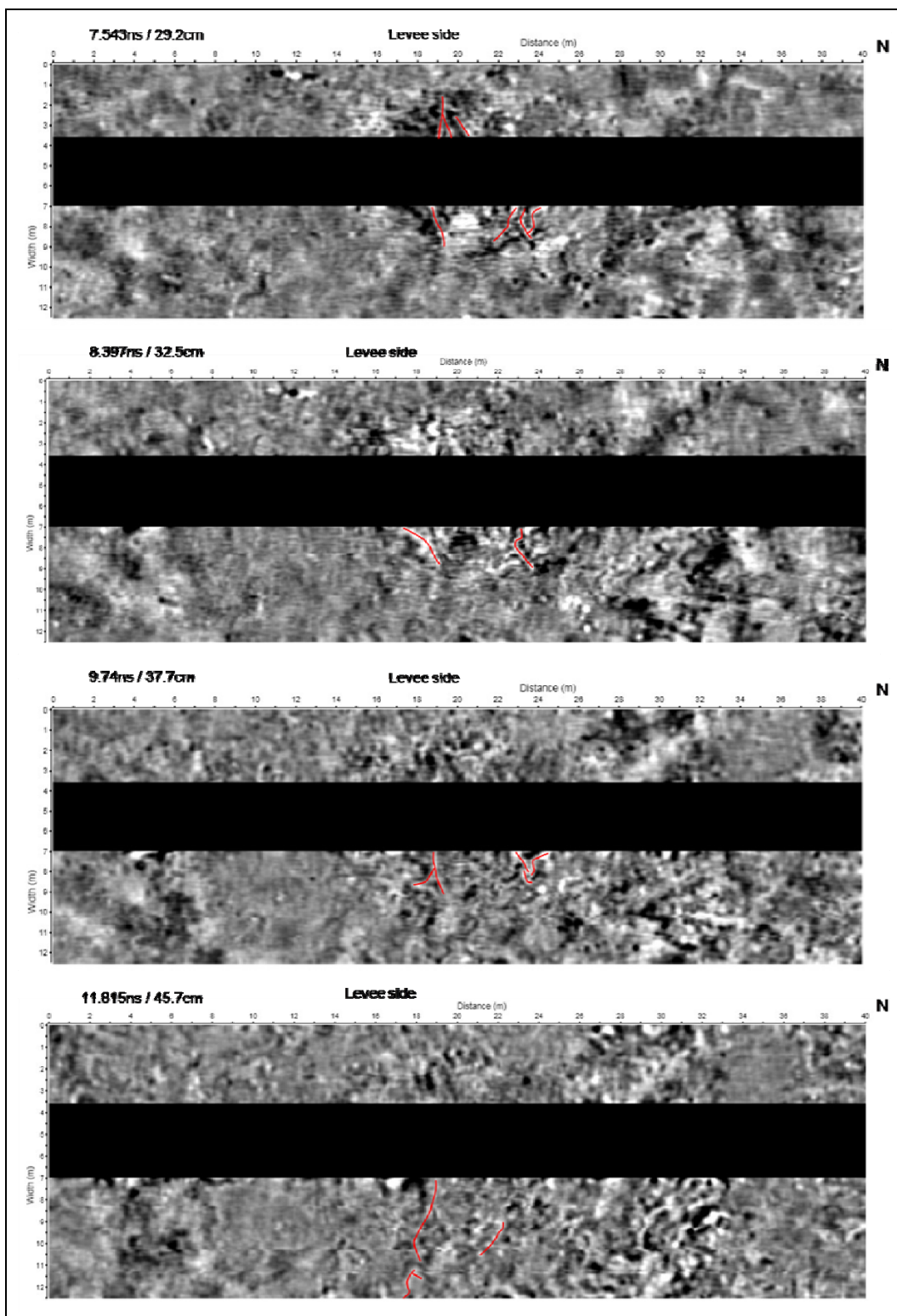


Figure 135. Continued.

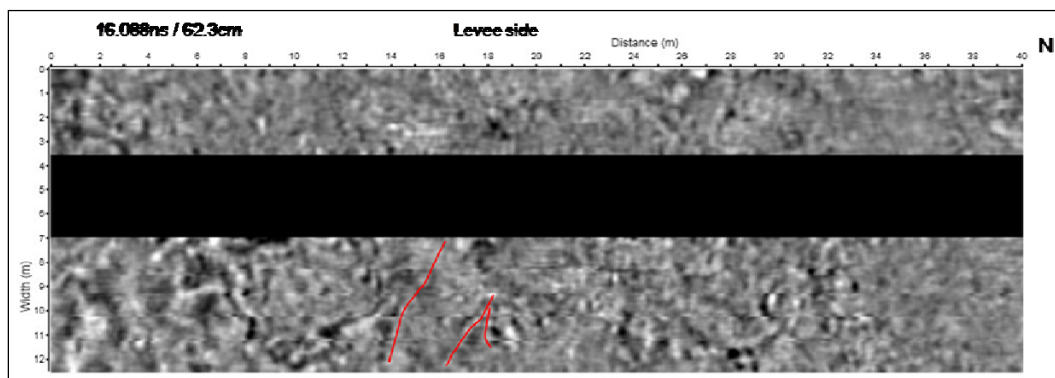


Figure 135. Concluded.

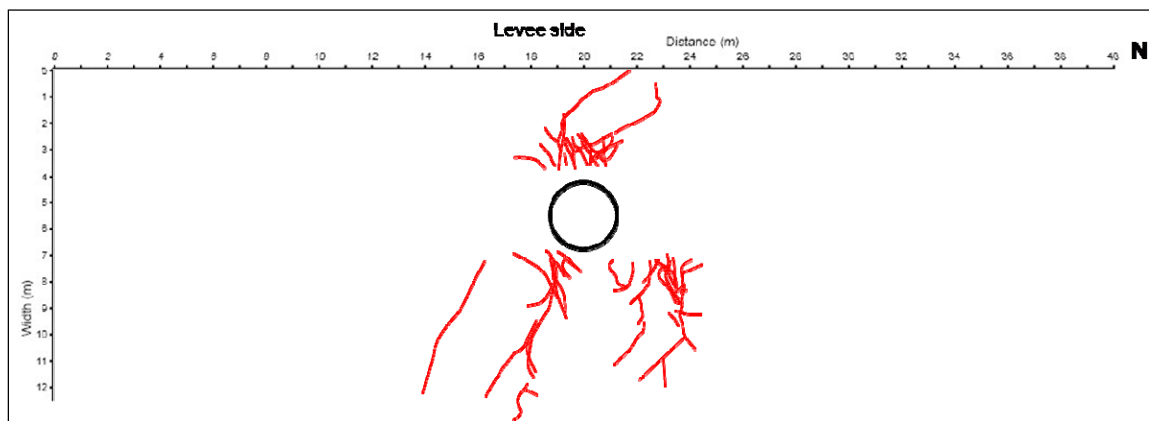


Figure 136. Location of possible tree roots interpreted from GPR data collected around a cedar tree on the Burlington Levee, Burlington, WA.

contents. The results also indicate a roughly circular area with much lower electrical resistivity than the surrounding overburden, with a diameter of approximately 10 m centered on the location of the tree. The circular area penetrates the entire thickness of the overburden and appears more like an anomalously low resistivity cylinder. The EM survey results also indicate an anomalous circular area centered on the tree with an approximate diameter of 10 m. The GPR results show possible root segments to a depth of approximately 0.62 m. These mapped root segments extend about 6 m from the tree. It is presumed that this approximately 10- to 12-m-diam circular area detected by the three survey methods defines the maximum detectable extent of the tree root zone.

Albuquerque, NM

Background

ERDC personnel conducted ERI surveys at two sites near Albuquerque, NM, to determine the extent of tree root distributions during 9 through

12 April 2010 (Figure 137). The two 13- by 11-m sites, designated Sites 1 and 2, are located on the unprotected toe of the Rio Grande levee.

Site 1 is located on the east bank of the river approximately 20 m from the levee toe. The site is flat and sandy. The tree studied, a 0.42-m-diam Rio Grande cottonwood (*Populus fremontii*), is located near the center of the site. There are also three cottonwood trees within 2 m of the site boundary with diameters ranging between 0.30 and 0.41 m.



Figure 137. Locations of test Sites 1 and 2, Albuquerque, NM.

Site 2, approximately 2.75 km upriver of Site 1, is located on the west bank of the river. This site is also flat and sandy and located approximately 10 m from the levee toe. There are two Rio Grande cottonwoods (*Populus fremontii*) within the site. The diameters of the two trees are approximately 0.58 and 0.27 m measured at chest height.

Data acquisition and processing

A 3-D ERI grid measuring 13 by 11 m was established at each site. Each rectangular grid consists of 168 electrode positions spaced 1 m apart. Stainless steel rods, approximately 1 cm in diameter, were driven vertically into the ground to a depth of about 0.3 m and used as electrodes for the

ERI survey. An Advanced Geosciences, Inc., SuperSting R8 resistivity meter with the Smart electrode switching system was used to collect data. A 3-D roll-along survey method was used to collect the ERI data. The ERI grid layouts for Sites 1 and 2 are shown in Figures 138 and 139, respectively.

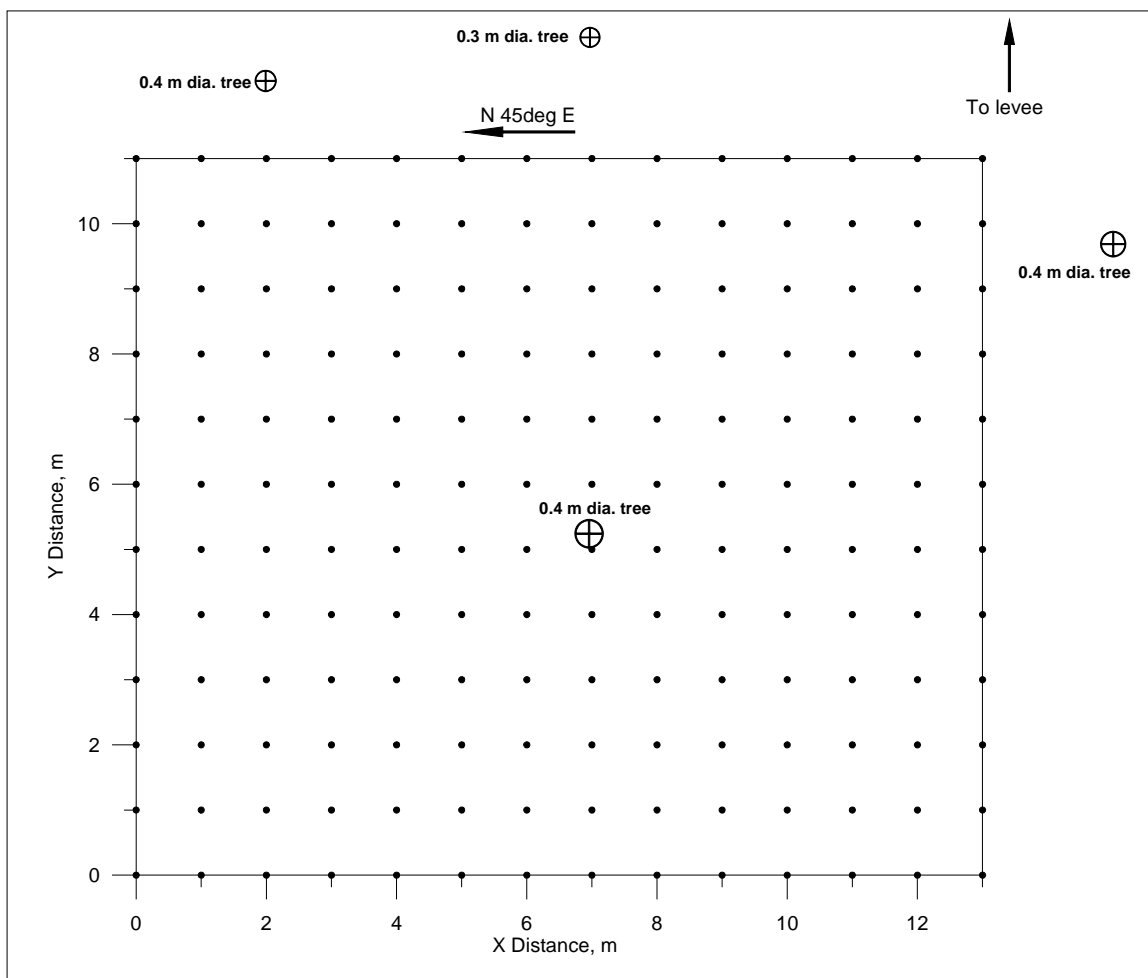


Figure 138. 3-D ERI layout, Site 1, Albuquerque, NM.

Results and interpretation

Site 1

The 3-D resistivity data for Sites 1 and 2 were inverted using EarthImager 3-D software (Advanced Geosciences, Inc.). The 3-D inversion image for Site 1 is shown in Figure 140. The black ovals represent trees' approximate position. The top 1.5 to 2.0 m of the site has resistivity values of approximately 100 to 300 $\Omega\text{-m}$ and overlies soils with resistivity values greater than 300 $\Omega\text{-m}$. The maximum depth of investigation is 3.25 m.

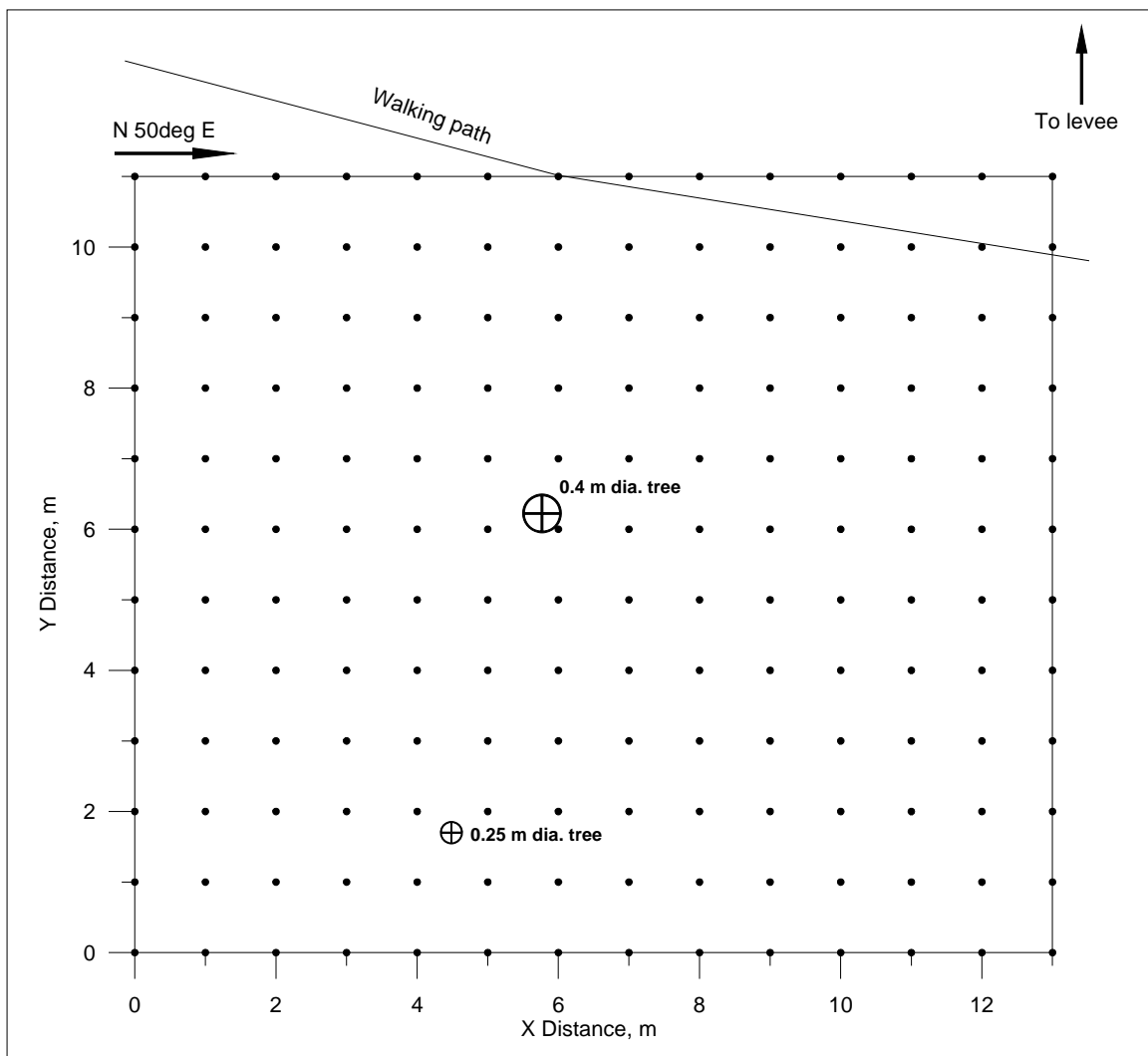


Figure 139. 3-D ERI layout, Site 2, Albuquerque, NM.

Figures C213 through C219, in Appendix C, are depth slices at 0.50-m depth intervals between depths of 0.00 and 3.00 m. The black ovals represent the approximate locations of the trees on the ground surface and the white ovals are the projected locations of the trees on the depth slice surface. The dots on the figures represent the electrode locations, which are spaced 1 m apart. The figures show that the deeper the depth slice, the higher the resistivity readings.

Figures C220 through C230, in Appendix C, present electrical resistivity slices (cross sections) taken parallel to x -axis between $Y = 3.00$ m and $Y = 8.00$ m at 0.50-m intervals. The figures show a relatively low resistivity surface layer approximately 1.5 m thick overlying a high resistivity layer. The low resistivity thins out away from the levee and towards the river.

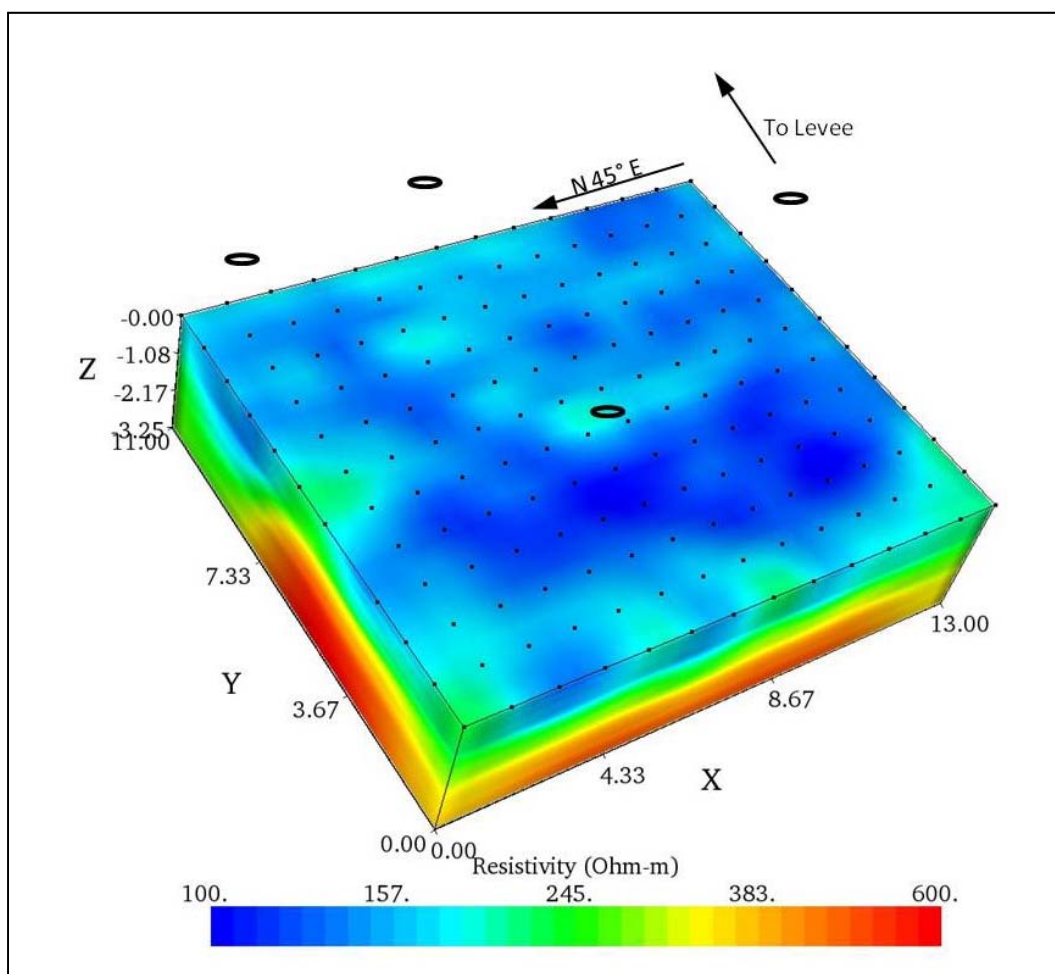


Figure 140. 3-D resistivity inversion image, Site 1, Albuquerque, NM.

No tree root zones were interpreted from the ERI results.

Site 2

The 3-D inversion image for Site 2 is shown in Figure 141. The black ovals represent the trees' approximate positions. The figure shows a partial 3-D distribution of resistivity values. The maximum depth of investigation is 3.25 m.

Figures C231 through C237, in Appendix C, are depth slices taken at 0.50-m depth intervals between depths of 0.00 and 3.00 m. The black ovals represent the approximate locations of the trees on the ground surface and the white ovals are the projected locations of the trees on the depth slice surface. The dots on the figures represent the electrode locations, which are spaced 1 m apart. The figures indicate that resistivity values increase with depth.

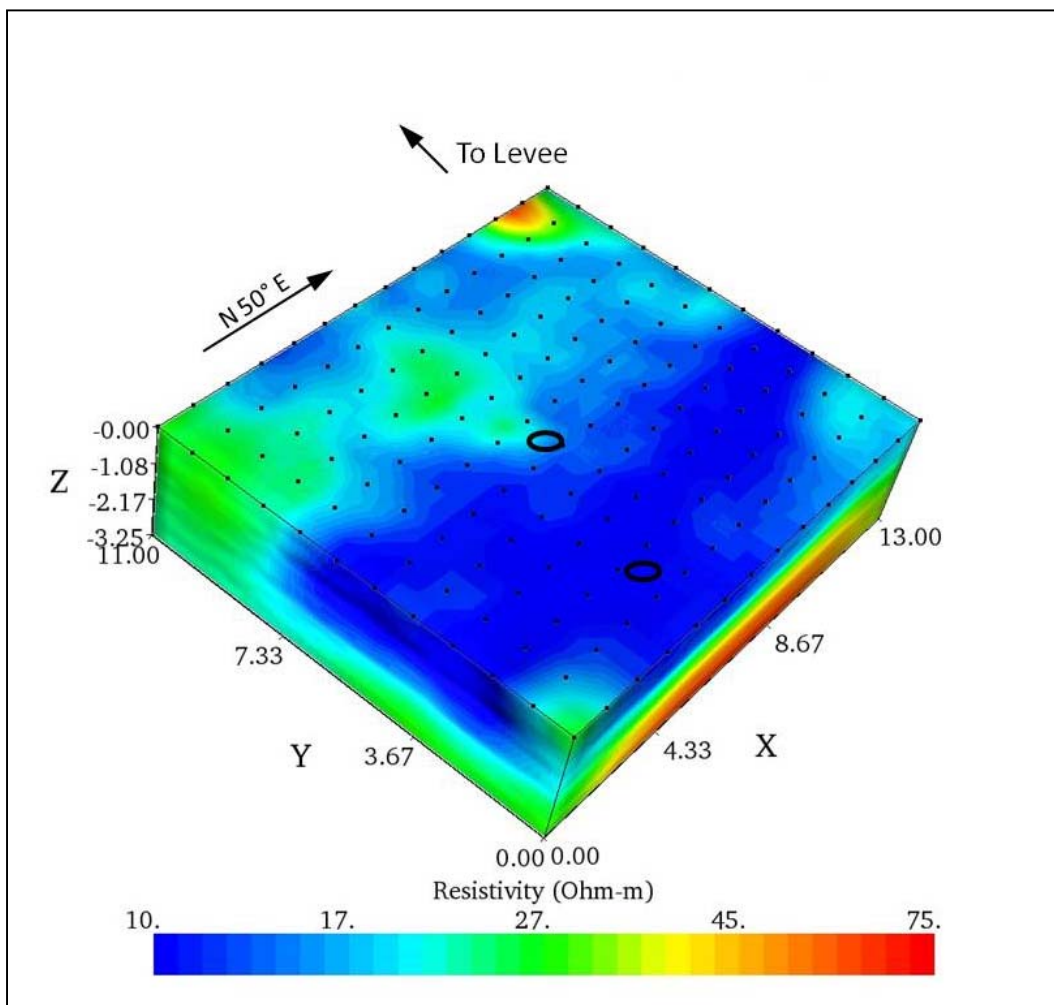


Figure 141. 3-D resistivity inversion image, Site 2, Albuquerque, NM.

Figures C238 through C252, in Appendix C, present electrical resistivity slices (cross sections) taken parallel to x -axis between $Y = 1.00$ m and $Y = 8.00$ m. The figures show the higher resistivity underlying layer thinning out towards the levee.

No tree root zones were interpreted from the ERI results.

Conclusions

ERI surveys were conducted at two sites along the Rio Grande levee near Albuquerque, NM, to noninvasively map the tree root distribution of several cottonwood trees. There was one cottonwood tree within Site 1 and two within Site 2. Three dimensional ERI surveys were run in a grid fashion to detect resistivity differences between materials beneath and

immediately around the tree associated with the tree root zone and from background readings.

The 3-D ERI results do not indicate any differences in resistivity readings between soils located immediately beneath or near the trees and from background. Both sites have an increase in resistivity values with depth presumed to be caused by an increase in coarse-grained material. The majority of the resistivity readings range between 100 and 600 $\Omega\text{-m}$ at Site 1 and between 10 and 75 $\Omega\text{-m}$ at Site 2. This may be an indication that the soils at Site 1 are drier or coarser grained than those at Site 2.

Lewisville Dam, Lewisville, TX

Background

During the period 11 through 13 March 2010, ERDC personnel conducted a geophysical investigation at Lewisville Dam, Lewisville, TX, located approximately 35 km NNW of Dallas (Figure 142). To map the extent of the root zone of a post oak (*Quercus stellata*), the tree was located on the downstream toe of the dam using noninvasive methods.

ERDC contacted the U.S. Army Engineer District, Ft. Worth (SWF), early in 2010 requesting permission to conduct a geophysical investigation near some trees along the Trinity River levees near Dallas, TX. SWF could not allow the work on the Trinity River levees at the time because of high river levels. During this time, SWF was in the process of installing a series of relief wells along the toe of the dam. The location of one of the planned relief wells was adjacent to a tree, and the tree would have to be removed. SWF suggested that ERDC conduct the geophysical investigation at Lewisville Dam because it would provide the opportunity to compare the geophysical-based measurements with the actual tree root zone. ERDC chose to conduct a geophysical study at Lewisville Dam based on the results of a site assessment.

The investigated tree has a relatively large diameter of 1.1 m at chest height, a crown width of about 15 m, and a height of approximately 10 m. The tree is located near the western portion of the dam (Figure 143) between the downstream toe and a paved service road (Figure 144).

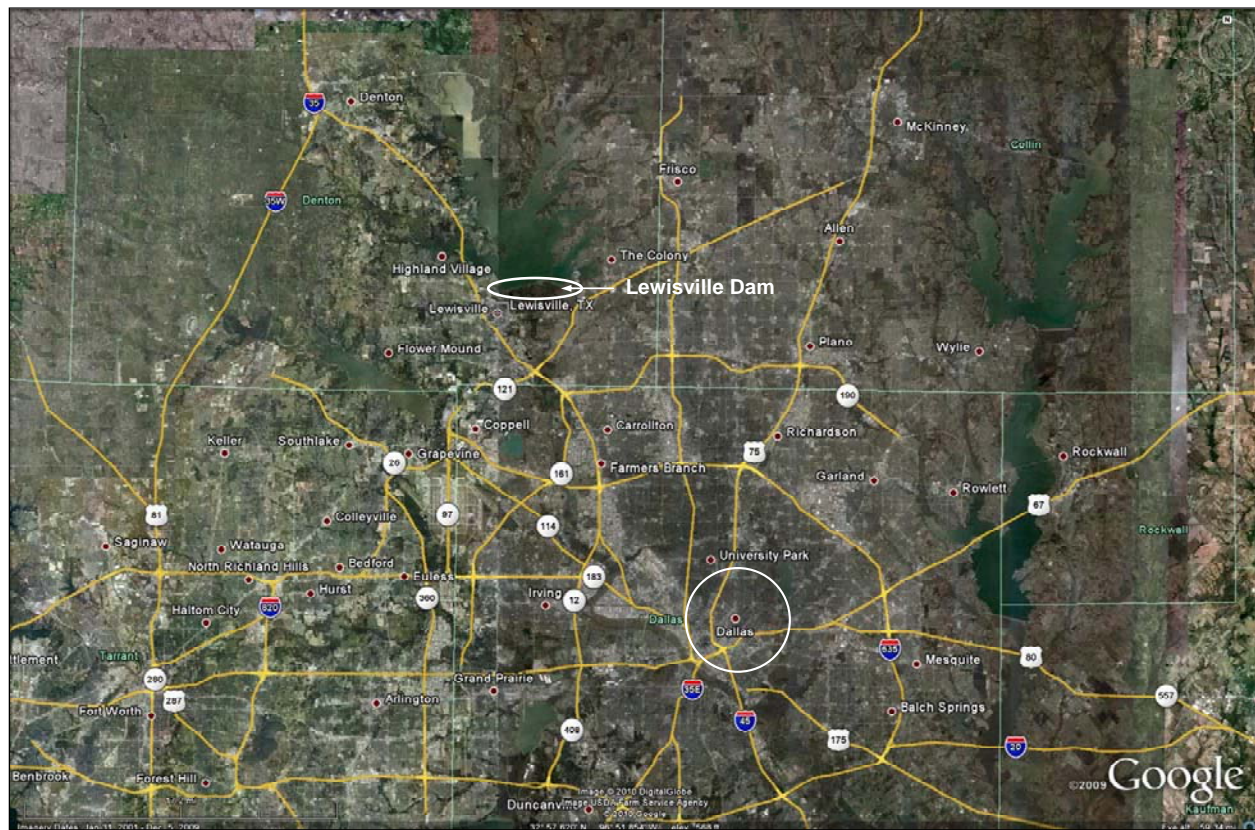


Figure 142. Lewisville Dam, Lewisville, TX.

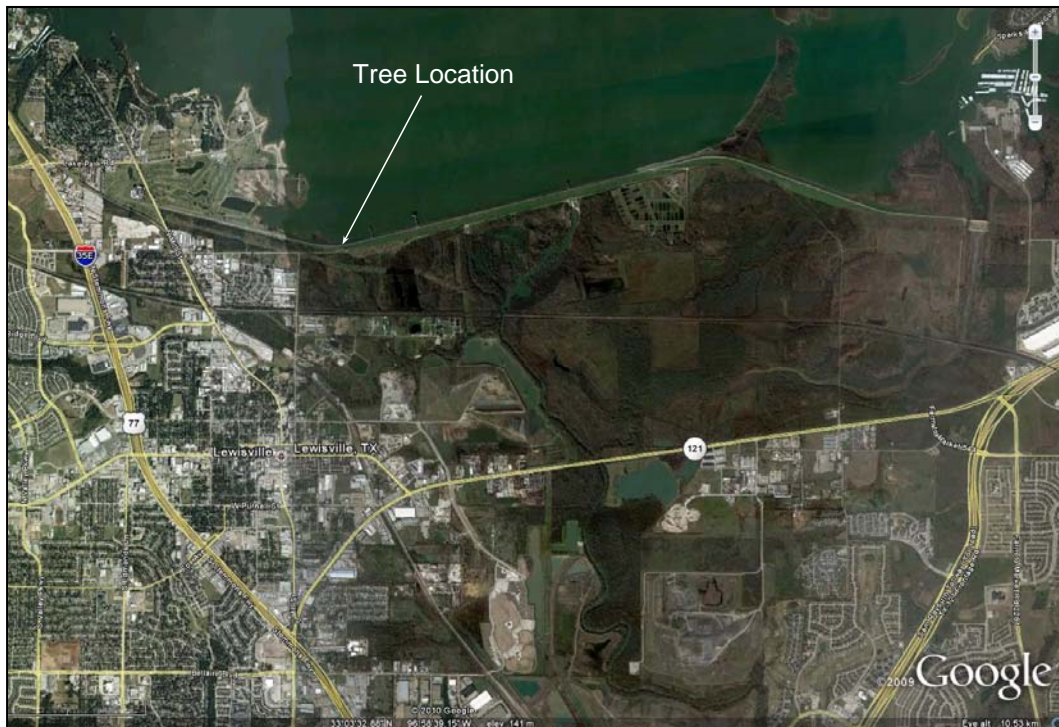


Figure 143. Location of study tree relative to Lewisville Dam, Lewisville, TX.

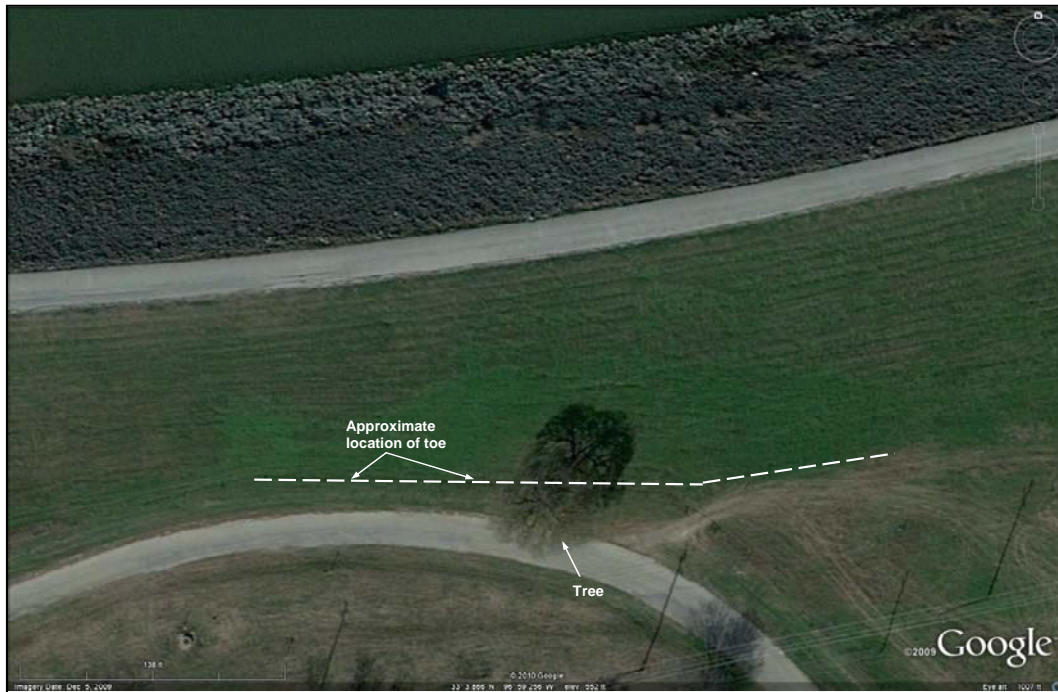


Figure 144. Location of study tree relative to the service road and Lewisville Dam toe, Lewisville, TX.

Geophysical investigation

ERI and EM induction methods were used to map the extent of the tree root zone during 11 through 13 March 2010. Principles of operation for these two methods are described earlier in this report.

Geophysical survey methods

ERI

Data acquisition and processing

A 3-D ERI grid measuring 13 by 11 m was established around the study tree (Figure 145). The rectangular grid consists of 168 electrode positions spaced 1 m apart. Stainless steel rods, approximately 1 cm in diameter, were driven vertically into the ground to a depth of about 0.3 m and used as electrodes. Holes were drilled through the asphalt road that covered the southern portion of the grid so that the electrodes could be emplaced and contact the underlying soil (Figure 146). An Advanced Geosciences, Inc., SuperSting R8 resistivity meter with the Smart electrode switching system was used to collect data.

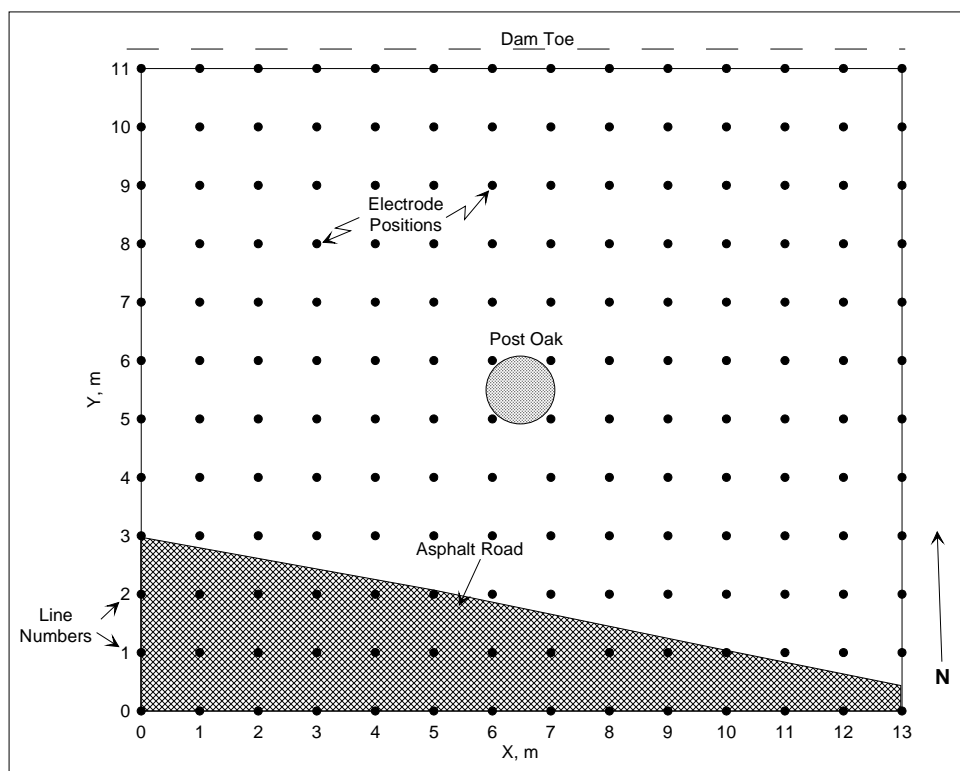


Figure 145. Plan view of 3-D ERI test layout,
Lewisville Dam, Lewisville, TX.



Figure 146. Drilling holes in asphalt service road for electrode
emplacement, Lewisville Dam, Lewisville, TX.

A 3-D roll-along survey was used to collect the ERI data. In this survey, 3-D data were initially collected from electrodes along lines 0 through 7. Upon completion of the initial survey, cables along lines 0 through 3 were disconnected from the electrodes and rolled-along to the front of the grid. The four rolled-along cables from lines 0 through 3 were then connected to electrodes along lines 8 through 11 allowing ERI data to be collected from lines 4 through 11, the last section of the survey. Figures 147 and 148 show the ERI survey layout for lines 0 through 7 (before roll-along) and lines 4 through 11 (after roll-along), respectively.

Results and interpretation

The 3-D resistivity data were inverted using EarthImager 3-D software. The resistivity inversion image is shown in Figure 149. The black oval in the center of the grid indicates the tree's approximate position. There is a circular, high resistivity anomaly, approximately 3 m in diameter, in the center of the site corresponding to the location of the tree. The maximum depth of investigation is 3.25 m.

Figures C155 through C162, in Appendix C, are depth slices at 0.25-m depth intervals between depths of 0.25 and 2.00 m. Figures C163 and C164, in Appendix C, are depth slices at depths of 2.50 and 3.25 m, respectively. The black oval represents the approximate location of the tree shown on the surface of the 3-D inversion image and the white oval is the vertical projected surface location of the tree on the depth slice surface. The dots on the figures represent the electrode locations, which are spaced 1 m apart. The high resistivity anomaly found on the surface in Figure 120 can be followed to a depth of approximately 1.50 m (Figure C160). At a depth of 1.75 m (Figure C161), the size and intensity of the anomaly have diminished considerably, and at a depth of 2.00 m (Figure C162), the anomaly is no longer evident.

Figures C165 through C175, in Appendix C, present electrical resistivity slices (cross sections) taken parallel to the y -axis between $X = 3$ m and $X = 10$ m. For this site, a resistivity value above $17 \Omega\text{-m}$ has been arbitrarily selected as the threshold above which resistivity values are considered anomalously high. Although the slices taken at $X = 3$ m and $X = 4$ m (Figures C165 and C166) show slightly elevated resistivity values near the center of the section, they are not considered anomalous because values do not exceed $17 \Omega\text{-m}$. Between $X = 5.0$ m and $X = 6.5$ m, an anomaly located midway along each slice increases laterally and vertically as well as in



Figure 147. 3-D ERI layout showing the extent of lines 0 through 7,
Lewisville Dam, Lewisville, TX.



Figure 148. 3-D ERI layout showing the extent of lines 4 through 11,
Lewisville Dam, Lewisville, TX.

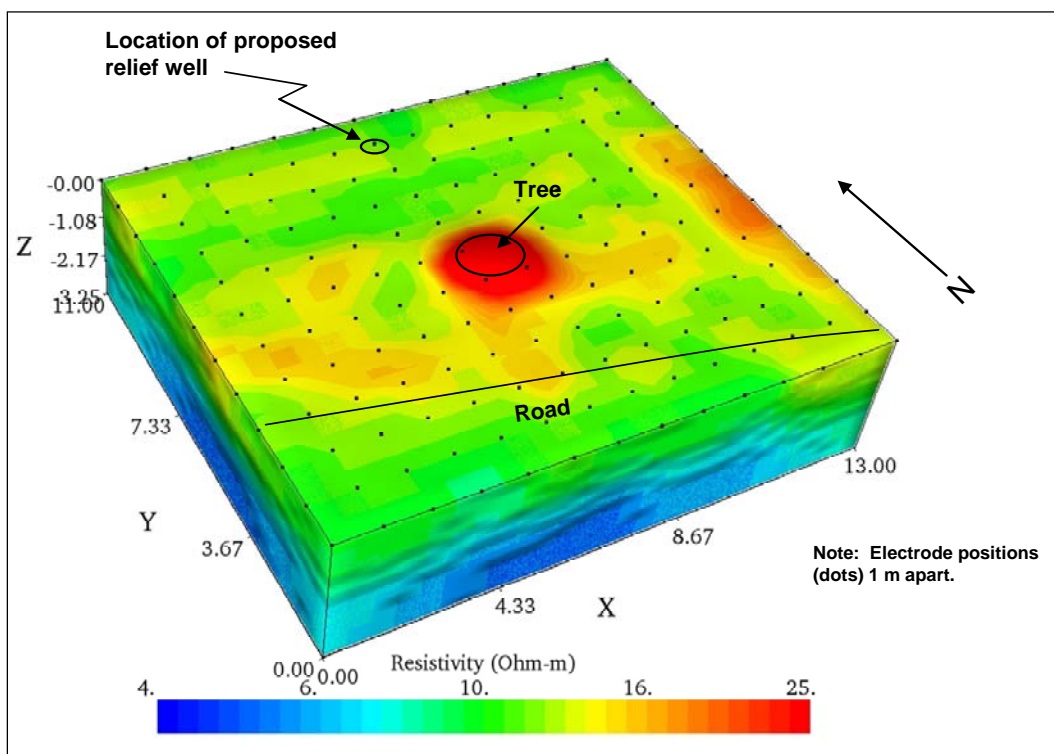


Figure 149. ERI inversion image, Lewisville Dam, Lewisville, TX.

resistivity magnitude. Between $X = 6.5$ m and $X = 8.0$ m, the anomaly begins to diminish laterally and vertically and the magnitude of the resistivity values also decrease. As in slices taken at $X = 3$ m and $X = 4$ m, the slices taken at $X = 9$ m and $X = 10$ m show slightly elevated resistivity values near the center of the section, but are not considered anomalous as resistivity values do not exceed $17 \Omega\text{-m}$. Table 34 presents the lateral and vertical extent and maximum resistivity values of the anomaly interpreted from slices normal to the x -axis.

Similar to the procedure already described, slices were also taken normal to the y -axis and analyzed to determine the maximum detectable extent of the tree's zone of influence. Again, a resistivity value of $17 \Omega\text{-m}$ was chosen as an anomaly threshold. Table 35 presents the lateral and vertical extent and maximum resistivity values of the anomaly interpreted from slices normal to the y -axis. The data in Table 35 show that the maximum detectable anomaly range along the x -axis is 3.5 m, whereas in Table 34 the maximum detectable anomaly range along the y -axis is 2.7 m, suggesting that there may be a preferential root growth parallel to the toe of the dam.

Table 34. Maximum detectable anomaly range and maximum resistivity magnitude for selected slices normal to the x-axis, Lewisville Dam, Lewisville, TX.

Slice Location Normal to x-axis, m	Maximum Detectable Anomaly Range along y-axis, m	Maximum Detectable Anomaly Depth Range, m	Anomaly Maximum Resistivity Value, $\Omega\text{-m}$
3	n/a	n/a	Less than 17
4	n/a	n/a	Less than 17
5	4.5-5.9 (1.4 m)	0.6-1.1	19
5.5	3.7-6.3 (2.6 m)	0-1.3	29
6	3.9-6.6 (2.7 m)	0-1.5	54
6.5	3.9-6.6 (2.7 m)	0-1.5	68
7	4.0-6.6 (2.6 m)	0-1.4	49
7.5	3.7-6.2 (2.5 m)	0-1.1	24
8	3.6-4.8 (1.2 m)	0.1-1.1	18
9	n/a	n/a	Less than 17
10	n/a	n/a	Less than 17

Table 35 Maximum detectable anomaly range and maximum resistivity magnitude for selected slices normal to the y-axis, Lewisville Dam, Lewisville, TX.

Slice Location Normal to y-Axis, m	Maximum Detectable Anomaly Range Along x-axis , m	Maximum Detectable Anomaly Depth Range, m	Anomaly Maximum Resistivity Value, $\Omega\text{-m}$
3.0	n/a	n/a	Less than 17
4.0	7.4-5.3 (2.1 m)	0-1.0	19
4.5	8.5-5.0 (3.5 m)	0-1.2	30
5.0	7.9-4.6 (3.3 m)	0-1.5	53
5.5	7.9-4.8 (3.1 m)	0-1.5	68
6.0	7.7-5.1 (2.6 m)	0-1.3	45
6.5	5.8-7.2 (1.4 m)	0-1.0	22
7.0	n/a	n/a	Less than 17

The electrical resistivity results indicate that tree's maximum detectable zone of influence extends approximately 2.7 m along the *y*-axis, 3.5 m along the *x*-axis and 1.5 m in depth. For this site, the tree's zone of influence is characterized as a relatively high electrically resistive anomaly.

EM survey

Data acquisition and processing

A 15- by 11-m grid was established around the study tree, as shown in Figure 150 for the EM survey. The rectangular grid overlaps the ERI grid and extends an additional 2 m to the east. A Geonics Ltd. EM38-MK2 conductivity meter was used with Tx-Rx coils set at fixed distances of 0.5 and 1.0 m and operated in the vertical dipole mode. Twelve survey lines were spaced 1.0 m apart and were oriented parallel to the toe of the dam.

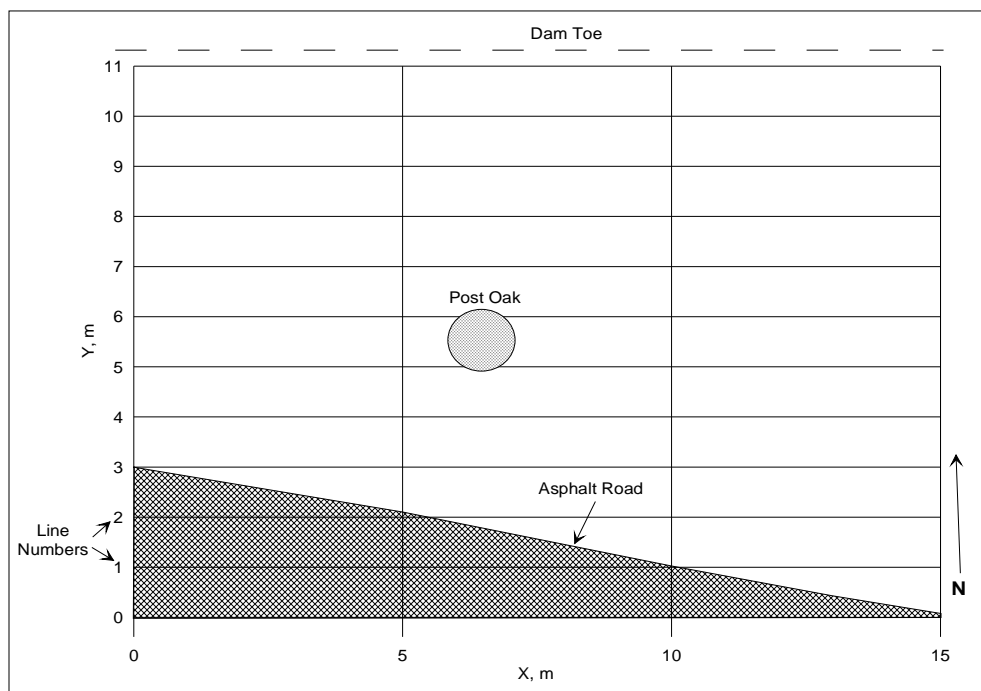


Figure 150. EM survey layout, Lewisville Dam, Lewisville, TX.

Conductivity and in-phase data for both coil separations were simultaneously collected. The EM data were contoured and plotted as maps of conductivity and in-phase values for the 0.5- and 1.0-m inter-coil separations.

Results and interpretation

Figures 151 and 152 present the conductivity survey results for the 0.5- and 1.0-m inter-coil spacings, respectively. Comparing Figures 151 and 152 shows that, in general, the measured conductivity values of the 1.0-m inter-coil spacing are significantly higher than those of the 0.5-m inter-coil spacing. This difference in conductivity indicates that the soil's electrical conductivity increases with depth and is caused by an increase in clay or

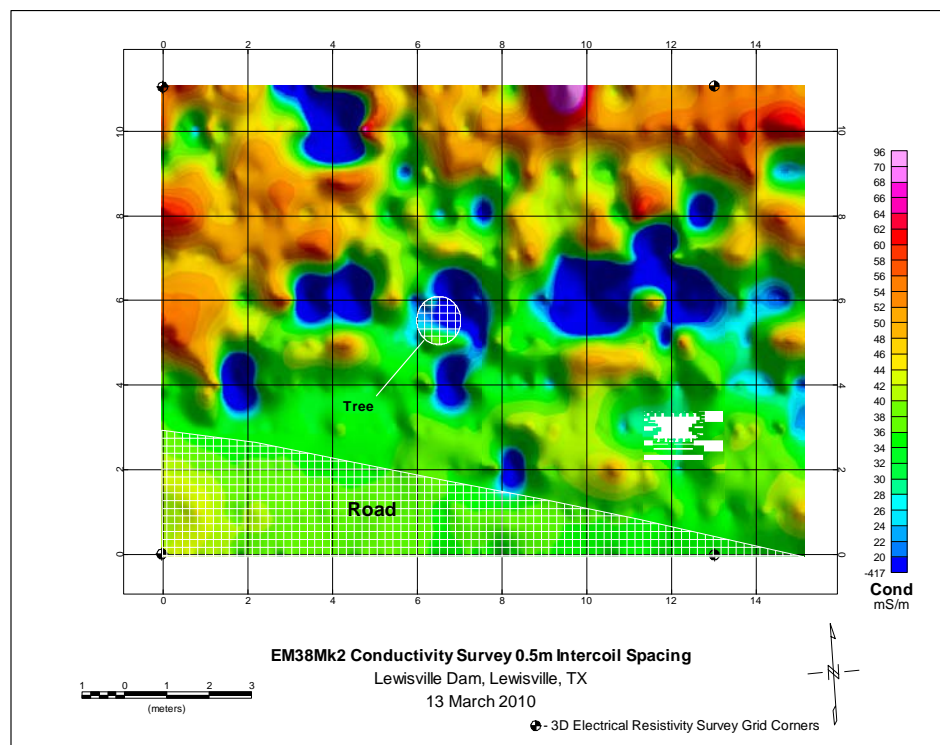


Figure 151. EM38-MK2 conductivity survey results, 0.5-m inter-coil separation, vertical dipole mode, Lewisville Dam, Lewisville, TX.

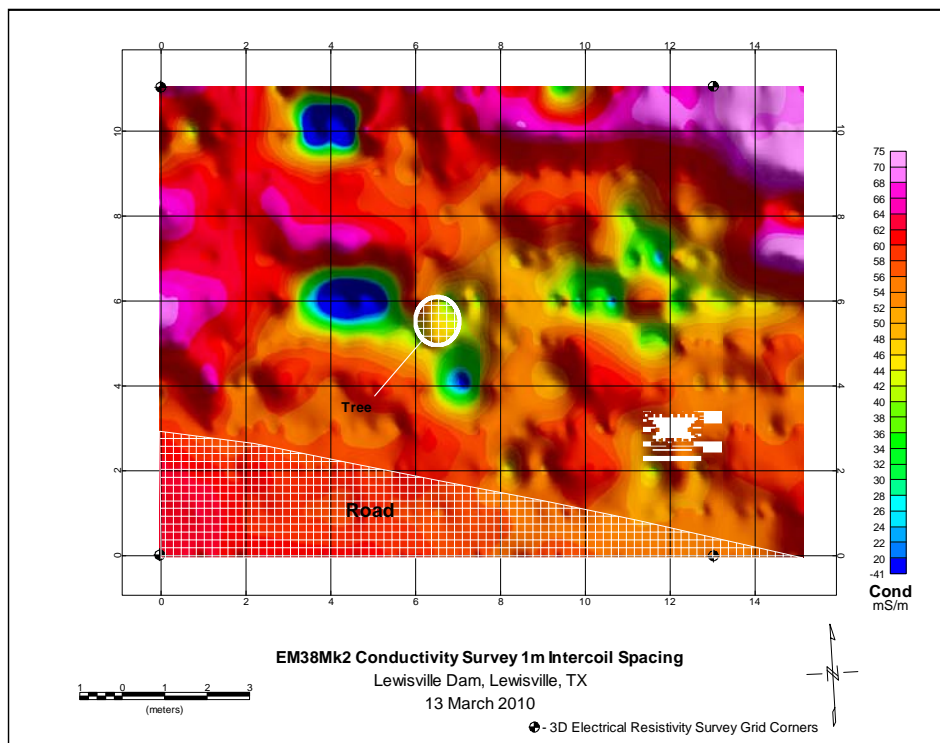


Figure 152. EM38-MK2 conductivity survey results, 1.0-m inter-coil separation, vertical dipole mode, Lewisville Dam, Lewisville, TX.

moisture with depth. Figure 151 suggests that the tree location is associated with a low conductivity zone, but there are other similar low conductivity zones also present in other portions of the site. Figures 153 and 154 present the in-phase survey results for the EM38-MK2 0.5- and 1.0-m inter-coil spacing, respectively. With the exception of several small high and low valued anomalies, the 0.5-m inter-coil in-phase values are fairly consistent across the test site. The 1.0-m inter-coil spacing data (Figure 154) show the same anomaly locations as those shown in Figure 153, however, the size of the anomalies have increased. The anomalies are most likely caused by small buried metallic objects. As with the conductivity surveys, no anomalous in-phase values indicating the presence of the root zone were interpreted.

Conclusions

ERI and EM induction investigations were conducted to noninvasively map the tree root distribution of a post oak (*Quercus stellata*) on the downstream toe of Lewisville Dam, Lewisville, TX. The electrical resistivity (inverse of electrical conductivity) values obtained from this survey were used to infer certain soil properties. The purpose was to see if ERI could measure a contrast in electrical resistivity values between a tree's root zone and surrounding soil.

A 3-D roll-along ERI survey grid measuring 13 by 11 m with 1-m electrode spacing was established around the base of the tree. The 3-D grid survey collected resistivity data from many surface electrode configurations and provided a 3-D representation of the distribution of resistivity values. The lateral and vertical extent of the root ball zone was interpreted for the tree-based 3-D inversion results. The tree root zone, in this case, is interpreted as the volume of soil beneath and around the tree having a significantly higher resistivity value than the surrounding soils. The increased electrical resistivity readings measured beneath and around the tree may be caused by the roots having relatively higher resistivity than the native soil and thus the combined soil/root matrix has a higher resistivity. The resistivity data indicate that the clay content or moisture increases to a depth of 3.25 m, the maximum depth of investigation. The survey also indicates that the tree's maximum detectable zone of influence extends approximately 2.7 m perpendicular to the toe of the dam, 3.5 m parallel to the toe of the dam and 1.5 m deep. For this site, the tree's zone of influence is characterized as a relatively high resistivity anomaly.

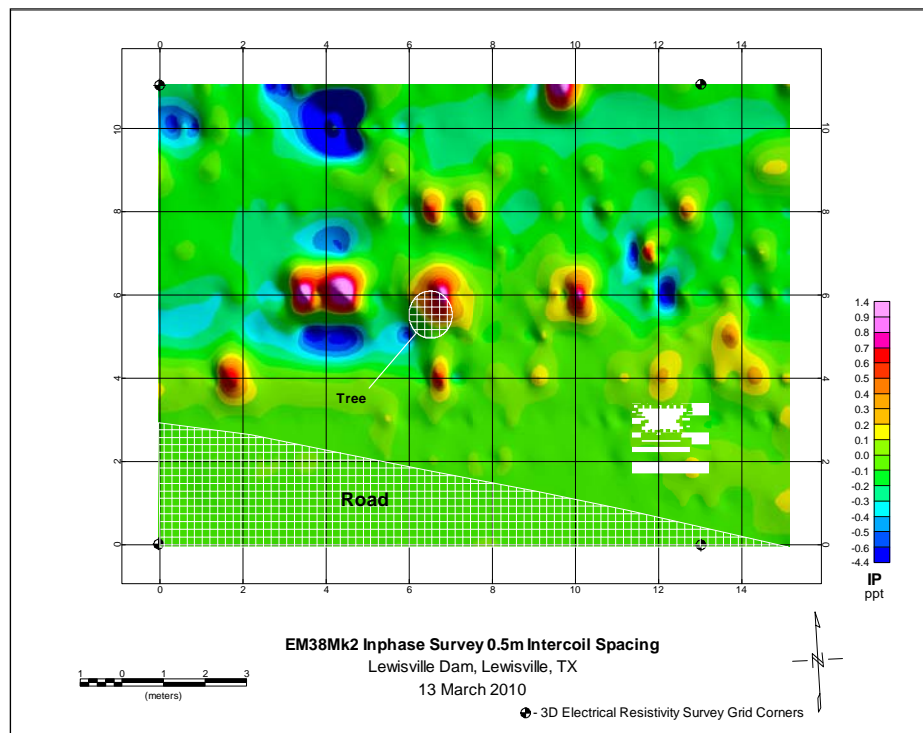


Figure 153. EM38-Mk2 in-phase survey results, 0.5-m inter-coil separation, vertical dipole mode, Lewisville Dam, Lewisville, TX.

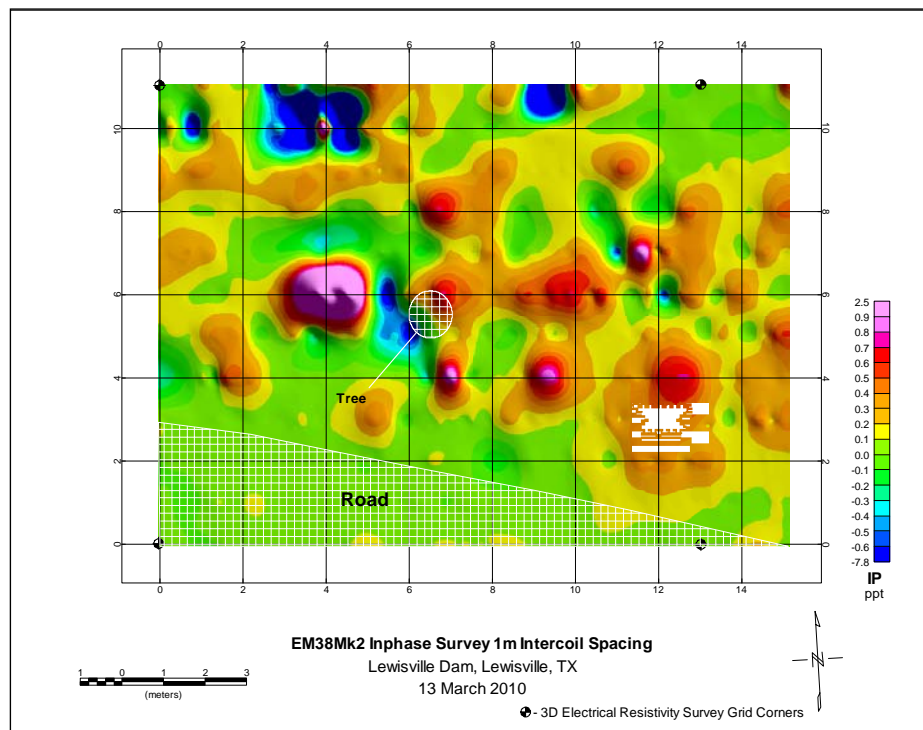


Figure 154. EM38-Mk2 in-phase survey results, 1.0-m inter-coil separation, vertical dipole mode, Lewisville Dam, Lewisville, TX.

The EM survey conductivity results also indicate an increase in clay or soil moisture to a depth of approximately 1.5 m, the maximum depth of investigation. The in-phase survey, which is sensitive to metallic objects, shows the presence of numerous localized anomalies, and it is presumed that they are caused by small buried metallic objects because of the intensity of the measured values. The site would have to be excavated to confirm the metallic nature of the anomalies. No anomalies suggestive of the tree's root zone location were interpreted from the EM survey results.

New Orleans, LA

Background

EM and GPR surveys were conducted at two sites near New Orleans, LA, during 16 through 19 May 2009 to non-intrusively determine the lateral and vertical extent of tree root zones. The two sites are called the Inner Harbor Navigation Canal (IHNC) and the 17th Street Canal sites and their locations are shown in Figure 155.

Inner Harbor Navigation Canal (IHNC) site

This study site is on the protected slope of the IHNC levee located approximately 6.5 km northeast of downtown New Orleans (Figure 155). The tree studied, a hackberry (*Celtis occidentalis*), was cut down within several days of the survey and is located at the toe of the levee. The tree's diameter at chest height is 0.64 m. Figure 156 shows the geophysical test grid established on the levee's protected slope adjacent to the recently cut hackberry tree. The levee is composed of dry clay (CL-CH) according to the Unified Soil Classification System (USCS).

EM survey

Data acquisition and processing

A Geonics Ltd. EM38-MK2 conductivity meter was used with Tx-Rx coils set at fixed distances of 0.5 and 1.0 m and operated in the vertical dipole mode. Data were collected along seven 8-m-long survey lines spaced 0.5 m apart and oriented parallel to the axis of the levee. Conductivity and in-phase data for both coil separations were collected simultaneously.

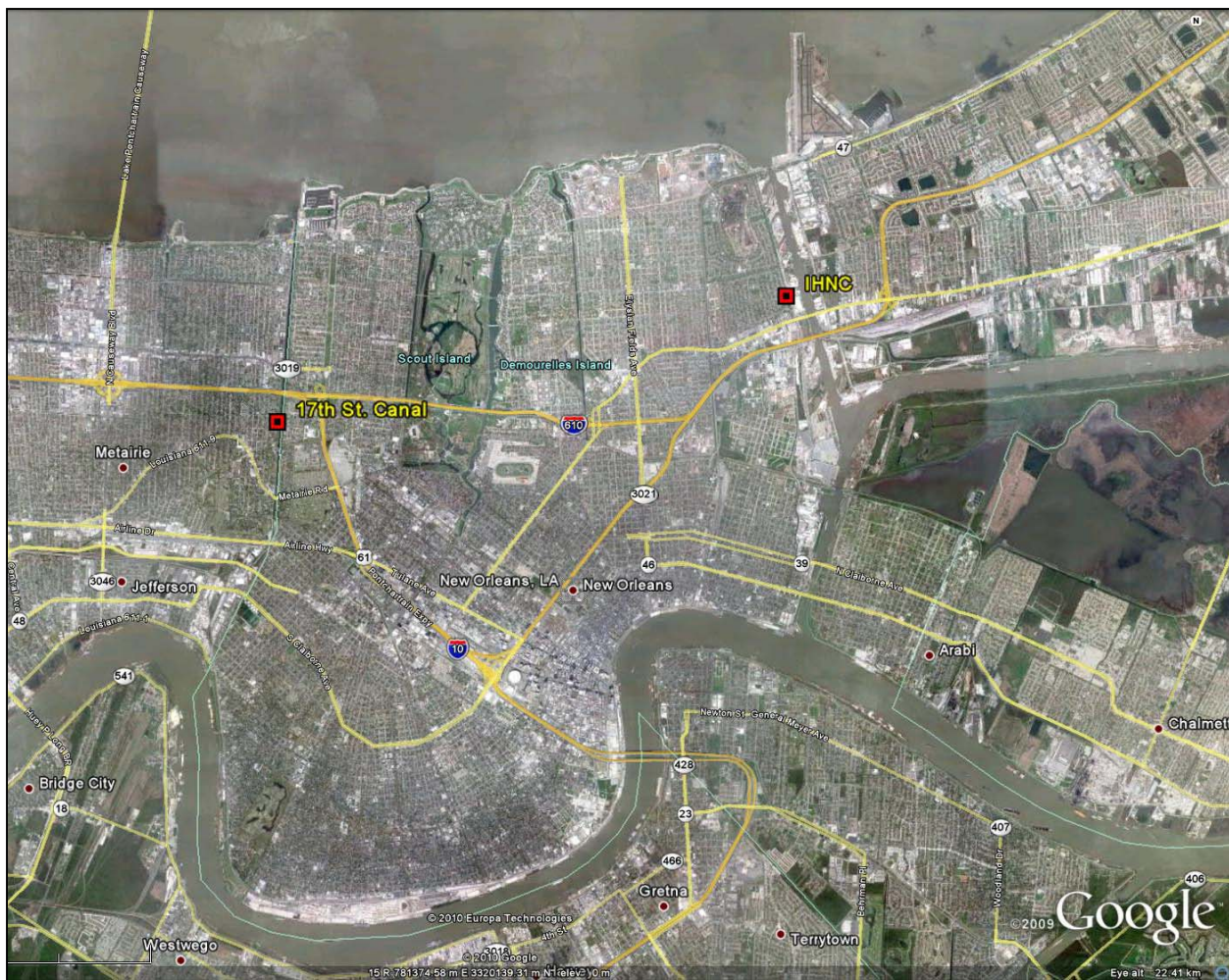


Figure 155. IHNC and 17th Street geophysical study sites, New Orleans, LA.

Data interpretation

The data are plotted as contour maps of conductivity and in-phase values for the 0.5- and 1.0-m inter-coil separations. Figures 157 and 158 present the conductivity survey results for the 0.5- and 1.0-m coil spacing, respectively. The conductivity results for the 0.5-m survey show that the majority of the values are below 50 millisiemens per meter (mS/m) whereas the majority of the conductivity readings for the 1.0-m survey range between approximately 65 and 105 mS/m. The increase in conductivity values for the 1.0-m surveys is presumed to be caused by an increase in soil moisture with increasing depth. No anomalous conductivity values were observed, indicating the presence of the root zone of the stump in the data.

Figures 159 and 160 present the in-phase survey results for the EM38-MK2 0.5- and 1.0-m coil spacing, respectively. The 0.5-m results (Figure 159) indicate that the majority of the readings are in the general range of



Figure 156. Geophysical test grid on levee slope near recently cut test tree, IHNC Site, New Orleans, LA.

-0.40 to -0.05 parts per thousand (ppt). Small anomalous features are indicated at ($X = 0, Y = 5.75$) and ($X = 1, Y = 11.5$).

The 1.0-m results (Figure 160) show that the majority of the readings generally range between 0.65 and 1.20 ppt. Anomalous features are again indicated at ($X = 0, Y = 5.75$) and ($X = 1, Y = 11.5$). The areal extents of the anomaly is relatively deep. No anomalous in-phase values were interpreted, which would indicate the presence of a tree root zone.

GPR survey

Data acquisition and processing

A 3-D-Radar Geoscope with B1831 antenna array was used in this study. The GPR antenna array was vehicle-towed at an antenna height 10 cm above the ground surface. The GPR data were acquired along survey lines parallel to the levee crest along the levee slope. The tree stump was located 0.8 m from the 0-m line at the toe of the levee. The survey lines were centered on meter markers and spaced 1 m apart providing approximately

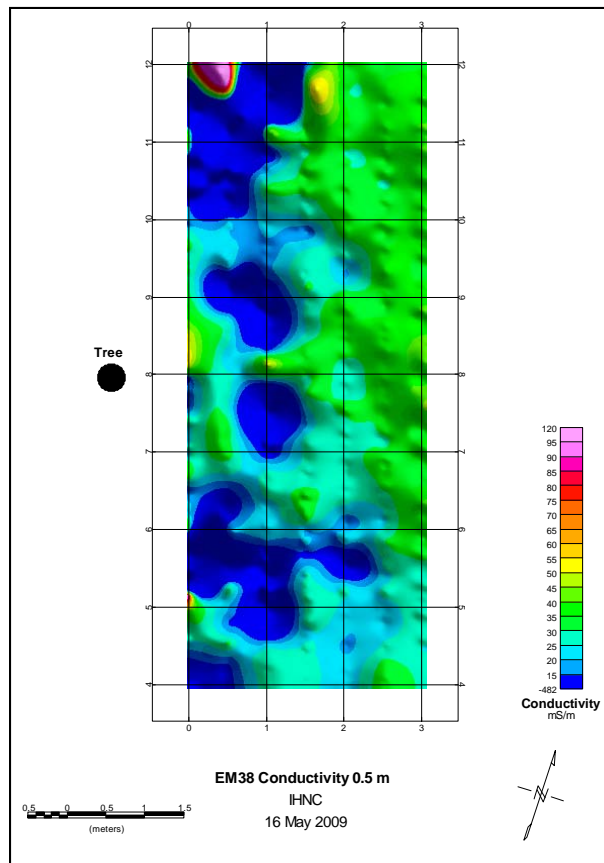


Figure 157. EM38 conductivity results, 0.5-m, IHNC Site, New Orleans, LA.

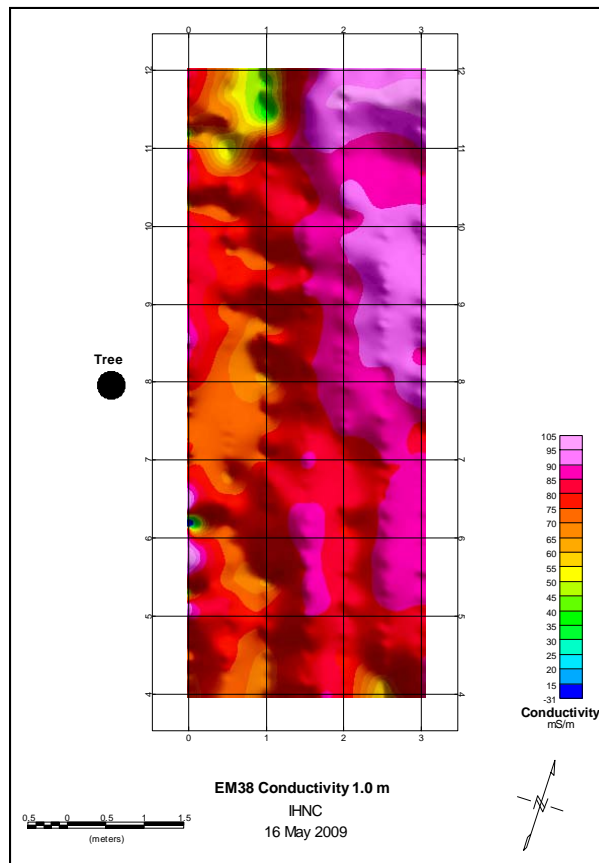


Figure 158. EM38 conductivity results, 1.0-m, IHNC Site, New Orleans, LA.

50 cm of overlap from line to line. Four lines were surveyed (1E-4E) (Figure 161). The levee crest is located east of the survey area. Depth of investigation is no greater than 0.5 m, based on a subsurface electromagnetic wave velocity of 0.07 m/ns. The processing steps used in the analysis of the GPR data are described earlier in this chapter.

Data interpretation

A plan view of the radar data at an approximate depth of 8 cm is shown in Figure 162. An in-line GPR section along line 0.44E (location of line in plan section) is also shown. Both the plan view and in-line section show an anomalous region adjacent to the stump location. This region extends about 1.8 m from the stump and is about 1 m wide.

Data interpretation

A plan view of the radar data at an approximate depth of 8 cm is shown in Figure 162. An in-line GPR section along line 0.44E (location of line in

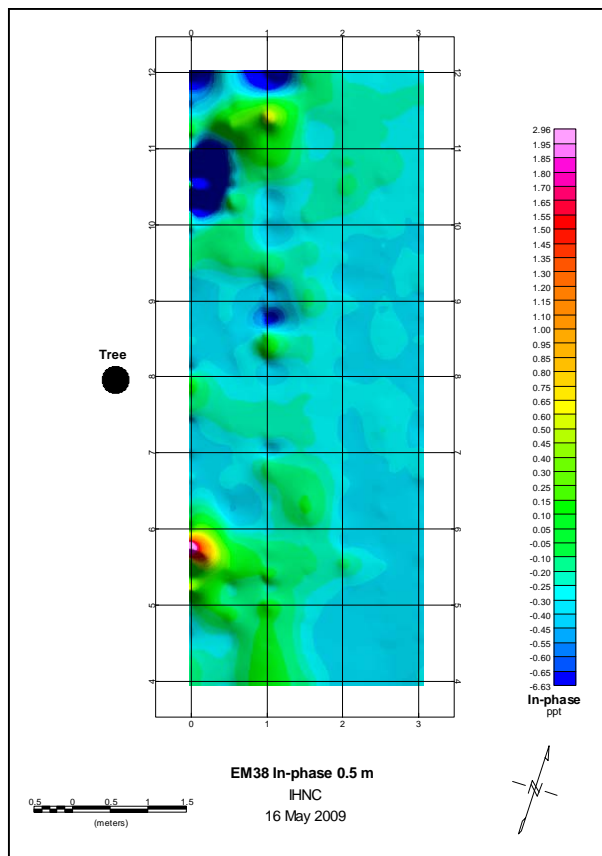


Figure 159. EM38 in-phase results, 0.5 m, IHNC Site, New Orleans, LA.

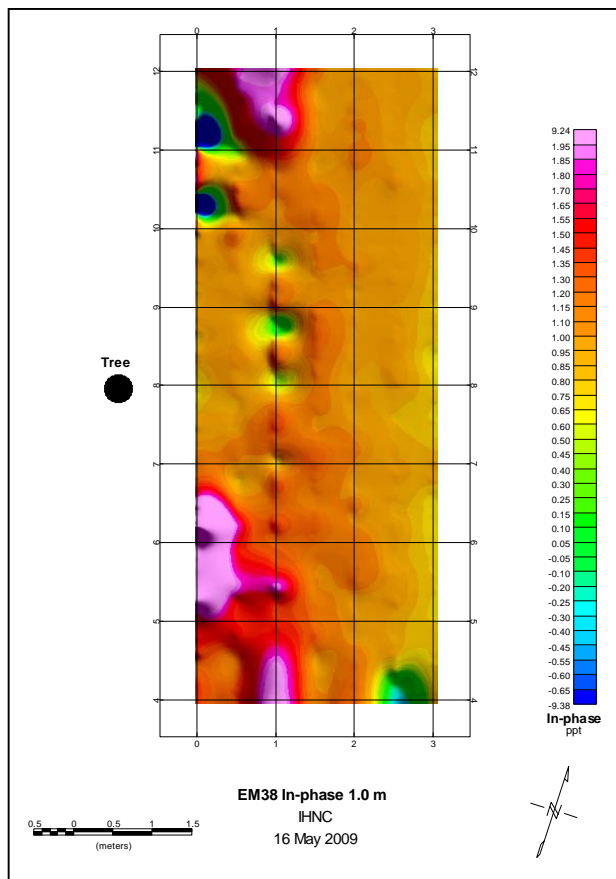


Figure 160. EM38 in-phase results, 1.0 m, IHNC Site, New Orleans, LA.

plan section) is also shown. Both the plan view and in-line section show an anomalous region adjacent to the stump location. This region extends about 1.8 m from the stump and is about 1 m wide.

17th Street Canal site

The study site is located on the protected slope of the west side of the 17th Street Canal approximately 6 km northwest of downtown New Orleans, LA (Figure 155). Reportedly, the levee consists of clay soils. Two oak tree stumps, approximately 37 m apart and located about half way up the grassy levee slope, are found within the site (Figure 163). The oak trees had been cut approximately two years prior to the survey. The diameters of the northern and southern stumps measure 1.1 and 0.9 m, respectively. The relative elevation difference between the toe and crest of the levee is approximately 4 m.

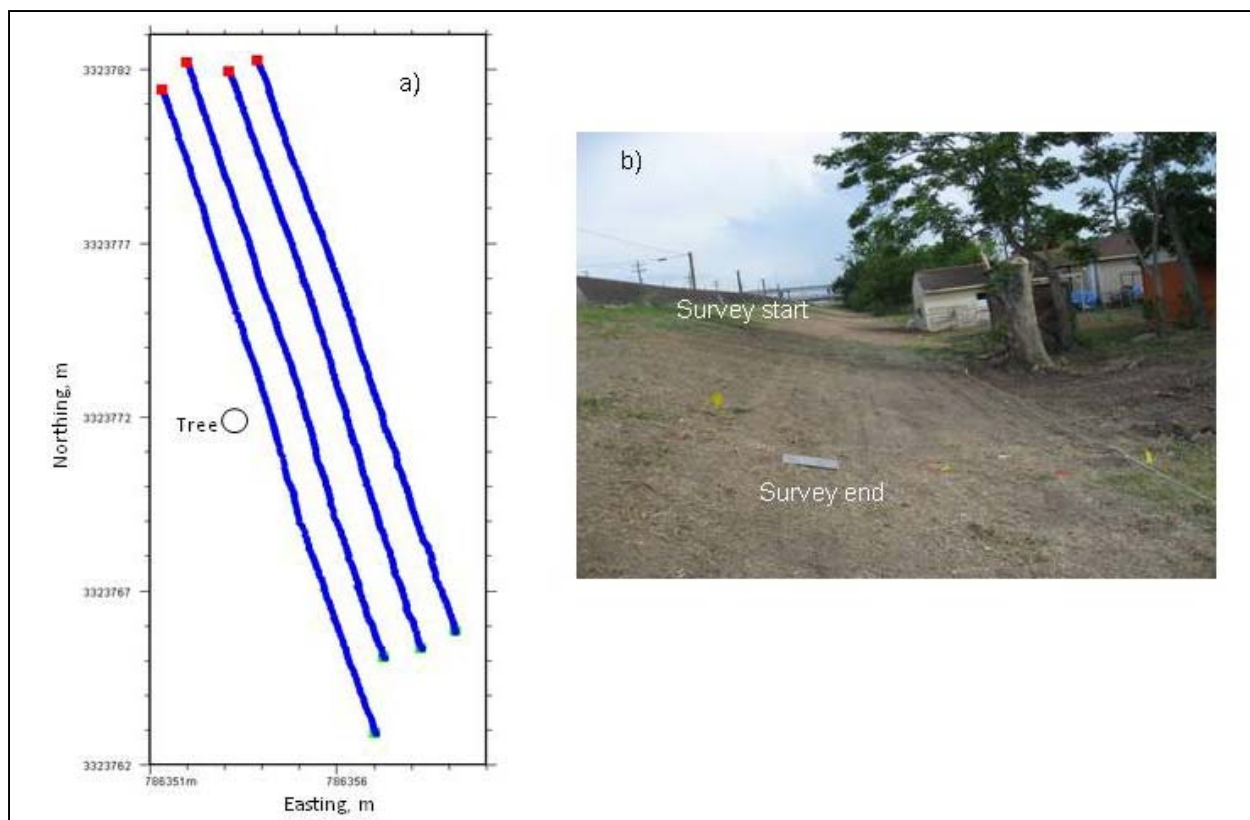


Figure 161. Survey area (a) and photograph looking towards the southeast (b), IHNC Site, New Orleans, LA. The GPR survey line locations (a) are represented by blue lines; the green and red squares mark the start and end, respectively, of a GPR survey line. The black circle indicates the tree stump location.

EM survey

Data acquisition and processing

A Geonics Ltd. EM38-MK2 conductivity meter was used with Tx-Rx coils set at fixed distances of 0.5 and 1.0 m and operated in the vertical dipole mode. Conductivity and in-phase data for both coil separations were collected simultaneously. Data were collected along thirteen 53-m-long survey lines spaced 0.5 m apart and oriented parallel to the axis of the levee (Figure 164).

Data interpretation

The data are plotted as contour maps of conductivity and in-phase values for the 0.5- and 1.0-m inter-coil separations (Figures 165 and 166). The conductivity results for the 0.5-m survey show that the majority of the values are in excess of 70 mS/m, whereas the majority of the conductivity readings for the 1.0-m survey range between approximately 40 and 66 mS/m. The decrease in conductivity values between the 0.5- and 1.0-m

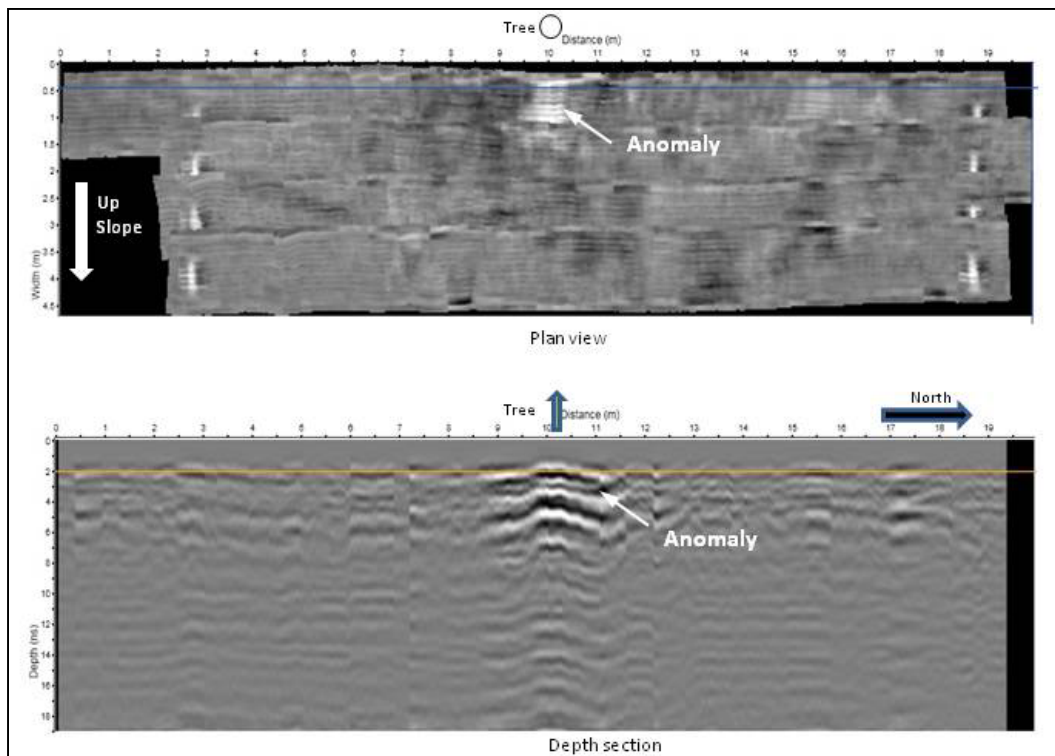


Figure 162. Plan view (top) of radar section at approximately 8-cm depth. The circle marks the location of the stump. Depth section (bottom) along line 0.44E (location of line in the top section), IHNC Site, New Orleans, LA.



Figure 163. Location of 17th Street Canal Site, New Orleans, LA.

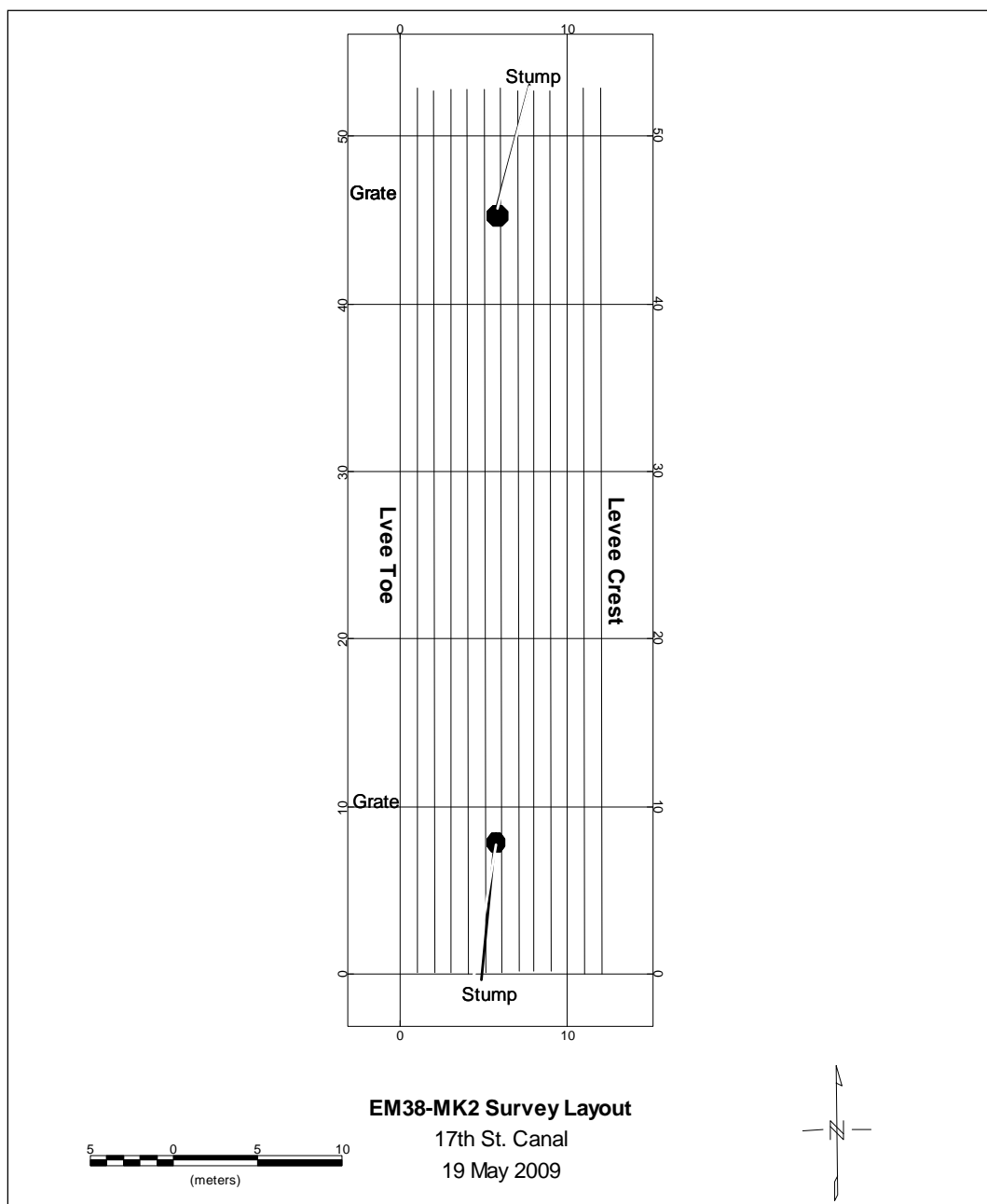


Figure 164. EM38 survey line layout, 17th Street Canal Site, New Orleans, LA.

surveys suggests a reduction in soil moisture or percentage of fine-grained soil with increasing depth, or both. The small (1- to 2-m-diam.) localized anomalous features seen in Figures 165 and 166 are presumed to be caused by shallowly buried metallic objects. The relatively high-valued northsouth oriented conductivity feature seen on the western edge of the site for both the 0.5- and 1.0-m surveys is caused by a buried steel drainpipe. The 0.5-m survey shows a relatively low-valued anomalous area in the vicinity of the northern stump. This anomaly is most likely caused by a buried

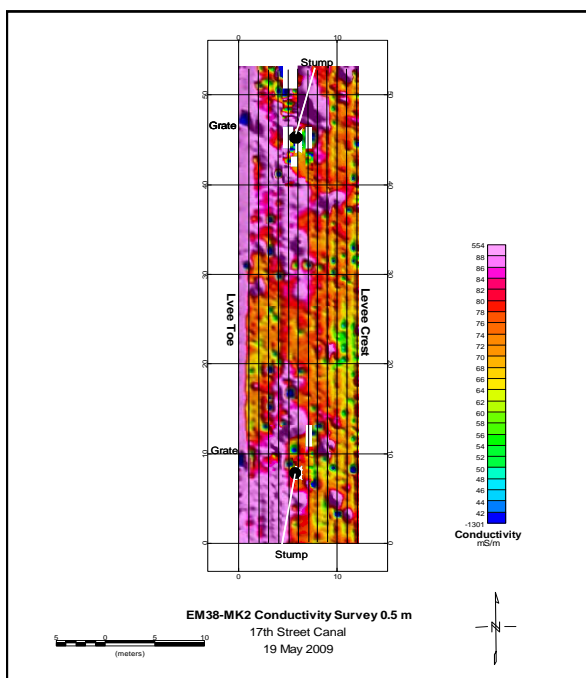


Figure 165. EM38 conductivity results, 0.5 m, 17th Street Canal Site, New Orleans, LA.

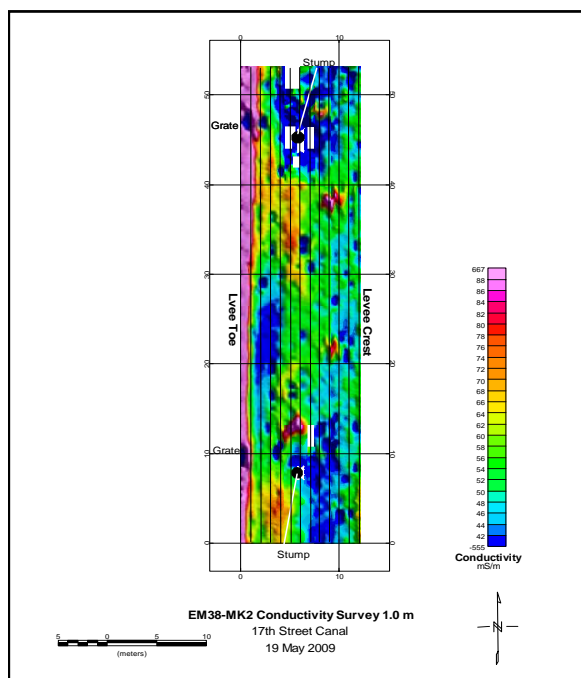


Figure 166. EM38 conductivity results, 1.0 m, 17th Street Canal Site, New Orleans, LA.

metallic object rather than by the tree's root zone. The 1.0-m conductivity survey indicates areas of relatively low-valued readings (less than 42 mS/m) in the vicinity of both stumps. However, as these low-valued conductivity zones exist in other portions of the site, they probably do not indicate the stumps' root zone. No anomalous conductivity values indicating the presence of the root zone of either stump were interpreted from the data results.

Figures 167 and 168 present the in-phase survey results for the EM38-MK2 0.5- and 1.0-m coil spacing, respectively. The 0.5-m results (Figure 167) indicate that the majority of the readings are in the general range of -0.2 to 0.6 ppt. In the northern portion of Figure 167, there is an area with relatively lower values. The 1.0-m results (Figure 168) shows that the majority of the readings generally range between -2.0 and -1.0 ppt. An area of high-valued readings that is greater than 2.0 ppt is visible in the northwestern portion of Figure 168 and is most likely caused by buried metallic debris. As also shown in the conductivity plots, a high-valued linear anomaly caused by a buried steel drainpipe along the western edge of the site is clearly evident. Several prominent localized anomalies are scattered throughout the site and are presumed to be caused by small, buried metallic objects. No anomalous in-phase values indicating the presence of the root zone of either stump were present in the data sets.

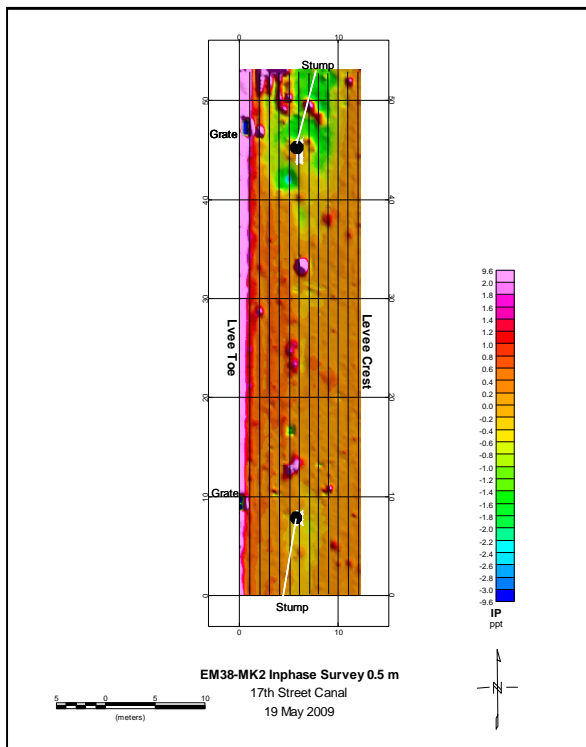


Figure 167. EM38 in-phase results, 0.5 m, 17th Street Canal Site, New Orleans, LA.

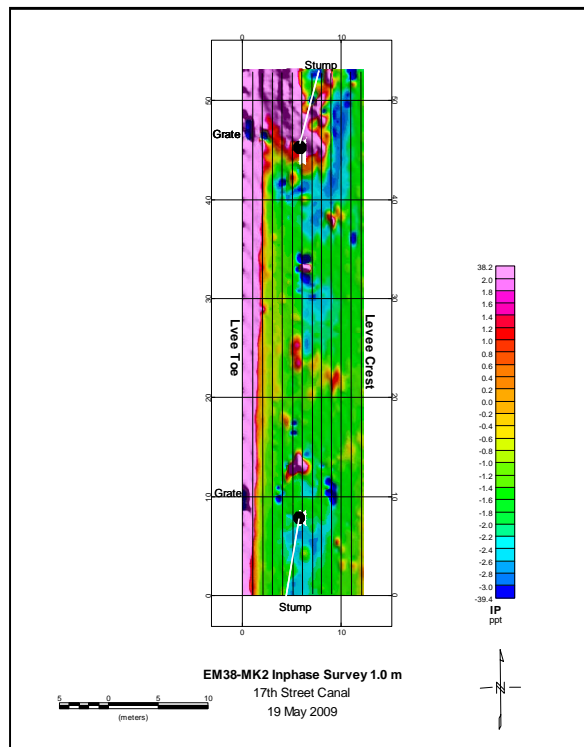


Figure 168. EM38 in-phase results, 1.0 m, 17th Street Canal Site, New Orleans, LA.

GPR survey

Data acquisition and processing

The GPR data were acquired along survey lines parallel to the levee crest along the levee slope. The survey lines were centered on meter markers and spaced 1 m apart. Ten lines (1E-5E, 6.5E, and 7E-10E) were surveyed. The data acquired along the first line (1E) were not usable. There are two drain grates along the line located at the toe of the levee (0-m). Figure 169 shows the location of the tree stumps, drain grates, and GPR survey lines. The GPR processing steps used in this study are described earlier in this chapter.

Data interpretation

Figure 170 shows a plan view of the GPR data at approximately 6-cm depth and a radargram along line 7E at 777429.534. The radar swaths adjacent to the stumps show a change in reflection characteristics near the stumps, especially on the east side. Because of the distance the east GPR track is from the northern stump, there is some doubt whether or not the variation in reflections is caused by the tree.

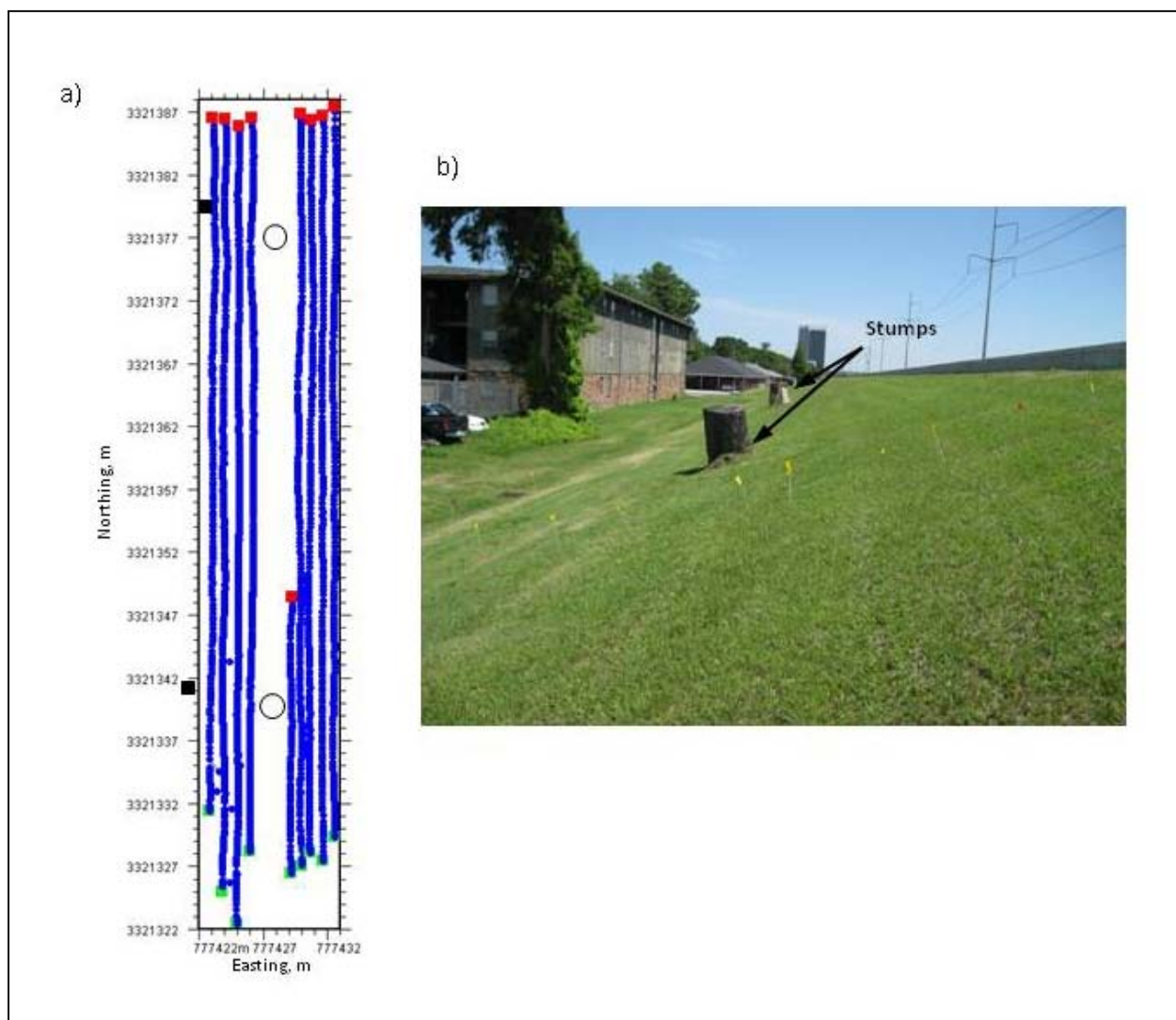


Figure 169. Survey area (a) and photograph (b) at 17th Street Canal, New Orleans, LA. The GPR survey lines (a) are represented by blue GPS-derived dots; the dots off of the survey line are outlier GPS points; the green and red squares mark the start and end, respectively, of a survey line. The circles indicate the stump locations; black squares the drain grates.

Summary

EM and GPR data were collected adjacent to tree stumps at two clay levee sites in New Orleans: IHNC and 17th Street Canal. The tree at the IHNC Site, located at the toe of the levee, had been cut within two weeks of the survey whereas the two trees at the 17th Street Canal Site, located on the levee slope, had been cut approximately two years prior to the survey.

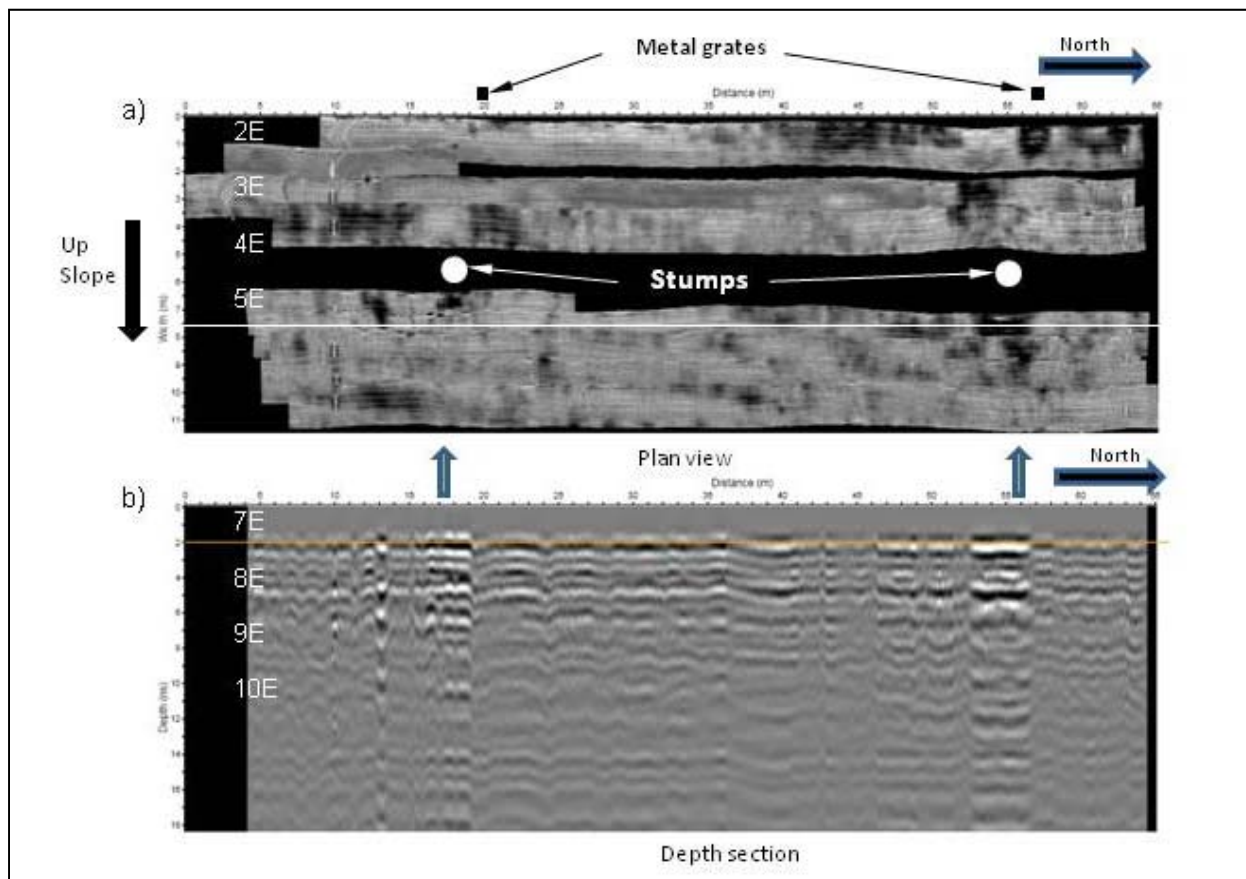


Figure 170. 17th Street Canal Site: (a) Plan view of radar section at approximately 6-cm depth. The solid white circles mark the locations of the stumps; black squares are drain grates. (b) Inline section along line 7E at 777429.534 (white line in a).

Influence of the tree stump on the surrounding soil is evident in the GPR section acquired at the IHNC Site. It is not definitive, however, that GPR signatures near the 17th Street Canal Site stumps are caused by the stumps because similar features are apparent elsewhere in the GPR section. It is likely that there is a correlation between the age of the stumps and the ability of GPR to detect a zone of influence around the stump. No indications of a tree root zone were observed in the EM data at either site.

Vicksburg, MS

Background

Two geophysical methods (ERI and GPR) were used to find the maximum detectable extent of the tree root distribution of an oak tree, located approximately 17 km southeast of Vicksburg, MS (Figure 171). The investigation was conducted by ERDC personnel on 25 and 30 March 2010.



Figure 171. Location of test site, Vicksburg, MS.

Study site

A 13- by 7-m test site, centered on the study tree, was established on a slight incline. The incline slopes downward towards the northeast. The long axis (x-axis) of the test site runs approximately parallel to the contours of the slope (Figure 172). The study tree, a southern red oak (*Quercus falcata*), has a crown width of 7.16 m cross slope and 7.83 m upslope, an approximate height of 7.6 m, and a trunk diameter of 0.29 m at chest height (Figure 172).

Geophysical survey methods

ERI survey

Data acquisition and processing

A 3-D ERI grid measuring 7 by 13 m was established around the study tree (Figure 173). The rectangular grid consisted of electrodes positioned 1 m apart. Stainless steel rods, approximately 1 cm in diameter, were driven vertically into the ground to a depth of about 0.3 m and used as electrodes.



Figure 172. Test grid layout and test tree, Vicksburg, MS.

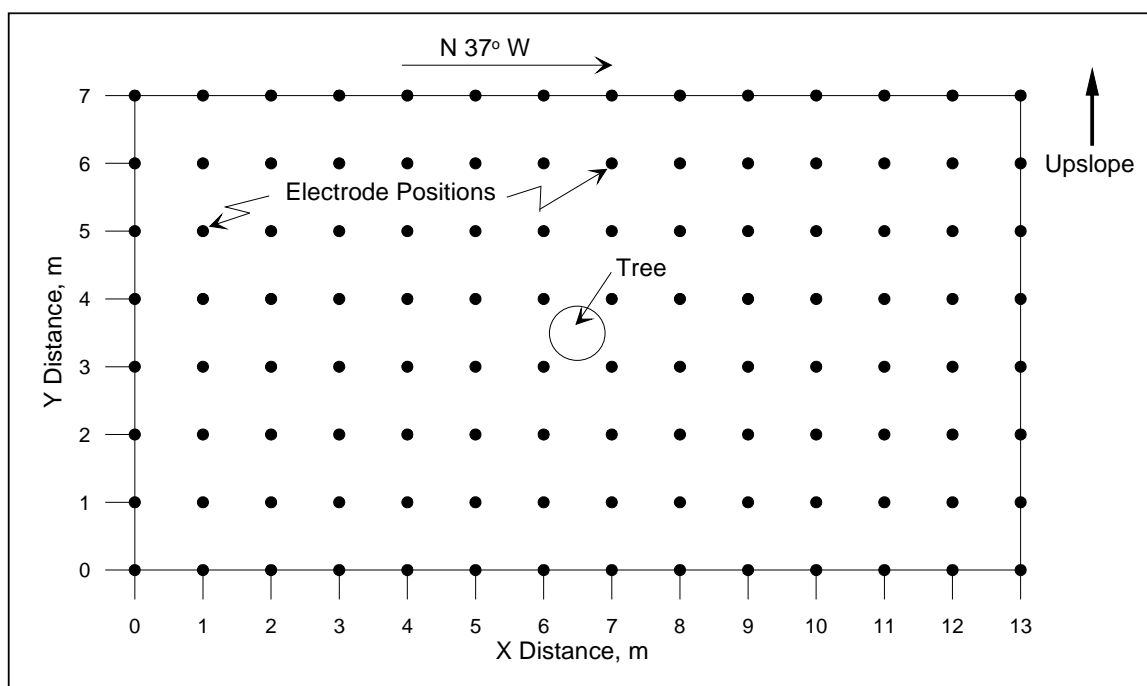


Figure 173. 3-D ERI layout, Vicksburg, MS.

The electrodes were connected to a multi-conductor cable, which was coupled to an Advanced Geosciences, Inc., SuperSting R8 resistivity meter with the Smart electrode switching system. Figure 174 shows the electrode layout and the location of the tree within the ERI grid. The 3-D resistivity data were inverted using EarthImager 3-D software.

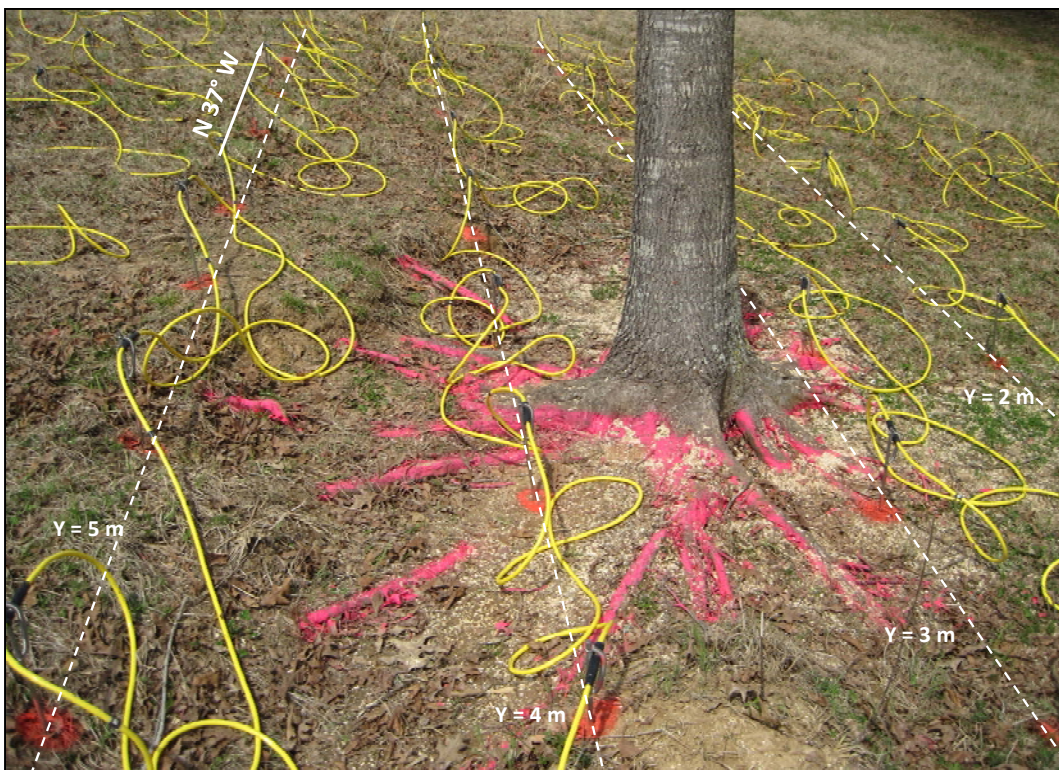


Figure 174. Location of electrical resistivity lines relative to the test tree, Vicksburg, MS.

Data interpretation

An inverted resistivity image of the 3-D grid is shown in Figure 175. The black oval in the center of the grid shows the tree's approximate position. The dots on the figure represent the electrode locations, which are spaced 1 m apart. The maximum depth of investigation is approximately 3.25 m. The inverted resistivity image shows the uppermost layer being about 2 m thick with resistivity values ranging between approximately 50 and 65 $\Omega\text{-m}$ and underlain by a lower resistivity layer. There is an area in the center of the grid surface with anomalously high resistivity values that corresponds to the location of the tree.

Figures C176 through C185, in Appendix C, show depth slices of the inverted resistivity image taken at 0.25-m depth intervals between depths

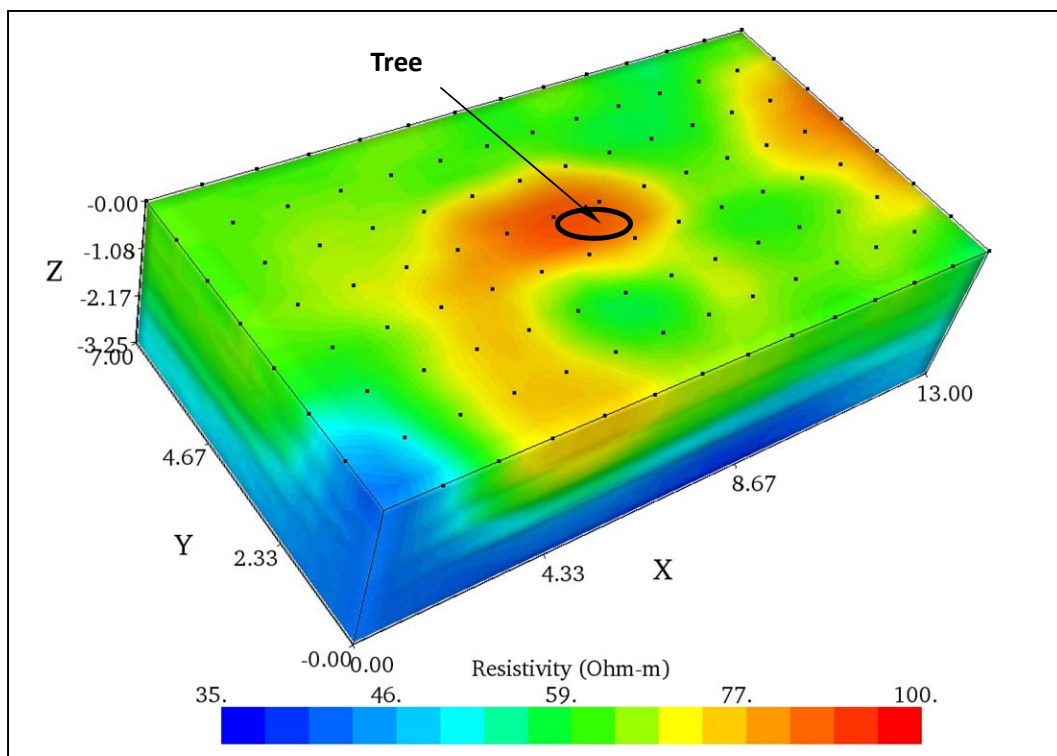


Figure 175. 3-D inverted resistivity image, Vicksburg, MS.

of 0 and 1.50 m and at 0.50-m intervals between 1.50 and 3.00 m. The black oval represents the approximate location of the base of the tree on the ground surface of the 3-D inversion image; the gray oval is the projected surface location of the tree on the depth slice surface.

There is a relatively high resistivity area, approximately 3.5 by 2 m, near the center of the test section, and it is evident from a depth of 0 to 1.25 m. This high resistivity area is presumed to indicate the maximum detectable extent of the tree root zone. As the depth of the slices increase, the intensity and size of the high resistivity zone decrease. At a depth of 1.50 m, the high resistivity zone is no longer visibly apparent. Based on the ERI results, the depth of the root zone is assumed to be between 1.25 and 1.50 m.

Figures C186 through C193, in Appendix C, show slices of the inverted resistivity image taken parallel to the x -axis between $Y = 2.00$ and $Y = 6.00$ m. The black oval represents the location of the tree on the ground surface. As the slices progress from 2.00 to 6.00 m, a high resistivity area occurs at $Y = 3.00$ m and reaches maximum values and extent between $Y = 3.5$ and 4.00 m—the vicinity of the tree. The high resistivity area fades

away between $Y = 5.00$ and 6.00 m. Another relatively high resistivity area with lower values than the area around the tree is seen along $X = 13$ m. No visible surface features were observed that would cause such an anomaly.

GPR survey

Data acquisition and processing

A pE 1000 GPR system, having 450- and 900-MHz frequency antennas in the profiling survey mode, was used for these tests. In this mode, the receiving and transmitting antennas are kept a fixed distance apart as the antenna pair is pulled slowly along a survey line. Separations of 0.25 and 0.17 m with the 450- and 900-MHz antennas, respectively, were used. Data traces were collected every 0.05 and 0.02 m along each survey line with the 450- and 900-MHz antennas, respectively. Although the pE 1000 system is flexible enough to vary the antenna separation, the separations used in this study are those suggested by the GPR manufacturer. The 450-MHz data were collected at 0.5-m line intervals between $Y = 3.5$ and 7.0 m and the 900-MHz data were collected at 0.5-m intervals between $Y = 1.0$ and 6.0 m. Figure 176 shows the locations of the GPR survey lines. The programs EKKO View Deluxe and EKKO View (Sensors & Software, Inc.) were used to analyze and present the GPR data.

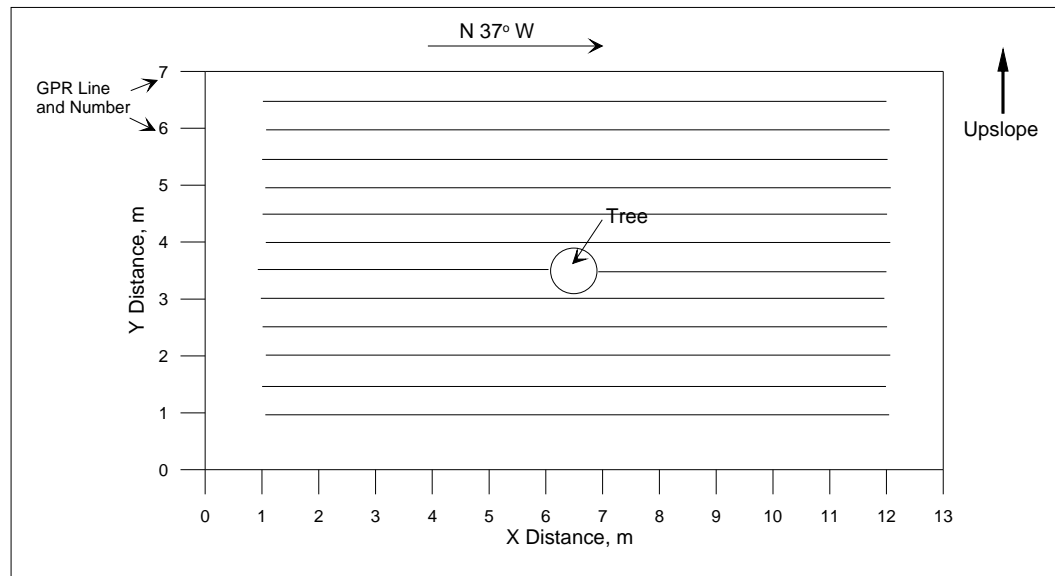


Figure 176. GPR survey line layout, Vicksburg, MS.

Data interpretation

The GPR results are presented as 2-D cross sections (radargrams), where the X-axis is distance along the survey line and the Y-axis is the two-way

travel time in nanoseconds (ns). Figure 177 shows a typical radar section. An assumed velocity of 0.075 m/ns, typical of the loess soils found in this area, was used to compute the depth scale shown on the right-hand side of each profile. The lack of coincidence between zero time and zero depth in the GPR profiles is ascribable to the separation of the transmitter and receiver antenna. The first arrival at the receiver is the direct wave traveling from the transmitter to the receiver, not the reflection from the ground surface. The time span between zero time and zero depth is the one-way travel time of the direct wave between the transmitter and the receiver.

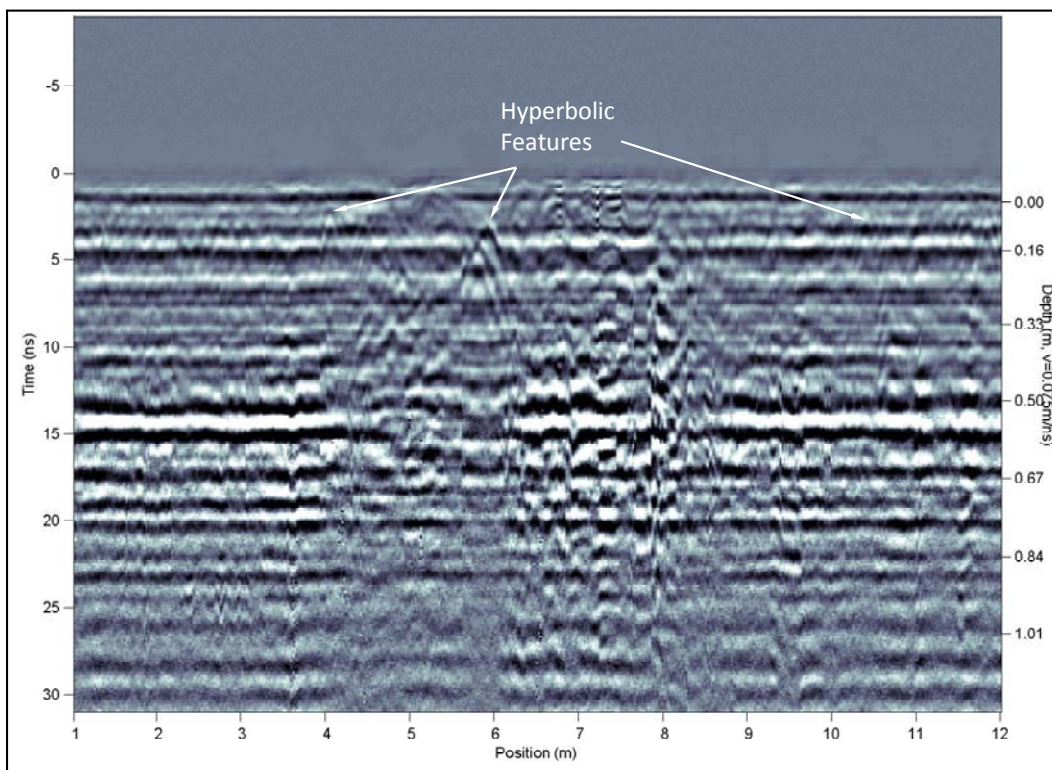


Figure 177. Typical GPR cross section showing hyperbolas presumably caused by tree roots.

The depth scale, in particular at very shallow depths, is nonlinear. The depth scale is based on the velocity of the transmitted EM pulse through the propagating media. Because the transmitter and receiver antenna are separated by a finite distance and the transmitted pulse has a lobe-shaped radiation pattern, the ray of the transmitted pulse that arrives at the receiver does not strike the subsurface interface at normal incidence, but at an acute angle. The depth scale is corrected for non-normal incidence of the transmitted ray path. The peaks of the hyperbolas indicate the lateral and vertical position of a buried object.

450-MHz Data

GPR surveys were run along the X direction between $X = 1$ and $X = 12$ m and between $Y = 3.5$ and $Y = 7.0$ m; they are presented as radargrams (Figures C194 through C201, in Appendix C). The depth of investigation for the 450-MHz antennas is approximately 1 to 1.25 m. A gap is present in the $Y = 3.5$ m radargram (Figure C194) because of the presence of the tree in the middle of the survey line. The radargrams between 3.5 and 5.0 m show areas of disturbance interpreted as caused by the tree root zone. As the GPR lines move away from the tree, the size of the disturbed area becomes smaller until, at line 5.5 m, there is little or no indication of the root zone.

900-MHz Data

GPR surveys were run along the X direction between $X = 1$ and $X = 12$ m and between $Y = 1.0$ and $Y = 7.0$ m; they are presented as radargrams (Figures C202 through C212, in Appendix C). The depth of investigation for the 900-MHz antennas is approximately 0.75 to 1 m. A gap is present in the $Y = 3.5$ m radargram (Figure C207) because of the presence of the tree in the middle of the survey line. The 900-MHz radargrams show greater resolution than those from 450-MHz. The 900-MHz radargrams are able to resolve much thinner layers and also can discriminate smaller objects as shown by the numerous hyperbolas. The radargrams collected within 1.5 to 2.0 m on either side show numerous hyperbolas at less than 0.25 m depth that may be caused by tree roots. Evidence of possible tree roots can be seen along individual lines between approximately $X = 4$ and $X = 8$ m, as indicated by numerous hyperbolas and discontinuities in layering.

Conclusions

GPR and 3-D ERI surveys were used to noninvasively map the root zone distribution of a lone southern red oak (*Quercus falcata*) tree located on a gentle slope. The tree is centered within a 13- by 7-m test site located approximately 17 km southeast of Vicksburg, MS. The tree has crown widths of 7.16 m cross slope and 7.83 m upslope, an approximate height of 7.6 m, and a trunk diameter of 0.298 m at chest height.

ERI was used to determine potential differences in electrical resistivity values between the root zone and the background soil. The ERI results point to a volume of soil with relatively high electrical resistivity, which is interpreted to be the maximum detectable root zone. It measured approximately 3.6 m long, 1.8 m wide, and 1.0 m deep in the vicinity of the tree.

A series of GPR survey lines using 450- and 900-MHz antennas were run within the test site to locate roots and the root zone. The 450-MHz antenna, while able to detect areas interpreted to be the location of the main root zone, was not able to discern individual roots. The 450-MHz antenna detected a maximum root mass diameter of approximately 5 m cross slope. The 900-MHz antenna, with the greater resolving power, was able to map the root zone and what appeared to be individual roots. Root mass lengths of approximately 4.5 m cross slope and 3.5 m upslope were interpreted from the 900-MHz antenna system. The maximum depth of investigation of the 450- and 900-MHz antennas is approximately 1.25 and 1 m, respectively.

The objective of conducting the surface-based geophysical investigations reported in this study was to determine which, if any, method could detect tree roots and, if so, to what depth and lateral extent they could be traced. GPR and ERI had the greatest success in detecting tree roots and the root zone extent. Each of the methods has its strengths and limitations. As mentioned previously in Section II, the ability of these methods to detect a tree's individual roots or root zone depends primarily on the degree of contrast in electrical and/or magnetic properties or between the root/root zone and the surrounding soil matrix. If the root diameter and or the root ball mass are too small then the contrast may be insufficient, thus making it impossible to detect them.

A limitation of the ERI method is that the measured reading at a given point is a weighted average of the effects over a large volume of material. This causes the detection or resolution of smaller targets to become more difficult as a function of depth. The distribution of resistivity readings on the ground surface can be accurately modeled given the number of layers, layer thicknesses and layer resistivity values (forward modeling). However, the ERI inversion process (the process by which the distribution of subsurface resistivity values are determined) does not provide a unique interpretation. The more information is known about the subsurface conditions (i.e., number of layers, layer thicknesses, etc.) and can be input into the resistivity inversion program the higher the confidence of the inversion results. This is why having prior information about subsurface conditions, whether from borings or other geophysical exploration methods, is so important in forming a more accurate picture of the subsurface. A high degree of subsurface heterogeneity, large topographical gradients and very dry surface soils can influence the quality of the readings and affect

interpretation results. High contact resistance problems occur when the near surface soils are so resistive (usually caused by extremely dry surface soil) that the current electrode has difficulty injecting current into the ground. In this case, salt water is usually poured around the base of the electrodes to lower the electrode-soil contact resistance. Other factors that affect electrical resistivity surveys are the presence of metallic fences, rails, pipes, or other soil-contacting conductors that could provide a short circuit path.

Perhaps a better way to map the extent of a root zone of a living tree is to monitor the electrical resistivity around the tree over a long time period rather than just taking a “snap shot” reading in time. By conducting periodic 3-D surveys over a long time period it may be possible, for example, to detect changes in resistivity values caused by water uptake by the tree during a growing season.

A summary table of the geophysical methods and the results of the application of these surveys are provided in Table 36.

In situ root architectural subsampling

Invasive samples were taken to validate the noninvasive techniques at the four sites summarized in Table 29. A subsampling approach was applied in Sacramento, Albuquerque, and Burlington while complete excavation was applied in Vicksburg. Regardless of the extent of excavation, each site required both field and laboratory analyses as well as significant post-processing. This section summarizes methods applied as well as properties of the root systems investigated.

Sample design

In Sacramento, Albuquerque, and Burlington, subsamples consisted of 1-m² cells randomly selected from a sampling grid oriented parallel to levee alignment and extending to the canopy line with the sample tree approximately in the center. Four subsamples were collected for each test tree. A stratified-random sampling protocol was used to select cells based on whether inner and outer domains were specified (Figures 178 through 181). Two domains were used to select cells with a range of root densities

Table 36. Summary of the geophysical methods and results of the application of these surveys.

Location	Site Description ^a	Survey Results Summary					
Sacramento, CA 38°29'20" N 121°33'05" W	<p>A reach of sandy levee in urban Sacramento on the east bank of the Sacramento River. The sample tree was located midslope on the landside of the levee. Mean annual temperature is 16.2°C. Mean annual rainfall is 4.5 cm. Prevailing winds are from the south.</p> <p>Valley oak (<i>Quercus lobata</i> Née) 75 cm DBH^c 16.8 m drip line 15 m height Soil: silty sand GPR: individual roots probably detected but subsurface clutter makes it difficult to identify them.</p>		Mapped lateral influence of tree root zone with respect to levee axis	Method	Parallel (m)	Perpendicular (m)	Depth (m)
		ERI (avg)	1.6	1.5	1.6		
		GPR	1.4	1.7	0.35		
		EM	No correlation with tree root zone				
	<p>Soil: silty sand</p> <p>GPR: individual roots probably detected but subsurface clutter makes it difficult to identify them.</p>	SME	Average Moistured ^d (%)	Average Root Volume (m ³)	Average Root Volume Ratio (= root vol / cell vol)		
			8.92	0.02104	0.02547		
Albuquerque, NM 35°08'33.35" N 106°40'34.54" W	<p>Site 1 – A reach of sandy levee in urban Albuquerque on the east bank of the Rio Grande River south of Montano Boulevard. The sample tree was located on the waterside of the levee approximately 15 m from the levee toe.</p> <p>Fremont cottonwood <i>Populus fremontii</i> 41 cm DBH 10.7 m drip line 11 m height Soil: sand (poorly graded)</p>	Site 1	Mapped lateral influence of tree root zone with respect to levee axis				
			Method	Parallel (m)	Perpendicular (m)	Depth (m)	
35°09'55.23" N 106°40'01.21" W	<p>Site 2 – A reach of sandy levee in urban Albuquerque on the west bank of the Rio Grande River north of Montano Boulevard. The sample trees were located on the waterside of the levee approximately 10 m from the levee toe.</p> <p>2 Fremont cottonwoods <i>Populus fremontii</i> 58 cm DBH 14 m drip line</p>	Site 2	Mapped lateral influence of tree root zone with respect to levee axis				
			Method	Parallel (m)	Perpendicular (m)	Depth (m)	
		ERI	No correlation with tree root zone				
		SME	Average Moistured ^d (%)	Average Root Volume (m ³)	Average Root Volume Ratio (= root vol / cell vol)		
			7.91	0.03814	0.03814		

Location	Site Description ^a	Survey Results Summary			
			13.17	0.06555	0.07782
	<p>12 m height 27 cm DBH 9.2 m drip line 9 m height</p> <p>Soil: sand (well graded)</p> <p>Mean annual temperature is 13.8°C. Mean annual rainfall is 22.6 cm. Prevailing winds are from the north.</p>				
Burlington, WA 48°27'47" N 122°18'47" W	<p>Sample tree was 5 m from the levee toe on the waterside of the west bank of the Skagit River levee system. Mean annual temperature is 10.5 °C. Mean annual rainfall is 83.1 cm. Prevailing winds are from the south-southeast.</p> <p>Western red cedar <i>Thuja plicata</i> 143 cm DBH 12.2 m drip line 20 m height</p> <p>Soil: silty sand</p> <p>GPR: Individual roots detected.</p>		Mapped lateral influence of tree root zone with respect to levee axis		
		Method	Parallel (m)	Perpendicular (m)	Depth (m)
		ERI (avg)	10	10	1.5 -2
		GPR	12	12	0.62
		EM	10	10	---
		SME	Average Moistured ^d (%)	Average Root Volume (m ³)	Average Root Volume Ratio (= root vol / cell vol)
			15.18	0.05117	0.05117
Vicksburg, MS 32°12'41" N 90°48'21" W	<p>Test site was in a rural pasture approximately 14 km south of Vicksburg. Sample tree was on an embankment sloping gently from SW to NE at approximately 5 deg. Mean annual temperature is 18.6°C. Mean annual rainfall is 147.3 cm. Prevailing winds are from the south.</p> <p>Southern red oak <i>Quercus falcata</i> 29 cm DBH 7.5 m drip line</p>		Mapped lateral influence of tree root zone with respect to levee axis		
		Method	Parallel (m)	Perpendicular (m)	Depth (m)
		ERI	3.6	1.8	1.0
		GPR	4.5	3.5	---
		SME	Average Moistured ^d (%)	Average Root Volume (m ³)	Average Root Volume Ratio (= root vol / cell vol)

Location	Site Description ^a	Survey Results Summary			
	7.5 m height Soil: clay (lean)		---	0.2020	---
New Orleans, LA 30°00'41" N 90°01'52.63" W	IHNC Site – A reach of clay levee on the Inner Harbor Navigation Canal in an urban environment. The studied tree had been cut several days prior to the field study. The tree was located on the toe of the levee. The survey was conducted only on the levee side of the tree. Hackberry <i>Celtis occidentalis</i> 64 cm DBH Soil: clay GPR: Individual roots not detected.	Site 1	Mapped lateral influence of tree root zone with respect to levee axis		
		Method	Parallel (m)	Perpendicular (m)	Depth (m)
		GPR	1	1.8	---
		EM	No correlation with tree root zone		
29°59'15.33" N 90°07'29.71" W	17 th Street Site – A reach of clay levee on the 17 th Street Canal. Two oak tree stumps that had been cut approximately 2 years prior to the study were located halfway up the levee slope. The survey was conducted only on the levee side of the tree. Oak trees 110 and 90 cm DBH Soil: clay Mean annual temperature is 20.3°C, Mean annual rainfall is 157.2 cm. Prevailing winds are from the south.	Site 2	Mapped lateral influence of tree root zone with respect to levee axis		
		Method	Parallel (m)	Perpendicular (m)	Depth (m)
		GPR	---	---	---
		EM	No correlation with tree root zone		
Portland, OR 45°33'32" N 122°26'14" W	Test site is located approximately half way up the protected slope of a sandy levee. Eight trees, roughly in a 150-ft long line and parallel to the crest of the levee, were sampled. 8 Fremont cottonwoods <i>Populus fremontii</i>		Mapped lateral influence of tree root zone with respect to levee axis		
		Method	Parallel (m)	Perpendicular (m)	Depth (m)
		ERI	No correlation with tree root zone		
		GPR	NA	6.0	0.5

Location	Site Description ^a	Survey Results Summary				
	Diameter range approximately 50-100 cm DBH Overlapping drip lines Height ranges approximately 10-15 m Soil: sand GPR: Individual roots detected. Mean annual temperature is 11.9°C Mean annual rainfall is 112.6cm. Prevailing winds in summer are from the NNW and from the ESE in the winter.	EM	No correlation with tree root zone			
Lewisville, TX 33°03'51" N 96°59'15" W	The studied tree is located on the toe of the western end of Lewisville Dam. The site consists of clay soils. Post oak <i>Quercus stellata</i> 110 cm DBH 15 m drip line 10 m height Soil: clay (fat) Mean annual temperature is 17.8°C Mean annual rainfall is 86.6 cm. Prevailing winds are from the south.	Method	Parallel (m)	Perpendicular (m)	Depth (m)	
		ERI	3.5	2.7	1.5	
		EM	No correlation with tree root zone			

^a Temperature and precipitation values are average annual from the weather station closest to the site. (USDC 2010). Prevailing wind data are from WRCC (2010).

^b GPR – ground-penetrating radar, ERI – electrical resistivity imaging, EM – electromagnetic, SME – sub-sampled manual excavation.

^c DBH – diameter at breast height.

^d Gravimetric moisture content.

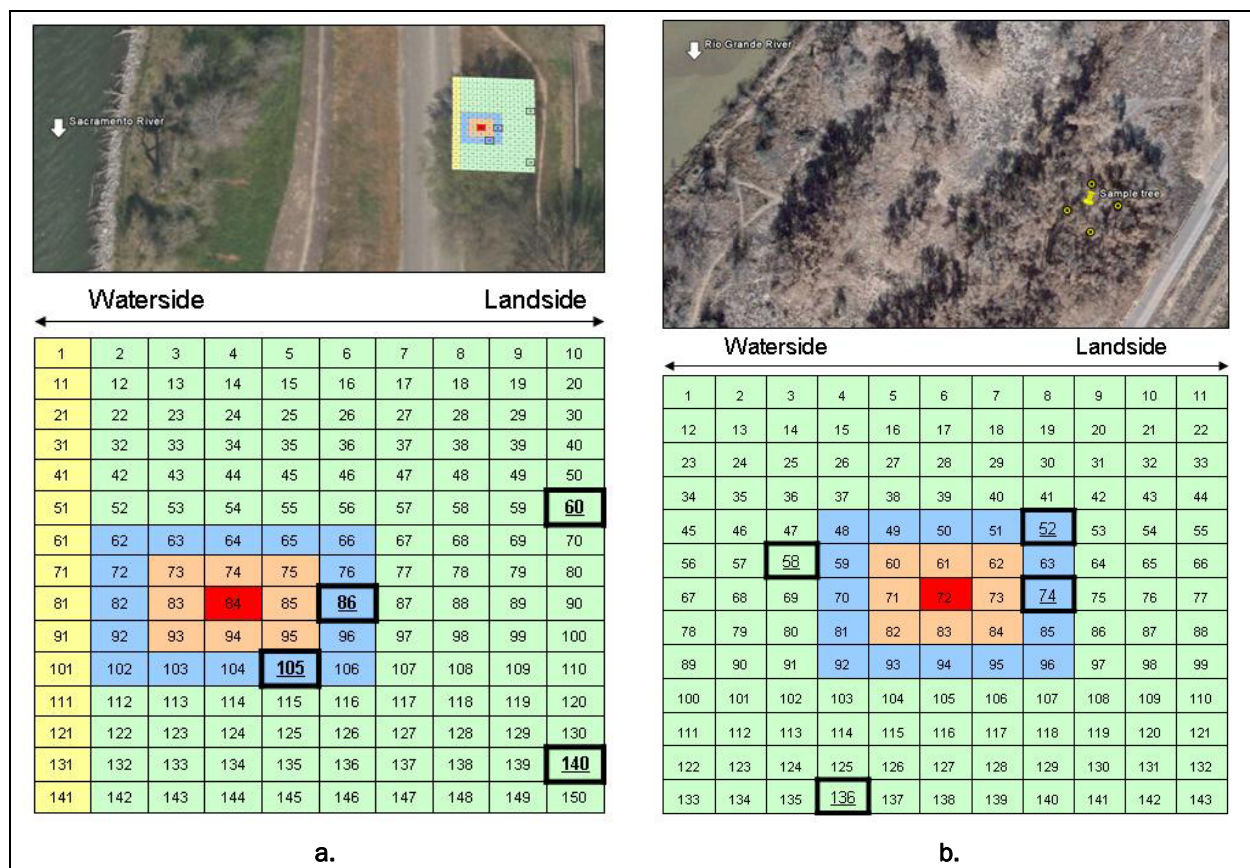


Figure 178. Stratified, random sample design for invasive measurement in:

- (a) Sacramento, (b) Albuquerque – Site 1, (c) Albuquerque – Site 2, and
- (d) Burlington. Cell colors indicate low-density root domain (green), high-density root domain (blue), tree location (red), cells excluded to prevent damage to the tree (tan), and cells excluded to prevent damage to the levee road (yellow).

to test for both Type I and Type II detection errors. The sample size of 1-m² was selected to create a large enough sample to adequately, but practically, define bulk root properties while conducting analyses (Retzlaff et al. 2001). Throughout this document, cells may be referred to as Site-Cell Number (e.g., SAC-60 refers to cell 60 in Sacramento).

In Vicksburg, complete manual excavation was undertaken. Five zones were established for data collection and processing, four zones were based on an orthogonal coordinate system (7-m cross-slope and 6-m downslope) and a fifth covering the area immediately surrounding the tree at a 0.5-m radius (Figure 179). In this document, these rooting zones may be referred to as Q1-Q4 for the four quadrants and S for the area nearest the stump.

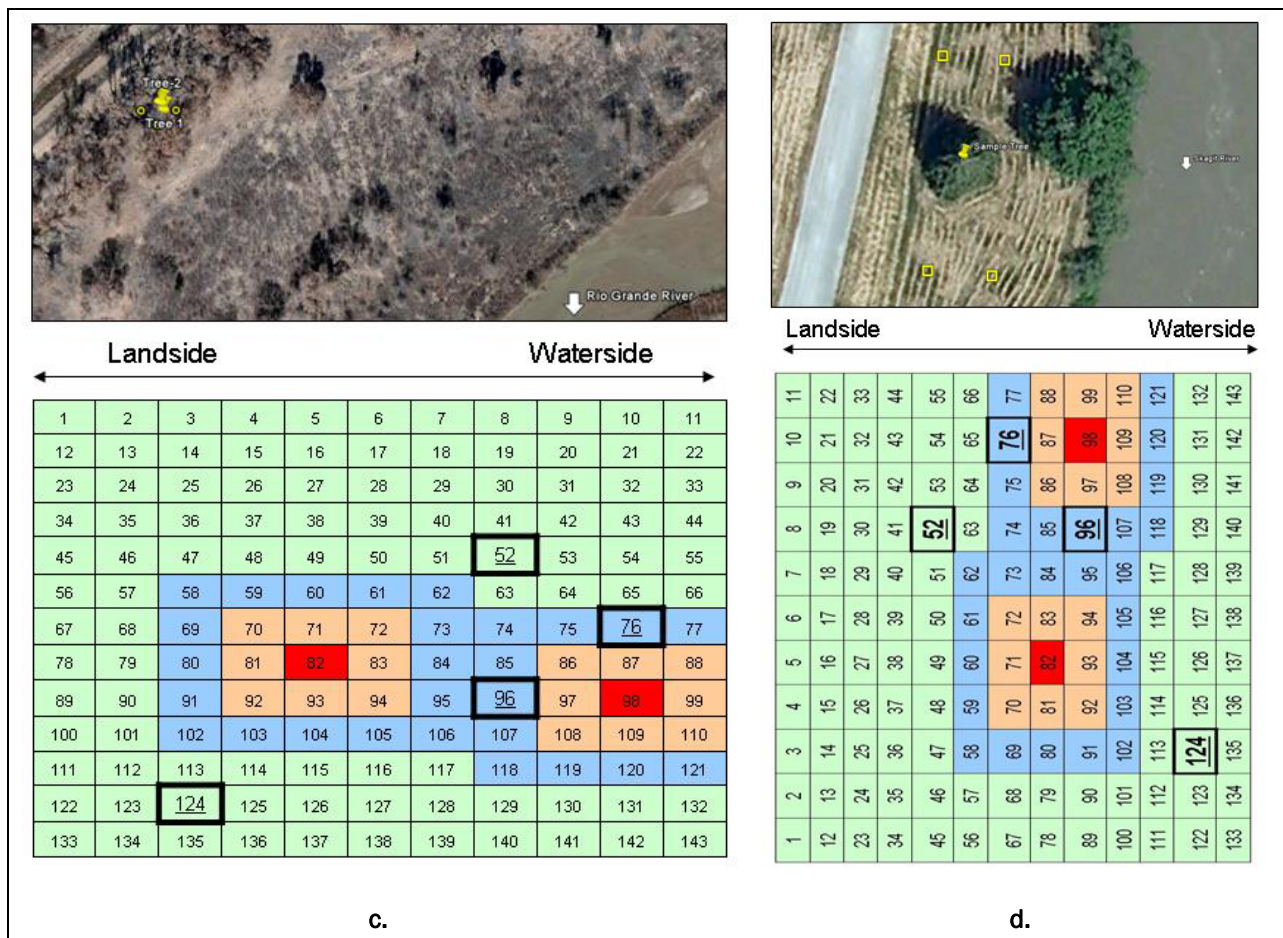


Figure 178. (Concluded).

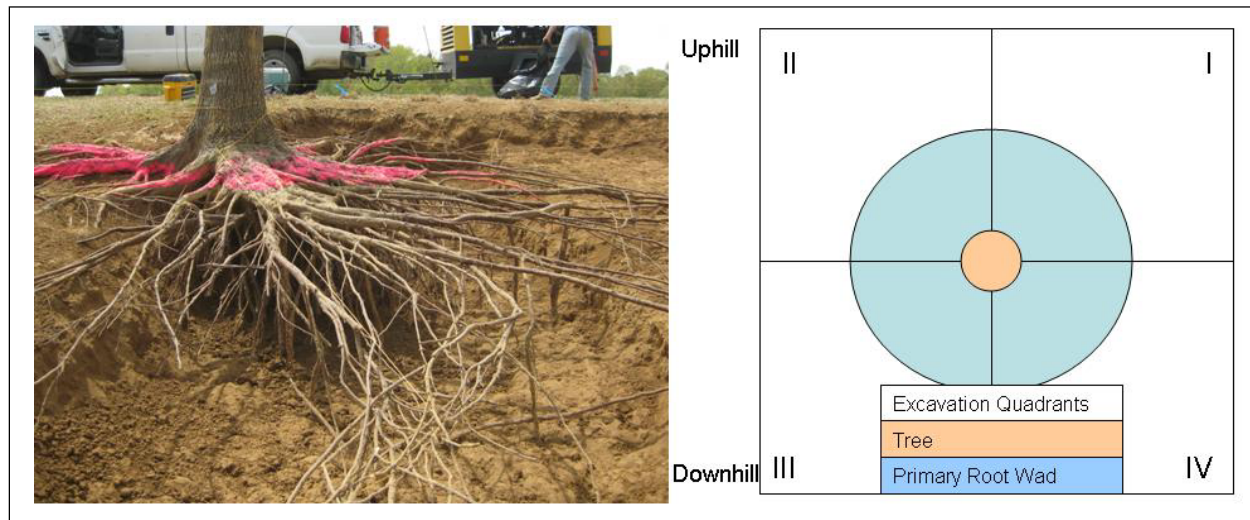


Figure 179. Stratified, random sample design for invasive measurement in Vicksburg, MS.



Figure 180. Invasive subsampling using (a) manual excavation and (b) compressed air.

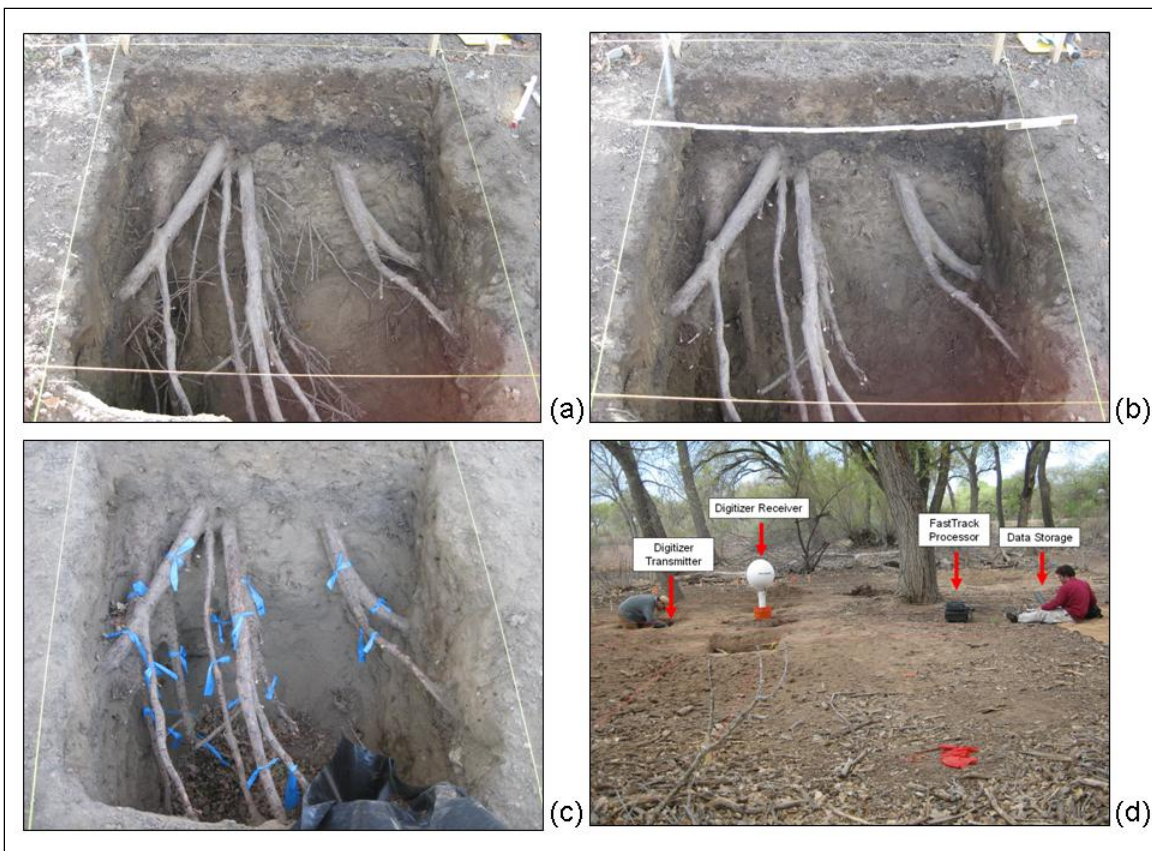


Figure 181. Excavation and digitization of subsamples: (a) unclipped roots, (b) clipped roots, (c) roots labeled and marked for digitization, and (d) digitization of subsample.

Field data collection

For subsampling sites, each 1-m² sample unit was excavated in 20-cm increments to capture changes in root properties as a function of depth. In Sacramento, cells were manually excavated (Figure 180a). In Albuquerque

and Burlington, cells were excavated using a GuardAir Air-Spade 2000 with a 225-ft³/min nozzle supplied by a 375-ft³/min air compressor (Figure 180b). Both techniques are expected to produce similar disturbance to the root system with roots as small as 1 to 2 mm remaining after excavation (Danjon et al. 2007). Techniques were selected based on site limitations with preference given to compressed air. Cells were excavated to a minimum of 60 cm and a maximum of 100 cm. Any significant disturbances to roots or anomalies encountered were noted (e.g., debris, animal burrows). For each depth increment, a representative soil sample was taken for analysis of grain size, texture, soil moisture, and total organic content (TOC).

Following excavation of each layer, a photograph was taken, roots less than 2-cm diam were clipped and reserved for laboratory analysis, and another photograph was taken showing only coarse roots (Figure 181 a,b). Roots were labeled and marked for digitization (Figure 181c). Root diameter was measured with a Vernier caliper at three locations along the root. Root position was measured with a 3-D digitizer (3SPACE Fastrak, Polhemus, Short and Long Ranger Options) using low-frequency electromagnetic field sensing (Figure 181d) and driven by Polhemus software (FTGui). Three digitization lines were taken for each root approximately 120 deg apart as viewed by root cross section with the primary line located on the top of the root. Points were taken at 10-cm intervals along a given root unless obvious changes in root diameter, shape, or orientation required smaller intervals. A local benchmark was established to verify instrument stability, with data points taken prior to and following measurement.

In Vicksburg, an entire tree was excavated (Figure 182a). Compressed air was applied to remove soil in the four quadrants shown in Figure 179. Excavation was conducted in three vertical intervals of 0 to 25 cm, 25 to 50 cm, and 50 to 100 cm. At each interval, roots less than 2 cm were clipped and reserved for laboratory analysis. The area immediately surrounding the tree was kept in contact so that roots may be measured with a minimum of movement (Figure 182b). Roots were measured in situ by the electromagnetic system previously described. Following measurement, coarse roots greater than 2 cm were also collected for laboratory analysis of mass and volume. The remaining root zone was removed by heavy machinery (Figure 182c). This root zone was then cleaned with compressed air, smaller roots were collected, and large roots were digitized. To maintain consistency between all digitization efforts,

five benchmarks were established on the trunk of the test tree (Figure 182d). Although mechanical removal can damage the root system directly below the tree, this approach provided for more reliable estimates of root location and extent for a majority of this root system. Additionally, few roots appeared to be damaged below the 1.5-m excavation depth.

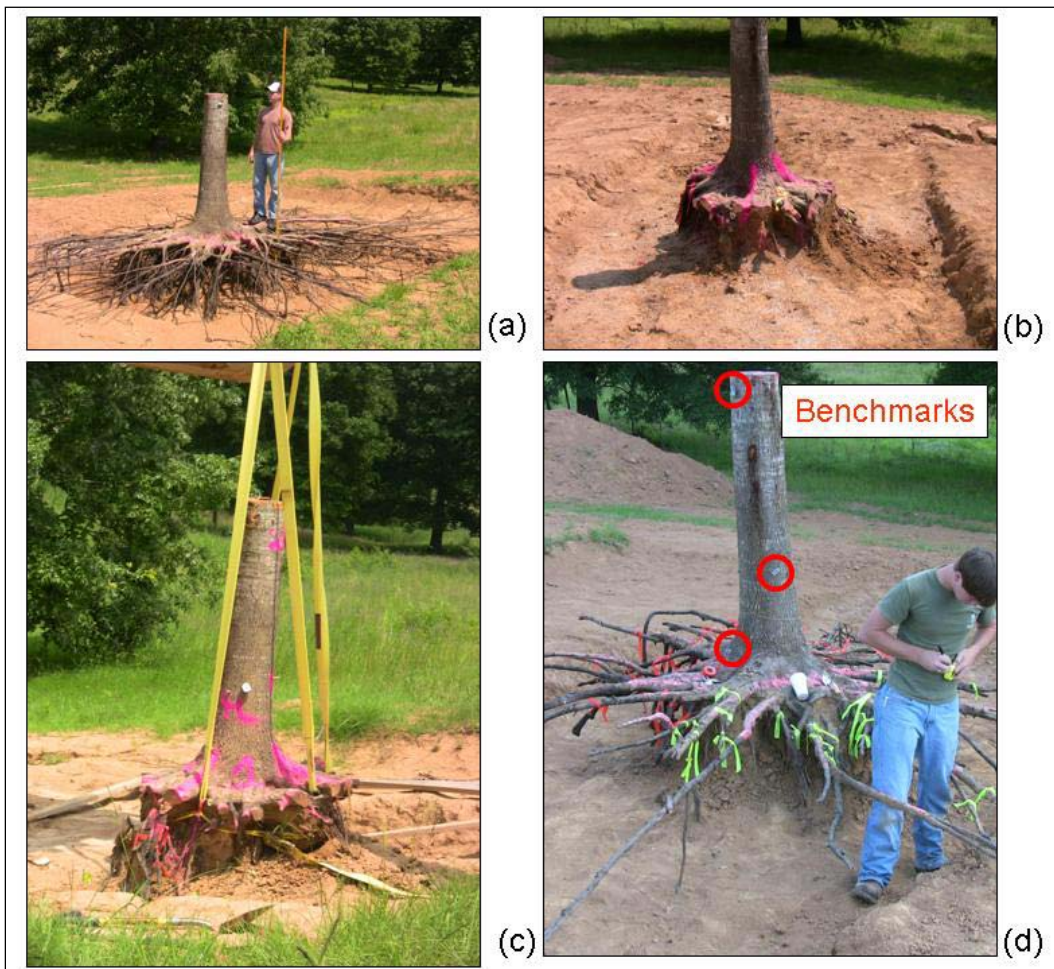


Figure 182. Excavation of a complete root system in Vicksburg, MS: (a) excavation of tree, (b) tree following compressed air excavation, (c) mechanical removal of remaining root system, and (d) digitization benchmarks.

Soil analysis

Soil samples from multiple depths in each subsampling unit were sealed and returned to the laboratory. Samples were weighed, oven dried at 180°C for 24 hr, and reweighed to determine moisture content. Samples were then subjected to grain size analysis by mechanical sieving and gravimetric analysis. Three subsamples were then dried in a 550°C furnace for 1.5 hr to determine total organic content by mass (TOC).

Tables 37 through 40 present a summary of soil analyses for Sacramento, Albuquerque Site 1, Albuquerque Site 2, and Burlington, respectively.

Clipped roots were oven dried at 180°C for 24 hours to determine organic dry mass. Root volume was estimated from mass measurements and an assumed specific gravity of root material (Table 41).

Table 37. Summary of soil analysis for Sacramento.

Sample Location	Depth Range (cm)	Average Moisture Content (%) ^a	Fine Material Content (%) ^b	D ₁₀ (mm)	D ₅₀ (mm)	D ₉₀ (mm)	TOC (%)
Sac-B-60	0-20	10.11	3.06	0.185	0.434	1.334	2.41
Sac-B-60	20-40	6.68	1.89	0.208	0.481	1.607	1.35
Sac-B-60	40-60	9.1	2.34	0.192	0.453	1.738	2.14
Sac-B-60	60-80	6.91	4.57	0.114	0.301	1.572	1.38
Sac-B-86	0-20	10.49	3.03	0.176	0.661	3.811	2.87
Sac-B-86	20-40	13.23	1.93	0.225	0.740	6.051	2.95
Sac-B-86	40-60	7.88	2.56	0.172	0.344	0.96	2.13
Sac-B-86	60-80	7.48	2.12	0.184	0.313	0.677	1.78
Sac-B-105	0-20	11.66	2.29	0.203	0.525	4.535	4.21
Sac-B-105	20-40	7.73	1.94	0.191	0.388	1.237	1.92
Sac-B-105	40-60	8.43	2.31	0.175	0.329	0.825	2.03
Sac-B-105	60-80	7.96	2.13	0.173	0.313	0.685	2.01
Sac-B-105	80-90	6.93	2.52	0.151	0.303	0.677	2.04
Sac-B-140	0-20	10.07	1.09	0.227	0.524	1.624	2.78
Sac-B-140	20-40	9.57	1.81	0.210	0.517	1.922	2.25
Sac-B-140	40-60	9.48	2.43	0.187	0.415	1.756	2.07
Sac-B-140	60-80	7.87	2.05	0.181	0.335	1.295	1.62

^a Averaged over three subsamples.

^b Percent of sample passing through a No. 200 sieve (<0.075 mm).

Post-processing of root architectural data

Digitized root locations provide two opportunities for validation of noninvasive tools: (1) some noninvasive tools operate at sufficient spatial resolution to potentially predict the location and orientation of roots and (2) digitized root locations may be used in conjunction with laboratory samples to estimate bulk properties of the sample volume. Root locations were plotted in three dimensions for visual comparison using Sigma-Plot 11.0 (Figures 183 through 187). To calculate bulk properties (e.g., root volume or surface area), root digitization was used to calculate root length. Assuming roots are cylindrical between digitization points, length was

Table 38. Summary of soil analysis for Albuquerque Site 1.

Sample Location	Depth Range (cm)	Average Moisture Content (%) ^a	Fine Material Content (%) ^b	D ₁₀ (mm)	D ₅₀ (mm)	D ₉₀ (mm)	TOC (%)
ABQ-1-52	0-20	17.65	3.25	-	-	-	4.34
ABQ-1-52	20-40	14.32	5.57	-	2.964	-	3.72
ABQ-1-52	40-60	6.76	35.83	3.939	0.128	3.939	3.40
ABQ-1-52	60-80	4.88	25.58	4.678	0.137	4.678	4.18
ABQ-1-52	80-100	4.23	25.05	4.660	0.133	4.660	3.67
ABQ-1-58	0-20	8.13	3.62	-	3.919	-	8.66
ABQ-1-58	20-40	7.38	23.78	0.366	0.108	0.366	3.23
ABQ-1-58	40-60	5.35	16.87	0.176	0.112	0.176	1.76
ABQ-1-58	60-80	5.61	20.26	1.033	0.115	1.033	1.76
ABQ-1-58	80-100	3.70	7.07	0.568	0.289	0.568	1.80
ABQ-1-74	0-20	15.96	4.54	-	8.565	-	4.40
ABQ-1-74	20-40	11.38	23.78	0.366	0.108	0.366	6.51
ABQ-1-74	40-60	7.05	0.03	7.066	1.600	7.066	-
ABQ-1-74	60-80	7.57	20.44	7.973	0.303	7.973	3.40
ABQ-1-74	80-100	3.87	14.75	2.583	0.288	2.583	1.96
ABQ-1-136	0-20	8.57	18.39	2.218	0.121	2.218	1.97
ABQ-1-136	20-40	6.93	18.57	0.790	0.113	0.790	1.88
ABQ-1-136	40-60	5.94	14.39	0.392	0.114	0.392	1.64
ABQ-1-136	60-80	7.40	23.92	8.027	0.121	8.027	2.71
ABQ-1-136	80-100	5.57	8.56	5.594	0.306	5.594	2.00

^a Averaged over three subsamples.^b Percent of sample passing through a No. 200 sieve (<0.075 mm).

combined with measurements of diameter to estimate coarse root volume. In this analysis, three components of root system properties were measured, which are combined to form a bulk or averaged estimate of root volume and density within each of the sampling units. The three components are: (1) very large, digitized roots, (2) moderate-sized, macro-scale roots collected through clipping, and (3) fine, micro-scale organic matter estimated from soil samples. Mass and volume measurements may be transferred using estimates of specific gravity obtained from field data and literature, mass and volume. Fine root mass and volume was estimated from measured Total Organic Content (TOC) and sample volume. Tables 42 through 46 present these estimates as well as the combined estimate of rooting mass and volume in each cell. Root volume and volumetric density(V_{root}/V_{cell}) provide appropriate metrics for assessing the efficacy of noninvasive techniques.

Table 39. Summary of soil analysis for Albuquerque Site 2.

Sample Location	Depth Range (cm)	Average Moisture Content (%) ^a	Fine Material Content (%) ^b	D ₁₀ (mm)	D ₅₀ (mm)	D ₉₀ (mm)	TOC (%)
ABQ-2-52	0-20	19.20	1.04	3.185	-	-	7.99
ABQ-2-52	20-40	11.20	9.76	0.076	0.385	9.274	10.47
ABQ-2-52	40-60	11.48	3.54	0.122	0.421	9.093	1.98
ABQ-2-76	0-20	11.38	5.87	0.101	7.581	-	6.80
ABQ-2-76	20-40	15.24	6.53	0.128	3.265	10.322	4.45
ABQ-2-76	40-60	12.11	0.27	0.386	2.541	8.849	19.74
ABQ-2-76	60-80	12.09	0.23	0.242	2.273	8.418	10.38
ABQ-2-96	0-20	20.97	1.31	1.192	7.738	-	11.11
ABQ-2-96	20-40	22.75	2.20	1.174	8.723	-	7.43
ABQ-2-96	40-60	11.47	4.06	0.138	0.423	7.457	1.93
ABQ-2-96	60-80	15.88	7.70	0.092	0.776	9.669	3.19
ABQ-2-96	80-100	21.53	10.12	0.074	1.858	9.852	3.12
ABQ-2-124	0-20	8.77	6.60	0.090	1.011	8.186	0.62
ABQ-2-124	20-40	4.83	12.06	0.071	0.148	0.420	10.39
ABQ-2-124	40-60	3.35	3.97	0.126	0.287	0.406	1.35
ABQ-2-124	60-80	8.52	3.20	0.150	0.337	7.826	1.43

^a Averaged over three subsamples.

^b Percent of sample passing through a No. 200 sieve (<0.075 mm).

Root architecture analysis

Large root characteristics were derived within each cell from digitization data using Python freeware (Python 2010). A numerical code was developed that circumscribes a circle around the digitized triangular root cross section (Figure 188a and b), generates an octagon of equivalent outer dimensions (Figure 188c and d), and triangulates a surface mesh from multiple octagonal cross sections. The triangular surface mesh was used to generate a tetrahedral volume mesh for computation of root volume. Previous studies have applied alternative representations of root structure, such as truncated cones (Di Iorio et al. 2005; Danjon et al. 2007) or discontinuous cylinders; however, surface and volume meshes provide a standardized platform for importing data into numerical models of slope stability and seepage in later analyses.

Table 47 presents digitized root volumes derived from this analysis.

Table 40. Summary of soil analysis for Burlington, WA.

Sample Location	Depth Range (cm)	Average Moisture Content (%) ^a	Fine Material Content (%) ^b	D ₁₀ (mm)	D ₅₀ (mm)	D ₉₀ (mm)	TOC (%)
BUR-24	0-20	12.14	13.41	0.064	0.573	8.479	4.86
BUR-24	20-40	10.10	19.35	0.061	0.195	0.951	3.19
BUR-24	40-60	16.92	17.17	0.058	0.152	1.757	3.90
BUR-24	60-80	13.54	22.18	0.056	0.118	0.402	2.59
BUR-24	80-100	23.33	21.30	0.020	0.305	4.043	4.04
BUR-41	0-20	12.50	13.55	0.065	0.307	5.822	5.96
BUR-41	20-40	13.13	23.31	0.050	0.126	1.853	3.96
BUR-41	40-60	15.77	25.33	0.048	0.119	0.722	4.41
BUR-41	60-80	18.20	17.27	0.056	0.189	2.193	4.64
BUR-41	80-100	20.26	18.82	0.052	0.164	1.587	5.30
BUR-103	0-20	13.79	13.11	0.066	0.270	4.758	4.97
BUR-103	20-40	7.49	17.27	0.065	0.118	0.311	2.06
BUR-103	40-60	10.58	19.00	0.065	0.110	0.225	2.21
BUR-103	60-80	18.27	17.62	0.056	0.134	2.399	3.96
BUR-103	80-100	20.06	18.44	0.055	0.157	0.820	5.30
BUR-142	0-20	15.14	17.49	0.057	0.155	5.086	4.89
BUR-142	20-40	9.56	15.74	0.067	0.125	0.358	2.06
BUR-142	40-60	15.57	17.97	0.058	0.144	0.654	3.59
BUR-142	60-80	16.13	19.08	0.058	0.134	0.604	2.57
BUR-142	80-100	21.18	16.82	0.051	0.244	1.580	2.68

^a Averaged over three subsamples.^b Percent of sample passing through a No. 200 sieve (<0.075 mm).

Table 41. Summary of root specific gravity.

Common Name	Scientific Name	Specific Gravity	Source
Shortleaf pine	<i>Pinus echinata</i>	0.458	Gibson et al. (1986)
Slash pine	<i>Pinus elliottii</i>	0.377	Gibson et al. (1986)
Longleaf pine	<i>Pinus palustris</i>	0.411	Gibson et al. (1986)
Loblolly pine	<i>Pinus taeda</i>	0.413	Gibson et al. (1986)
Fremont cottonwood	<i>Populus fremontii</i>	0.613 (n=6)	This study
White oak	<i>Quercus alba</i>	0.48 (<0.5cm) 0.54 (0.5-1cm) 0.59 (1-2cm) 0.62 (>2cm)	Danjon et al. (2007)
Southern red oak	<i>Quercus falcata</i>	0.575 (n=3, <0.5cm) 0.680 (n=3, 0.5-2cm) 0.796 (n=3, >2cm)	This study
Western red cedar	<i>Thuja plicata</i>	0.525 (n=11)	This study

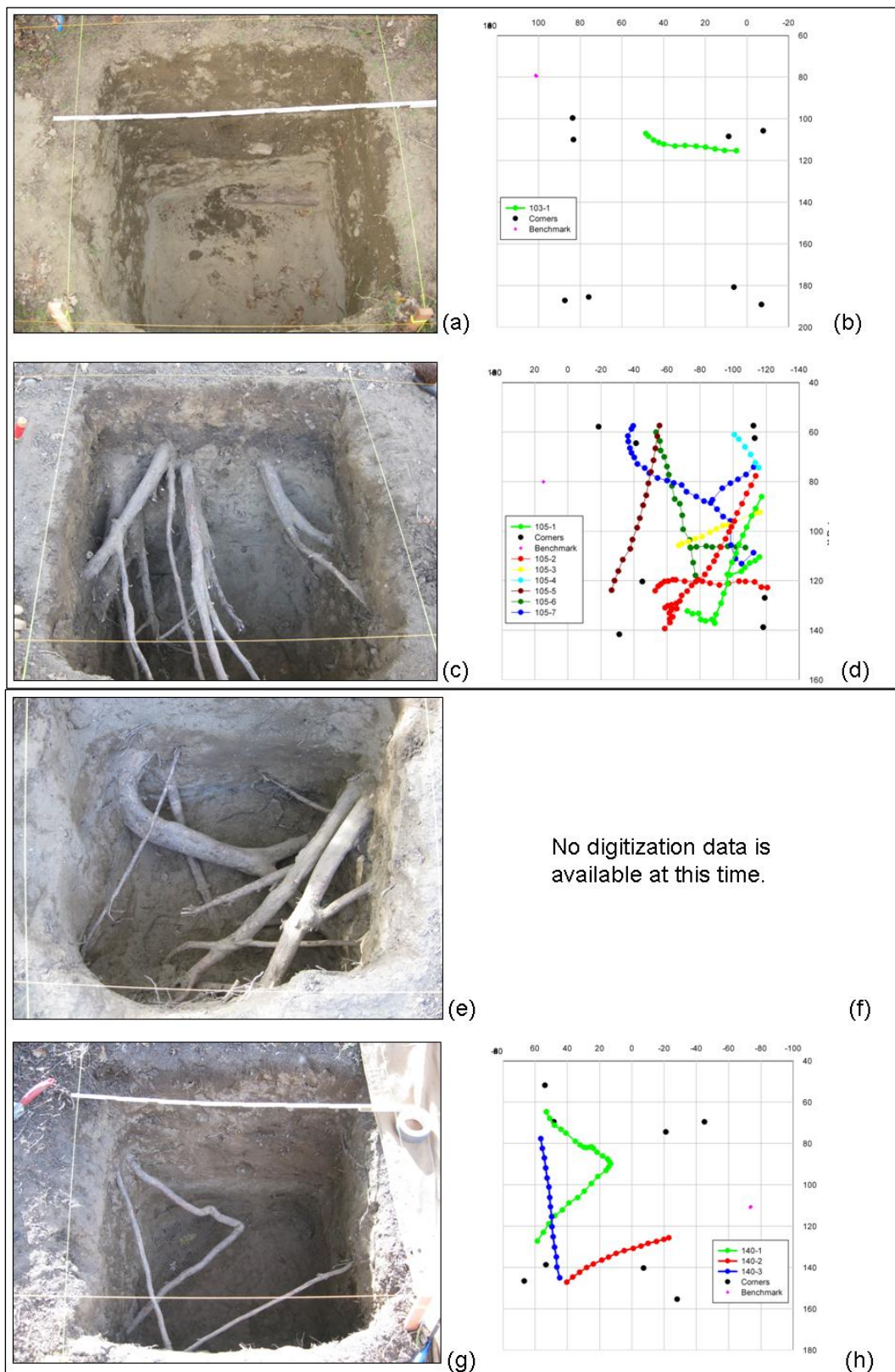


Figure 183. Photographs and digital renderings of invasive subsample locations in Sacramento (a/b) Cell B60, (c/d) Cell B86, (e/f) Cell B105, and (g/h) Cell B140.

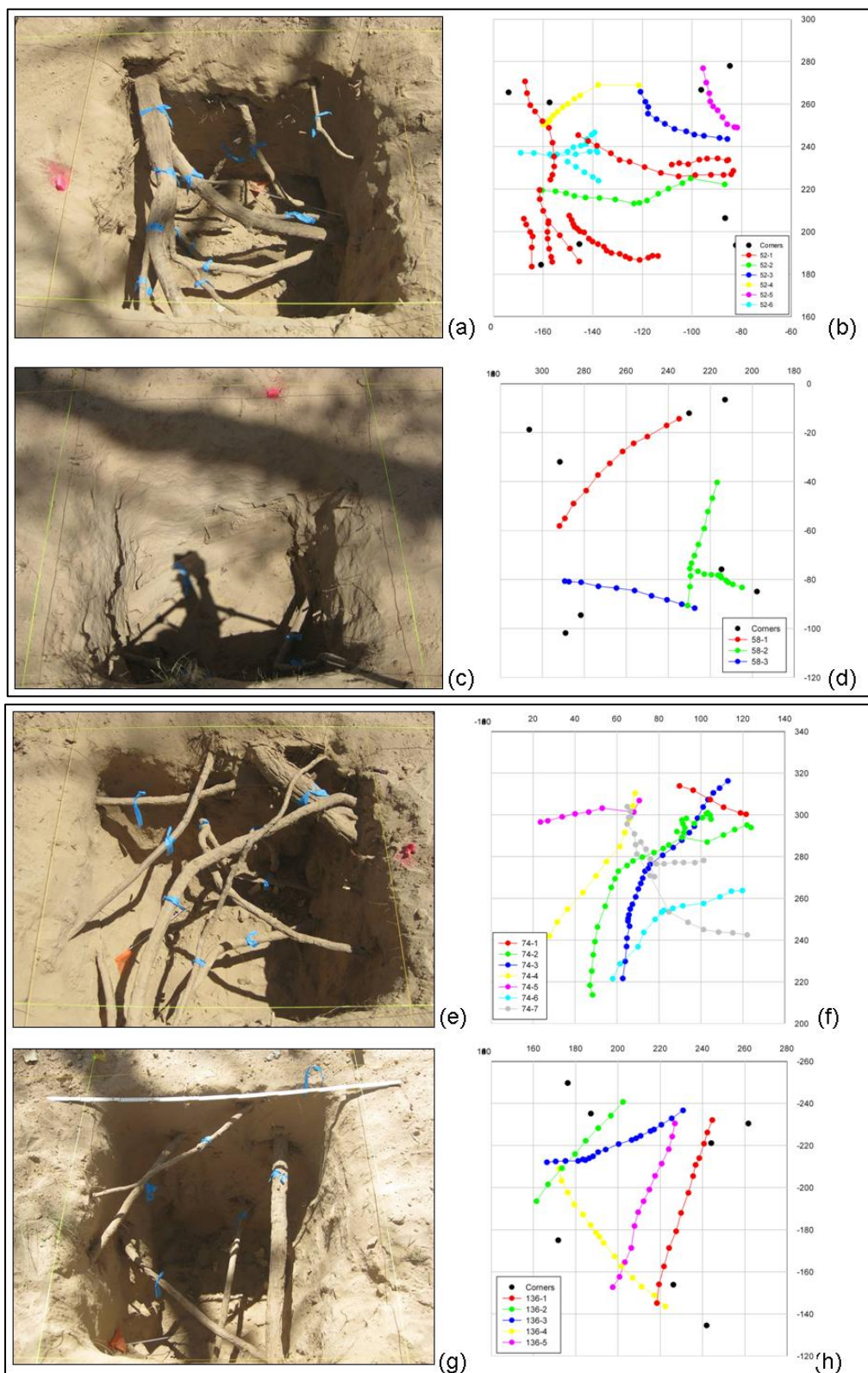


Figure 184. Photographs and digital renderings of invasive subsample locations in Albuquerque – Site 1 (a/b) Cell 52, (c/d) Cell 58, (e/f) Cell 74, and (g/h) Cell 136.

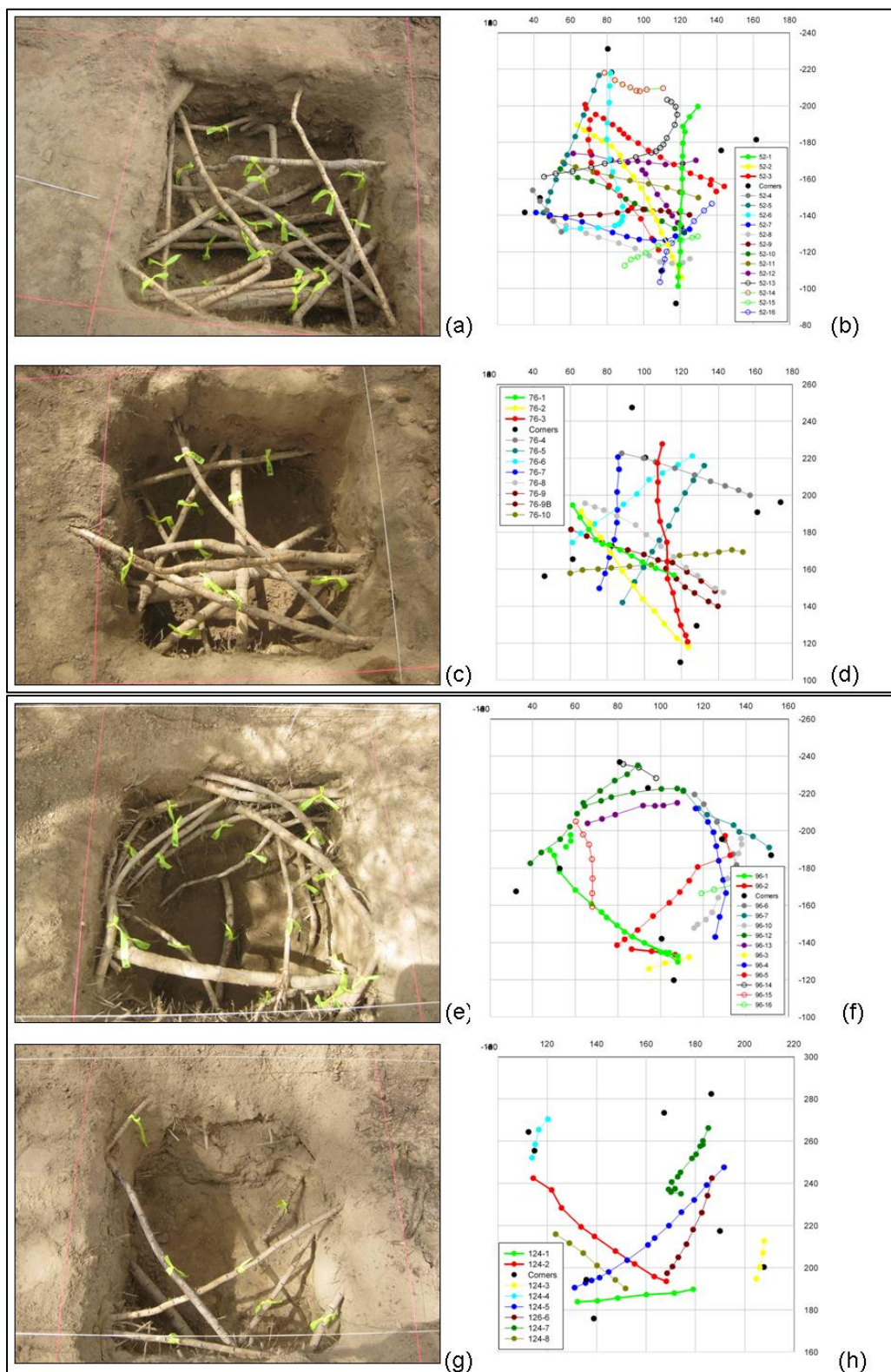


Figure 185. Photographs and digital renderings of invasive subsample locations in Albuquerque – Site 2 (a/b) Cell 52, (c/d) Cell 76, (e/f) Cell 96, and (g/h) Cell 124.

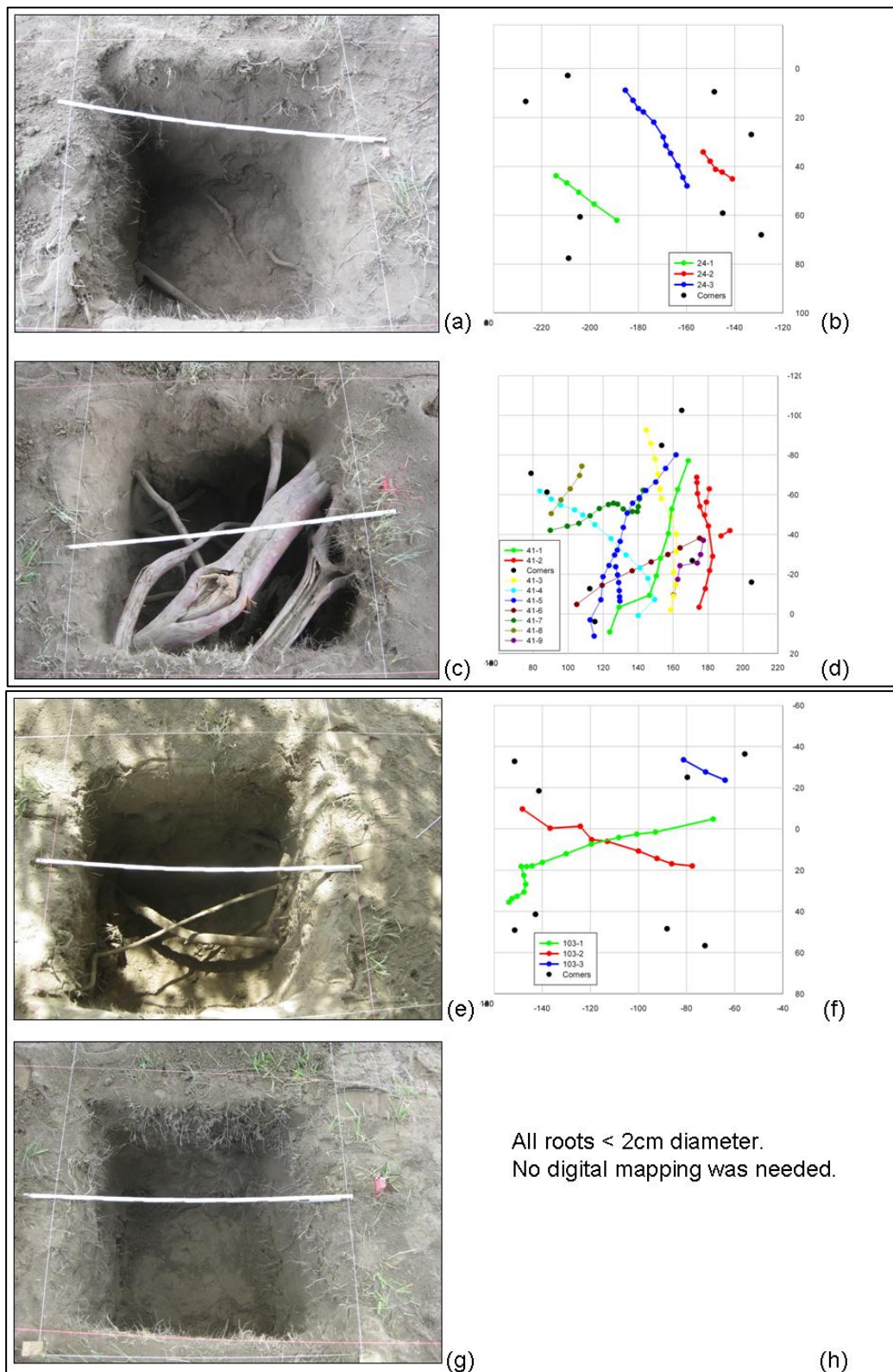


Figure 186. Photographs and digital renderings of invasive subsample locations in Burlington (a/b) Cell 24, (c/d) Cell 41, (e/f) Cell 103, and (g/h) Cell 142.

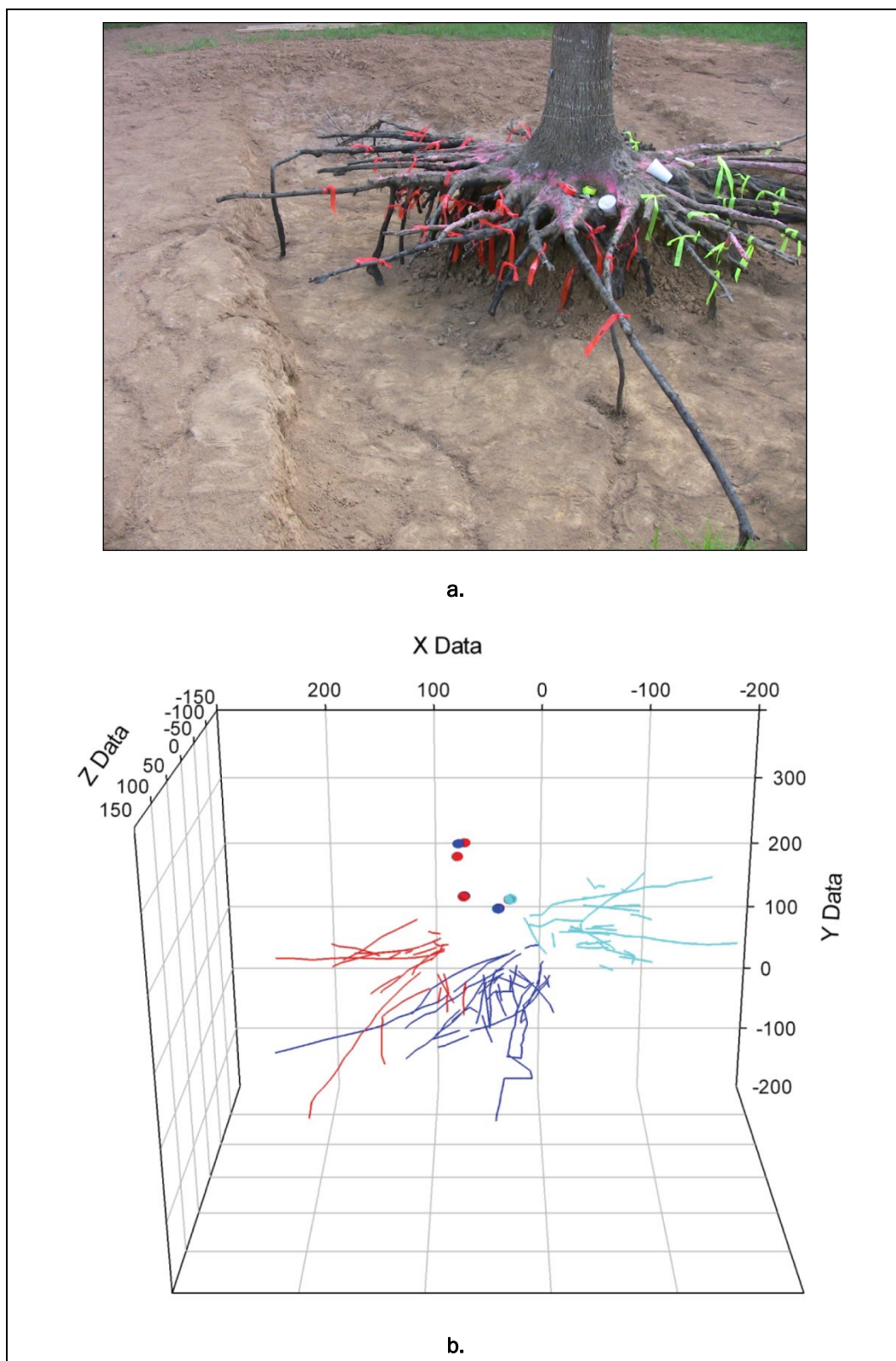


Figure 187. Comparative photograph (a) and digital rendering (b) of invasive root architecture data collection in Vicksburg, MS.

Table 42. Summary of root properties – Sacramento, CA.

Sample Location	Depth Range (cm)	Unsampled Fine Roots			Clipped Roots		Unclipped Roots		All Roots		Volumetric Density
		TOC	V (m³)	M (g)	V (m³)	M (g)	V (m³)	M (g)	V (m³)	M (g)	
Sac-B-60	0-20	0.024	0.00482	2,612	0.00119	646	0.00224	1,214	0.01838	9,964	0.02298
Sac-B-60	20-40	0.014	0.00270	1,463	0.00023	122					
Sac-B-60	40-60	0.021	0.00428	2,320	0.00011	62					
Sac-B-60	60-80	0.014	0.00276	1,496	0.00005	28					
Sac-B-86	0-20	0.029	0.00574	3,111	0.00018	97	-	-	0.02138	11,588	0.02673
Sac-B-86	20-40	0.030	0.00590	3,198	0.00070	381					
Sac-B-86	40-60	0.021	0.00426	2,309	0.00104	563					
Sac-B-86	60-80	0.018	0.00356	1,930	-	-					
Sac-B-105	0-20	0.042	0.00842	4,564	0.00022	120	-	-	0.02407	13,048	0.02675
Sac-B-105	20-40	0.019	0.00384	2,081	0.00013	73					
Sac-B-105	40-60	0.020	0.00406	2,201	0.00050	271					
Sac-B-105	60-80	0.020	0.00402	2,179	0.00048	261					
Sac-B-105	80-90	0.020	0.00204	1,106	0.00036	193	0.00123	665	0.02034	11,026	0.02543
Sac-B-140	0-20	0.028	0.00556	3,014	0.00081	440					
Sac-B-140	20-40	0.023	0.00450	2,439	0.00054	292					
Sac-B-140	40-60	0.021	0.00414	2,244	0.00024	132					
Sac-B-140	60-80	0.016	0.00324	1,756	0.00008	45					

Table 43. Summary of root properties – Albuquerque, NM – Site 1.

Sample Location	Depth Range (cm)	Unsampled Fine Roots			Clipped Roots		Unclipped Roots		All Roots		Volumetric Density
		TOC	V (m³)	M (g)	V (m³)	M (g)	V (m³)	M (g)	V (m³)	M (g)	
ABQ-1-52	0-20	0.043	0.00867	5,315	0.00007	44	0.00538	3,298	0.04510	27,649	0.04510
ABQ-1-52	20-40	0.037	0.00745	4,566	0.00053	325					
ABQ-1-52	40-60	0.034	0.00680	4,171	0.00026	161					
ABQ-1-53	60-80	0.042	0.00836	5,125	0.00011	69					
ABQ-1-52	80-100	0.037	0.00733	4,494	0.00013	82					
ABQ-1-58	0-20	0.087	0.01732	10,617	0.00036	223	0.00729	4,468	0.04229	25,923	0.04229
ABQ-1-58	20-40	0.032	0.00645	3,956	0.00004	23					
ABQ-1-58	40-60	0.018	0.00351	2,153	0.00008	47					
ABQ-1-58	60-80	0.018	0.00351	2,154	0.00011	68					
ABQ-1-58	80-100	0.018	0.00361	2,212	0.00000	2					
ABQ-1-74	0-20	0.044	0.00879	5,389	0.00041	252	0.00675	4,138	0.04015	24,612	0.04015
ABQ-1-74	20-40	0.065	0.01302	7,982	0.00017	103					
ABQ-1-74	40-60	-	-	-	0.00021	130					
ABQ-1-74	60-80	0.034	0.00680	4,167	0.00003	17					
ABQ-1-74	80-100	0.020	0.00393	2,407	0.00005	28					
ABQ-1-136	0-20	0.020	0.00395	2,419	0.00039	239	0.00354	2,173	0.02503	15,345	0.02503
ABQ-1-136	20-40	0.019	0.00377	2,309	0.00029	178					
ABQ-1-136	40-60	0.016	0.00329	2,014	0.00023	138					
ABQ-1-136	60-80	0.027	0.00543	3,328	0.00015	89					
ABQ-1-136	80-100	0.020	0.00400	2,452	0.00001	6					

Table 44. Summary of root properties – Albuquerque, NM – Site 2.

Sample Location	Depth Range (cm)	Unsampled Fine Roots			Clipped Roots		Unclipped Roots		All Roots		Volumetric Density
		TOC	V (m3)	M (g)	V (m3)	M (g)	V (m3)	M (g)	V (m3)	M (g)	
ABQ-2-52	0-20	0.080	0.01597	9,792	0.00093	568	0.01330	8,150	0.06036	37,000	0.07545
ABQ-2-52	20-40	0.105	0.02094	12,838	0.00210	1,288					
ABQ-2-52	40-60	0.020	0.00397	2,433	0.00315	1,931					
ABQ-2-76	0-20	0.068	0.01359	8,333	0.00183	1,119					
ABQ-2-76	20-40	0.044	0.00889	5,452	0.00168	1,027	0.01247	7,646	0.10297	63,121	0.12871
ABQ-2-76	40-60	0.197	0.03948	24,199	0.00263	1,611					
ABQ-2-76	60-80	0.104	0.02077	12,729	0.00164	1,004					
ABQ-2-96	0-20	0.111	0.02221	13,616	0.00073	447					
ABQ-2-96	20-40	0.074	0.01486	9,108	0.00126	775	0.00759	4,652	0.06585	40,369	0.06585
ABQ-2-96	40-60	0.019	0.00385	2,363	0.00122	750					
ABQ-2-96	60-80	0.032	0.00637	3,907	0.00042	260					
ABQ-2-96	80-100	0.031	0.00623	3,821	0.00109	671					
ABQ-2-124	0-20	0.006	0.00125	764	0.00152	933	0.00265	1,623	0.03301	20,236	0.04126
ABQ-2-124	20-40	0.104	0.02077	12,734	0.00078	478					
ABQ-2-124	40-60	0.013	0.00270	1,655	0.00019	115					
ABQ-2-124	60-80	0.014	0.00286	1,754	0.00029	181					

Table 45. Summary of root properties – Burlington, WA.

Sample Location	Depth Range (cm)	Unsampled Fine Roots			Clipped Roots		Unclipped Roots		All Roots		Volumetric Density
		TOC	V (m³)	M(g)	V (m³)	M(g)	V (m³)	M (g)	V (m³)	M (g)	
BUR-24	0-20	0.049	0.00973	5,106	0.00041	216	0.00078	409	0.03968	20,831	0.03968
BUR-24	20-40	0.032	0.00638	3,347	0.00023	119					
BUR-24	40-60	0.039	0.00780	4,094	0.00026	138					
BUR-24	60-80	0.026	0.00519	2,723	0.00044	230					
BUR-24	80-100	0.040	0.00808	4,243	0.00039	204					
BUR-41	0-20	0.060	0.01193	6,262	0.00032	169	0.04210	22,104	0.09202	48,311	0.09202
BUR-41	20-40	0.040	0.00792	4,157	0.00006	30					
BUR-41	40-60	0.044	0.00882	4,629	0.00009	47					
BUR-41	60-80	0.046	0.00929	4,875	0.00050	264					
BUR-41	80-100	0.053	0.01060	5,567	0.00039	207					
BUR-103	0-20	0.050	0.00995	5,224	0.00024	124	0.00237	1,244	0.04078	21,412	0.04078
BUR-103	20-40	0.021	0.00413	2,168	0.00006	30					
BUR-103	40-60	0.022	0.00441	2,317	0.00038	201					
BUR-103	60-80	0.040	0.00791	4,154	0.00044	230					
BUR-103	80-100	0.053	0.01060	5,566	0.00029	154					
BUR-142	0-20	0.049	0.00979	5,138	0.00022	116	0.00000	0	0.03221	16,913	0.03221
BUR-142	20-40	0.021	0.00413	2,167	0.00003	18					
BUR-142	40-60	0.036	0.00719	3,773	0.00004	19					
BUR-142	60-80	0.026	0.00513	2,694	0.00015	77					
BUR-142	80-100	0.027	0.00535	2,809	0.00020	103					

Table 46. Summary of root properties – Vicksburg, MS.

	Root Size Class	Quad-I	Quad-II	Quad-III	Quad-IV	Stump	Total
Mass (g)	< 0.5 cm	2,560	2,200	2,923	2,887	6,100	16,669
	0.5-2.0 cm	4,050	8,100	5,400	8,000	0	25,550
	> 2.0 cm	11,800	16,150	10,750	23,700	206,150	268,550
	Total	18,410	26,450	19,073	34,587	212,250	310,769
Volume (m ³)	< 0.5 cm	0.0045	0.0038	0.0051	0.0050	0.0106	0.0290
	0.5-2.0 cm	0.0060	0.0119	0.0079	0.0118	0.0000	0.0376
	> 2.0 cm	0.0148	0.0203	0.0135	0.0298	0.2590	0.3374
	Total	0.0252	0.0360	0.0265	0.0466	0.2696	0.4039
Percent by Mass	< 0.5 cm	14	8	15	8	3	
	0.5-2.0 cm	22	31	28	23	0	
	> 2.0 cm	64	61	56	69	97	
	Total	100	100	100	100	100	
Percent by Volume	< 0.5 cm	18	11	19	11	4	
	0.5-2.0 cm	24	33	30	25	0	
	> 2.0 cm	59	56	51	64	96	
	Total	100	100	100	100	100	

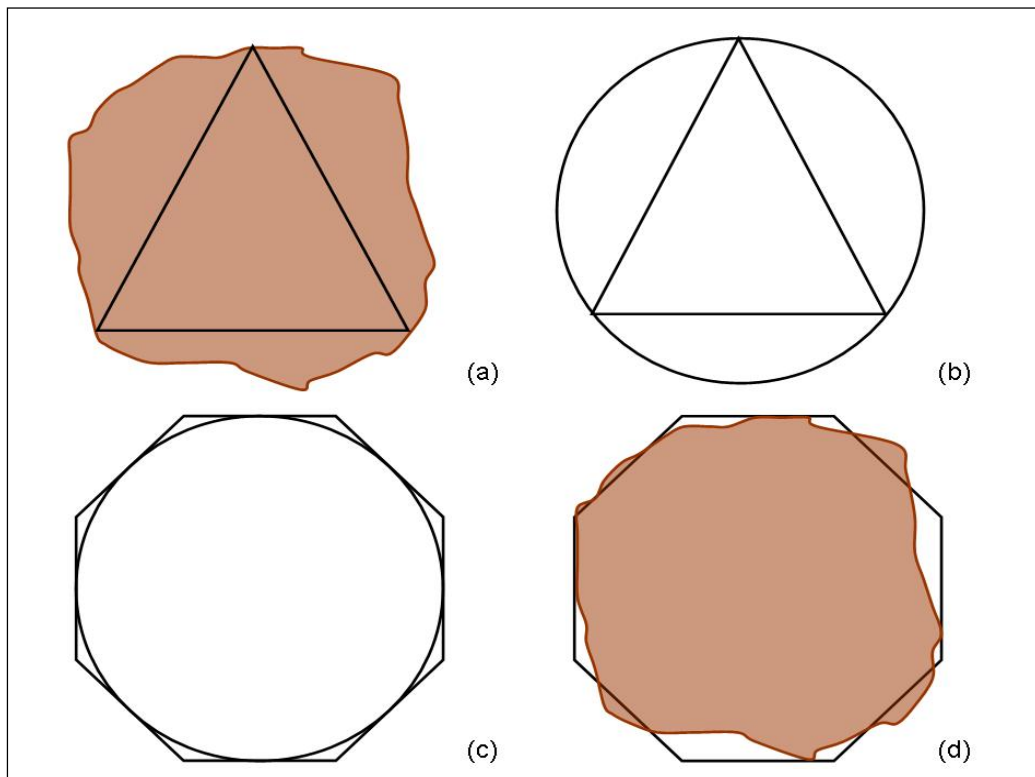


Figure 188. Example of numerical representation of root cross section:
(a) triangular digitization of irregular root, (b) circumscription of circle around triangular data, (c) octagonal fitting of circle, and
(d) comparison of sample root cross section to octagon.

Surface and volume meshes of large roots were generated using the Python model previously described for each cell. Data were imported to Paraview, an open source scientific visualization software (ParaView 2010), for additional visualization and computation. Figure 183 shows side-by-side comparisons of photographs of the root system and 3-D renderings in Paraview.

Bulk properties of root system

In this analysis, three components of root system properties were measured, which are combined to form a bulk or averaged estimate of root volume and density within each of the sampling units. The three components are:

- Very large, digitized roots
- Moderate-sized, macro-scale roots collected through sieving and clipping
- Fine, micro-scale organic matter estimated from soil samples.

Table 47. Root properties from invasive subsamples.

Sample	Sample Size (m ³)	Unsampled Fine Roots			Clipped Roots		Unclipped Roots		Total Roots		Volumetric Density
		TOC	V (m ³)	M (kg)							
B-60-0-20 cm	0.2	0.0241	0.00481	2.608	0.00119	0.646	0.002352	1.275	0.01849	10.02394	0.02312
B-60-20-40 cm	0.2	0.0135	0.00271	1.468	0.00023	0.122					
B-60-40-60 cm	0.2	0.0214	0.00427	2.316	0.00011	0.062					
B-60-60-80 cm	0.2	0.0138	0.00277	1.500	0.00005	0.028					
B-86-0-20 cm	0.2	0.0287	0.00573	3.107	0.00018	0.097	0.000000	0.000	0.02137	11.58176	0.02671
B-86-20-40 cm	0.2	0.0295	0.00589	3.194	0.00070	0.381					
B-86-40-60 cm	0.2	0.0213	0.00426	2.310	0.00104	0.563					
B-86-60-80 cm	0.2	0.0178	0.00356	1.930							
B-105-0-20 cm	0.2	0.0421	0.00842	4.564	0.00022	0.120	0.000000	0.000	0.02406	13.04047	0.02673
B-105-20-40 cm	0.2	0.0192	0.00383	2.076	0.00013	0.073					
B-105-40-60 cm	0.2	0.0203	0.00405	2.196	0.00050	0.271					
B-105-60-80 cm	0.2	0.0201	0.00402	2.181	0.00048	0.261					
B-105-80-90 cm	0.1	0.0204	0.00204	1.106	0.00036	0.193	0.001342	0.727	0.02046	11.09026	0.02558
B-140-0-20 cm	0.2	0.0278	0.00555	3.011	0.00081	0.440					
B-140-20-40 cm	0.2	0.0225	0.00450	2.441	0.00054	0.292					
B-140-40-60 cm	0.2	0.0207	0.00414	2.246	0.00024	0.132					
B-140-60-80 cm	0.2	0.0162	0.00324	1.758	0.00008	0.045					

Danjon et al. (2007) estimated a root specific gravity (0.542); this provides a mechanism for transferring mass estimates to volume and vice versa for all root size classes. Fine root mass and volume were estimated from measured Total Organic Content (TOC) and sample volume. Table 47 presents these estimates as well as the combined estimate of rooting mass and volume in each cell. Root volume and volumetric density (V_{root}/V_{cell}) are the metrics used to assess the efficacy of noninvasive techniques.

Comparison of GPR data with root characterization

The following discussion presents radargram depth sections corresponding to the in situ root characterization. Figure 189 shows the locations of the cells where the root characterization was done. The locations of the cells relative to the tree are given in Table 48. The root characterization removed soil in depth increments of 20 cm. Only fine roots were revealed above a depth of 40 cm. The radargrams at a depth of 40 cm are presented in Figure 190. An enlargement of the GPR section in each cell, along with photographs showing the roots present in the four cells, is shown in Figure 191. The radar sections have been rotated so they are oriented in the same direction as the cells in the photographs. Figures 192 to 193 and Figures 194 to 195 are similar presentations for depths 60 cm and 80 cm, respectively. There are differences in the parallel and perpendicular expanded radar sections (for example, cell 105 in Figure 191). The reflection characteristics of an object can differ, depending on the shape of the object and the angle at which the GPR antenna crosses over the object. It is possible that a reflection may be visible in data collected in one direction and not another. Also, in data collected using local grid coordinates, the possibility of the antenna array sliding on the levee slope could cause some positioning error. A comparison of the radar sections and the root photographs for each cell (Figures 191, 193, and 195) does not suggest that the GPR imaged the tree roots. At depths of 40 cm and 60 cm, there is clutter present in the radar sections that overwhelms any signature that may be present from the roots.

Summary

GPR data were collected parallel and perpendicular to the levee crest using a 31-channel antenna array. There was a significant amount of clutter in the subsurface that hindered the detection of individual roots. However, the lateral extent of the root zone of influence determined using the GPR is comparable to that determined from the electrical resistivity survey.



Figure 189. Location of the root characterization cells.

Table 48. Location of root characterization cells relative to tree.

Cell	Local Grid Location	
	West (m)	South (m)
Tree	6-7	8-9
60	0-1	5-6
86	4-5	8-9
105	5-6	10-11
140	0-1	13-14

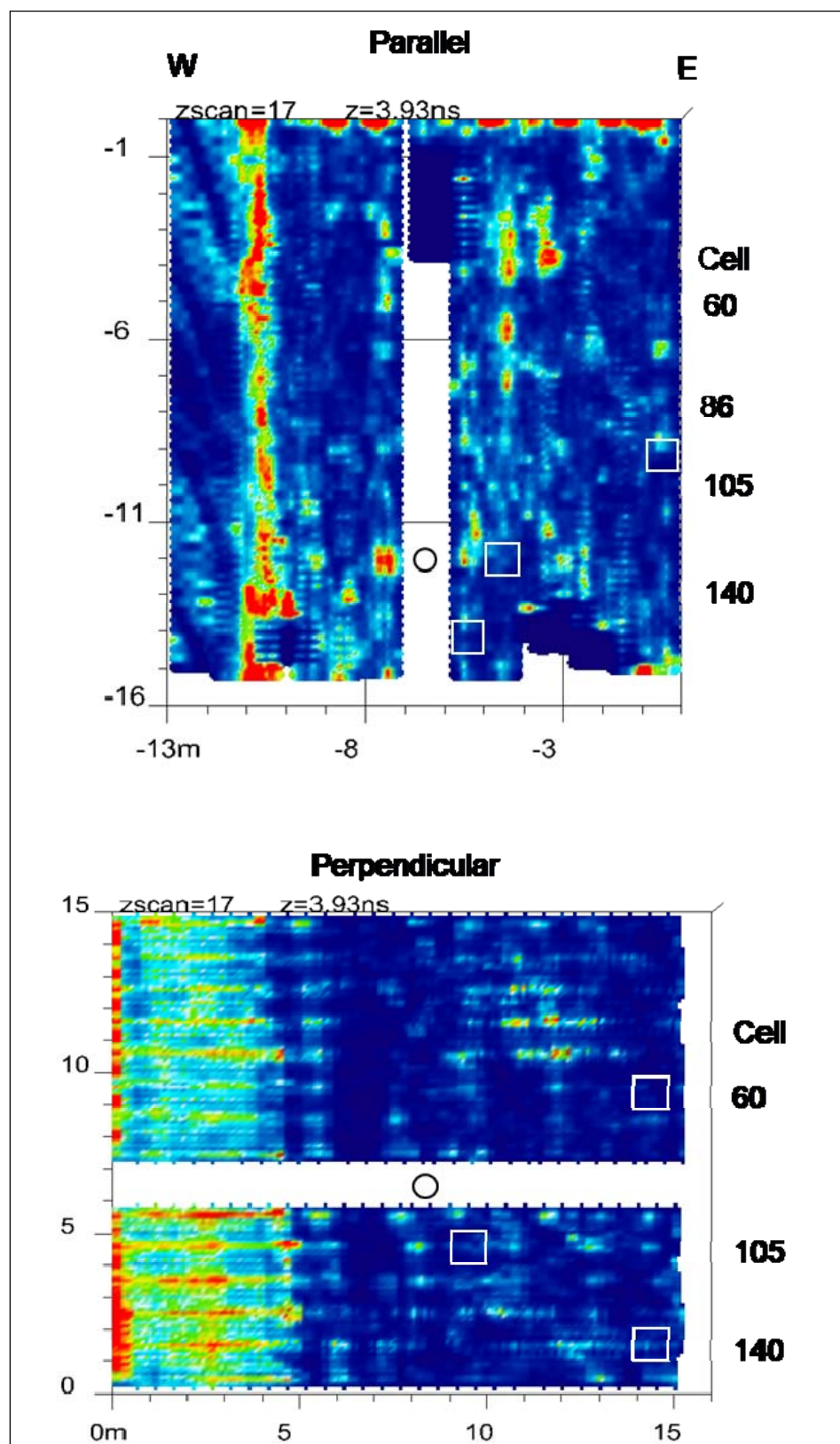


Figure 190. GPR depth slices at 40 cm (actual 39.3 cm) parallel and perpendicular to the crest with outline of root characterization cells and tree position (circle).

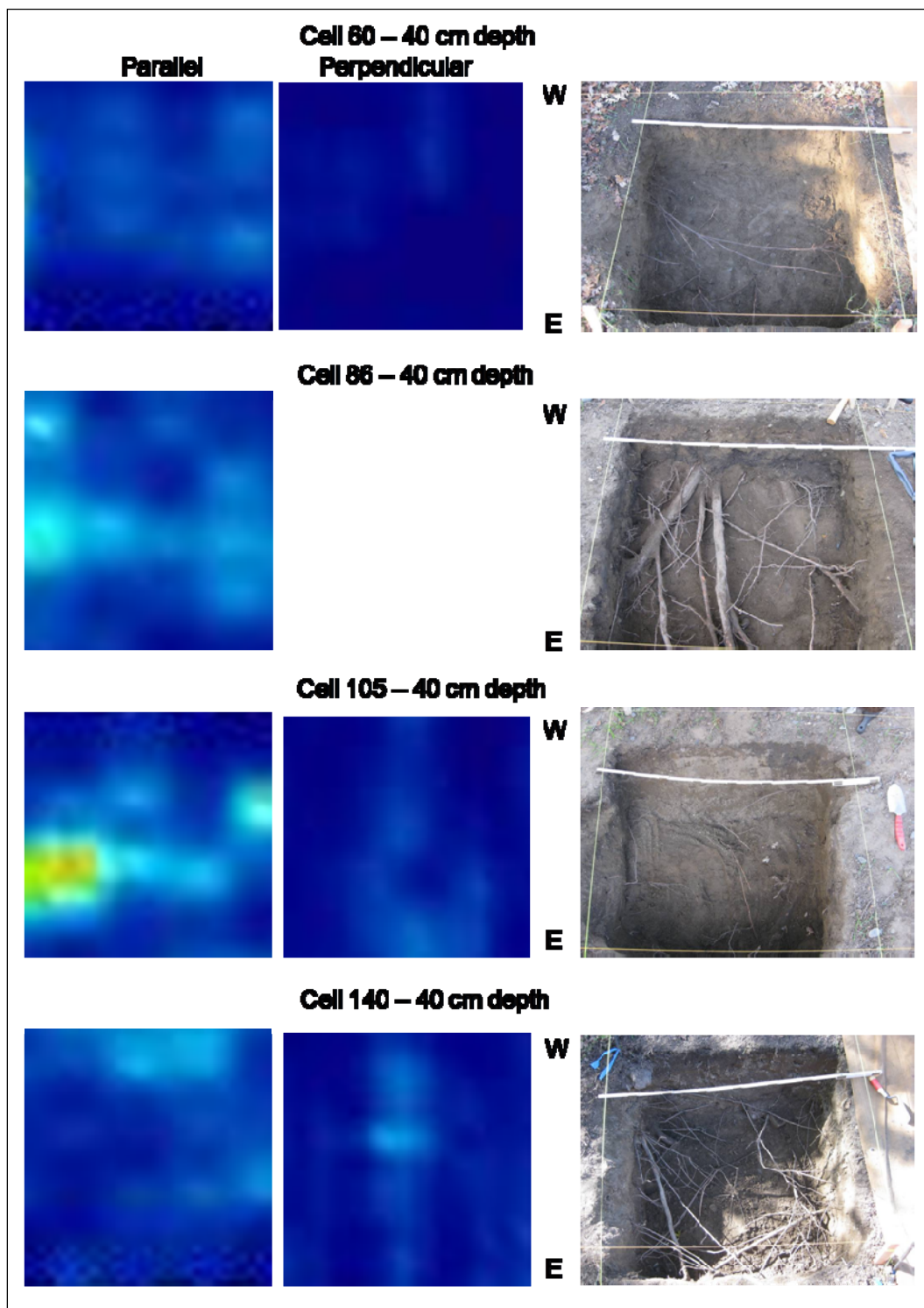


Figure 191. Comparison of GPR sections and photographs of root characterization cells at 40-cm depth.

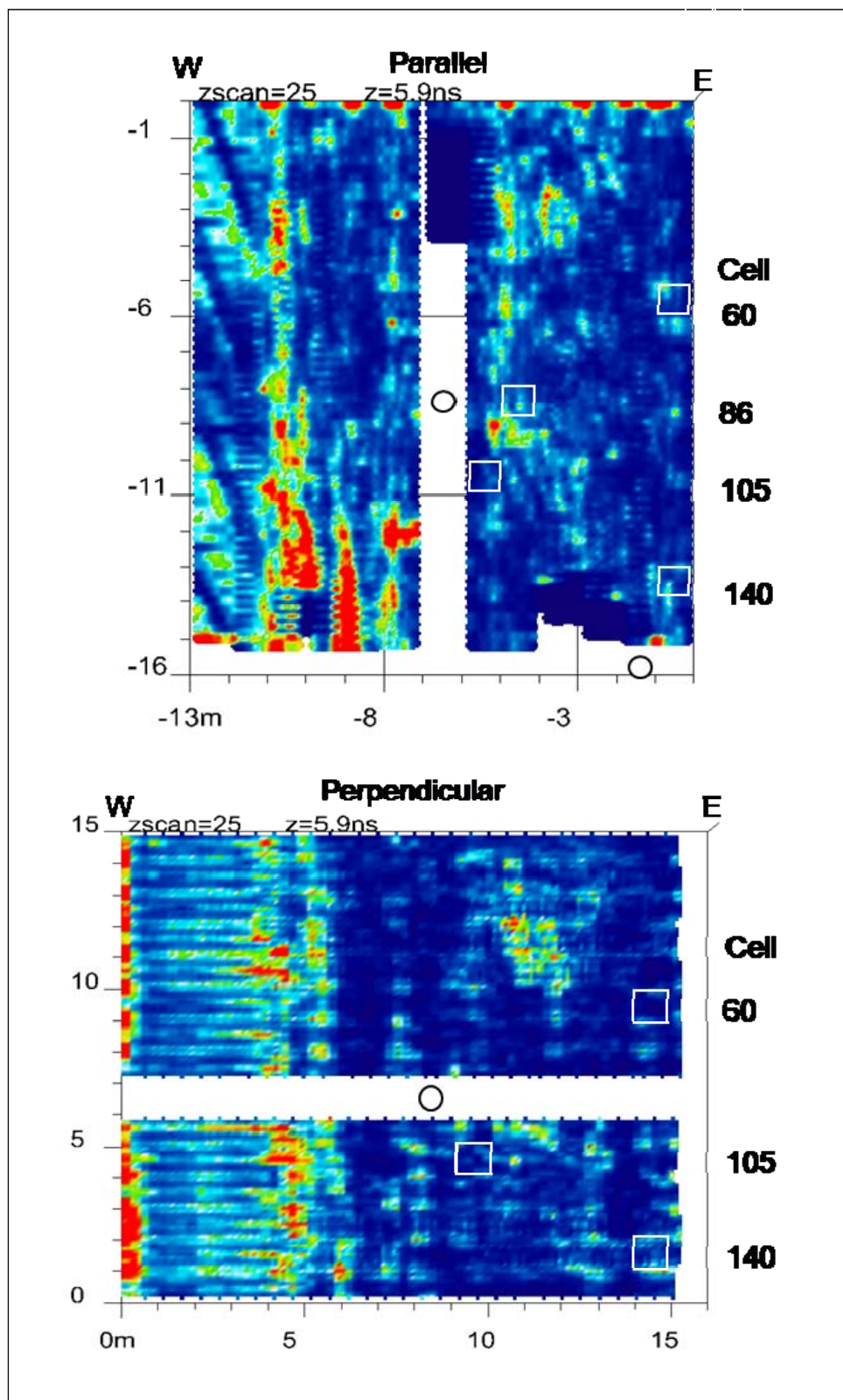


Figure 192. GPR depth slices at 60 cm (actual 59 cm) parallel and perpendicular to the crest with outline of root characterization cells and tree position (circle).

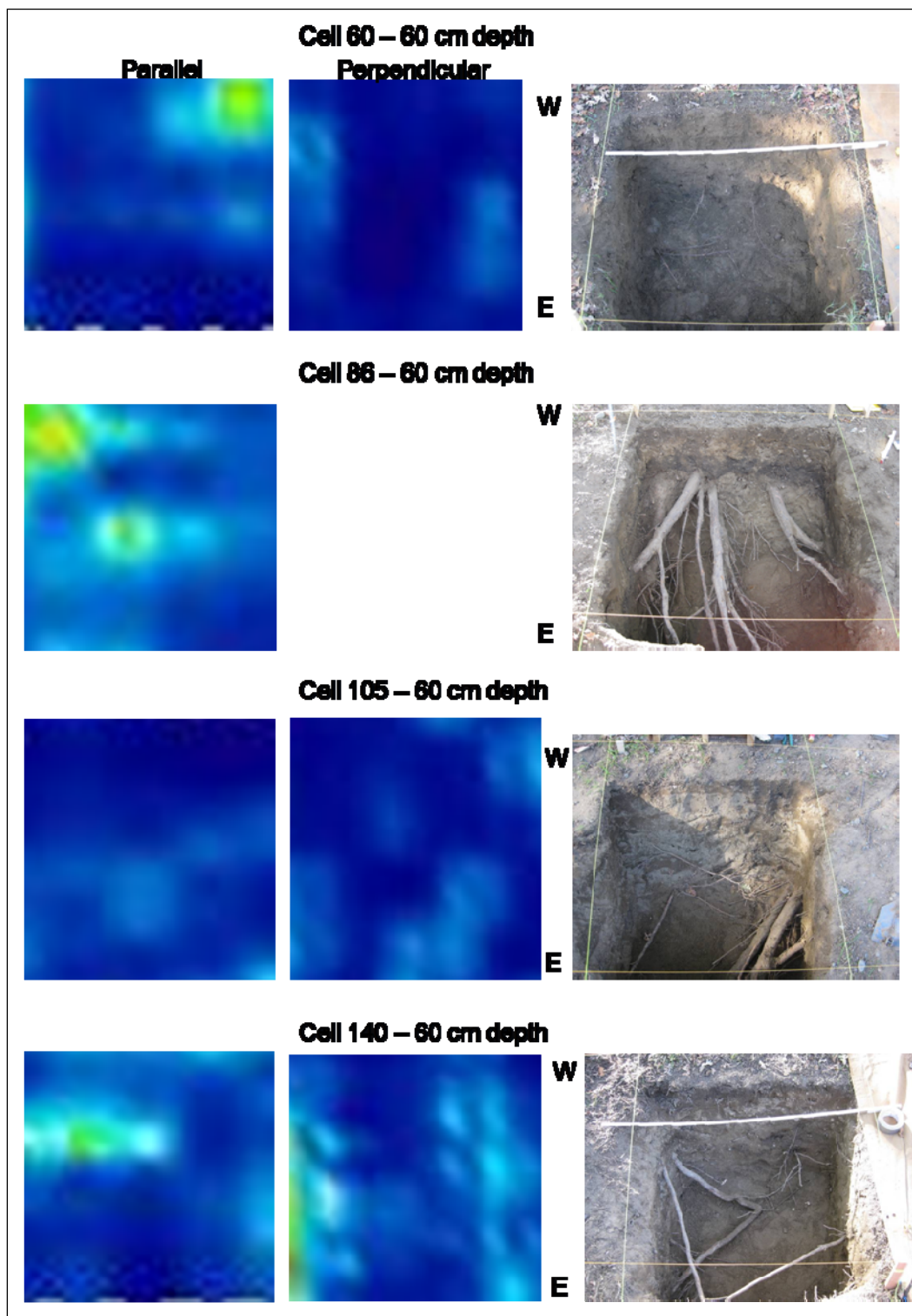


Figure 193. Comparison of GPR sections and photographs of root characterization cells at 60-cm depth.

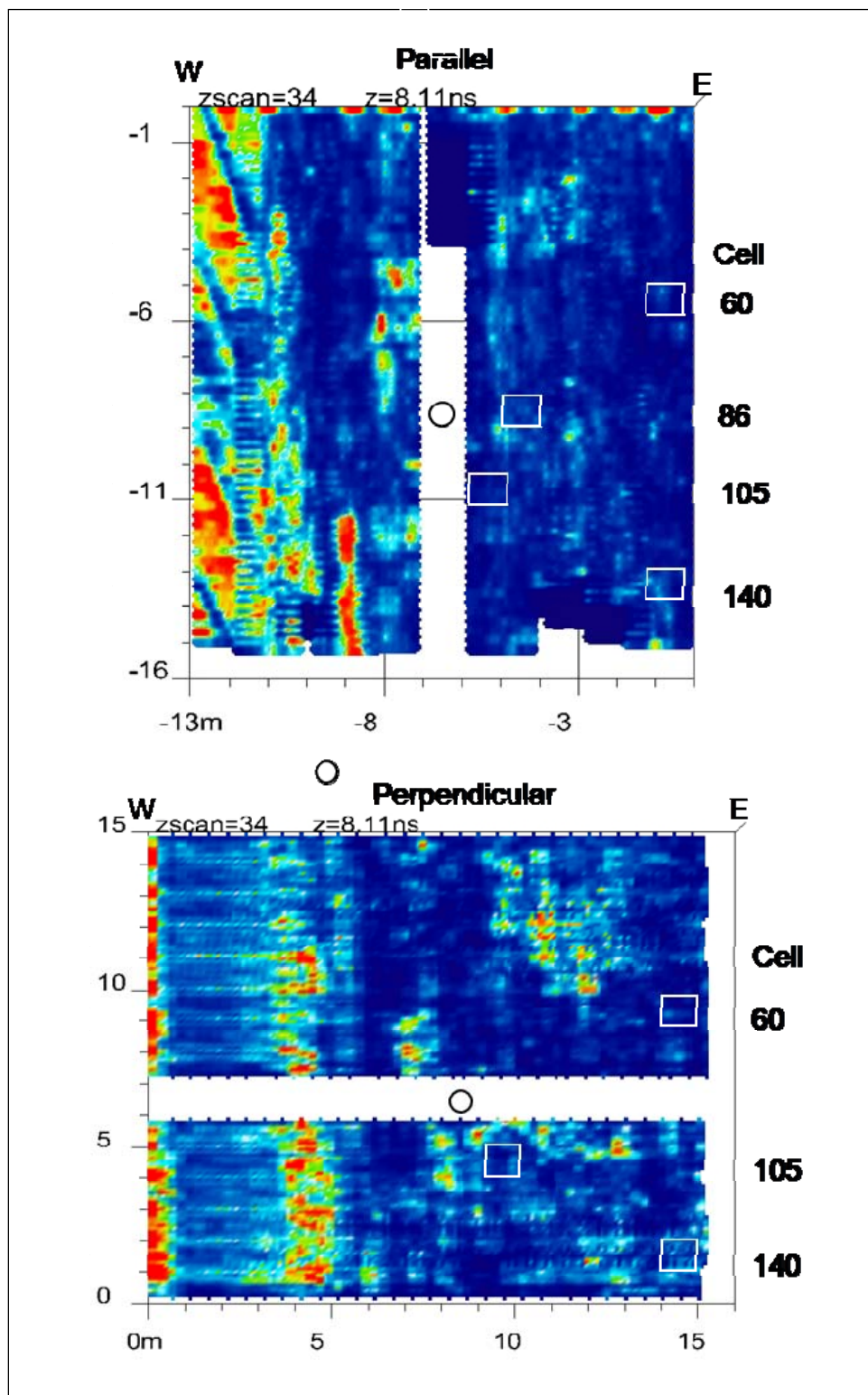


Figure 194. GPR depth slices at 80 cm (actual 81.1 cm) parallel and perpendicular to the crest with outline of root characterization cells and tree position (circle).

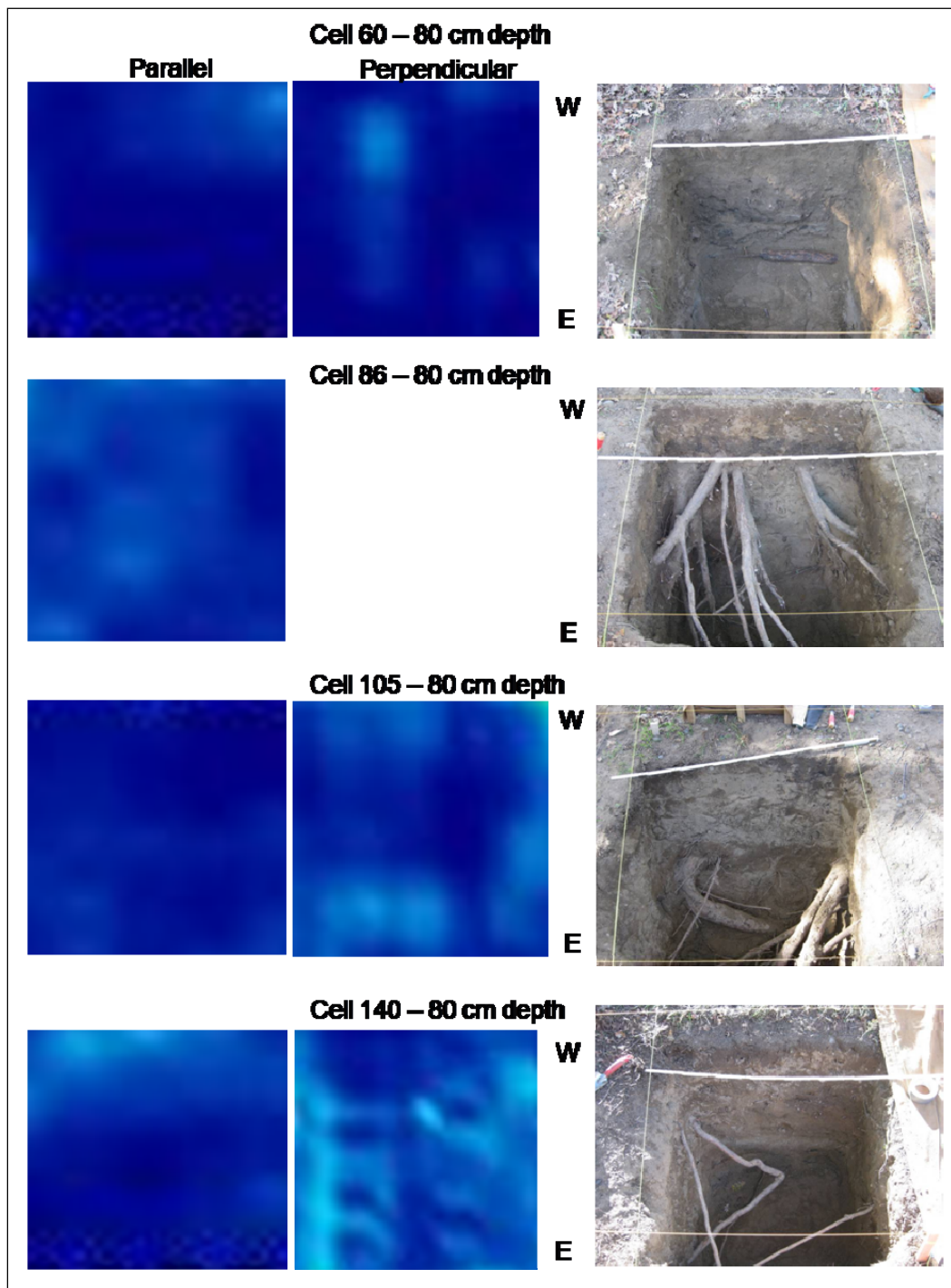


Figure 195. Comparison of GPR sections and photographs of root characterization cells at 80-cm depth.

Calibration of GPR

In addition to bulk properties of root systems, individual root location, size, and orientation is likely required for some applications (e.g., roots in proximity to infrastructure such as pipes, slurry walls, or T-Walls). As discussed in previous sections of this report, root architectural data are challenging, time-consuming, and in many cases costly to collect. Ideally, root measurements would be rapidly conducted with noninvasive tools such as GPR (Danjon and Reubens 2008).

Existing work has shown that under favorable soil moisture and texture conditions, i.e., moist, sandy soils, GPR can effectively identify known roots (Butnor et al. 2001; Barton and Montagu 2004; Hirano et al. 2008; Zanetti et al. 2011). However, few studies have attempted to measure root architecture in situ with GPR (Hruska et al. 1999; Stokes et al. 2002; Cermak et al. 2006b; Danjon and Reubens 2008). These studies have shown that GPR accuracy increases when coupled with invasive sampling with cores, pits, or trenches (Butnor et al. 2003; Nadezhda and Cermak 2003b).

The objective of this study is to examine GPR efficacy for in situ measurement of root location, size, and orientation (i.e., root architecture) under favorable instrument conditions. To do so, 9 m² of high resolution, multi-frequency GPR data were collected around a loblolly pine (*Pinus taeda*), excavated six 1-m³ sub-samples from this zone, and measured three-dimensional (3-D) root locations with an electromagnetic digitizer as well as a photographic registration, rectification, and modeling software.

Methods

Study site

Soil properties have the potential to limit penetration depth and reduce signal-to-noise ratio of ground-penetrating radar (GPR, Butnor et al. 2003). As such, a study site was selected in favorable conditions for GPR (i.e., sandy soils) in proximity to ERDC laboratories in Vicksburg, MS (Figure 196). Mean annual temperature and rainfall at the site are 18.6°C and 147.3 cm, respectively. A single loblolly pine (*Pinus taeda*) was chosen that was isolated from neighboring trees by more than 10 m (dbh = 40 cm, tree height = 8.8 m, canopy width = 10.4 m north-south × 8.8 m eastwest). A 3-m × 3-m sampling grid was established on the east side of the tree

oriented N23E as a consistent spatial reference for subsequent analyses (Figure 197). The tree is situated in a well-drained, coarse-grained sandy soil ($D_{50} = 0.68$ mm, $n = 24$).



Figure 196. Aerial (top) and panoramic (bottom) photographs of the study site, Vicksburg, MS.

Ground-penetrating radar

A ground-penetrating radar (GPR) survey was performed to map the subsurface location of roots extending from the study tree. The GPR survey used a Sensors and Software, Inc. pulseEkko 1000 high frequency system (Figure 198). Three antenna frequencies were used: 450 MHz, 900 MHz, and 1,200 MHz. Data were collected in the north-south (N-S) direction with the 450- and 1,200-MHz antenna, but were collected in both the N-S and east-west (E-W) directions with the 900-MHz antenna. A wheel odometer was used to track distance traveled, with a 2-cm along-line step increment used with the 450-MHz antenna, and a 1-cm step with the 900- and 1,200-MHz antenna. Survey line spacing for the 450- and 900-MHz antenna was 25 cm, whereas 10-cm line spacing was used with the 1,200-MHz antenna. Average volumetric moisture content was 23.1, 24.7,

26.4, 31.4, and 33% at depths of 10, 20, 30, 40, and 50 cm, respectively. The survey was conducted after a heavy rain the previous night.

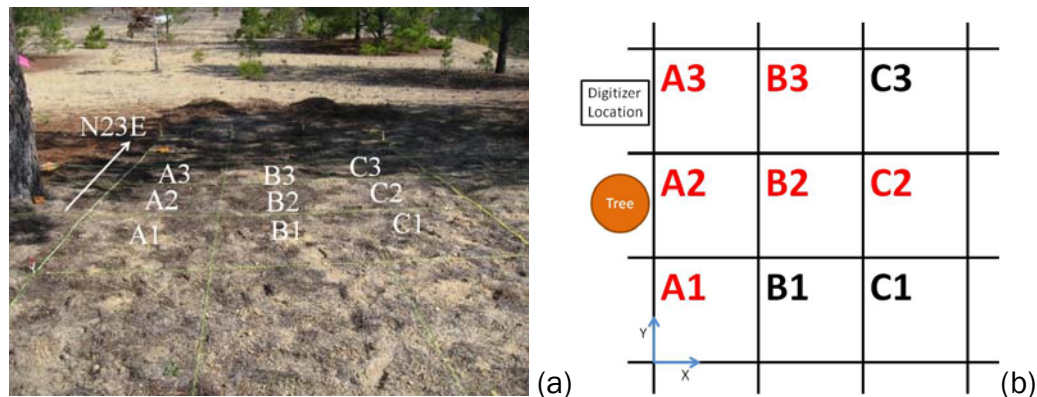


Figure 197. (a) Survey grid located on the east side of the pine tree divided into nine 1-m × 1-m cells. (b) Schematic of sampling grid showing local coordinate system (blue arrows) and cells selected for excavation (red font).

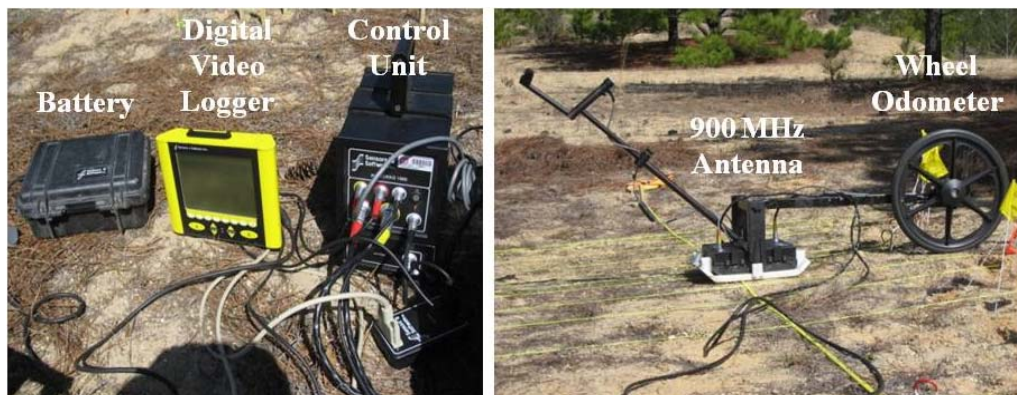


Figure 198. Sensors and Software pulseEkko 1000 antenna system using a wheel odometer to measure distance traveled.

In situ measurement

To verify GPR predictions, six of the nine cells within the sampling grid were excavated and roots were measured in situ. GPR was expected to detect roots no smaller than 2 cm in diameter (Hirano et al. 2008). Thus, verification cells were selected to maximize root size (Figure 197). Each 1.0 m² cell was excavated in 0.25-m increments to a depth of 1 m to capture changes in root properties and GPR efficacy as a function of depth. Soil was removed using a GuardAir Air-Spade 2000 with a 225-ft³/min nozzle supplied by a 375-ft³/min air compressor (See Danjon and Reubens 2008 for a review of root architectural methods). This technique has been shown to produce minimal disturbance to small roots with roots as small as 1 to 2 mm remaining after excavation (Cermak et al. 2006, Danjon et al.

2007). For each depth increment, a representative soil sample was taken for analysis of grain size, gravimetric soil moisture on the excavation date, and total organic content.

Following excavation of each 0.25-m layer, roots less than 2 cm in diameter were clipped and reserved for laboratory analysis. Remaining coarse roots were labeled, marked for digitization, and diameter was measured with a Vernier caliper at each digitization point. Digitization points were taken at 5-cm intervals along a given root unless changes in root diameter, shape, or orientation required smaller intervals (Di Iorio et al. 2005). Root position was measured with a 3-D digitizer (3SPACE Fastrak, Polhemus, Long Ranger Option) using low-frequency electromagnetic field sensing and driven by Polhemus software (FTGui). Three digitization lines were taken for each root approximately 120 deg apart as viewed by root cross-section with the primary line located on the top of the root. Numerous local benchmarks were established to verify instrument stability with data points taken prior to and following measurement. Benchmarks were also used to assess precision of the Polhemus Long Ranger by surveying each benchmark a minimum of 60 times. Root locations were plotted in three dimensions for visual comparison using SigmaPlot 11.0. Root digitization was used to calculate root length, and assuming roots are cylindrical between digitization points, length was combined with measurements of diameter to estimate coarse root volume.

Photogrammetry is the process of generating 3-D coordinates using two-dimensional (2-D) photographs. Photomodeler Scanner (PMS, Eos Systems Incorporated) uses this technology to generate 3-D point clouds of high definition 2-D images (Alby et al. 2009). Image-based modeling with the PMS software provides an alternative to electromagnetic digitization for estimating coarse root length and volume (Cermak et al. 2006b, Danjon and Reubens 2008). Image based modeling has become popular because of ease of use and affordability of alternative software (Remondino and El-Hakim 2006). Once a line of sight was created via excavation, photographs were taken of each root at several stations with a calibrated Nikon D300S single lens reflex camera. Photographs were uploaded to PMS and cross referenced using multiple benchmarks. Using one photograph as a reference, benchmarks were identified in as many photographs as possible. Throughout this process, the reference photograph was changed several times because each image does not capture all benchmarks required for accurate cross referencing. After each

photograph has obtained a sufficient number of reference points, the PMS software produces a 3-D point cloud, which can be extracted and analyzed using computer aided design (CAD) software. Cylinders were manually fit in CAD and used to estimate root length and volume.

Laboratory analyses

Soil samples from multiple depths in each sub-sampling unit were sealed and returned to the laboratory. Samples were weighed, oven dried at 180°C for 24 hr, and reweighed to determine gravimetric moisture content. Samples were then subjected to grain size analysis by mechanical sieving and gravimetric analysis. Three sub-samples were then dried in a 550°C furnace for 1.5 hr to determine total organic content by mass (TOC). Clipped roots (i.e., those < 2 cm) were oven dried at 180°C for 24 hr to determine organic dry mass. Root volume was measured for all samples greater than 100 g by measuring the change in volume in a graduated cylinder after submerging roots.

Results

Ground-penetrating radar

The moist sand on the sample date and lack of subsurface targets other than the tree roots provided a good medium for GPR signal propagation. Example radar profiles acquired using each frequency are shown in Figure 199. Based on a subsurface electromagnetic wave velocity of 0.1 m/ns, the depth of investigation was about 0.9 m, 1.6 m, and 2.0 m for the 1,200-MHz, 900-MHz, and 450-MHz antenna frequencies, respectively. Figure 200 presents a comparison of a plan view image at a similar depth range for the three antenna frequencies. This figure clearly illustrates how the resolution improves as the frequency of the antenna increases. As stated previously, data were acquired in the N-S direction only with the 450- and 1,200-MHz antennas, while it was collected in both the N-S and E-W directions with the 900-MHz antenna. Figure 201 demonstrates the improvement in root delineation achieved by using a combined orthogonal data set as opposed to a data set acquired in a single direction. This is because the GPR response is strongest when the long axis of a target is oriented perpendicular to the direction the antenna travels. Observe in Figure 201 the root within the circle outline in each image. The N-S traverse images the E-W section of the root, whereas the E-W traverse images the N-S section. Combining both the N-S and E-W data sets provides a more

complete image of the root. In the following discussion, only images of the combined 900-MHz data will be presented, although final root delineations will be presented for each of the three antenna frequencies.

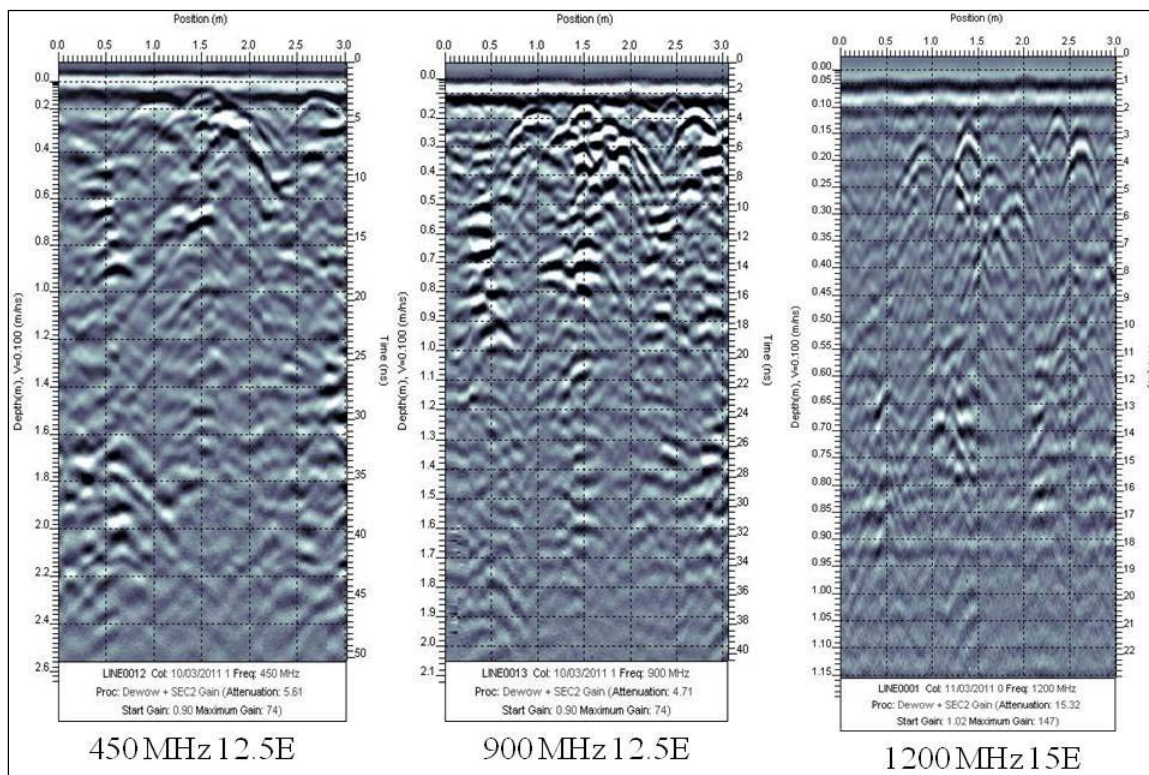


Figure 199. GPR profiles showing data acquired with the three antenna frequencies, and the difference in depth of signal penetration and resolution for each frequency.

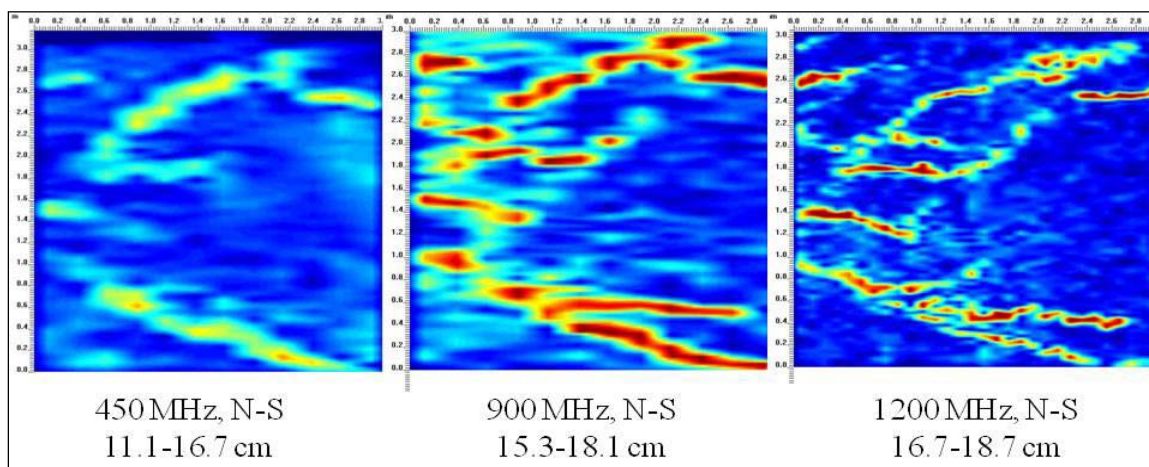


Figure 200. GPR depth images showing an improvement in target resolution with an increase in antenna frequency.

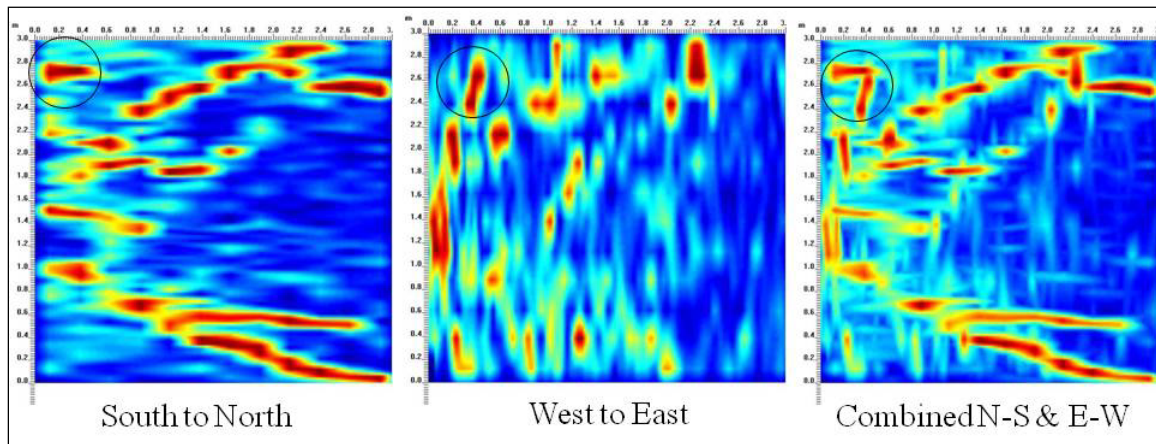


Figure 201. 900 MHz (15.3-18.1 cm) depth images illustrating the dependence of root delineation on the direction of survey traverse.

The depth images presented in Figure 202 are representative of the 900-MHz data. These images and others were used to map the roots identified in Figure 203. Figure 203 shows all roots mapped with each antenna frequency and a combined map within the depth range 0 to 50 cm. No roots were excavated deeper than 50 cm.

Figure 204a is a comparison of the roots mapped with a combined signal using GPR at depth ranges of 0 to 25 cm and 25 to 50 cm with the excavation photographs prior to clipping the roots. Figure 204b is a photograph taken after the excavation was completed to give a better view of the roots with a diameter of 2 cm and greater. This photograph has not been rotated to orient it with the grid to allow a better view of the roots. Note the numerous small diameter roots present in the excavation photographs. The tree has some roots greater than 2-cm diam, but roots < 2-cm diam dominate the root system. The majority of roots are located in the upper 25 cm. The GPR was successful at imaging the larger roots (≥ 2 cm) and also mapped roots of lesser diameter. The root enclosed by the red ovals in Figures 204a and 204b is an example of an odd-shaped root imaged by the GPR. The other roots seen in the clipped photograph were also mapped with the GPR, along with numerous smaller roots.

In situ measurement

Thirteen local benchmarks were surveyed with 60 independent observations each to check the accuracy of the digitizer. Benchmarks were distributed at varying distances throughout the sampling grid, and thus, provide the opportunity to examine instrument accuracy with increasing

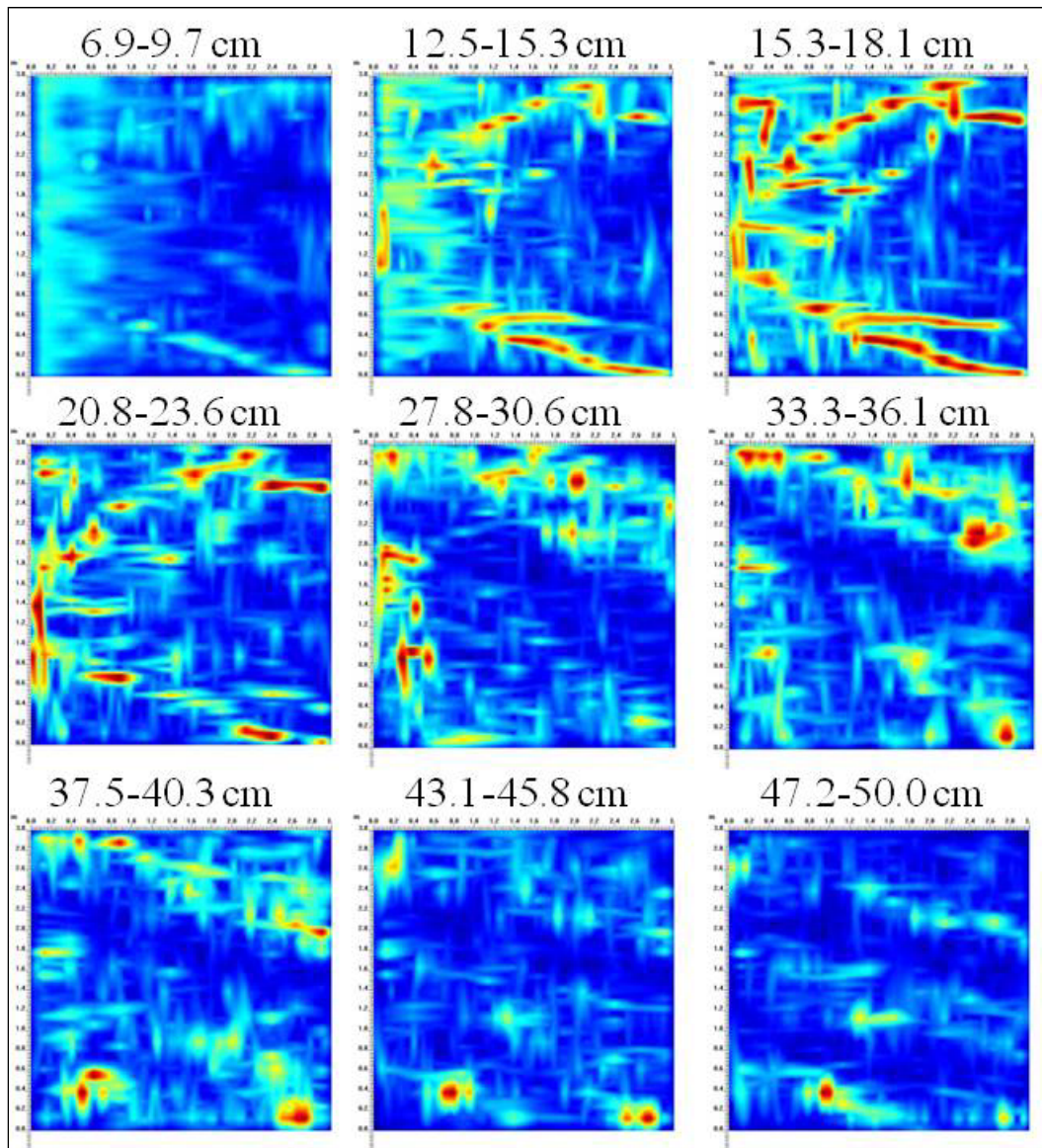


Figure 202. Select depth images of the combined 900 MHz GPR data.

distance from the digitizer. Figure 205 shows the standard deviation and range of these measurements as well as the maximum root distance sampled. Given that only two roots extend beyond 250 cm (Roots 4 and 4B), the accuracy of the digitizer is well within needed accuracy limits of this study.

Eleven roots greater than 2 cm in diameter were digitized. Each root was marked at 5-cm intervals for digitization unless an anomaly required greater resolution. Roots varied in length from 11 cm (Root 1A, 4 digitization points) to 247 cm (Root 4, 59 digitization points), and varied in maximum diameter from 2.27 cm (Root 6) to 8.02 cm (Root 4). For each root,

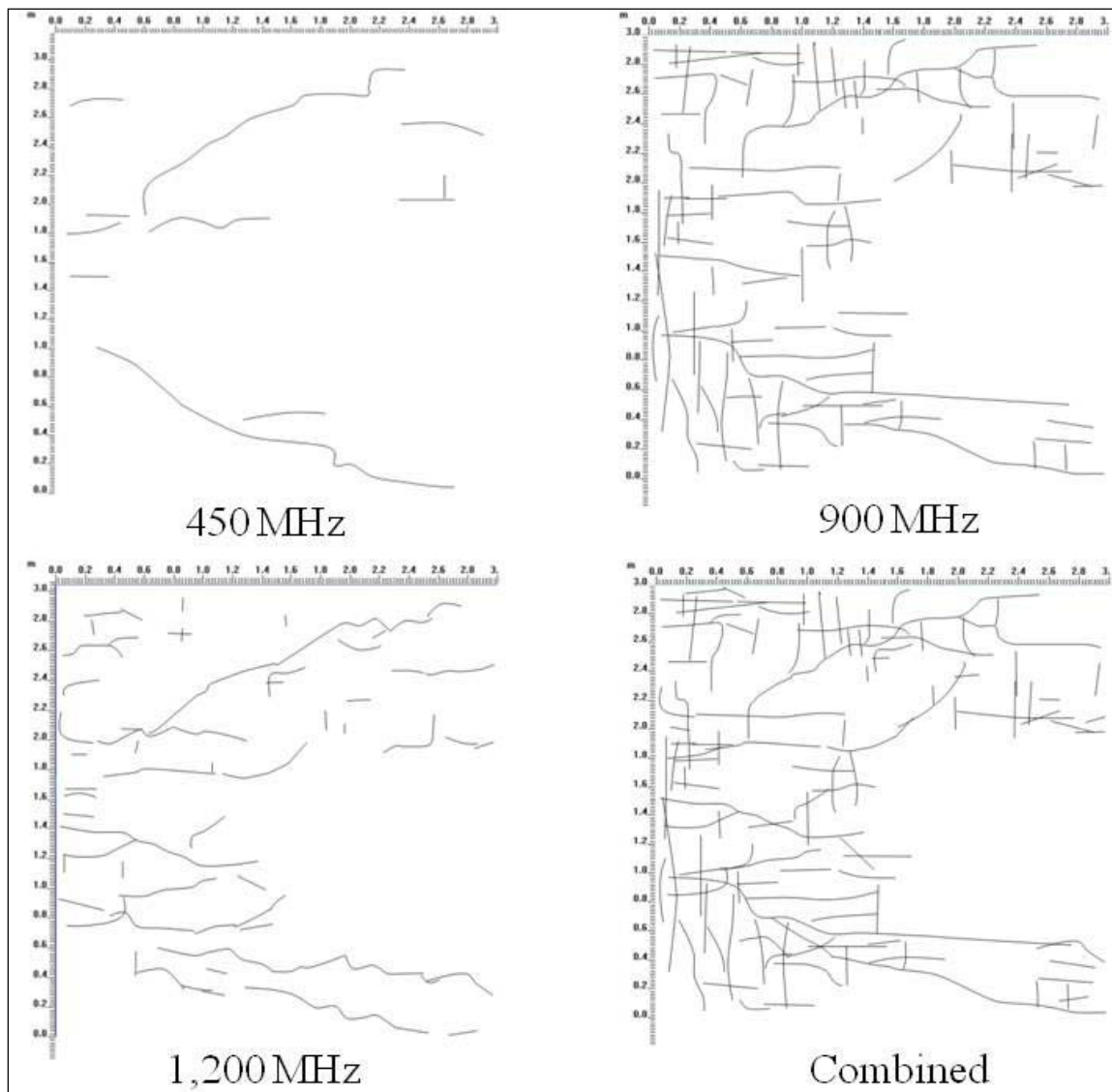
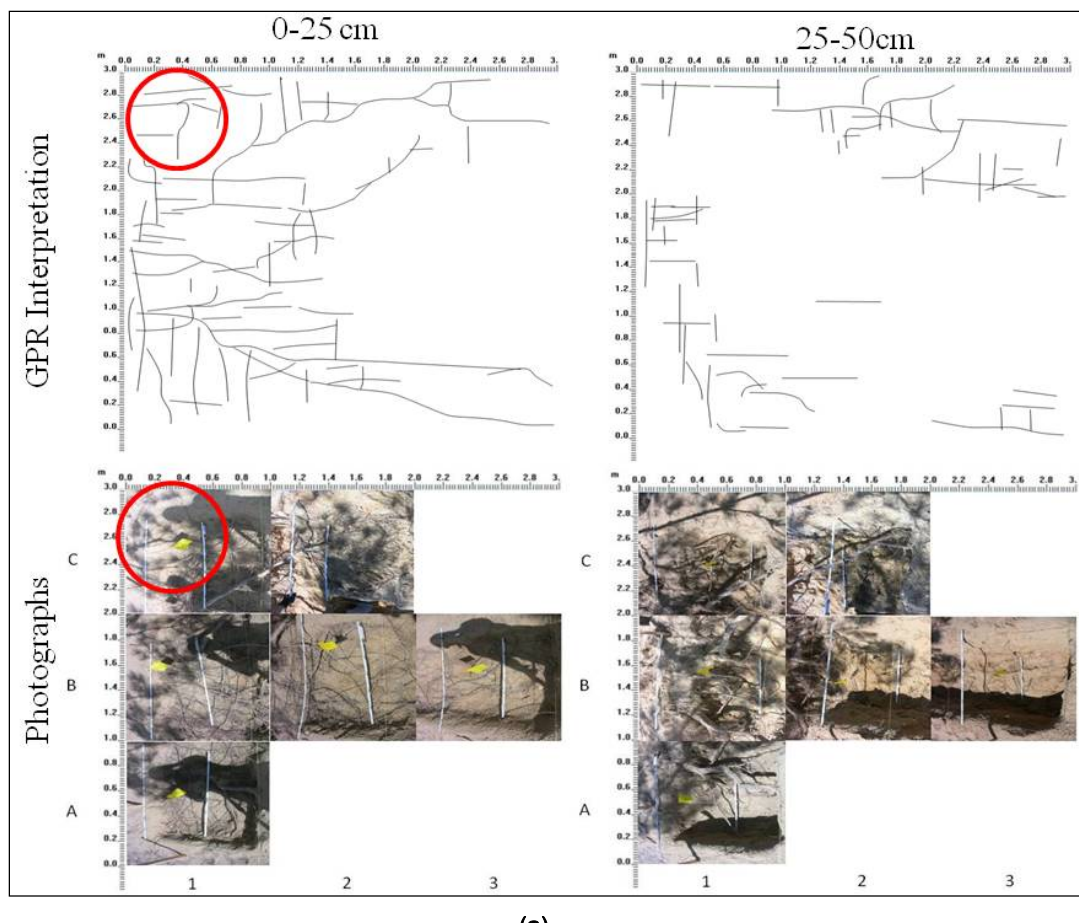


Figure 203. Root interpretations between the depth range 0 to 50 cm for GPR data collected with the 450-, 900-, and 1,200-MHz antennae.

three digitization lines were taken approximately 120 deg apart as viewed by root cross-section with the primary line located on the top of the root. The primary digitization line was used to plot the location of roots. Root diameter and digitization were applied to estimate coarse root length and volume by assuming cylindrical geometry. Additionally, Photomodeler Scanner (PMS) was applied to estimate root length and volume from calibrated photographs. Table 49 presents estimates of root length and volume for each technique, and Figure 206 shows virtual renderings of the root system from digitization and photo-modeling.



(a)



(b)

Figure 204. (a) Comparison of interpreted roots with excavation photographs for depth ranges 0 to 25 cm and 25 to 50 cm. (b) Photograph of excavated roots >2 cm.

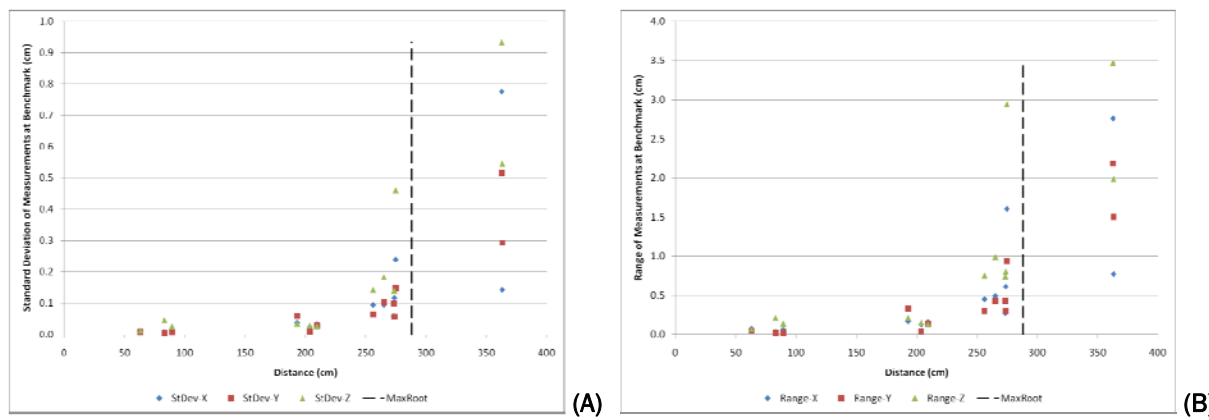


Figure 205. Error in 60 digitization measurements at 13 local benchmarks with increasing distance between transmitter and received: (a) standard deviation and (b) range.

Table 49. Coarse root properties.

Root	Diameter (cm)	Digitizer (DG)		Photo-Modeler (PM)		Percent Difference	
		L (cm)	V (cm ³)	L (cm)	V (cm ³)	L (%)	V (%)
1	7.99	99.0	2453.7	87.9	2918.3	11.2	-18.9
1A	4.44	11.1	135.3	10.2	109.7	7.8	18.9
1A-1	5.42	37.0	181.3	24.0	141.8	35.1	21.8
1B	3.82	20.1	169.6	22.0	196.5	-9.6	-15.8
2	2.28	35.7	132.1	29.1	166.6	18.4	-26.1
4	8.02	246.7	3875.3	185.5	3352.7	24.8	13.5
4A	2.83	15.3	75.2	11.0	83.0	27.9	-10.3
4A-1	2.27	15.5	49.3	11.8	45.8	23.7	7.2
4B	2.73	23.8	127.8	19.5	166.8	17.9	-30.5
5	2.59	47.3	147.0	31.4	129.3	33.6	12.0
6	2.27	36.5	107.7	28.4	88.1	22.1	18.2

+ Calculated as (DG-PM)/DG.

Soil samples collected during excavation were subjected to grain size, soil moisture, and organic content analyses (Table 50). Grain size was remarkably uniform across each of the six cells and can be classified as medium to coarse sand (e.g., for D₅₀, mean = 0.68 mm, standard deviation = 0.09, n = 24). Organic content was typically low (mean = 0.72%). Fine root samples (< 2 cm) were weighted and specific gravity was determined for all samples greater than 100 g (mean = 0.56, standard deviation = 0.06). Specific gravity was within range of values reported elsewhere for loblolly pines (0.413, Gibson et al. 1986). Site specific root densities were used to estimate fine root volume.

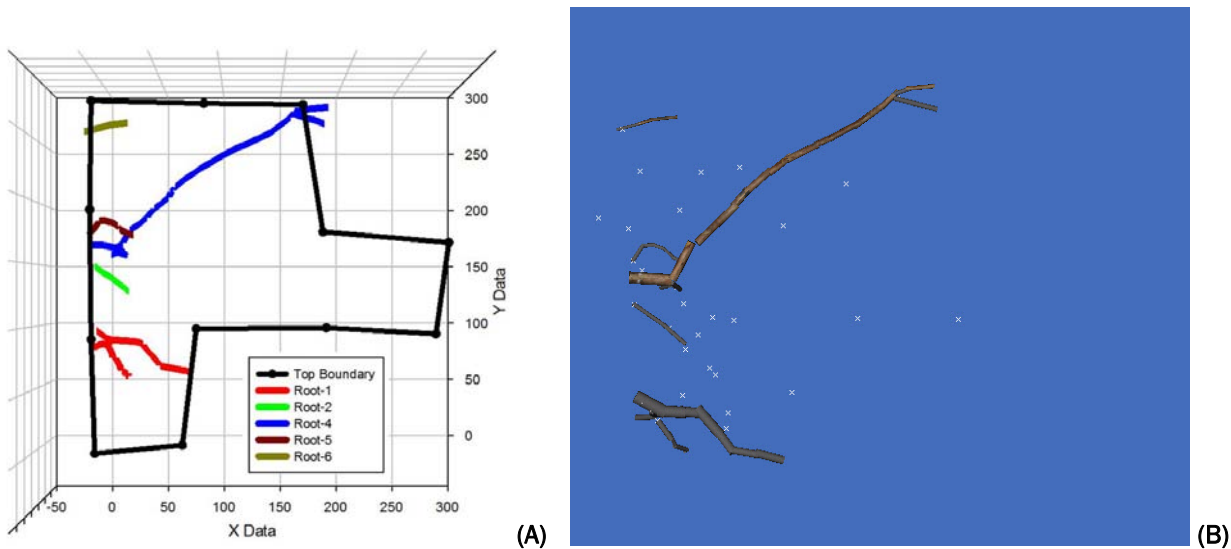


Figure 206. Virtual representation of the study root system generated from electromagnetic digitizer (a) and calibrated photographic modeling (b).

Conclusions

The clean, moist sand at this location provided a conducive environment for ground-penetrating radar survey. Based on visual comparison amongst methods (Figure 207), roots smaller than 2 cm in diameter were able to be mapped. Use of orthogonally collected data sets provided a more complete image of the tree root system, and the position of the mapped roots agreed with excavation data. No attempt was made to estimate tree root diameter and/or volume based on the GPR data. Butnor et al. (2001, 2003) have had limited success in correlating GPR signal strength with root diameter because of influences such as signal attenuation with depth, oblique angle crossing, and dielectric properties of the medium. Barton and Montagu (2004) found a correlation between waveform zero crossings with root diameter; however, it was only applicable to the 500-MHz data they collected and not the 800-MHz or 1-GHz data. The high quality GPR data set acquired in this study, along with detailed excavation data, will provide an opportunity for studying correlations between GPR waveform characteristics and root diameter/volume estimations.

Opportunities for future research

This study has assessed the feasibility of measuring the location, size, and orientation of individual roots with ground-penetrating radar. This analysis was conducted under favorable GPR conditions on a single tree, and thus the results may be limited by sample size and location. The

Table 50. Summary of soil and fine root properties.

Cell	Depth	Organic Content (%)	Moisture ^a Content (%)	Grain Size			Fine Roots (< 2 cm)	
				D ₉₀ (mm)	D ₅₀ (mm)	D ₁₀ (mm)	Mass (g)	Volume (cm ³) ^b
A1	0-25 cm	1.45	2.82	4.21	0.50	0.26	272.4	486.5
	25-50 cm	0.96	4.90	6.48	0.58	0.26	150.4	268.6
	50-75 cm	0.36	4.04	> 8	0.81	0.38	84.7	151.3
	75-100 cm	0.98	6.51	4.75	0.62	0.29	121.9	217.7
A2	0-25 cm	1.04	2.43	6.07	0.60	0.28	392.5	700.9
	25-50 cm	0.48	3.84	6.64	0.72	0.30	760.5	1358.1
	50-75 cm	0.75	4.04	6.77	0.69	0.31	91.2	162.9
	75-100 cm	0.64	3.97	6.86	0.69	0.32	91.0	162.5
A3	0-25 cm	0.52	2.57	7.05	0.57	0.27	207.3	370.2
	25-50 cm	0.34	3.44	7.22	0.60	0.26	194.1	346.6
	50-75 cm	0.96	5.00	5.94	0.71	0.32	24.6	43.9
	75-100 cm	0.36	4.40	4.26	0.65	0.28	79.0	141.1
B2	0-25 cm	0.52	3.00	5.36	0.48	0.25	279.5	499.1
	25-50 cm	2.06	3.37	> 8	0.82	0.37	15.9	28.4
	50-75 cm	1.05	5.14	6.17	0.75	0.37	18.5	33.0
	75-100 cm	0.38	7.99	4.86	0.75	0.34	8.3	14.8
B3	0-25 cm	0.59	2.30	6.33	0.69	0.30	234.7	419.1
	25-50 cm	0.75	4.86	7.53	0.74	0.31	126.1	225.2
	50-75 cm	0.26	4.75	6.88	0.72	0.34	32.5	58.0
	75-100 cm	0.41	5.74	5.64	0.86	0.43	37.8	67.5
C2	0-25 cm	1.34	3.00	7.32	0.64	0.28	80.7	144.1
	25-50 cm	0.15	4.54	7.19	0.69	0.28	33.1	59.1
	50-75 cm	0.66	5.17	6.52	0.71	0.32	7.7	13.8
	75-100 cm	0.27	5.66	5.56	0.77	0.35	0.6	1.1

^a Gravimetric moisture content.^b Estimated from mass (lab sample) and root density (0.560 g/cm³).

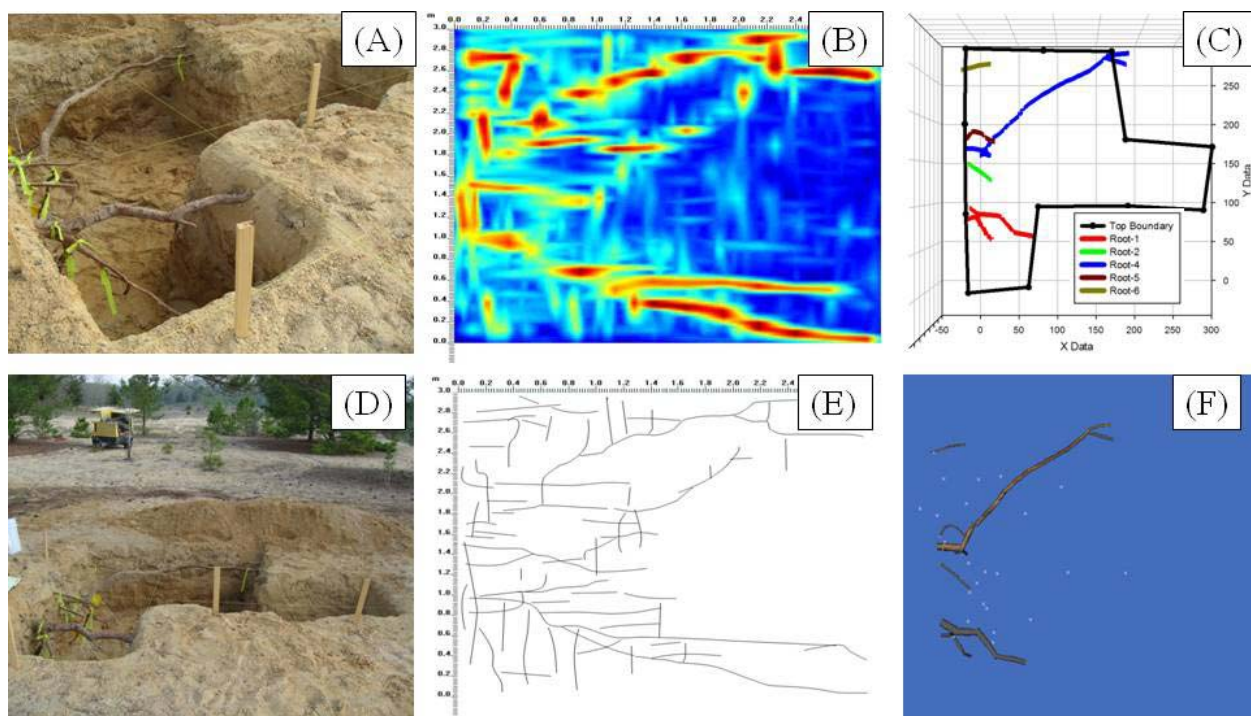


Figure 207. Qualitative comparison of root detection techniques: photographs of sampling area (a/d), GPR data (b) and interpreted roots (e), electromagnetic digitization (c), and calibrated photographic modeling (f).

following topics highlight potential areas of future research related to in situ detection and measurement of roots.

- *Quantitative validation:* This comparison between GPR predictions and excavated root morphology has been primarily qualitative in nature. Additional quantitative comparisons among root detection methods should be conducted to better refine the strengths and limitations of the tool. Key topics to be addressed include detection thresholds in root size, soil type, and depth, application of spatial statistics to examine the accuracy of root predictions with respect to location and orientation, and the capacity to predict bulk properties.
- *Calibration of noninvasive tools:* This analysis has focused primarily on verification of GPR; however, there is potential to calibrate these tools with limited sub-sampling. For instance, a tree with a root zone of 10 m could be assessed with GPR, and a small amount of sub-sampling (e.g., a few 1 m³ excavation pits) could be used to assist with interpretation of radar data (i.e., “train” the instrument). At present, the amount of improvement in predictive resolution and the number of subsamples required for this improvement is unknown.

- *Increasing GPR signal strength:* This study has examined a single tree in a favorable soil environment. The soil conditions suitable for GPR are relatively well-known (Doolittle et al. 2007). However, the interaction between soil and plant conditions has not been adequately addressed. For instance, taxa with greater wood density (i.e., higher specific gravity) may provide a stronger contrast between soil and roots and thus a better prediction of root morphology (Butnor et al. 2001). Additionally, there may be techniques for increasing the signal strength of the GPR by modifying the root environment with moisture or electrical current.

Geo-referenced LiDAR collection for root characterization

Background

In April 2010, ERDC identified the need for an additional method to collect root distribution information. Although geophysical and in situ methods proved successful in identifying roots within the capabilities of the techniques, a more detailed characterization of roots was needed for the 3-D model.

LiDAR was tested at a site in Vicksburg, MS. A southern red oak, typical of species found along slopes, banks, toes of levees or canals and rivers, was selected for the scan. The tree is situated on a moderate slope with a clay soil. Scans were performed prior to soil disturbance, and after excavation of soil to expose the roots.

Method

ERDC used two Trimble GXA LiDAR scanner systems simultaneously to collect LiDAR points of the roots, ground, trunk, and canopy of the tree at evenly spaced 5-mm intervals. The tree was in a leafed out state at the time, and it was a good opportunity to compare the canopy size and geometry to that of the root size and geometry using ground-based, high density LiDAR data.

The tree was georeferenced so that the tree and root positions, their geometry, and the density could be compared to the sun angle, and other sampling methods that may have used a global positioning system (GPS) during their data collection processes. To accomplish this, two

independent, autonomous GPS positions were established within 100 m of the tree using two Trimble R8 GNSS receivers on geodetic tripods.

Each Trimble GXA LiDAR system independently initiates the scanning sequence by collecting point data of prepositioned targets. These are flatfaced targets affixed to a 2-m-tall prism pole supported by a bi-pod. It takes a minimum of three targets to align additional scans to the initial scan, but Trimble, the company producing the LiDAR system, recommends acquiring data from four or more targets during each scan. These additional targets can be used in subsequent scans for additional scan alignment. Five spherical, 37-mm-diam targets were affixed to the tree trunk at this time, and position data were collected on them as well. These targets will be used when the top portion of the tree is removed, and in case some of the surrounding ground-based target locations are destroyed during soil removal.

The tree point cloud data were collected in three phases, and the GPS was used in Phase 1. These phases are as follows:

1. Tree canopy and ground scan
2. Partial excavation and root scan
3. Full (completed) excavation and root scan

Tree canopy and ground scan

The tree and surrounding ground surface, within the approximate drip line plus 10 ft, were scanned from six different locations approximately 60 deg apart, considering a 360-deg circumference about the tree. While acquiring the four LiDAR targets near the tree during the first two scans, the two positions occupied with the GPS equipment were also acquired, as well as the three spheres attached to the tree that could be seen from scanner position 1. Each scan took about 2 hr to complete, and the entire process, including the GPS, took approximately 2 days.

The data from the 6-hr GPS data collection from the two temporary bench marks (TBM) were submitted to the Online Positioning User Service (OPUS) branch of the National Geodetic Survey (NGS) approximately 3 days after the data were collected. This allows the OPUS to collect information from the Continuously Operating Reference Stations (CORS). After submission, the results are usually returned to the submitter within 1 hr. When the results were received, personnel returned to the tree

excavation site, and using RTK-GPS techniques, determined the positions of the four other LiDAR TBM.

The LiDAR scans could then be geopositioned by using a LiDAR processing program called PointScape offered by Trimble. A process of acquiring LiDAR data on targets located at three known spots, and applying a technique called resection, locates the position of each scanner. This correctly orients the first scanner and the now georeferenced LiDAR points (point cloud) to grid north, and then, using the point clouds created by this scanner, all the other target locations, including the spheres on the tree trunk, are queried and these positions are used to geoposition all the other point clouds created by the other scan locations. Each time the scanner is moved to a new location, the operator must require data on at least four of the targets that previously had positions calculated for them.

By use of another Trimble program called RealWorks, the six georeferenced point clouds created in PointScape are combined and edited into a single 3-D point cloud of the tree and ground. The point cloud of the tree canopy and ground contains 10,116,139 points. Figure 208 is a photograph of the tree and the LiDAR scan prior to soil excavation.



Figure 208. (a) Photograph of the southern red oak prior to the LiDAR scan, and
(b) the LiDAR scan of the tree canopy and ground prior to soil excavation.

Partial excavation and root scan

Several weeks after the initial scans of the tree and canopy, ERDC returned to the site for the next set of scans. The tree canopy and partial trunk had

been removed, and the soil to a depth of 0.5 m on the north side of the tree had been excavated.

Removal of the soil left the top surface of the tree root zone exposed, which included both small and larger roots. A LiDAR scan was done at this time so that the smaller roots could be clipped and removed and the soil removal could continue to greater depth.

There were 2,549,934 points in the combined point cloud for the partial root excavation. Figure 209 shows the partial soil excavation around the tree and the LiDAR scan after excavation.

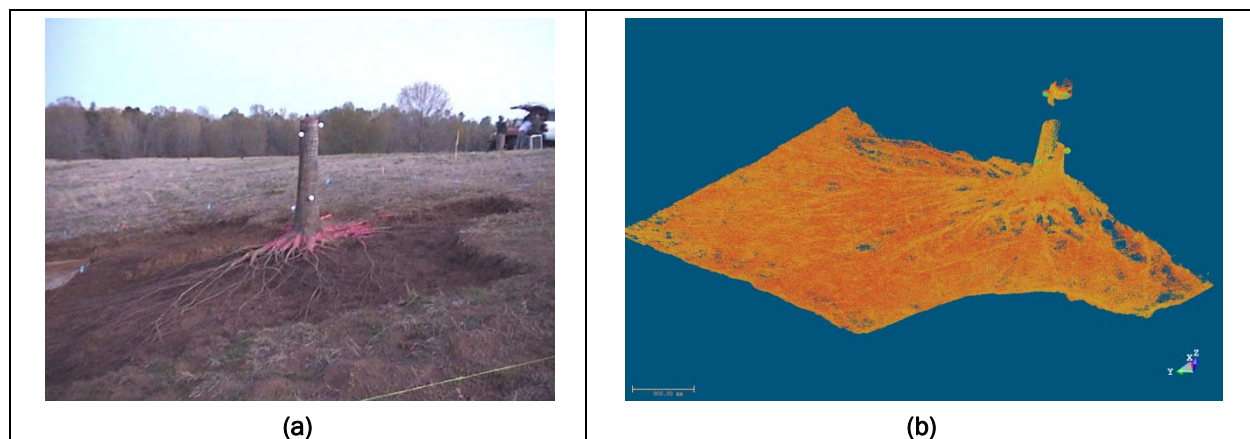


Figure 209. (a) Photograph of the southern red oak with tree canopy removed and soil excavated to 0.5 m, and (b) LiDAR scan after partial excavation.

Full excavation and root scan

The following week the root excavation was completed and ERDC again returned to the site for the next set of scans. This time the tree canopy and partial trunk had been removed, as had the soil to a depth of 1 to 1.5 m around the tree.

The smaller roots had been removed, and the LiDAR could penetrate deeper into the root zone, which mainly now consisted of larger roots. The scanning took about a day and a half. There are 26,399,855 points in the combined point cloud for the full root excavation. Figure 210 is a photograph of the tree and the LiDAR scan of the full excavation.

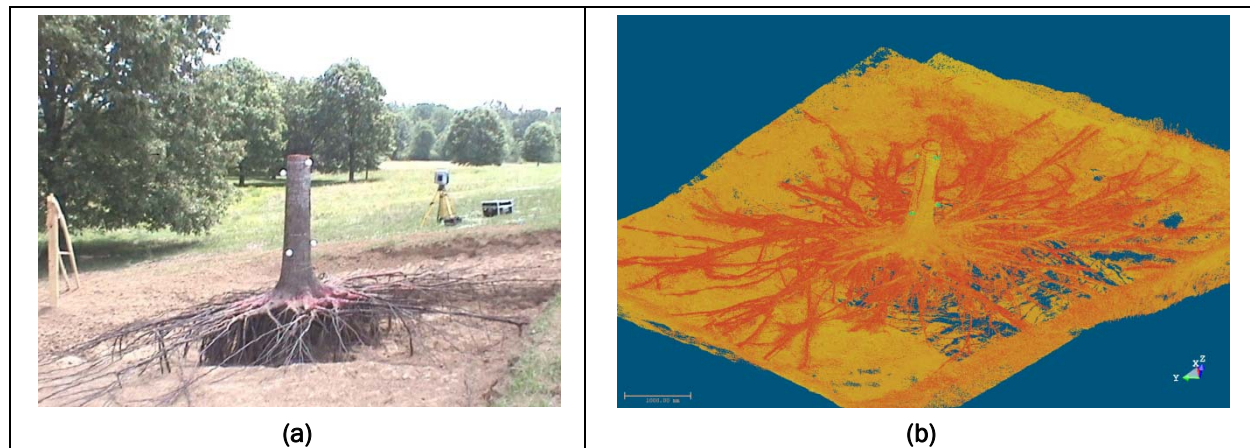


Figure 210. (a) Photograph of the southern red oak tree after full excavation, and
(b) LiDAR scan of tree trunk and exposed roots.

Conclusions

The initial product delivery from this effort was three large, comma-delimited ASCII files containing seven sets of characters in the following format: X , Y , Z (in WGS 84, Zone 15N UTM coordinates), Intensity, Red, Blue, Green. There was also a subsequent delivery of an additional three comma delimited ascii files with 10 characters that contained X , Y , Z , Intensity, Red, Blue, Green, x_{norm} , y_{norm} , and z_{norm} . The data files are used in the 3-D numerical model discussed in Volume III.

5 In Situ Hydraulic Conductivity Tests

Objectives

The objective of the in situ hydraulic conductivity tests is to provide comparative study to determine if root growth alters hydraulic conductivity within a soil horizon. To accomplish this objective, hydraulic conductivity of the soil/root matrix was measured in situ within and around the root mass of a tree and compared to the hydraulic conductivity measured around a control site within the same reach of a levee. These tests were conducted at nine tree sites and nine corresponding control sites. Test locations, tree species, and soil types are listed in Table 51.

Table 51. Locations of in situ hydraulic conductivity tests.

Site Name	Latitude Longitude	Tree Type	Soil Type
Sacramento, CA	38°29'20.4" -121°33'4.64"	valley oak tree, (<i>Quercus lobata</i> Née)	Silty sand
Portland, OR	45°33'32.05" -122°26'15.0"	cottonwood (<i>Populus fremontii</i>)	Silty sand
Burlington, WA	48°27'47.88" -122°18'46.38"	red cedar (<i>Thuja plicata</i>)	Silty sand
Lewisville, TX	33°03'51.14" -96°59'15.2"	post oak (<i>Quercus stellata</i>)	Clay
Vicksburg, MS	32°12'40.13" -90°48'18.36"	red oak (<i>Quercus falcate</i>)	Clay
Albuquerque (1), NM	35°08'31.65" -106°40'36.62"	cottonwood (<i>Populus fremontii</i>)	Silt
Albuquerque (2), NM	35°09'55.07" -106°40'1.07"	cottonwood (<i>Populus fremontii</i>)	Silty sand
Boca Raton, FL	26°21'18.66" -80°17'52.43"	strangler fig tree (<i>Ficus Aurea</i>)	Silty sand
Danville, PA	40°57'47" -76°37'36"	silver maple (<i>Acer saccharinum</i>)	Sandy clay

Hydraulic conductivity is the most important soil parameter for estimating flow of water through soil. It is a required input parameter to every seepage analyses conducted by USACE for design and construction of levees.

To efficiently conduct seepage analyses, levee systems are broken into segments called reaches that are typically 500 to 1000 ft in length. Specific

reach boundaries are chosen such that input parameters can be represented by average values using the best available data about that location. If hydraulic conductivity is influenced by the presence of woody vegetation on levees, the magnitude of its influence must be found to assess the end effect on the seepage analyses. Hence, a secondary objective of this investigation is to obtain realistic boundaries of the parameter to verify ranges used in the ERDC seepage analyses and parameter sensitivity analyses. The purpose of this field effort was to provide comparable data sets for hydraulic conductivity. Hydraulic conductivity values from detailed geotechnical reports were used in the seepage models discussed in Volume III. The ERDC seepage analyses are discussed in Volume III and include subsurface zones of woody vegetation with variable hydraulic conductivity in the simulations.

Approach

The objective was to assess the hydraulic conductivity, thus in situ measurements were taken using a Guelph permeameter manufactured by Soilmoisture Equipment Corporation. The permeameter measures the infiltration rate of water into the borehole at a steady state and the hydraulic conductivity is calculated thereafter. To ensure that conductivity values were consistent with the soil type tested, soil samples were collected and analyzed. These common properties are soil grain size distribution, type, consistency, structure, plasticity, in situ water content and in situ density. Two types of samples were taken: grab samples and undisturbed core samples. Grab samples were used for grain-size analysis, identification of soil type, specific gravity, natural water content, and Atterberg limits. Core samples were analyzed for dry density.

For in situ measurements of hydraulic conductivity, ERDC followed standard operating procedures written by the U.S. Department of Agriculture (USDA), National Sedimentation Laboratory (NSL), Oxford, MS, for calculating hydraulic conductivity of the shallow subsurface within both forested and non-forested areas. This included using the Guelph Permeameter. The Guelph permeameter test is essentially a constant head test conducted at the bottom of a borehole. The permeameter delivers a constant influx of water into the borehole at a constant head, typically 5 to 10 cm. The rate of flow at steady state is recorded in addition to the radius of the borehole and applied head. These three parameters are used in calculating the hydraulic conductivity of the tested soil interval. The volume of soil tested is dependent upon the head in the borehole, size of

the borehole, and soil structure. Literature regarding this device is abundant (Wilson et al. 1989; Amoozegar 1989; Reynolds and Elrick 1985 and 1986; Jabro and Evans 2006; and Reynolds 1993).

Soil samples were taken from each boring in which a permeameter test was conducted. Samples were collected for visual observation of roots and for the purpose of obtaining additional soil properties. A selection of the samples was tested in the laboratory for grain size distribution, specific gravity, water content, dry density, and Atterberg limits. In situ volumetric moisture content measurements were also collected using a soil moisture probe (Aquaterr M-300 Moisture Meter) manufactured by Aquaterr Instruments. Additionally, soil moisture and density measurements were made using a Troxler nuclear density gauge. These measurements were taken within 2 to 12 in. of the ground surface and are discussed in Chapter 3. These data were collected for verification of soil properties at the tree and corresponding control sites. Pertinent studies that influenced this investigation include: Brizendine (1997a); Gray et al. (1991); Gabr et al. (1995); Wilson et al. (1989); Amoozegar (1989); Reynolds and Elrick (1986); Jabro and Evans (2006); Fatahi et al. (2009); and Indraratna et al. (2006).

Background

Definition of hydraulic conductivity

Hydraulic conductivity is a measure of the ability of a soil to transmit water and was first described by Henry Darcy in 1856 (Freeze and Cherry 1979). Darcy found that the amount of water (specific discharge, v) transmitted through a specified column of soil per unit time is proportional to the applied hydraulic pressure gradient (i). Through experimentation, Darcy found that finer grained soils transmitted less water than coarser grained soils when subjected to the same gradient. Therefore, he concluded that the amount of water that a soil will transmit is dependent upon the gradient *and* an intrinsic property of the soil related to the geometry and the size distribution of the pores within the soil body (Amoozegar and Wilson 1999). This intrinsic property was defined by Darcy as the constant of proportionality or hydraulic conductivity (K) and is expressed mathematically by Darcy's law:

$$v = -K i$$

where:

v = specific discharge through the column (flow velocity)

K = hydraulic conductivity

i = hydraulic gradient

Typical values of K for different soil types are given in Table 52.

**Table 52. Values of hydraulic conductivity for typical soils
(Freeze and Cherry 1979).**

Soil Type	Typical Range of Saturated Hydraulic Conductivity Values (cm/s)	Typical Range of Saturated Hydraulic Conductivity Values (ft/day)
Unweathered marine clay	10^{-10} to 10^{-7}	2.83^{-7} to 2.83^{-4}
Glacial till	10^{-10} to 10^{-4}	2.83^{-7} to 2.83^{-1}
Silt, loess	10^{-7} to 10^{-4}	2.83^{-4} to 2.83^{-1}
Silty sand	10^{-5} to 10^{-1}	2.83^{-2} to 2.83^2
Clean sand	10^{-3} to 10^0	2.83 to 2.83^3
Gravel	10^{-1} to 10^2	2.83^2 to 2.83^5

Specific discharge (v) is a macroscopic concept. It is calculated using the total volume of water passing through the soil column, divided by the cross-sectional area of the soil column, when the flow rate into the column equals the flow rate exiting the column. Actual flow rate around individual soil grains is not computed. By adopting Darcy's law and using K to define soil behavior, the soil matrix of individual grains (microscopic concept) is being replaced by a representative continuum of porous media (macroscopic concept). Thus, calculation of K will provide an average value representative of the soil matrix within the radius of influence of the test. Further, the in situ measurement of K within a volume of soil containing tree roots should express the influence of flow around individual roots within the tested volume of soil.

Measurement of in situ hydraulic conductivity

Hydraulic conductivity is measured in the laboratory or in the field (in situ). For this study, field measurements were taken because the objective was to measure hydraulic conductivity of a volume of soil containing roots to compare to the conductivity measured in the same volume of a control soil without roots. The challenge was to choose a test volume that would include a representative range of root sizes. Root-size distribution studies (Gray et al. 1991; Dupuy et al. 2007; Brizendine 1997; and Marks and Tschantz

2002) showed that root sizes from hairline to 2 cm (0.39 in.) in diameter represent a significant percent of most trees' root masses. For example, Gray et al. (1991) found that 100% of the roots at the drip line of 10 individual trees were within this range. In this study, approximately 40% of the roots digitized at the Vicksburg site for the root architecture study discussed in Chapter 4 were within this range. The ERDC root study recorded root size and location from the tree's stem to its drip line and to a depth of 1 m (3.05 ft). Further, both the ERDC study and Gray et al. (1991) found this range of root sizes to be located within 2 to 3 ft of the surface. Therefore, a test volume that would include these sizes was assumed valid to test the effects of roots on soil hydraulic conductivity.

Laboratory permeability tests were not considered an efficient means for measuring hydraulic conductivity of the soil/root matrix for several reasons. The first was the high costs associated with these tests. Secondly, the field test could sample a larger volume of soil than a typical lab sample (i.e., 2-in. diameter by 4-in. length). To collect a similarly large sample for the lab would require greater effort and time in the field. In addition, many more tests could be conducted in the field versus the lab for the same cost and the tested interval in the field is undisturbed. For these reasons and others, field measurements were chosen to evaluate the soil/root matrix.

There are several ways to measure hydraulic conductivity in the field, including large scale pumping tests, ring infiltration tests, and borehole tests. Pumping tests were not considered because they are usually conducted in the saturated zone and tree roots are contained mostly in the vadose (unsaturated) zone. Smaller scale infiltration tests were not considered because they do not test deeper than 10 to 18 in. from the surface, requiring excavation to conduct deeper tests. The borehole permeameter can test anywhere within the first 6 ft of soil. It is a portable device and was easily shipped to the field sites and hand-carried between sampling locations. Also, the size of the sample interval was assumed to accommodate the desired test size, or soil volume of concern. That is, the test boreholes were 5 cm in diameter and depending on the applied head, (usually 10 to 5 cm), the volume of soil tested was assumed to be a bulb shape with the height equal to twice the applied head (Figure 211). The operating manual for the device is available from the manufacturer on their website (Soilmoisture Equipment Corp 2010).

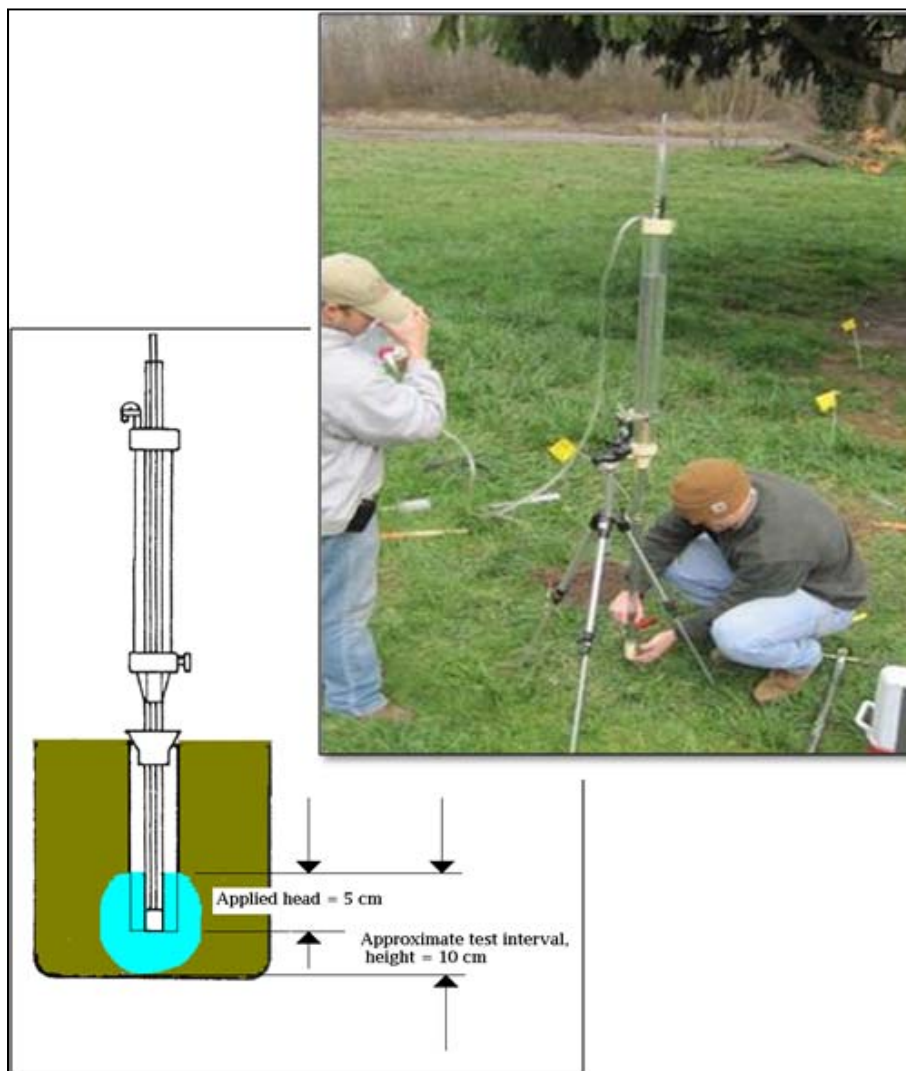


Figure 211. Diagram of the Guelph Permeameter constant head, in situ, hydraulic conductivity measuring device (modified from Reynolds and Elrick 1986).

Test plan

An ambitious test plan was designed after review of the literature and consideration of a limited time schedule. The goal was to measure the hydraulic conductivity within the first 5 ft of the surface where the majority of roots were presumed to reside (Fatahi et al. 2009; Brizendine 1997; and Gray et al. 1991). Further, a reasonably high number of tests per location site (48 tests per location) were desired to provide reasonable confidence in the results while allowing for a substantial number of locations to be investigated (8 locations total, including a total of 9 trees and 9 control sites).

To establish an objective sampling distribution from which to determine inherent soil property variation, sampling points were selected randomly using the random number generator in Microsoft Excel. Coordinates were randomly generated for 12 borings using bounds of 0 to 360 deg in 22.5-deg increments for the azimuth coordinate and bounds of 3 ft to a maximum of the drip line radius as bounds for the radial coordinates. Thus, a unique sampling pattern was made for each geographic location as illustrated by Figure 212. The origin of the plot coincides with the tree location and represents the center of the tree stem. The tree's diameter is not plotted but should be noted when reviewing the distance data. The identical sample plot was applied to the tree's respective control sites. Some of the test boreholes had to be moved a few inches or feet from their planned locations because of large tree roots or gravel being intercepted in the borehole or other man-made obstacles (e.g., fences, pavement).

Equipment selection

Permeameter

Because of their expertise in collecting in situ hydraulic conductivity along riverbanks and forested lands, the NSL provided input to ERDC on the instruments and standard operating procedures used by their organization to measure in situ hydraulic conductivity. At the recommendation of NSL, a Guelph Permeameter manufactured by Soilmoisture Equipment Corporation was selected for the ERDC field tests. The Guelph Permeameter is a constant head permeameter; it measures the steady-state rate of water recharge into an unsaturated soil (inside a borehole) in which a constant head of water is maintained. Figure 213 is a schematic diagram of the device. Permeameter testing was guided by the manufacturer's operating manual and NSL field experience.

The Guelph Permeameter primarily measures horizontal K in a granular porous medium and an average of the vertical and horizontal K in a structured medium (Reynolds and Elrick 1985). A constant head is maintained in the well bore until a constant infiltration rate is observed. This constant infiltration rate, the radius of the well bore, and the head applied in the well are used to calculate the hydraulic conductivity. There are a variety of analytical methods for calculation of the hydraulic conductivity using the Guelph Permeameter and these are described in detail in the literature. The precision of the available methods is still being tested by the developers and users of the instrument. Because the primary

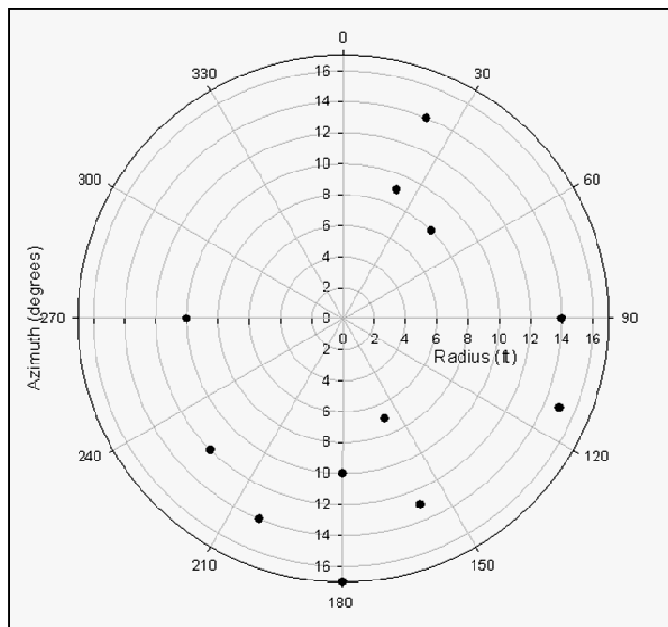


Figure 212. Plan view of hydraulic conductivity field test locations plotted in polar coordinates. The tree's center is located at the origin of the plot, and test locations are plotted along random azimuths and radii.

objective of this investigation is to compare measurements of the tree site to its respective control site, the precision of the instrument is not critical to the investigation. However, keeping the testing procedures consistent between tree and control site is important and the Guelph Permeameter is a reliable instrument for this purpose.

Soil moisture probe

A small moisture probe (M-300) (Figure 214) was used to capture volumetric soil moisture measurements prior to hydraulic conductivity tests. The M-300 is a handheld device approximately 30 in. in length and 0.5 in. in diameter. The moisture sensor is approximately 4 in. in length and located at the end of the probe. At the top of the device is a digital screen for reading the measurement and two handles for pushing the probe into the ground. The user simply pushes the probe to the desired depth and takes the moisture reading by pressing a small button on the read-out device. It is manufactured by Aquaterr Instruments and distributed by Soilmoisture Corporation.

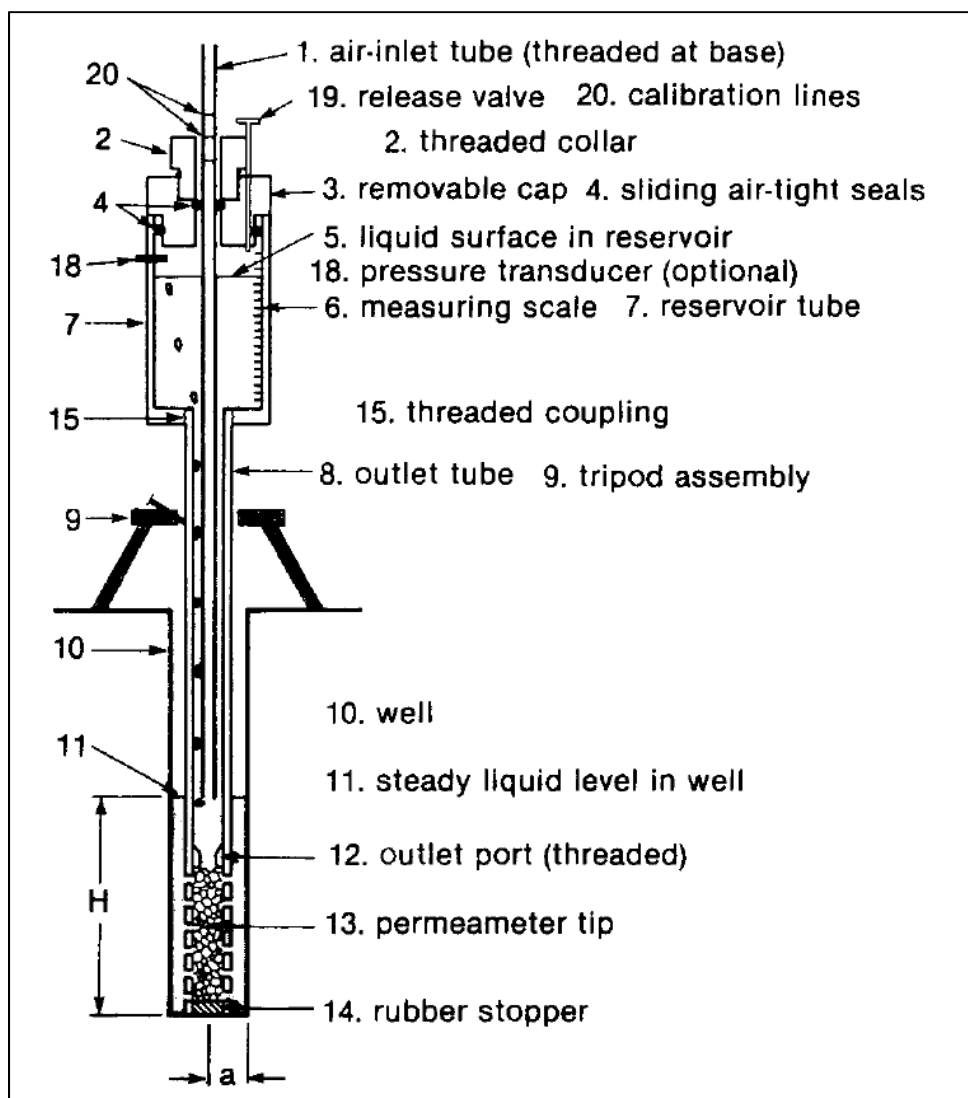


Figure 213. Schematic diagram of the Geulph Permeameter
(Reynolds and Elrick 1986).

Density soil sampling auger kit

After each hydraulic conductivity test, the borehole was cleaned out with a hand auger, and a cylindrical core sampler was hammered into the hole to obtain an undisturbed laboratory soil sample. A soil sample was captured by a stainless steel ring with dimensions of 53-mm diam by 51-mm height placed inside the core sampler. The volume of the ring is 100 cc. The sampling kit is manufactured by Eijkelkamp Agrisearch Equipment in Giesbeek, The Netherlands, and distributed by Soilmoisture Corp. Figure 215 is a photograph of the core sampler and ring.



Figure 214. M-300 soil moisture probe.

Test procedures

Determining meaningful test boundaries

The lateral extent and depth of the root mass for the purpose of hydraulic conductivity testing were estimated from the literature (Fahati et al. 2009; Indraratna et al. 2006; Brizendine 1997; Marks and Tschantz 2002; and Gray 1991) and geophysical surveys conducted early in this investigation. Indraratna et al. (2006) used a conical shape to represent the root mass in his mathematical model of root water uptake where the largest diameter of the cone is proportional to the tree's drip line and the maximum depth of the cone is equal to the height of the tree. Although the maximum depth of roots is estimated at no greater than the height of a tree, he notes an



Figure 215. Eijkelkamp soil core sampler and ring (ring dimensions are 53-mm diam by 51-mm length).

exponential decrease in root mass with depth as does Gray et al. (1991). Further, Brizendine (1997) discusses Francis' (1979) study where trenches were dug to study yellow poplar trees from 8 to 34 years of age. The majority of these poplar roots were found in the top 4 ft of the soil horizon.

Marks and Tschantz (2002) discussed the extensive root studies conducted by K. D. Coder. These studies related tree trunk size to root ball and root system diameter. The root ball defined by Coder is the roots directly below the trunk that provide vertical support. The root system refers to the lateral transport root system that provides nutrients and the lateral support for the tree. Table 53 summarizes the empirical data collected by Coder (Marks and Tschantz 2002).

Early in this study at the Pocket Levee in Sacramento, CA, the ERDC geophysical survey noted a change in soil properties near the valley oak tree at a radius of 6 ft around the trunk and a depth of 5 ft. The height of

**Table 53. Root characteristics as documented by Coder
(after Marks and Tschantz 2002).**

Tree Diameter, cm	Rootball Diameter, m	Root System Diameter, m
10.2 - 12.7	1.8	3.0 - 3.7
15.2 - 17.8	2.4	4.9 - 5.5
20.3 - 22.9	3.0	6.1 - 6.7
25.4 - 27.9	3.7	7.9 - 8.5
30.5 - 35.6	4.3	9.1 - 9.8
38.1 - 40.6	4.9	11.6 - 14.0
48.3 - 58.4	5.5	14.6 - 17.7
61.0 - 91.4	6.1	18.3 - 27.4
94.0 - 114.3	6.7	28.0 - 34.1

this tree was approximately 50 ft and the drip line diameter was approximately 55 ft. The excavation of a red oak at the Vicksburg, MS, site conducted at the end of this investigation revealed that approximately 90% of its root mass was within the first 2 ft of the surface. The height of the tree was 25 ft and the drip line had a radius of 25 ft. Tree roots depend on the abundance of oxygen and nutrients in the vadose zone to survive, thus the majority of root masses are positioned in shallow soil horizons.

Because of these observations, the majority of tests for the ERDC study were conducted within the boundary of the tree's drip line and no deeper than 5 ft from the ground surface. Two depths of testing were conducted for each tree and control site. Because the majority of roots are located within the first 3 ft of soil, this is the depth interval that was tested. Another suite of tests were conducted at 5 ft (at most sites) because it was assumed that less roots were located at this depth, and therefore a difference from the shallower depth may be detected. Also, if the weight of the tree causes an increase in soil consolidation (i.e. density) a change in conductivity may be noticeable at this depth compared to the control site.

Borehole testing and sampling protocol

The field procedure began with surveying the site and marking the boring locations corresponding to the randomly generated sampling pattern (Figure 216). Moisture content readings were taken at approximately 2.5 ft near each flag marking the test locations with a soil moisture probe (Figure 217).



Figure 216. Surveying test locations for permeameter tests, Burlington, WA.

Boreholes were advanced by hand auger or hand rotary-drill one boring at a time (Figure 218). Borings were drilled to approximately 6 in. above the testing depth (e.g., 2.5 ft for the 3.0-ft testing depth). A grab sample was taken at this depth using a hand auger (Figure 219). After securing the grab sample in an airtight bag, a sizing auger was used to prepare the bottom of the borehole and to ensure that the walls and floor were free of debris and level. The permeameter was positioned at depth 3.0 ft



Figure 217. Measurement of in situ moisture content measurement using the M-300 Aquaterr, Burlington, WA.

(Figure 220), and the borehole was filled with water up to 5 or 10 cm prior to the start of the test. After completion of the permeameter test, the sizing auger was used again to remove any debris from the hole. A handheld core sampler was then hammered into the hole to collect an undisturbed soil sample (Figure 221) for laboratory analysis. Core samples were sealed with plastic caps and black electrician's tape.

This sequence was repeated to the next selected depth. For each control site and tree site, 24 permeameter tests were conducted. Twenty-four grab samples were retrieved, and at most sites an additional 24 undisturbed core-samples were retrieved for analyses. The core samples were taken at approximately the same location in the borehole as the permeability test and were used for laboratory analysis to calculate dry density. Grab samples were taken for evaluation of soil type. After soil sampling and permeameter tests were completed, the hole was backfilled and compacted by tamping. Both grab samples and core samples were packed in hard-cased



Figure 218. Handheld drill with auger used to drill a hole for placement of permeameter, Vicksburg, MS.



Figure 219. Removal of grab sample prior to permeameter test, Burlington, WA.



Figure 220. Guelph Permeameter seated inside boring and ready to test boring interval at 3 ft, Burlington, WA.



Figure 221. Undisturbed soil sample collected for laboratory analysis, Burlington, WA.

containers and shipped to the ERDC soil-testing laboratory. Specific gravity, grain size, Atterberg limits, water content, and dry density were measured in the lab on selected samples from each site location.

Calculation of field saturated hydraulic conductivity

Hydraulic conductivity of the test intervals were calculated using the Glover Equation as described in Amoozegar (1989). Glover's solution of the Compact Constant Head Permeameter (CCHP) was used for calculating the hydraulic conductivity, based on review of the available solutions in the literature and guidance provided by NSL. The Glover solution, which is based on gravitational flow from a cylindrical hole at a constant head, is given as (Amoozegar 1989):

$$K_s = CQ/2(\pi)H^2$$

where:

$$C = \sinh^{-1}(H/r) - (r^2/H^2 + 1)^{1/2} + r/H$$

Q = measured steady flow rate into the well

H = constant height of water in the well

r = radius of the well.

Wilson et al. (1989) used the Glover solution and the Guelph Permeameter to evaluate saturated hydraulic conductivity of the subsoil in two forested watersheds. Their findings included a log normal distribution of the infiltration rates as measured in both watersheds. Calculated conductivity values for each field test performed by ERDC are provided in Appendix D.

Field test results

Calculated hydraulic conductivity values for each tree site and its control were plotted as a function of distance from the center of the tree. Conductivities were plotted on a log scale for visual clarity. Each plot has the same scale and range for ease in comparing results from different locations. The randomly generated sampling pattern is shown below each plot of conductivities. Results for each site are summarized in this section.

Sacramento, CA

Field derived hydraulic conductivity values range from 10^{-2} to 10^{-3} cm/sec for both the tree and control sites at the 3-ft depth (Figure 222). For the 5-ft depth, the range of K values varies between 10^{-2} and 10^{-4} cm/sec (Figure 223). The range of values reflects the range of grain sizes. Boring data from the study site indicate that shallow soils at the Pocket Levee are composed of silty sand to uniform sand (SM to SP). Test results show the near surface hydraulic conductivity values obtained from field methods are slightly more permeable than those recommended by URS (2010a), which were used in evaluating levee underseepage. The range in conductivity data increases slightly (i.e., less permeable by one order of magnitude) for the 5-ft depth as compared for the 3-ft depth, but no obvious difference in values between the tree and control sites is noted. Both control and tree data cluster together equally within the distribution of the measured values in Figures 222 and 223. Values for the 3-ft data appear to reflect a slight decrease in hydraulic conductivity beneath the tree. A comparison of distance from the center of the tree to variations in conductivity do not show any distance relationships with conductivity. A total of 24 tests were completed at the 3-ft depth and 24 tests were completed at the 5-ft depth.

Burlington, WA

Field-derived hydraulic conductivity values generally range from near 10^{-3} to 10^{-4} cm/sec for both the tree and control site at the 3-ft depth (Figure 224). At the 5-ft depth, the range of K values is nearly similar to the 3-ft depth (Figure 225). The range of K values calculated are consistent with the silty sand collected at this site. Also, the data are consistent with boring information obtained prior to the field testing. Boring data indicate that the shallow soils in the Burlington area are mainly composed of silty sand (SM). Hydraulic conductivity values for the 3-ft depth in Figure 224 suggest that the control data are slightly more permeable than the tree data. No trend is noted between conductivity in Figures 224 and 225 and distance from the tree. A total of 24 tests were completed at 3-ft depth and 23 tests were completed at the 5-ft depths.

Albuquerque, NM Site 1

Hydraulic conductivity measurements were made in the vicinity of cottonwood trees. The field sampling plan was modified for the two Albuquerque sites. Instead of sampling at 3 and 5 ft, the sampling interval

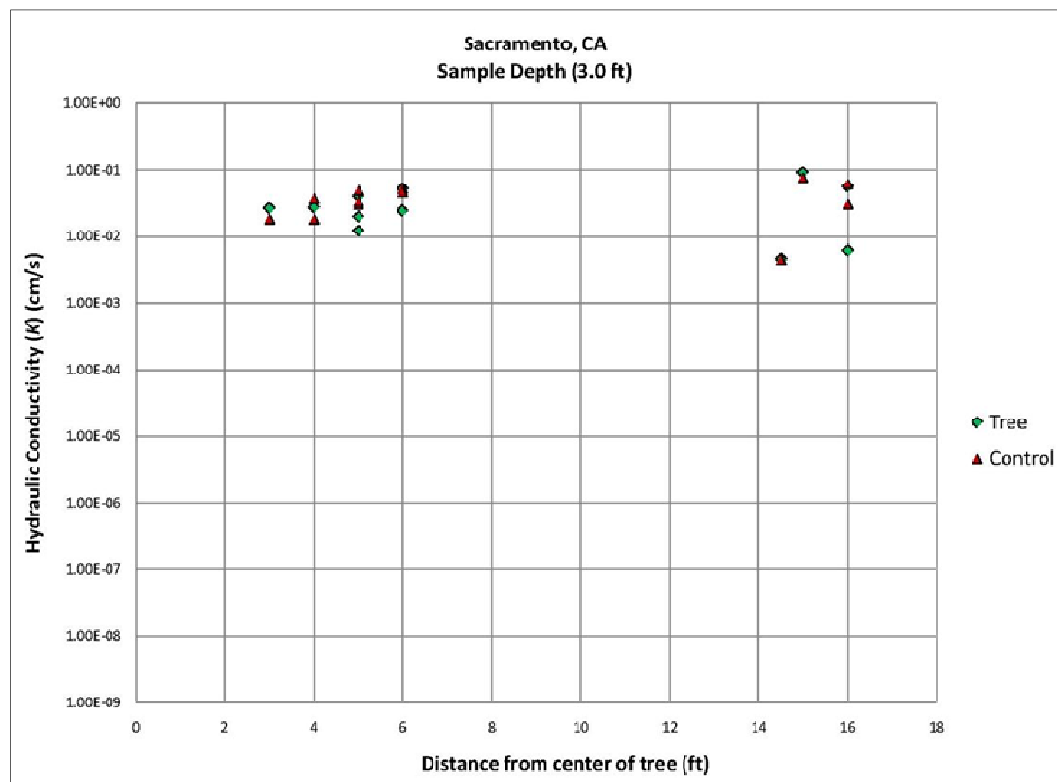


Figure 222a. Hydraulic conductivity calculated from in situ permeameter tests at a depth of 3.0 ft, Sacramento, CA.

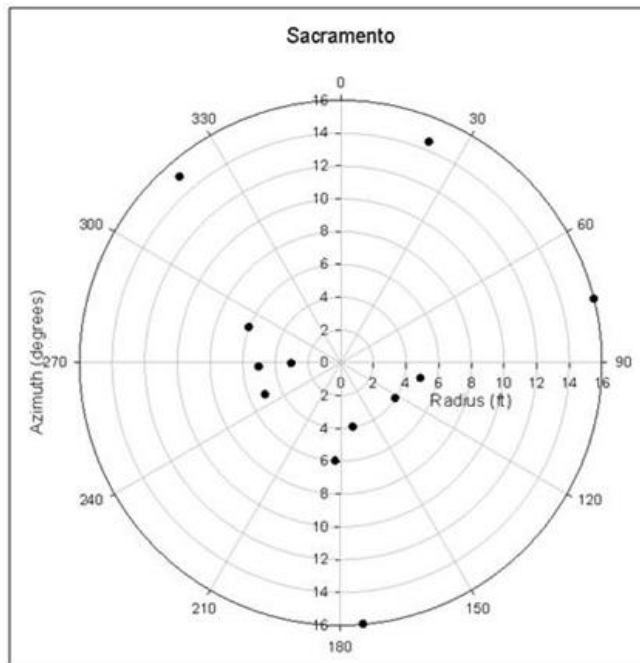


Figure 222b. The locations of the random samples for permeameter tests in Sacramento, CA. The x-y axes are in feet.

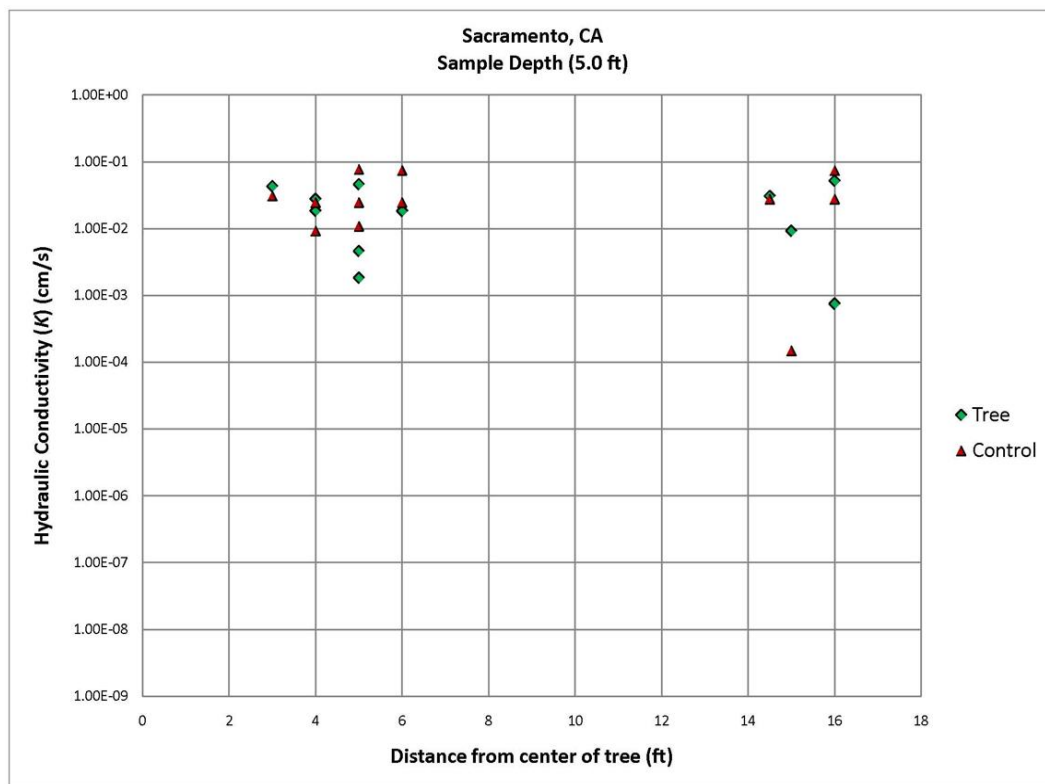


Figure 223a. Hydraulic conductivity calculated from in situ permeameter tests at a depth of 5.0 ft, Sacramento, CA.

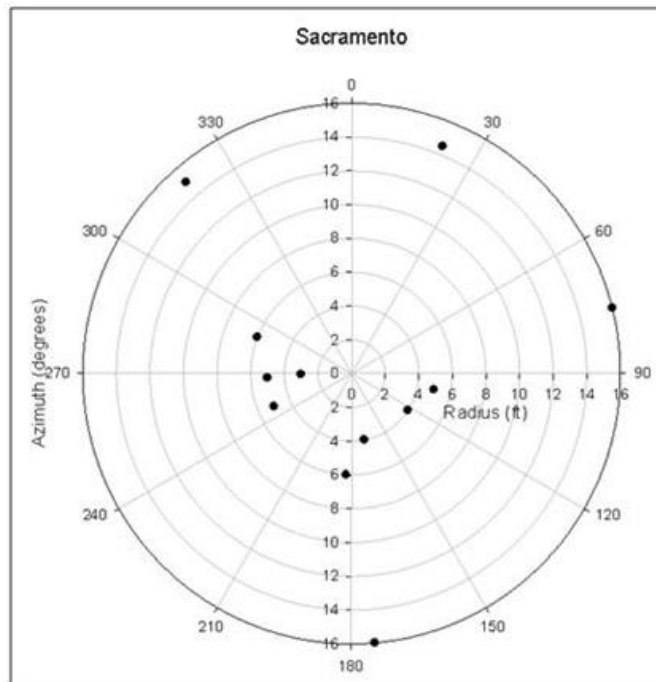


Figure 223b. The locations of the random samples for permeameter tests in Sacramento, CA. The x-y axes are in feet.

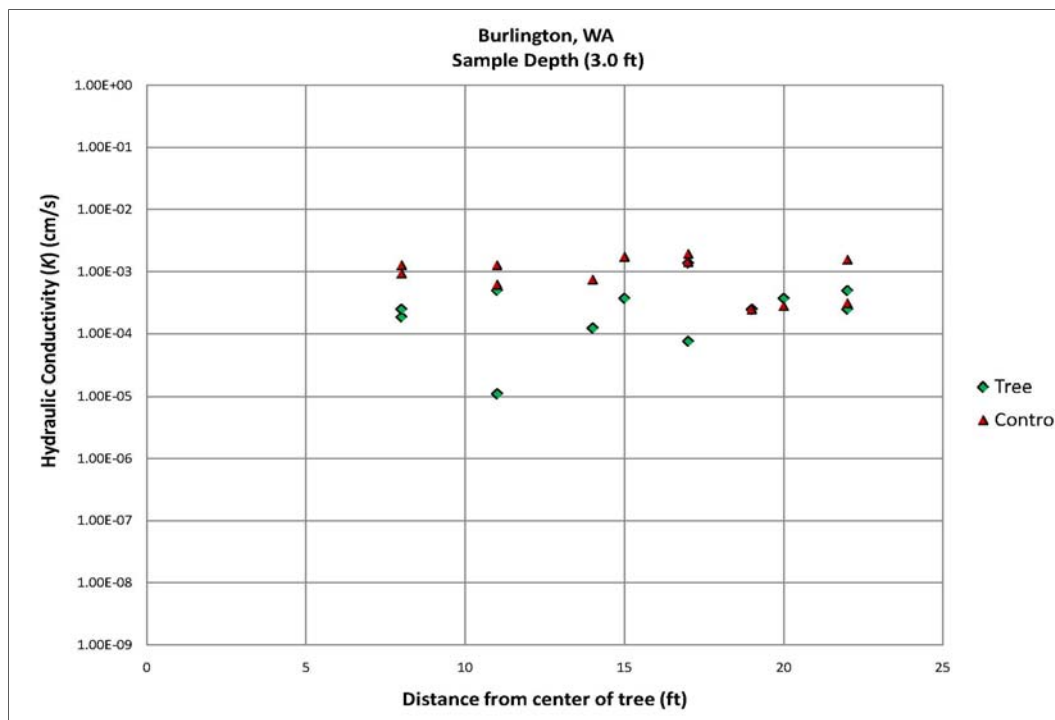


Figure 224a. Hydraulic conductivity calculated from in situ permeameter tests at a depth of 3.0 ft, Burlington, WA.

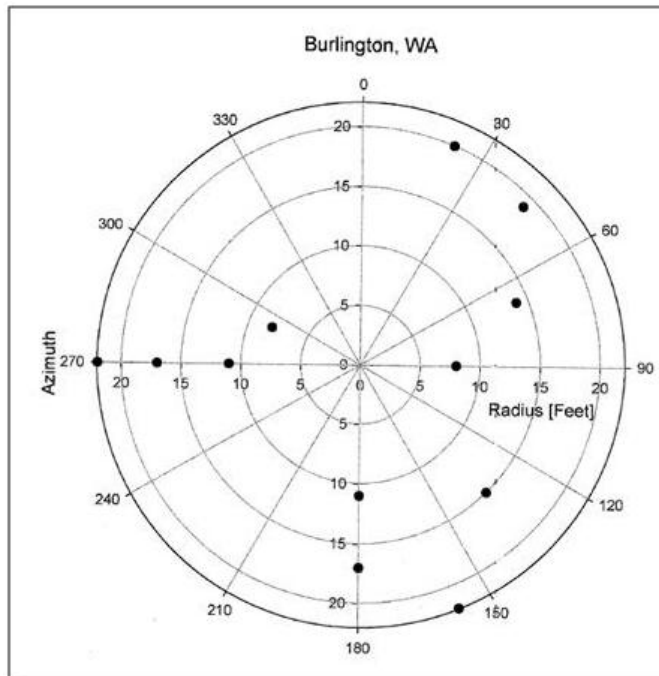


Figure 224b. The locations of the random samples for permeameter tests in Burlington, WA. The x-y axes are in feet.

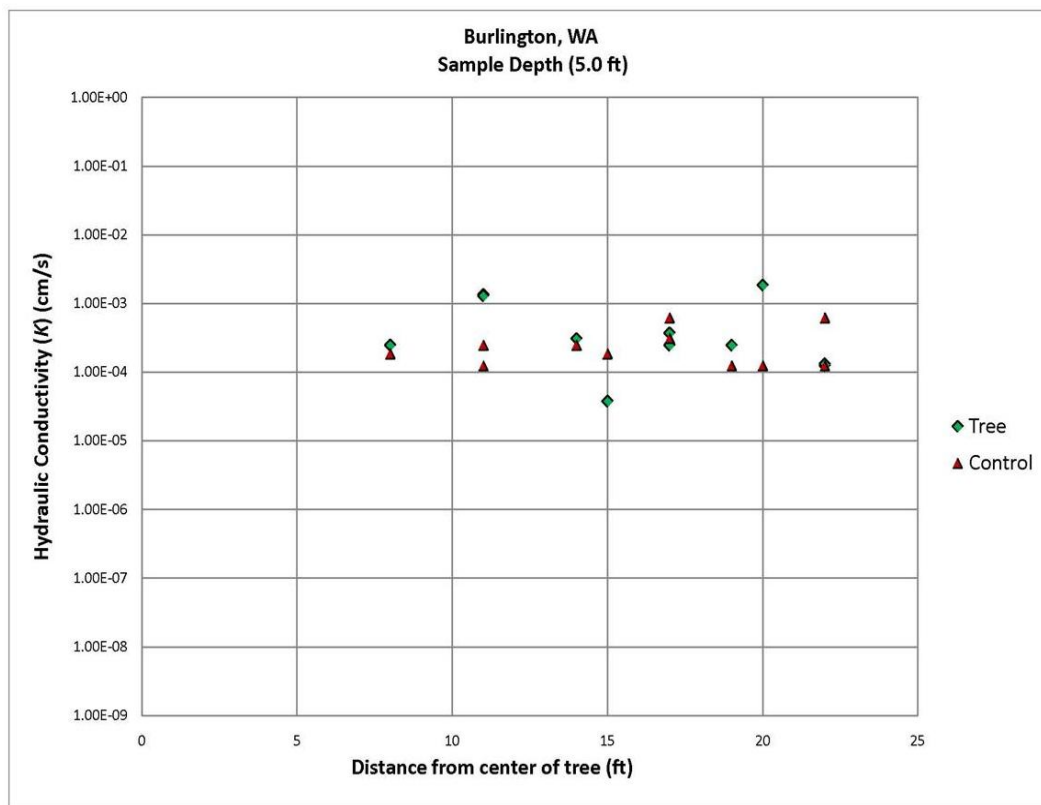


Figure 225a. Hydraulic conductivity calculated from in situ permeameter tests at a depth of 5.0 ft, Burlington, WA.

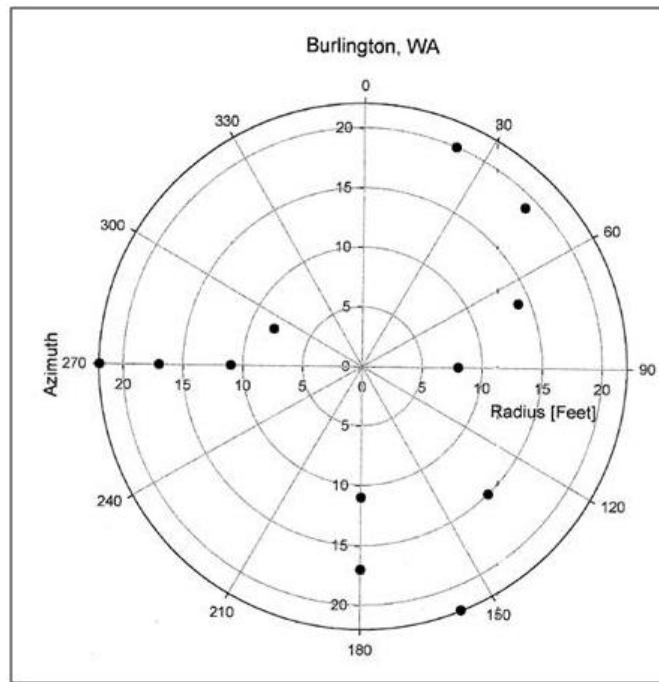


Figure 225b. The locations of the random samples for permeameter tests in Burlington, WA. The x-y axes are in feet.

was changed to 1.5 and 2.5 ft. The change was made to obtain more data from the root zone, as opposed to below the root zone. Field-derived hydraulic conductivity values for the east Rio Grande levee (Site 1) at the 1.5-ft depth are between 10^{-2} to 10^{-3} cm/sec range for both the tree and control site (Figure 226) with one value at 10^{-4} cm/sec. For the 2.5-ft depth, the range of K values was an order magnitude wider, from 10^{-2} to less than 10^{-4} cm/sec (Figure 227). A slight increase in K values occurs between 6 to 10 ft from the tree for both the 1.5- and 2.5-ft depths. The 2.5-ft data also display a difference between the control and tree values. Control values are higher by about one-half order of magnitude (Figure 227). Hydraulic conductivity values from the floodplain of the east Rio Grande levee site identify these soils as being sandy silt. No apparent trend in conductivity is evident with distance from the tree. A total of 31 tests were completed in the 1.5-ft horizon, and 31 tests were completed in the 2.5-ft depth, as well.

Albuquerque, NM Site 2

Hydraulic conductivity values from the west Rio Grande levee site (Site 2) reflect the cohesionless nature of these soils. Boring data from the floodplain identify these soils as silty sand. Field-derived hydraulic conductivity values for the west Rio Grande levee at the 1.5-ft depth are clustered between the 10^{-2} to 10^{-3} cm/sec range for the control site and the tree site (Figure 228). Shallow data indicate that hydraulic conductivity values for tree site are about 1 order of magnitude less permeable than the control site. For the 2.5-ft depth, the range of K values show greater variability, extending from greater than 10^{-1} to nearly 10^{-4} cm/sec (Figure 229). The overall trend is similar for both the shallow and deep tests with hydraulic conductivity values from soils containing trees being noticeably less permeable than the control data. Figures 228 and 229 do not show a correlation of hydraulic conductivity to distance from the tree. A total of 24 tests were conducted at the 1.5-ft depth and 24 tests were completed at the 2.5-ft depth.

Portland, OR

Field-derived hydraulic conductivity values generally range from near 10^{-2} to 10^{-7} cm/sec for the tree and control site for the 3- and 5-ft depth (Figures 230 and 231). This range of hydraulic conductivity values encompasses a broad range in soil types. Samples obtained by hand augering indicate the composition of the shallow soils at the Portland site were

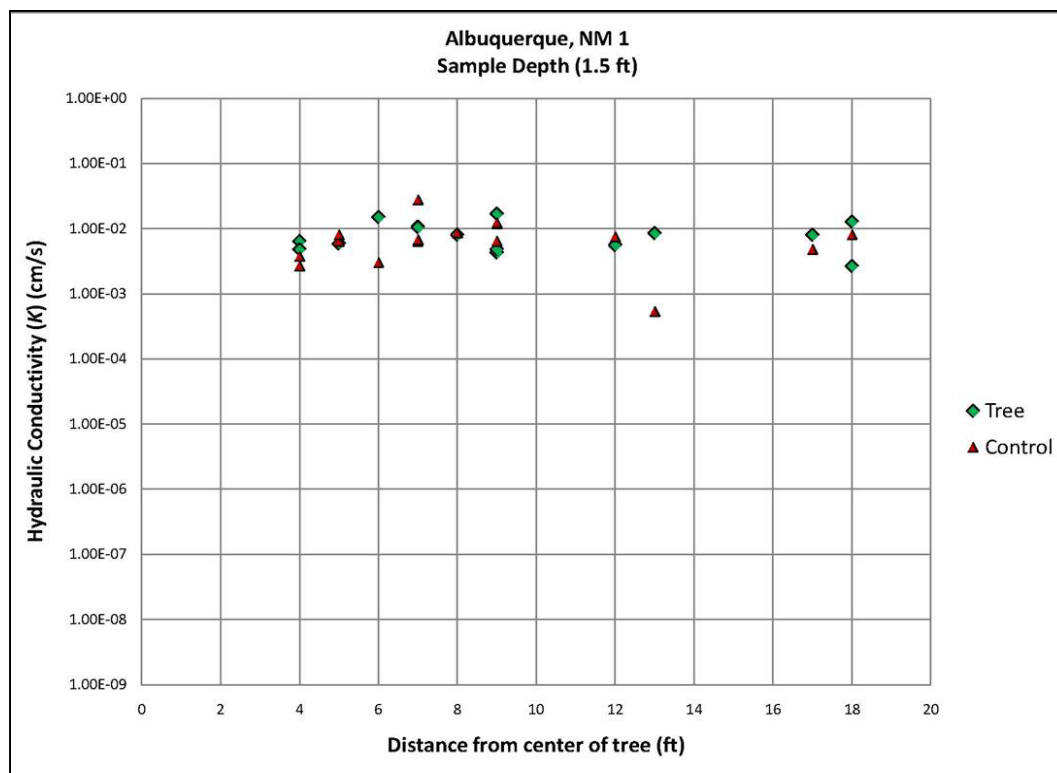


Figure 226a. Hydraulic conductivity calculated from in situ permeameter tests at a depth of 1.5 ft. Albuquerque, NM 1.

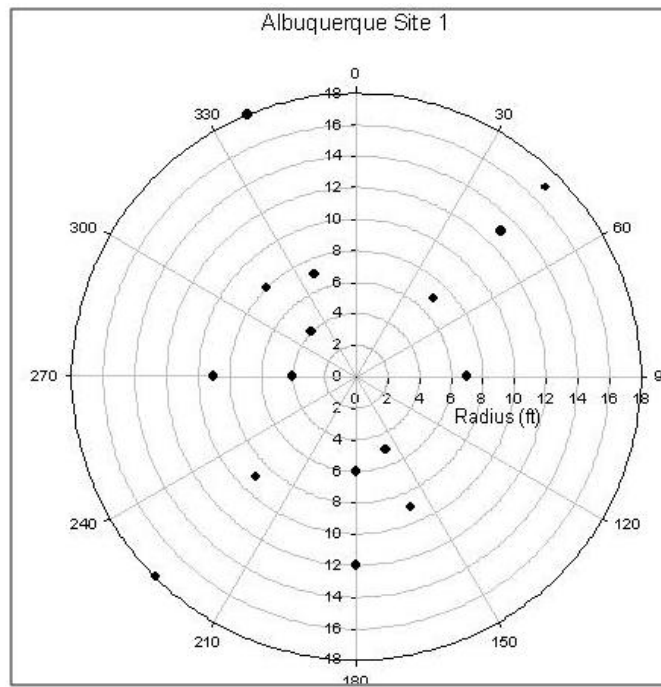


Figure 226b. The locations of the random samples for permeameter tests in Albuquerque, NM 1. The x-y axes are in feet.

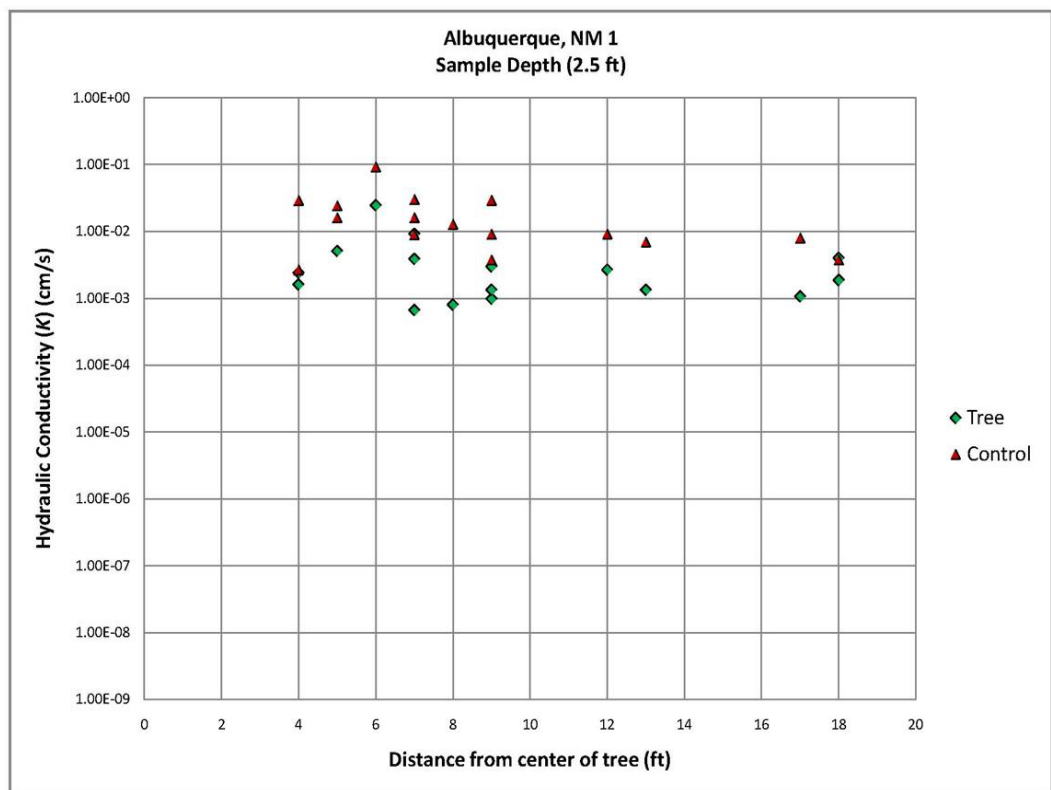


Figure 227a. Hydraulic conductivity calculated from in situ permeameter tests at a depth of 2.5 ft, Albuquerque, NM 1.

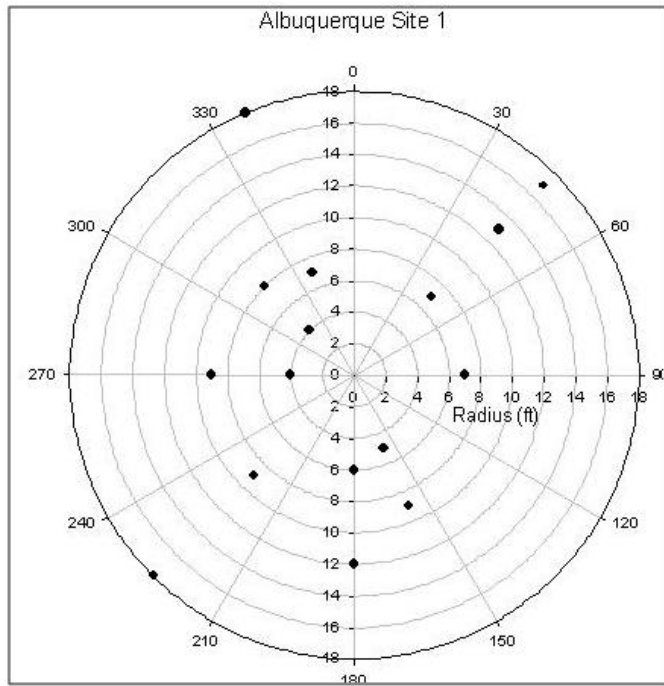


Figure 227b. The locations of the random samples for permeameter tests in Albuquerque, NM 1. The x-y axes are in feet.

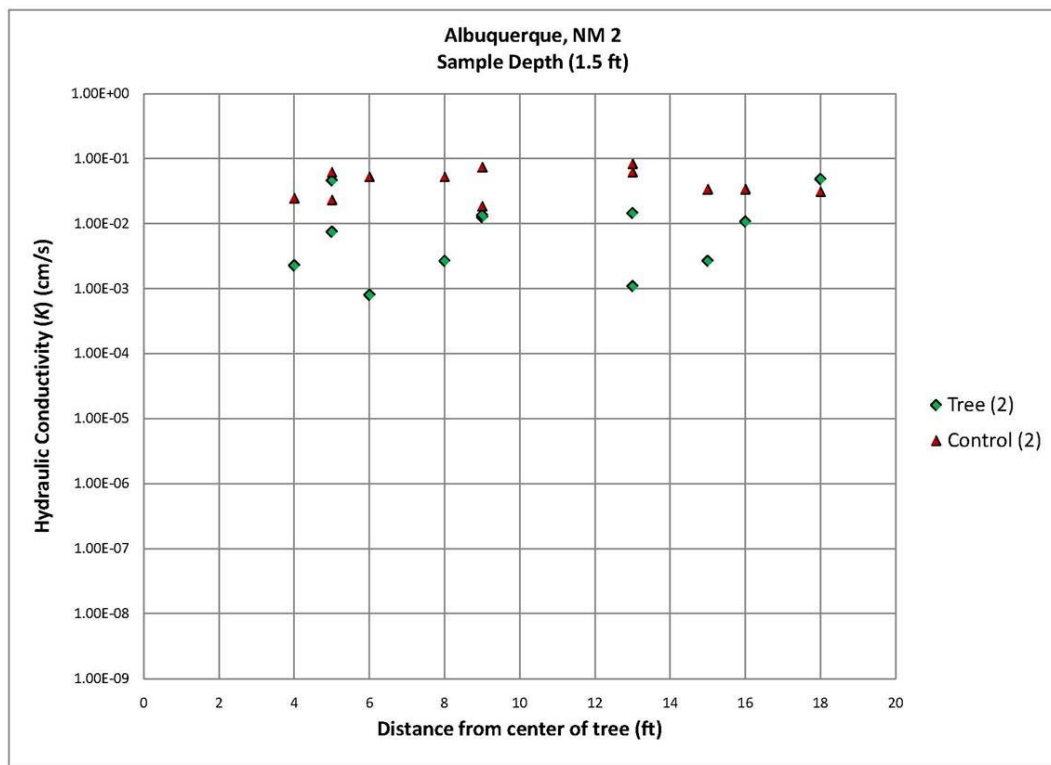


Figure 228a. Hydraulic conductivity calculated from in situ permeameter tests at a depth of 1.5 ft, Albuquerque, NM 2.

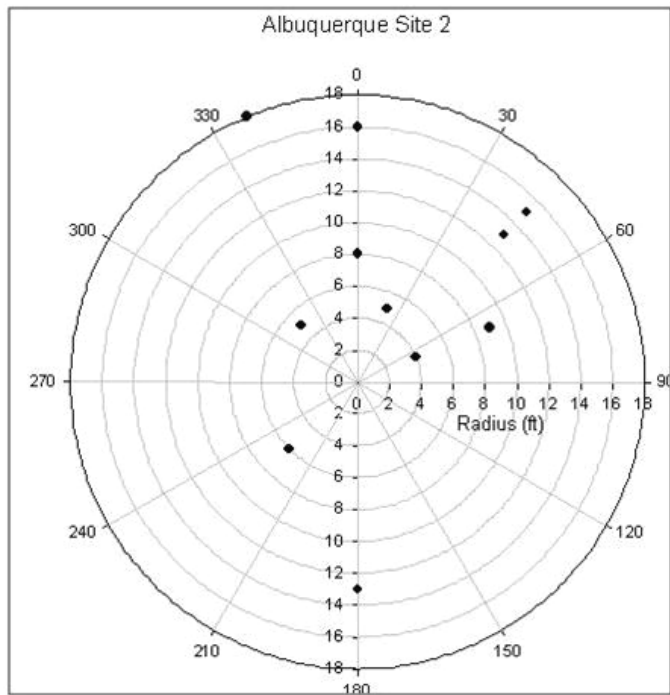


Figure 228b. The locations of the random samples for permeameter tests in Albuquerque, NM 2. The x-y axes are in feet.

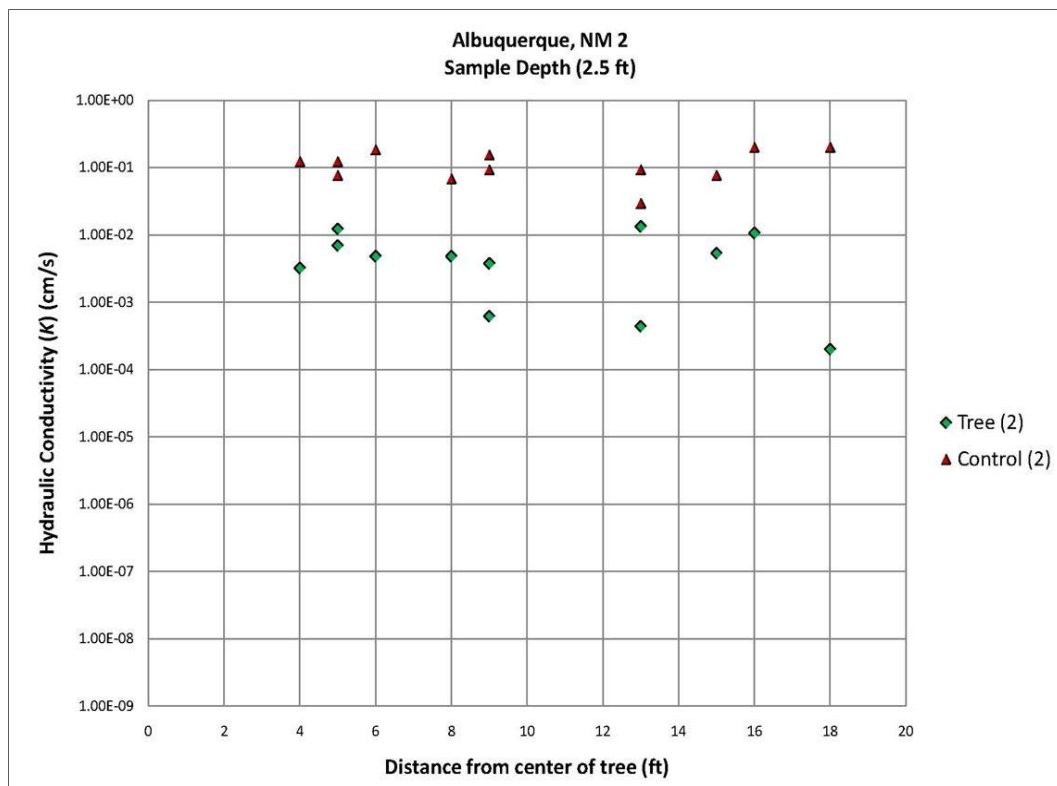


Figure 229a. Hydraulic conductivity calculated from in situ permeameter tests at a depth of 2.5 ft, Albuquerque, NM 2.

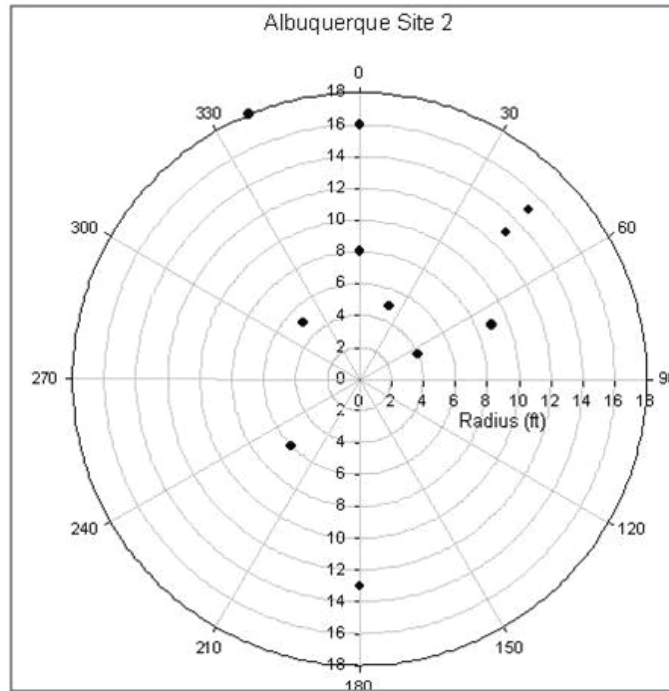


Figure 229b. The locations of the random samples for permeameter tests in Albuquerque, NM 2. The x-y axes are in feet.

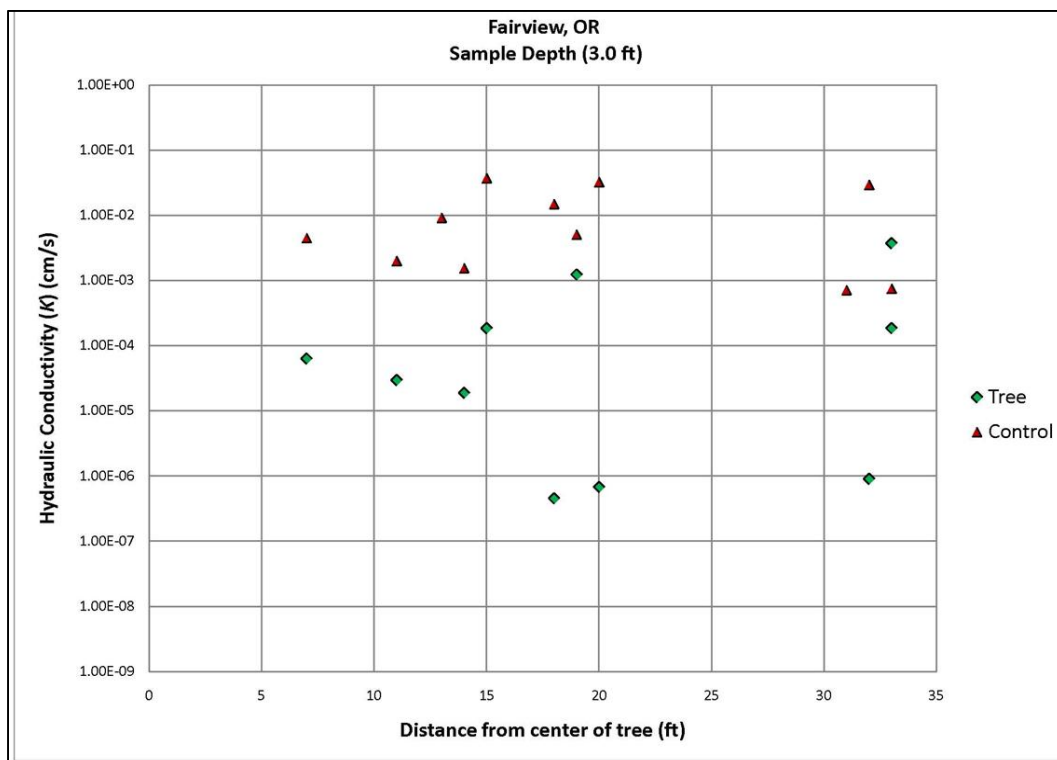


Figure 230a. Hydraulic conductivity calculated from in situ permeameter tests at a depth of 3.0 ft, Portland, OR.

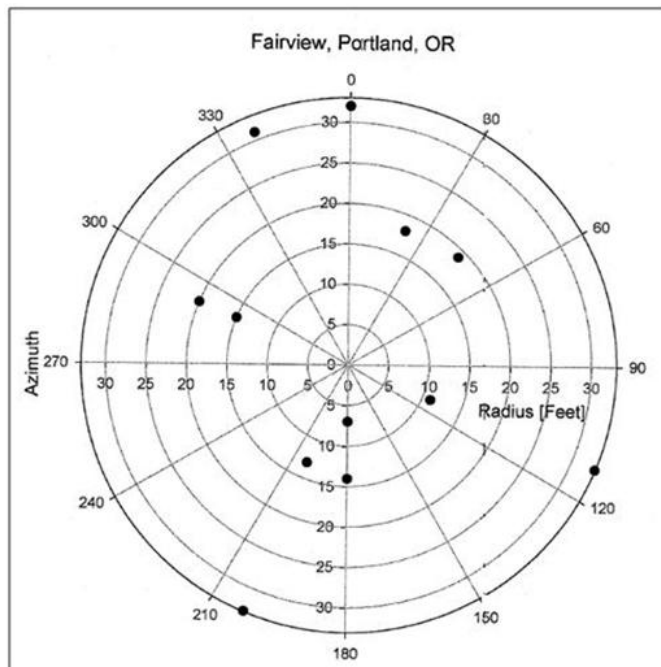


Figure 230b. The locations of the random samples for permeameter tests in Portland, OR. The x-y axes are in feet.

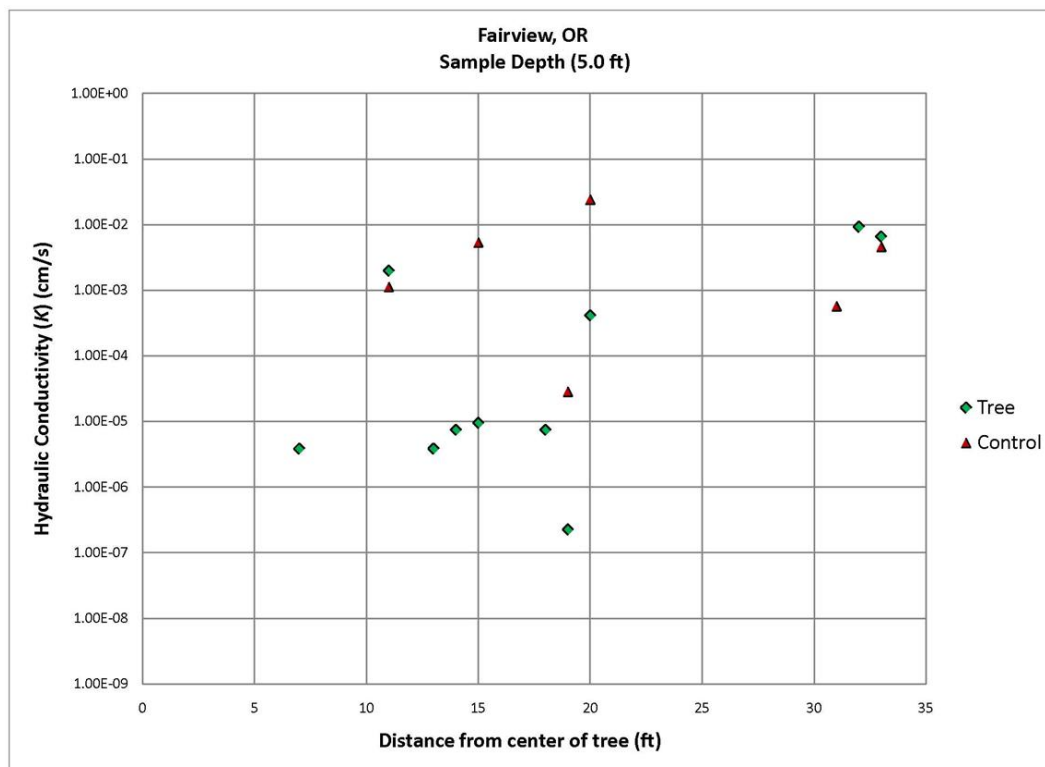


Figure 231a. Hydraulic conductivity calculated from in situ permeameter tests at a depth of 5 ft, Portland, OR.

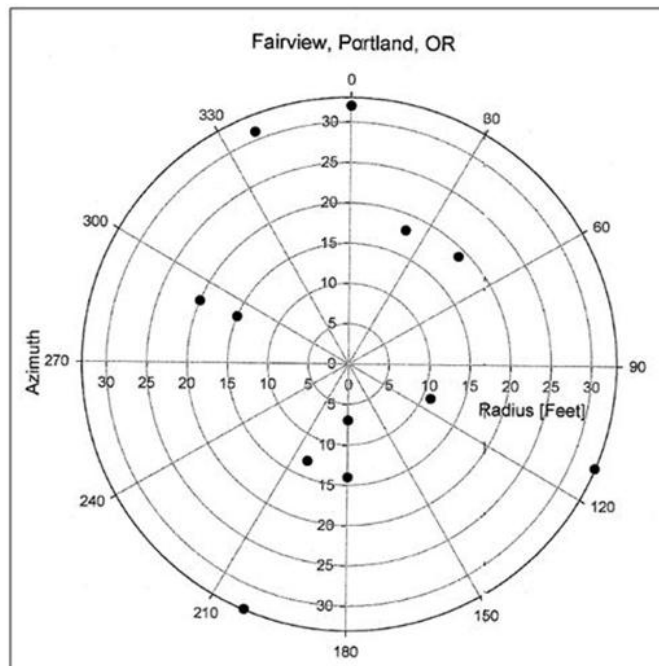


Figure 231b. The locations of the random samples for permeameter tests in Portland, OR. The x-y axes are in feet.

highly variable. The presence of a very fine-grained, discontinuous volcanic ash layer probably influenced the range in hydraulic conductivity values at this site. A comparison of the distance from the center of the tree to variation in hydraulic conductivity values in Figures 230 and 231 does not indicate any distance to conductivity correlation. However, data do show that measurements performed adjacent to the tree are less permeable than the control site.

The Portland levee site was not well suited for this testing, but this was not determined until laboratory analyses were concluded. Infiltration rates were measured in the field with the permeameter, and hydraulic conductivity values were calculated after completion of the field tests. Grain-size analyses revealed that the average soil type at the tree site is ML, and the average soil type for the control site is SM. Thus, the assumption that the control sites consists of similar soils as the tree site was incorrect in this case. A total of 22 tests were conducted at the 3-ft depth and 16 tests were conducted at the 5-ft depth.

Boca Raton, FL

The testing protocol was modified to test 1- and 2-ft depths because of shallow bedrock conditions encountered at this site. Field-derived hydraulic conductivity values adjacent to a fig tree are generally fairly narrow (~1/2 order in magnitude in range) at the 10^{-2} cm/sec range for both the tree and control sites for the 1-ft depth (Figure 232). The range of values broadens appreciably for the 2-ft depth (~2 orders of magnitude) between 10^{-3} to 10^{-5} cm/sec range (Figure 233), and reflects the silty to clayey nature of the sands and decomposed shell overlying the limestone bedrock. The hydraulic conductivity values plotted do not exhibit any trends with distance from the tree. Test data suggest that soils at the control site are less permeable than the soils at the tree site. No obvious differences are exhibited between the control site and tree site with respect to depth or distance from the tree. A total of 24 tests were completed in the 1-ft soil horizon and 24 tests were completed in the 2-ft horizon.

Lewisville, TX

Conductivity data are highly variable at this site with over three orders of magnitude difference at both the 3- and 5-ft test depths shown in Figures 234 and 235, respectively. Overall, conductivity values range between 10^{-4} to 10^{-7} cm/sec. Data suggest that the control site is less

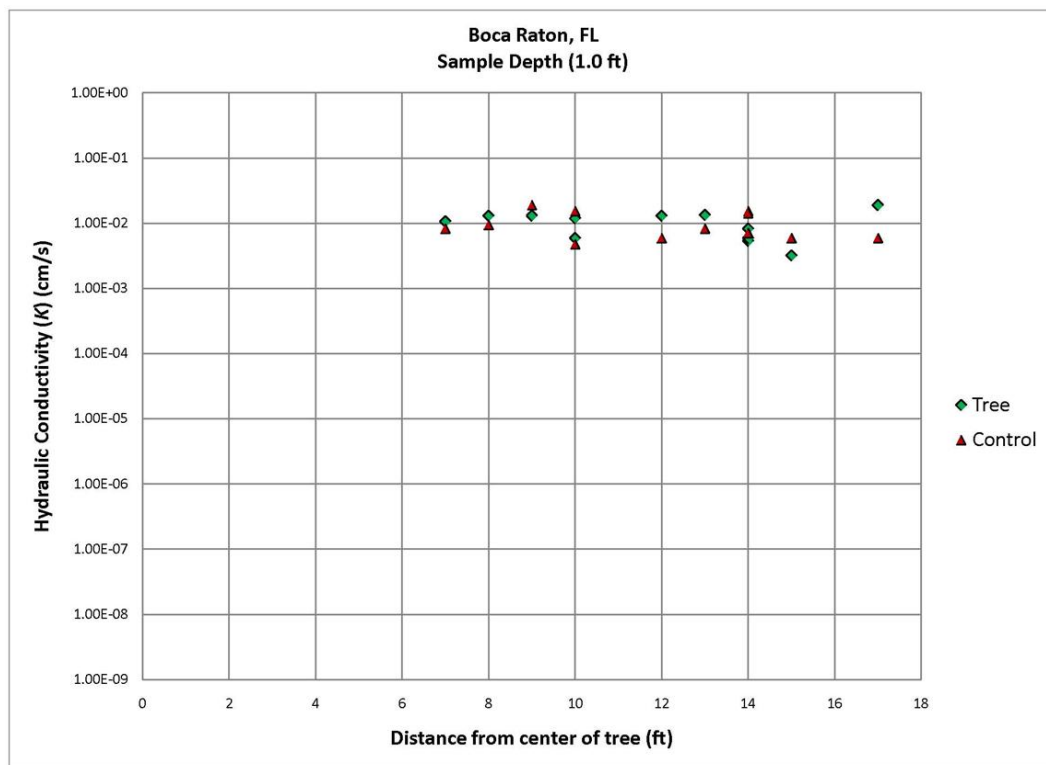


Figure 232a. Hydraulic conductivity calculated from in situ permeameter tests at a depth of 1.0 ft, Boca Raton, FL.

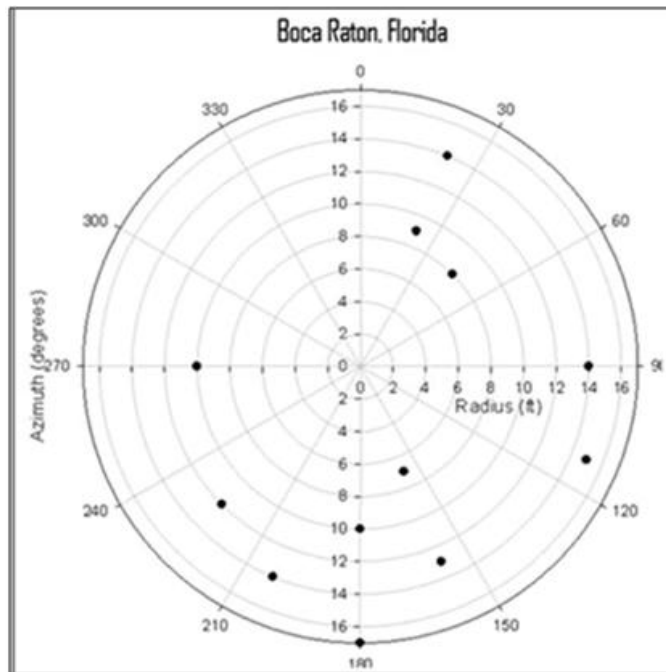


Figure 232b. The locations of the random samples for permeameter tests in Boca Raton, FL. The x-y axes are in feet.

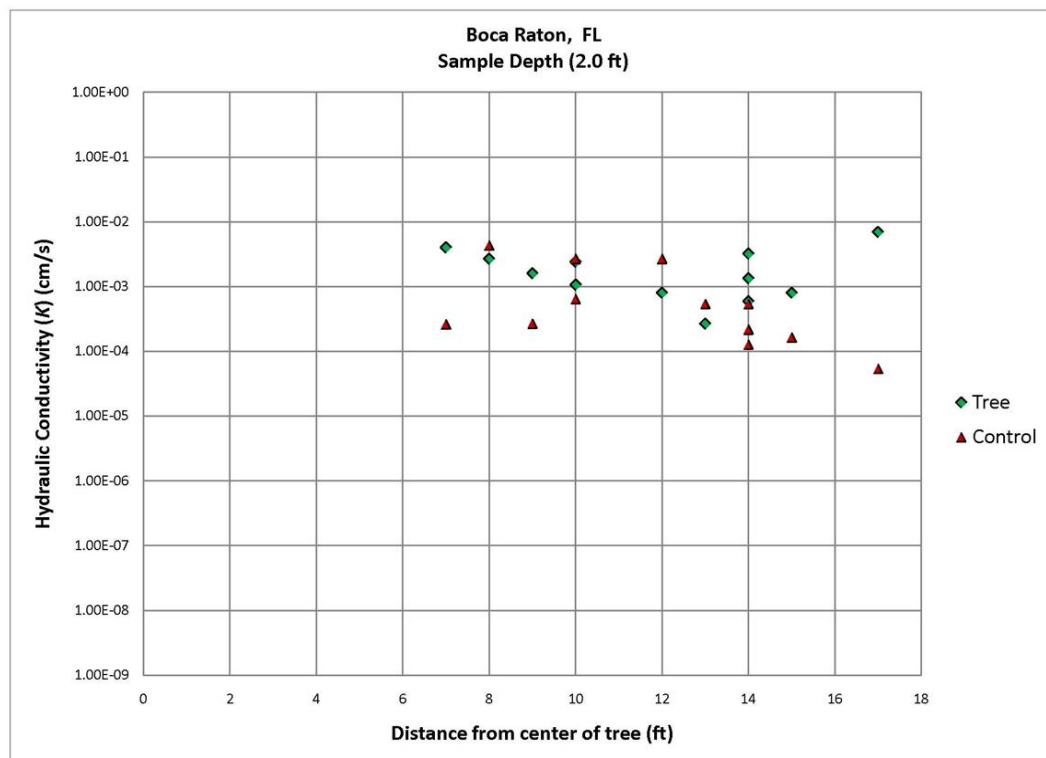


Figure 233a. Hydraulic conductivity calculated from in situ permeameter tests at a depth of 2.0 ft, Boca Raton, FL.

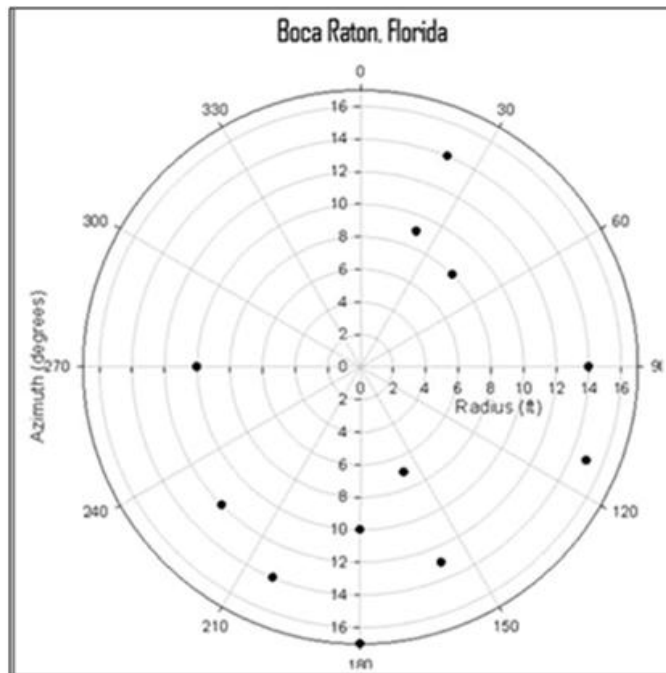


Figure 233b. The locations of the random samples for permeameter tests in Boca Raton, FL. The x-y axes are in feet.

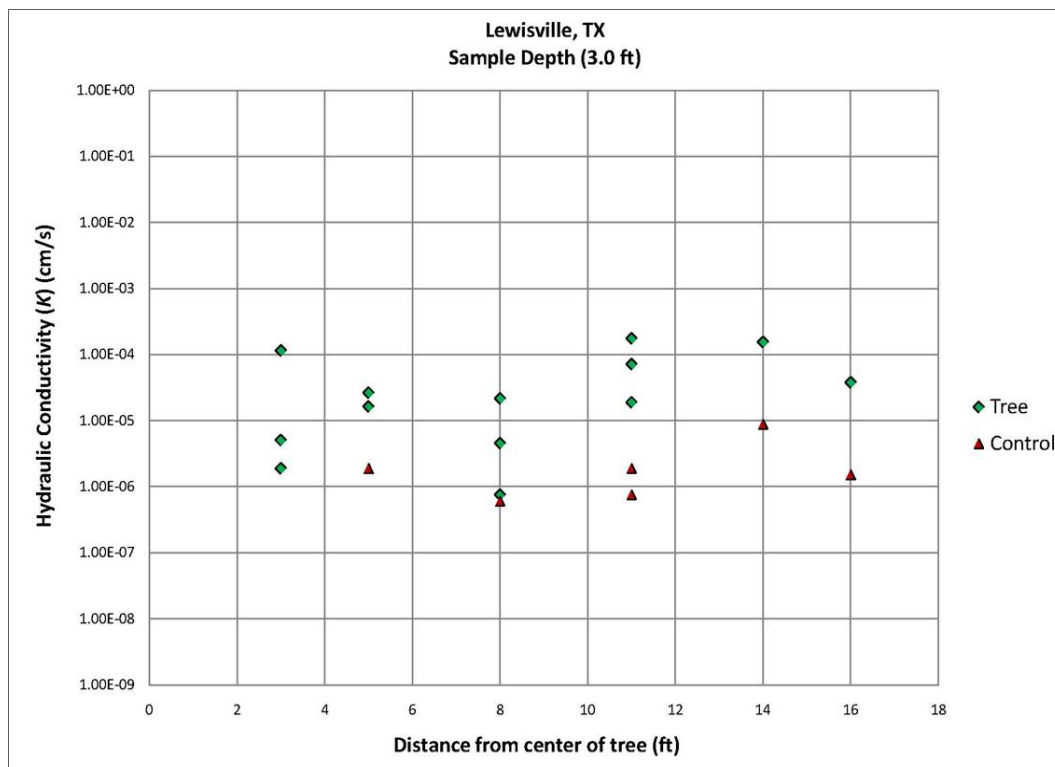


Figure 234a. Hydraulic conductivity calculated from in situ permeameter tests at a depth of 3.0 ft, Lewisville, TX.

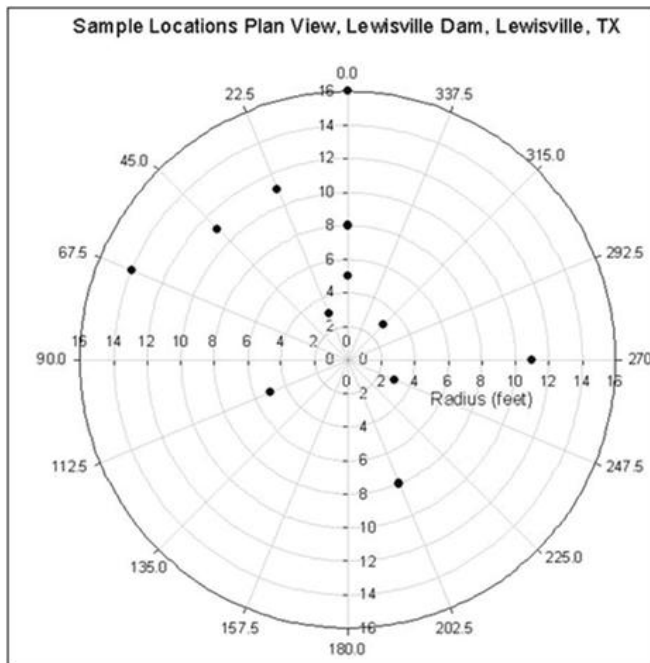


Figure 234b. The locations of the random samples for permeameter tests in Lewisville, TX. The x-y axes are in feet.

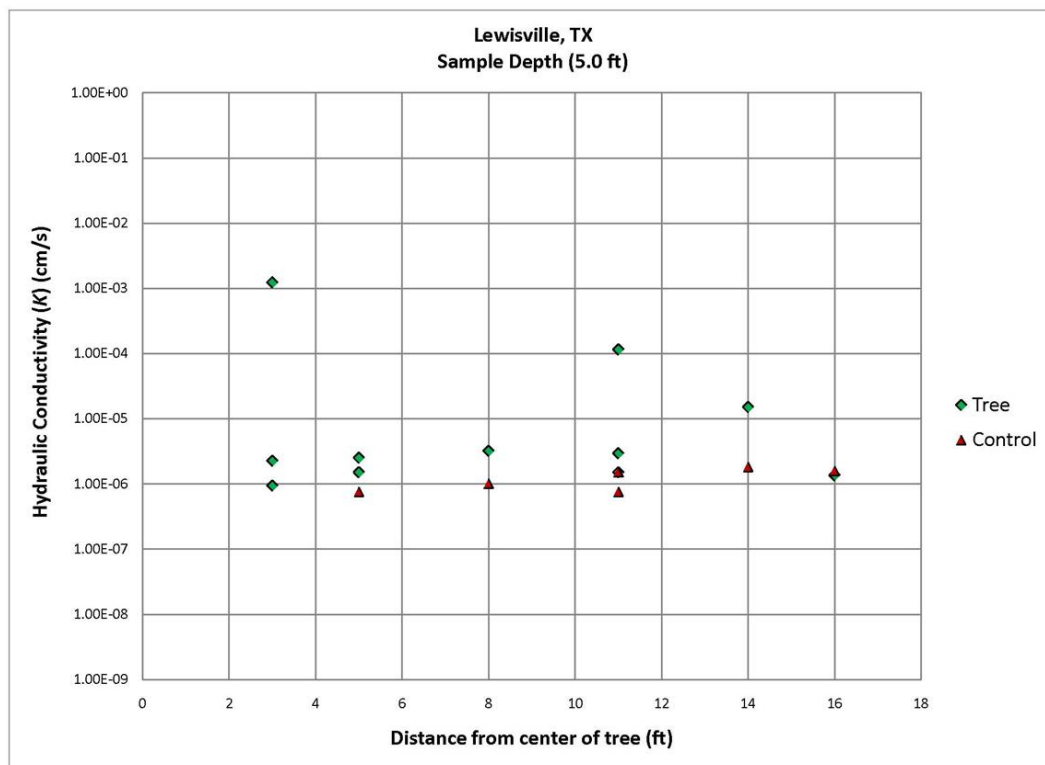


Figure 235a. Hydraulic conductivity calculated from in situ permeameter tests at a depth of 5.0 ft, Lewisville, TX.

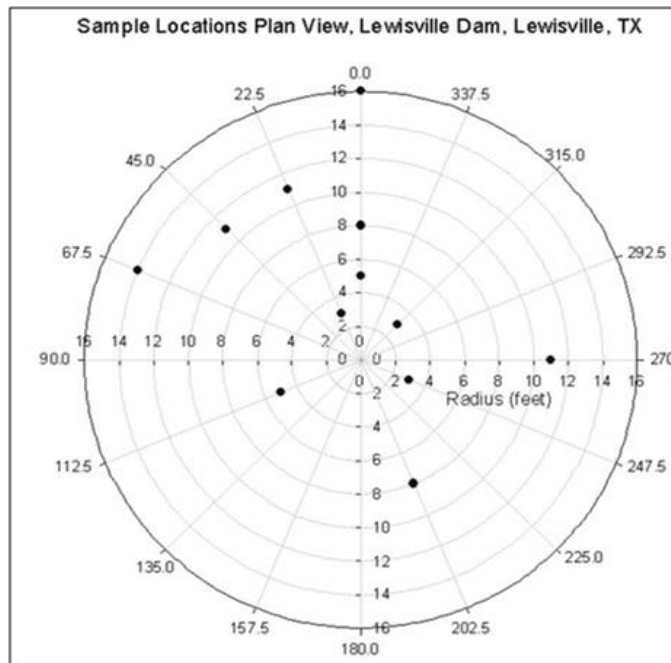


Figure 235b. The locations of the random samples for permeameter tests in Lewisville, TX. The x-y axes are in feet.

permeable than the tree site for both the 3- and 5-ft depths. The low conductivity values calculated are consistent with the clayey soil collected at the site. A total of 19 tests were completed at the 3-ft depth and 17 tests were completed at the 5-ft depth. Fewer tests were possible because of the time required to complete these tests in low permeability soils. Also, precipitation during the test period resulted in boreholes filling with rain water. No trend was noted between conductivity and distance from the tree.

Danville, PA

Hydraulic conductivity testing at the Danville site was at the levee toe adjacent to a recently cut silver maple tree, but the stump was left in place. The roots appeared intact. Field-derived hydraulic conductivity values range between 10^{-2} to 10^{-3} cm/sec for both the tree and control sites at depths of 3- and 5-ft as shown in Figures 236 and 237, respectively. The range of K values is generally less than two orders of magnitude and reflects the sandy nature of the floodplain deposits along the Susquehanna River. Hydraulic conductivity values for the 3-ft depth in Figure 236 show slightly lower values for tree data than the control data. Control data may be slightly less permeable than the tree data for the 5-ft depth as shown in Figure 237. The conductivity values plotted do not show a relationship with distance from the tree. A total of 23 tests were completed in the 3-ft depth and 24 tests were completed at the 5-ft depth.

Vicksburg, MS

Field-derived hydraulic conductivity values adjacent to an oak tree generally range from near 10^{-5} to 10^{-6} cm/sec for both the tree and control sites for the 3- and 5-ft depths, Figures 238 and 239, respectively. The range of K values is narrow and reflects the uniform nature of the loess deposit. Hydraulic conductivity values for the 3-ft depth in Figure 238 do not show any clear trends between the control and tree data. However, hydraulic conductivity values from the tree sites are slightly less permeable ($\sim 1/2$ order of magnitude) than the control sites for the 5-ft data values. One extremely high value was calculated at the 5-ft depth. This test was located 3 ft from the center of the tree and probably tested an interval adjacent to a vertical root. Pictures of the excavated root system show a large mass of vertical roots extending approximately 3 to 4 ft from the tree's center. No trend in conductivity with distance from the tree was

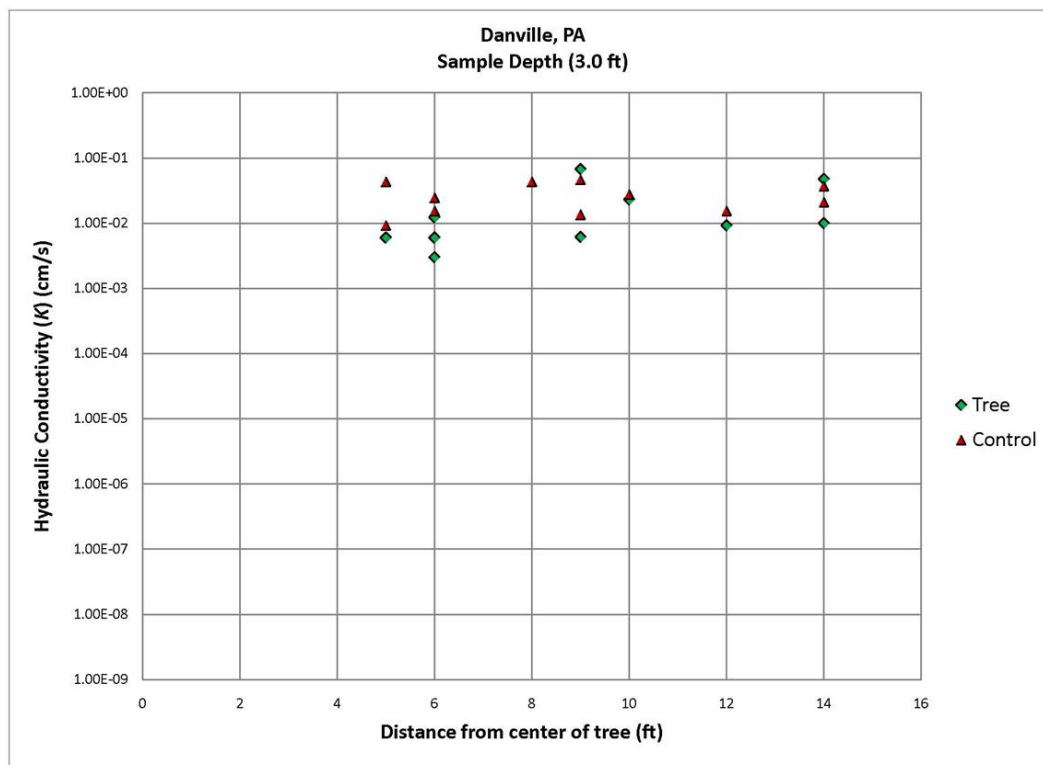


Figure 236a. Hydraulic conductivity calculated from in situ permeameter tests at a depth of 3.0 ft, Danville, PA.

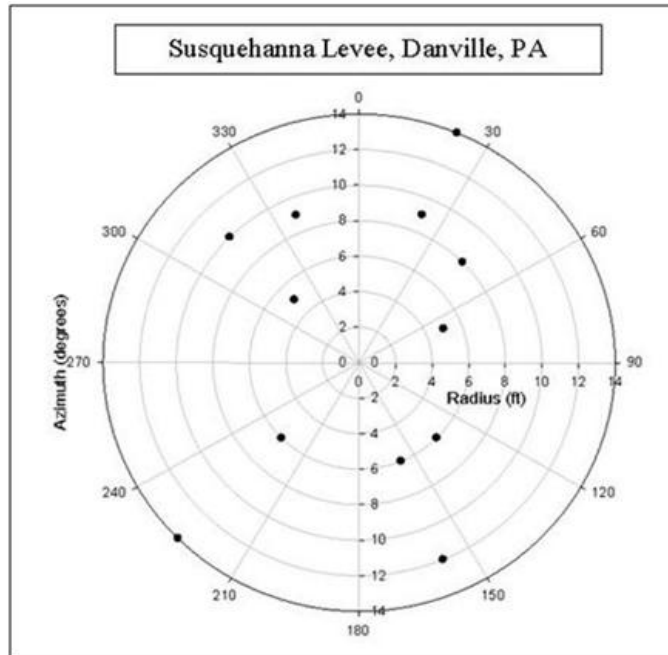


Figure 236b. The locations of the random samples for permeameter tests in Danville, PA. The x-y axes are in feet.

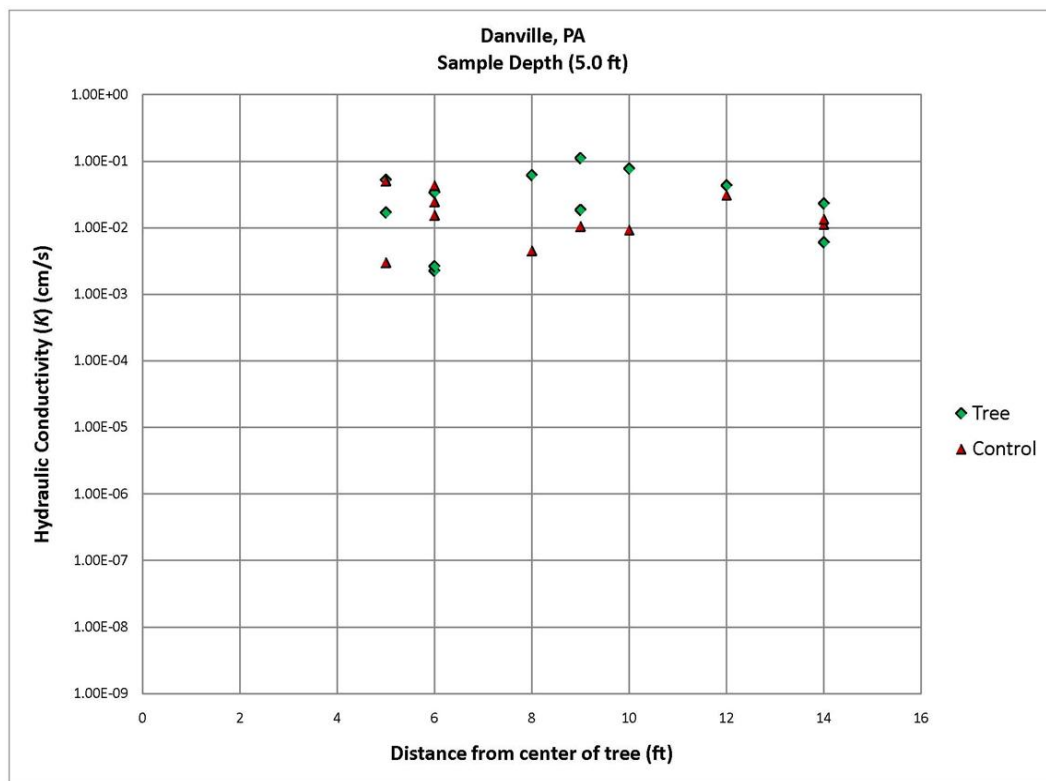


Figure 237a. Hydraulic conductivity calculated from in situ permeameter tests at a depth of 5.0 ft, Danville, PA.

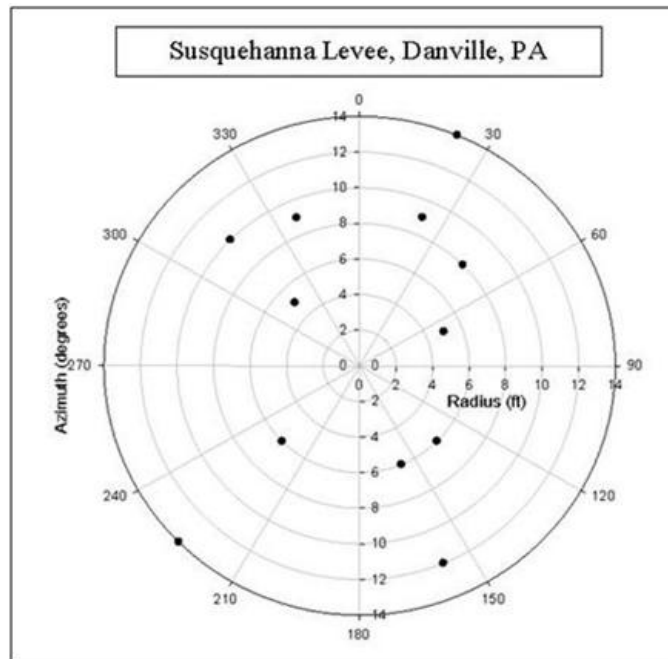


Figure 237b. The locations of the random samples for permeameter tests in Danville, PA. The x-y axes are in feet.

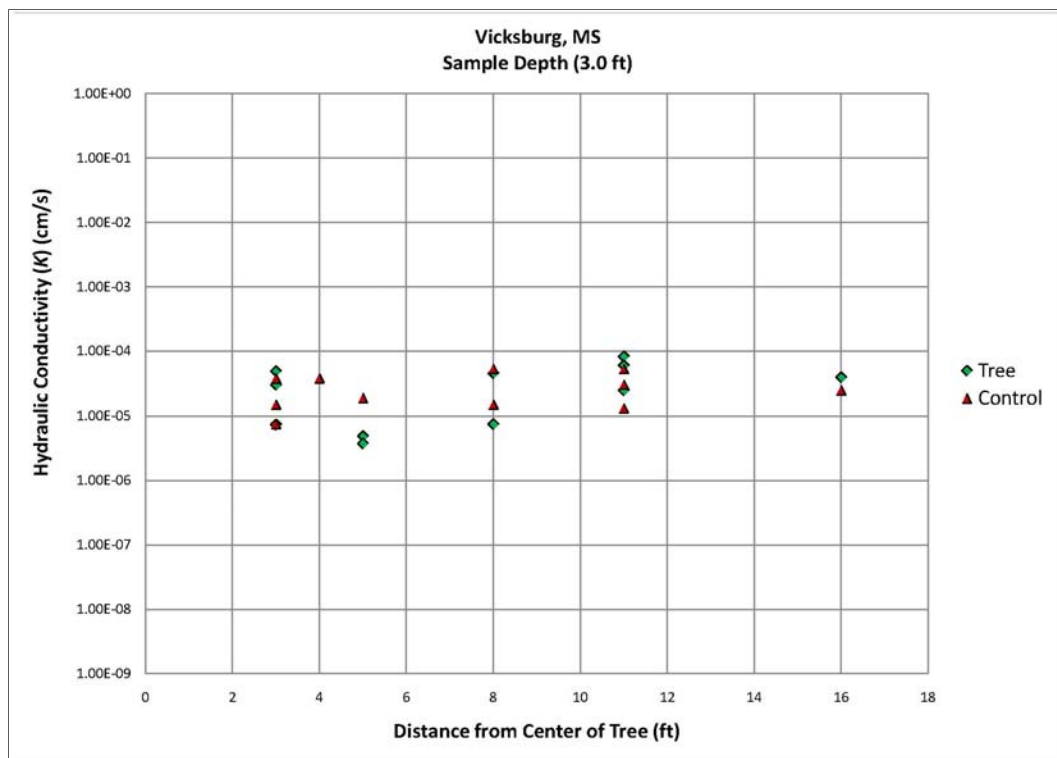


Figure 238a. Hydraulic conductivity calculated from in situ permeameter tests at a depth of 3.0 ft, Vicksburg, MS.

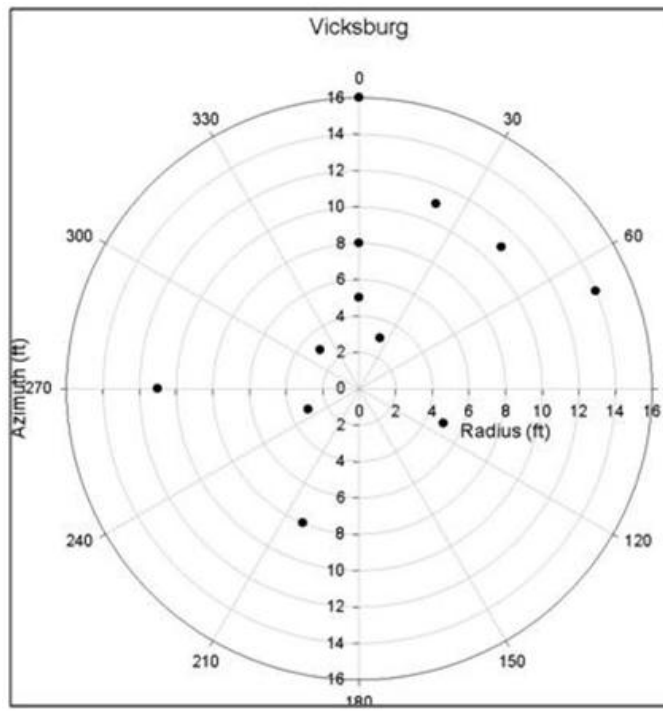


Figure 238b. The locations of the random samples for permeameter tests in Vicksburg, MS. The x-y axes are in feet.

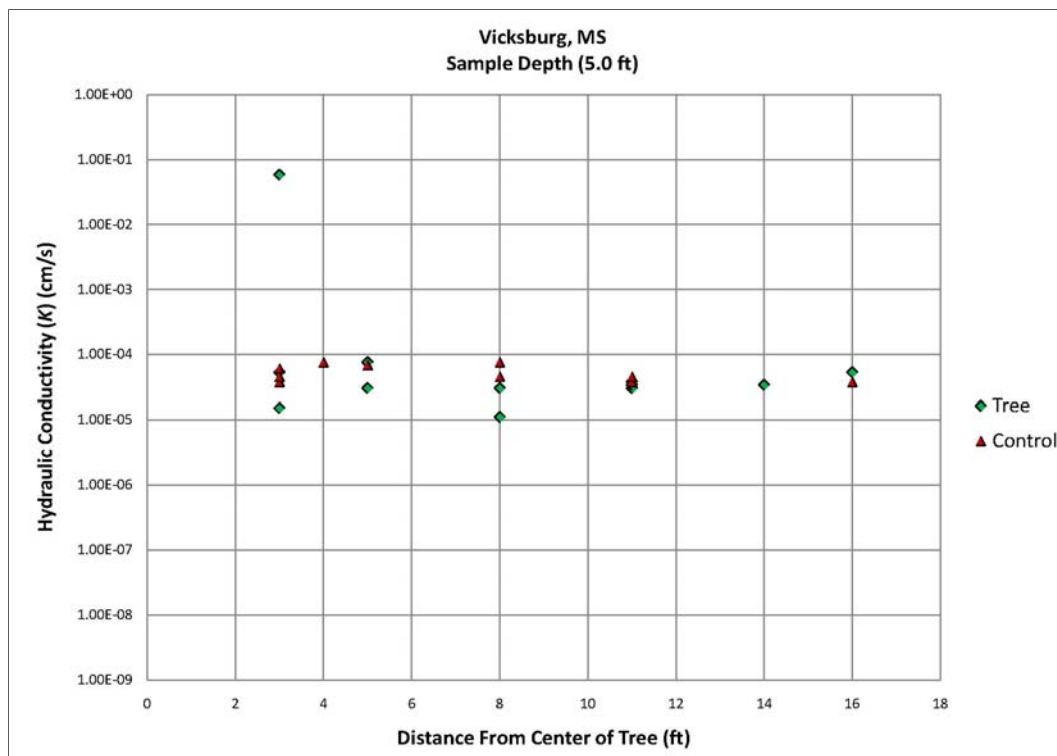


Figure 239a. Hydraulic conductivity calculated from in situ permeameter tests at a depth of 5.0 ft, Vicksburg, MS.

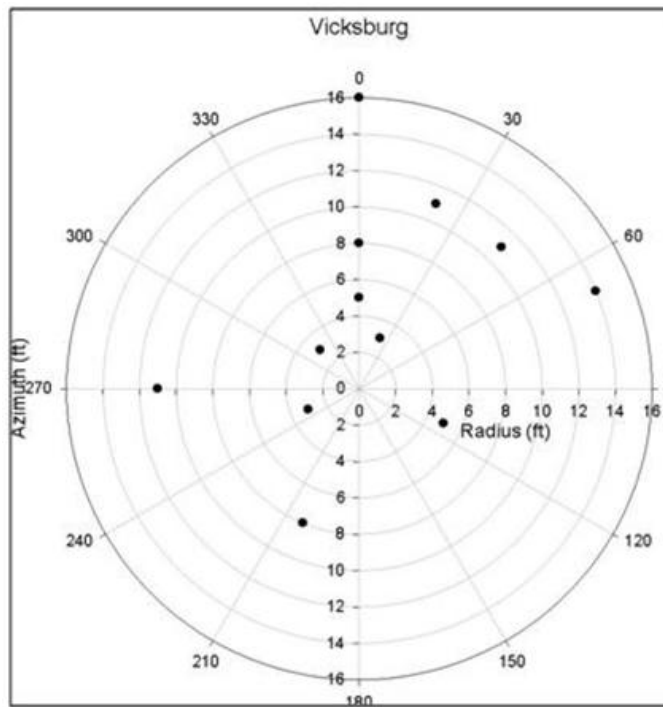


Figure 239b. The locations of the random samples for permeameter tests in Vicksburg, MS. The x-y axes are in feet.

observed. A total of 24 tests were completed in the 3-ft horizon and 24 tests were completed in the 5-ft soil horizon.

Summary of field tests for hydraulic conductivity

Testing was conducted around nine trees at eight locations across the United States. Table 54 lists the site names (city and state) along with the latitude and longitude of the selected tree. A control site was selected for comparison of soil property values for each tree site. Control sites were selected within a maximum of 500 ft of the tree site and a minimum of 40 ft from the tree's drip line because of similar geologic and topographic characteristics as the tree, with respect to both soil type and position on the levee slope or toe. Each test was conducted within the boundaries of the selected tree's root zone, as estimated by the geophysical testing by ERDC and by extensive empirical studies by Coder (Marks and Tschantz 2002).

At most sites, 12 conductivity tests were conducted at two depths around the tree and the same sample pattern was followed for the control site. At some sites difficulties were encountered during sampling, therefore, less than 12 tests were conducted in some soil horizons. Grab samples were taken before each conductivity tests for visual observation. Undisturbed core samples were obtained from the same boring at the completion of each conductivity test, after cleaning out the material in the bottom of the hole. Specific gravity, grain size distribution, Atterberg limits, water content and dry density were determined for selected soil samples. A full multivariate correlation analysis of laboratory testing results to conductivity results was outside the scope of this study; however soil laboratory test data have been retained for future analyses.

Statistical analysis of the hydraulic conductivity test data

The study was planned with the assumption that in situ hydraulic conductivity could be measured quickly with the Guelph Permeameter and that nearly identical tests could be conducted at the tree and control areas of each site. Thus, holding the soil type constant and using random sampling locations, an unbiased comparison of the measured hydraulic conductivities between the tree site and its respective control site could be accomplished using statistical analyses.

Table 54. Details of locations used for in situ hydraulic conductivity tests.

Site Name/Location	Tree Species	Tree Location with Respect to Levee	Major Soil Type (USCS) Tree/Control ^a	Diameter of Tested Area	Tree Dimensions	Estimated Width to Length of Root Ball and Depth ^b	Estimated Root Ball Diameter, Root System Diameter ^c
Sacramento, CA	valley oak (<i>Quercus lobata</i> Née)	On landside, at midslope	Silty sand (SM)/SM	10 m	75 cm DBH 16.8 m drip line 15 m height	Geophysics unsuccessful at estimating root extent	6 m root ball 22 m root system
Burlington, WA	red cedar (<i>Thuja plicata</i>)	4 m from riverside toe	SM/SM	13.4 m	143 cm DBH 12.2 m drip line 20 m height	10 m by 12 m Depth 0.6 m	>6.5 m root ball >34 m root system
Albuquerque, NM Site 1	cottonwood (<i>Populus fremontii</i>)	21 m from riverside toe	ML/ML	10.8 m	41 cm DBH 10.7 m drip line 11 m height	Geophysics unsuccessful at estimating root extent	16 m root ball 14 m root system
Albuquerque, NM Site 2	cottonwood (<i>Populus fremontii</i>)	20 m from riverside toe	SM/SM	10.8 m	58 cm DBH 14 m drip line 12 m height	Geophysics unsuccessful at estimating root extent	5.5 m root ball 17.5 m root system
Portland, OR	cottonwood (<i>Populus fremontii</i>)	15 m from landside toe	Silt (ML)/SM	20 m (center of boring plot is located between two cottonwood trees)	91 cm DBH ^d 20 m drip line ^e 24.6 m height Average dimensions	Geophysics unsuccessful at estimating root extent (geophysics survey conducted on different tree)	6.5 m root ball 32 m root system
Boca Raton, FL	strangler fig tree (<i>Ficus aurea</i>)	38 m landside of canal	SM/SM	10.2 m	73 cm DBH 10 m drip line 6 m height	No surveys conducted	6.1 m root ball 23 m root system

Site Name/Location	Tree Species	Tree Location with Respect to Levee	Major Soil Type (USCS) Tree/Control ^a	Diameter of Tested Area	Tree Dimensions	Estimated Width to Length of Root Ball and Depth ^b	Estimated Root Ball Diameter, Root System Diameter ^c
Lewisville, TX	post oak (<i>Quercus stellata</i>)	On landside toe, Lewisville Dam	Clay (CL)/CL	9.6 m	110 cm DBH 15 m drip line 10 m height	2.7 m by 3.5 m Depth 1.5 m	6.5 m root ball 32 m root system
Danville, PA	silver maple (<i>Acer saccharinum</i>)	5 m from riverside toe	SC	8.4 m	Stump diam 73.2 cm drip line N/A height N/A	No surveys conducted	6.1 m root ball 23 m root system
Vicksburg, MS	red oak (<i>Quercus falcate</i>)	natural, Loess deposit	CL/CL	9.6 m	29 cm DBH 7.5 m drip line 7.5 m height	4.5 m by 3.5 m Depth 1.25 m	13 m root ball 9 m root system

^aSource: ERDC lab testing.

^b Source: ERDC geophysical surveys.

^c Source: Empirical Data (Marks and Tschantz 2002).

^d Average DBH of both trees.

^e Combined drip line, drip line dimension given as diameter, of two adjacent trees was 20 m.

Note: Soil types used in ERDC modeling efforts were obtained from available sources at the time of modeling. Field testing was conducted during and after completion of the numerical models for the ERDC research.

Note: DBH = diameter of tree stem at breast height.

Hydraulic conductivity was measured using a Guelph Permeameter, which is essentially a constant head test conducted in a 5-cm-diam borehole. On average, 12 tests were conducted on two soil horizons for each tree and each control site. The resulting data were analyzed for normality, and appropriate means (geometric/arithmetic) for each soil horizon and site were then calculated. Jabro and Evans (2006), Wilson et al. (1989), and Reynolds and Elrick (1986) observed that hydraulic conductivity is lognormally distributed when observing many in situ measurements. Its variability in the field is dependent upon intrinsic (natural, e.g., geologic, grain size distribution) and extrinsic (cultural, e.g., farming) processes (Warrick and Van Es 2002). Thus, it was not surprising that most of the data collected in this study were also log-normally distributed. To assess normality, this analysis employed the Shapiro-Wilk's test, Coefficient of Variation, Q-Q plots, and histograms of the untransformed and logtransformed permeability data. Analyses were conducted using SAS version 9.1 (© SAS Institute Inc. 2003).

If non-normality is caused by one or more extreme outliers, no transformation will succeed in imposing normality. Outlier(s) should be dropped if there is reason to believe they are erroneous; if not, nonparametric tests can be used for data analysis. In this study, no data points were dismissed as erroneous; when normality could not be achieved by log transformation, comparison of tree and control data was performed using the nonparametric Kruskal-Wallis test.

Equality of variances

An assumption of parametric tests for comparing treatments is equality of treatment variances. The t-test procedure in SAS uses the Folded F test to check equality of variances. Significantly unequal variances are indicated by a P value < 0.05. If variances are unequal, a t-test for unequal variances may be used for comparing two treatments. SAS uses a Satterthwaite adjustment of the degrees of freedom for this test.

Comparison of tree and control data

At each test location and depth, tree and control data were compared using either the untransformed or log transformed data based on the normality tests (Table 55). T-tests were used with a two-tailed significance level of $\alpha = 0.05$. As a check, nonparametric Kruskal-Wallis tests were also performed. The procedures used to check normality indicated that log-

transformed data provided a better fit to the normal distribution than untransformed data for both depths at Albuquerque (both sites), Boca Raton, Burlington, Danville, and Portland, and the 3-ft depth at Lewisville.

Table 55. Difference of log means and confidence intervals plotted in Figures 240 and 241.

Location	Depth (ft)	Difference between Log Means (Tree - Control)	Confidence Interval	t-test Significant (P<0.05)
Sacramento, CA	3	-0.1239	0.3157	no
	5	-0.1518	0.5577	no
Burlington, WA	3	-0.5752	0.365	yes
	5	0.168	0.3423	no
Albuquerque, NM Site 1	1.5	0.098	0.222	no
	2.5	-0.6785	0.2947	yes
Albuquerque, NM Site 2	1.5	-0.7977	0.3732	yes
	2.5	-1.5197	0.3862	yes
Portland, OR	3	-2.2591	0.9092	yes
	5	-1.4746	1.5675	no
Boca Raton, LA	1	0.007	0.1795	no
	2	0.513	0.423	yes
Lewisville, TX	3	1.227	0.561	yes
	5	0.71	0.8649	no
Danville, PA	3	-0.3113	0.2888	yes
	5	0.19	0.3998	no
Vicksburg, MS	3	-0.0519	0.3449	no
	5	0.084	0.5818	no

The 5-ft depth at Lewisville included several high outliers, and the 5-ft Vicksburg data contained one extremely high outlier. Log transformation did not succeed in improving normality for either of these data sets, so nonparametric statistical procedures were used. At Sacramento (both depths) and Vicksburg (3-ft depth), the untransformed data provided a better fit to normality than did log transformation, as did the untransformed 5-ft Vicksburg data if the high outlier was removed. Histograms of each data set are shown in Appendix F.

Correlation of hydraulic conductivity and distance from tree

This study also examined whether a correlation exists between changes in hydraulic conductivity and distance from the tree. The Pearson correlation coefficient with a significance level of $\alpha = 0.05$ was used to test the association of untransformed and log transformed hydraulic conductivity with distance from the tree for each location and depth. Control data were not included in this analysis. When the hydraulic conductivity data were severely non-normal even with transformation (e.g., Lewisville, 5-ft depth), nonparametric Spearman correlation was also used.

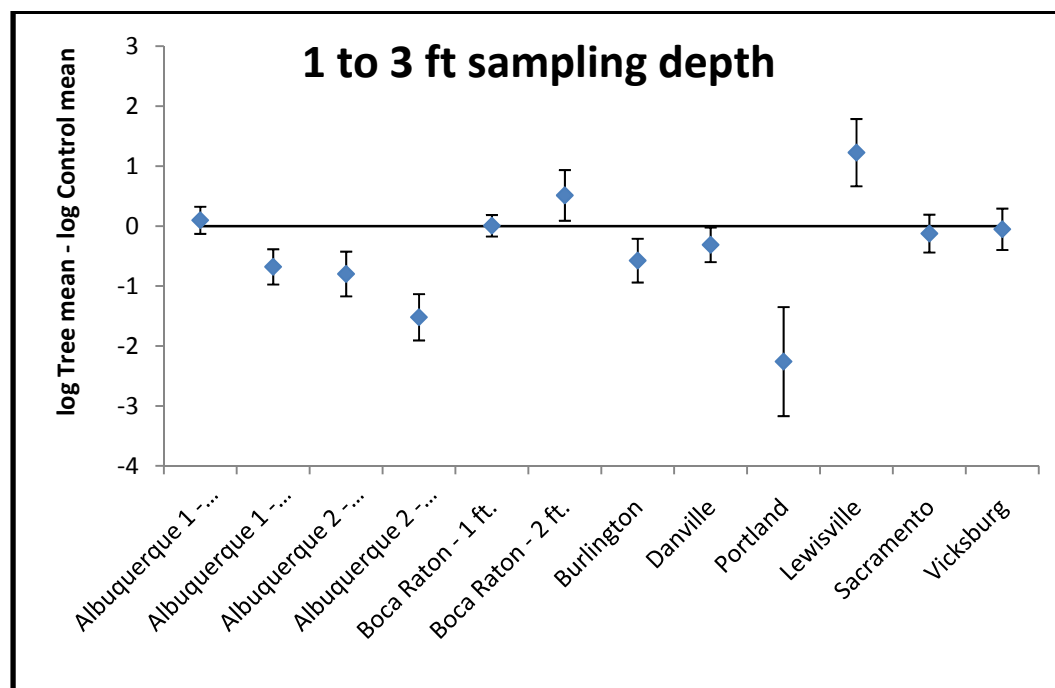


Figure 240. Difference between mean hydraulic conductivities for shallow depth (1 to 3 ft) for the tree and control sites with 95% confidence interval.

Results of statistical analyses

Comparison of tree and control data

Table 56 shows a summary of the statistical analyses. The table provides the difference in mean values between the locations with trees and those without, and also gives the percent difference with respect to the control. For the shallower sampling depths (1 to 3 ft), control hydraulic conductivity data were significantly greater than tree hydraulic conductivity data at Albuquerque (Tree 2; and Tree 1, 2.5 ft only), Burlington, Danville and Portland; while tree data were significantly greater than control at Boca Raton (2 ft only) and Lewisville. For the deeper sampling depth (5 ft), there

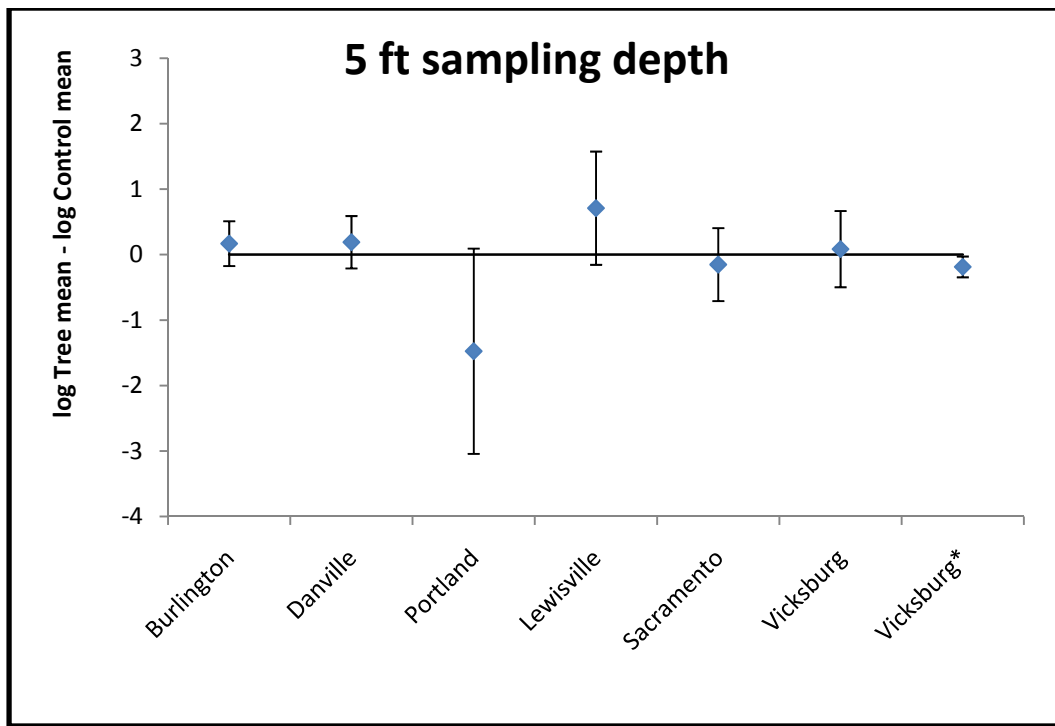


Figure 241. Chart showing difference between tree and control mean hydraulic conductivities and the 95% confidence intervals for tests conducted at 5 ft. Vicksburg is shown with and without the outlier included in the data set. The Vicksburg data without the outlier (Vicksburg *) shows a smaller confidence interval.

were no significant differences between tree and control hydraulic conductivity data at any site, except Vicksburg when the high outlier was excluded from the tree data.

Figures 240 and 241 are graphical representations of the statistical results. For comparison between sites, the graphs display the difference in means of the log transformed data, and the error bars represent the 95% confidence intervals for the difference in means. If the confidence interval lies entirely above the zero reference line, then log tree mean is statistically significantly greater than log control mean, and vice versa if the confidence interval lies entirely below the zero line. Confidence intervals that include zero indicate that the difference in means is not statistically significant. Although only the log transformed data intervals are displayed for uniformity, the statistical interpretation is identical to that of the t-tests using untransformed data at the appropriate locations (Sacramento, Lewisville, Vicksburg), and the nonparametric Kruskal-Wallis test used with the 5-ft Lewisville data and 5-ft Vicksburg data (outlier included).

Table 56. Summary of calculated mean hydraulic conductivities per tree and control site.

Location	Depth (ft)	Geometric Mean of Calculated Hydraulic Conductivities		
		Calculated Mean Hydraulic Conductivity Tree Site, K (cm/s)	Calculated Mean Hydraulic Conductivity Control Site, K (cm/s)	Percent Difference in Mean Hydraulic Conductivities (Tree – Control)/Control
Sacramento	3	3.31E-02	3.84E-02 ^b	-25
	5	2.27E-02	3.38E-02 ^b	-29
Burlington	3	2.21E-04	8.31E-04	-73
	5	3.20E-04	2.17E-04	47
Albuquerque 1	1.5	7.44E-03	5.94E-03	25
	2.5	2.39E-03	1.24E-02	-81
	1.5	6.57E-03	4.13E-02	-84
Albuquerque 2	2.5	3.17E-03	1.05E-01	-97
	3	4.55E-04	1.24E-02	-90
Portland ^c	5	1.83E-03	4.47E-03	1500
	3	9.18E-03	9.03E-03	2
Boca Raton	1	1.51E-03	4.63E-04	226
	2	2.52E-05	1.49E-06	1588
Lewisville ^a	3	1.16E-04 ^b	1.24E-06 ^b	9200
	5	1.12E-02	2.29E-02	-51
Danville	3	2.17E-02	1.40E-02	55
	5	3.20E-05	2.8E-05 ^b	-11
Vicksburg	3	6.08E-05	5.00E-05	21

^a At Lewisville, 12 tests were conducted at 3 and 5 ft at the tree site and 7 and 6 tests were conducted at the control site for 3- and 5-ft depths, respectively. The low permeability of the soil increased the length of time needed to conduct the test and the field time was exhausted before tests could be completed.

^b Arithmetic means.

^c Portland control site was not suitable—however, results are shown.

Correlation of hydraulic conductivity and distance from tree

Correlations were not significant at any location or at either sampling depth.

Conclusions of statistical analysis

Results of statistical comparisons between the mean hydraulic conductivities of the tree data and control data were inconsistent for the shallow soil horizon. No significant differences between tree and control data were found at the deeper soil horizon. It was not determined why shallow soil horizon data for some of the control areas were higher than the respective tree data and some were lower, but it could possibly be linked to soil type, texture, or structure. Additional factors that might affect the

results should also be considered such as, if the scale of the test was appropriate and were enough data points taken to evaluate the variability of the data. At the time of field testing, the test and analysis plan, scale of measurement, and test apparatus were assumed appropriate. In the future, it is recommended that more testing locations be added per tree; that testing be conducted closer to the tree trunk; that larger scale tests (infiltration tests) be added to the investigation; and that study design include more rigorous control of tree species, soil type, and ambient conditions (climate and season).

In summary, in situ hydraulic conductivity tests were conducted around nine trees and their respective control sites at shallow (1.5 to 3 ft) and deep (5 ft) depths. The generalized results are shown in Figures 240 and 241, which compare the differences in log mean of the tree and control hydraulic conductivity values and confidence levels associated with these differences. A thorough multivariate correlation analysis between the soil properties collected in the field and the differences in mean hydraulic conductivity was not within the scope of this investigation. However, instead of a multivariate study, it is recommended that additional field tests be conducted with a more rigorous study design, keeping the number of variables at a minimum by keeping the tree species and geographic location constant, and increasing the number of tests per tree and control site.

The purpose of the statistical analysis is to answer two questions:

- Is there a measurable difference in the average hydraulic conductivity values representing the tree data sets versus the average value of their respective control data?
- If a difference is found at the tree location, does it vary with distance from the tree?

Table 56 summarizes the differences in the geometric (arithmetic for some) means of the calculated hydraulic conductivities for each tree and control site. The purpose of this table is to emphasize that the magnitudes of the differences are small. The difference could be within the order of natural variance for the tested soil. Thus, statistically there were measurable differences in the calculated means of the tree and control sites, but the magnitudes of the differences are not significant when considering the use of the parameter in a seepage analysis. It was not

determined whether or not the differences lie within the natural variance of the soil.

Gray et al. (1991) found no appreciable difference in hydraulic conductivities when testing laboratory samples with and without roots. Brizendine found no appreciable difference in hydraulic conductivity when testing in situ hydraulic conductivity at the drip line of trees and outside of the drip line where no roots were present. This study has found a statistically measurable difference in 8 of the 12 shallow soil horizons tested. Of the seven deep soil horizons tested, no statistically measurable differences between the tree and control data sets were found. However, the magnitude of the differences is not significant considering practical use of the parameter in a seepage analysis. Additional studies are needed to better understand the contribution of roots to macroporosity and hydraulic conductivity. Because of limited field data, in Volume III, a sensitivity analysis was conducted for the ERDC research on the premise that roots might influence hydraulic conductivity.

With the exception of Portland, Lewisville, and Boca Raton, all mean differences were less than one order of magnitude. Portland was not a suitable test site because the control soil was a different classification (ML) than the tree site (SM). Not enough tests were conducted at the Lewisville control site to make a strong comparison. Finally, Boca Raton was a difficult site because of the rocky nature of the soil. It may not be possible to measure the effect of tree roots in hard soils.

6 Root Reinforcement for Slope Stability

Purpose

Knowing in situ root strength provides a better understanding of the response of root systems against external loads. The pullout tests show not only the possible tensile strength of a root, but also the interaction between the root and the surrounding geological materials. Data from the pullout tests are used as part of root reinforcement parameters in the slope stability analysis conducted by ERDC for this research (Volume III).

Root pullout device development

By considering the variation of root sizes in a levee environment, ERDC constructed, but modified, the root tree pullout apparatus and procedure described by Norris and Greenwood (2000; 2003). The modifications included using a T-System configuration at the base of the aluminum frame instead of a diagonal rod to accommodate pulling of larger roots. In the ERDC device, the root was pulled directly without a lever system as used by Norris and Greenwood et al. (2000; 2003), and a string pot was used to measure displacement. The ERDC device uses a steel post to resist shear rather than anchors.

The ERDC device is composed of several parts:

- T-System – an aluminum reaction frame for supporting the pistons, pulley system, and string pot
- Hydraulic pump – an automatic Enerpac hydraulic system with a double-acting piston used to pull the root at a constant rate
- Root holder – a multiple root clamping device, with inserts to accommodate tree root size variations
- Load cell – for pulling force measurements
- String potentiometer (pot) – for root displacement measurements
- Computer (data logger) – records pullout displacement

A schematic diagram of the ERDC root pullout apparatus is shown in Figure 242. Figure 243 is a field photograph of the ERDC apparatus in operation.

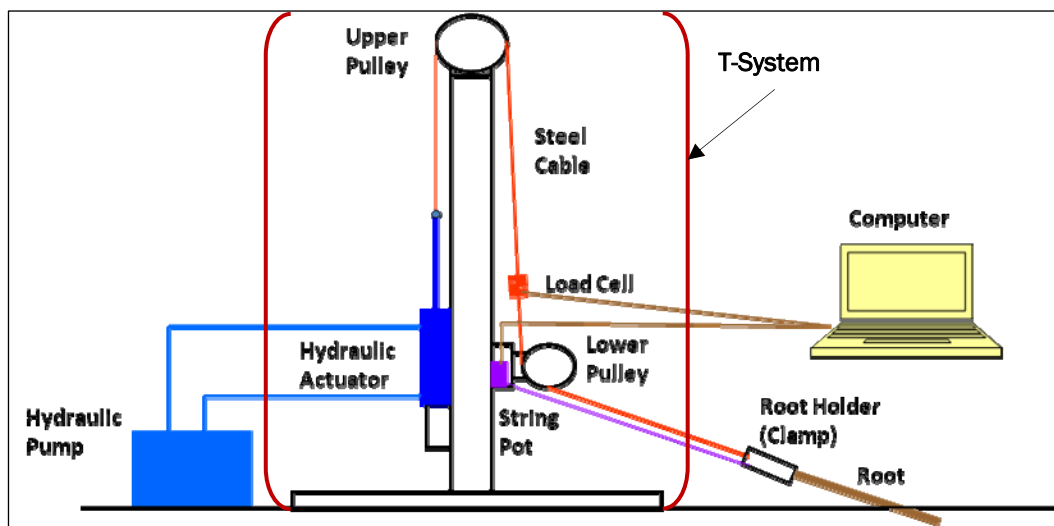


Figure 242. Schematic diagram of the ERDC root pullout device.

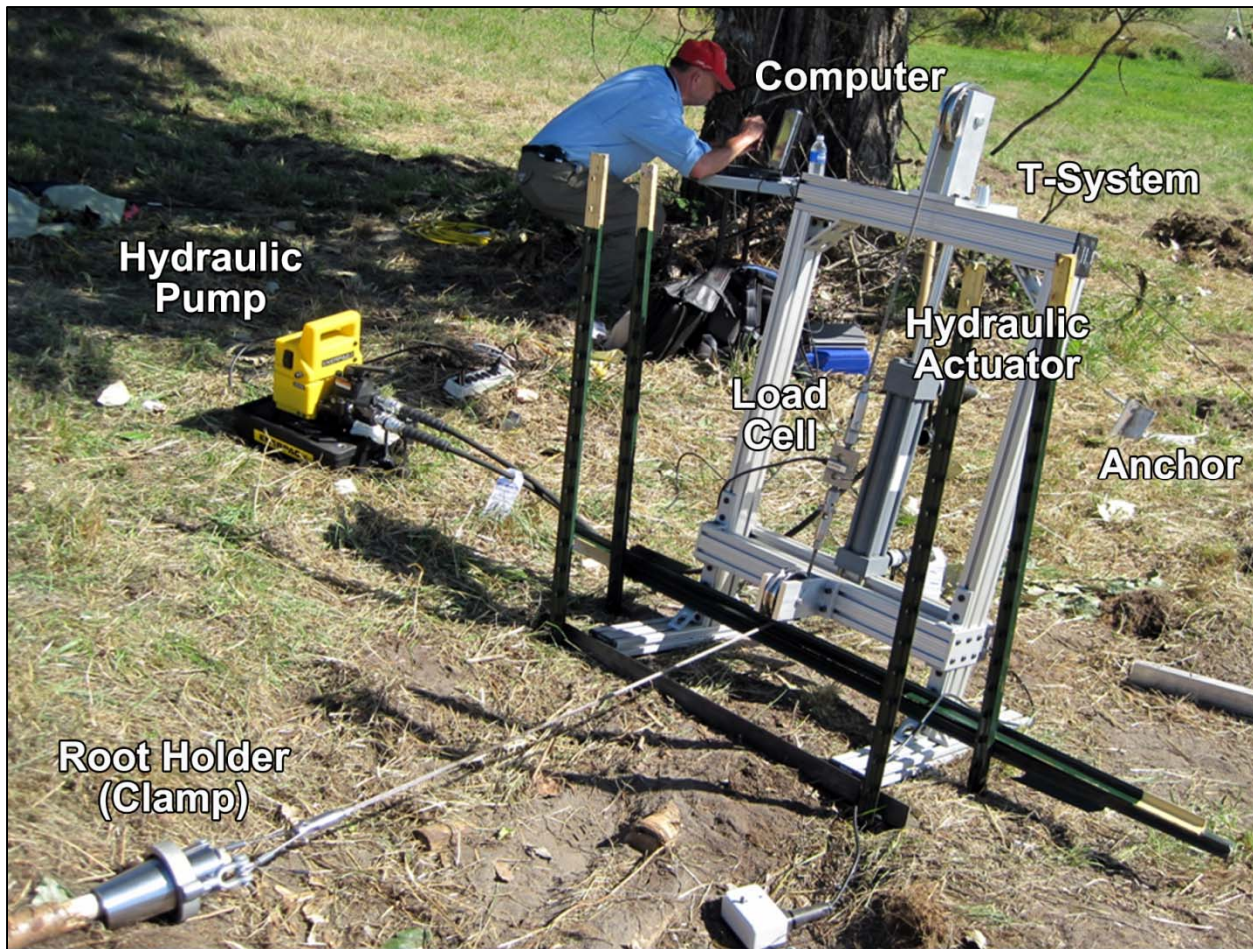


Figure 243. Field operation of the ERDC root pullout device.

Root pullout testing procedure

Site preparation

In general, pullout tests were conducted approximately 60 deg around the tree selected for the tests. The location of a test depended on the availability of a root near the ground surface. At present, the root size that can be tested by the ERDC device cannot exceed 2.5 in. (diameter of root with bark) because of the design of the root clamp.

A backhoe was used to remove soil around the tree to locate roots. Once a root was located, the soil surface was cleared of debris prior to the test.

Once the tree root is exposed, the root bark is removed to allow the hard surface of the root, known as the secondary xylum, to be in direct contact with the root holding mechanism for secure holding during the pullout process. Previous tests done by Sharma and Webster (1994) and Turmanina (1965) indicated that tree bark contributes little to the ultimate tensile strength of tree roots. Before the root was secured in the clamp, the root diameter was measured and recorded, and the root was photographed.

Equipment preparation

The T-System is placed in front of the root perpendicular to the root path. A 6-ft distance between the frame and the root is required because the frame needs to be anchored firmly to the ground. The frame is held in place by an anchoring system with steel posts (Figure 243). The string pot is positioned in front of the frame, slightly away from the root path to avoid a direct hit by the root clamp when the root fails.

The tree species, dip angle and dip direction of the root, root location with respect to the tree, tree location, dates, weather, and soil type are recorded. The following mechanical connections are made prior to the test: the steel cable is attached to the double-acting piston and the load cell, the string pot is connected to the root holder, and the laptop computer is attached to the load cell and the string pot for data recording.

For each root pullout experiment, Tosi (2007) finished the test in 3 min. Based on previous research using pullout devices (Norris and Greenwood 2003), the needle valve on the hydraulic pump, which controls the rate of

loading, was adjusted for a relatively slow pulling displacement rate of 0.08 in./sec. The hand operated Enerpac hydraulic actuator is a displacement control device with a displacement rate ranging from 0.1 and 0.08 in./sec.

Testing execution

The test begins when the hydraulic pump is started. The load cell and displacement transducers immediately start recording the measurements, and the measurements are stored on a laptop computer. The tests are always conducted with the pulling force toward the tree. Failure occurs when the root breaks or is pulled out of the soil. Maximum forces and root failure location are noted, as well as any additional observations during and after the test.

Root pullout field test

Pullout tests were conducted at three locations: Portland, OR; Burlington, WA; and Albuquerque, NM, under dry field conditions. A variety of tree species were tested: maple, alder, Oregon ash, cottonwood, and cedar. In general, cottonwood roots are straighter than other species tested and located near the ground surface. The trees tested are shown in Figures 244 through 248.

The length and root diameter at different positions along the root are measured. All root branches, if found, are also measured. The failure mechanism is recorded: whether the root breaks or there is a bonding failure. If the root breaks, it happens abruptly so the force versus displacement curve usually shows a steep slope, and there is no residual strength. In a bonding failure, the force versus displacement curve shows a gentler slope, and there is residual strength. A combined failure mode may also occur, which includes both a root break failure and a bonding failure.

Root pullout test results

Root pullout strength can be expressed in two ways: pullout force, which is a direct output from the load cell (measured in pounds), and pullout stress (pullout force divided by root cross-section area (measured in psi)).



Figure 244. Two trees, cottonwood and Oregon ash, selected for root pullout tests, in Portland, OR, approximately 10 miles east of Portland Airport, near Columbia River.



Figure 245. Three trees, two maples and one cedar, selected for root pullout tests, east of Burlington, WA, along the Skagit River.



Figure 246. Three trees, alder, cottonwood, and cedar, selected for root pullout tests, east of Burlington, WA, along the Skagit River.



Figure 247. Five cottonwood trees, selected for root pullout tests, in Albuquerque, NM, approximately 4 miles northwest of the intersection of I-25 and I-40, near the Rio Grande River.



Figure 248. Four cottonwood trees, selected for root pullout tests, in Albuquerque, NM, approximately 5 miles northwest of the intersections of I-25 and I-40, near the Rio Grande River.

Figures 249 and 250 show examples of pullout force versus displacement curves for cottonwood trees from two different test sites. Results of the other pullout tests are located in Appendix G. Figure 249 shows the pullout test results of a cottonwood in Portland, OR. The cottonwood tree is 81 ft high with diameter at breast height (DBH) of 42 in. and with a root diameter of 1.74 in. The major root break occurred at approximately 0.5 in. of displacement, and the load cell recorded a pullout force of 2,467 lb. Dividing the pullout force by the cross-sectional area of the root, the maximum pullout stress is 1,038 psi. After the major root broke, the curve showed the remaining force resistance until reaching almost zero resistance at a displacement of 6 in. The failure mode of this root is a combination of a root break failure and a bonding failure.

Figure 250 shows the pullout test results for a cottonwood from Albuquerque, NM. The cottonwood tree has height of 40.5 ft with a DBH of 18.2 in., and a root diameter of 1.78 in. The major root break happened at approximately 6.9 in. of displacement and a pullout force of 2,722 lb. However, this is not considered the maximum pullout force. The ERDC team considers the maximum allowable displacement to be 4 in. This number is used because although the pullout resistance was still

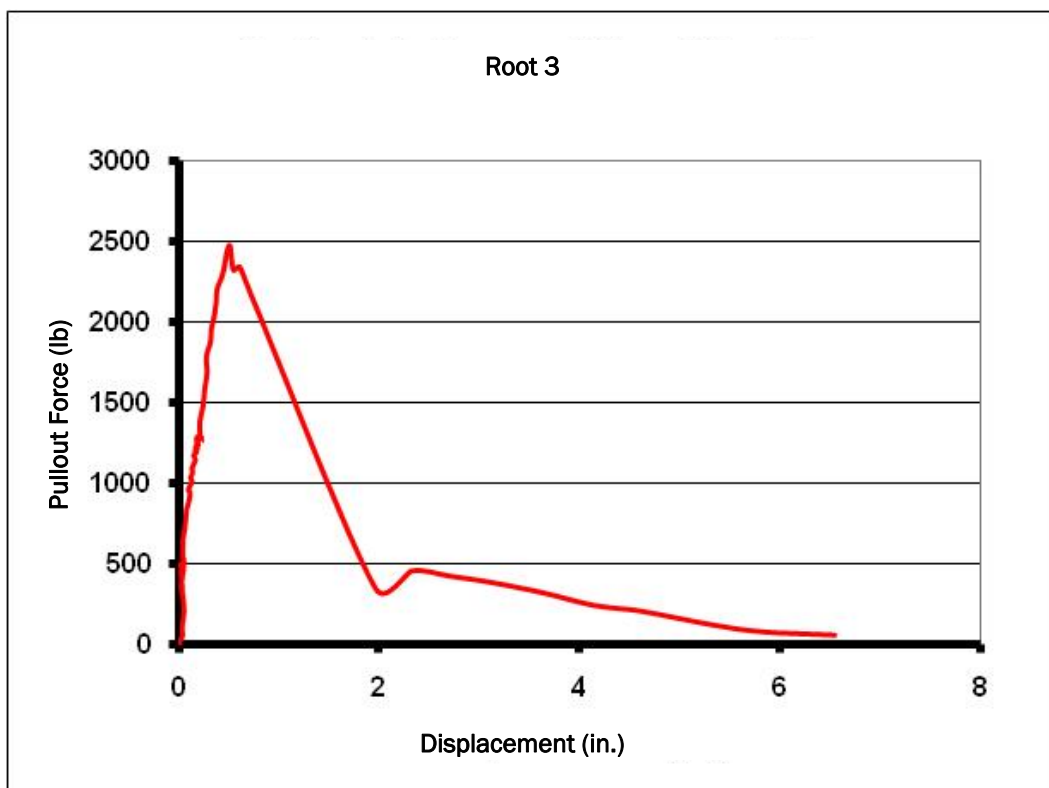


Figure 249. Pullout force vs. displacement of a cottonwood, Portland, OR.

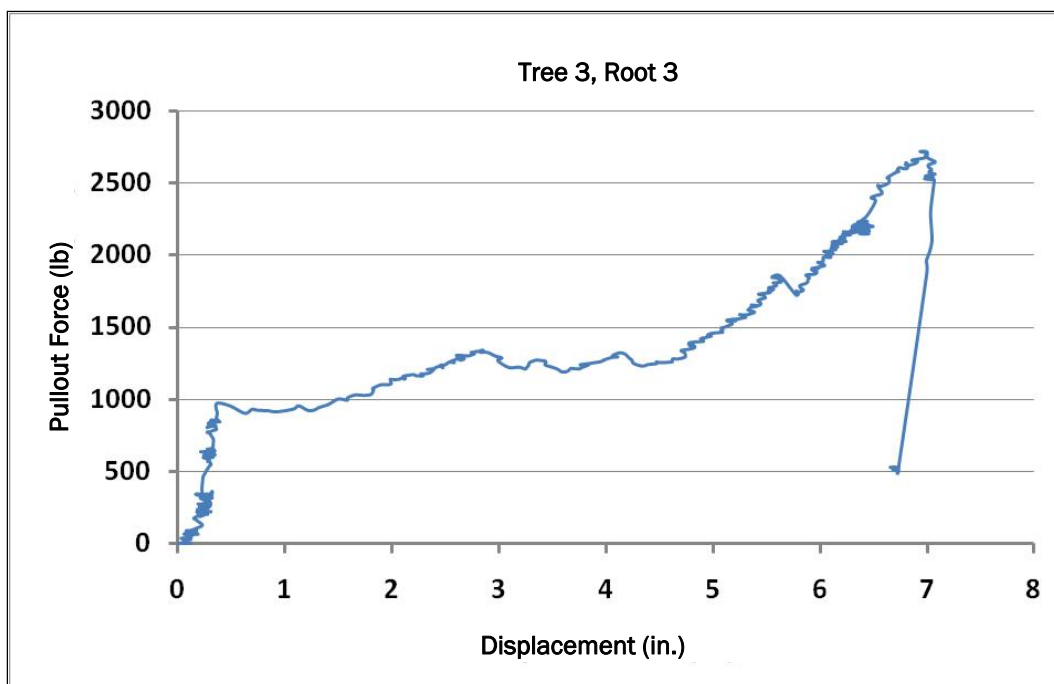


Figure 250. Pullout force vs. displacement of a cottonwood, Albuquerque, NM.

increasing, the root had moved more than 4 in. so the root is considered to have failed. For this particular test, the maximum pullout force was the load cell reading when the root reached the 4-in. displacement, 1,292 lb, or the maximum pullout stress of 519 psi.

Table 57 is the summary of pullout test results from Portland, OR, Burlington, WA, and Albuquerque, NM. Root diameters (root with bark) range between 0.7 and 2.33 in., the pullout force ranges from 86 to 3513 lb, and the pullout stresses are between 56 and 2,645 psi.

Figure 251 shows the relationship between pullout stress and root diameter for test results from Portland, OR, Burlington, WA, and Albuquerque, NM. The solid line shows the equation line developed by Abernethy and Rutherford (2001) after converting it to English units. The trend is also similar to data collected by Norris (2005) as well as Tosi (2007). The data collected by ERDC populated the vertical component of the Abernethy and Rutherford (2001) equation line.

Statistical analysis of root pullout data

An analysis of covariance was used to assess the statistical significance between severed root diameter and the force required to displace severed roots. This analysis is modeled after that of Abernethy and Rutherford (2001), who found that root diameter at the point of rupture was a significant predictor of tensile strength of roots. Results from the ERDC study are qualitatively similar to those of Abernethy and Rutherford, although the analyses differ in several respects. The ERDC study considered a larger range of root diameters (up to 2 in.) and root diameters were measured at the point where the roots were severed and force was applied, rather than at the point of rupture. ERDC performed the analysis after converting the force applied to the roots to a cumulative measure of work required to displace the root up to 4 in. at half-inch increments. The explanatory variables included root displacement distance, root diameter, location, and species (Table 58).

Data consisted of force in pounds resulting in displacement in inches of tree roots measured at half-second intervals. Data were collected for several different tree species at four locations (Portland, OR; Burlington, WA; and two at Albuquerque, NM). Displacements were sectioned into half-inch increments up to a maximum of 4 in., and work was calculated as

Table 57. Pullout tests summary.

Species	Location	DBH (in.)	Height (ft)	Root No.	Root Diameter with Bark (in.)	Pullout Force (lb)	Pullout Stress (psi)	Failure Mode
Cottonwood	Portland, OR	42.0	81	1	1.10	1294	1362	Bonding
				2	1.08	394	430	Root break
				3	1.74	2467	1038	Combined
				4	1.07	352	392	Root break
				5	1.99	1839	592	Combined
				6	1.84	1979	745	Root break
Oregon ash	Portland, OR	12.6	48	1	1.27	1888	1491	Root break
				2	1.09	1575	1689	Bonding
				3	1.50	2039	1154	Bonding
				4	0.72	837	2057	Root break
				5	1.17	2842	2645	Root break
Maple 1	Burlington, WA	50.4	72	1	0.83	524	969	Root break
				2	0.70	896	2329	Root break
				3	1.01	237	296	Combined
				4	0.81	1039	2017	Root break
				5	0.80	1087	2164	Bonding
Maple 2		50.8	53.5	1	1.25	1657	1351	Bonding
Alder	Burlington, WA	16.8	69	1	1.71	862	376	Combined
				2	1.62	777	377	Bonding
				3	1.78	638	257	Root break
Cottonwood	Burlington, WA	23.6	96	1	1.71	3252	1417	Root break
				2	1.24	1289	1068	Root break
				3	1.85	1320	491	Bonding
				4	1.77	2972	1208	Bonding
				5	1.48	452	263	Bonding
Cedar 1	Burlington, WA	22.2	28	1	0.74	546	1270	Root break
Cedar 2				1	1.37	1488	1010	Combined
				2	1.3	1777	1339	Root break
Cottonwood 1	Albuquerque, NM, Site 1	13.4	49	1	0.92	207	312	Root break
Cottonwood 2				2	2.11	2543	728	Root break
Cottonwood 3				3	1.94	1042	353	Root break
Cottonwood 4		16.8	41.5	1	1.64	2539	1203	Root break
Cottonwood 5		9.9	44	2	1.27	2223	1756	Root break
		25.6	44.5	1	2.33	1974	463	Root break
		20.3	36	2	1.26	2062	1655	Root break
				1	1.67	663	303	Root break
				2	2.04	436	133	Combined
				3	1.37	1507	1023	Combined

Species	Location	DBH (in.)	Height (ft)	Root No.	Root Diameter with Bark (in.)	Pullout Force (lb)	Pullout Stress (psi)	Failure Mode
Cottonwood 1	Albuquerque, NM, Site 2	24.1	51	1	1.09	1064	1141	Root break
				2	1.18	1072	981	Root break
				3	1.40	86	56	Bonding
				4	1.84	3513	1322	Combined
Cottonwood 2		10.3	33	5	2.14	1932	537	Combined
				1	1.30	829	625	Combined
				2	1.41	2330	1493	Root break
				3	1.63	1613	773	Bonding
Cottonwood 3		18.2	40.5	4	1.81	680	264	Root break
				1	2.28	1322	324	Bonding
				2	1.90	1810	639	Bonding
				3	1.78	1292	519	Bonding
Cottonwood 4		14.1	31	4	1.03	1115	1339	Root break
				1	1.30	1218	918	Bonding
				2	1.13	211	211	Combined
				3	1.25	816	665	Root break

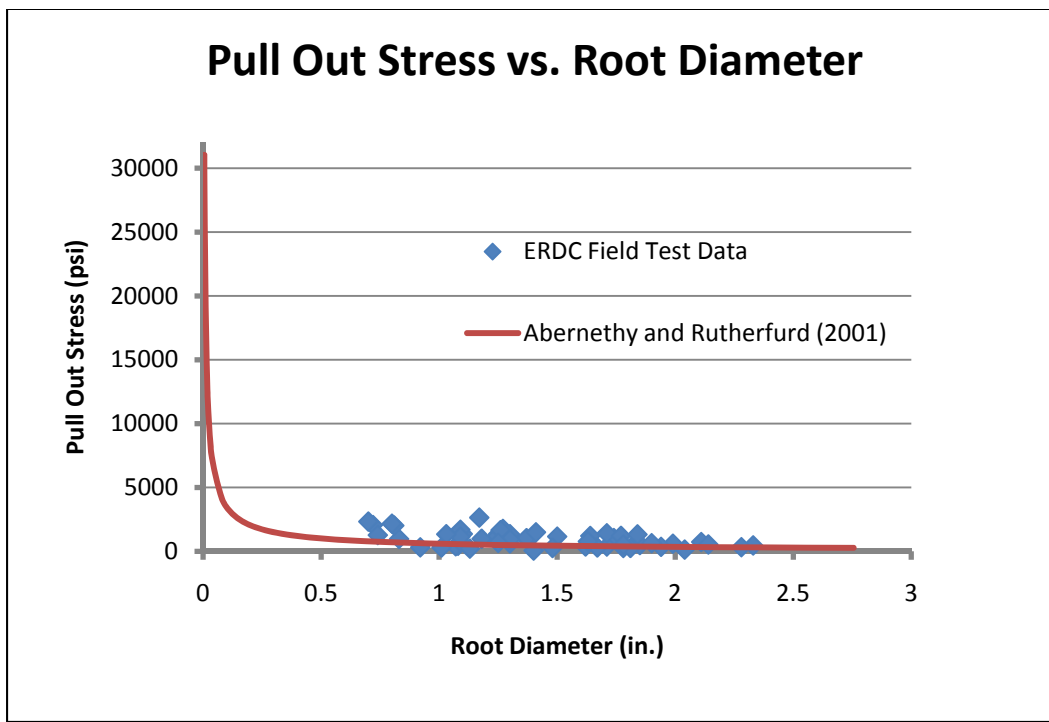


Figure 251. Comparison of ERDC and Abernathy and Rutherford (2001) pullout stress vs. root diameter tests.

the cumulative sum of all force measurements up through each displacement increment. Data were analyzed using an analysis of covariance (ANCOVA) test, which was implemented using the generalized linear model (GLM) procedure in the Statistical Analysis System (SAS) software. The null hypotheses were that no significant relationships exist between the work required to displace a root and the three explanatory variables.

**Table 58. Displacement increment data for pullout tests at
Albuquerque, NM, Burlington, WA, and Portland, OR.**

Location	Species	Tree	Root	Diameter (in.)	Work	Displacement (in.)	Log Transformed Work
ALBUQUERQUE1	Cottonwood	1	1	0.92	281.343833	0.5	5.639577526
ALBUQUERQUE1	Cottonwood	1	2	2.11	86621.0229	0.5	11.36929782
ALBUQUERQUE1	Cottonwood	1	3	1.94	284.017324	0.5	5.649035236
ALBUQUERQUE1	Cottonwood	1	3	1.94	859.828971	1	6.756733499
ALBUQUERQUE1	Cottonwood	1	3	1.94	1535.191826	1.5	7.33641062
ALBUQUERQUE1	Cottonwood	1	3	1.94	1927.932629	2	7.564203531
ALBUQUERQUE1	Cottonwood	1	3	1.94	3064.488862	2.5	8.027636068
ALBUQUERQUE1	Cottonwood	1	3	1.94	11719.02953	3	9.368969255
ALBUQUERQUE1	Cottonwood	1	3	1.94	17022.03937	3.5	9.742264217
ALBUQUERQUE1	Cottonwood	1	3	1.94	19938.30171	4	9.90039787
ALBUQUERQUE1	Cottonwood	2	1	1.64	202170.8021	0.5	12.21686817
ALBUQUERQUE1	Cottonwood	2	2	1.27	119832.354	0.5	11.69384899
ALBUQUERQUE1	Cottonwood	3	1	1.09		0.5	
ALBUQUERQUE1	Cottonwood	4	1	2.33	390.053265	0.5	5.966283307
ALBUQUERQUE1	Cottonwood	4	1	2.33	1807.110552	1	7.499484469
ALBUQUERQUE1	Cottonwood	4	1	2.33	34136.26496	1.5	10.43811559
ALBUQUERQUE1	Cottonwood	4	1	2.33	76323.74682	2	11.2427394
ALBUQUERQUE1	Cottonwood	4	1	2.33	103629.0112	2.5	11.5485726
ALBUQUERQUE1	Cottonwood	4	1	2.33	129129.0145	3	11.7685673
ALBUQUERQUE1	Cottonwood	4	1	2.33	149693.6339	3.5	11.91634604
ALBUQUERQUE1	Cottonwood	4	1	2.33	191316.7612	4	12.16168577
ALBUQUERQUE1	Cottonwood	4	2	1.26	377.097845	0.5	5.93250469
ALBUQUERQUE1	Cottonwood	4	2	1.26	34038.07624	1	10.43523507
ALBUQUERQUE1	Cottonwood	4	2	1.26	152619.518	1.5	11.93570329
ALBUQUERQUE1	Cottonwood	4	2	1.26	248795.6684	2	12.42438723
ALBUQUERQUE1	Cottonwood	5	1	1.67	27018.05856	0.5	10.20426076
ALBUQUERQUE1	Cottonwood	5	2	2.04	23838.99357	0.5	10.0790779
ALBUQUERQUE1	Cottonwood	5	2	2.04	36348.70654	1	10.5009139
ALBUQUERQUE1	Cottonwood	5	2	2.04	42366.85383	1.5	10.65412159
ALBUQUERQUE1	Cottonwood	5	2	2.04	46368.20656	2	10.7443693
ALBUQUERQUE1	Cottonwood	5	2	2.04	47684.40164	2.5	10.77235961
ALBUQUERQUE1	Cottonwood	5	2	2.04	49008.09748	3	10.79974082
ALBUQUERQUE1	Cottonwood	5	2	2.04	50334.63068	3.5	10.8264486
ALBUQUERQUE1	Cottonwood	5	2	2.04	51250.81363	4	10.84448677
ALBUQUERQUE1	Cottonwood	5	3	1.37	156505.9856	0.5	11.96084953
ALBUQUERQUE1	Cottonwood	5	3	1.37	211425.2907	1	12.26162698
ALBUQUERQUE1	Cottonwood	5	3	1.37	219997.9365	1.5	12.30137345
ALBUQUERQUE1	Cottonwood	5	3	1.37	227886.9554	2	12.33660498

Location	Species	Tree	Root	Diameter (in.)	Work	Displacement (in.)	Log Transformed Work
ALBUQUERQUE1	Cottonwood	5	3	1.37	236083.1588	2.5	12.37193939
ALBUQUERQUE1	Cottonwood	5	3	1.37	243102.3478	3	12.40123782
ALBUQUERQUE1	Cottonwood	5	3	1.37	251919.6108	3.5	12.43686531
ALBUQUERQUE2	Cottonwood	1	1	1.09	20800.57943	0.5	9.942736123
ALBUQUERQUE2	Cottonwood	1	2	1.18	1005.513096	0.5	6.913253233
ALBUQUERQUE2	Cottonwood	1	2	1.18	56164.79559	1	10.93604543
ALBUQUERQUE2	Cottonwood	1	3	1.4	93.45041	0.5	4.537430921
ALBUQUERQUE2	Cottonwood	1	3	1.4	195.047705	1	5.27324417
ALBUQUERQUE2	Cottonwood	1	3	1.4	317.222911	1.5	5.759604716
ALBUQUERQUE2	Cottonwood	1	3	1.4	1604.000245	2	7.380255941
ALBUQUERQUE2	Cottonwood	1	3	1.4	1943.655186	2.5	7.572325596
ALBUQUERQUE2	Cottonwood	1	3	1.4	3111.759538	3	8.042943613
ALBUQUERQUE2	Cottonwood	1	3	1.4	6111.124808	3.5	8.717866128
ALBUQUERQUE2	Cottonwood	1	3	1.4	6519.798862	4	8.782598805
ALBUQUERQUE2	Cottonwood	1	4	1.84	3628.01931	0.5	8.196442134
ALBUQUERQUE2	Cottonwood	1	4	1.84	187075.0426	1	12.13926511
ALBUQUERQUE2	Cottonwood	1	4	1.84	229831.3223	1.5	12.34510094
ALBUQUERQUE2	Cottonwood	1	4	1.84	281919.2098	2	12.54937582
ALBUQUERQUE2	Cottonwood	1	5	2.14	34214.62491	0.5	10.44040846
ALBUQUERQUE2	Cottonwood	1	5	2.14	93601.91213	1	11.44680609
ALBUQUERQUE2	Cottonwood	1	5	2.14	105972.5428	1.5	11.57093531
ALBUQUERQUE2	Cottonwood	1	5	2.14	115406.6796	2	11.65621751
ALBUQUERQUE2	Cottonwood	1	5	2.14	116935.9626	2.5	11.66938174
ALBUQUERQUE2	Cottonwood	1	5	2.14	123143.408	3	11.72110487
ALBUQUERQUE2	Cottonwood	1	5	2.14	129412.161	3.5	11.77075764
ALBUQUERQUE2	Cottonwood	1	5	2.14	135699.4926	4	11.81819811
ALBUQUERQUE2	Cottonwood	2	1	1.3	24832.5579	0.5	10.11991089
ALBUQUERQUE2	Cottonwood	2	1	1.3	70280.96223	1	11.16025623
ALBUQUERQUE2	Cottonwood	2	1	1.3	73265.53668	1.5	11.20184561
ALBUQUERQUE2	Cottonwood	2	1	1.3	77076.09776	2	11.2525485
ALBUQUERQUE2	Cottonwood	2	1	1.3	79328.58549	2.5	11.28135382
ALBUQUERQUE2	Cottonwood	2	2	1.41	187756.2113	0.5	12.14289965
ALBUQUERQUE2	Cottonwood	2	3	1.63	458.346653	0.5	6.127625782
ALBUQUERQUE2	Cottonwood	2	3	1.63	4299.528781	1	8.36626071
ALBUQUERQUE2	Cottonwood	2	3	1.63	10574.16254	1.5	9.266168808
ALBUQUERQUE2	Cottonwood	2	3	1.63	32125.10768	2	10.37739317
ALBUQUERQUE2	Cottonwood	2	3	1.63	52968.30844	2.5	10.87744906
ALBUQUERQUE2	Cottonwood	2	3	1.63	123630.264	3	11.72505065
ALBUQUERQUE2	Cottonwood	2	3	1.63	161308.6314	3.5	11.99107477
ALBUQUERQUE2	Cottonwood	2	3	1.63	170169.9906	4	12.04455316

Location	Species	Tree	Root	Diameter (in.)	Work	Displacement (in.)	Log Transformed Work
ALBUQUERQUE2	Cottonwood	2	4	1.81	8258.405328	0.5	9.018986788
ALBUQUERQUE2	Cottonwood	2	4	1.81	15375.00577	1	9.640498468
ALBUQUERQUE2	Cottonwood	2	4	1.81	30682.89805	1.5	10.33146071
ALBUQUERQUE2	Cottonwood	2	4	1.81	43759.8497	2	10.686472
ALBUQUERQUE2	Cottonwood	2	4	1.81	51744.18721	2.5	10.85406738
ALBUQUERQUE2	Cottonwood	2	4	1.81	59414.41542	3	10.99229216
ALBUQUERQUE2	Cottonwood	2	4	1.81	64735.30627	3.5	11.07806202
ALBUQUERQUE2	Cottonwood	2	4	1.81	68603.57445	4	11.13609992
ALBUQUERQUE2	Cottonwood	3	1	2.28	33048.08439	0.5	10.40571888
ALBUQUERQUE2	Cottonwood	3	1	2.28	47479.68537	1	10.76805722
ALBUQUERQUE2	Cottonwood	3	1	2.28	69601.3246	1.5	11.15053888
ALBUQUERQUE2	Cottonwood	3	1	2.28	74642.19665	2	11.22046127
ALBUQUERQUE2	Cottonwood	3	1	2.28	82747.35624	2.5	11.32354734
ALBUQUERQUE2	Cottonwood	3	1	2.28	90850.02025	3	11.4169653
ALBUQUERQUE2	Cottonwood	3	1	2.28	102206.7896	3.5	11.53475339
ALBUQUERQUE2	Cottonwood	3	1	2.28	112295.5381	4	11.62888941
ALBUQUERQUE2	Cottonwood	3	2	1.9	80189.90806	0.5	11.29215295
ALBUQUERQUE2	Cottonwood	3	2	1.9	93069.485	1	11.44110164
ALBUQUERQUE2	Cottonwood	3	2	1.9	103956.7595	1.5	11.55173032
ALBUQUERQUE2	Cottonwood	3	2	1.9	112196.427	2	11.62800643
ALBUQUERQUE2	Cottonwood	3	2	1.9	119000.8613	2.5	11.68688601
ALBUQUERQUE2	Cottonwood	3	2	1.9	125964.9464	3	11.74375894
ALBUQUERQUE2	Cottonwood	3	2	1.9	131239.915	3.5	11.78478234
ALBUQUERQUE2	Cottonwood	3	2	1.9	136538.8186	4	11.82436424
ALBUQUERQUE2	Cottonwood	3	3	1.78	100246.1945	0.5	11.51538438
ALBUQUERQUE2	Cottonwood	3	3	1.78	104871.5051	1	11.56049112
ALBUQUERQUE2	Cottonwood	3	3	1.78	111586.8058	1.5	11.62255809
ALBUQUERQUE2	Cottonwood	3	3	1.78	122211.7178	2	11.71351021
ALBUQUERQUE2	Cottonwood	3	3	1.78	145665.1342	2.5	11.88906566
ALBUQUERQUE2	Cottonwood	3	3	1.78	178015.2365	3	12.08962442
ALBUQUERQUE2	Cottonwood	3	3	1.78	193000.1375	3.5	12.17044618
ALBUQUERQUE2	Cottonwood	3	3	1.78	205180.351	4	12.23164463
ALBUQUERQUE2	Cottonwood	3	4	1.03	391.148887	0.5	5.969088273
ALBUQUERQUE2	Cottonwood	3	4	1.03	119298.8828	1	11.68938724
ALBUQUERQUE2	Cottonwood	4	1	1.3	36358.56708	0.5	10.50118514
ALBUQUERQUE2	Cottonwood	4	1	1.3	105073.899	1	11.56241918
ALBUQUERQUE2	Cottonwood	4	1	1.3	163411.7362	1.5	12.00402828
ALBUQUERQUE2	Cottonwood	4	1	1.3	165834.2176	2	12.01874388
ALBUQUERQUE2	Cottonwood	4	1	1.3	179031.7572	2.5	12.09531848
ALBUQUERQUE2	Cottonwood	4	1	1.3	203875.0699	3	12.22526268

Location	Species	Tree	Root	Diameter (in.)	Work	Displacement (in.)	Log Transformed Work
ALBUQUERQUE2	Cottonwood	4	2	1.13	13983.58309	0.5	9.545639284
ALBUQUERQUE2	Cottonwood	4	2	1.13	27636.58517	1	10.22689572
ALBUQUERQUE2	Cottonwood	4	2	1.13	29914.78711	1.5	10.30610819
ALBUQUERQUE2	Cottonwood	4	2	1.13	30625.67788	2	10.32959408
ALBUQUERQUE2	Cottonwood	4	2	1.13	31271.29523	2.5	10.35045587
ALBUQUERQUE2	Cottonwood	4	2	1.13	31560.91237	3	10.35967468
ALBUQUERQUE2	Cottonwood	4	2	1.13	31961.55191	3.5	10.37228896
ALBUQUERQUE2	Cottonwood	4	2	1.13	32229.87477	4	10.38064909
ALBUQUERQUE2	Cottonwood	4	3	1.25	17799.35536	0.5	9.78691752
ALBUQUERQUE2	Cottonwood	4	3	1.25	127848.7641	1	11.75860331
BURLINGTON	Maple	2	1	1.25	43822.57414	0.5	10.68790435
BURLINGTON	Maple	2	1	1.25	114830.1435	1	11.6512093
BURLINGTON	Maple	2	1	1.25	129772.7431	1.5	11.77354007
BURLINGTON	Maple	2	1	1.25	146206.1251	2	11.89277272
BURLINGTON	Maple	2	1	1.25	158825.2754	2.5	11.97555998
BURLINGTON	Maple	2	1	1.25	174214.0964	3	12.06804026
BURLINGTON	Maple	1	1	0.83		0.5	
BURLINGTON	Maple	1	2	0.7	62003.51334	0.5	11.03494633
BURLINGTON	Maple	1	2	0.7	76978.34204	1	11.25127939
BURLINGTON	Maple	1	3	1.01	6204.822113	0.5	8.733082029
BURLINGTON	Maple	1	3	1.01	11143.31117	1	9.318594702
BURLINGTON	Maple	1	3	1.01	13737.81493	1.5	9.527907523
BURLINGTON	Maple	1	3	1.01	14615.51865	2	9.589839164
BURLINGTON	Maple	1	3	1.01	15137.84027	2.5	9.624952866
BURLINGTON	Maple	1	3	1.01	15440.01205	3	9.644717604
BURLINGTON	Maple	1	3	1.01	15945.9185	3.5	9.676958182
BURLINGTON	Maple	1	3	1.01	16369.18474	4	9.703155867
BURLINGTON	Maple	1	4	0.81	52447.92705	0.5	10.86757609
BURLINGTON	Maple	1	5	0.8	3629.37957	0.5	8.196816995
BURLINGTON	Maple	1	5	0.8	21231.80612	1	9.963255625
BURLINGTON	Maple	1	5	0.8	46897.65542	1.5	10.75572296
BURLINGTON	Maple	1	5	0.8	83750.9508	2	11.3356028
BURLINGTON	Maple	1	5	0.8	101742.4576	2.5	11.53019997
BURLINGTON	Maple	1	5	0.8	112975.3942	3	11.63492532
BURLINGTON	Maple	1	5	0.8	124383.9657	3.5	11.73112856
BURLINGTON	Alder	1	1	1.71	143609.2929	0.5	11.87485165
BURLINGTON	Alder	1	1	1.71	148696.0233	1	11.90965939
BURLINGTON	Alder	1	1	1.71	152928.3142	1.5	11.93772456
BURLINGTON	Alder	1	1	1.71	156214.6287	2	11.95898617
BURLINGTON	Alder	1	1	1.71	159470.4045	2.5	11.97961363

Location	Species	Tree	Root	Diameter (in.)	Work	Displacement (in.)	Log Transformed Work
BURLINGTON	Alder	1	1	1.71	163668.8299	3	12.00560034
BURLINGTON	Alder	1	1	1.71	165931.5249	3.5	12.01933048
BURLINGTON	Alder	1	1	1.71	168162.3596	4	12.03268522
BURLINGTON	Alder	1	2	1.62	50952.68637	0.5	10.83865276
BURLINGTON	Alder	1	2	1.62	92258.22114	1	11.43234668
BURLINGTON	Alder	1	2	1.62	98560.81105	1.5	11.49842901
BURLINGTON	Alder	1	2	1.62	101564.7552	2	11.52845186
BURLINGTON	Alder	1	2	1.62	103862.1439	2.5	11.55081976
BURLINGTON	Alder	1	2	1.62	106079.9383	3	11.57194822
BURLINGTON	Alder	1	2	1.62	109017.7142	3.5	11.59926566
BURLINGTON	Alder	1	2	1.62	112175.0216	4	11.62781562
BURLINGTON	Alder	1	3	1.78	8392.554204	0.5	9.035100187
BURLINGTON	Alder	1	3	1.78	21294.4719	1	9.966202783
BURLINGTON	Alder	1	3	1.78	28784.27139	1.5	10.26758438
BURLINGTON	Cottonwood	1	1	1.71	12692.47685	0.5	9.448764723
BURLINGTON	Cottonwood	1	1	1.71	79767.36609	1	11.28686975
BURLINGTON	Cottonwood	1	1	1.71	135954.6271	1.5	11.82007648
BURLINGTON	Cottonwood	1	1	1.71	158483.5433	2	11.97340604
BURLINGTON	Cottonwood	1	1	1.71	158483.5433	2.5	11.97340604
BURLINGTON	Cottonwood	1	1	1.71	158483.5433	3	11.97340604
BURLINGTON	Cottonwood	1	1	1.71	161879.0351	3.5	11.99460464
BURLINGTON	Cottonwood	1	1	1.71	166458.6707	4	12.02250233
BURLINGTON	Cottonwood	1	2	1.24	64920.16899	0.5	11.08091362
BURLINGTON	Cottonwood	1	2	1.24	71590.04115	1	11.17871125
BURLINGTON	Cottonwood	1	2	1.24	79142.41849	1.5	11.27900427
BURLINGTON	Cottonwood	1	3	1.85	8492.667427	0.5	9.046958415
BURLINGTON	Cottonwood	1	3	1.85	39264.07293	1	10.5780652
BURLINGTON	Cottonwood	1	3	1.85	73973.87889	1.5	11.21146732
BURLINGTON	Cottonwood	1	3	1.85	95734.08149	2	11.46932964
BURLINGTON	Cottonwood	1	3	1.85	117176.6926	2.5	11.67143827
BURLINGTON	Cottonwood	1	3	1.85	141249.403	3	11.85828242
BURLINGTON	Cottonwood	1	3	1.85	173124.9836	3.5	12.06176906
BURLINGTON	Cottonwood	1	3	1.85	207223.3757	4	12.2415526
BURLINGTON	Cottonwood	1	4	1.77	6194.243579	0.5	8.731375685
BURLINGTON	Cottonwood	1	4	1.77	39481.50298	1	10.58358756
BURLINGTON	Cottonwood	1	4	1.77	131499.0185	1.5	11.78675467
BURLINGTON	Cottonwood	1	4	1.77	136527.4563	2	11.82428102
BURLINGTON	Cottonwood	1	4	1.77	160973.3904	2.5	11.98899435
BURLINGTON	Cottonwood	1	4	1.77	224049.7035	3	12.3196232
BURLINGTON	Cottonwood	1	4	1.77	258166.8307	3.5	12.46136129

Location	Species	Tree	Root	Diameter (in.)	Work	Displacement (in.)	Log Transformed Work
BURLINGTON	Cottonwood	1	4	1.77	274675.9414	4	12.52334729
BURLINGTON	Cottonwood	1	5	1.48	5977.136842	0.5	8.695696943
BURLINGTON	Cottonwood	1	5	1.48	17712.04344	1	9.782000108
BURLINGTON	Cottonwood	1	5	1.48	25153.40571	1.5	10.13274858
BURLINGTON	Cottonwood	1	5	1.48	26182.44206	2	10.17284431
BURLINGTON	Cottonwood	1	5	1.48	27457.808	2.5	10.22040585
BURLINGTON	Cottonwood	1	5	1.48	28756.52045	3	10.26661982
BURLINGTON	Cottonwood	1	5	1.48	30389.12612	3.5	10.32184013
BURLINGTON	Cottonwood	1	5	1.48	32142.96238	4	10.37794881
BURLINGTON	Cedar	1	1	0.74	17208.99575	0.5	9.753187535
BURLINGTON	Cedar	1	1	0.74	21985.17092	1	9.998123456
BURLINGTON	Cedar	1	1	0.74	31472.86172	1.5	10.35688092
BURLINGTON	Cedar	1	1	0.74	45531.66575	2	10.72616331
BURLINGTON	Cedar	2	1	1.37	269261.8464	0.5	12.50343959
BURLINGTON	Cedar	2	1	1.37	294143.8177	1	12.5918241
BURLINGTON	Cedar	2	1	1.37	195902.2175	1.5	12.18537092
BURLINGTON	Cedar	2	1	1.37	340517.1889	2	12.73822088
BURLINGTON	Cedar	2	2	1.3	67052.56938	0.5	11.11323221
BURLINGTON	Cedar	2	2	1.3	118860.1433	1	11.68570281
BURLINGTON	Cedar	2	2	1.3	156682.6567	1.5	11.96197774
BURLINGTON	Cedar	2	2	1.3	181629.0379	2	12.10972163
BURLINGTON	Cedar	2	2	1.3	202474.8352	2.5	12.21837089
BURLINGTON	Cedar	2	2	1.3	218190.238	3	12.29312261
PORTLAND	Cottonwood	1	1	1.1	26098.03782	0.5	10.16961541
PORTLAND	Cottonwood	1	1	1.1	33475.63392	1	10.41857311
PORTLAND	Cottonwood	1	1	1.1	40566.03552	1.5	10.61068643
PORTLAND	Cottonwood	1	1	1.1	47900.2738	2	10.7768765
PORTLAND	Cottonwood	1	1	1.1	51997.94504	2.5	10.85895948
PORTLAND	Cottonwood	1	1	1.1	53247.85726	3	10.88271284
PORTLAND	Cottonwood	1	2	1.08	11721.25377	0.5	9.369159034
PORTLAND	Cottonwood	1	2	1.08	19832.34516	1	9.895069478
PORTLAND	Cottonwood	1	3	1.74	127655.5667	0.5	11.75709103
PORTLAND	Cottonwood	1	3	1.74	134755.9655	1	11.81122076
PORTLAND	Cottonwood	1	3	1.74	134755.9655	1.5	11.81122076
PORTLAND	Cottonwood	1	3	1.74	135210.7007	2	11.81458959
PORTLAND	Cottonwood	1	3	1.74	135632.3504	2.5	11.8177032
PORTLAND	Cottonwood	1	3	1.74	136014.8567	3	11.8205194
PORTLAND	Cottonwood	1	3	1.74	136333.2933	3.5	11.82285785
PORTLAND	Cottonwood	1	3	1.74	136575.2383	4	11.82463094
PORTLAND	Cottonwood	1	4	1.07	11173.19482	0.5	9.321272869

Location	Species	Tree	Root	Diameter (in.)	Work	Displacement (in.)	Log Transformed Work
PORLAND	Cottonwood	1	5	1.99	76679.14814	0.5	11.24738509
PORLAND	Cottonwood	1	5	1.99	103511.2655	1	11.54743573
PORLAND	Cottonwood	1	5	1.99	104249.1567	1.5	11.55453905
PORLAND	Cottonwood	1	5	1.99	109956.2175	2	11.60783754
PORLAND	Cottonwood	1	5	1.99	114901.7656	2.5	11.65183283
PORLAND	Cottonwood	1	5	1.99	120670.2557	3	11.70081695
PORLAND	Cottonwood	1	5	1.99	127086.4046	3.5	11.75262249
PORLAND	Cottonwood	1	5	1.99	132344.011	4	11.79315996
PORLAND	Cottonwood	1	6	1.84	7946.661804	0.5	8.980507221
PORLAND	Cottonwood	1	6	1.84	39560.56406	1	10.58558804
PORLAND	Cottonwood	1	6	1.84	58430.72185	1.5	10.97559709
PORLAND	Cottonwood	1	6	1.84	120129.7719	2	11.69632787
PORLAND	Cottonwood	1	6	1.84	134516.2184	2.5	11.80944005
PORLAND	Cottonwood	1	6	1.84	146082.1634	3	11.89192451
PORLAND	Cottonwood	1	6	1.84	146082.1634	3.5	11.89192451
PORLAND	Cottonwood	1	6	1.84	146082.1634	4	11.89192451
PORLAND	Oregon Ash	1	1	1.27	76647.85497	0.5	11.2469769
PORLAND	Oregon Ash	2	2	1.09	22990.35877	0.5	10.04283022
PORLAND	Oregon Ash	2	2	1.09	27615.9245	1	10.22614786
PORLAND	Oregon Ash	2	2	1.09	32543.1572	1.5	10.3903224
PORLAND	Oregon Ash	2	2	1.09	39790.72806	2	10.5913892
PORLAND	Oregon Ash	2	2	1.09	51167.70577	2.5	10.84286387
PORLAND	Oregon Ash	2	2	1.09	65336.104	3	11.08730006
PORLAND	Oregon Ash	2	2	1.09	87964.60591	3.5	11.38468981
PORLAND	Oregon Ash	2	3	1.5	49309.71772	0.5	10.80587645
PORLAND	Oregon Ash	2	3	1.5	129863.5937	1	11.7742399
PORLAND	Oregon Ash	2	3	1.5	281970.3499	1.5	12.5495572
PORLAND	Oregon Ash	2	3	1.5	355606.3452	2	12.78157963
PORLAND	Oregon Ash	2	3	1.5	432753.6744	2.5	12.97792396
PORLAND	Oregon Ash	2	4	0.72	25007.83598	0.5	10.12694449
PORLAND	Oregon Ash	2	5	1.17	125796.881	0.5	11.74242383
PORLAND	Oregon Ash	2	5	1.17	229264.6866	1	12.34263245

Log transformation was found to marginally improve normality of the work calculations, but not the diameter measurements. The log transformed work calculations were used in the ANCOVA model that initially included work as the dependent variable; displacement increment, location, and tree species nested within location as the main factors; diameter as the covariate; and all possible interaction terms. None of the interaction terms was significant so they were dropped from the model. In

the final ANCOVA model, location, displacement increment, and diameter were all significant, while species was not. This indicates that the amount of work is directly related to the displacement increment and differs among locations, but not tree species. The amount of work is also significantly related to the root diameter. Results are shown in Table 58.

Table 59. Analysis of covariance for root pullout data collected in Albuquerque, NM, Burlington, WA, and Portland, OR.

08:04 Friday, September 10, 2010 51																																			
The GLM Procedure																																			
Class Level Information																																			
<table style="width: 100%; border-collapse: collapse;"> <thead> <tr> <th style="text-align: left; width: 15%;">Class</th><th style="text-align: left; width: 15%;">Levels</th><th style="text-align: left; width: 70%;">Values</th><th style="text-align: right; width: 10%;"></th></tr> </thead> <tbody> <tr> <td>SPECIES</td><td>5</td><td>ALDER CEDAR CW MAPLE OA</td><td></td></tr> <tr> <td>LOCATION</td><td>4</td><td>ALBUQUERQUE1 ALBUQUERQUE2 BURLINGTON PORTLAND</td><td></td></tr> <tr> <td>DISPLACEMENT</td><td>8</td><td>0.5 1 1.5 2 2.5 3 3.5 4</td><td></td></tr> </tbody> </table>						Class	Levels	Values		SPECIES	5	ALDER CEDAR CW MAPLE OA		LOCATION	4	ALBUQUERQUE1 ALBUQUERQUE2 BURLINGTON PORTLAND		DISPLACEMENT	8	0.5 1 1.5 2 2.5 3 3.5 4															
Class	Levels	Values																																	
SPECIES	5	ALDER CEDAR CW MAPLE OA																																	
LOCATION	4	ALBUQUERQUE1 ALBUQUERQUE2 BURLINGTON PORTLAND																																	
DISPLACEMENT	8	0.5 1 1.5 2 2.5 3 3.5 4																																	
<table style="width: 100%; border-collapse: collapse;"> <tr> <td style="width: 60%;">Number of Observations Read</td><td style="width: 40%; text-align: right;">270</td></tr> <tr> <td>Number of Observations Used</td><td style="text-align: right;">268</td></tr> </table>						Number of Observations Read	270	Number of Observations Used	268																										
Number of Observations Read	270																																		
Number of Observations Used	268																																		
08:04 Friday, September 10, 2010 52																																			
The GLM Procedure																																			
Dependent Variable: LNWORK																																			
<table style="width: 100%; border-collapse: collapse;"> <thead> <tr> <th style="text-align: left; width: 15%;">Source</th><th style="text-align: left; width: 15%;">DF</th><th style="text-align: left; width: 30%;">Sum of Squares</th><th style="text-align: left; width: 15%;">Mean Square</th><th style="text-align: left; width: 15%;">F Value</th><th style="text-align: left; width: 15%;">Pr > F</th></tr> </thead> <tbody> <tr> <td>Model</td><td>15</td><td>162.7322626</td><td>10.8488175</td><td>6.04</td><td><.0001</td></tr> <tr> <td>Error</td><td>252</td><td>452.7212813</td><td>1.7965130</td><td></td><td></td></tr> <tr> <td>Corrected Total</td><td>267</td><td>615.4535439</td><td></td><td></td><td></td></tr> </tbody> </table>						Source	DF	Sum of Squares	Mean Square	F Value	Pr > F	Model	15	162.7322626	10.8488175	6.04	<.0001	Error	252	452.7212813	1.7965130			Corrected Total	267	615.4535439									
Source	DF	Sum of Squares	Mean Square	F Value	Pr > F																														
Model	15	162.7322626	10.8488175	6.04	<.0001																														
Error	252	452.7212813	1.7965130																																
Corrected Total	267	615.4535439																																	
<table style="width: 100%; border-collapse: collapse;"> <thead> <tr> <th style="text-align: left; width: 15%;">Source</th><th style="text-align: left; width: 15%;">DF</th><th style="text-align: left; width: 30%;">Type I SS</th><th style="text-align: left; width: 15%;">Mean Square</th><th style="text-align: left; width: 15%;">F Value</th><th style="text-align: left; width: 15%;">Pr > F</th></tr> </thead> <tbody> <tr> <td>LOCATION</td><td>3</td><td>32.9920709</td><td>10.9973570</td><td>6.12</td><td>0.0005</td></tr> <tr> <td>SPECIES(LOCATION)</td><td>4</td><td>11.4418776</td><td>2.8604694</td><td>1.59</td><td>0.1769</td></tr> <tr> <td>DISPLACEMENT</td><td>7</td><td>103.0557679</td><td>14.7222526</td><td>8.19</td><td><.0001</td></tr> <tr> <td>DIAMETER</td><td>1</td><td>15.2425462</td><td>15.2425462</td><td>8.48</td><td>0.0039</td></tr> </tbody> </table>						Source	DF	Type I SS	Mean Square	F Value	Pr > F	LOCATION	3	32.9920709	10.9973570	6.12	0.0005	SPECIES(LOCATION)	4	11.4418776	2.8604694	1.59	0.1769	DISPLACEMENT	7	103.0557679	14.7222526	8.19	<.0001	DIAMETER	1	15.2425462	15.2425462	8.48	0.0039
Source	DF	Type I SS	Mean Square	F Value	Pr > F																														
LOCATION	3	32.9920709	10.9973570	6.12	0.0005																														
SPECIES(LOCATION)	4	11.4418776	2.8604694	1.59	0.1769																														
DISPLACEMENT	7	103.0557679	14.7222526	8.19	<.0001																														
DIAMETER	1	15.2425462	15.2425462	8.48	0.0039																														
<table style="width: 100%; border-collapse: collapse;"> <thead> <tr> <th style="text-align: left; width: 15%;">Source</th><th style="text-align: left; width: 15%;">DF</th><th style="text-align: left; width: 30%;">Type III SS</th><th style="text-align: left; width: 15%;">Mean Square</th><th style="text-align: left; width: 15%;">F Value</th><th style="text-align: left; width: 15%;">Pr > F</th></tr> </thead> <tbody> <tr> <td>LOCATION</td><td>3</td><td>51.72477392</td><td>17.24159131</td><td>9.60</td><td><.0001 Signif.</td></tr> <tr> <td>SPECIES(LOCATION)</td><td>4</td><td>15.94677667</td><td>3.98669417</td><td>2.22</td><td>0.0674 Not Sig.</td></tr> <tr> <td>DISPLACEMENT</td><td>7</td><td>83.48708509</td><td>11.92672644</td><td>6.64</td><td><.0001 Signif.</td></tr> <tr> <td>DIAMETER</td><td>1</td><td>15.24254621</td><td>15.24254621</td><td>8.48</td><td>0.0039 Signif.</td></tr> </tbody> </table>						Source	DF	Type III SS	Mean Square	F Value	Pr > F	LOCATION	3	51.72477392	17.24159131	9.60	<.0001 Signif.	SPECIES(LOCATION)	4	15.94677667	3.98669417	2.22	0.0674 Not Sig.	DISPLACEMENT	7	83.48708509	11.92672644	6.64	<.0001 Signif.	DIAMETER	1	15.24254621	15.24254621	8.48	0.0039 Signif.
Source	DF	Type III SS	Mean Square	F Value	Pr > F																														
LOCATION	3	51.72477392	17.24159131	9.60	<.0001 Signif.																														
SPECIES(LOCATION)	4	15.94677667	3.98669417	2.22	0.0674 Not Sig.																														
DISPLACEMENT	7	83.48708509	11.92672644	6.64	<.0001 Signif.																														
DIAMETER	1	15.24254621	15.24254621	8.48	0.0039 Signif.																														

References

- Abernethy, B., and I. D. Rutherford. 2001. The distribution of riparian tree root in relation to riverbank reinforcement. *Hydrological Processes* 15:63-79.
- al Hagery, S. A. 2007. Geophysical imaging of root-zone, trunk, and moisture heterogeneity. *Journal of Experimental Botany* 58(4):839-854.
- al Hagrey, S. A., and R. Meissner. 2004. Botanical problems, studied by applied geophysics. *Deutsche Geophysikalische Gesellschaft e. 14384(2):2-9.*
- Alby, E., E. Smigiel, P. Assali, P. Grussenmeyer, and I. Kauffman-Smigiel. 2009. Low cost solutions for dense point clouds of small objects: Photomodeler scanner vs. David laserscanner. *22nd CIPA Symposium. October 11-15, 2009.*
- Allsop, W., A. Kortenhaus, M. Morris, F. Buijs, R. Hassan, M. Young, N. Doorn, J. van der Meer, P. Van Gelder, M. Dyer, M. Redaelli, M. Uilly, P. Visser, R. Bettess, D. Lesniewska, and W. ter Horst. 2007. *Failure mechanisms for flood defence structures*, FLOODsite Project Report To4_06_01 (<http://www.floodsite.net>) (accessed 6 June 2011).
- Amato, M., B. Basso, G. Celano, G. Bitella, G. Morelli, and R. Rossi. 2008. In situ detection of tree root distribution and biomass by multielectrode resistivity imaging. *Tree Physiology* 28:1441-1448.
- AMEC Earth and Environmental. 2008. *Geotechnical and hydrogeological investigation and analysis report, Albuquerque west levee project*. Albuquerque, NM.
- Amoozegar, A. 1989. A compact constant head permeameter for measuring saturated hydraulic conductivity of the vadose zone. *Soil Sci. Soc. Am. J.* 53: 1356-1361.
- Amoozegar, A., and G. V. Wilson. 1999. Methods for measuring hydraulic conductivity and drainable porosity. In: *Agricultural drainage*, ed. W. Skaggs and J. Van Schilfgaarde. Am. Soc. Agron. Special Monograph No. 38, Chpt. 37, pp. 1149-1206. (Book Chapter)
- Ayyub, B. 2003. *Risk analysis in engineering and economics*. Boca Raton, FL: Chapman Hall/CRC Publishers.
- Baker, D. L. 2003. Sensing breaches in earthen dams. *IEEE Instrumentation and Measurement Magazine* 6(2):13-18.
- Banks, D. C., and W. E. Strohm. 1965. *Methods of preventing flow slides*. Potamology Investigations Report 12-16. Vicksburg, MS: U.S. Army Engineer, Waterways Experiment Station.
- Barthelemy, D., and Y. Caraglio. 2007. Plant architecture: A dynamic, multilevel and comprehensive approach to plant form, structure and ontogeny. *Annals of Botany* 99:375-407.

- Barton, C. V. M., and K. D. Montagu. 2004. Detection of tree roots and determination of root diameters by ground penetrating radar under optimal conditions. *Tree Physiology* 24:1323-1331.
- Beeson, M. H., T. L. Tolan, and I. P. Madin. 1991. *Geologic map of the Portland quadrangle, Multnomah and Washington counties, Oregon, and Clark county, Washington*. Map GMS-75, 1:24,000 scale, Oregon Department of Geology and Mineral Industries.
- Berg, T. M., and C. M. Dodge. 1981. Atlas of preliminary geologic quadrangle maps of Pennsylvania. Commonwealth of Pennsylvania. Harrisburg, PA: Bureau of Topographic and Geologic Survey.
- Berg, T. M., W. D. Sevon, and R. Abel. 1984. Rock types of Pennsylvania. Map 63, 1:500,000 scale map. Commonwealth of Pennsylvania. Harrisburg, PA: Bureau of Topographic and Geologic Survey.
- Berry, K. L., and K. Lewis. 1997. *Historical documentation of middle Rio Grande flood protection projects, Corrales to San Marcial*, Contract DACW47-94-D-0019, Office of Archaeology. Albuquerque, NM: University of New Mexico.
- Bibalani, G. H., B. Majnonian, E. Adeli, and H. Sanni. 2007. Protection roles of forest and non-forest woody species on slopes in Iran. In Stokes et al. (eds.) *Eco- and ground bio-engineering: The use of vegetation to improve slope stability*, 73-79, Springer.
- Brizendine, A. 1997a. *Probabilistic analysis of hydraulic conductivity in woody vegetation*. Vicksburg, MS: U.S. Army Engineer Waterways Experiment Station.
- Brizendine, A.L. 1997b. *Risk based analysis of levees*. PhD. Dissertation submitted to the College of Engineering and Mineral Resources, West Virginia University, Morgantown, WV.
- Brown, C. B., and M. S. Sheu. 1975. Effects of deforestation on slopes. *Journal of Geotechnical Engineering Division* 101(GT2 Feb.):147-165.
- Butnor, J. R., J. A. Doolittle, K. H. Johnsen, L. Samuelson, T. Stokes, and L. Kress. 2003. Utility of ground-penetrating radar as a root biomass survey tool in forest systems. *Soil Science Society of America Journal* 67:1607-1615.
- Butnor, J. R., J. A. Doolittle, L. Kress, S. Cohen, and K. H. Johnsen. 2001. Use of ground-penetrating radar to study tree roots in the southeastern United States. *Tree Physiology* 21:1269-1278.
- Cermak, J., J. Neruda, N. Nadezdina, R. Ulrich, M. Martinkova, R. Gebauer, E. Pokorny, V. Nadezdin, J. Hruska, J. Gasparek, and I. Culek. 2006b. Identification of tree root system damage caused by heavy machinery using new measurement technology suitable for precision forestry. *Proceedings of the International Precision Forestry Symposium*, 291-304. South Africa: Stellenbosch University.
- Cermak, J., R. Ulrich, Z. Stanek, J. Koller, and L. Aubrecht. 2006a. Electrical measurement of tree root absorbing surfaces by the earth impedance method: 2. Verification based on allometric relationships and root severing experiments. *Tree Physiology* 26:1113-1121.

- Childress, S. C. 1973. Mississippi geologic names. Bulletin 118. Jackson, MS: Mississippi Geological, Economic and Topographical Survey.
- Chu-Agor, M. L., G. A. Fox, and G. V. Wilson. 2009. Empirical sediment transport function predicting seepage erosion undercutting for cohesive bank failure protection. *Journal of Hydrology* 377:155-164.
- Clark, P. U., A. R. Nelson, W. D. McCoy, B. B. Miller, and D. K. Barnes. 1989. Quaternary aminostratigraphy of Mississippi Valley loess. *Geological Society of America Bulletin* 101:918-926.
- Connell, S. 1997. *Geology of the Alameda quadrangle, Bernalillo and Sandoval Counties, New Mexico*, Map Series OF-GM-10, Scale 1:24,000, New Mexico Bureau of Mines and Mineral Resources.
- Connell, S. 2008. *Geologic map of the Albuquerque-Rio Rancho metropolitan area and vicinity, Bernalillo and Sandoval Counties, New Mexico*. Map Series GM-78, Scale 1:50,000, New Mexico Bureau of Mines and Mineral Resources.
- Corcoran, M. K., D. H. Gray, D. Biedenharn, C. D. Little, F. Pinkard, P. Bailey, and L. T. Lee. 2011. Literature review: Vegetation on levees. ERDC Technical Report (in review), Vicksburg, MS.
- Cornforth Consultants. 2008. *Summary report: Bridgeton levee tree stump removal (2007 and 2008)*. Portland, OR.
- Coutts, M. P. 1983. Root architecture and tree stability. *Plant and Soil* 71:171-188.
- Coutts, M. P. 2004. *Wind and trees*. Cambridge University Press.
- Crow, T. R., and G. G. Erdmann. 1983. Weight and volume equations and tables for red maple in the lake states. Research Paper NC-242, U.S. Department of Agriculture, Forest Service. St. Paul, MN: North Central Forest Experiment Station.
- Cunny, R. W. 1987. *Inspection and control of levee underseepage during flood fights*, Vicksburg, MS: U.S. Army Engineer Waterways Experiment Station.
- Danjon, F., and B. Reubens. 2008. Assessing and analyzing 3D architecture of woody root systems, a review of methods and applications in tree and soil stability, resource acquisition and allocation. *Plant and Soil* 303:1-34.
- Danjon, F., D. H. Barker, M. Drekhage, and A. Stokes. 2007a. Using three-dimensional plant root architecture in models of shallow-slope stability. *Annals of Botany* 1-13.
- Danjon, F., D. H. Barker, M. Drekhage, and A. Stokes. 2007b. Using three-dimensional plant root architecture in models of shallow-slope stability. *Annals of Botany* 101(8):1281-1293.
- Danjon, F., D. Bert, C. Godin, and H. Stokes. 1999. Structural root architecture of 5-year-old *Pinus pinaster* measured by 3D digitising and analysed with AMAPmod. *Plant and Soil* 217:49-63.

- Danjon, F., H. Sinoquet, C. Godin, F. Colin, and M. Drexhage. 1999. Characterisation of structural tree root architecture using 3D digitizing and AMPmod software. *Plant and Soil*. Kluwer Academic, Vol. 211, pp. 241-258.
- Danjon, F., T. Fourcaud, and D. Bert. 2005. Root architecture and wind-firmness of mature *Pinus pinaster*. *New Phytologist* 168:387-400.
- Dethier, D. P., and J. T. Whetten. 1981. Preliminary geologic map of the Mount Vernon 7-1/2 min quadrangle, Skagit County, Washington. U.S. Geologic Survey.
- Di Iorio, A., B. Lasserre, G. S. Scippa, and D. Chiatante. 2005. Root system architecture of *Quercus pubescens* trees growing on different sloping conditions. *Annals of Botany* 95:351-361.
- Dickenson, S. E., B. J. Wavra, and J. Sunitsakul. 2000. *Seismic performance of the Columbia River levee adjacent to the Portland International Airport (PDX), Portland, OR*. Geotechnical Group, Department of Civil, Construction, and Environmental Engineering, Oregon State University.
- Doolittle, J. A., F. E. Minzenmayer, S. W. Waltman, E. C. Benham, J. W. Tuttle, and S. D. Peaslee. 2007. Ground-penetrating radar soil suitability map of the conterminous United States. *Geoderma* 141:416-421.
- Dunbar, J. B., and L. D. Britsch. 2008. Geology of the New Orleans area and the canal levee failures. *Journal of Geotechnical and Geoenvironmental Engineering* 134(5):566-582.
- Dunbar, J. B., M. Blaes, S. Dueitt, and J. May. 1995. *Geological investigation of the Mississippi River deltaic plain, Report 3 of a Series*. Technical Report GL-84-15, Vicksburg, MS: U.S. Army Engineer Waterways Experiment Station.
- Dunbar, J. B., M. Blaes, S. Dueitt, and K. Stroud. 1994. *Geological investigation of the Mississippi River deltaic plain, Report 2 of a Series*. Technical Report GL-84-15, Vicksburg, MS: U.S. Army Engineer Waterways Experiment Station.
- Dupuy, L., T. Foucaud, and A. Stokes. 2005. A numerical investigation into the influence of soil type and root architecture on tree anchorage. *Plant and Soil* 278:119-134.
- Dupuy, L. X., T. Fourcaud, P. Lac and A. Stokes. 2007. A generic 3D finite element model of tree anchorage integrating soil mechanics and real root system architecture. *American Journal of Botany* 94(9):1506-1514.
- Endo, T, and T. Tsuruta. 1969. The effects of tree root upon the shearing strength of soil. Annual Report of the Hokkaido Branch, Tokyo Forest Experiment Station, 18:168-179.
- Fatahi, B., H. Khabbaz, and B. Indraratna. 2009. Parametric studies on bioengineering effects of tree root-based suction on ground behavior. *Ecological Engineering* 35:1415-1426.
- Fauchard, C., and P. Meriaux. 2007. Geophysical and geotechnical methods for diagnosing flood protection dikes. French Ministry for Infrastructure, Transportation, Spatial Planning, Tourism and the Sea.

- Federal Emergency Management Agency (FEMA). 2005. Technical manual for dam owners: Impacts of plants on earthen dams.
- Fisk, H. N. 1944. *Geological investigation of the alluvial valley of the Lower Mississippi River*. Vicksburg, MS: Mississippi River Commission.
- Fourcaud, T., J. N. Ji, Z. Q. Zhang, and A. Stokes. 2008. Understanding the impact of root morphology on overturning mechanisms: A modeling approach. *Annals of Botany* 101:1267-1280.
- Fourcaud, T., X. Zhang, A. Stokes, H. Lambers, and C. Körner. 2008. Plant growth modeling and applications: The increasing importance of architecture in growth models. *Annals of Botany* 101:1053-1063.
- Francis, John K. 1979. Yellow-poplar rooting habits. Report No. 7, SKN/SO-246. Southern Forest Experiment Station, New Orleans, LA. pg. 29.
- Freeze, R. A., and J. A. Cherry. 1979. *Groundwater*. Englewood Cliffs, NJ: Prentice-Hall, Inc.
- Gabr, M. A., M. Akram, and H. M. Taylor. 1995. Effect of simulated roots on the permeability of silty soil. *ASTM Geotechnical Testing Journal (GTJ)* 18(1):112-115.
- Gartner, H., and C. Denier. 2006. Application of a 3D laser scaling device to acquire the structure of whole root systems – A pilot study. In Heinrich I., et al. (eds.), *TRACE – Tree Rings in Archaeology, Climatology and Ecology* 4: 288-294.
- Ghani, M. A., A. Stokes, and T. Foucaud. 2008. The effect of root architecture and root loss through trenching on the anchorage of tropical urban trees (*Eugenia grandis* Wight). *Trees* 23(2):197-209.
- Gharibi, M., and L. R. Bentley. 2005. Resolution of 3-D electrical resistivity images from inversions of 2-D orthogonal lines. *Journal of Environmental and Engineering Geophysics* 10(4):339-349.
- Gibson, M. D., C. W. McMillin, and E. Shoulders. 1986. Moisture content and specific gravity of the four major southern pines under the same age and site conditions. *Wood and Fiber Science* 18(3):428-435.
- Godin, C., and Y. Caraglio. 1998. A multiscale model of plant topological structures. *Journal of Theoretical Biology* 191:1-46.
- Golder Associates Inc. 2009. *Final Report: Geotechnical investigation and levee analysis. City of Burlington and Dike District 12 levee certification project*. Burlington, WA. Prepared for: Pacific International Engineering. Edmonds, WA.
- Grassel, K. 2002. *Taking out the jacks, issues of jetty jack removal in Bosque and river restoration planning*. Water Resources Program, Publication No. WRP-6, Albuquerque, NM: University of New Mexico.
- Gray, D. H. 1978. Role of woody vegetation in reinforcing soils and stabilising slopes. *Symposium on Soil Reinforcing and Stabilising Techniques, Sydney, Australia*, 253-306.

- Gray, D. H., and A. T. Leiser. 1982. *Biotechnical slope protection and erosion control*. New York: Van Nostrand Reinhold Company.
- Gray, D. H., A. MacDonald, T. Thomann, I. Blatz, and F. D. Shields, Jr. 1991. *The effects of vegetation on the structural integrity of sandy levees*. Technical Report REMR-EI-5:117. Department of the Army. Vicksburg, MS: Waterways Experiment Station, Corps of Engineers.
- Gray, D. H., and H. Ohashi. 1983. Mechanics of Fiber Reinforcement in Sand. *Journal of Geotechnical Engineering* 109(3):335-353.
- Greenway, D. R. 1987. Vegetation and slope stability. In: *Slope stability*, ed. M. G. Anderson, and K. S. Richards, 187-230. Chichester: John Wiley & Sons Ltd.
- Greenwood, J. R., J. E. Norris, and J. Wint. 2004. Assessing the contribution of vegetation to slope stability. *Proceedings of the Institution of Civil Engineers, Geotechnical Engineering* 157, October 2004 Issue GE4, 199-207.
- Griffin, J. R. 1973. Xylem sap tension in three woodland oaks of central California. *Ecology* 54(1):152-159.
- Griffin, J. R. 1977. Oak woodland. In: *Terrestrial vegetation of California*, ed. Michael G. Barbour and Jack Malor, 383-415. New York: John Wiley and Sons.
- Guardo, M., and K. P. Rohrer. 2000. Calibration of a steady-state seepage model from transient recovery of field data. *Journal of the American Water Resources Association* 36(1):87-94.
- Gurwin, J., and M. Lubczynski. 2005. *Modeling of complex multi-aquifer systems for groundwater resources evaluation - Swidnica study case (Poland)* 4(4):1431-2174.
- Hall, J. W., R. J. Dawson, P. B. Sayers, C. Rosu, J. B. Chatterton, and R. Deakin. 2003. *Proceedings of the Institution of Water & Maritime Engineering*, 156(WM3): 235-247.
- Harris, S. C. 1989. *Proceedings of the 16th Annual Conference sponsored by the Water Resources Planning and Management Division*. 842.
- Hawley, J. W., R. M. Chamberlin, and S. D. Connell. 1996. *Geology of the Albuquerque east quadrangle, Bernalillo County, New Mexico*, Map Series OF-GM-3, Scale 1:24,000, New Mexico Bureau of Mines and Mineral Resources.
- Hazen, A. 1911. Discussion: Dams on sand foundations, *Transactions, American Society of Civil Engineers* 73:199.
- Holley, E. J., and D. S. Harwood. 1985a. *Geologic map of the late Cenozoic deposits of the Sacramento valley and Northern Sierran Foothills, California*. Miscellaneous Field Studies. Map MF-1790, Sheet 1 of 5, Scale: 1:62500. Reston, VA: U.S. Geological Survey.

- Holley, E. J., and D. S. Harwood. 1985b. *Description and legend to the geologic map of the late Cenozoic deposits of the Sacramento valley and Northern Sierran Foot-hills, California*. Miscellaneous Field Studies. Map MF-1790, Scale: 1:62500. Reston, VA: U.S. Geological Survey.
- Henderson, R., E. D. Ford, and E. Renshaw. 1983. Morphology of the structural root system of Sitka spruce: 1. Analysis and quantitative description. *Forestry* 56:121-135.
- Hirano, Y., M. Dannoura, K. Aono, T. Igarashi, M. Ishii, K. Yamase., N. Makita, and Y. Kanazawa. 2008. Limiting factors in the detection of tree roots using ground-penetrating radar. *Plant and Soil* 319(1-2):15-24.
- Horton, J. S. 1949. *Trees and shrubs for erosion control of southern California mountains*. Berkeley, CA: U.S. Department of Agriculture, Forest Service, California [Pacific Southwest] Forest and Range Experiment Station; California Department of Natural Resources, Division of Forestry. 72.
- Hoskins, D. M. 1976a. Danville geologic quadrangle. Map 160, 1:24,000 scale map. Atlas of Preliminary Geologic Quadrangle Maps of Pennsylvania. Harrisburg, PA: Pennsylvania Geological Survey.
- Hoskins, D. M. 1976b. Riverside geologic quadrangle. Map 483, 1:24,000 scale map. Atlas of Preliminary Geologic Quadrangle Maps of Pennsylvania. Harrisburg, PA: Pennsylvania Geological Survey.
- Hruska, J., J. Cermak, and S. Sustek. 1999. Mapping tree root systems with ground-penetrating radar. *Tree Physiology* 19:125-130.
- Hsi, G., and J. H. Nath. 1970. Wind drag within a simulated forest. *Journal of Applied Meteorology* 9:592-602.
- Interagency Performance Evaluation Team (IPET). 2006. Performance evaluation of the New Orleans and southeast Louisiana hurricane protection system, Volume V—The Performance—levees and floodwalls. Washington, DC: U.S. Army Corps of Engineers.
- Indraranta, B., B. Fatahi, and H. Khabbaz. 2006. Numerical analysis of matric suction effects of tree roots. *Proceedings of the Institution of Civil Engineers, Geotechnical Engineering* 159, April 2006, 77-90.
- Isphording, W. C., and G. M. Lamb. 1971. Age and origin of the Citronelle Formation in Alabama. *Geological Society of America Bulletin* 82:775-780.
- Jabro, J. D., and R. G. Evans. 2006. Discrepancies between analytical solutions of two borehole permeameters for estimating field-saturated hydraulic conductivity. *Applied Engineering in Agriculture* 22(4):549-554.
- JESCO Environmental and Geotechnical Services, Inc. 2008. *Documentation and analysis of tree root extent and soil behavior along and in levees and floodwalls in the New Orleans District*. Final Report Jennings, LA.
- Jones, N. L. 1999. *SEEP2D Primer*. Groundwater Modeling System, Environmental Modeling Research Laboratory. Provo, UT: Brigham Young University.

- Kaestner, A., M. Schneebeli, and F. Graf. 2006. Visualizing three-dimensional root networks using computed tomography. *Geoderma* 136:459-469.
- Keller, G. V., and F. C. Frischknecht. 1966. *Electrical methods in geophysical prospecting*. Oxford: Pergamon Press.
- Kelly, J. R., and Noah Vroman. 2009. *The Spring 2008 Midwest Flood, Observations of Missouri and Iowa Levee Breaches, 21-23 July 2008*. Technical Report GSL SR-09-01. U.S. Army Engineer Research and Development Center, Vicksburg, MS.
- Kolb, C. R., and C. O. Durham. 1967. Field trip guidebook, Lower Mississippi Alluvial Valley and Terraces. *Geological Society of America 1967 Annual Meeting*. New Orleans, Louisiana.
- Kolb, C. R., and R. T. Saucier. 1982. *Engineering geology of New Orleans*, Geological Society of America, Review in *Engineering Geology*, Volume V, 75-93
- Kolb, C. R., and J. R. VanLopik. 1958a. *Geology of the Mississippi River deltaic plain*. Technical Report No. 3-483, Vol 1 and 2. Vicksburg, MS: U.S. Army Engineer Waterways Experiment Station.
- Kolb, C. R., and J. R. VanLopik. 1958b. *Geological investigation of the Mississippi River-Gulf Outlet Channel*. Miscellaneous Paper No. 3-259. Vicksburg, MS: U.S. Army Engineer Waterways Experiment Station.
- Kolb, C. R., and J. R. VanLopik. 1965. Depositional environments of the Mississippi River deltaic plain – southeastern Louisiana. In *Deltas in their geologic framework*, edited by M. L. Shirley and J. A. Ragsdale. Houston Geological Society, 17-61.
- Krinitzsky, E. L. 1965. *Geological influences on bank erosion along meanders of the lower Mississippi River*. Potamology Investigations Report 12-15. Vicksburg, MS: U.S. Army Corps of Engineers Waterways Experiment Station.
- Krinitzsky, E. L., and W. J. Turnbull. 1967. *Loess deposits of Mississippi*. Special Paper 94. New York: Geological Society of America.
- Lagasse, P. F. 1980. An assessment of the response of the Rio Grande to Dam Construction – Cochitti to Isleta Reach, a technical report for the U.S. Army Corps of Engineers, Albuquerque District, Albuquerque, NM.
- Landau Associates. 2003. *Report of geotechnical engineering services, proposed Home Depot Store, George Hopper Road and Burlington Blvd.*, one volume.
- Lewis, D. C., and R. H. Burgy. 1964. The relationship between oak tree roots and groundwater in fractured rock as determined by tritium tracing. *Journal of Geophysical Research* 69(12):2579-2587.
- Lindgren, O., and G. Orlander. 1978. A study on root development and stability of 6- to 7-year-old container plants. 142-144 in *Van Eerden and Kinghorn*.
- Locke, M. H. 2000. Electrical imaging surveys for environmental and engineering studies. Lecture notes. <http://www.geoelectrical.com/> (accessed July 2010).

- Mabey, M. A., T. L. Youd, and C. F. Jones. 1993a. *Liquefaction susceptibility map, Portland Quadrangle, Multnomah and Washington Counties, Oregon and Clark County Washington, Plate 1*, Map GMS-79, 1:24,000 scale, Oregon Department of Geology and Mineral Industries.
- Mabey, M. A., and I. P. Maudin. 1993b. *Ground motion amplification map, Portland Quadrangle, Multnomah and Washington Counties, Oregon and Clark County Washington, Plate 2*, Map GMS-79, 1:24,000 scale, Oregon Department of Geology and Mineral Industries.
- Mabey, M. A., and I. P. Maudin. 1993c. *Lateral displacement and dynamic slope instability map, Portland Quadrangle, Multnomah and Washington Counties, Oregon and Clark County Washington, Plate 3*, Map GMS-79, 1:24,000 scale, Oregon Department of Geology and Mineral Industries.
- Mabey, M. A., I. P. Maudin, D. B. Meier, and S. P. Palmer. 1995. *Relative earthquake hazard map of the Mount Tabor Quadrangle, Multnomah County, Oregon and Clark County Washington*. Map GMS-89, 1:24,000 scale, Oregon Department of Geology and Mineral Industries.
- Mansur, C. I., R. I. Kaufman, and J. R. Schultz. 1956. *Investigation of underseepage and its control, Lower Mississippi River levees*. Technical Memorandum No. 3-424. Vicksburg, MS: U.S. Army Engineer Waterways Experiment Station.
- Marks, B. D., and B. A. Tschantz. 2002. *A technical manual on the effects of tree and wood vegetation root penetrations on the safety of earthen dams*. Funded by Federal Emergency Management Agency and Association of State Dam Officials. Report developed from ASDSO/FEMA Workshop on Plant and Animal Impacts on Earth Dams, held at University of Tennessee, Knoxville, TN, 1999.
- Massman, J. W., 2003. A design manual for sizing infiltration ponds, final research report for Washington Department of Transportation.
- Mellen, F. F., T. E. McCutcheon, and M. R. Livingston. 1941. Warren County mineral resources. Bulletin 43. University, MS: Mississippi State Geological Survey.
- Michigan State University. 1962. *A dictionary of agricultural and allied terminology*. John N. Winburne, editor-in-chief. East Lansing, MI: Michigan State University Press.
- Middle Rio Grande Conservancy District (MRGCD). 2010. <http://www.mrgcd.com/> (accessed 18 September 2010).
- Moore, W. H. 1976. Geologic map of Mississippi. University, MS: Mississippi Mineral Resources Institute.
- Morelli, G. F., T. Zenone, M. Teobaldelli, F. Fischanger, M. Matteucci, and G. Seufert. 2007. Use of Ground-Penetrating Radar (GPR) and Electrical Resistivity Tomography (ERT) to study tree roots volume in pine forest and poplar plantation. *Proceedings of the 5th International Workshop on Functional-Structural Plant Models*, ed. Prusinkiewicz, Hanan, and Lane, 21:1-4. New Zealand: Napier.
- Mualem, Y. 1976. A new model predicting the hydraulic conductivity of unsaturated porous media. *Water Resources Research* 12:513–522.

- Mulder, J. 2009. *Digital reproduction of the geologic map of the late Cenozoic deposits of the Sacramento valley and Northern Sierran Foothills, California.* Scale: 1:126,720. Sacramento, CA: Department of Water Resources, Northern District, Geological Investigations Unit.
- Mussetter Engineering, Inc. 2006. *Hydraulic analysis Rio Grande levees evaluation,* Albuquerque Reach, Rio Grande, New Mexico. Fort Collins, CO, 52 p.
- Myers, C., D. Polak, and L. Stortz. 1976. Full tree weight equations and tables for selected central hardwoods. In *Proceedings of the Central Hardwood Forest Conference, 17-19 October 1976, Carbondale, IL*, ed. J. S. Fralish, G. T. Weaver, and R. C. Schlessinger, 401-407. Carbondale, IL.
- Nadezhina, N., and J. Cermak. 2003. Instrumental methods for studies of structure and function of root systems of large trees. *Journal of Experimental Botany* 54(387):1511-1521.
- Norris, J. E. 2005. Root reinforcement by hawthorn and oak roots on a highway cut-slope in Southern England. *Plant and Soil* 278:43-53.
- Norris, J. E., and J. R. Greenwood. 2000. In situ shear and pull out testing to demonstrate the enhanced shear strength of root reinforced soil. *Proceedings of the 8th International Symposium on Landslides, Cardiff, 26-30 June 2000*, 1123-1128. Thoma Telford, London.
- Norris, J. E., and J. R. Greenwood. 2003. In situ shear box and root pullout apparatus for measuring the reinforcing effects of vegetation. In *Field Measurements in Geomechanics*, ed. F. Myrvoll, Oslo. Swets and Zeitlinger, Lisse, 593-597.
- Norris, J. E., J. R. Greenwood, A. Achim, B. A. Gardiner, B. C. Nicoll, E. Cammeraat, and S. B. Mickovski. 2008. Hazard assessment of vegetated slopes. *Slope stability and erosion control: Ecotechnological solutions*, ed. J. E. Norris, A. Stokes, S. B. Mickovski, E. Cammeraat, E. Van Beek, B. C. Nicoll, and A. Achim. Springer Dordrecht, The Netherlands.
- Norris, J. E., A. Stokes, S. B. Mickovski, E. Cammeraat, R. van Beek, B. C. Nicoll, and A. Achim. 2007. *Slope stability and erosion control: Ecotechnological solutions*. Springer. Dordrecht, The Netherlands. 287.
- ParaView. 2010. <http://www.paraview.org> (accessed 18 September 2010).
- Pollen, N., and A. Simon. 2005. Estimating the mechanical effects of riparian vegetation on stream bank stability using fiber bundle model. *Water Resources Research* 41:1-11.
- Pradal, C., S. Dufour-Kowalski, F. Boudon, and N. Dones. 2007. The architecture of OpenAlea: A visual programming and component based software for plant modeling. *5th International Workshop on Functional-Structural Plant Models*, page 25, 1-4.
- Python. 2010. Python programming language. <http://www.python.org> (accessed 18 September 2010).

- Read, J., and A. Stokes. 2006. Plant biomechanics in an ecological context. *American Journal of Botany* 93(10):1546-1565.
- Remondino, F., and S. El-Hakim. 2006. Image based 3D modeling: A review. *The Photogrammetric Record Journal* 21(115):269-291.
- Retzlaff, W. A., J. A Handest, D. M. O'Malley, S. E. McKeand, and M. A. Topa. 2001. Whole-tree biomass and carbon allocation of juvenile trees of loblolly pine (*Pinus taeda*): Influence of genetics and fertilization. *Canadian Journal of Forest Research* 31:960-970.
- Reubens, B., J. Poesen, F. Danjon, G. Geudens, and B. Muys. 2007. The role of fine and coarse roots in shallow slope stability and soil erosion control with a focus on root system architecture: A review. *Trees* 21:385-402.
- Reynolds, W. D. 1993. Saturated hydraulic conductivity: field measurement. In: *Soil Sampling and Methods of Analysis*, ed. M. R. Carter, 599-613. Canadian Society of Soil Science. Boca Raton, FL: Lewis Publishers.
- Reynolds, W. D., and D. E. Elrick. 1985. In situ measurement of field-saturated hydraulic conductivity, sorptivity, and the alpha-parameter using the Guelph Permeameter. *Soil Science* 140(4):292-302.
- Reynolds, W. D., and D. E. Elrick. 1986. A method for simultaneous in situ measurement in the vadose zone of field-saturated hydraulic conductivity, sorptivity, and the conductivity-pressure head relationship. *Ground Water Monitor. Rev.* 16:84-95.
- Riestenberg, M., and S. Sovonick-Dunford. 1983. The role of woody vegetation in stabilizing slopes in the Cincinnati area, Ohio. *Geological Society of America Bulletin* 94(4):506-518.
- Robertson, P. K., and R. G. Campanella. 1983. Interpretation of Cone Penetration Tests (Part I (Sand) and Part II (Clay)). *Canadian Geotechnical Journal* 20(4):718-733.
- Rucker, D. F., M. T. Levitt, J. Greenwood, and X. Yang. 2008. Inversion of large electrical resistivity surveys on multi-processor platforms. *Proceedings of the Symposium on the Application of Geophysics to Environmental and Engineering Problems (SAGEEP '08)*, 1316-1327.
- Saucier, R. T. 1963. "Recent geomorphic history of the Pontchartrain Basin, Louisiana," *Technical Report 16, Part A*, United States Gulf Coastal Studies, Coastal Studies Institute, Contribution No. 63-2, Louisiana State University, Baton Rouge, LA.
- Saucier, R. T. 1994. *Geomorphology and quaternary geologic history of the Lower Mississippi Valley*. Volumes I and II. Vicksburg, MS: Mississippi River Commission.
- Schnabel Engineering. 2010. Phase 2 - Geotechnical data collection and evaluation/assessment Danville Area Flood Protection System (FPS) Borough of Danville, Montour County Pennsylvania. Project 09150010.A2. West Chester, PA: Schnable Engineering.
- Scott, T. M. 1993. Geologic map of Palm Beach County. Florida Geological Survey, Open File Map Series No. 65. Tallahassee, FL: Department of Natural Resources.

- Scott, T. M., K. M. Campbell, F. R. Rupert, J. D. Arthur, R. C. Green, G. H. Means, T. M. Missimer, J. M. Lloyd, J. W. Yon, and J. G. Duncan. 2001. Geologic map of the State of Florida. 1:1,000,000 scale, Map Series 145. Tallahassee, FL: Department of Natural Resources.
- Sevon, W. D., and D. D. Braun. 2000. Glacial deposits of Pennsylvania. Map 59, Commonwealth of Pennsylvania, Department of Conservation and Natural Resources, Bureau of Topographic and Geologic Survey, Harrisburg, PA. www.dcnr.state.pa.us/topogeo/index.aspx (accessed 8 June 2011).
- Shannon and Wilson. 2000. *Geotechnical report, riverside bridge replacement, Mount Vernon and Burlington, Washington*, one volume.
- Sharma, S., and A. D. Webster. 1994. The tensile strength of small diameter woody roots of apple rootstocks in relation to poor anchorage. *Gartenbauwissenschaft* 59(5): 229-234.
- Shepherd, R. G. 1989. Correlations of permeability and grain size. *Ground Water* 27(5):633-38.
- Shields, F. D., and D. H. Gray. 1993. Effects of woody vegetation on sandy levee integrity. *Water Resources Bulletin* 28(5):917-931.
- Shlemon, R. J. 1967. *Quaternary geology of Northern Sacramento County, California*. Annual Field Trip Guidebook of the Geological Society of Sacramento. Department of Geology. Davis, CA: University of California.
- Shlemon, R. J. 1971. Quaternary deltaic and channel system in the Central Great valley, California. *Annals of the Association of American Geographers* 61(3):427-440.
- Shlemon, R. J., and E. L. Begg. 1973. Late Quaternary evolution of the Sacramento-San Joaquin Delta, California. *Quaternary Studies, Bulletin* 13:259-266.
- Society of American Foresters. 1971. *Terminology of forest science, technology, practice, and products*. F. C. Ford-Robertson, ed. Washington, DC: Society of American Foresters.
- Soilmoisture Equipment Corp. 2010. Operating instructions. Model 2800K1 Guelph Permeameter. <http://www.soilmoisture.com/operating.html> (accessed 1 May 2011).
- Steenbergen, H. M. G. M., B. L. Lassing, A. C. W. M. Vrouwenvelder, and P. H. Waarts. 2004. Reliability analysis of flood defence systems. *HERON* 49(1):51-73.
- Stoeckler, J. H., and W. A. Kluender. 1938. The hydraulic method of excavating the root systems of plants. *Ecology* 19(3):355-369.
- Stokes, A. 1999. Strain distribution during anchorage failure in root systems of Maritime pine (*Pinus pinaster* Ait.) at different ages and tree growth response to wind-induced root movement. *Plant and Soil* 217:17-27.
- Stokes, A., T. Fourcaud, J. Hruska, J. Cermak, N. Nadyezdina, and L. Praus. 2002. An evaluation of different methods to investigate root system architecture of urban trees in situ: I. Ground-penetrating radar. *Journal of Arboriculture* 28(1):1-9.

- Stokes, A., T. Fourcaud, J. Hruska, J. Cermak, N. Nadyezdhina, V. Nadyezhdin, and L. Praus. 2002. An evaluation of different methods to investigate root system architecture of urban trees in situ: I. Ground-penetrating radar. *Journal of Arboriculture* 28(1):2-10.
- Sutton, R. F., and R. W. Tinus. 1983. *Root and root system terminology*. Forest Sciences Monograph 24. Washington, DC: Society of American Foresters.
- Ter Horst, W. L., S. N. Jonkman, and J. K. Vriling. 2006. Probabilistic analysis of safety of dikes during flood waves, In C Guedes Soares & E Zio (ed.), *Safety and reliability for managing risk* (2073-2080). London: Taylor & Francis.
- Tharp, B. C., and C. H. Muller. 1940. A rapid method for excavating root systems of native plants. *Ecology* 21(3):347-350.
- Tosi, M. 2007. Root tensile strength relationships and their slope stability implications of three shrub species in Northern Apennies (Italy). *Geomorphology* 87:268-283.
- Toto, E., L. Zouhri, and A. Jgounni. 2009. Direct and inverse modelling of the ground-water flow in porous media. *Hydrological Sciences Journal* 54(2): 327-337.
- Tracy, F. T. 2006. Clean two- and three-dimensional analytical solutions of Richards equation for testing numerical solvers. *Water Resources Research* 42:1-11.
- Tracy, F. T. 1983. *User's guide for a plane and axisymmetric finite element program for steady-state seepage problems*. Instruction Report No. IR K-83-4. Vicksburg, MS: U.S. Army Engineer Waterways Experiment Station.
- Turmania, V. 1965. The strength of tree roots. *Bulleten Moskovskigo Obscestva Ispytatelej Prirody (Otdel Biologiceskij)* 70(5):36-45.
- Turnbull, W. J., E. L. Krinitzsky, and F. J. Weaver. 1966. Bank erosion in soils of the Lower Mississippi Valley. *Journal of Soil Mechanics and Foundation Division* 92(SM1):121-136.
- U.S. Army Corps of Engineers (USACE). 1941. *Investigation of underseepage, Lower Mississippi River levees*. Technical Memorandum 184-1. Vicksburg, MS: U.S. Army Engineer Waterways Experiment Station.
- U.S. Army Corps of Engineers (USACE). 1953. *Detailed design memorandum on initial contract for Rio Grande floodway, Albuquerque Unit*. Design Memorandum 1. Albuquerque, NM: U.S. Army Engineer District, Albuquerque.
- U.S. Army Corps of Engineers (USACE). 1954a. *Detailed design memorandum on Rio Grande floodway, Albuquerque unit phase II, June 1954*. Design Memorandum 2. Albuquerque, NM: U.S. Army Engineer District, Albuquerque.
- U.S. Army Corps of Engineers (USACE). 1954b *Detailed design memorandum on Rio Grande floodway, Albuquerque unit phase II, November 1954*. Design Memorandum 3. Albuquerque, NM: U.S. Army Engineer District, Albuquerque.
- U.S. Army Corps of Engineers (USACE). 1955. *Detailed design memorandum on Rio Grande floodway, Albuquerque unit phase III, July 1955*. Design Memorandum 4. Albuquerque, NM: U.S. Army Engineer District, Albuquerque.

U.S. Army Corps of Engineers (USACE). 1968. *General supplement No. 8, inner harbor navigation canal remaining levees*. Design Memorandum No. 2. New Orleans, LA: U.S. Army Corps of Engineers, New Orleans District.

U.S. Army Corps of Engineers (USACE). 1979. *Skagit River, Washington, general design memorandum levee improvements*, Two Volumes. Seattle, WA: U.S. Army Engineer District.

U.S. Army Corps of Engineers (USACE). 1990. *General design, 17th St. outfall canal*. Volumes I and II, Design Memorandum No. 20. New Orleans, LA: U.S. Army Corps of Engineers, New Orleans District.

U.S. Army Corps of Engineers (USACE). 1993. *Middle Rio Grande flood protection project Bernalillo to Belen, New Mexico*. Feature Design Memorandum. Albuquerque, NM: U.S. Army Engineer District, Albuquerque District.

U.S. Army Corps of Engineers (USACE). 1995. *Earthquake design and evaluation for civil works projects*. EM 1110-2-1806. Washington, DC: Department of the Army, Office of the Chief of Engineers.

U.S. Army Corps of Engineers (USACE). 1996. *Rio Grande and tributaries, Corrales, New Mexico, plans for middle Rio Grande flood protection project, Bernalillo to Belen, New Mexico, Corrales Unit*. Albuquerque, NM: U.S. Army Engineer District, Albuquerque District.

U.S. Army Corps of Engineers (USACE). 1999. *Evaluating the reliability of existing levees*, Appendix B in risk-based analysis in geotechnical engineering for support of planning studies. Engineering Technical Letter (ETL) 1110-2-556, 28 May, Washington, DC.

U.S. Army Corps of Engineers (USACE). 2000. *Design and construction of levees*. Engineer Manual EM-1110-2-1913. Washington, DC.

U.S. Army Corps of Engineers (USACE). 2001. *Seismic Performance of the Columbia River Levee along NE Marine Drive*. Portland, OR: U.S. Army Engineer District, Portland.

U.S. Army Corps of Engineers (USACE). 2004. *FEMA levee stability for pocket area to Freeport, Explorations*. Volume 1, American River (Common Features) California. Sacramento, CA: U.S. Army Corps of Engineers, Soil Design Section, Sacramento District.

U.S. Army Corps of Engineers (USACE). 2005a. *Geotechnical evaluation of safety, Sacramento Rivers east bank levees from approximately RM 53.7 to RM 45.3, Pocket Area to New North Beach Levee*. Draft, American River Watershed Project (Common Features) California. Sacramento, CA: U.S. Army Corps of Engineers, Soil Design Section, Sacramento District.

U.S. Army Corps of Engineers (USACE). 2005b. *Albuquerque levee investigations*, Albuquerque, NM: U.S. Army Engineer District, Albuquerque.

- U.S. Army Corps of Engineers (USACE). 2009. *Guidelines for Landscape Planting and Vegetation Management at Levees, Floodwalls, Embankment Dams, and Appurtenant Structures*. Engineering Technical Letter (ETL) 1110-2-571, 10 April, Washington, DC.
- U.S. Army Engineer Research and Development Center (ERDC). *Groundwater Modeling System*. <http://chl.erdc.usace.army.mil/gms> (accessed 19 August 2010).
- U.S. Department of Agriculture (USDA). 1964. Soil survey of Warren County, Mississippi. Washington, DC: U.S. Department of Agriculture.
- U.S. Department of Agriculture (USDA). 1978. Soil survey of Palm Beach County area, Florida. Washington, DC: U.S. Department of Agriculture.
- U.S. Department of Agriculture (USDA). 1985. Soil survey of Montour County, Pennsylvania. Washington, DC: U.S. Department of Agriculture.
- U.S. Department of Commerce (USDC). 2010. National Environmental Satellite, Data, and Information Service (NESDIS): National Climatic Data Center. <http://www.ncdc.noaa.gov/oa/ncdc.html> (accessed 19 August 2010).
- U.S. Department of Agriculture Natural Resources Conservation Service. 2010. Plants database. <http://plants.usda.gov/index.html> (accessed 20 July 2010).
- Urban Forests Ecosystem Institute, California Polytechnic State University. 2010. SelecTree. <http://www.ufei.org/about.html> (accessed 20 July 2010).
- URS. 2007. *Guidance Document for geotechnical analyses*, Urban Levee Geotechnical Evaluations Program, Revision 5, Contract 4600007418, Prepared for Department of Water Resources, Division of Flood Management, URS, Gateway Oaks Drive, Sacramento, CA, 139 p.
- URS. 2008. *Phase 1 geotechnical data report (P1GDR), Sacramento River study area*. Urban Levee Geotechnical Evaluations Program Contract 4600007418, Task Order 40, Prepared for Department of Water Resources, Division of Flood Management, URS, Gateway Oaks Drive, Sacramento, CA, 1274 p.
- URS. 2010a. *Phase 1 geotechnical evaluation report (P1GER), Sacramento River study area*. Urban Levee Geotechnical Evaluations Program Contract 4600007418, Prepared for Department of Water Resources, Division of Flood Management, URS, Gateway Oaks Drive, Sacramento, CA, 369.
- URS. 2010b. *Geomorphology and reaches, Sacramento River Study Area, plate 3, Phase 1 geotechnical evaluation report (P1GER), Sacramento River study area*. Urban Levee Geotechnical Evaluations Program Contract 4600007418, Prepared for Department of Water Resources, Division of Flood Management, URS, Gateway Oaks Drive, Sacramento, CA, 99.
- URS. 2010c. *Sacramento River plan and profile, Station 1500+00 to Station 1550+00, plate 14, Phase 1 geotechnical evaluation report (P1GER), Sacramento River study area*. Urban Levee Geotechnical Evaluations Program Contract 4600007418. Prepared for Department of Water Resources, Division of Flood Management, URS, Gateway Oaks Drive, Sacramento, CA, 110.

URS. 2010d. *Sacramento River plan and profile, Station 1550+00 to Station 1600+00, Plate 15, Phase 1 geotechnical evaluation report (P1GER), Sacramento River study area*. Urban Levee Geotechnical Evaluations Program Contract 4600007418. Prepared for Department of Water Resources, Division of Flood Management, URS, Gateway Oaks Drive, Sacramento, CA, 111.

Van Eerden, E., and J. M. Kinghorn. 1978. *Root Form of Planted Trees Symposium*, Victoria, B.C, May 1978. Proceedings, British Columbia Ministry of Forestry, Canadian Forestry Services., Joint Rep. No.8, 357.

Van Gelder, P., F. Buijs, C. M. Van, W. ter Horst, W. Kanning, M. Nejad, S. Gupta, R. Shams, N. van Erp, B. Gouldby, G. Kingston, P. Sayers, M. Wills, A. Kortenhaus, and H-J Lambrecht. 2008. *Reliability analysis of flood sea defence structures and systems*, FLOODsite Project Report T o 7 -08-01. <http://www.floodsite.net> (accessed 18 September 2010).

van Genuchten, M. Th., 1980. A closed-form equation for predicting the hydraulic conductivity of unsaturated soils. *Soil Science Society of America Journal* 44(5):892-898.

Vorogushyn, S., B. Merz, and H. Apel. 2009. Development of dike fragility curves for piping and micro-instability breach mechanisms. *Natural Hazards and Earth System Sciences* 9(2009):1383-1401.

Vrouwenvelder, A. C. W. M. 1987. *Probabilistic design of flood defenses*. Report # B-87-404. IBBC-TNO (Institute for Building Materials and Structures of the Netherlands, Organization of Applied Scientific Research), The Netherlands.

Wahler and Associates. 1986. *Initial appraisal report, investigation for levee repair, American River Flood Control District (ARFCD) and California Department of Water Resources, maintenance area no. 9, Sacramento River, Sacramento County, California*. Project COE-251D. Palo Alto, CA: Wahler and Associates.

Wahler and Associates. 1989a. *Sacramento River flood control project, Sacramento urban area levee reconstruction, basis of design*. Vol. 1. Prepared for the U.S. Army Corps Engineers, Sacramento District. Palo Alto: Wahler and Associates.

Wahler and Associates. 1989b. *Sacramento River flood control project, Sacramento urban area levee reconstruction, basis of design*. Vol. 2, Appendices. Prepared for the U.S. Army Corps Engineers, Sacramento District. Palo Alto, CA: Wahler and Associates.

Waldron, L. J. 1977. The shear resistance of root-permeated homogeneous and stratified soil. *Soil Science Society American Journal* 41:843-849.

Warrick, A. W., and H. M. Van Es. 2002. Soil Science of America, 677 /s. Segoe Rd., Madison, WI 53711, USA. Methods of Soil Analysis. Part 4. Physical Methods. SSSA Book Series, no. 5.

Watson, A. J., C. J. Phillips, and M. Marden. 1999. Root strength, growth, and rates of decay: root reinforcement changes of two tree species and their contribution to slope stability. *Plant and Soil* 217: 39-47.

Wells, O. O., and R. C. Schmidling. 1990. *Platanus occidentalis L. sycamore*. In: Burns, Russell M.; Honkala, Barbara H., technical coordinators. *Silvics of North America. Volume 2. Hardwoods*. Agric. Handbook 654. Washington, DC. U.S. Department of Agriculture, Forest Service: 511-517.

Western Regional Climate Center (WRCC). Prevailing Wind Direction.
<http://www.wrcc.dri.edu/htmlfiles/westwinddir.html> (accessed 19 August 2010).

Wilson, G. V., J. M. Alfonsi, and P. M. Jardine. 1989. Spatial variability of saturated hydraulic conductivity of the subsoil of two forested watersheds. *Soil Science Society of America Journal* 53:679-685.

Wright, S. G. 1999. UTEXAS4, a computer program for slope stability calculations. Tutorial prepared for Department of the Army, U.S. Army Corps of Engineers Washington, DC. Shinoak Software, Austin Texas.

Wright, S. G. 2009. Tutorial for UTEXAS Preprocessor Software. Shinoak Software, Austin Texas.

Wu, T. H. 1976. Investigation of landslides on Prince of Wales Island, Alaska, Geotechnical Engineering Report No. 5, Dept. of Civil Engineering, Ohio State University, Columbus, Ohio, 94 pp.

Wu, T. H., W. P. McKinnel III, and D. N. Swanston. 1979. Strength of tree root and landslides on Prince of Wales Island, Alaska. *Canadian Geotechnical Journal* 16:19-33.

Wynia, A. 1977. Monitoring nursery shipping stock. In *Plantation Establishment Symposium Proceedings*, p. 105-106, R. F. Sutton, ed. Department of Environmental Canadian Forestry Services., Sault Ste. Marie, Ont. Symp. Proc. O-P-5.

Yang, F. R., C. H. Lee, W. J. Kung, and H. F. Yeh. 2009. The impact of tunneling construction on the hydrogeological environment of Tseng-Wen Reservoir Trans-basin Diversion Project in Taiwan. *Engineering Geology* 103(1-2):39-58.

Zanetti, C., A. Weller, M. Vennetier, and P. Meriaux. 2011. Detection of buried tree root samples by using geoelectrical measurements: A laboratory experiment. *Plant and Soil* 339: 273-283.

Zee, C. H., and R. Zee. 2006. Earthquake hydrodynamic pressure on dams. *Journal of Hydraulic Engineering* 132(11):1128-1133.